Crystallographic analyses of apo and reduced azurins

A thesis presented in partial fulfilment of the requirements for the degree of Doctor of Philosophy in Chemistry at Massey University.

William E. Botelho Shepard

1991

Acknowledgements

I would like to sincerely thank my supervisors Prof. E.N. Baker and Dr. B.F. Anderson for their assistance and advice throughout this work. I would also like to thank Dr. G.E. Norris and Mrs. H.M. Baker for their kind support, encouragement and many helpful discussions during this study.

Thanks are also due to the following:

Kate McPherson and Musa Shongwe for helping with the mounting of the photographs in this thesis.

Dr. R.C. O'Driscoll for help with problems related to the word processor hardware used in the typing of this thesis.

Computer Centre Staff for help with computing problems.

Central Photographic Unit for processing the photos of this thesis.

Dr. G.E. Norris and Mrs. H.M. Baker for assistance in purification and crystallisation experiments.

Prof. E.N. Baker, Dr. B.F. Anderson and Dr. G.E. Norris for proof-reading and comments.

Dr. B.F. Anderson for help in computing and programming.

Special thanks and appreciation go to my parents and sister, and many friends who have given me much moral support and encouragement during this time; especially Dave Leithwick, Lawrence Mantjika, Kate McPherson, Joanna Nilsen, Mike O'Hara, Jeff Sluka, Karen Tyrrell, Hugo Vitalis and members of the Massey University Tae Kwon Do Club.

Finally, I would like to thank the Massey University for my appointment as Graduate Assistant, and the Society of the Crystallographers in Australia for the "1987 Scholarship" to attend the 15th I.U.Cr. Congress held in Bordeaux, France.

Abstract

Crystals of the blue copper protein azurin, from *Alc. denitrificans*, have been prepared in the apo (metal-free) and reduced (Cu(I)) forms by soaking oxidised (Cu(II)) azurin crystals in solutions containing cyanide and ascorbic acid, respectively. The apo and reduced azurin crystals are isomorphous with the oxidised crystals, containing two protein molecules in the asymmetric unit. A CAD4 diffractometer was used to collect X-ray diffraction data from these crystals, to 2.2Å resolution for apo-azurin and 1.9Å for reduced azurin. Both crystal structures have been refined using restrained least-squares methods, treating the two protein molecules of the asymmetric unit independently, to give final R-factors of 0.158 for apo-azurin (1956 protein atoms and 275 solvent atoms) and 0.166 for reduced azurin (1967 protein atoms and 269 solvent atoms).

Analysis and comparison of these structures with that of the oxidised form show that the protein structure is essentially identical between all three forms. However, very small changes, which are consistent between the two independent molecules of the asymmetric unit, are apparent at and near the copper binding site. Upon reduction of the oxidised form, all copper distances (left unrestrained during refinement) increase by 0.05-0.10Å, while the geometry remains unchanged. Thus the copper in reduced azurin is bound strongly by one thiolate sulphur (Cys-112) and two imidazole nitrogens (His-46 and His-117) in a trigonal arrangement, while a thioether sulphur (Met-121) and a carbonyl oxygen (Gly-45) approach the copper from axial directions to complete a distorted trigonal bipyramidal geometry. The Cu...S_δ 121 distance is 3.2Å, and does not agree with the 2.7Å distance predicted by EXAFS studies despite attempts to restrain this distance during refinement. Two S...HN hydrogen bonds, between the cysteine sulphur and peptide NH groups, are shortened by ≈0.2Å upon reduction of Cu(II) to Cu(I).

The configuration of the copper ligands and the surrounding structure are maintained when the copper is removed. This shows that the folding of the polypeptide chain determines the conformation of the metal ligands, enforcing a distorted geometry on the copper centre in both oxidised and reduced forms. The structure of the copper binding site in the apo form is more similar to the oxidised form than to the reduced form.

The observations made in the analysis of these three forms of azurin have implications for the biological function of the protein, which is thought to be electron transfer. The distorted geometry of the copper, which is enforced upon the metal by the protein, supports the concept of the entatic state, whereby the copper is held in a geometry approximating the transition state between the coordination preferences of Cu(II) and

Cu(I). Since minimal changes at the active site occur upon reduction, the protein accomplishes its function of fast electron transfer by minimising the activation energy of the process.

Erratum

p. 45 Reference number 395 should be 210.

Table of Contents

Chapter 1 : Introduction

1.1 Copper in Biology

Copper is an essential element for many biological systems, being the third most abundant trace metal in humans, after zinc and iron[1]. In many proteins, copper is necessary for biological function. Of the copper proteins currently known to date, the metal provides for a wide variety of functions including electron transfer, O_2 transport, substrate catalysis and copper acquisition[2,3,4].

In recent years, there has been considerable research into copper proteins. The emphasis has focussed on the role of the metal in the active sites of these proteins, because of the diversity of functions performed. Also, many of the copper centres display unusual physical and chemical properties, which are seldom observed in low molecular weight copper complexes. These unusual properties have encouraged chemists to design models of these active sites in an effort to understand the nature of the copper and its role in the protein. Several reviews on copper proteins have appeared in the literature over the years (for examples see Fee (1975)[5] or Adman (1991)[2], including a comprehensive series edited by R. Lontie (1984)[3]).

Classification of copper proteins has been based on the different spectroscopic properties of the copper centres. Vänngård proposed a classification which differentiated them into three types, namely, *type 1*, *type 2* and *type 3* [5,6]. Type 1 copper in the cupric form is intensely blue coloured and exhibits an unusual electron paramagnetic spectrum. Hence, proteins containing this copper centre are often called the "blue" copper proteins. Type 2 copper is more typical of inorganic copper complexes, and is sometimes referred to as the "non-blue" copper. The last class of copper centres, type 3, is diamagnetic instead of paramagnetic, as is expected for Cu(II), in the cupric state. Of course, some metalloproteins contain active copper centres which do not conform to this classification, but these copper centres have received less attention than the other three types. Although this classification has some drawbacks, it does have the advantage of also separating the copper sites according to their most likely biological functional roles.

1.1.1 Type 1 Copper centres

Metalloproteins with type 1 copper centres have been studied extensively, because of their unique spectral properties (for reviews see Fee (1975)[5], Lappin (1981)[7], Farver and Pecht (1984)[8], Ryden (1984)[9] and Adman (1985)[10]). These proteins are found in plants,

bacteria, vertebrates, fungi and some algae, either as a single type 1 centre as in the small blue copper proteins[2,5,9,10], or in conjunction with other types of copper centres (type 2 and type 3) as in the larger blue oxidases[2,3,4,5]. In both groups, the type 1 copper is vital for activity. The small blue copper proteins (e.g. plastocyanin and azurin) range in molecular weight from 10-20kDa, and are found in bacteria, plants and some algae. The multi-copper blue oxidases which contain type 1, 2 and 3 copper centres (e.g. ascorbate oxidase and laccase), however, are found in the more highly evolved plants and in animals, and range in size between 80-140kDa. The type 1 copper centre in these multi-copper oxidases acts in conjunction with the other copper centres to perform the overall function of the protein. Some of the blue oxidases (e.g. ceruloplasmin[11] and ascorbate oxidase[7,12,13]) are thought to contain more than one type 1 copper centre. However, recent crystallographic analysis has shown only one type 1 copper present in ascorbate oxidase[14].

The function of the type 1 centre in all of the blue copper proteins is assumed to be electron transfer, although the specific physiological redox partners are known only for some of these proteins (e.g. amicyanin[15-20], plastocyanin[9,21] and pseudoazurin[22]). The transfer of electrons may take place either between two redox proteins (as for the small blue copper proteins), or between a substrate and a copper centre (as for the blue copper oxidases). Kinetic studies show that the electron transfer exchange rates are very fast both between small blue copper proteins and their physiological partners ($\approx 10^7$ Ms^{-1})[23,7,24,25], as well as between copper centres in the multi-copper proteins ($\approx 10^6$ Ms^{-1})[11,26]. Electron transfer in the self-exchange (ESE) reaction between two molecules of the same protein was also found to have a high rate ($\approx 10^6$ Ms^{-1}) from NMR experiments[27,28].

Early interest in the blue copper proteins focussed on the unique spectral properties of the type 1 copper site. The most prominent feature in the UV-Visible spectra of type 1 copper centres is the intense absorption near 600nm (ε_{max} = 3000 - 5000 cm^{-1}), which gives these proteins their characteristic deep blue colour. Raman and metal substitution studies have suggested this absorption is mainly due to a S(Cys)$\sigma \rightarrow$ Cu charge transfer band with small contributions from the other ligands[2,7,10]. Type 1 copper centres also show very unusual electron paramagnetic resonance (EPR) spectra in the oxidised, paramagnetic Cu(II), state. The EPR spectral parameters, $g_{\|}$ and $g_{\perp}$, are similar to those of small Cu(II) complexes, but the the hyperfine splitting constant, $A_{\|}$, is unusually small (<100 cm^{-1}). Also, the redox potential for these proteins is unusually high ranging from $\approx$200-600mV[5,7,8,10]. These properties will be discussed in more detail in Section 1.2.

Prior to the availability of hard structural data, type 1 copper sites were thought to contain nitrogen and sulphur ligands, but little was known about their coordination until the structure of the copper site was determined by X-ray diffraction methods [14,29-41]. These studies show that the copper generally has four ligands arranged in a irregular geometry (see Figure 1.1.1.1). The distorted geometry is a special feature of these copper sites, and is thought to explain some of their unusual properties. The structure of the blue copper proteins will be discussed in more detail below (see section 1.2.7).

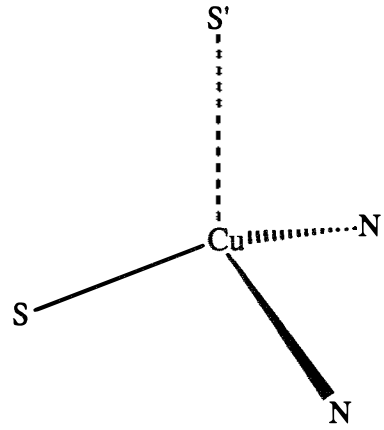

Figure 1.1.1.1 The basic arrangement of ligands in the "type 1" copper site.

1.1.2 Type 2 copper centres

Most type 2 copper centres are involved in the biological oxidation of substrates[2,4,5,42], although the role of the copper ion in these processes is as yet unclear. The mono-copper oxidases (e.g. amine oxidase[43] and glactose oxidase[44]), the multi-copper blue oxidases[11,26,45] and Cu/Zn superoxide dismutase[46] all contain type 2 copper centres which are critcal to the function of these proteins[42]. In some cases, other cofactors participate with the type 2 copper site in the protein function, especially when a two electron oxidation is involved (e.g. galactose oxidase[2]). Type 2 copper containing proteins are located in many biological systems. For example, the mono-copper oxidases are found in fungal, plant and mammalian tissues[42].

The type 2 copper centre has spectral properties similar to those found in low molecular weight Cu(II) complexes with nitrogen and/or oxygen ligands arranged in square planar or distorted tetragonal geometries[47]. These copper sites absorb weakly in the 320, 450-480, and/or 600nm regions of the visible spectrum[2,4,5,42] and have EPR parameters of $g_{||}$ $\approx$2.3, $g_{\perp}$ $\approx$2.0 and $A_{||}$ $\approx 200 \times 10^{-4}$ cm^{-1} [43,44,46,48,49]. Originally, the type 2 classification was intended to include only the copper centers which were neither type 1 nor type 3 in the multi-copper oxidases, but superoxide dismutase and the mono-copper

oxidases have since been included in this classification despite the differences in chemical reactivity, because of their similar spectroscopic properties[5].

X-ray crystal structures have been determined for two proteins with type 2 copper centers, bovine Cu/Zn superoxide dismutase[50] and galactose oxidase from the fungus *Dactylium dendroides* [51]. These proteins, each of which has only one type 2 copper centre have been refined to 2.0Å resolution and 1.7Å resolution, respectively. The structure of superoxide dimutase has shown the type 2 copper atom to be coordinated to four imidazole nitrogens of histidine side-chains with a distorted tetrahedral or square planar geometry. The type 2 copper site in ascorbate oxidase[14] is actually part of a trinuclear copper site, and will be dealt with in section 1.1.4. In the structure of galactose oxidase, the copper is bound in a square pyramidal geometry by two histidines, two tyrosines and one acetate (one tyrosine forms the axial ligand). Figure 1.1.2.1 depicts the copper geometries of type 2 centres.

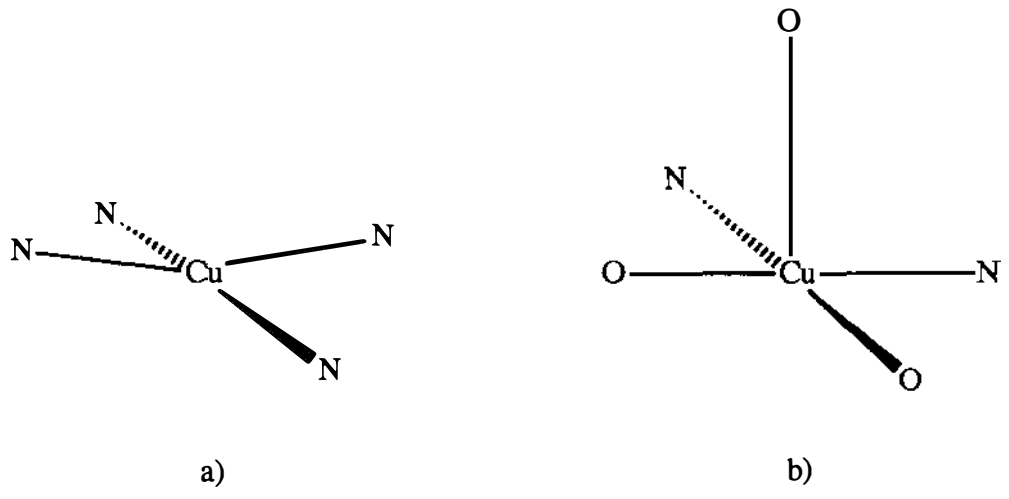

Figure 1.1.2.1. Two examples of type 2 copper centers from a) superoxide dimutase and b) galactose oxidase.

1.1.3 Type 3 copper centres

Type 3 copper centres have received much attention because they are binuclear and have the ability to bind molecular oxygen. The proteins which contain this copper centre fulfil a variety of different biological functions, including oxygen transport (e.g. hemocyanin[52]), hydroxylation (e.g. tyrosinase[53]), and the four electron reduction of O_2 to H_2O (e.g. laccase and ascorbate oxidase[6,11,26,45,54,55]). Type 3 copper centres may occur as an isolated binuclear site, as in hemocyanin, or as part of a trinuclear cluster as in the blue oxidase ascorbate oxidase[14]. Hemocyanin is typically found in arthropods and molluscs[2,52], the blue oxidases in plants and vertebrates, while tyrosinase can be found

in bacteria, fungi, plants and mammals[53]

In the oxidised Cu(II)-Cu(II) state, the normally paramagnetic Cu(II) ions are EPR silent. This EPR silence is the result of the two copper atoms lying within close proximity (3-4Å) to each other, and coupling through a strong antiferromagnetic interaction [2,56,52]. This coupling of the coppers also accounts for the intense optical absorption at 330nm, which is assigned to a $O_2^{2-} \rightarrow$Cu(II) charge transfer band[55,57]. An endogenous bridging ligand has been proposed on the basis of spectroscopic analysis[58], but has not been seen in structural analyses[14,59]. How the O_2 molecule binds to the copper pair has not yet been fully established, but a model where the dioxygen binds as a peroxide bridging two the coppers in a cis μ-1,2 fashion (Figure 1.1.3.1b) explains EPR, resonance Raman[60-62] and UV/visible spectra[52,53,55].

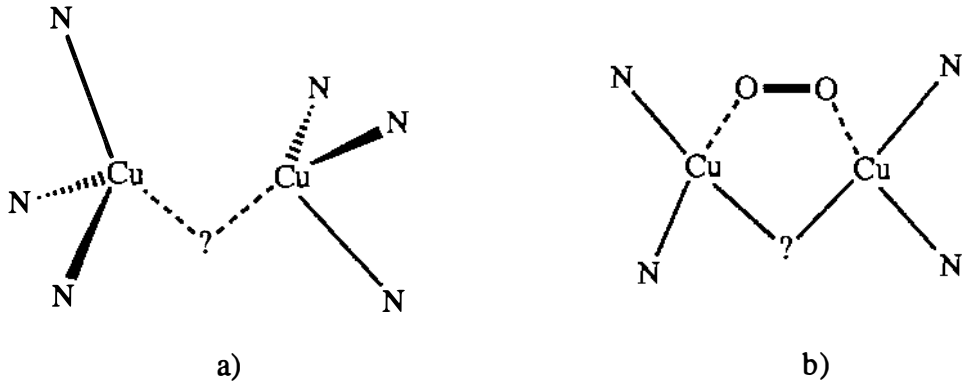

Figure 1.1.3.1. Schematic diagrams of a) the copper pairs in hemocyanin as seen in the crystal structure at 3.2Å resolution[59], and b) a possible model for O_2 binding from resonance Raman studies. A question mark (?) indicates a possible endogenous bridging ligand.

X-ray crystallographic analyses have been carried out on two copper proteins with type 3 centres; hemocyanin from *Panulirus interruptus* [59] and the multi-copper protein ascorbate oxidase from zucchini[14]. In both structures, the two copper atoms are approximately 3.4Å apart and are coordinated by a total of six imidazole nitrogens, three bound to each copper (see Figures 1.1.3.1a and 1.1.3.2). It should be mentioned, however, that in ascorbate oxidase, the ligand assignment is tentative, as the primary sequence is only partially known[14]. For ascorbate oxidase, the partial structural analysis has established that the type 2 and type 3 copper centres are close enough together to be considered as a trinuclear type 2-type 3 copper cluster (with a type 2 to type 3 copper separation of 4.0Å)[14]. The copper which is labelled type 2 in ascorbate oxidase[14] has two imidazole nitrogen ligands from histidines and a possible third ligand as OH^- or H_2O , which may suggest that this copper centre is directly involved with O_2 or an oxygen complex during the biological activity of the protein. On the basis of EPR studies, such a trinuclear cluster is also thought to occur in mammalian ceruloplasmin, where the cluster is essential for

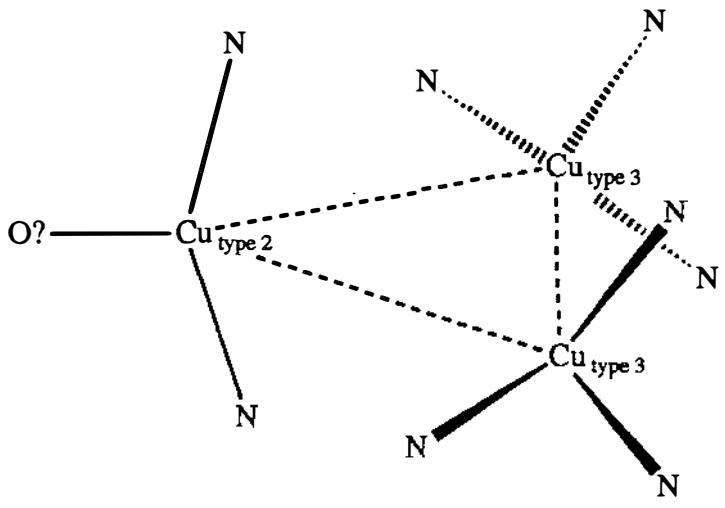

Figure 1.1.3.2. A schematic diagram of the trinuclear copper site of ascorbate oxidase. A hydroxyl group (designated O?) may possibly bind to the type 2 copper.

efficient transfer of an electron to O_2[63].

1.1.4 Other copper centres

Other types of copper centres exist apart from the those classified as type 1, 2 or 3. Technically, the trinuclear copper centre in ascorbate oxidase does not come under the type1-3 classification, but *spectroscopically* the coppers are distinct, and prior to X-ray structural studies the two copper types were considered separate[11,14,26,45]. Examples of other copper proteins which have copper centres that can not be classed as type 1-3, are copper-metallothionein[64], cytochrome c oxidase[65,66], nitrous oxide reductase[67,68], nitrite reductase[2,69] and uricase[2,69]. Here, only three of these copper centres will be discussed.

The metallothioneins are low molecular weight proteins rich in cysteine (approximately 33% of amino acid residues)[4,64]. These proteins are thought to be in involved in acquisition and/or detoxification of metals such Hg, Cd, Zn or Cu. A recent report has suggested that a possible role for copper-metallothionein is the reconstitution of plantacyanin, a basic blue copper protein[70]. The structure of the copper sites in metallothionein, as determined by EXAFS[71], is thought to be four coordinate with cysteine sulphurs as single ligands and/or bridging ligands, giving rise to CuS clusters.

A novel copper site has been proposed for the copper in cytochrome c oxidase[72-74] and nitrous oxide reductase[68], designated Cu_A. Although the EPR spectrum of Cu_A is like that of type 1 copper centres, the visible spectrum is not (nitrous oxide reductase has a pink form and a purple form)[2]. EXAFS measurements have indicated that Cu_A has two

nitrogen (or oxygen) and two sulphur ligands[75]. This is supported by EPR spectroscopy and electron nuclear double resonance (ENDOR) which confirms that the Cu_A site may be accounted for by a monomeric Cu(II) ion with two histidine nitrogen and two *cysteine* sulphur ligands[73,76] (not to be confused with the N_2SS' coordination of the type 1 copper centre). In the case of cytochrome c oxidase which also contains a heme group, a second copper site, Cu_B, is proposed to bind O_2 in association with the heme[65] as a binuclear Cu/Fe heme centre. This was suggested by Palmer *et al.*[77] after the discovery of the absence of any EPR signal for both Cu_B and Fe heme. Many researchers now favour a model where the molecular oxygen binds as a μ-peroxo ligand between the Cu_B and Fe heme a_3 centres (see Figure 1.1.4.1)[78-80].

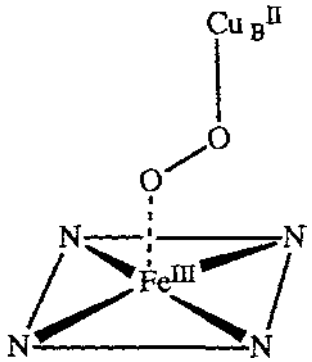

Figure 1.1.4.1. The proposed model for the binuclear Cu_B/Fe heme centre in cytochrome c oxidase[78-80].

1.2 Properties of the blue copper proteins

1.2.1 Electronic Absorption spectra

The ultraviolet and visible spectrum of the blue copper proteins is made up of several bands[81]. The most prominent feature of the spectra is the intense absorption ($\varepsilon \approx 2000$-$5000\ M^{-1}cm^{-1}$) in the visible region near 600nm giving the proteins their characteristic blue colour. This band is flanked on both sides by weaker bands at about 450nm and 780nm, and a poorly resolved d-d absorption is found in the near infrared between 900nm and 1100nm[10,82,83]. The two bands near 600nm and 780nm are assigned as $S(Cys)\sigma \rightarrow Cu(d_{x2-y2})$ and $S(Cys)\pi \rightarrow Cu(d_{x2-y2})$ ligand→metal charge-transfer transitions (respectively) between the cysteine sulphur and the copper(II) atom[81,82,83]. The higher energy band near 450nm is assigned to a $N(His)\pi \rightarrow Cu(d_{x2-y2})$ charge transfer transition[84]. Table 1.2.1.1 gives the λ_{max} of these transitions for some of the blue copper proteins.

Table 1.2.1.1. Electronic Spectral Assignments for some selected Blue Copper Proteins, λ_{max} (nm).

Assignment	*Alc. denitricans* azurin	*Ps. aeruginosa* azurin	Spinach plastocyanin	*Rhus vernicifera* stellacyanin
$N(His)\pi \rightarrow Cu(d_{x2-y2})$	460	481	490	450
$S(Cys)\sigma \rightarrow Cu(d_{x2-y2})$	619	625	597	608
$S(Cys)\pi \rightarrow Cu(d_{x2-y2})$	780	779	780	850
d-d	900-1000	≈1100	-	-
Reference	82	81	5	5

Comparison of the intense $S(Cys)\sigma \rightarrow Cu(d_{x2-y2})$ charge transfer band in azurins and plastocyanins shows that the band is at a characteristically higher energy, lower wavlength, in plastocyanins than in azurins (λ_{max} ≈600nm compared to ≈620nm)[7,82]. The origin of this difference is not understood, but it does imply that there is some variation in the electron density on the copper atom. Since the Cu-S(Cys) bondlength appears to be very similar in both proteins from EXAFS results, two other possible explanations that have been put forward are; 1) a variation in the weak axial interaction of the methionine sulphur, which may withdraw electronic charge from the copper atom[85], and 2) a variation in the number and strength of the S...HN hydrogen bonds made to the cysteine sulphur may affect the charge transfer band[31].

A shift to shorter wavlengths is observed in the 600nm absorption band at higher pH values, and appears to be a general feature of the blue copper proteins. In azurin, when the pH is increased from 10.5 to 11.4, the band at 619nm moves to 610nm[82]. A similar change is seen in stellacyanin which shows a change from 604 to 588nm between pH 9

and 11[5,87]. Shifts of this nature are seen in other blue copper proteins, for example laccase[87,88], mavicyanin[89], umecyanin[90] and ascorbate oxidase[88]. Since these bands are assigned to charge transfer transitions at the copper center, the shift to higher energy suggests a build up in the electron density at the copper possibly associated with changes in the copper bond lengths and angles[91]. Note that these changes parallel modifications seen in the EPR spectrum of the blue copper proteins (see section 1.2.2).

1.2.2 Electron paramagnetic resonance spectra

One of the most distinctive features of the blue copper proteins is their unique electron paramagnetic resonance (EPR) spectra. The EPR spectra of these copper centres are axial ($2.0 < g_{\perp} < g_{||}$), with some proteins displaying a small rhombic distortion[5,7,10,81], with a characteristically small hyperfine coupling constant ($A_{||} < 100 \times 10^{-4}$ cm^{-1}). The g-values of the spectrum indicate that the d_{x2-y2} orbital is the ground state of the unpaired electron. Initially, the spectra were explained in terms of an asymmetric copper geometry tetragonally flattened from a tetrahedral geometry[7,10,81,93]. Since then, however, the X-ray crystal structures of several blue copper proteins suggest that a N_2S donor set is sufficient to define these spectra[82]. Also, the variation of the Cu...S(Met) distance between proteins has little effect on the EPR spectrum[82]. Futhermore, analysis of single crystal EPR spectra, and ligand field calculations on plastocyanin show that the d_{x2-y2} orbital of the unpaired electron lies roughly in the plane of imidazole nitrogens and thiolate sulphur[83]. On theoretical grounds, because of the rhombicity of the g-values, the density of the unpaired electron in plastocyanin is 40% localised over the d_{x2-y2} orbital of the copper and 36% delocalised over the p_{π} orbital of the thiolate sulphur[92,93]. Theoretical analysis of model complexes with C_s or C_1 geometry rationalises the low $A_{||}$ value seen in the blue copper proteins as a result of a high degree of delocalisation of the unpaired electron in the d_{x2-y2} orbital onto the p_{π} orbital of the thiolate sulphur[92]. In general, the g-values and the hyperfine splitting constant, $A_{||}$, can be largely accounted for by a high degree of delocalisation of the unpaired electron over the copper and thiolate sulphur, which results in copper-sulphur bonding with a high covalent character[92].

Studies involving model compounds have had little success in mimicking the EPR properties of the blue copper site (for a recent reveiw see Bouwman *et al.* (1990)[94]). What has been shown, however, is that thiolate coordination alone does not produce the low $A_{||}$ value, although the g-values of these model complexes are similar to the blue copper centres. A low $A_{||}$ value was reported to be observed in the cluster $[Cu^{I}_{10}Cu^{II}_{2}L_{12}(MeCN)_4](BPh_4)_2$, where the Cu(II) centres have a distorted square pyramidal geometry and N_3S_2 donor set[95]. Upon re-examination of the spectra,

however, there are five unevenly spaced hyperfine lines in the $g_{\|}$ region, and it was concluded that the initial interpretation was over simplified[82]. One model, a Cu(II) substituted insulin incorporating a coordinated pentafluorothiophenol, mimics remarkably well the spectroscopic characteristics of the blue coppper proteins (λ_{max} = 626nm, ε_{max} = 2.0 $mM^{-1}cm^{-1}$; $A_{\|} = 80 \times 10^{-4}$ cm^{-1}, $g_{\|}$ = 2.281, $g_{\perp}$ = 2.079)[96]. The Cu(II) ion is presumed to be bound to three histidine residues supplied by three protein subunits, with the fourth ligand as the pentafluorothiophenol completing a distorted tetrahedral geometry. In site directed mutagenesis studies on azurin, the characteristic EPR spectrum disappears when one of the histidine ligands is mutated into a glycine[97]. However, the spectrum returns after the addition of N-methylimidazole to the mutant protein, indicating that the imidazole ligands are also necessary for the blue copper site. In another site directed mutagenesis experiment, replacing the methionine with a leucine only slightly alters the EPR parameters, implying that the methionine sulphur is not necessary to produce the characteristically small hyperfine splitting (see Section 1.2.8)[98].

Table 1.2.2.1. EPR parameters of some blue copper proteins and the type 1 copper centres of the blue oxidases.

Protein/Source	EPR	$g_{\perp}$	$g_{\|}$	$A_{\|}$ ($\times 10^{-4}cm^{-1}$)
azurin				
Pseudomonas aeruginosa[93]	rhombic	2.035,2.052	2.263	56
pH 5.2				
pH 9.2		2.035,2.051	2.276	51
azurin				
Alcaligenes denitrificans[82]				
pH 6.5	axial	2.059	2.255	60
pH 11.4		2.058	2.278	69
rusticyanin				
Thiobacillus ferroxidans[99]	rhombic	2.019, 2.064	2.229	65, 2, 45
plastocyanin				
spinach[100]	axial	2.053	2.26	50
umecyanin				
horseradish root[101]	axial	2.05	2.317	35
stellacyanin				
lacquer tree[87]	rhombic	2.03, 2.08	2.29	57, 29, 35
cucumber basic protein				
cucumber seedlings[102]	rhombic	2.02, 2.08	2.207	60, 10, 55
mavicyanin				
green squash fruit[89]	rhombic	2.03, 2.08	2.29	57, 29, 35
laccase				
Rhus vernicifera[88]	axial	2.055	2.298	48
ascorbate oxidase				
Cucumis sativus[88]	axial	2.050	2.230	65

EPR spectra have been measured under different pH conditions for many of the blue copper proteins [82,93,87,88,103-106]. In the pH range of 4-10, the EPR properties remain unchanged. Above pH 10, the EPR spectrum is modified slightly for some proteins, although the copper coordination site maintains its type 1 properties (e.g. azurin[82],

stellacyanin[87,106], umecyanin[90] and plantacyanin[105]). Other proteins (e.g. plastocyanin[103], ascorbate oxidase[88] and laccase[87,88]) are observed to undergo an autoreduction of the copper centre at alkaline pH. In plastocyanin this occurs at pH 10.2. Note that for laccase, the pH dependence of the EPR spectrum was originally interpreted as a modification[87] instead of an autoreduction[88] at high pH.

For *Ps. aeruginosa* and *Alc. denitrificans* azurins, the effect of pH on the EPR properties is similar to those seen in other blue copper proteins. Between pH 5.2 and 9.2, the EPR spectrum of *Ps. aeruginosa* azurin changes from 2.263 to 2.276 in $g_{||}$, and from 56 to 51 $\times 10^{-4}$ cm^{-1} in $A_{||}$ [93]. This effect has been tentatively assigned to changes in the conformation of His-35 which is in the second coordination sphere of the copper site[93]. The EPR spectrum of *Alc. denitrificans* azurin does not change in the pH range 4.0-10.5 ($g_{||}$ = 2.255 and $A_{||} = 60 \times 10^{-4}$ cm^{-1}), but over the pH range 10.5-11.4 the values of $g_{||}$ and $A_{||}$ increase slightly to 2.278 and 69×10^{-4} cm^{-1}, respectively.

1.2.3 Redox potential

Another special feature of the blue copper proteins is their relatively high redox potential (E°) with respect to the aqueous Cu(II)/Cu(I) couple (+153mV). The redox potential for blue copper proteins ranges from +184mV in stellacyanin[10] to +680mV for rusticyanin[107] (see Table 1.2.3.1[7,82,85,91,109-111]). Azurins as a group have E° values between 230mV and 308mV[82]. The high redox potentials are attributed to the mixture of imidazole nitrogen and sulphur ligands in the copper site, and reflect a stabilisation of the Cu(I) state.

Table 1.2.3.1. Redox potentials of some blue copper proteins.

Protein	E° (mV)	Protein	E° (mV)
azurin (*Alc. denitrificans*)	276	pseudoazurin (*Ach. cycloclastes*)	245
azurin (*Ps. aeruginosa*)	308	rusticyanin (*Th. ferrooxidans*)	680
azurin (*Alc. faecalis*)	266	mavicyanin (zucchini)	285
plastocyanin (spinach)	370	umecyanin (horseradish)	283
stellacyanin (*R. vernicifera*)	184	plantacyanin (cucumber seedlings)	317

Recent studies on copper complexes show that several factors govern the value of the redox potential. Although ligand type is important, other factors such as the metal geometry and the surrounding environment of the copper site are just as important. In general, sulphur ligands raise E° (thioether sulphurs more than thiols[112-114]), oxygen ligands lower E°, and nitrogen ligands can do either, lowering E° if saturated or raising E° if aromatic[114-116]. The geometry of the copper greatly effects E°, as is clearly shown in the comparison of two similar N_2S_4 macrocycles, where a change in the copper

geometry from octahedral (N_2S_4) to tetrahedral (N_2S_2) is accompanied by an increase in E° of 316mV[117]. Ainscough *et al.*[82] have suggested that the ≈100mV difference in E° between plastocyanin (370mV) and azurin (276mV) is due to the differences in copper-ligand distances and geometry. Furthermore, substitution of the methionine ligand in *Ps. aeruginosa* azurin with the softer ligand seleno-methionine raises the E° by 25mV. This effect is expected since the softer Se(Met) group is Cu(I) stabilising[118]. The surrounding environment of the copper site also effects the value of E° as shown by site directed mutagenesis studies (see Section 1.2.8), where a more hydrophobic environment destabilises the oxidation state with the higher electronic charge, resulting in a higher E°.

The redox potential for many blue copper proteins varies with pH[119], usually dropping with increasing pH (e.g. pseudoazurin, plantacyanin and stellacyanin). The redox potentials of both plastocyanins and azurins also have been shown to decrease with increasing pH[100,120,121]. In the case of plastocyanin, the change in E° with respect to pH is thought to be correlated with a change in the copper site resulting from protonation of one of the copper ligands in the reduced Cu(I) state[122]. NMR studies on azurin from *Ps. aeruginosa* have suggested that the structure undergoes a pH-dependent conformational change[28,123-127]. Protonation of a histidine residue (His-35)[123-127], and/or changes in the Cu-S(Met) interaction[123] have been proposed as explanations for the pH dependence of E° in *Ps. aeruginosa* azurin. X-ray crystallographic studies on this protein at two pH values (5.5 and 9.0), however, show that the copper site is identical at high and low pH[41]. In addition, the azurins from *Alc. denitrificans* and *Alc. faecalis* do not appear to undergo similar conformational changes with pH, despite the pH dependence of E° [110,128]. An interesting point is that the E° values for these two proteins (276mV[82] and 266mV[110], respectively) are more typical of those found for azurins than the value for *Ps. aeruginosa* (308mV[109]). The latter is the highest of the azurins[82].

1.2.4 Resonance Raman Spectra

Resonance Raman (RR) spectroscopy has been used as a probe of the internal vibrational modes of the copper site in analysing several blue copper proteins. Several approaches have been used, including isotopic substitution of copper, hydrogen-deuterium exchange[82,129], spectral enhancement at cryogenic temperatures[130-132] and theoretical analysis[133-135]. Although the spectra are not understood in detail, basic features have been established, despite subtle variations which reflect minor differences in structure.

In the blue copper proteins, RR peaks due to vibrational fundamentals appear below 500cm^{-1}, and are enhanced by wavelengths near 600nm, arising from the Cu-S(Cys)

charge transfer chromophore. Above 500cm^{-1}, the spectra are dominated by overtones and combinations of the fundamentals[82,129,132,136]. Two sets of fundamental RR bands at ≈270cm^{-1} and ≈400cm^{-1} are characteristic of blue copper centres. Four very strong peaks are usually observed in the 400cm^{-1} region, and are assigned to Cu-S(Cys) stretching modes[129,132]. Normal coordinate analysis calculations on tetrahedral CuN_2SS' models predicts a considerable mixing of vibrational modes, particularly from the Cu-S(Cys) coordinate[134]. Originally, variations in the RR spectra were thought to reflect differences in the coupled vibrations of Cu-S(Cys) modes with other ligands[82], but more recent studies show that the diversity stems from the difference in the peptide structure surrounding the copper site[135]. Although no single peak in the 400cm^{-1} region is due to pure Cu-S(Cys) stretch, this stretch is the main contributor to peaks in this region, with extensive coupling to skeletal deformations from the protein structure[135]. For azurin and plastocyanin, two of four peaks in the 400cm^{-1} region are thought to have contributions from the S_γ-C_β-C_α angle bend. The other two have mixed modes involving as yet unestablished internal ligand coordinates, which could arise from deformations of the histidines and/or the C_α of the cysteine[129,132].

The bands at 270cm^{-1} have been assigned to the Cu-N(imidazole) stretching modes with contributions from the other ligand coordinates, because of a marked deuterium isotope effect[129,137]. In *Alc. denitrificans* azurin and laccase, however, the assignment of these bands to Cu-S_γ-C_β deformation may be more appropriate[82,134,137], since no deuterium isotope effect is shown. Consequently, the assignments of these peaks for some proteins may include internal deformations due to the cysteine ligand coupling to the Cu-N(His) stretches[129]. Previously these bands were assigned to Cu-S(Met) stretching modes based on model copper thioether complexes[129,139], but this assignment has been questioned[134] because refined crystal structures of blue copper proteins show the Cu-S(Met) distance to be very long for a bond (2.7-3.1Å)[31,32,34,41]. Also, where Met-121 has been replaced by seleno-methionine in *Ps. aeruginosa* azurin, the RR spectrum was shown to be indistinguishable from that of the native protein[134].

Of particular interest is the RR spectrum of stellacyanin[132,140,129,137], which shows the greatest variation among blue copper proteins. Some of the RR peaks are proposed to contain contributions from a Cu-S(disulphide) stretch[129,139], but one peak at 1233cm^{-1} has been unambiguously assigned to the amide vibration of a peptide group, which is thought to coordinate to the copper through a backbone carbonyl oxygen[129].

Although there is a wealth of RR spectral data available, it is still difficult to relate the subtle differences in spectra to differences in structure[82]. The current knowledge of these

spectra has only laid down a partial framework for interpreting those from other less well characterised copper sites (e.g. nitrite reductase[130]). Once the RR spectra of different blue copper proteins can be interpreted precisely in terms of bonding and structure, the variations in the blue copper proteins will be better understood.

1.2.5 Nuclear Magnetic Resonance Spectra

Experiments in nuclear magnetic resonance (NMR) have provided much information on structure and behaviour of the blue copper proteins[141-146]. Initially NMR experiments were carried out to identify the copper ligands, and the residues making up the surrounding environment[125,147,148]. Later, more sophisticated experiments were carried out to determine structural changes dependent on pH, to measure the electron self exchange rate[27,28,128] and to compare the Cd-substituted binding sites of different blue copper proteins[143]. Three-dimensional structures of three plastocyanins have also been determined by high field NMR experiments[145,149,150,151]. Here, only the main points regarding the NMR spectra of azurin are discussed, since the work on all of the blue copper proteins is very extensive.

The copper ligands of azurin were determined by utilising the paramagnetic broadening effects of the Cu(II) ion, and comparing the spectra of the apo, Cu(I) and Cu(II) forms[125,147,149]. The paramagnetic Cu(II) ion broadens resonances in the aromatic and aliphatic region indicating that the copper site is buried in the hydrophobic interior, inaccessible to the solvent medium[125,148]. The appearance of two non-titratable histidine side-chains was considered evidence for these as possible copper ligands[125,147,148]. Ugurbil *et al.*[125] also suggested the possibility of an amide group coordinated to the copper on the basis of ^{13}C NMR data. The assignment of the Met-121 copper ligand was not clear in early NMR experiments, but after the determination of the crystal structure, the methyl group of Met-121 was found to lie above an aromatic ring, and could be easily identified from the ring current shifts of their signals. Several papers have noted that this aromatic ring appears to be structurally conserved in all blue copper proteins [10,31-36,40].

NMR spectroscopy has also been utilised to determine changes which occur upon the oxidation or removal of the Cu(I) ion in reduced azurin. The experiments show that on oxidation the overall structural changes are small, with a few effects distant from the copper center[126]. Similarly, comparison of the apo spectra with the reduced, Cu(I), spectra shows that removal of the copper does produce some shifts, which are interpreted as only small changes in the structure[126]. One of the histidines, presumed to be bound to the copper becomes freely titratable upon removal of the copper[126,148], while the pK_a of

another histidine becomes distinctly lower in the apo form than in the Cu(I) form[126]. Futhermore, removal of the metal from azurin markedly increases the NH proton lability and presumably their accessibility to solvent[126]. This increased NH proton lability has been noticed in plastocyanin[152], and the authors concluded that the presence of the copper did not alter the overall organisation of the protein, but did stabilise the structure somewhat.

In the recent past, interest has focussed on the pH dependence of the redox activity of azurin[27,28,123,128]. NMR experiments have suggested two different conformers of His-35 are involved in the pH dependent electron exchange mechanism between *Ps. aeruginosa* azurin and cytochrome c_{551}[28,125,126,153]. The imidazole ring of His-35 (pK_a ≈7.1) appears to become protonated under acidic conditions and this is followed by a considerable reorientation of the side-chain (a 1.37ppm difference in the resonance of the $C_{\varepsilon 1}$ proton occurs between low and high pH forms)[28,123]. The conformational shifts at His-35 in *Ps.aeruginosa* azurin are thought to cause changes in the environment of His-46 and Met-121 and possibly alter the geometry of the copper[28]. However, similar experiments have shown no significant pH-dependent conformational changes in His-35 or the copper site for either *Alc. faecalis* or *Alc. denitrificans* azurins[93,128,154]. In *Alc. denitrificans* azurin, the side-chain of His-35 becomes protonated below pH 4.5[99] (pK_a ≈4.8[93,128]). This is accompanied by a small shift of 0.39ppm[128] in the $C_{\varepsilon 1}$ proton resonance, but has no effect on the copper site. Very recently, the crystal structure analysis of *Ps. aeruginosa* azurin at pH 5.5 and pH 9.0 has clarified the behaviour ofHis-35, and has shown that the protonation of this residue does not affect the copper site. Other results from the crystal structure analyses of native *Alc. denitrificans* azurin[31] and *Ps. aeruginosa* azurin mutants[155], show that the combined effect of sequence changes between the two bacterial strains is a shift in one of the β-strands which opens a cleft in *Ps. aeruginosa* azurin allowing His-35 to become protonated at higher pH, while the corresponding side-chain in *Alc. denitrificans* azurin remains buried and inaccessible to solvent[155]. As far as the pH-dependent redox reaction between *Ps. aeruginosa* azurin and cytochrome c_{551} is concerned, temperature jump experiments on site directed azurin mutants show that His-35 is not the site of electron transfer, although these studies also demonstrated that the protonation of His-35 is responsible for a second relaxation phase in the electron transfer kinetics[156] (see section 1.2.8).

A mixture of oxidised and reduced azurin molecules will undergo electron self-exchange (ESE). The ESE rate has been measured directly by NMR techniques for azurins in partially reduced protein solutions [27,28,128], and found to be independent of pH, buffer and ionic strength, and very fast (1.3×10^6 $M^{-1}s^{-1}$ and 4×10^5 $M^{-1}s^{-1}$ for *Ps. aeruginosa*

and *Alc. denitrificans* proteins, respectively). This also suggests that the site of the ESE reaction is not at His-35[128], but is more likely to be at His-117 which is located at the centre of the hydrophobic patch of azurin[31,157]. Note that, the hydrophobic patch is a surface feature which appears to be conserved in all structurally characterised blue copper proteins, suggesting it has some functional importance.

Substitution of the copper atoms of plastocyanin, stellacyanin, and azurin (*Ps. aeruginosa* and *Alc. denitrificans* strains) with ^{113}Cd has allowed study of the metal binding sites by ^{113}Cd NMR[143]. The ^{113}Cd chemical shifts of these proteins appear in the same region as those of other Cd(II) thiolate containing complexes[158,159], and there is little doubt that the Cd(II) ion binds in the blue copper site. Resonances of the Cd(II) derivatives of stellacyanin, *Ps. aeruginosa* azurin and *Alc. denitrificans* azurin are virtually identical (380ppm, 372ppm and 379ppm, respectively), whereas the plastocyanin derivative resonates 50 ppm further down-field at 432ppm. The differences in these chemical shifts reflects a difference in the geometry and coordination number of the cadmium sites in these proteins[143]. Since the stellacyanin ^{113}Cd shift is much closer to that of *Alc. denitrificans* azurin, it has been suggested that the copper site of stellacyanin may be more like that of azurin (distorted trigonal bipyramid[31]) than plastocyanin (distorted tetrahedral[32])[143,82]. In *Ps. aeruginosa* azurin, the ^{113}Cd resonance varies only slightly as the pH is decreased (372.5ppm to 371.7ppm), which indicates a subtle change in the cadmium environment, presumably the result of the changes at His-35 as discussed above[27,28,41,123,128,143]. Unfortunately, the ^{113}Cd spectrum for *Alc. denitrificans* azurin was only measured between pH 7.7 and 8.7, where no change in the resonance was observed, so no comparison of the pH dependence of the two azurins can be made.

1.2.6 X-ray Absorption Spectra Studies

X-ray absorption spectroscopy has provided a method for determining the metal-ligand distances in the primary metal environment of several metalloproteins. The copper absorption edge fine structure of the X-ray spectra (EXAFS) has been measured for azurin[160,161], plastocyanin[162,163], umecyanin[164], amicyanin[165], stellacyanin[166,167] and rusticyanin [168]. The EXAFS results clearly indicate that models fitting the spectra of the blue copper proteins all have in common two nitrogen (or oxygen) ligands at normal distances to the copper, and a short copper to sulphur bond. Presumably, these ligands correspond to the two histidine side-chains and a cysteine side-chain. The copper-ligand distances agree with those values determined from crystallographic studies[32,33,36,38].

The presence of other copper ligands, especially the methionine sulphur, have been

difficult to establish from these spectra. Copper-S(Met) distances could be determined for only a few of the proteins, and usually this distance is associated with a large error, so that the value is assigned only tentatively. Table 1.2.6.1 gives copper-ligand distances determined from EXAFS studies of blue copper proteins.

Table 1.2.6.1. Copper distances of some type 1 blue copper sites determined from EXAFS experiments in both the oxidised and reduced forms. Where references gave more than one copper-ligand distance, average values are given. "n.d." indicates a contribution not dedected. The Cu-S and Cu-S' correspond to the first and second (if any) copper to sulphur distances.

	Cu-N distance (Å)		Cu-S distance (Å)		Cu-S' distance (Å)	
	oxidised	reduced	oxidised	reduced	oxidised	reduced
azurin[160,161]						
pH 4.1-5.5	1.95	1.97	2.19	2.24	n.d.	2.70
pH 9.1-9.2	1.95	1.97	2.23	2.21	n.d.	2.74
amicyanin[165]						
pH 5.2-6.6	1.91	1.89	2.13	2.18	n.d.	2.41
pH 9.2-8.9	1.95	2.02	2.11	2.19	n.d.	n.d.
plastocyanin[160,169]	1.97	2.05	2.10	2.22	n.d.	n.d.
rusticyanin[168]	1.99	2.07	2.16	2.17	2.84	2.80
stellacyanin[166,167]	1.93	1.98	2.21	2.25	n.d.	2.66
umecyanin[164]						
pH 7.5	1.99	2.03	2.13	2.21	n.d.	n.d.
pH 10.5	1.99	2.03	2.13	2.21	n.d.	n.d.

The case of plastocyanin illustrates the difficulties in determing the Cu-S(Met) distance. The presence of a Cu-S(Met) bond could not be detected by preliminary EXAFS studies, and so the thermal motion of the copper and methionine sulphur was presumed to be uncorrelated. It was thought that this uncorrelated motion could be the result of disorder in the methionine side-chain. To detect any such disorder, low temperature (4K) X-ray absorption spectra for Cu(II) plastocyanin were recorded. It was reasoned that if the lack of contribution from the methionine sulphur is the result of uncorrelated thermal disorder, then it should be possible to reduce this effect by lowering the temperature. Edge spectra were tested for a fit with two possible conformations of the methionine sulphur, but the analysis revealed that the methionine sulphur does not contribute significantly to the EXAFS at 4K[162].

Further experiments on plastocyanin were conducted to establish the influence of the methionine sulphur and provide a possible explanation for the absence of its contribution[163]. From the crystal structure of plastocyanin, it is known that the Cu-S(Met) bonds lie approximately parallel to the a axis of the crystal[32,38]. This unique situation was exploited by measuring the 'polarised' X-ray absorption spectra of oriented

plastocyanin crystals. The ability to detect the contribution from the methionine sulphur should be enhanced when the Cu-S(Met) bonds are parallel to the polarisation vector of the incident X-rays. Comparison of the X-ray spectra from two orientations, one expecting maximum contribution and the other expecting minimum contribution from the methionine sulphur showed little difference, confirming that the methionine sulphur in plastocyanin makes little or no contribution to the copper EXAFS and that the interaction between the copper and methionine sulphur is very weak.

Another finding from the EXAFS experiments on the blue copper proteins is the increase in the copper-ligand distances upon reduction from Cu(II) to Cu(I). Although the effect varies in magnitude from protein to protein, results show that for all proteins, especially azurin[161], plastocyanin[167] and umecyanin[164], the copper-sulphur distance increases by as much as 0.1Å upon reduction. The effect is less prominent for copper-nitrogen distances, with an increase of roughly 0.05Å for most of the blue copper proteins. For amicyanin, however, distances actually decrease between pH 5.2-6.6, possibly due to a conformational change at the copper site[165].

Experiments on the copper EXAFS of azurin (*Ps. aeruginosa*) have been conducted on the oxidised and reduced forms at both low and high pH to determine whether any changes occur at the copper site[161]. In the oxidised state, the Cu-N distances and Cu-S distance were calculated at 1.95Å and 2.21Å, respectively, while no second Cu-S distance could be detected. Upon reduction, the copper-ligand distances increase slightly, and a tentative second copper-sulphur distance of 2.7Å appears. The effect of pH (pH 4.2-9.2) is very small on the EXAFS in either redox state, with no significant changes occuring in the bond-lengths for the major ligands. These results indicate that the copper site is independent of pH despite the structural changes suggested by NMR studies on azurin[27,28,123,128].

1.2.7 Three-Dimensional Structural Studies

The structures of several blue copper proteins have been analysed by single crystal X-ray diffraction methods. Structures have been reported for three azurins (*Ps. aeruginosa*, *Alc. denitrificans* and *Ps. denitrificans*)[29,30,31,35,36,41,155], two plastocyanins (*Poplus nigra* and *Enteromorpha prolifera*)[32,33,38], cucumber basic blue protein[40], pseudoazurin or cupredoxin (*Alc. faecalis* S-6)[34,37,39], and ascorbate oxidase (zucchini)[14]. Although the crystal structure of stellacyanin is as yet undetermined, the structure of this protein from *Rhus vernicifera* has been modelled by potential energy calculations[170]. These results, however, should be treated with caution since they are based on a sequence alignment

with plastocyanin[170], and conflict with other results based on sequence alignment with cucumber basic blue protein[40]. The fold of the polypeptide chain of two plastocyanins (*Scendesmus obliquus* and spinach) has been determined from 2-dimensional NMR techniques[145,149,150], and these structures were found to be identical to the crystal structure of plastocyanin[32,33,38].

All of the single type 1 blue copper proteins structurally characterised to date share several common structural features, supporting the proposal that they have evolved from a common ancestor[171]. In each case, the polypeptide chain is folded into a single domain, the main part of which forms a β-sandwich; eight β-strands for all of these proteins, except for cucumber basic blue protein which has five. Two β-sheets are packed face-to-face, with hydrophobic side-chains in the interior and charged side-chains on the exterior of the protein. The single copper atom is bound by side-chains from the loops which interconnect the β-strands at the "north" end of the molecule. Figures 1.2.7.1-1.2.7.5 illustrate the folding patterns of four of these proteins. A similar β-sandwich topology is also found in the tertiary structure of ascorbate oxidase from zucchini, and it has been suggested that the ancestral gene of the type 1 copper proteins may have been inserted into the larger copper protein somewhere along its evolutionary pathway[14].

Several important structural differences are apparent in the type 1 copper proteins. The most obvious of these are the insertions in the polypeptide sequence which have given rise to folded sections separate from the main structural element, the β-sandwich. Two examples are the "flap" region of azurin[31] and the "C-terminal extension" of pseudoazurin[34] which fold into α-helices and loops. It is possible that these differences have a functional significance, since the insertions occupy a region which is spatially equivalent to the "negative patch" in plastocyanin, a possible binding site for physiological redox partners[32].

The copper site of each protein is buried in the interior of the structure by several loops at the "north" end of the molecule. Three strongly binding copper ligands are provided by the side-chains of two of these loops; two histidine imidazole nitrogens (Cu-N = 1.9-2.1Å) and one cysteine thiolate sulphur (Cu-S = 2.1-2.2Å). The Cu-S(Cys) bond is short compared to those in small molecule Cu(II) complexes (2.19-2.65Å), while the two Cu-N(imidazole) bond lengths are similar to those found in Cu(II) complexes with tetrahedral geometry (1.98-2.05Å)[172,173].

A fourth ligand, a methionine thioether sulphur, forms a weak bond with the copper with a bond distance ranging from 2.7Å in *Alc. faecalis* pseudoazurin[39] to 3.1Å in *Alc.*

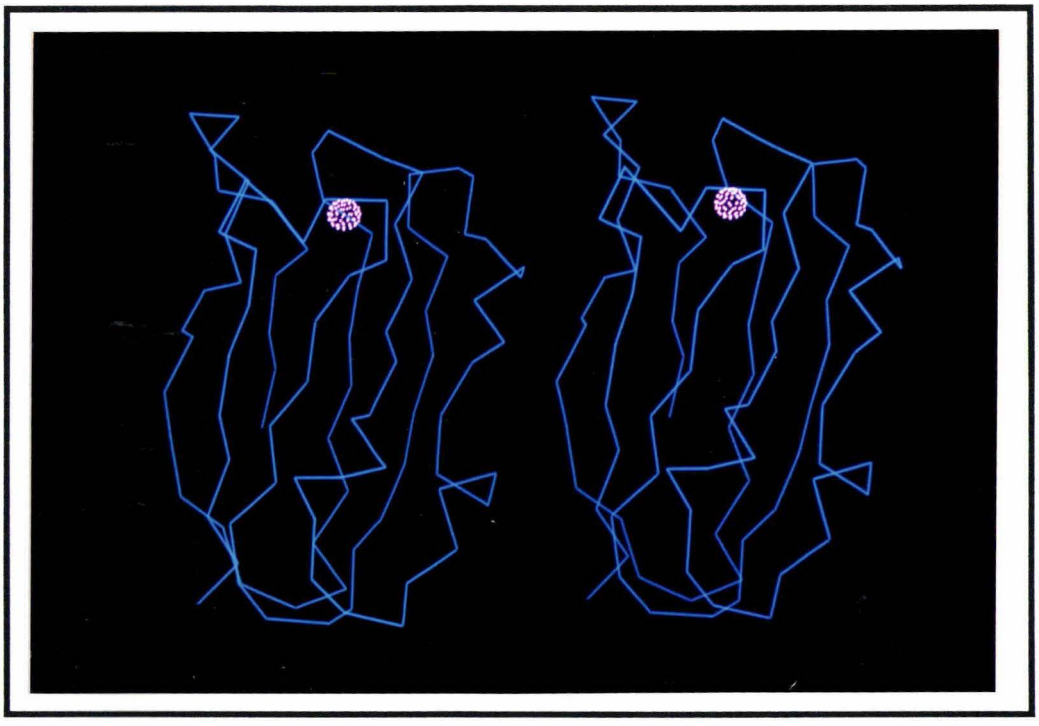

Figure 1.2.7.1. A C_α trace (blue) of the folding pattern of poplar plastocyanin (copper atom in pink). Coordinates obtained from the Protein Data Bank.

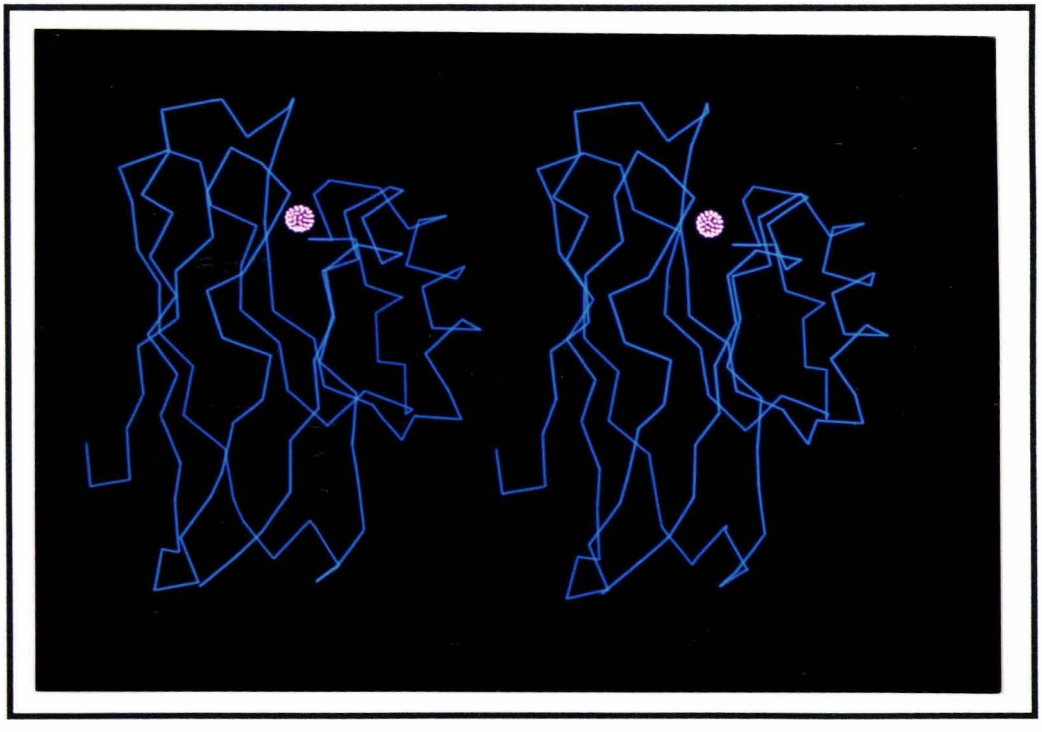

Figure 1.2.7.2. A C_α trace (blue) of the folding pattern of azurin from *Alc. denitrificans* (copper atom in pink).

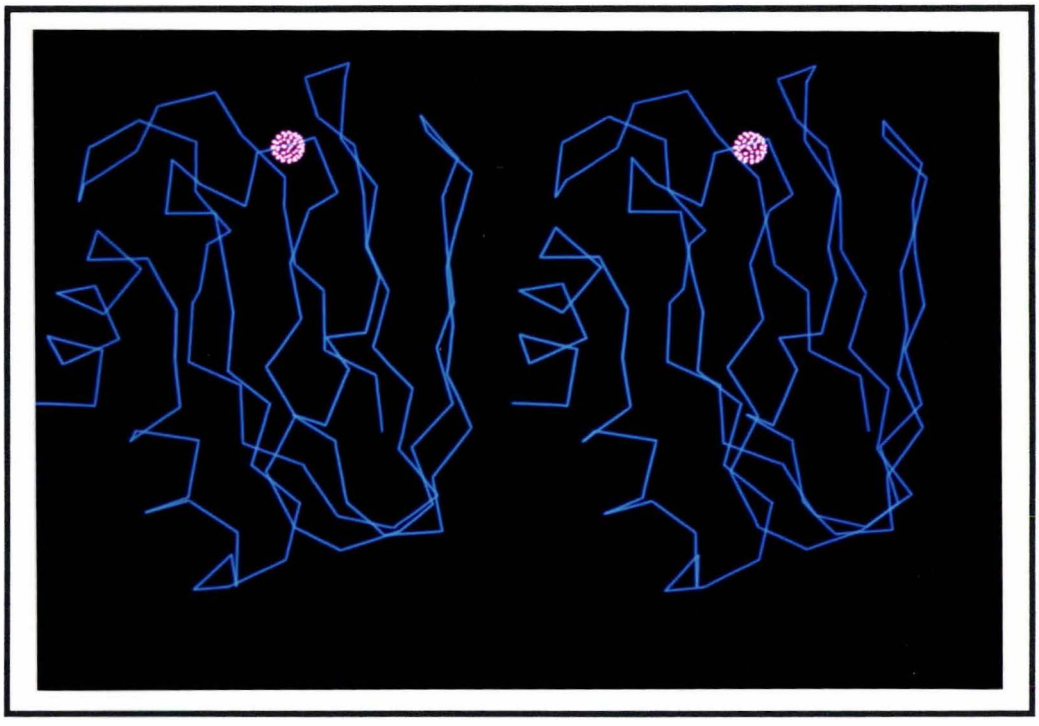

Figure 1.2.7.3. A C_α trace (blue) of the folding pattern of pseudoazurin from *Alc. faecalis* S-6 (copper atom in pink). Coordinates obtained from the Protein Data Bank.

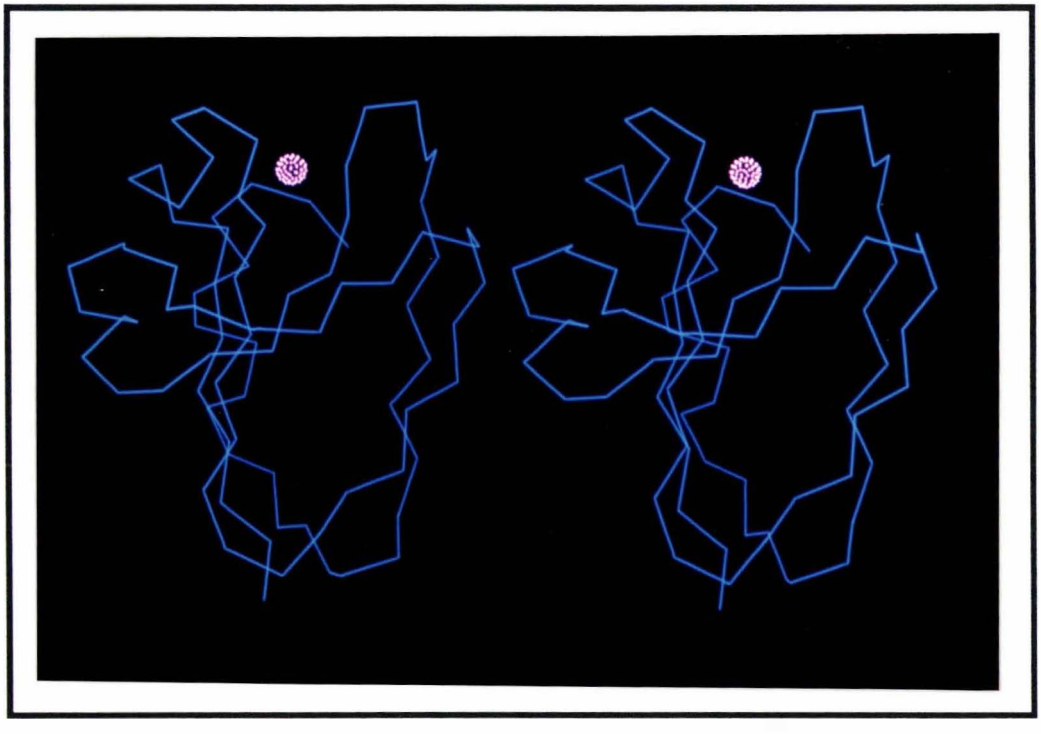

Figure 1.2.7.4. A C_α trace (blue) of the folding pattern of cucumber basic protein (copper in pink). Coordinates obtained from the Protein Data Bank.

denitrificans azurin[31]. In the case of stellacyanin, which has no methionine, the fourth ligand has been proposed to be either a side-chain carbonyl oxygen from a Gln[102], or a sulphur from a disulphide bridge[170,174-178]. The Cu-S(Met) distance is long compared with Cu(II)-S(thioether) bond lengths of 2.24-2.45Å in tetrahedral low molecular weight complexes , and 2.57-2.92Å in tetragonal complexes (for reviews on copper coordination chemistry see, e.g. Hathaway and Billings[47]). Variations in the length of the Cu-S(thioether) bond may provide a possible means for tuning the redox potential of the copper site[82,10].

Structure analyses of azurin from both *Alc. dentrificans* and *Ps. aeruginosa* have shown a possible fifth ligand may be provided by a main-chain carbonyl oxygen at ≈3.1Å from the copper[31,41,155]. The corresponding distance in the other blue copper protein structures is greater than 3.5Å (e.g. 3.8Å in pseudoazurin[34]). A distance of 3.1Å between a copper and the carbonyl oxygen is far greater than typical Cu-O axial distances (≈2.6Å), and consequently, it is considered to be at the extreme limit for a Cu-O interaction[31]. The possibility of a fifth ligand in the copper site is important because RR spectra[129], ^{113}Cd NMR[143] and potential energy calculations[170] suggest that a carbonyl oxygen might be a copper ligand in stellacyanin.

Several features near the copper site are conserved in the structures of all of these proteins. At least one peptide NH...S hydrogen bond is made to the cysteine sulphur atom of the copper site. A hydrogen bond is also formed between a main-chain carbonyl oxygen and the more buried histidine ligand, while the other histidine ligand is on the protein surface at the center of a hydrophobic patch. Some residues near the the copper site are conserved. For instance, Asn-11 and Thr-79 of pseudoazurin[39] link together the loops containing the copper ligands by means of a hydrogen bond. Corresponding residues appear in plastocyanin[32] and azurin[31], and function in the same manner. Similarly, the methyl group of the methionine copper ligand is capped by a phenyl ring in all of these proteins. Although, this aryl residue is not invariant, the aromatic nature is conserved (e.g. as Tyr-15 in *Alc. dentrificans* azurin[31], but Phe-18 in pseudoazurin[39], and Trp-11 in cucumber basic blue protein[40]).

1.2.8 Site Directed Mutagenesis Studies on azurin

Very recently, the genes encoding azurin (*azu*) from *Alc. denitrificans* [179], *Alc. faecalis* [179] and *Ps. aeruginosa* [180] along with their structural flanking regions have been cloned and sequenced. A 19 amino acid signal peptide precedes the mature protein of 128-129 amino acids, and is designed to enable transport of the protein across one or more

membranes[181,182]. The azurin gene from *Ps. aeruginosa* has also been expressed in *E. coli* [183]. Analyses of the *azu* gene sequence have strengthened the assumption that azurins are involved in the nitrite/nitrate respiration pathway [180,179,184].

A primary reason for cloning and expressing azurin is to study its structure-function relationships by altering the residues in and around the copper site using site directed mutagenesis techniques. To date, changes have been made at seven different locations in the sequence of azurin. These are listed in Table 1.2.8.1. One of the most significant of these changes is the mutation at Met-121 to all other amino acids and the stop codon[98,185]. All of these mutants display the strong blue colour and characteristic EPR signal of type 1 Cu(II) proteins at both low pH and high pH, except for Met-121→Glu (M121E) and Met-121→Lys (M121K)[185] which change at high pH. Differences in the spectral properties of all these mutants are small when compared to the wild type, indicating that the blue copper site remains intact. This implies that the methionine is not an essential component of the blue copper site. The same conclusion was previously drawn from the observation that stellacyanin does not contain any methionine in its sequence yet has similar properties to the other blue copper proteins. The optical absorption maximum (λ_{max}) for these mutants varies between 608nm (M121R) and 631nm (M121T), with the extinction coefficients ranging from 4.0-6.0 $mM^{-1}cm^{-1}$. The EPR parameters for the Leu, Ala, Thr, Val, Ile and Trp mutants closely resemble those of the wild type, while Asn, Asp, Gln, and His mutants have stellacyanin-like EPR spectra, and the spectra of Gly, Ser, Phe and Tyr mutants fall in between these categories. A pH dependence is observed for the Lys, Glu and "Stop" mutants, where at low pH (≈pH 4) the EPR and optical spectra are stellacyanin-like, but at high pH (≈pH 7) $A_{\|}$ increases to over 100×10^{-4} cm^{-1}. An increase of 70mV in E° is also seen in M121L mutant (the only mutant for which E° was reported), presumably because the active site becomes more hydrophobic and has lost any apical Cu-S(Met) interaction. Interestingly, the copper occupancy of all of these mutants is less than 100%, and it is thought that, even if the methionine is not a vital part of the blue copper site, it may confer a greater stability on the structure, which may explain why this methionine is conserved in most blue copper proteins[98].

Another important azurin mutation is the His-117→Gly mutant, removing one of the histidine side-chains that binds the copper[97]. This change drastically alters the visible and EPR spectra of the protein so that it becomes characteristic of a type 2 copper centre. The optical spectrum exhibits a strong absorption near 420nm ($\varepsilon > 2.0$ $mM^{-1}cm^{-1}$), and the EPR parameters are 2.283 and 139×10^{-4} cm^{-1} for $g_{\|}$ and $A_{\|}$, respectively. However, addition of N-methylimidazole to the protein solution causes the reappearance of the

characteristic EPR and visible spectra of a type 1 copper centre that is almost identical to the wild type protein (λ_{max} = 630nm, $\varepsilon > 4.7$ $mM^{-1}cm^{-1}$, $g_{\parallel} = 2.266$, $g_{\perp} = 2.055$ and $A_{\parallel} = 57 \times 10^{-4}$ cm^{-1}).

Table 1.2.8.1. Spectral and redox properties of site directed azurin mutants from *Ps. aeruginosa* currently known to date. "k_{ese}" refers the electron self exchange rate between two azurin molecules. "k_{12}" refers to the second order rate constant for the electron exchange with cytochrome c_{551}. † EPR values for Met-121→Leu azurin[98].

Mutant	Ref.	λ_{max} (nm)	ε_{max} ($M^{-1}cm^{-1}$)	$A_{\parallel}$ (cm^{-1})	E° (pH 7) (mV)	E° (pH 6) (mV)	k_{12} or k_{ese} (Ms^{-1})
Wild type	156, 188,189	628	5300/5700	56×10^{-4}	311/319	338	$k_{12} \approx 6 \times 10^6$ $k_{ese} \approx 1.3 \times 10^6$
His-35→Lys	188	628	-	56×10^{-4}	306	334	$k_{12} \approx 9 \times 10^6$
His-35→Gln	155,156 189	628	5500	-	268	-	$k_{ese} \approx 1.3 \times 10^6$ $k_{12} \approx 2.7 \times 10^6$
His-35→Leu	155,156	622	5300	-	299	-	$k_{12} \approx 4.8 \times 10^6$
His-35→Phe	156	628	5500	-	301	-	$k_{12} \approx 2.5 \times 10^6$
Met-44→Lys	156,189	625	5300	64×10^{-4}	372	361±10	$k_{ese} < 10^3$ pH 5 $k_{ese} > 10^5$ pH 9
Glu-91→Gln	188	628	-	56×10^{-4}	306	324	$k_{12} \approx 10 \times 10^6$
Phe-114→Ala	188	621	-	52×10^{-4}	350	359	$k_{12} \approx 6 \times 10^6$
His-117→Gly	97	630	>4700	57×10^{-4}	-	-	-
Met-121→All	98,185	608-631	4000-6000	39×10^{-4}†	375†	375†	-

Other mutations in the vicinity of the copper site have been made to try and identify loci concerned with electron transfer by the protein. Of particular interest are the mutations at His-35, a proposed site of electron transfer with cytochrome c_{551} (a presumed physiological partner) [127,186,187]. This residue has been mutated to Lys[188], Gln[189,156], Leu[156] and Phe[156], all of which have produced little or no changes in E° or in the spectra. Similar results have been obtained for the mutant Glu-91→Gln[188], on the surface of the protein, near His-35[31,36]. These experiments have conclusively shown that changes to the His-35 do not alter the electron transfer rate between azurin and cytochrome c_{551}. Futhermore, the electron transfer rates between these mutants and nitrite reductase, the other physiological partner of azurin are similar to the rate with the wild type protein[156]. These findings have led to the conclusion that His-35 is not part of the pathway which transfers electrons to or from cytochrome c_{551} or nitrite reductase[156].

Although the spectra of the Met-44→Lys mutant remain unaltered from the wild type, the mutation is of particular interest because it places a potentially charged side-chain in the hydrophobic patch which has been proposed as a site for the ESE reaction[27,28,123,128]. This mutant shows an ESE rate which is dependent on pH (faster with increasing pH), while the wild type shows pH independent behaviour. Presumably, the pH dependence is caused by the protonation of the Lys side-chain at low pH conditions, where the positive

charge causes a repulsion of the two azurin molecules. The redox potential also increases by 50mV, possibly because of the extra positive charge near the copper site[156,189].

One mutation in the second coordination sphere of the copper site does alter both the spectra and redox potential of azurin. Changing Phe-114 to Ala[188], increases the redox potential by 20-30mV, shifts the optical absorption maximum 7nm to a shorter wavelength and drops the hyperfine splitting constant, $A_{\parallel}$, slightly, by 4×10^{-4} cm^{-1}. Yet, the rate constant for electron exchange with cytochrome c_{551} is the same as for wild type azurin. The Phe-114→Ala mutant is also considerably slower than the wild type in binding copper. The changes to the spectra, redox potential, and the fact that Phe-114 is somehow involved indirectly with copper uptake is of interest, because this side-chain lies adjacent to the copper ligand His-117 in the hydrophobic patch.

In the expression of azurin in *E. coli*, no differences were observed between the expressed protein and the *Ps. aeruginosa* azurin, except that a non-reconstitutable azurin-like protein could be separated from the holo-protein[183]. This azurin-like protein, referred to as azurin*, resembles apo-azurin in electrophoretic (SDS-PAGE and IEF) and spectroscopic (UV/Vis, ^1H NMR, static and dynamic fluorescence) properties, but has lost the ability to bind copper ions. Crystallographic and chemical studies have shown, however, that azurin* contains Zn(II) bound in the copper binding site, which explains the inability of azurin* to bind copper ions[190]. This may also explain why less than 100% of the protein molecules, for many mutants, do not appear to bind copper.

Several points can be made regarding the site directed mutagenesis studies on azurin from *Ps. aeruginosa*. The Met-121 mutations have shown that methionine is not vital for the formation of the type 1 copper centre[98], although the His-117→Gly mutant strongly indicates that the presence of the imidazole ring of residue His-117 is essential if the characteristics of a type 1 centre are to be maintained[97]. This suggests that cysteine and two histidine ligands form the basis of the blue copper site. The studies also have implications for the two proposed sites for electron transfer for azurin, His-35 and the hydrophobic patch. Mutations at the His-35 site[156,188,189] have had little effect on electron exchange with either cytochrome c_{551} or nitrite reductase, indicating that this is not a part of the electron transfer pathway. Certain changes at the hydrophobic patch (Met-44→Lys[189] and Phe-114→Ala[188]), on the other hand, have shown an effect on the electron exchange rate with cytochrome c_{551} compared to the wild type. The small effect observed on the electron transfer rate as a result of the Phe-114→Ala mutation is not unexpected, because this mutation maintains the hydrophobic character of the side-chain. However, the most direct evidence to date implicating the hydrophobic patch as a site of

electron transfer is given by the Met-44→Lys mutant[189], where ^{1}H NMR experiments have found that the ESE rate becomes pH-dependent. The most likely cause of this pH effect is the protonation of the lysine side-chain, which could prevent the formation of the ESE association complex between the two protein molecules prior to electron transfer[189]. Finally, E° and spectral properties show larger changes when the mutation is closer to the copper site. This makes structural sense, since changes near the copper site (e.g. Met-121) will perturb its configuration more than those further away and at the surface of the protein (e.g. Glu-91[188]).

1.3 Structure-function relationships of azurin and plastocyanin

1.3.1 General description of the structure of azurin

With the interest in the spectroscopic and redox properties of azurin, it soon became evident that structural information was required in order to gain a better understanding of its properties. Structures of oxidised azurin from three different bacterial strains (*Alc. denitrificans, Ps. aeruginosa* and *Ps. denitrificans*) have been determined by X-ray crystallographic methods. In all three structures, the folding of the polypeptide chain is virtually the same. Crystal structures have been solved for wild type *Ps. denitrificans* azurin at 3.0Å resolution[35], wild type *Alc. denitrificans* azurin (pH 6.0) at 1.8Å resolution[31], wild type and two mutants of *Ps. aeruginosa* azurin (pH 5.5 and pH 9.0) at 1.9Å resolution[41] and 2.0Å resolution[155], respectively.

Azurin is a single domain protein of 128-129 amino acid residues. The main secondary structural element is an eight-stranded twisted β-sandwich, consisting of two β-sheets, one of $3\frac{1}{2}$ and the other of $4\frac{1}{2}$ β-strands (see Figure 1.3.0.1). These are connected by loops of varying length. The only disulphide bridge in the structure links the first and third β-strands at the 'south' end of the molecule. Between residues 51 and 81, the polypeptide chain breaks away from the β-barrel motif to form a "flap" region which lies against one of the β-sheets. The first half of the "flap" region contains three turns of the only α-helix in the structure, while the remainder of this region folds into three consectutive turns (see Figure 1.3.0.2).

The single copper atom of azurin is located at the 'northern' end of the molecule, in a crevice between the two β-sheets. Loops in the polypeptide chain surround the copper site, effectively burying the copper atom 6-7Å in the hydrophobic interior of the protein. The copper geometry found in the refined structures of azurin from *Alc. denitrificans* and *Ps. aeruginosa* is best described as distorted trigonal or trigonal bipyramidal (see Figure 1.3.0.3). The copper is bound strongly in a trigonal plane by two imidazole nitrogens from His-46 and His-117, and the thiolate sulphur from Cys-112. Two axial approaches are made to the copper, from the thioether sulphur of Met-121 and the peptide carbonyl oxygen of Gly-45. The copper atom is displaced 0.1Å out of the plane defined by the nitrogen and thiolate sulphur ligand atoms (N_2S plane), towards the sulphur of Met-121. It is thus much closer to the N_2S plane than in any of the other blue copper proteins structurally characterised, where the copper atom is usually displaced about 0.3Å from the N_2S plane[7,14,32,33,34,40]. Average copper distances and angles for the four refined structures of azurin[31,41,155] are listed in Tables 1.3.0.1 and 1.3.0.2. Interestingly, the

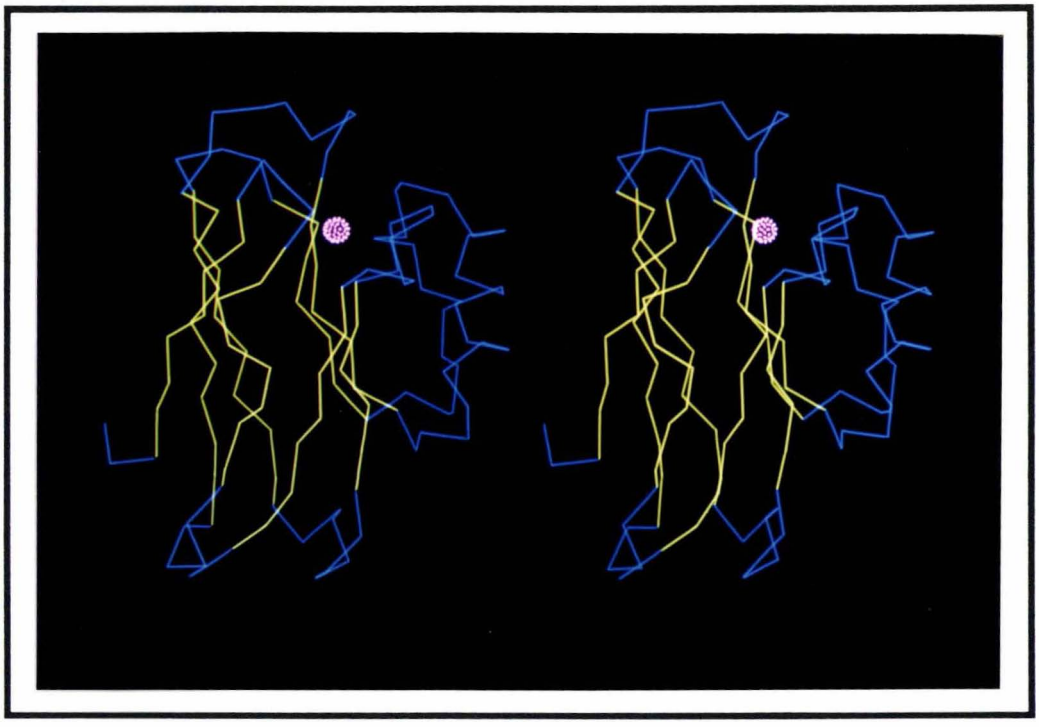

Figure 1.3.0.1. C_α trace (blue) of the polypeptide chain folding of azurin (*Alc. denitrificans*), β-strands are highlighted in yellow (copper atom in pink).

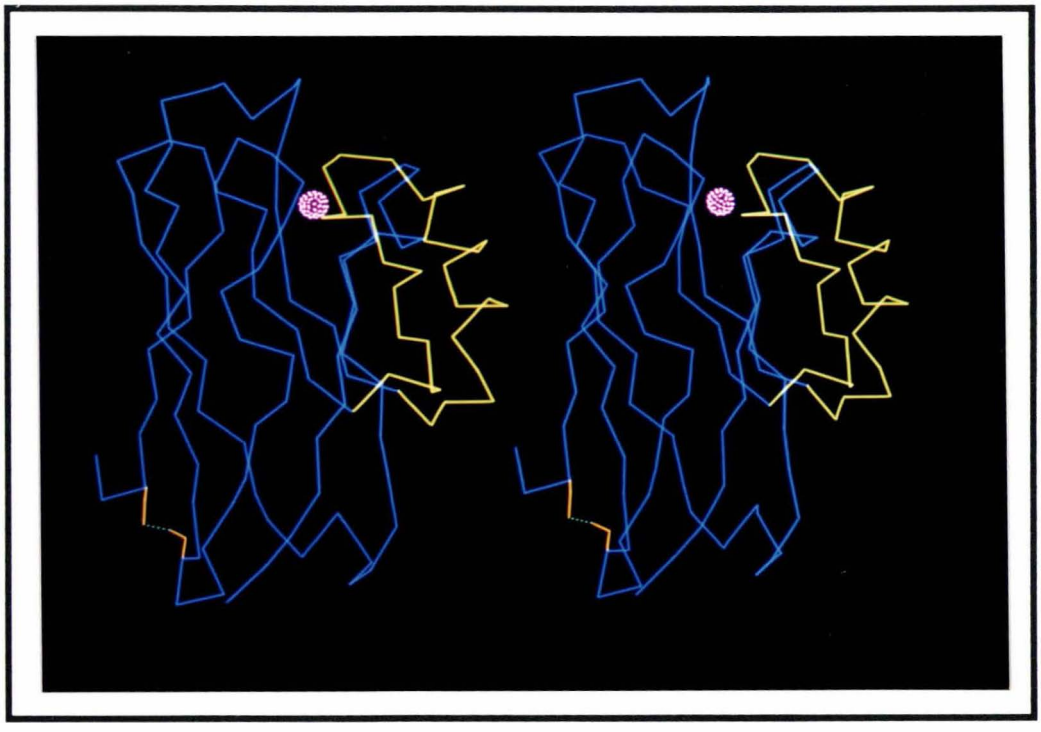

Figure 1.3.0.2. Stereo view of the C_α trace (blue) of the polypeptide chain folding in azurin (*Alc. denitrificans*) showing the 'flap' region and α-helix in yellow, and the disulphide bridge in orange. (Copper atom in pink.)

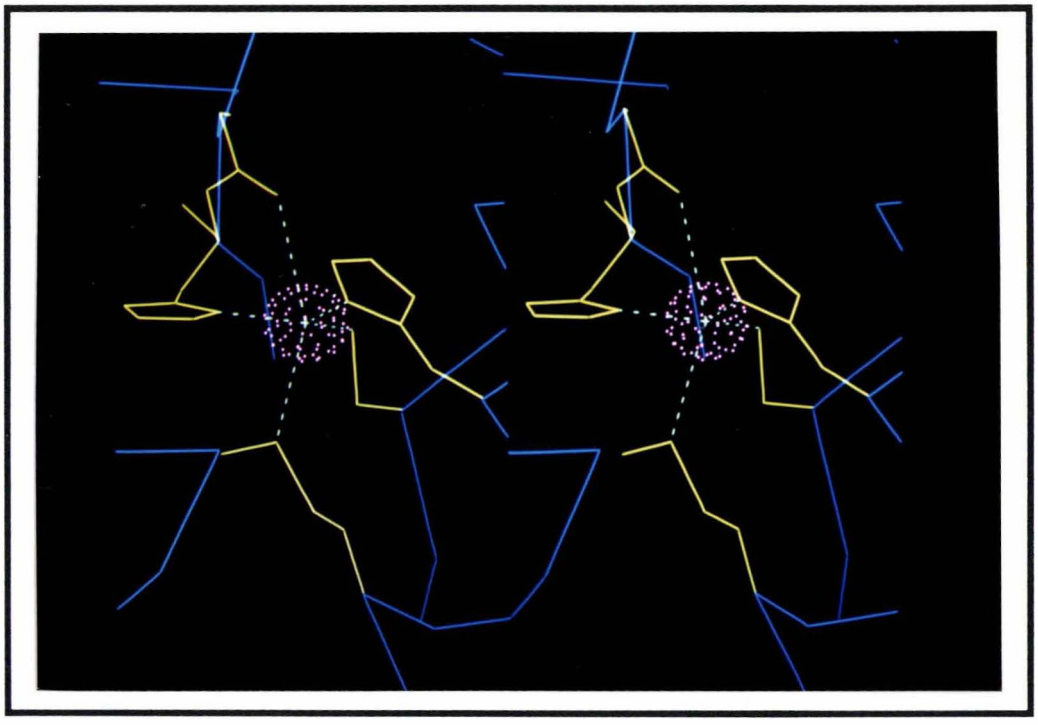

Figure 1.3.0.3. Stereo view of the copper site of azurin (*Alc. denitrificans*) with the C_α trace in blue, the copper ligands in yellow and the copper in pink.

copper site of *Ps. aeruginosa* azurin was originally described as a distorted tetrahedron[36]. Now, with the refined structures of the wild type and two mutants[41,155], the copper site is seen to be essentially identical to that of *Alc. denitrificans* azurin. Also noteworthy is the fact that E° varies somewhat despite the virtually identical copper sites (*Alc. denitrificans* wild-type: E° = 276mV, *Ps. aeruginosa* wild-type: E° = 308mV, *Ps. aeruginosa* mutants His-35→Gln: E° = 268mV and His-35→Leu: E° = 299mV).

Table 1.3.0.1. Average copper distances of oxidised (Cu(II)) azurin from *Alc. denitrificans* (*A.d.*) and *Ps. aeruginosa* (*P.a.*); wild-types (WT), His-35→Gln (H35Q) and His-35→Leu (H35L) mutants. A dash "-" indicates a value not supplied by published results.

Average copper distances (Å)	WT (*A.d.*) pH 6.0	WT (*P.a.*) pH 5.5	WT (*P.a.*) pH 9.0	H35Q (*P.a.*)	H35L (*P.a.*)
Cu...Gly-45 O	3.12	2.97	2.95	3.09	3.09
Cu...His-46 $N_{\delta 1}$	2.08	2.11	2.09	2.03	2.09
Cu...Cys-112 S_γ	2.15	2.25	2.26	2.05	2.20
Cu...His-117 $N_{\delta 1}$	2.00	2.03	2.04	2.05	2.03
Cu...Met-121 S_δ	3.11	3.15	3.12	3.04	3.01
Other distances					
O 45...S_δ 121	5.99	-	-	-	-
S_γ 112...N 47	3.49	-	-	3.56	3.60
S_γ 112...N 114	3.58	-	-	3.75	3.56

Table 1.3.0.2. Average copper angles of oxidised (Cu(II)) azurin from *Alc. denitrificans* (*A.d.*) and *Ps. aeruginosa* (*P.a.*); wild-types (WT), His-35→Gln (H35Q) and His-35→Leu (H35L) mutants.

Average copper angles (°)	WT (*A.d.*) pH 6.0	WT (*P.a.*) pH 5.5	WT (*P.a.*) pH 9.0	WT (*P.a.*) H35Q	WT (*P.a.*) H35L
O 45-Cu-$N_{\delta 1}$ 46	74	73	77	80	73
O 45-Cu-S_{γ} 112	103	98	98	95	97
O 45-Cu-$N_{\delta 1}$ 117	79	89	88	91	87
O 45-Cu-S_{δ} 121	147	149	149	152	149
$N_{\delta 1}$ 46-Cu-S_{γ} 112	135	133	134	133	135
$N_{\delta 1}$ 46-Cu-$N_{\delta 1}$ 117	104	103	103	100	101
$N_{\delta 1}$ 46-Cu-S_{δ} 121	78	78	74	72	77
S_{γ} 112-Cu-$N_{\delta 1}$ 117	119	123	122	127	122
S_{γ} 112-Cu-S_{δ} 121	107	110	110	107	109
$N_{\delta 1}$ 117-Cu-S_{δ} 121	96	87	88	89	93

The copper to imidazole nitrogen bondlengths of 2.0Å and 2.1Å (His-46 and His-117, respectively) in azurin are typical for blue copper proteins, as is the copper to thiolate sulphur (Cys-112) bond-length of 2.1Å. The Cys-112 sulphur makes two hydrogen bonds to NH groups of the polypeptide chain (S_{γ} 112...HN 47 and S_{γ} 112...HN 114). A striking feature of the copper site of azurin is the long copper to methionine sulphur distance of 3.1Å, which is much longer than Cu-S(thioether) bond distances found in small molecule copper complexes, and is also the longest Cu-S(Met) distance reported for the blue copper proteins. The distance of 3.1Å between the copper and carbonyl oxygen of Gly-45 is unique to azurin, since the corresponding distances in other proteins are greater than 3.8Å[34,39]. Although the distance is at the limit for any interaction, the carbonyl may be considered as a possible fifth ligand because it is favourably orientated towards the copper, and is surrounded by a hydrophobic environment without any nearby potential hydrogen bonding partners.

Two important surface features appear in the structure of azurin. The most significant is an extensive hydrophobic patch of 14 or more residues surrounding the outer edge of one of the copper ligands, His-117, illustrated in Figure 1.3.0.4. Of the 17 residues of the hydrophobic patch in *Alc. denitrificans* azurin[31], seven are invariant and another six maintain their hydrophobic character in other azurins[10]. The hydrophobic patch is a conserved feature of the blue copper proteins, and is an obvious candidate for the electron transfer site. The other main surface feature found in *Alc. denitrificans* azurin, is a sulphate binding site located in a cleft formed between the flap region and the β-sandwich (see Figure 1.3.0.5). The sulphate anion binds weakly to the protein, and bridges the gap of the cleft via two hydrogen bonds from His-83 and Gly-76[31]. Interestingly, the sulphate binding site of azurin spatially corresponds to a patch of negatively charged side-chains in plastocyanin[32] which has been suggested as a site for physiological redox

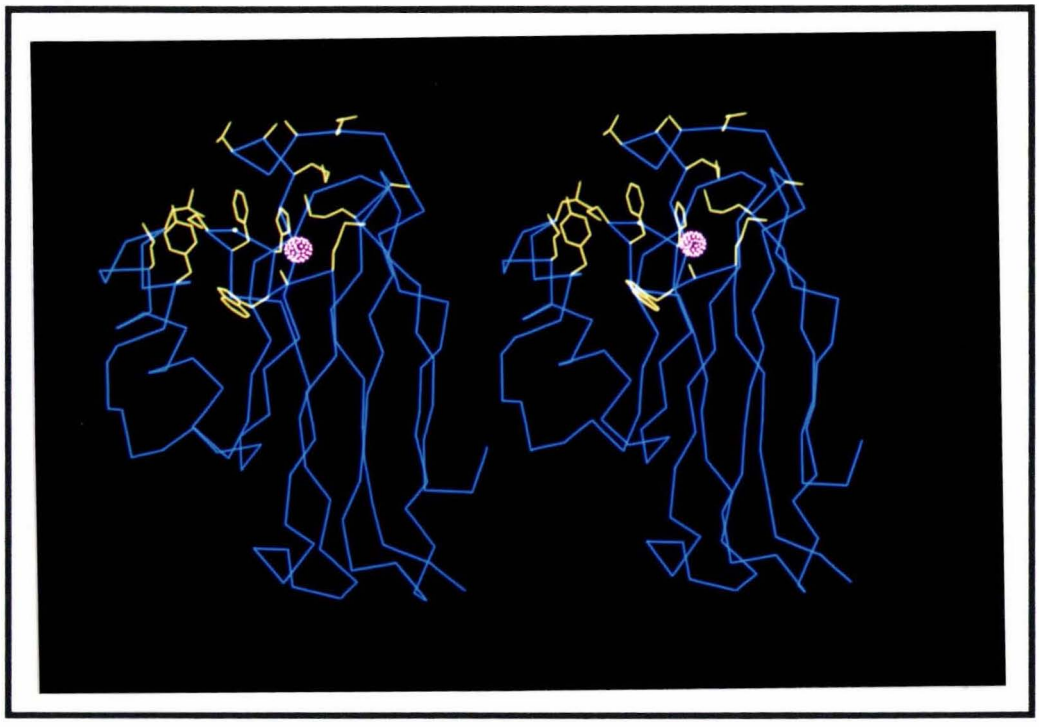

Figure 1.3.0.4. The hydrophobic patch of *Alc. denitrificans* azurin, with the C_α atoms of the polypeptide chain in blue, the side-chains of the patch in yellow and the copper atom in pink.

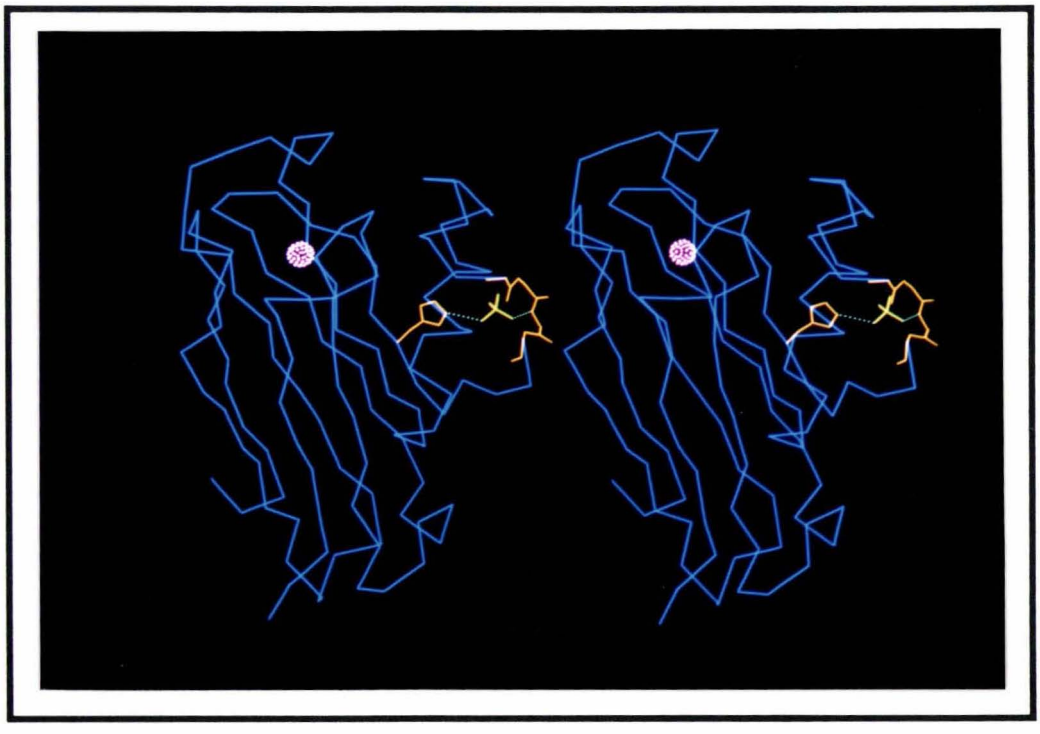

Figure 1.3.0.5. The sulphate binding site of *Alc. denitrificans* azurin, showing the sulphate in yellow and the two parts of the protein to which it binds to in orange.

partners.

The proposed pH-linked conformational change in *Ps. aeruginosa* azurin, thought from NMR studies to involve His-35, has been explained by the analyses of the crystal structures of this azurin at two pH values (pH 5.5 and pH 9.0)[41]. In the high pH form, the imidazole ring of His-35 makes two hydrogen bonds to other parts of the protein; $N_{\delta 1}$ 35...N 37 and $N_{\varepsilon 2}$ 35...O 44. Upon protonation of the side-chain of His-35, the peptide bond linking Pro-36 and Gly-37 rotates 180° so that a new hydrogen bond, $N_{\delta 1}$ 35...O 36, is formed (see Figure 1.3.0.6).The imidazole ring, however, only moves by a small amount (≈0.2Å), and does not affect the copper site at all.

Alc. denitrificans azurin does not undergo a similar pH-dependent change because of a crucial difference in the amino acid sequence between *Alc. denitrificans* and *Ps. aeruginosa* azurins[41]. In *Alc. denitrificans* azurin, residue 36 is a valine not a proline, as in *Ps. aeruginosa* azurin. This allows the formation of a hydrogen bond between N 36 and O 9 in *Alc. denitrificans* azurin, that is prohibited in *Ps. aeruginosa* azurin. This sequence difference shifts the polypeptide chain so that it covers the cleft in which the imidazole ring of His-35 is located, preventing its interaction with the solvent.

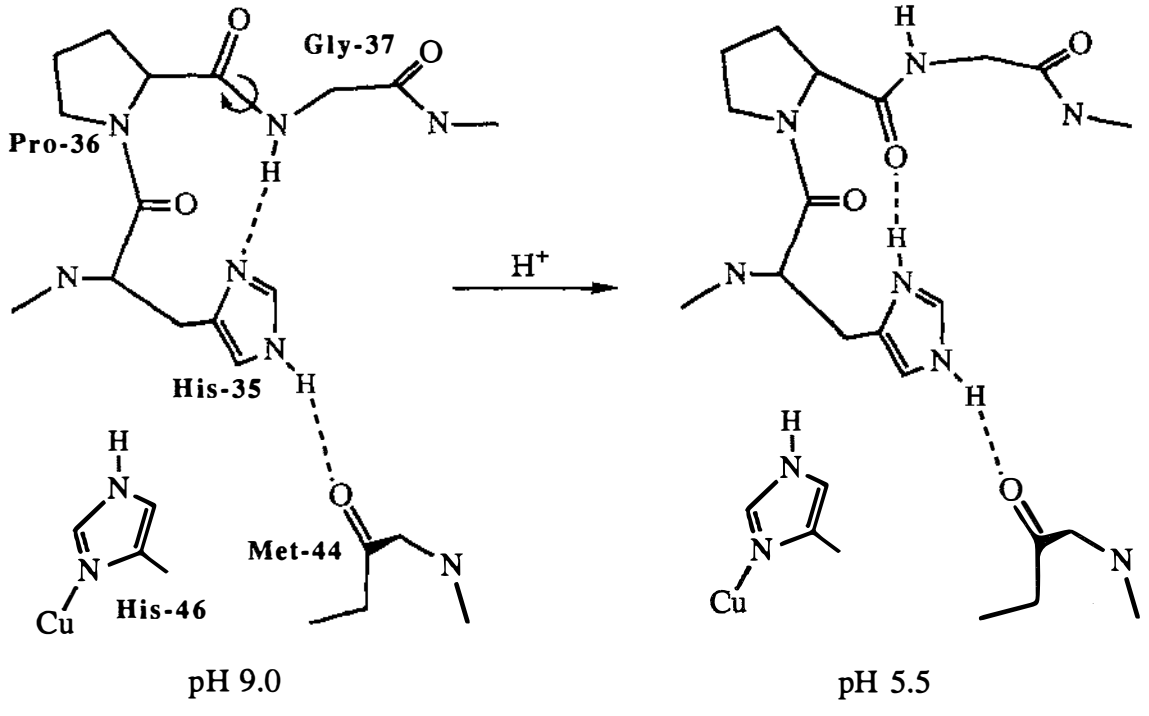

Figure 1.3.0.6. Schematic diagram of the peptide flip in *Ps. aeruginosa* azurin showing the change in hydrogen bonding at His-35.

1.3.2 Comparison of azurin and plastocyanin

Of all the blue copper proteins, the azurins and plastocyanins have been the most extensively studied. At present, plastocyanin is the only blue copper protein for which crystal structure analyses have been completed on its oxidised, Cu(II)[32], reduced, Cu(I)[122], and apo forms[191]. By comparing the structures of the different forms of plastocyanin, the redox behaviour of the protein could be explained. Structural studies on the reduced and apo forms of azurin, however, have not been reported. Despite the many similarities between azurins and plastocyanins, there are some important differences that suggest that some of the changes upon reduction or release of the copper are not the same. Below is a short summary of the differences between azurin and plastocyanin, and how they relate to the properties of the two proteins. The review on the structure and function of the blue copper proteins by Adman[10] covers more thoroughly the differences between azurin and plastocyanin.

Despite having similar characteristic properties (which have led to the suggestion that the blue copper proteins have evolved from a common ancestor[171,192]), azurin and plastocyanin are isolated from very different sources. Azurins have been found in denitrifying bacteria (e.g. *Pseudomonas, Alcaligenes* [10]), and are thought to play an electron transfer role in the denitrification pathway between cytochrome c_{551} and nitrite reductase[8,10,187]. Plastocyanins on the other hand, are found in many plants and some algae[193]. They are known to function as an electron transport protein in photosystem I, passing an electron between cytochrome f and $P700^+$ [194,195].

The changes during evolution which have led to differences between azurin and plastocyanin are mainly concerned with insertions and deletions in some of the loops connecting secondary structural elements. The loop which holds the first histidine ligand is much larger in azurin than in plastocyanin, and this may be the reason for the closer approach of the carbonyl oxygen to the copper[31]. The loop which provides the other three ligands is of the same length in the two proteins, but changes in sequence have slightly altered the positions of the copper ligands.

The general organisation of the azurin and plastocyanin molecules is the same, although there are several small differences in and around the β-sandwich. Within the β-sandwich, small conservative sequence changes have resulted in a shift of the relative disposition of the two β-sheets, because the different volumes of the internal residues has caused the opposing β-sheets to modify their packing[196]. Plastocyanins do not have any disulphide bridges in their structures, while azurins contain one which links the two β-strands at the

'south' end of the molecule, probably contributing to the overall structural stability of the β-sandwich. The largest difference in the sequence and the structure between these two proteins occurs as a large insertion in azurin which forms the "flap" region. This "flap" region is separate from the β-sandwich structure, and folds into three turns of an α-helix, followed by several β-turns. The area which the flap region covers in azurin corresponds to a cluster of negatively charged side-chains, known as the "negative patch" in plastocyanin. This patch has been suggested as a possible binding site for inorganic redox reagents and physiological redox partners in plastocyanin[122].

The most important contrast between azurin and plastocyanin is at the copper site. In azurin, the copper geometry may be described as distorted trigonal bipyramidal with two imidazole nitrogens and a thiolate sulphur in the equatorial plane, while a thioether sulphur and a carbonyl oxygen approach the axial positions. The copper atom is approximately 0.1Å above the plane of the equatorial ligands towards the thioether sulphur[31]. The copper geometry of plastocyanin, however, is closer to a flattened tetrahedron, with the two imidazole nitrogens and thiolate sulphur acting as the base, and the thioether sulphur as the apical ligand. The copper atom, however, lies 0.3Å above the plane of the base ligands[38]. The length of the Cu-S(Met) interaction in plastocyanin at 2.9Å is significantly shorter than the 3.1Å distance for azurin. These differences in the copper geometry and the Cu-S(Met) distance may account for the difference in the E° of the two proteins[31,82], and are presumably due to the differences in the sequence near the copper site. Figure 1.3.2.1 shows the two oxidised copper sites superimposed on each other.

The structure surrounding the copper site also shows important differences. In azurin the copper ligand His-46 has its side-chain oriented by a hydrogen bond to the main-chain carbonyl oxygen of residue 10, whereas in plastocyanin the corresponding ligand, His-37, is bound to O 33 from a different part of the structure. An extra S...HN hydrogen bond between the main-chain and the cysteine sulphur ligand is also found in azurin. This extra S...HN interaction has been suggested as the cause of the different λ_{max} of the charge transfer band in azurin compared to plastocyanin[82].

Some significant changes in internal residues also occur between azurin and plastocyanin. For instance, the side-chain of His-35, which packs against the ligand His-46 in azurin, is an asparagine in plastocyanin. Similarly, the residues which sandwich the histidine ligand on the surface of the protein (His-117 in azurin) are different in the two proteins. In azurin, the hydrophobic patch near the copper site is more extensive than in plastocyanin, being composed of as many as 17 residues compared to eight[10]. It has,

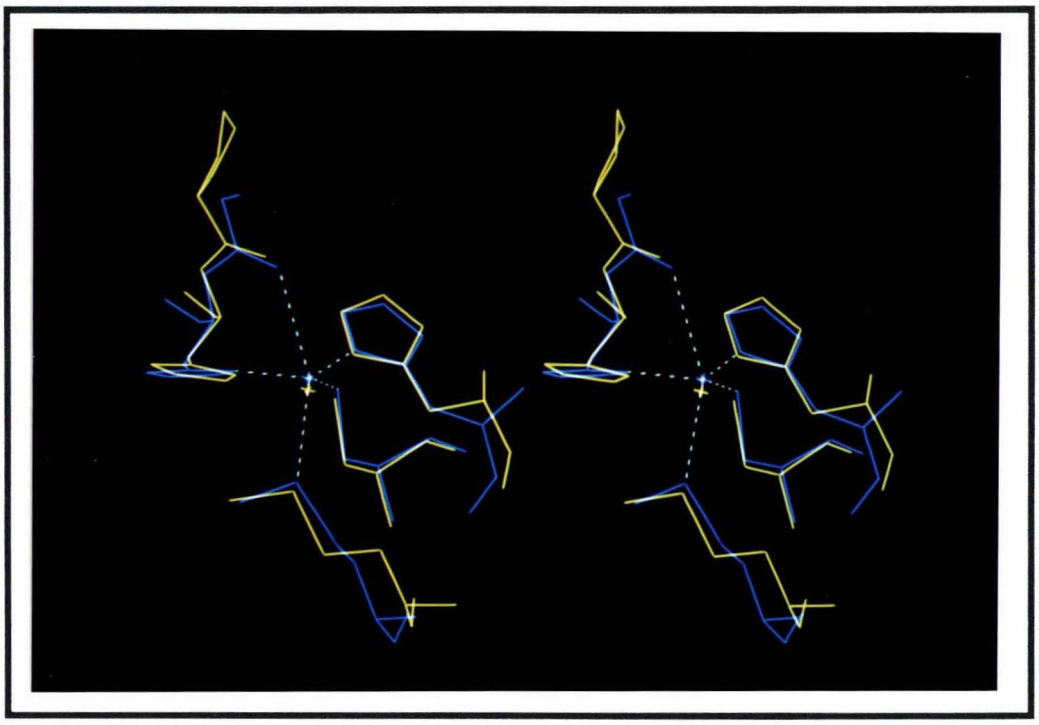

Figure 1.3.2.1. The superimposed Cu(II) sites of azurin[31] (blue) and plastocyanin[32] (yellow). The superposition was done using the side-chain atoms of the cysteine, methionine and two histidines of the copper site.

however, been proposed as a site of electron transfer for both proteins[186].

1.3.3 Reduction of plastocyanin and azurin

The crystal structure analysis of reduced poplar plastocyanin at different pH values has answered many questions regarding its redox behaviour and function[122]. Changes in the protein structure upon reduction showed why the electron transfer rate of plastocyanin is fast with physiological partners, and why it "switched off" at low pH[172,193].

Upon reduction, the bulk of the structure of plastocyanin remains essentially unchanged from the oxidised form. However, small but significant changes occur at the copper site. The initial structure analysis of reduced plastocyanin gave cause for concern since one of the copper-ligand distances appeared to lengthen drastically, such that it could be no longer considered a bond. Such a change was unexpected because in order for plastocyanin to function as a fast electron transfer protein, changes at the active site need to be kept to a minimum[122]. Further investigation revealed that in the reduced state, the copper site geometry was found to alter with pH. Two forms of reduced plastocyanin were proposed to exist; an "active" high pH form and an "inactive" low pH form.

At alkaline pH (pH ≥ 7), the Cu(I) geometry shows negligible differences from the Cu(II) site of the oxidised structure. The virtually identical geometries between the two oxidation states at high pH have been attributed to the rigid surrounding structure of the copper sites, and satisfy the requirements for fast electron transfer. Since no bonds are broken and the structural changes are small upon reduction, the process must have a low Franck-Condon reorganisational barrier. A low barrier will optimize the blue copper site of plastocyanin for fast, efficient, outer sphere electron transfer[122].

Under conditions of low pH (pH ≤ 4), the copper site of reduced plastocyanin is appreciably different from the oxidised form. The Cu(I) becomes three coordinate instead of four coordinate, with one nitrogen (His-37) and two sulphurs (Cys-84 and Met-92) as ligands. The Cu-Nδ1 (His-87) bond is broken after Nδ1 87 becomes protonated and then rotates 180° to interact with the solvent. With a more trigonal copper geometry, one less nitrogen ligand and a shorter Cu-S(thioether) bond, the metal strongly prefers its reduced state. Thus the low pH form has a higher redox potential, and electron transfer is prevented until the copper geometry reverts to the high pH form. Consequently, the low pH form is regarded as redox 'inactive'[122].

The existence of two pH-dependent forms of reduced plastocyanin explains the pH-dependent behaviour of the redox potential[172,193]. For spinach plastocyanin, the redox potential increases by approximately 60mV per pH unit below pH 5.4[38]. This is supported by crystal structures determined at intermediate pH values (pH 3.8-7.8)[122] which show the copper geometry to undergo a gradual change from the distorted tetrahedron of the high pH form to the trigonal arrangement of the low pH form. This can be related to three progressive changes noted in the crystal structures analysed between pH 7.8 and pH 3.8: 1) a lengthening or breaking of the Cu-Nδ1 (His-87) bond, 2) a shortening of the Cu-Sδ(Met-92) bond and 3) a 0.68Å shift of the copper atom into the NSS' plane. The authors proposed that the structures at intermediate pH values were weighted averages of both extreme pH forms of plastocyanin, so that when the pH drops, the average copper geometry converts from an 'active' to an 'inactive' form. This proposal is also supported by studies of electron transfer rates with inorganic oxidants[172,193].

Like plastocyanin, azurin is involved in biological electron transfer. One of the presumed physiological partners of azurin, cytochrome c_{551}[153,197], exchanges electrons with azurin at a very fast rate, between 1.4×10^6 and 8×10^7 $M^{-1}s^{-1}$ [24,198], which approaches the diffusion limit of 10^8-10^9 $M^{-1}s^{-1}$. Similarly, the ESE rates for azurins, ranging from 7×10^5 to 2×10^6 $M^{-1}s^{-1}$, are also very fast as judged from NMR experiments[27,28,128]. The

rates with physiological partners are far greater than with inorganic redox reagents[198].

The effect of pH on the electron transfer rates of azurin has been the subject of considerable debate. The redox potential, E°, for several azurins drops approximately 60mV between pH 5 and pH 9[199]. The electron transfer rates were discovered to be pH-dependent with a number of inorganic redox reagents†, including $FeEDTA^{2-}$ [200], $Co(phen)_3^{3+}$ [199] and $Fe(CN)_6^{3-}$ [199], while with others the reaction is pH-independent (e.g. $Co(4,7\text{-DPSphen})_3^{3-}$ [199]). Originally, the electron exchange rate between azurin and cytochrome c_{551} was reported to be pH-independent[24], but later it was proposed that there were pH-dependent transitions between the redox forms of these proteins[153,200]. This proposal was also supported by the redox reactivity of flavocytochrome b_2 derivatives with azurin and stellacyanin[23]. Contrary to the results with inorganic and biological redox partners, however, the ESE rate deduced from NMR spectra was pH-independent[27,28,123,128]. This varied redox behaviour of azurin led to the conclusion that there must be different sites for electron transfer[10].

It has since been shown conclusively by crystal structure analysis, that the pH induced conformational changes in *Ps. aeruginosa* azurin at His-35, suggested by ^1H NMR experiments, do not structurally affect the copper site[27,28,41,123]. This agrees with results from other methods (EPR[82,93] and EXAFS[161]) which suggest that the copper site is not affected by pH. Crystal structure analyses also show why the pH-dependence seen in *Ps. aeruginosa* azurin does not occur for *Alc. denitrificans* and *Alc. faecalis* azurins[128] (see Section 1.3.1). Finally, site directed mutagenesis studies on *Ps. areuginosa* azurin, in which His-35 has been changed to Gln, Leu and Phe, have discredited the possibility that pH-dependent changes at His-35 cause a deactivation of the copper site[156]. These studies did, however, show that His-35 is responsible for a second relaxation phase in the electron transfer kinetics found in the wild type protein, but not in the mutants. Any pH-dependent redox activity with inorganic reagents is probably a reflection of a conformational change on the surface of the protein where the reagent binds (e.g. at the sulphate binding site, where the protonation of His-83 may have an effect).

1.3.4 Apo-plastocyanin and apo-azurin

The structure of apo plastocyanin has been determined by X-ray diffraction methods to 1.8Å resolution[191]. Comparison of this structure with that of oxidised plastocyanin[32] shows shows that the apo structure closely resembles the holo form. Superimposing the

† Abbrevations used: phen, 1,10-phenanthroline; 4,7-DPSphen, 4,7-(di(phenyl-4'-sulphonate)-1,10-phenanthroline.

apo structure onto the oxidised and reduced (pH 3.8) structures (using only the main-chain atoms) gives r.m.s. deviations in main-chain atom positions of 0.12Å and 0.21Å, respectively. Five residues, however, do undergo significant changes upon copper removal. The most interesting change is at the His-87 imidazole ring, which provides the shortest route between the copper atom and the solvent. The position of the His-87 imidazole ring shifts on average by 0.39Å, but an examination of the surrounding solvent structure shows that it has rotated 180° about the C_β-C_γ bond. The other significant changes also occur in the copper binding site, and in the nearby residue Pro-36. The other copper binding groups (except for His-87) move into the space vacated by the copper atom, although by amounts less than the movements seen for His-87 (His-37 ≈0.31Å, Cys-84 ≈0.20Å and Met-92 ≈0.12Å). The change at Pro-36, which forms part of the rim of the hydrophobic patch in plastocyanin, on the other hand, is a movement away from the copper binding site, and may be a relaxation of the polypeptide chain related to the 180° rotation of the His-87 imidazole ring.

The fact that the bulk of the structure of plastocyanin is essentially identical between the apo and holo forms suggests that the folding of the polypeptide chain is stable and independent of copper binding. Small conformational changes of 0.1-0.4Å at the vacant copper site show this region to be relatively rigid in structure, held by the hydrogen bonds and packing interactions surrounding the active site. This implies that the distorted tetrahedral geometry of the copper is dictated by the protein, which imposes the particular ligand geometry found. Consequently, it has been suggested that the protein "tunes" the copper coordination to acquire the high redox potential[191].

Some insight was also gained into a possible mechanism of copper incorporation into apo plastocyanin[191]. The 180° rotation of His-87 in apo-plastocyanin has led to a proposed "revolving door" mechanism which would allow the copper atom access to the active site. The proposal implies that the copper binds first to $N_{\delta 1}$ 87, which then undergoes a 180° rotation to carry the copper into its eventual binding site. Unfortunately, there is no published kinetic data on the uptake of copper by apo-plastocyanin to test this proposal, but results from kinetic studies on azurin and stellacyanin show two-step mechanisms[201,202] which could agree with the proposal. However, other conformational changes may just as easily explain the two-step kinetics of copper incorporation.

For azurin, NMR studies indicate that the apo protein has similar secondary structure to the holo-protein[126,148]. This suggests that, like plastocyanin, most of the tertiary structure in azurin is stable and unchanged in the absence of the copper. However, small changes in the ^1H NMR spectra are discernible, suggesting that copper removal may

cause some small structural changes. One of the most notable of these is the release of one histidine residue for titration[126]. Another significant observation is that the removal of the metal markedly increases the lability of several N-H protons[126], a phenomena also found in plastocyanin[203].

Results from differential scanning calorimetry[204] and Fourier transform infrared spectral analysis (FT-IR)[205]show that the thermal stability of azurin drops when the copper is removed. While Cu(II) azurin shows remarkable thermal stability, with a single melting transition at ≈80°C in calorimetric scans, the apo protein shows an extra irreversible melting phenomenon at ≈65°C[204]. The temperature of the extra transition is pH sensitive and drops from 69°C to 58°C between pH 5.5 and 9.0, suggesting the involvement of histidine side-chains which titrate in this pH range. In addition, the copper binding ability is irreversibly lost when apo azurin is annealed above 75°C. The authors speculated that the extra melting phenomena may be due to the unfolding of the flap" region of azurin, while the majority of the β-sandwich structure remains intact[204]. Interestingly, this extra melting phenomena is not seen for apo-plastocyanin, but does occur for apo-stellacyanin[204]. FT-IR spectra also indicate that although the secondary structure of apo-azurin is practically indistinguishable from Cu(II) protein at room temperature, there is a slight reduction in the content of the β-structure at 67°C, and complete melting of the β-strands at 86°C[205].

Similarly, enzymes such as trypsin or chymotrypsin can digest apo-azurin while the holo-protein is resistant to this degradation[206]. Binding Co(II) to apo-azurin can protect the protein from digestion[206], and in calorimetric scans, metal substituted derivatives of azurin (Hg(II), Cd(II), Zn(II), Ag(I) and Co(II)) show a single melting transition at ≈80°. Presumably, incorporation of most metal ions into the protein is able to "tighten" the structure in a way that protects it from thermal denaturation and proteolytic digestion.

The evidence above suggests that the protein structure is largely unchanged by metal removal, although the metal does confer extra stability. This stabilising effect appears to be greater for azurin than for plastocyanin, and may relate to deeper burial of the metal in azurin, making it more difficult to remove.

1.3.5 Proposed structural studies on reduced and apo-azurin

Reduced, Cu(I), azurin

There are many reasons for a crystallographic analysis of the reduced structure of azurin.

First, fast electron transfer, the presumed biological function of azurin, requires that the reorganisation of the structure upon oxidation/reduction be small. To quantify this, the structures of both the oxidised and the reduced forms need to be known and compared. Furthermore, it would be interesting to see whether changes in the copper geometry reflect the coordination preferences for Cu(I) and Cu(II). For instance, does the copper atom move closer to the methionine sulphur and further away from the carbonyl oxygen upon reduction as suggested by EXAFS experiments[160,161]? And if so, does this result in a more tetrahedral like copper geometry for the reduced protein?

Although high resolution structures are available for both oxidised and reduced plastocyanin, the comparison was complicated by the pH-dependent conformational change which inactivated the protein[32,122]. This meant that at intermediate pH values the reduced structure was a mixture of two forms, so that *true* active reduced structure had to be deduced by extrapolation[122]. For azurin, however, the protein is not inactivated at low pH, and there is no evidence of a pH-dependent conformational change at the copper site. Futhermore, the only pH-dependent change near the copper site is that by *Ps. aeruginosa* azurin alone. It involves a peptide flip at residues 36-37, and has no effect on the copper site and function[41].

The copper site of azurin is also different in many important respects from that of plastocyanin. The Cu-S(Met) bond is longer in azurin, and there is the close approach of a carbonyl oxygen (Gly-45) which may interact weakly with the copper (a shift in this oxygen atom may support the suggestion of a Cu...O 45 interaction[31]). The cysteine sulphur makes two S...HN hydrogen bonds compared to only one in plastocyanin, possibly further constraining the position of the side-chain of Cys-112. The copper is also more deeply buried in azurin, and the loop preceding the first histidine ligand, which is flexible and moves in plastocyanin, is longer and different in azurin. Therefore, the structural relationships between the oxidised and reduced forms may be different for azurin. Eventually, the structural knowledge of the changes made upon reduction will also aid the classification of the blue copper proteins into different sub-classes as has recently been proposed by Adman[2,10].

Apo, copper free, azurin

Determination of the apo-azurin structure will test the hypothesis that the metal site of azurin is result of the protein imposing structural constraints on the configuration of the metal ligands. This concept is referred to as "rack-induced bonding" [129,207], or as the "entatic state" [208], where the protein structure imposes a transition-state like geometry,

which has functional advantages, on the metal. The alternative to "rack-induced bonding" or the "entatic state", is that the active site is modified by binding of the metal, so that there is some element of an induced fit.

Calorimetric scans have shown that for all metals examined (except for Ni(II)), the presence of a metal ion thermally stabilises the protein structure, and that removal of this ion adds an extra melting transition at lower temperatures, which is irreversible and renders the protein incapable of binding metals again[204]. This extra melting transition does not occur in the calorimetric scans of plastocyanin[204]. A structural analysis of apo-azurin and examination of the thermal parameters may be able to establish which part of the polypeptide chain is likely to unfold in this extra melting transition.

It will also be of interest is to determine whether the apo site resembles the Cu(I) site or the Cu(II) site of azurin since this would have relevance to the redox potential of the protein. A more Cu(I) like site in apo-azurin would imply that the high redox potential is the result of a structural preference for Cu(I) over Cu(II).

A comparison of the apo structure with the oxidised and reduced structures has been done for plastocyanin[191], but the findings made could not be related directly to published kinetic data on the uptake of copper by plastocyanin. However, kinetic data on the uptake of copper by azurin has been published[201,202], and so any structural changes which lead to a proposed mechanism for copper uptake can be tested against the kinetic data. Futhermore, the proposed "revolving door" mechanism for plastocyanin may not apply to azurin because the metal binding site is more deeply buried. Finally, any changes in the loop preceding Gly-45 may bear on the suggestion that the Cu...O 45 distance in oxidised azurin is a weak interaction[31].

Chapter 2 : Experimental

2.1 Preparation of reduced and apo-azurin crystals

2.1.1 Preparation of reduced (Cu(I)) azurin crystals

Crystals of oxidised Cu(II) azurin were prepared from buffered ammonium sulphate solutions according to the protocol set out in the thesis of Dr. G. Norris[209]. Needle-like crystals as long as 1mm were grown by vapour diffusion against reservoirs of 70% saturated ammonium sulphate, buffered to pH 5.5-6.5. Crystals appeared after 3-4 months at 37°.

Azurin was reduced by soaking the oxidised crystals in a stabilising solution (75% saturated ammonium sulphate buffered to pH 5.5 with phosphate) containing 0.1M ascorbate. The crystals were soaked over a 8-12 hour period, to allow the reducing agent to diffuse completely through the solvent channels of the crystal lattice. The colourless crystals were then removed from the reducing solution and mounted in X-ray capillary tubes in the presence of the mother liquor. Under these conditions the crystals were stable in the X-ray beam for approximately 3-4 days, at the end of which time they appeared pale blue in colour as irradiation with X-rays caused the protein to oxidise.

Table 2.1.1.1 lists the axial lengths of the reduced azurin crystal and shows that the reduced crystals are isomorphous with the oxidised crystals. These observations indicate that the molecular structure of the protein is only slightly changed when the copper site is reduced. Full details of the unit cell for reduced azurin are given in Appendix C.1.

Table 2.1.1.1. Average unit cell dimensions in Å of oxidised and reduced azurin.

	a (Å)	b (Å)	c (Å)
oxidised azurin	75.0	74.2	99.6
reduced azurin	75.1	73.8	100.1

2.1.2 Preparation of apo-azurin crystals by soaking in cyanide

The method used to prepare crystals of copper-free azurin is similar to that used for removing copper in solution[209], and has been used by Guss *et al.* in the preparation of apo-plastocyanin crystals[191]. Crystals of oxidised Cu(II) azurin were soaked in stabilizer solutions of 0.1M potassium phosphate buffer and 75% saturated ammonium sulphate containing 0.1-0.2M potassium cyanide. The solutions were replaced every 1-2 months, for up to one year. Depending on the pH of the soaking solution, the crystals slowly lost

their blue colour over a period of 2-6 months. Even after several months, however, some apo-azurin crystals soaking under acidic conditions (pH 5-7) had not completely lost their blue colour, indicating that some copper still remained bound. Eventually, such crystals were transferred to fresh potassium cyanide solutions under more basic conditions (pH 7-8), and the remaining blue colour disappeared over several months.

The dependence of the rate of copper removal on pH can be understood as a function of the relative concentrations of cyanide ion and hydrogen cyanide. In the presence of hydrogen ions, cyanide forms hydrogen cyanide according to the equlibrium;

$$HCN \rightleftharpoons H^+ + CN^- \qquad K_{diss} = 4 \times 10^{-10} \text{ mol } l^{-1}$$

At pH 5, the ratio between the concentrations of cyanide ion and hydrogen cyanide is 4×10^{-5}, while at pH 8, this ratio is a thousand fold higher at 4×10^{-2}. The difference in the relative cyanide ion and hydrogen cyanide concentrations between pH 5 and pH 8 may explain the pH-dependence of copper removal.

The other possibility is that there are pH-dependent changes in the protein conformation which prevent the removal of copper. The reconstitution of the copper into apo-azurin was noted to be faster at higher pH[201], and the pH profile suggested the involvement of a residue with a pK_a of 6.75. This suggests that the side-chain of His-117 needs to be deprotonated before the copper is incorporated into the protein. Also, in the structural analysis of reduced copper(I) plastocyanin at several pH values[122], it was suggested that a possible biological function of the low pH form of reduced plastocyanin is to prevent the loss of copper[122].

The above experiments indicate that the optimum conditions for soaking the crystals are 0.2M potassium cyanide, 0.150-0.175M potassium dihydrogen phosphate and 75% saturated $(NH_4)SO_4$, pH 7.2-8.0. The cyanide solutions were replenished periodically, since the pH drops over time through the loss of ammonia. Replenishing with fresh solution also removes any copper in the form of $Cu(CN)_4^{3-}$, preventing it from re-entering the protein.

The apo-azurin crystals, judged copper free by the absence of any blue colour, were transferred to a 0.1M potassium phosphate buffer stabilizer solution, 75% saturated with ammonium sulphate, pH 6.0, just prior to data collection. This served to adjust the pH to a value similar to that used for the oxidised and reduced structures, and to remove any excess copper in solution. No detectable trace of blue colour returned to the crystals

during or after data collection. This is evidence that all of the copper has been removed, and not reduced, since a blue colour did return to the reduced crystals during the data collection.

Finally, as a test to ensure that the apo-azurin crystals were truly copper free and not just converted to the reduced copper(I) form, crystals were transferred to 0.01M $K_3Fe(CN)_6$ solutions to reoxidise any remaining copper. At first, a sample of small colourless crystals were soaked for 24 hours in 0.1M potassium phosphate stabilizer solution pH 5.7 to dialyse out the potassium cyanide, and were then transferred to a stabilizer solution containing 0.01M $K_3Fe(CN)_6$. After 24 hours and several changes of oxidising solution, the crystals of apo-azurin remained colourless, indicating no copper present in the protein. The above reoxidation procedure was repeated on one of the crystals used for X-ray data collection to further verify that no copper had been present in that crystal. No blue colour returned even after 120 hours. After six months, the crystal still had no colour apart from a faint yellow tinge (presumably due to remaining $K_3Fe(CN)_6$), indicating an absence of copper in the protein.

Conclusions regarding the removal of copper from azurin crystals

Unlike plastocyanin, azurin does not appear to have a fast mechanism for copper removal when in the crystalline state. This is clear when the length of soaking times is compared between the two proteins. In the case of plastocyanin, removal of the copper took 72 hours, while for azurin, the time required for complete removal was as long as a year. This difference in the rate of copper removal can be explained by comparing the contacts between neighbouring protein molecules for azurin and plastocyanin. In plastocyanin, the closest intermolecular contact to His-87 is 5.6Å away[32]. In addition, the side-chain of His-87 is very accessible to solvent since it is part of the protein surface adjacent to a large cavity in the crystal lattice (see Figure 2.2.1.1). The corresponding side-chain in azurin (His-117) is buried away from the bulk solvent by the packing of an opposing molecule at the hydrophobic patch. Figure 2.2.1.2 shows this packing arrangement of the two molecules of azurin which effectively blocks off any easy access to the copper site from the solvent.

2.1.3 Crystallization of apo-azurin from solution

Although crystals of the apo form of azurin could be obtained by soaking oxidised crystals in potassium cyanide solutions, attempts were also made to grow crystals directly

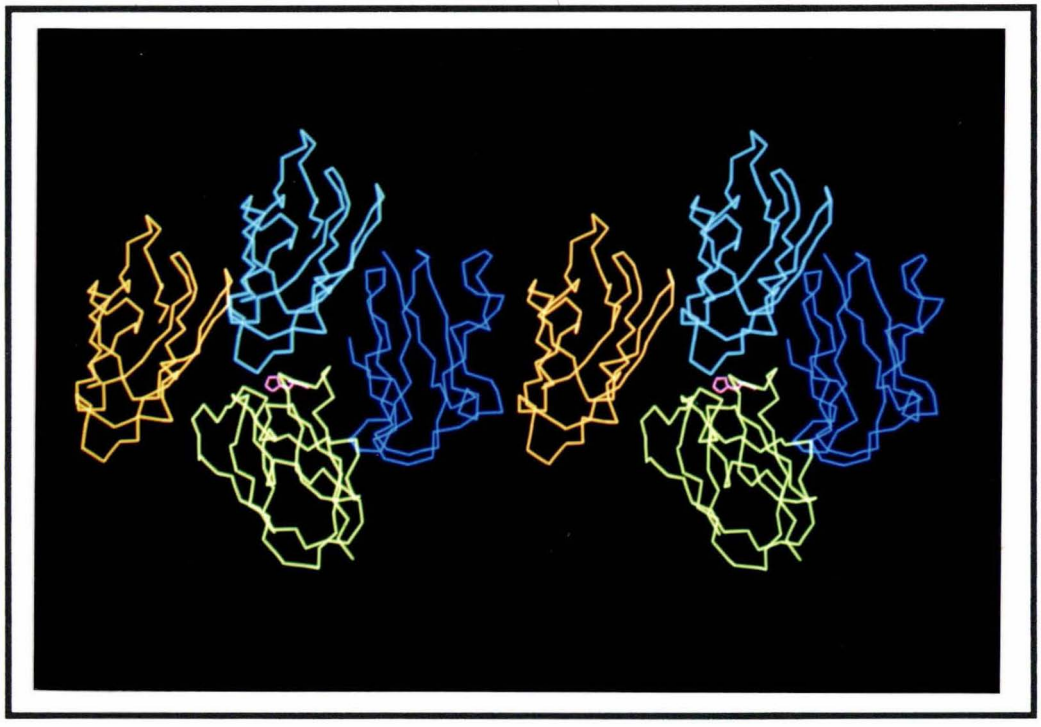

Figure 2.2.1.1. The solvent channel which provides easy access to the copper site through the side-chain of His-87 (pink) in plastocyanin. Coordinates obtained from the Protein data bank[395].

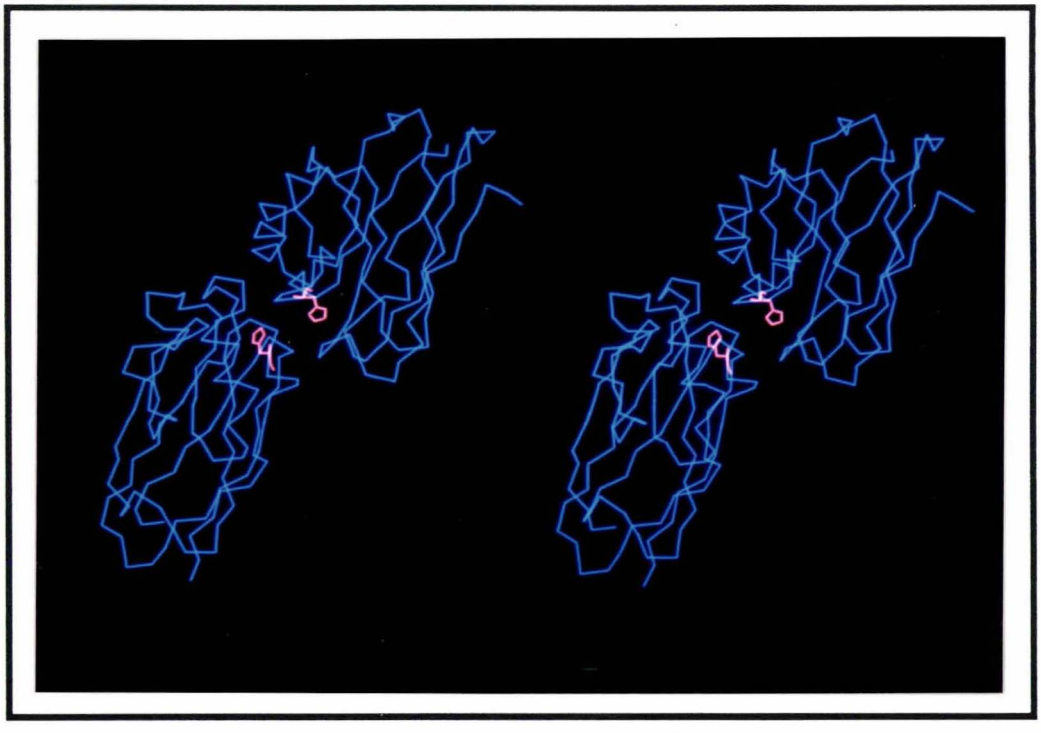

Figure 2.2.1.2. The crystal packing which effectively excludes solvent access to the copper site through His-117 (pink) in azurin.

from solutions of apo-azurin. This would determine whether the constraints of the crystal lattice prevent the protein from taking up its preferred conformation if the copper is removed from azurin in the crystalline state.

Apo-azurin was prepared by treating oxidised azurin solutions with 0.1-0.2M potassium cyanide, 0.10-0.18M potassium phosphate at pH 8.0-8.5[211]. Material for the preparation came from two sources; 1) dissolved small crystals and 2) further purified frozen protein from a previous preparation of azurin. The initial protein solution was concentrated to approximately 200µl using Centricon YM-10 centrifuge microconcentrators. Then fresh potassium cyanide solution was added (approximately 2ml), and the solution was concentrated to 200µl again. The procedure was repeated every 2-4 hours for 16 hours or until all visible trace of blue colour disappeared. After the total loss of blue colour from the protein solution, the cyanide solution was replaced in the same manner over 8 hours with 0.1M potassium phosphate, 50% saturated ammonium sulphate buffer solutions pH 5.6-7.6. The optical densities of these freshly prepared apo-azurin solutions (concentration ≈1mg/ml) were then measured at 280nm and 625nm, and found to have negligible absorbance at 625nm indicating either the removal of the copper atom or its reduction to copper(I). No colour returned to the protein solutions after ≈24 hours, indicating that they were copper-free, since the reduced protein slowly oxidises in the absence of reducing agents.

Two vapour diffusion methods were employed to crystallize apo-azurin from solution. In the first method, 10µl droplets of apo-azurin solutions (10-12mg/ml protein in 0.1M potassium phosphate, 50% ammonium sulphate buffer) were placed on siliconised glass slides, and were hung over a solution of 60-75% saturated ammonium sulphate (referred to as the "hanging drop" method). The other method used involved setting up 50-100µl of protein solution in siliconised or plastic tubes, which were then placed in sealed bottles containing 1 ml of 60-70% saturated ammonium sulphate solution (referred to as the "batch" method).

Although the best oxidised azurin crystals are obtained at 37°C[209], a report by Engeseth and McMillin[204] suggests that apo-azurin is less thermally stable than the oxidised form. To avoid the possibility of denaturation during the crystallization experiments, it was decided to keep the crystallizations at room temperature (18-25°C). Microcrystals of apo-azurin appeared after three months, but larger crystals took 6-18 months to grow. All crystals contained some faint blue colouration depending on their size. The addition of chelating agents (potassium cyanide, thiourea and EDTA) at approximately 0.01M concentration to the crystallizing solutions had no effect on completing the removal of the

copper from the protein solution. Buffer and stabilizer solutions for the crystallizations were made up of ultra pure chemical stock (less than 0.2ppm of copper and 0.5ppm of other metals) and put down a Chelex column to remove residual metal ions. All glassware used in setting up the crystallizations were acid washed (except for siliconised and plastic tubes), then rinsed repeatedly with deionised distilled water. Nevertheless, it must be assumed that either some copper contamination of the buffers, etc. did occur, or that a small amount of the copper remained as Cu(I) after cyanide treatment. The concentrations of the solutions which the protein solutions diffuse against were occasionally increased by 2-4% if no further sign of crystallization occurred within 3-6 months. Table 2.1.3.1 lists the results of the crystallization experiments, and the details for each experiment are given in the footnote.

The best apo-azurin crystals were grown after 1-2 years by vapour diffusion from "batch" method crystallization experiments with 10mg/ml protein buffered to pH 5.6-6.4 with 0.1M potassium phosphate and 70% saturated ammonium sulphate. The first signs of crystallization appear after three months, after which the concentrations of the reservoirs need to be increased to 70% saturated ammonium sulphate. Large crystals also appeared in the hanging drop experiments under similar conditions, at pH values between 6.8-7.6 and reservoir concentrations of 70-75% ammonium sulphate. These crystals grew faster (3-9 months) than those at lower pH and in the batch method, but often appeared twinned. Stringent methods were used to keep the protein solutions copper-free,but despite this, completely colourless large crystals could not be grown, reflecting the high affinity of apo-azurin for copper[201]. Futhermore, apo-azurin crystals regained some blue colour after removal from the crystallization solution, indicating that the protein can still easily pick up copper from solution.

One crystallization experiment produced a new crystal form of apo-azurin mixed in with the usual crystal form. A single large crystal with hexagonal habit was found, but has not yet been characterised.

Full details of the unit cell for apo-azurin are given in Appendix C.1.

Table 2.1.3.1. Crystallisation results of apo-azurin solutions†.

Initial $(NH_4)_2SO_4$ concentration	pH 5.3	pH 5.4	pH 5.6	pH 6.0	pH 6.4	pH 6.8	pH 7.2	pH 7.6
60% saturated	-	-	m^1 L^2	m^1 L^2	m^1 s^2	p^3	mp^3	m^3
64% saturated	-	-	m^1 L^2	c^1 L^2	m^1 L^2	p^3	mp^3	m^3
66% saturated	s^9	s^{10}	p^6 p^7 p^8 s^9	p^6 p^7 p^8	p^6 p^7 p^8 s^{10}	-	-	-
68% saturated	s^9	s^{10}	m^1 LH^2 p^6 p^7 p^8 s^9	m^1 L^2 p^6 p^7 p^8	m^1 s^2 p^6 p^7 p^8 p^{10}	p^3	L^3	m^3
70% saturated	s^9	s^{10}	p^6 p^7 s^9	p^6 p^7	p^6 p^7 p^{10}	-	-	-
72.5% saturated	-	-	-	-	-	L^3	s^3	p^3
75% saturated	-	-	-	-	-	L^3 L^{*4} L^5	s^3 L^{*4} sc^5	c^3 s^4 d^5

† Descriptions of results are given a one letter code:

c = cluster of crystals.
d = dried out solution.
H = hexagonal crystal form.
L = Large crystals.
m = microcrystalline material.
p = precipitate.
s = small crystals (too small for X-ray work).
* = crystals transferred to potassium cyanide solutions.

Each experiment is denoted with a superscript number:

1 = Hanging Drop Method (purified frozen protein), 10 µL of 12 mg/ml apo-azurin, 0.1M potassium phosphate, 50% saturated ammonium sulphate, 4 months
2 = Batch Method (purified frozen protein), 12 mg/ml apo-azurin, 0.1M potassium phosphate, 50% saturated ammonium sulphate, precipitant concentrations increased by 2% then to 70%, 18 months.
3 = Hanging Drop Method (purified frozen protein), 10 µL of 12 mg/ml apo-azurin, 0.1M potassium phosphate 50% saturated ammonium sulphate, 3 months.
4 = Hanging Drop Method (purified frozen protein), as for #3, plus 10 µL of precipitant, 3 months.
5 = Hanging Drop Method (purified frozen protein), as for #3, plus 10 µL of 0.2 M potassium cyanide buffer, 3 months.
6 = Batch method (dissolved crystals), 50 µl in siliconised tubes, 10mg/ml protein, 0.1M potassium phosphate buffer, potassium cyanide added as chelating agent, 1 month.
7 = Batch method (dissolved crystals), as for #6, but EDTA added as chelating agent, one month.
8 = Batch method (dissolved crystals), as for #6, but thiourea added as chelating agent, one month.
9 = Batch Method (dissolved crystals), 100 µl in plastic tubes, 10 mg/ml apo-azurin, 50% saturated ammonium sulphate, 0.05M ammonium/acetate buffer, 4°C then later 20°C, 9 months.
10 = Batch Method (dissolved crystals), as for #9, plus 0.01M EDTA, 4°C then later 20°C, 9 months.

2.2 X-ray data collection and processing

2.2.1 Data collection

X-ray diffraction data were collected from reduced and apo-azurin crystals on an Enraf-Nonius CAD4 diffractometer with Cu-K_α radiation using a 600mm helium filled long arm detector. Data to 1.9Å resolution were collected from a total of eight crystals of reduced azurin; four for data to 2.1Å resolution, and four for data from 2.1Å to 1.9Å resolution. Data to 2.2Å resolution were collected on two crystals of apo-azurin, but an attempt to collect higher resolution data to 1.9Å resolution was unsuccessful because of poorly diffracting crystals.

Unit cell parameters were initially determined from low angle reflections and then refined using higher angle reflections for the final cell parameters. A similar list of reflections was used for each crystal to determine the final unit cell parameters, which are given in Table 2.2.1.1. The average unit cell axial lengths (standard deviations in parentheses) from the eight crystals of reduced azurin are a=75.2(1)Å, b=73.8(1)Å and c=100.1(1)Å, and a=75.1(1)Å, b=74.3(1)Å and c=99.0(1)Å for the two crystals of apo-azurin.

Table 2.2.1.1. Data collection information for reduced azurin and apo-azurin crystals. [a] "Resolution limits" apply to the regions where the bulk of the data was collected for each crystal. [b] "Number of reflections" are the total number of measurements made including common reflections for each crystal. Note that for crystals 5 and 6 of reduced azurin the data collection was stopped because ≈90% of reflections were very weak (see below).

Crystal	Unit cell parameters			Resolution limits[a]	No. refs.[b]	% decay	Max. abs. corr.	steps × scan width
	a	b	c					
Reduced azurin								
1	75.21Å	73.82Å	100.07Å	∞ - 2.80Å	7918	16	1.486	7 × 0.04°
2	75.15Å	73.80Å	100.00Å	3.60 - 2.40Å	5576	20	1.667	7 × 0.05°
3	75.15Å	73.87Å	99.96Å	2.40 - 2.10Å	4268	22	1.323	7 × 0.05°
4	75.11Å	73.72Å	100.16Å	2.80 - 2.10Å	3191	26	1.393	7 × 0.04°
5	75.23Å	73.82Å	100.00Å	2.10 - 1.90Å	1604	9	1.374	7 × 0.05°
6	75.24Å	73.85Å	100.27Å	2.10 - 1.90Å	2284	12	1.597	7 × 0.05°
7	75.24Å	73.81Å	100.04Å	2.10 - 1.90Å	4562	20	1.233	8 × 0.05°
8	75.31Å	73.87Å	99.99Å	2.10 - 1.90Å	5728	22	1.473	8 × 0.04°
Apo-azurin								
1	75.12Å	74.35Å	99.01Å	∞ - 2.64Å	8233	25	1.565	7 × 0.04°
2	75.14Å	74.31Å	99.08Å	2.64 - 2.19Å	7970	38	1.212	8 × 0.04°

Fast data collection techniques were employed, for three reasons, 1) the large number of reflections to be measured, 2) the relatively high rate of intensity decay and 3) the reoxidation of reduced azurin crystals in the X-ray beam. For these reasons a limited step scan routine[212] was used to record the intensity of each reflection. This involves scanning across a reflection in a limited number of discrete steps so that the profile of each peak is recorded[213]. Variations in peak position are also tolerated using this method, which is

desirable because protein crystals are subject to slight movements during the data collection[213]. Later, during data processing, the profiles are fitted to a Gaussian curve to give an integrated intensity, I, and standard deviation, σ_I[214]. Reflection intensities were measured at constant scan speeds as 7-8 steps of 0.04-0.05° to give total scan widths of 0.28-0.40°. Scan speeds were adjusted to allow for differences in crystal size and intensity of diffraction.

A set of five standard reflections were measured every three hours to monitor the decay in intensities and check for any crystal movement. Reduced azurin crystals deteriorated 25% in 3-4 days, by which time the crystal colour had also become faintly blue, a sign of reoxidation. Apo-azurin crystals deteriorated at a faster rate, 25-40% in 3-4 days. No background intensity measurements were made, since this would waste valuable time in data collection; instead backgrounds were estimated from weak reflections of the data (see below). At the end of the data collection, absorption curves were measured for each crystal using the method of North *et al.* for each crystal[215].

2.2.2 Data processing

Data reduction

Processing the X-ray diffraction data was done using a set of three programs designed to handle raw intensity data from a CAD4 diffractometer[216]. The program PREPRO determines a background function from weak reflections[217] and a deterioration curve from the intensity standards. FITC3 determines a seven-parameter function to fit the profiles of strong reflections to a Gaussian curve. The seven-parameter function is then applied in REDUCER to determine I and σ_I, and corrections are made for deterioration, absorption and Lorentz polarization effects.

A key part of the fast data collection stategy was the ability to estimate background levels for the data as a whole using the weak reflections[217]. Reflections are defined as weak and used for background estimation if Peak < Ratio × BG; where Peak is the average of the two highest adjacent step counts, and BG is the average of the two outer most steps or the average of the two smallest adjacent steps (which ever is least). The value for Ratio was generally taken as either 1.35 or 1.50 depending on the number of weak reflections available.

The program PREPRO begins by calculating a deterioration correction from the fall off of the intensities of the standard reflections. These intensities are integrated using a Gaussian

fit to their profiles, and a polynomial is determined as a function of intensity decay and exposure time. The deterioration correction for each reflection is computed from this curve and applied to the intensites in REDUCER.

PREPRO then finds the weak reflections below the threshold and extracts the steps to be used for the background. A polynomial first determines the variation as a function of θ, then applies it to put all backgrounds on a common level prior to constructing a look-up table. These corrected backgrounds are tabulated into 10° blocks of ϕ and χ, and then smoothed by averaging over adjacent blocks to give the look-up table from which backgrounds could be obtained for the data as a whole. As a check, the smoothed backgrounds were compared against a small sample of weak reflection profiles from the raw intensity data to ensure that they reflected the true background level.

The advantage of averaging the backgrounds is the removal of statistically random errors which can seriously affect weak reflections. The backgrounds are used by the programs FITC3 and REDUCER to determine peak profiles and integrated intensities respectively.

Absorption corrections were determined empirically from azimuthal scans, measured at 10° intervals of ϕ, of a single strong reflection near $\chi = 90°$. Absorption curves were drawn by hand to smooth any statistical errors in the azimuthal scans, and then were written into a file for later use by REDUCER. Table 2.2.2.1 gives the maximum and minimum absorption corrections for the crystals of reduced azurin and apo-azurin.

Table 2.2.2.1 Absorption corrections. Values in parentheses are the ϕ angles for the minimum and maximum absorption corrections.

Crystal	reflection	maximum correction	minimum correction
Reduced azurin			
1	2 0 19	1.486 (286°)	1.000 (196°)
2	-2 0 19	1.667 (65°)	1.000 (325°)
3	-2 0 19	1.323 (233°)	1.000 (128°)
4	2 0 19	1.393 (85°)	1.013 (355°)
5	2 0 19	1.374 (165°)	1.000 (245°)
6	-2 0 19	1.597 (356°)	0.971 (86°)
7	-1 1 15	1.233 (149°)	1.000 (49°)
8	0 0 20	1.471 (289°)	1.000 (19°)
Apo-azuirn			
1	0 0 -20	1.565 (133°)	1.014 (223°)
2	0 0 -20	1.215 (103°)	1.000 (193°)

Intensities were determined from the step-scan data using the method developed by Hanson *et al.*[214]. The method involves a two-pass procedure, where the profiles of strong reflections are fitted to a Gaussian curve, and the information from these profiles is then applied to the weaker reflections to give their integrated intensities. One advantage of

using a profile fitting method for determining the intensities is that the curve fitting procedure, which removes some of the statistical fluctuations in the step intensities, can reduce the standard deviation of intensity measurements by 50% for the weak and moderate reflections[213,214,218].

More specifically, the program FITC3 determines a seven-parameter function for the peak width (C_3) by selecting and then fitting the profiles of all reflections above a certain threshold. Typically the threshold is Peak/Background $\geq$ 2.0, where Peak is the average of the highest two adjacent steps, and Background is taken from the smoothed function calculated in PREPRO. The Gaussian curve fitted to the steps of the reflection profiles has the form;

$$y_i = C_1 \exp -((x_i-C_2)^2 / (C_3)^2) \qquad (1)$$

where y_i = intensity at step i (background corrected)
C_1 = peak height
C_2 = the centroid of the scan (°)
C_3 = peak width (°)
x_i-C_2 = displacement of step i from the centroid (°).

A seven-parameter function is then refined against these reflections to derive an empirical formula, which describes the peak width, C_3, as a function of location in reciprocal space.

$$C_3 = \Sigma_i \Sigma_j a_i a_j A_{ij} - k\tan\theta \qquad (2)$$

or

$$C_3 = a_1a_1A_{11}+a_1a_2A_{12}+a_1a_3A_{13}+a_2a_2A_{22}+a_2a_3A_{23}+a_3a_3A_{33} - k\tan\theta$$

Aij are the elements of a symmetric tensor, which describes the variation of the peak width anisotropically in reciprocal space, and a_i are the direction cosines of the diffraction vector. The $k\tan\theta$ term acounts for the spectral dispersion effect on the peak width[214]. An advantage of this function is that it allows for variation in the peak width due to the non-uniform mosaic structure and shape of a protein crystal[214]. This profile information is then used in the program REDUCER to derive the integrated intensities of all the reflections.

The most important practical aspect in calculating the C_3-function, is to obtain plenty of well defined profiles for determining the coefficients of the function. This assumes that

the only difference in the profile of a strong and weak reflection is a scale factor[213]. Shells with many weak reflections will typically have fewer profiles for fitting. This can be resolved to some extent by lowering the threshold level, but difficulties arise when the step scan data has very few clear profiles from which to determine an accurate C_3-function, even with a low threshold level. Experience has shown that at least 500 reflections above a threshold of 1.5, for Peak/background, are required for accurate determination. Lowering the threshold below 1.5 does not improve the C_3 function, despite the extra reflections, because statistical fluctuations in the step intensities of these weak reflections give poor profiles (See Table 2.2.2.2 below).

The program REDUCER converts the step scan data into integrated intensities. All integrated intensities were determined using the calculated peak width (C_3) values which were calculated for each reflection from the seven parameter function provided by FITC3 (equation 2). These can then be used in equation 1, along with the individual steps (y_i) and peak centroid (C_2), to determine the peak height (C_1). The intensity of each reflection is proportional to the product of C_1 and C_3 (i.e. $I \propto C_1 \times C_3$). Corrections are then applied to the intensities for absorption, deterioration, Lorentz and polarization effects, and the data is output as structure factor amplitudes.

Arguably, a Gaussian curve is only an approximation to the actual peak profile, and may be crude in some instances. Stepping across the entire peak with as many as 20 steps is a more accurate method (e.g. see the method proposed by Diamond[213]), but using only the top of the peak and a limited number of steps is faster without losing too much information[214]. Usually the shape of a reflection profile is symmetrical, and a Gaussian curve should give a good estimate of the intensities of reflections[214]. This assumption breaks down, however, when the profiles of the data are significantly asymmetric, as may arise from twinned or poor quality crystals. Table 2.2.2.2 outlines the results of data reduction from reduced azurin and apo-azurin crystals.

For some of the shells the number of reflections with $I>2\sigma_I$ is zero. This is because there are very few (<500) strong reflections which could be used to define the parameters in the C_3-function. Consequently, the C_3-function parameters are poorly determined (i.e. they are associated with a high level of error), and this reflects in the levels of the standard deviations. Also it was noted that in the low resolution shells (∞-4.5Å or $\theta<10°$), it can be difficult to obtain enough weak reflections to calculate an acccurate background function, because most reflections in this region are strong and well defined.

Merging of the data

Data for both apo and reduced azurins were collected as a set of shells, which covered different resolution limits. In some cases, the data were collected in blocks which spanned different values of the *l* index (e.g. in reduced azurin crystal 1, the data in shells 2 and 3 span the resolution limits of 3.6-2.8Å, but shell 2 contains data with l=0→14, while shell 3 contains data with l=14→36).

As a general strategy, a certain amount of overlap was allowed for when choosing the limits of each shell. This was done so that there would be a pool of common reflections which could be used in the scaling and merging of the data sets. Two methods of generating common reflections were used: 1) A small shell of "scaling data" would be collected at the end of the data collection for the crystal. This small shell would typically span a wide resolution range, but would be collected over a small range in one of the indices (e.g. apo-azurin crystal 2 shell 4 consists of two sets of data between ∞ and 2.2Å resolution, where the indices ranged from h,k=0→5, l=10→45 for one set and h=6→34, k=0→5, l=0→10 for the other). These "scaling data" shells are labelled "‡" in Table 2.2.2.2. 2) The limits of each shell were set to give a small overlap in the indices. For example, between reduced azurin crystals 6 and 7, the shells spanned l=13→31 (crystal 6) and l=30→52 (crystal 7) to give an overlap with indices in the range l=30→31. By generating a pool of common reflections, each shell contained some data which overlapped with one of the other shells, thereby ensuring that the its scale factor could be calculated. It should be noted that some shells (denoted "†") are repeats of earlier shells which contained data made up of mostly weak reflections.These repeat shells are from reduced azurin crystals 7 (shell 2) and 8 (shells 1 and 2), and have generated a large overlap in the data between 2.1Å and1.9Å resolution.

Two programs were utilised to merge together the data from different crystals and shells. The program INTAV3[219] calculates the scale factors for each crystal or shell, while the program INTAV4 applies these scale factors and then merges all of the reflections into one data set. In an initial pass of the data, INTAV3 calculates a set of scale factors from all of the common reflections with I above a threshold value ($I > \sigma_I$), and then the scale factors are recalculated after rejecting those common reflections which give poor agreement with the average F, i.e. reject F_i if;

$$| k_i|F_i| - |F_{av}| | > 6\sigma_{av}$$

where

$$F_{av} = \frac{\sum w_i|F_i|}{\sum w_i}$$

k_i = scale factor of crystal i

w_i = weight for $|F_i| = \frac{1}{(k_i\sigma_i)^2}$

Two types of discrepancy factors are calculated;

$$R_{2a} = \sqrt{\frac{\Sigma\Sigma_i\Sigma_j\, w_{ij}\,(k_i|F_i| - k_j|F_j|)^2}{\Sigma\Sigma_i\Sigma_j\, w_{ij}\,|F_{av}|^2}}$$

where

$$w_{ij} = \frac{1}{(k_i\sigma_i)^2} + \frac{1}{(k_j\sigma_j)^2}$$

and

$$R_{2b} = \sqrt{\frac{\Sigma\Sigma_i\, w_i\,(|F_{av}| - k_i|F_i|)^2}{\Sigma\Sigma_i\, w_i\,|F_i|^2}}$$

where

$$w_i = \frac{1}{(k_i\sigma_i)^2}$$

Different sets of scale factors were generated and compared by adjusting the threshold and rejection criteria of the reflections. The final criteria used to scale the reduced azurin data (1.9Å resolution) were set at $F > \sigma_F$ and $|F-F_{av}| < 6\sigma_F$. (A threshold of $F > 2\sigma_F$ would have been used, but there are few common reflections above this threshold in the higher resolution shells.) The data gave discrepancy factors of $R_{2a} = 0.146$, $R_{2b} = 0.069$ for a total of 6177 common reflections. The criteria chosen for the apo-azurin data set (2.2Å resolution) were $F > 2\sigma_F$ and $|F-F_{av}| < 6\sigma_F$, which gave discrepancy factors of $R_{2a} = 0.0949$, $R_{2b} = 0.0421$ for 1303 common reflections. Table 2.2.2.3 lists the scale factors of the reduced azurin and apo-azurin data sets along with their standard deviations.

The second program, INTAV4, applies the calculated scale factors from INTAV3 (or from elsewhere) for the merging of F and σ_F. INTAV4 uses the following formulae to calculate the final Fs and σ_Fs:

$$F_{av} = \frac{k_{true}\,\Sigma_i w_i k_i |F_i|}{\Sigma_i w_i}$$

$$\sigma_{av} = \frac{k_{true}}{\sqrt{\Sigma_i w_i}}$$

where

w_i = weight for $F_i = \frac{1}{(k_i\sigma_i)^2}$

Table 2.2.2.2. Data reduction results for apo-azurin and reduced azurin shells. "Fitted" = number of reflections used to determine the C_3 function. "Total" = total number of reflections in the shell. "I>0" = number of reflections with I greater than zero (i.e. not negative or misset). "Misset" = number of reflections with the two adjacent highest steps at scan edge. "Negative" = number of reflections with negative I. "I>2σ_I" = number of reflections with I>2σ_I.

Crystal	Shell	Fitted	Total	I > 2σ_I	I > 0	Misset	Negative
Reduced azurin							
1	∞ -3.6Å	2934	3545	3165	3306	51	188
1	3.6-2.8Å	976	1695	1219	1482	81	132
1	3.6-2.8Å	1108	2218	1492	1813	146	259
1‡	∞ -2.8Å	298	460	191	397	28	35
2	2.8-2.4Å	1563	4745	2365	3953	450	342
2‡	3.6-2.8Å	468	831	589	742	47	42
3	2.4-2.1Å	997	4268	1999	3538	520	210
4	2.4-2.1Å	791	2528	1272	2088	290	150
4‡	2.8-2.4Å	186	663	29	540	71	52
5	2.1-1.9Å	186	1604	0	1207	306	91
6	2.1-1.9Å	38	2284	0	1746	481	57
7	2.1-1.9Å	286	2443	944	2013	227	203
7†	2.1-1.9Å	77	2119	0	1732	340	47
8†	2.1-1.9Å	737	4459	1499	3591	543	325
8†	2.1-1.9Å	109	1269	0	1027	199	43
Totals			**35131**	**14764**	**29175**	**3780**	**2176**
Apo-azurin							
1	∞ -3.56Å	3009	3522	3314	3453	38	31
1	3.56-2.64Å	2155	4711	3550	4308	220	183
2	2.80-2.64Å	151	300	0	266	16	18
2	2.64-2.38Å	1055	3162	2373	2908	147	107
2	2.38-2.19Å	636	2981	1830	2683	223	75
2‡	∞ -2.19Å	842	1527	1226	1395	58	74
Totals			**16203**	**12293**	**15013**	**702**	**488**

Table 2.2.2.3. Scale Factors of apo-azurin and reduced azurin data sets.

Crystal	Shell	scale factor	standard deviation	Number of common reflections
Reduced azurin				
1	∞-2.8Å	30.5086	0.1375	655
2	2.8-2.4Å	29.9857	0.1247	2338
3	2.4-2.1Å	28.1778	0.5907	145
4	2.8-2.1Å	29.1093	0.1330	1736
5	2.1-1.9Å	1.4817	0.0406	670
6	2.1-1.9Å	1.0990	0.1553	14
7	2.1-1.9Å	1.0000	0.0201	1385
7	2.1-1.9Å	1.1765	0.0283	1213
8	2.1-1.9Å	1.2343	0.0246	1780
8	2.1-1.9Å	1.4873	0.0412	771
Apo-azurin				
1	∞ -3.56Å	1.8094	0.0031	709
1	3.56-2.64Å	1.6281	0.0126	377
2	2.80-2.64Å	1.1802	0.2686	42
2	2.64-2.38Å	1.0000	0.0306	106
2	2.38-2.19Å	1.0985	0.0464	90
2	∞ -2.19Å	1.4301	0.0020	1240

k_i = scale factor of batch i

k_{true} = externally applied scale factor

Any badly agreeing measurements are rejected from the calculation of the final data set. The criteria for rejection were set down as in Table 2.2.2.4 and the worst measurements identified by these criteria are removed from the data and F_{av} recalculated.

Table 2.2.2.4. Rejection criteria used for reduced and apo-azurin data sets.

Reject F if	reduced azurin criteria	apo-azurin criteria
$\|F-F_{av}\| > N\,\sigma_{av}$	$3\,\sigma_{av}$	$2\,\sigma_{av}$
$\|F_{max}-F_{min}\| > N\,\sigma_{av}$	$4\,\sigma_{av}$	$4\,\sigma_{av}$
$\|F_{max} - F_{av}\| > N\,\sigma_{av}$	$3\,\sigma_{av}$	$2\,\sigma_{av}$
$\|F_{av}-F_{min}\| > N\,\sigma_{av}$	$3\,\sigma_{av}$	$2\,\sigma_{av}$

Decisions on the final data set were made after comparing the merging R-factors and the number of discarded reflections generated from different rejection criteria. INTAV4 determines merging R-factors according to the formula;

$$R = \frac{\sum_i |\,|F_i|^2 - |F_{av}|^2\,|}{\sum_i |F_{av}|^2}$$

Merging R-factors were calculated between individual batches, for each batch with respect to the entire merged data, and for the merged data set with and without badly agreeing measurements. Examination of these R-factors also gave a good indication of the least reliable shells. The overall merging R-factors after omitting poorly agreeing reflections are 0.052 for apo-azurin (129 rejected reflections out of 16203) and 0.116 for reduced azurin (461 rejected reflections out of 35131). The relatively high merging R-factor for reduced azurin is due to the large number of common reflections in the 2.1-1.9Å resolution range which contains much weak data. Tables 2.2.2.5 and 2.2.2.6 give the merging R-factors between individual shells for both reduced and apo-azurin data sets.

As a check on the data, the scale factors and the merging R-factors of the final data were compared to those calculated from two other sources; 1) scale factors based on the intensity standards, and 2) scale factors based on another azurin data set (e.g. oxidised azurin). Scale factors based on intensity standards were calculated from the first set of five standards after correcting for absorption. Scaling against a data set of another azurin form was done using the program INTAV3 after combining this data together with the data shells. Scaling by the latter method assumes that the differences in intensities are random between both azurin forms. Results are listed in Tables 2.2.2.7 and 2.2.2.8.

Table 2.2.2.5. Inter-batch R-factors for reduced azurin 1.9Å resolution data. Values in parentheses are the number of contributing reflections common between the two shells.

crystal	shell								
2	2.8-2.4Å	0.055 (706)							
3	2.4-2.1Å	–	–						
4	2.8-2.1Å	0.066 (13)	0.087 (>1000)	0.064 (24)					
5	2.1-1.9Å	–	–	0.102 (36)	–				
6	2.1-1.9Å	–	–	0.115 (40)	–	0.121 (52)			
7	2.1-1.9Å	–	–	0.091 (39)	0.095 (23)	–	0.126 (188)		
7	2.1-1.9Å	–	–	0.111 (52)	–	0.131 (>1000)	0.128 (369)	–	
8	2.1-1.9Å	–	–	0.109 (82)	0.102 (26)	0.122 (131)	0.142 (>1000)	0.105 (>1000)	0.128 (474)
8	2.1-1.9Å	–	–	0.110 (32)	–	0.121 (784)	–	–	0.119 (858)
resolution (Å)		∞-2.8	2.8-2.4	2.4-2.1	2.8-2.1	2.1-1.9	2.1-1.9	2.1-1.9	2.1-1.9
crystal		1	2	3	4	5	6	7	7

Table 2.2.2.6. Inter-batch R-factors for apo-azurin 2.2Å resolution data. Values in parentheses are the number of contributing reflections common between the two shells.

crystal	shell					
1	3.56-2.64Å	–				
2	2.80-2.64Å	–	0.086 (69)			
2	2.64-2.38Å	–	0.065 (6)	–		
2	2.38-2.19Å	–	–	–	–	
2	∞ -2.19Å	0.044 (722)	0.052 (357)	0.113 (6)	0.089 (134)	0.114 (110)
shell		∞-3.56Å	3.56-2.64Å	2.80-2.64Å	2.64-2.38Å	2.38-2.19Å
crystal		1	1	2	2	2

For the data sets of both reduced and apo-azurin the best merging R-factors are obtained when the internal common reflections are used. Comparison of the final scale factors with those based on intensity standards or from another azurin form shows that the general trend between shells is similar for the different scale factor sets. For the apo-azurin data, scale factors vary on average by only 10%, where the largest difference is in the set of scale factors based on intensity standards in the ∞-3.56Å resolution shell. A significant difference is seen in the scale factors of reduced azurin data for batches below 2.1Å

Table 2.2.2.7. Comparison of different scale factors for reduced azurin. [a] R-merge calculated using all reflections. [b] R-merge calculated using only reflections with $F > \sigma_F$.

Crystal	Shell	Scale factors from INTAV3	Scale factors based on Intensity standards	Scale factors based on Oxidised azurin data
1	∞-2.8Å	30.5086	23.4448	21.3826
2	2.8-2.4Å	29.9857	23.1014	23.3363
3	2.4-2.1Å	28.1778	22.6061	25.3728
4	2.8-2.Å	29.1093	22.5389	24.2288
5	2.1-1.9Å	1.4817	1.2093	1.5005
6	2.1-1.9Å	1.0990	1.2807	1.0926
7	2.1-1.9Å	1.0000	1.0000	1.0000
7	2.1-1.9Å	1.1765	1.0582	1.1890
8	2.1-1.9Å	1.2343	0.9497	1.2186
8	2.1-1.9Å	1.4873	0.9746	1.4900
R-merge		0.116[a]	0.182[a]	0.156[b]

Table 2.2.2.8. Comparison of different scale factors for apo-azurin. [a] Scale factors based on Reduced azurin data were calculated with $F>\sigma_F$ reflections.

Crystal	Shell	Scale factors from INTAV3	Scale factors based on Intensity standards	Scale factors based on Reduced azurin data[a]
1	∞-3.56Å	1.8094	1.6049	1.9110
1	3.56-2.64Å	1.6281	1.5840	1.7827
2	2.80-2.64Å	1.1802	1.2183	1.2636
2	2.64-2.38Å	1.0000	1.1192	1.0744
2	2.38-2.19Å	1.0985	1.0000	1.0000
2	∞-2.19Å	1.4301	1.3796	1.5486
R-merge		0.052	0.098	0.079

resolution. This difference is presumably a temperature factor effect between each crystal and is corrected for in part by the scale factors from INTAV3, since the X-ray data was collected in shells. The other two sets of scale factors, however, do not take this into account. Also, using the intensity standards as a basis for scaling does not allow for the fact that they may not be representative of the shell being collected. This is particularly true of higher resolution shells where no reflections are strong enough to use as intensity standards. Note that the scale factors of reduced azurin from intensity standards are similar to those based on the oxidised azurin data, a data set which was also scaled using the intensity standards.

As a means of determining the quality of the X-ray data for apo-azurin and reduced azurin, the final data sets were divided into even shells of resolution and the percentage of "observed" reflections ($I > \sigma_I$ or $2\sigma_I$) in each shell were plotted against resolution. Figure 2.2.2.1 clearly shows that the data in both forms of azurin is weak at high resolution. In particular, the apo-azurin data shows a marked drop in the percentage of $I > 2\sigma_I$ at the upper limit of the data (2.2Å resolution).

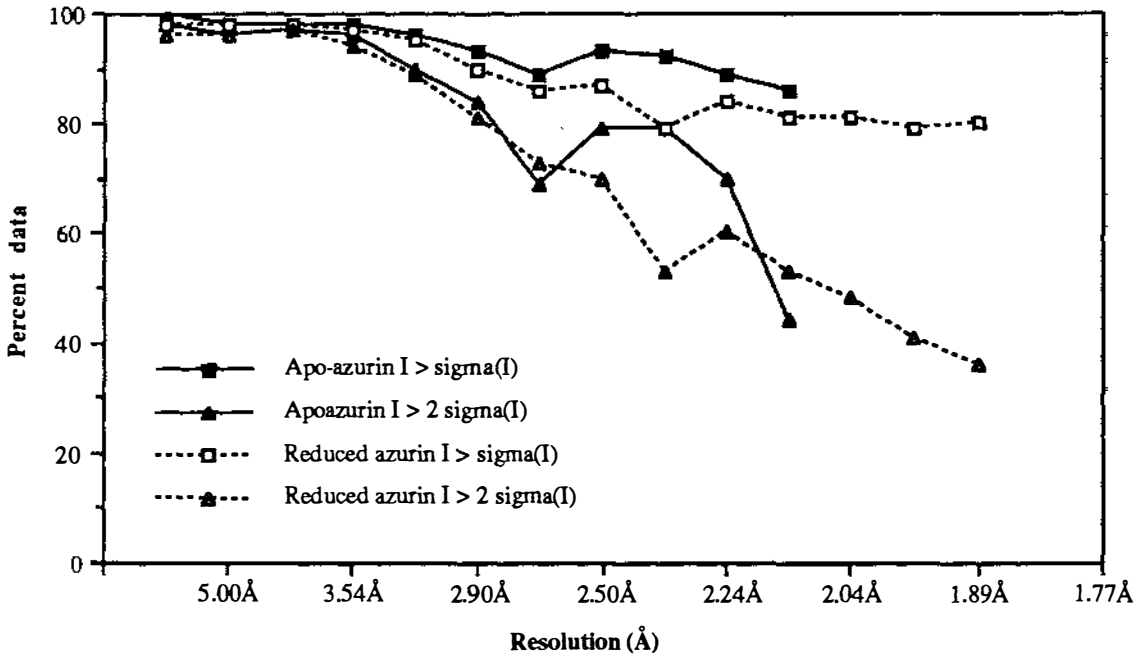

Figure 2.2.2.1. Plot of the percentage of reflections with $I>2\sigma_I$ and $I>\sigma_I$ as a function of resolution for apo and reduced azurin data sets.

2.3 Refinement methods

2.3.1 The starting model

Since crystals of apo and reduced azurins are isomorphous with the oxidised form, only small changes were expected in the overall structure of the protein. Consequently, the coordinates of oxidised azurin, refined to 1.8Å resolution[31], were used as a starting model for refinement of both apo and reduced structures .

2.3.2 Restrained refinement

For small molecule crystallography, full matrix least squares routines can be used in refining the structure because the ratio between the number of observations (X-ray diffraction data) and atom parameters (x,y,z,B) is relatively high (e.g. 3000-6000 observations for a 30-40 atom structure) . In protein crystallography, this method is inappropriate because this ratio is low (e.g. 20000 observations for a 2000 atom structure at 2.0Å resolution), and much of the X-ray data from protein crystals at high resolution is weak. Thus a method of restrained refinement is necessary.

Refinement of both the reduced and apo structures of azurin was completed by employing the restrained least squares program of Konnert and Hendrickson, PROLSQ[220-224]. The restrained least-squares method of PROLSQ utilises structural knowledge, acquired from previously deterrmined small molecule crystal structures, to restrain the stereochemistry of the model close to "ideal" values. The method treats the geometrical restraints as "observations", much like the X-ray diffraction data, and these are then combined into the equations to supplement the X-ray data. Thus a composite function (P) of X-ray and geometrical "observation" terms is minimised in PROLSQ to determine the shifts in the atomic parameters of the model. The types of geometrical restraints imposed on the protein model are the distances, planes, chiral volumes, thermal parameters, van der Waal's contacts and torsion angles (non-crystallographic symmetry can also be imposed, but this was not used); i.e the composition function minimised is;

$$P = P_{x\text{-}ray} + P_{distances} + P_{planes} + P_{chiral} + P_{thermal\ factors} + P_{van\ der\ Waal} + P_{torsion}$$

where

$P_{x\text{-}ray} = k_{x\text{-}ray} \Sigma |F_o - F_c|^2$ for all reflections

$P_{distances} = k_{distances} \Sigma |d_{ideal} - d_{model}|^2$ for all 1-2, 1-3 and 1-4 distances

etc...

The relative weighting for each contribution ($k_{x\text{-}ray}$, $k_{distances}$,...) to the function P is controlled by the input file of PROLSQ. The geometrical "observations" (i.e all of the bonds, angles, planes, chiral centres, etc.) are defined in a file created by the program PROTIN which uses a dictionary of "ideal" geometrical values[220-224]. This allows the user to adjust the restraints and redefine any of the "ideal" geometry as required. The benefit of restrained refinement is that the ratio between contributions from experimental observations (X-ray data) and ideal geometry can be varied, but the main drawback with this method is that geometrical restraints may prevent the model from reaching the correct minimum.

Normally, the restraints on the geometry of the model were kept relatively tight throughout the refinements of reduced and apo-azurin. But, when improvement of the R-factor ceased, the restraints on the geometry were loosened for a few cycles, and then gradually retightened by decreasing the weight of the X-ray contribution to the function P. By this method the refinement allowed the structure to move out of local minima, and then refine closer to the correct solution when the constraints were tightened. More specific changes to the weights of the geometrical restraints were also made, for example by loosening and retightening only the distances. The success of this method can be seen in the sections which describe the course of refinement of the reduced and apo structures.

2.3.3 PROLSQ and HKPROLSQ(FFT)

An important difference in the method of refinement used for apo and reduced azurin structures was the version of the PROLSQ program used. The structure of reduced azurin was refined with a version of PROLSQ which uses conventional least squares methods for the calculation of structure factors and shifts, while the apo structure was refined with a version of PROLSQ which uses fast Fourier transform algorithms[225] (FFT) for its calculations[226]. The main advantage of the FFT version (HKPROLSQ) is the enhanced speed of the calculations, which cuts down on refinement time and computer costs.

Both of these programs minimise the function ;

$$\Sigma_{hkl}\, w_{hkl}\, (|F_{o\,hkl}| - |F_{c\,hkl}|)^2,$$

where $F_{o\,hkl}$ and $F_{c\,hkl}$ are the observed and calculated structure factors for the reflection hkl, and w_{hkl}, is some applied weight. What makes these versions different is the approach to calculating structure factors and shifts. In PROLSQ, the program employs

standard analytical methods to calculate structure factors and to generate the normal equations to be solved for the shifts in the parameters[227,228]. HKPROLSQ on the other hand, uses FFTs to calculate the structure factors, and to give the elements of the normal matrix and gradient vector, which determines the shifts in the atom parameters. For example, the computation of the structure factors is done in two steps; first, an electron density map of the model is built from the atomic coordinates, and then the three dimensional FFT of this map is done to give F_c[226,229]. For a more detailed description of how FFTs are utilised in crystallographic refinement see Agarwal[226] or Ten Eyck[230].

2.3.4 Rebuilding the models

At periodic intervals during the refinements, when convergence of the least-squares process had been reached, the protein structure would be examined visually and where necessary manually rebuilt. Parts of the protein structure were selected for checking and/or rebuilding if 1) the B-value of any atom in the main-chain was above 35Å^2, in which case the whole residue was rebuilt, 2) the B-value of any atom in the side-chain was above 50Å^2, in which case the side-chain was rebuilt, or 3) the group was involved in a contact less than 2.6Å (for potential hydrogen bonds), or less than 3.0Å (between a carbon and any other atom).

The groups selected for rebuilding were omitted from the model, and the structure refined over three cycles of PROLSQ. Two Fourier maps were then calculated, one map with the coefficients ($2F_o$-F_c), and the other a difference map with coefficients (F_o-F_c map), i.e.;

$$(2|F_o|-|F_c|)e^{-i\alpha_c}$$
$$(|F_o|-|F_c|)e^{-i\alpha_c}$$

where $|F_o|$ = observed structure factor amplitude
$|F_c|$ = calculated structure factor amplitude
α_c = calculated phase

The first map should show the electron density of the molecule including that of the omitted residues or side-chains, while the latter map shows only the electron density of the group concerned with minimal bias towards the current model.

Rebuilding of the selected parts of the protein was then done manually, with an interactive graphics system (Evans & Sutherland PS-330) and the program FRODO[231], using the F_o-F_c and $2F_o$-F_c maps as guides to fit the groups correctly into the density. For a few

side-chains, on the surface of the molecule, the groups could not be adequately built into the density, since the Fourier maps were unclear. This is caused either by the group being flexible and its electron density becoming smeared out over several different conformations, or by errors in the X-ray data.

Non-crystallographic symmetry restraints were never imposed on the two independent protein molecules of the asymmetric unit at any stage of either refinement. At one point in the apo-azurin refinement, however, advantage was taken of the non-crystallographic symmetry to help rebuild sections of the protein which were clearer in one molecule than in the other. Also, it was noted that the "poor" molecule had consistently higher B-values in these regions than in the "good" molecule. Rebuilding was done by superimposing the clearer protein molecule onto the poorer one, and then rebuilding the unclear region using the clearer molecule as a guide. Unfortunately, this did not significantly improve the structure as judged by the the change in the B-values of the rebuilt region. The structures of these regions may therefore be different because of crystal packing or genuine structural microhetereogenity, or have refined back to their false minima.

2.3.5 Inclusion of the solvent structure

During refinement, solvent molecules were included in the model. This was done only after the protein structure had been refined after one "round" of rebuilding. Most of the solvent molecules included into the two structures of azurin were treated as water molecules. Exceptions to this were a sulphate anion bound to each of the protein molecules, and another possible sulphate anion (disordered) on a two-fold crystallographic axis. Peaks were located in difference Fourier maps and were labelled as water molecules if 1) the density was well defined, 2) the peak height was above $\approx$2 r.m.s. deviations ($\approx 2\sigma$) of the F_o-F_c density and 3) the geometry of interactions with potential hydrogen bonding partners was good. A decrease in the size and quality of the F_o-F_c peaks assigned to water molecules could be observed during the progress of refinement. For the apo-azurin refinement, in the first round, water molecules appeared as difference Fourier peaks greater than 4σ, and made good contacts with to hydrogen bonding partners. In the following rounds, the assignable peaks were smaller ($\approx 3\sigma$) and geometry poorer, until only peaks just greater than 2σ could be labelled as water molecules. This trend makes sense, since the most well ordered solvent molecules will be clearly resolved in the F_o-F_c maps and consequently entered into the structure early in the refinement, whereas the least well ordered solvent molecules will be poorly resolved in the F_o-F_c maps and entered into the structure towards the end of the refinement. Although occupancies for solvent molecules were not refined, these will be largely taken up by the

individual B-values.

At several stages of each refinement, the solvent structure was checked against omit maps to find any errors. Solvent molecules were omitted from the model and checked as described earlier (i.e. if B > 50-60Å^2 or if it made a contact of less than 2.6Å). In many cases, recentring the position of the solvent molecule was required, but in a few instances this created a short hydrogen bonding contact (<2.6Å) despite repeated attempts at rebuilding and refinement. Presumably, such short contacts in the solvent structure are a result of statistical errors in the X-ray data, errors in the model or the limited resolution. Near the end of refinement, the difference Fourier maps of both reduced and apo-azurin structures were checked against the solvent structure of oxidised azurin[31], to locate any overlooked solvent molecules.

Chapter 3 : Reduced azurin

3.1 Course of the refinement

The initial model for the refinement of reduced azurin was the refined structure of oxidised azurin at 1.8Å resolution[31]. The program PROLSQ was used throughout the refinement. In the first half of the refinement (cycles 1-85), the structure was refined against 12629 observations ($F > 0.6\sigma_F$ between 10Å and 2.1Å), after which the data was extended to 1.9Å resolution (19278 observations) and the refinement completed (cycles 86-157). Initially, unit weights were used for the X-ray data, but at cycle 44 this was changed to a function applying a Sin θ/λ term (see below) which emphasised and gave better agreement for the higher resolution data. Later at cycle 75, the X-ray weights were returned to unity, but were again reset at cycle 119 to the previous function in Sin θ/λ for the same reasons. Restraints on the geometry of the protein molecule were kept fairly tight during refinement, but at cycles 32, 43, 57, 65 and 118, the restraints were relaxed and then retightened to allow the structure to escape from local minima. The geometrical restraints used and the r.m.s deviations for the final model with respect to ideal geometry are listed in Table 3.1.1. The course of the refinement is outlined in Table 3.1.2.

Table 3.1.1. Values of geometrical constraints and the r.m.s. deviations in the final model of reduced azurin. [a] An upper limit for shifts in the atom coordinates and the thermal parameters was set to prevent any excessive shifts in the model. The values under "R.m.s. deviations" here represent the r.m.s. shift in the positions and B-values in the last cycle of refinement.

Geometry	Restraint	R.m.s. deviation
Distances		
1-2 bonded distances	0.020Å	0.021Å
1-3 angle distances	0.040Å	0.059Å
1-4 intraplanar distances	0.050Å	0.060Å
Planar groups		
deviation from plane	0.020Å	0.018Å
Chiral centers		
chiral volume	0.15Å^3	0.225Å^3
Non-bonded contacts		
single torsion	0.50Å	0.214Å
multiple torsion	0.50Å	0.225Å
Thermal factors		
main-chain bond	2.50Å^2	2.989Å^2
main-chain angle	3.50Å^2	4.315Å^2
side-chain bond	3.00Å^2	4.118Å^2
side-chain angle	3.50Å^2	5.905Å^2
Excessive shifts [a]		
positional parameters	0.30Å	0.026Å
thermal parameters	3.00Å^2	0.38Å^2

The initial model, consisting of the protein atoms of the oxidised structure, gave an R-factor of 0.250. This demonstrated that the reduced structure is similar to the oxidised

structure. Ten cycles of refinement dropped the R-factor to 0.198, at which point the copper and its ligands were removed, and the structure refined for another three cycles (R = 0.218). The copper site was then rebuilt and 43 water molecules input followed by 21 refinement cycles (R = 0.188, cycle 32). A further 76 water molecules were input and refinement contined for 11 cycles (R = 0.170). At this stage the weights on the X-ray data were changed because the agreement in the shells at higher resolution had not improved, while the lower resolution shells had. The weight for the X-ray data was changed from unit weights to :

$$w = \frac{1}{\sigma^2}$$

$$\sigma = 60 - 100\left(\frac{\text{Sin }\theta}{\lambda} - \frac{1}{6}\right)$$

Within three cycles this reduced the R-factor in the highest resolution shell (2.25-2.10Å) by 0.034. The geometrical restraints were then loosened (r.m.s.$\Delta_{distances}$ = 0.081Å) and retightened (r.m.s.$\Delta_{distances}$ = 0.017Å) over 10 cycles (R = 0.168, cycle 57). In the next 34 cycles, another 99 water molecules were input, the protein structure and the copper site rebuilt, and two sulphate anions input (R = 0.153, cycle 90). The X-ray data was then extended to 1.9Å resolution (R = 0.177). The refinement continued with several rounds of rebuilding of the protein, inclusion of solvent molecules and refinement cycles until the R-factor reached 0.166 at cycle 148. Three hydrogen bond distances (O 17...O_{η} 110, $O_{\gamma 1}$ 30...$O_{\gamma 1}$ 96 and $O_{\varepsilon 1}$ 4...$N_{\varepsilon 2}$ 32) were restrained because these interactions kept refining below 2.5Å. At cycle 142, four side-chains were modelled as disordered groups (see below). These were to be the final cycles, but nine cycles of HKPROLSQ refinement on just three residues were necessary, while the rest of the structure was fixed, to make sequence corrections as determined by the DNA sequence (Asp-16→Asn, Ser-42→Val and Glu-57→Gln)[179]. The final model contains 1956 protein atoms, 259 water molecules, three sulphate anions (one as a sulphur atom) and 11 disordered atoms, for a final R-factor of 0.168.

Various parts of the protein were rebuilt manually during the refinement to correct and improve the structure. Rebuilding of the protein was done in six rounds at cycles 57, 77, 91, 118, 145 and 149. Omit maps were generated for the regions which either had high B-values or made short van der Waals contacts. These were rebuilt manually as described earlier. During the rebuilding of the protein structure, four side-chains were modelled as disordered (Lys-34A, Lys-41A, Thr-61A and Gln-57B), since two conformations were clear enough to be included into the structure (total 11 atoms). The relative occupancies of each pair of the alternate conformations were adjusted to make the B-values roughly

Table 3.1.2. Course of the refinement for reduced azurin

Cycle	R-factor	rms Δ_{dist} (Å)	Total atoms	Comments
1	0.250	0.019	1954	Protein atoms of oxidised azurin
10	0.198	0.019	1954	10 cycles
13	0.218	0.019	1924	3 cycles with copper ligands removed (except for C_βs).
32	0.188	0.018	1997	Copper ligands built in, restraints loosened then retightened. 1954 protein atoms, 43 water molecules
43	0.170	0.017	2073	Input 76 water molecules, restraints loosened and retightened.
47	0.169	0.017	2073	Changed X-ray weight to emphasise the higher resolution data (i.e. dependent on sin θ/λ), which improved R-factor by 0.034 for data at 2.1Å resolution.
57	0.168	0.017	2073	Loosened distance restraints to rmsΔ(dist)= 0.082Å, then retighted to rmsΔ(dist)= 0.017Å.
65	0.173	0.017	2073	Rebuilt copper site, protein side-chains and waters with B>50Å^2. Loosened and retightened restraints.
74	0.162	0.019	2173	Input 100 waters
77	0.157	0.017	2173	Changed to unit weights for X-ray data (Total 1954 protein atoms and 219 waters)
85	0.153	0.016	2182	Rebuilt side-chains, input 2 sulphate anions and 12 waters, removed 13 waters
91	0.177	0.021	2182	Introduced new X-ray data (1.9Å resolution).
103	0.183	0.017	2200	Rebuilt side-chains and waters, input 18 waters
118	0.174	0.021	2200	1954 protein atoms 236 waters 10 sulphate atoms Restraints on distances and planes loosened and retightened.
130	0.167	0.021	2265	Side-chains, waters and copper site rebuilt, input 65 waters (total 301). Changed X-ray weight to emphasise the higher resolution data (i.e. dependent on sin θ/λ), which improved the R-factor for the higher resolution data.
139	0.167	0.021	2228	Removed 37 waters. Afterwards, protein and water structure were checked against the oxidised structure.
142	0.167	0.021	2240	Input 11 atoms of disordered side-chains.
145	0.169	0.020	2240	Repositioned waters with short hydrogen bonding contacts.
148	0.166	0.021	2235	Rebuilt short van der Waals contacts involving carbon, 5 waters removed.
151	0.167	0.021	2236	DNA sequence changes Ser-42 to Val, only Val-42 refined.
157	0.168	0.021	2236	DNA sequence changes Asp-16 to Asn and Glu-57 to Gln, only Asn-16, Val-42, Gln-57 and sulphate refined. Final model : 1956 protein atoms 258 water molecules 2 sulphates as SO_4^{2-} 1 sulphate as S atom 11 atoms of disordered side-chains

equal.

Solvent molecules were located from difference Fourier maps, and included in the structure as water molecules if good contacts were made to the surrounding structure. At cycles 57, 85, 118, 130, 139 and 142 selected solvent molecules were checked (see section 2.3 for the criteria). This was done by omitting them from the structure and then calculating difference Fourier maps to see if the corresponding peaks reappeared. Finally towards the end of the refinement (cycle 139), the solvent structure was checked against the positions of the solvent molecules in oxidised azurin, but no extra solvent molecules were found in this way. At cycle 77, a large F_o-F_c peak was found in the crevice formed between Gly-76 and His-83 in each of the protein molecules. These peaks were assigned as sulphate anions because, 1) the measured distances from the centre of the peaks to the NH groups of Gly-76 and the imidazole ring of His-83 are too long (≈4Å) for the them to be water molecules, 2) the shape of each peak is tetrahedral, and it is possible to orient a sulphate anion so that the oxygen atoms make good hydrogen bonds to the protein, and 3) the protein was crystallized from a solution 70% saturated with $(NH_4)_2SO_4$. Sulphate anions are also present in the same region in oxidised azurin[31]. A large peak was also found on a two-fold crystallographic axis. This was also found in oxidised azurin[31], and has been tentatively assigned as a disordered sulphate because the distances it makes to its nearest neighbours, which are hydrogen bond donors, are ≈4Å.

No constraints were imposed on the copper...protein distances, so that the copper geometry could refine freely. The structure of the copper site was closely monitored thoughout the refinement, but it became apparent early on that any changes due to reduction were minimal. Initially, the structure was allowed to refine for 22 cycles without the copper and its ligands. The copper site was then built into the F_o-F_c density.

Accuracy of the structure

The accuracy of the atomic coordinates of the final model can be estimated from the discrepancies between the observed and calculated structure factors[232]. Figure 3.1.1 shows the plot of R-factor against resolution for the refined structure. Apart from the data at low resolution (10-5Å), where the disordered solvent is inadequately modelled, the analysis suggests that the maximum average error in atomic coordinates of the model is 0.20Å. Since the Luzzati analysis assumes that differences in the observed and calculated structure factors only arise from discrepancies in the model[233,234], a more realistic average error should be less than this, considering that much of the weak data has been included in the structure refinement. (Weak X-ray data contains a significant component of statistical error, and this will be reflected in the discrepancies between the observed and

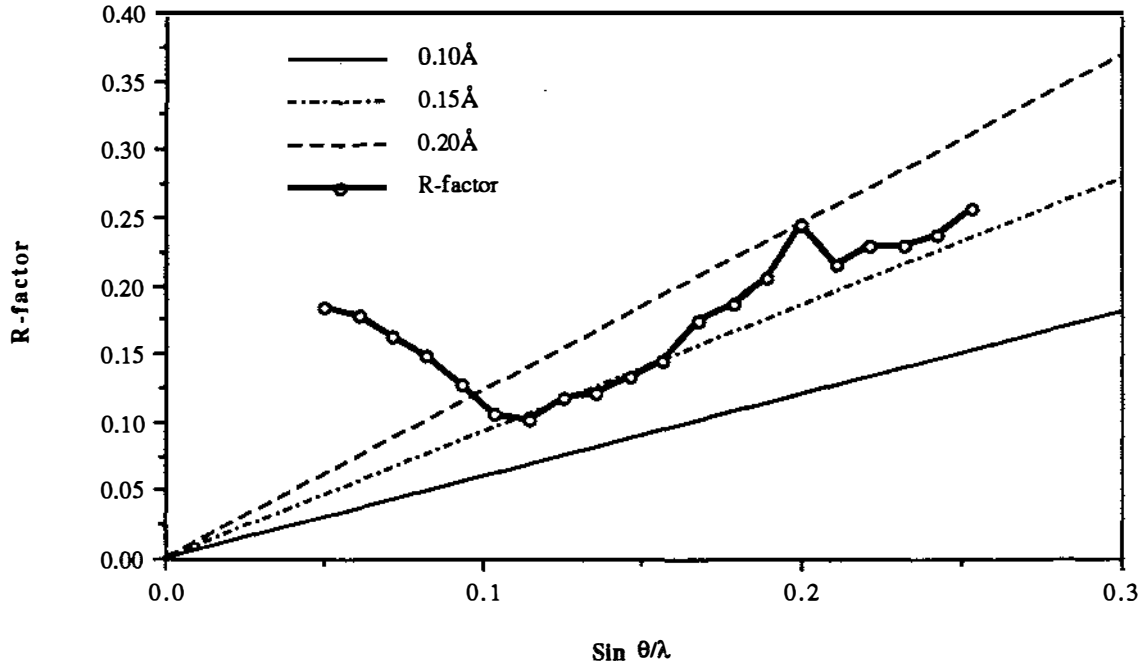

Figure 3.1.1. Luzzati plot of the refined structure of reduced azurin. Error lines are for non-centric data, and indicate a maximum error of 0.20Å.

calculated structure factors.)

An alternative indication of the accuracy of the reduced azurin structure can be obtained by the comparison of the two independent molecules in the asymmetric unit, and a complete analysis of this is presented in Section 3.3. A summary of these results is given here for the benefit of the comparison of the reduced and oxidised structures in Section 3.2. In general, the two reduced azurin molecules agree best for those parts of the structure which are well defined. Superposition of 95% of the main-chain atoms gives an r.m.s. deviation of 0.30Å in their positions. However, a breakdown of this shows that the main-chain atoms in the α-helix and β-strands agree within 0.25Å, while those main-chain atoms contained in the polypeptide loops show less agreement (0.3-0.6Å). Differences in side-chain atom positions are generally greater than those for main-chain atom positions. The smallest differences are seen for internal side-chain groups (≤0.3Å), while those on the surface of the protein differ in position by as much as 1-4Å. At the active site, a well defined part of the structure, the r.m.s. deviations in copper distances and angles are 0.06Å and 3.7°, respectively. The r.m.s. deviations of other structural parameters are 8.1° for main-chain torsion angles, 13.2° and 63.2° for internal and external side-chain torsion angles, and 0.20Å and 10.3° for hydrogen bond distances and

angles.

Restrained refinement of the Cu...S(Met) distance

EXAFS experiments have been done on *Ps. aeruginosa* azurin at the copper edge in both oxidised and reduced states[160,161]. The results give values for the metal-ligand distances of the primary coordination sphere around the copper site. For oxidised azurin, EXAFS measurements reveal the presence of a short copper to sulphur bond (2.10Å) and two coordinated nitrogens at normal distances (1.97Å), but no clear evidence for a second Cu...S interaction can be determined. Later experiments on the reduced form suggested a second Cu...S distance of 2.70Å[161]. If this result is correct, then the Cu...S(Met) distance changes from ≈3.1Å (from the crystallographic structure[31]) to ≈2.7Å upon reduction. Such a change could occur if the copper atom moves towards the methionine sulphur into a more tetrahedral geometry characteristic of Cu(I) coordination. The effect of pH was also investigated, and the results clearly show no significant dependance on pH of the bond lengths at the copper site[161].

During the course of the refinement, it became apparent that the results of the EXAFS experiments on reduced azurin did not agree totally with those from crystallography. The distances to the three main ligands of the copper site agree within experimental error, but the fourth distance, to S_γ 121, differs markedly from the crystallographic value (2.70Å versus 3.23Å), and the possibility of a fifth interaction, with the carbonyl oxygen of Gly-45, was not detected. To check the validity of the crystallographic distance and to ensure that the refinement was proceeding towards the correct structure, restrained refinement was carried out on a model on which the EXAFS distance of 2.7Å between the copper and the Met-121 sulphur was imposed. At two stages in the refinement (following cycles 118 and 151) the Cu...S(Met) distance was rebuilt, each time trying two different approaches.

Table 3.1.3 Comparison of crystal structure copper distances with those determined by EXAFS for reduced azurin. A hyphen "-" indicates no detected copper distance.

Copper ligand	Crystal structure distance (Å)	EXAFS distance (Å)	Difference (Å)
O 45	3.23	-	-
$N_{\delta 1}$ 46	2.13	1.89 / 2.04	0.24 / 0.09
S_γ 112	2.27	2.24	0.03
$N_{\delta 1}$ 117	2.05	1.89 / 2.04	0.16 / 0.01
S_δ 121	3.23	2.70	0.53

In the first method, the copper atom was moved 0.5Å directly towards the sulphur of Met-121. This rebuilt model was then refined with the Cu...S(Met) distance restrained at 2.70Å. Distances to other copper ligands were reasonable, and were allowed to refine freely. Two sets of PROLSQ refinement were completed; one with a moderate constraint (σ = 0.05Å) and another with a very tight constraint (σ = 0.01Å) on the Cu-S(Met-121) distance. When using moderate constraints on the Cu...S(Met-121) distance, six cycles of refinement saw the copper shift back to its original position and the Cu...S(Met-121) distance return to ≈3.2Å. Consequently, a tighter constraint was tried, and the experiment repeated. During this refinement, the target value for the Cu...S(Met) distance was periodically updated to the mean value for the two independent molecules. Refinement continued in this way until the model converged. During this procedure the copper atom shifted back to within 0.11Å of its original position in the first six cycles, but dragged the S_δ atom 0.31Å towards the original copper position to maintain the Cu...S(Met) distance (see Figure 3.1.2). After 35 further cycles, the methionine side-chain eventually returned to its original position and a Cu...S(Met) distance of 3.17Å. Results of this test are listed in Table 3.1.4 and illustrated schematically in Figure 3.1.2.

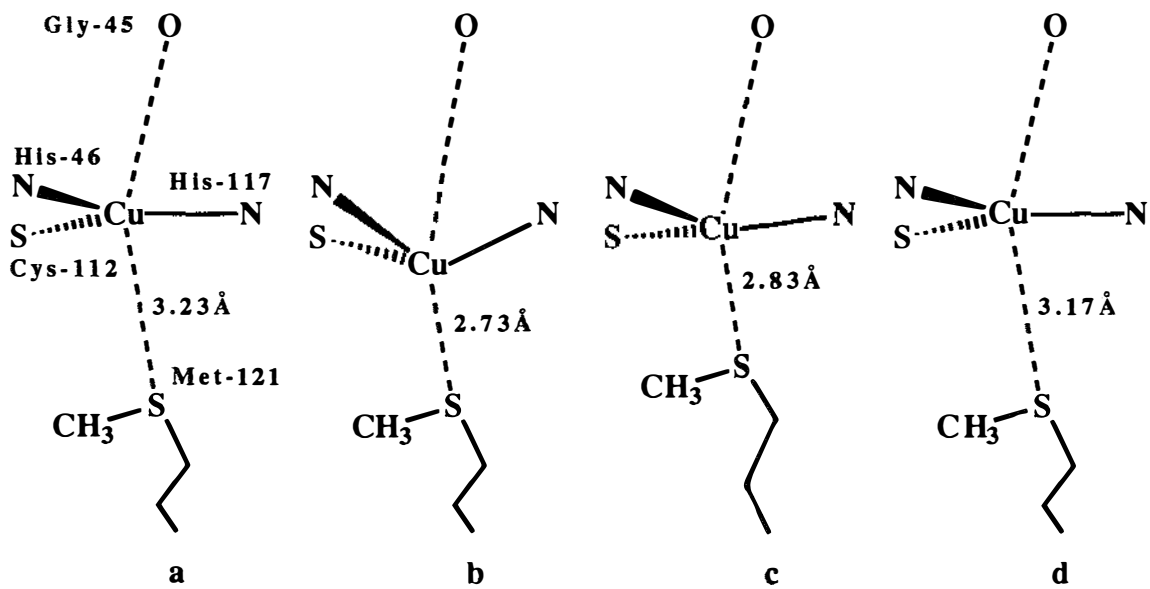

Figure 3.1.2. Schematic diagram of the test refinement of the Cu...S(Met) distance tightly restrained (σ = 0.01Å). In **a** the copper site is shown after unrestrained refinement of copper distances. In **b**, the copper is shifted 0.5Å towards S_δ 121. After six cycles of refinement, the copper returns to its normal position, but drags the sulphur closer to the copper postion (**c**). 41 cycles later, the Cu...S(Met) distance returns to its original value despite the tight restraint imposed.

The test refinement of the Cu...S(Met-121) distance was also repeated at the end of refinement, using FFT refinement procedures (HKPROLSQ). The results were essentially identical to those obtained at an earlier stage of refinement. Within 14 cycles of HKPROLSQ refinement, the copper returned close to its original position with a mean Cu...S(Met) distance of 3.15Å.

Table 3.1.4. Course of the test refinement on the tightly restrained Cu...Sδ 121 distance using PROLSQ (cycle 118) and HKPROLSQ (cycle 151). Values are the mean distances between the original position (Cu and Sδ 121) and those during refinement (Cu' and Sδ 121'), so that before cycle 1 <Cu'...Cu>=0.5Å and <Sδ 121'...Sδ 121>=0Å.

PROLSQ Cycle of refinement	<Sδ 121'...Sδ 121> (Å)	<Cu'...Cu> (Å)	<Cu'...Sδ 121'> (Å)	HKPROLSQ Cycle of refinement	<Cu'...Sδ 121'> (Å)
6	0.308	0.105	2.83	2	2.82
12	0.257	0.069	2.91	4	2.92
15	0.213	0.057	2.97	6	2.99
18	0.176	0.048	3.02	8	3.06
21	0.148	0.043	3.05	10	3.09
29	0.091	0.032	3.12	12	3.13
35	0.064	0.026	3.16	14	3.15
41	0.048	0.022	3.17		

In the second method the copper atom was left in place and the methionine side-chain was rebuilt so that its sulphur atom was moved to within ≈2.7Å of the copper. Upon rebuilding this side-chain, however, it became evident that the methionine side-chain could not extend far enough to reach the desired position by simply adjusting the side-chain torsion angles. Instead, rebuilding the side-chain required the "stretching out" of the side-chain bonds. To improve the geometry in the "stretched out" side-chain, the sulphur atom was fixed ≈2.7Å from the copper atom, and then the residue regularised so that better agreement with "ideal" geometry was obtained. The first six cycles of HKPROLSQ refinement were completed with the sulphur atoms of both Met-121 side-chains frozen in position approximately 2.7Å from the copper atoms. This allowed the rest of Met-121 and surrounding protein structure to accomodate to the rebuilt copper site, and to minimise any non-ideal geometry, without affecting the Cu...S(Met) distance. These six cycles were necessary to prevent the geometrical restraints on the side-chain from pulling the sulphur atom back to the original position. A significant improvement was seen in the geometry of the side-chain before the sulphur atom was released for refinement (see Figure 3.1.3).

The refinement was then continued with the Sδ 121 atoms released, and a very tight restraint (σ = 0.01Å) on the Cu...Sδ 121 distance. Over 15 cycles of HKPROLSQ refinement, the Cu...Sδ 121 distance gradually increased to ≈3.1Å, close to the original value of ≈3.2Å. Figure 3.1.4 plots the Cu...Sδ 121 distance with respect to the refinement cycle number. Also it was found that the B-value of Sδ 121 increased, until the Cu...Sδ 121 distance refined above 2.95Å (cycle 12) after which the B-value then gradually dropped over the remaining cycles.

These refinement tests clearly show that, despite tightly restraining the Cu...S(Met)

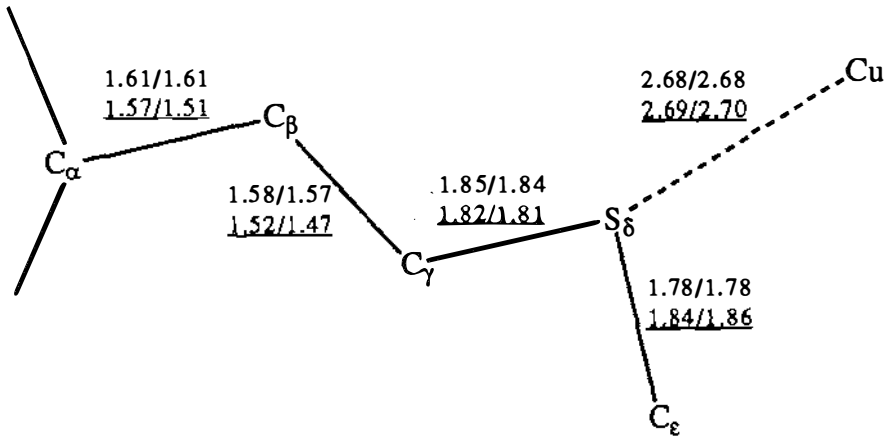

Figure 3.1.3. Geometry of the rebuilt Met-121 side-chain prior to refinement and after six cycles with the Sδ 121 atom positions frozen (underlined values). Ideal geometry values are C_α-C_β=1.522Å, C_β-C_γ=1.509Å, C_γ-S_δ=1.829Å and S_δ-C_ε=1.803Å.

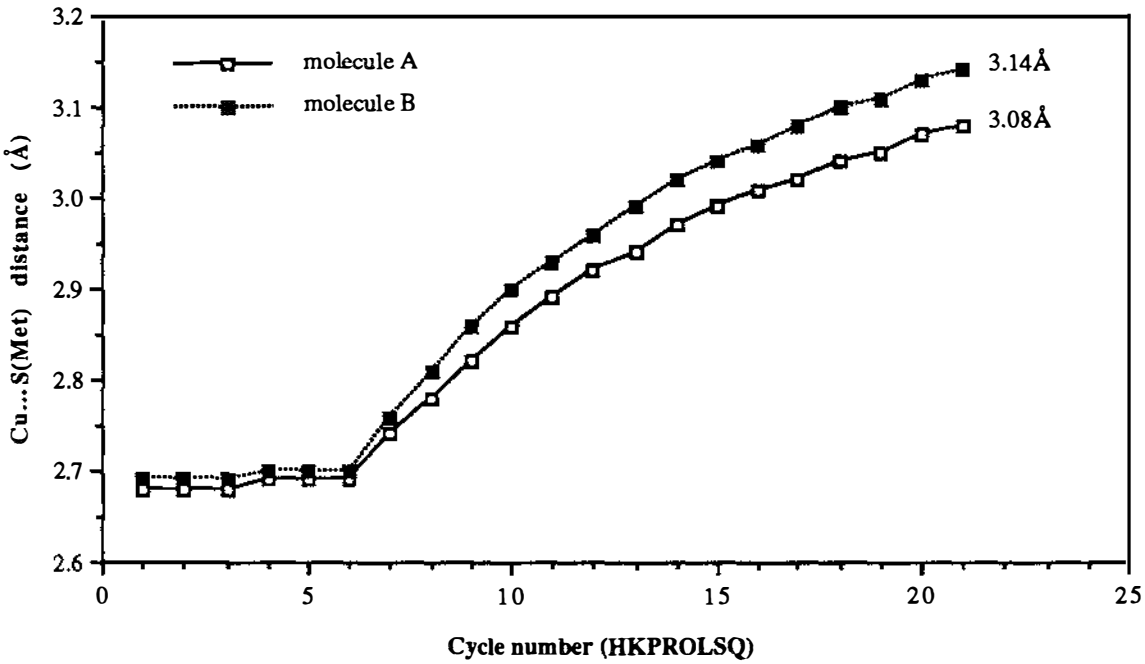

Figure 3.1.4. Change of Cu...Sδ 121 distance after rebuilding the side-chain of Met-121 towards the copper atom, and refining with this distance restrained at 2.7Å (σ = 0.01Å).

distance to 2.7Å (the result from the EXAFS studies), this distance reverted back to the crystallographic value of ≈3.2Å. Hence, it seems likely that the EXAFS value is incorrect.

EXAFS studies on other blue copper proteins have also revealed difficulties in accurately

determining the Cu...S(Met) distance[162,163]. The difficulty in determining this distance in plastocyanin was originally attributed to a very large thermal motion of the methionine sidechain[162], but even at cryogenic temperatures thermal motion could not be frozen out and the contact detected[162]. Eventually, polarised X-ray absorption spectra were taken on single crystals of plastocyanin in order to maximise the Cu-S(Met) contribution, yet still no definitive result regarding this distance to the methionine sulphur was found[163]. The absence of a clear Cu...S(Met) signal from EXAFS spectra may indicate that the methionine sulphur contributes only weakly to the ligand field of the copper, a conclusion supported by EPR spectra which show that the methionine sulphur has, at most, a small effect the ligand field of the copper[83].

3.2 The structure of reduced azurin and its comparison with oxidised azurin

The structure of reduced azurin is essentially the same as that of oxidised azurin[31]. The polypeptide chain folds into a single domain, with an eight stranded β-sandwich as the dominant secondary structural element. The remaining parts of the structure consist of loops and turns connecting the β-strands, and a three-turn α-helix in the "flap" region. The single copper atom is deeply buried in the "northern" end of the molecule in a cavity which is formed between the two sheets of the β-sandwich and several interconnecting loops. A general description of the oxidised structure was given in Chapter 1 to outline the main features of the protein. In this section a detailed discussion of the reduced azurin structure, including a comparison with the oxidised structure, will be given. Figure 3.2.1 is a schematic diagram of the overall structure of azurin, depicting the β-strands as arrows, the single α-helix as a coil, and showing the relative location of the copper binding site. A C_α plot showing the location of specific residues is given in Appendix C.2, together with the amino acid sequence of azurin.

Despite the overall similarities between the oxidised and reduced structures of azurin there are some differences. The problem, however, is that the largest differences are almost certainly not due to the process of reduction. These involve the side-chains on the surface of the molecule and some of the loops of the polypeptide chain, and simply reflect the the poor definition, or flexibility, of these regions. Any real structural changes due to reduction are at a much lower level, and the problem is then to identify them. For this, changes which are consistent between the two independent molecules of the asymmetric unit offer the best indication.

3.2.1 Crystal packing

The crystal packing of reduced azurin (*Alc. denitrificans*) is essentially identical to the crystal packing of oxidised azurin[31]. The space group is orthorhombic, $C222_1$, with 16 molecules in the unit cell (a=75.13Å, b=74.82Å and c=100.10Å). This gives two independent, but virtually identical protein molecules in the asymmetric unit. The two molecules are related to each other by a two-fold non-crystallographic axis which runs approximately parallel to the a-b diagonal in the x-y plane of the unit cell, and also passes through the interface between hydrophobic patches of the two molecules (see Figure 3.2.1.1). The crystal packing of the azurin molecules is shown in Figure 3.2.1.2. The transformation of best fit for superimposing molecule B (x_B,y_B,z_B) on to molecule A

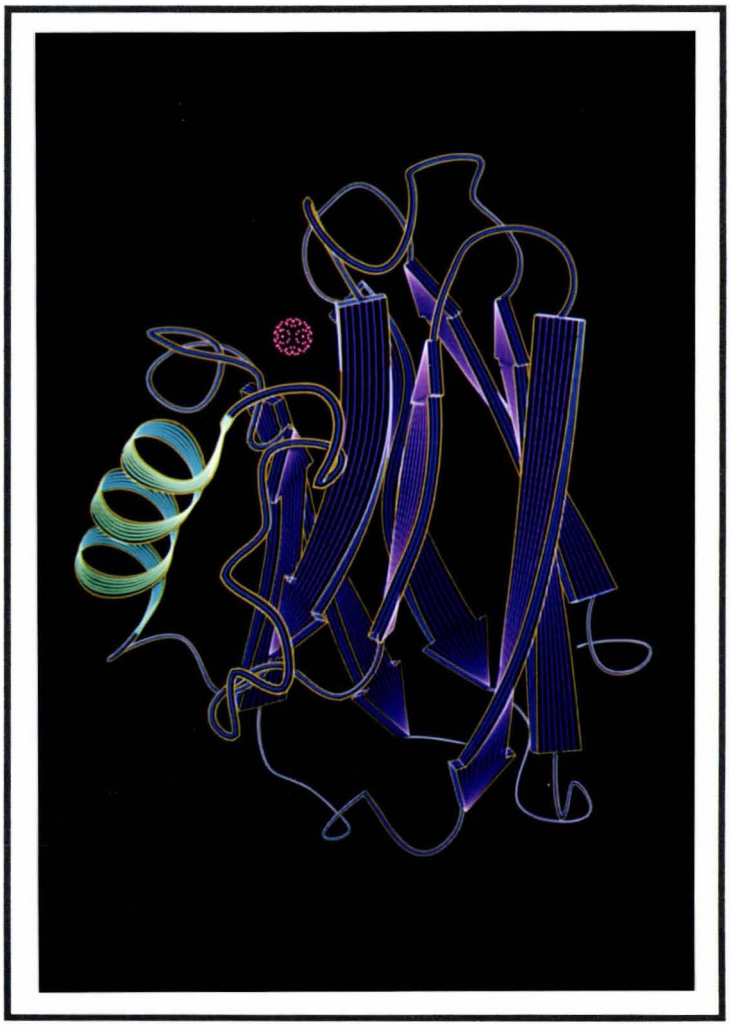

Figure 3.2.1. A schematic diagram of the structure of reduced azurin. β-sheets in purple, α-helix in green, and copper in pink.

(x_A,y_A,z_A) using all of the main-chain atoms except for the N- and C-termini (residues 1-2 and 128-129) is $X_A=R \cdot X_B+T$, or;

$$\begin{bmatrix} x_A \\ y_A \\ z_A \end{bmatrix} = \begin{bmatrix} -0.09673 & 0.99505 & 0.02277 \\ 0.99495 & 0.09605 & 0.02930 \\ 0.02697 & 0.02549 & -0.99931 \end{bmatrix} \times \begin{bmatrix} x_B \\ y_B \\ z_B \end{bmatrix} + \begin{bmatrix} 19.897 \\ -17.635 \\ -12.395 \end{bmatrix}$$

where R=rotation matrix and T=translation vector. The corresponding transformation for the oxidised structure is almost identical, the differences presumably due to the small changes in the unit cell parameters, i.e.;

$$\begin{bmatrix} x_A \\ y_A \\ z_A \end{bmatrix} = \begin{bmatrix} -0.10162 & 0.99460 & 0.02093 \\ 0.99438 & 0.10093 & 0.03184 \\ 0.02956 & 0.02404 & -0.99927 \end{bmatrix} \times \begin{bmatrix} x_B \\ y_B \\ z_B \end{bmatrix} + \begin{bmatrix} 19.839 \\ -17.375 \\ -12.540 \end{bmatrix}$$

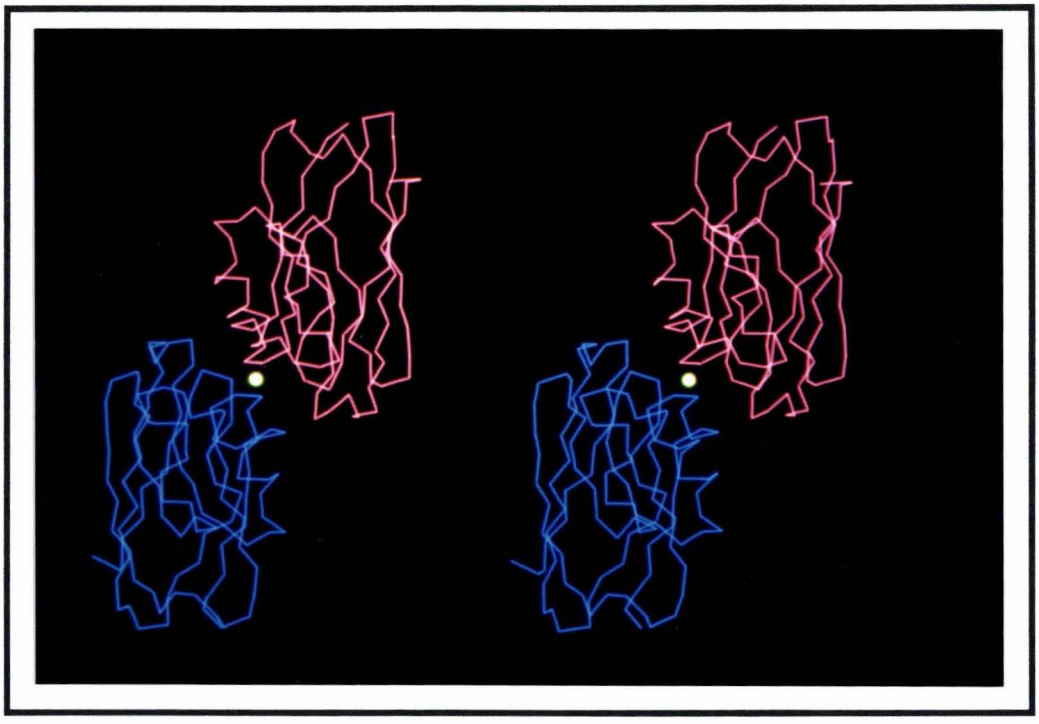

Figure 3.2.1.1. The packing of the two molecules of reduced azurin. The non-crystallographic 2-fold axis passes through the interface between the hydrophobic patches, and runs through the white sphere normal to the page.

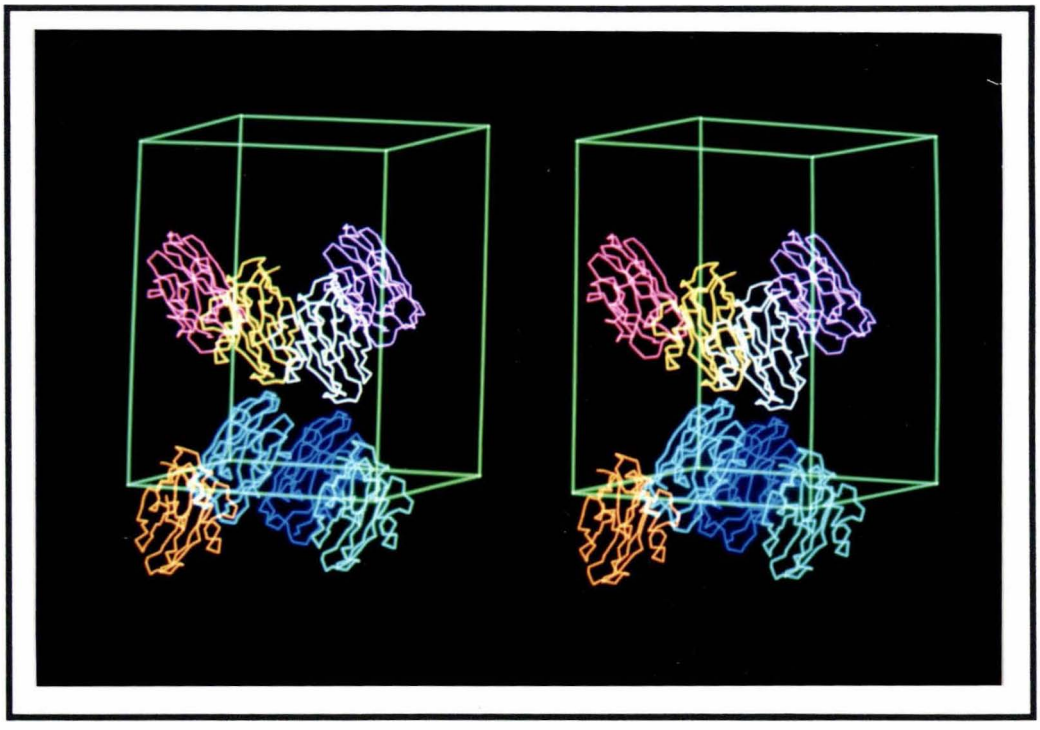

Figure 3.2.1.2 Crystal packing of reduced azurin from *Alc. denitrificans*. Only one protein molecule of the asymmetric unit is shown for clarity.

(Note that the transformation published for the oxidised structure[31] is different because of a different choice of the asymmetric unit.)

The non-crystallographic symmetry is noticeable in X-ray diffraction photographs as pseudo-tetragonal symmetry. The unit cell dimensions of the pseudosymmetric unit cell are a=b=53.12Å and c=100.10Å. It is interesting to note that crystals of azurin from *Ps. denitrificans* grow in the tetragonal space group $P4_122$ or $P4_322$ (a=b=52.3Å, c=99.3Å) with only one molecule per asymmetric unit[35]. The converse is also true; azurin from *Ps. aeruginosa* crystallizes in the space group $P2_12_12_1$ (a=58.9Å, b=79.0Å and c=108.5Å), with four molecules in the asymmetric unit, that are related by 222 symmetry[36].

3.2.2 Conformational angles

Main-chain torsion angles (ϕ,ψ)

The Ramachandran plots in Figure 3.2.2.1, which plot the torsion angles (ϕ,ψ) of the backbone of the polypeptide chain, shows the predominance of β-character in the structure of azurin through the concentration of values about (-120°, 135°). Another cluster around (-60°, -30°) represents residues of α-character i.e. some turns and the α-helix in the flap region. Residues Met-13, Asp-71 and Tyr-72 are the only non-glycine residues in the left-handed α region. Of these, residues 71-72 are part of a type III' turn, and the conformation of Met-13 may be a result of the intermolecular contacts made to its side-chain.

The main-chain conformational angles of reduced azurin closely resemble the angles of the oxidised structure. The overall difference between the redox forms gives a r.m.s. deviation in ϕ and ψ of 6.3° and 6.3°, respectively. These differences are smaller than the differences found in ϕ and ψ between the two molecules of the asymmetric unit of reduced azurin (rms $\Delta\phi$=8.5° and rms $\Delta\psi$=7.7°). The ϕ and ψ angles differ least for the residues which make up the β-strands (r.m.s. $\Delta\phi$=5.5° and r.m.s. $\Delta\psi$=5.6°) while those for the α-helix (r.m.s. $\Delta\phi$=6.3° and r.m.s. $\Delta\psi$=6.2°) are comparable with the overall values for the whole structure. The largest differences appear at residues 53-54, 74-76 and 105-106 which are surface residues with high thermal parameters in both the reduced and oxidised structures (see Table 3.2.2.1).

Very few of the changes in the main-chain torsion angles can be attributed to reduction. The only indication of a change in ϕ or ψ is in the stretch of residues between Met-44 and Asn-47. In this segment, six of eight ϕ,ψ angles change by 8-14° (see Table 3.2.2.2).

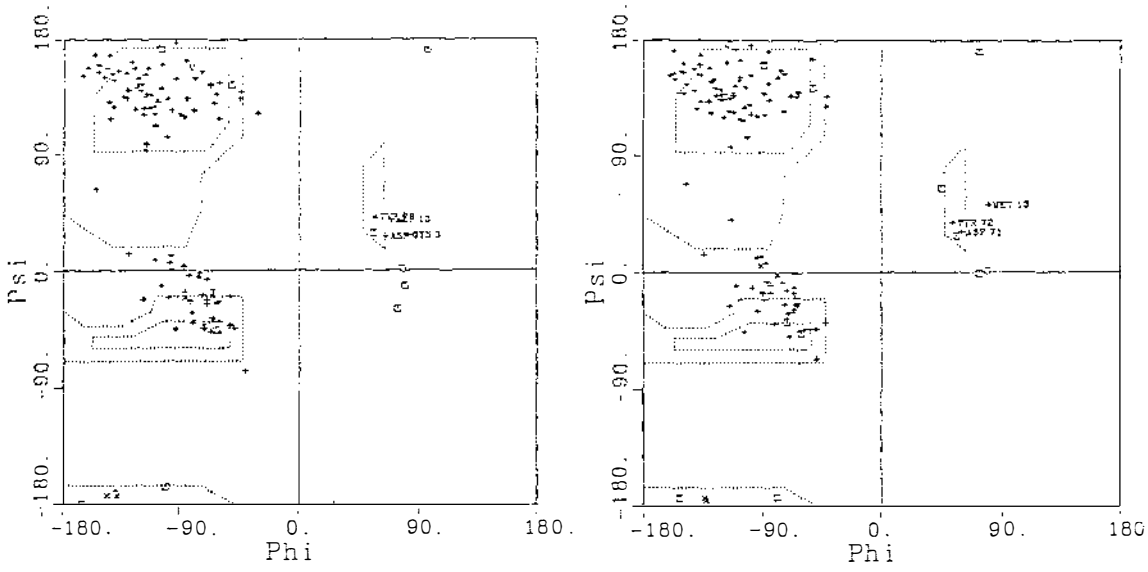

Figure 3.2.2.1 Ramachandran plot of the main-chain torsion angles (ϕ,ψ) for both molecules of reduced azurin (molecule A on the left and molecule B on the right).

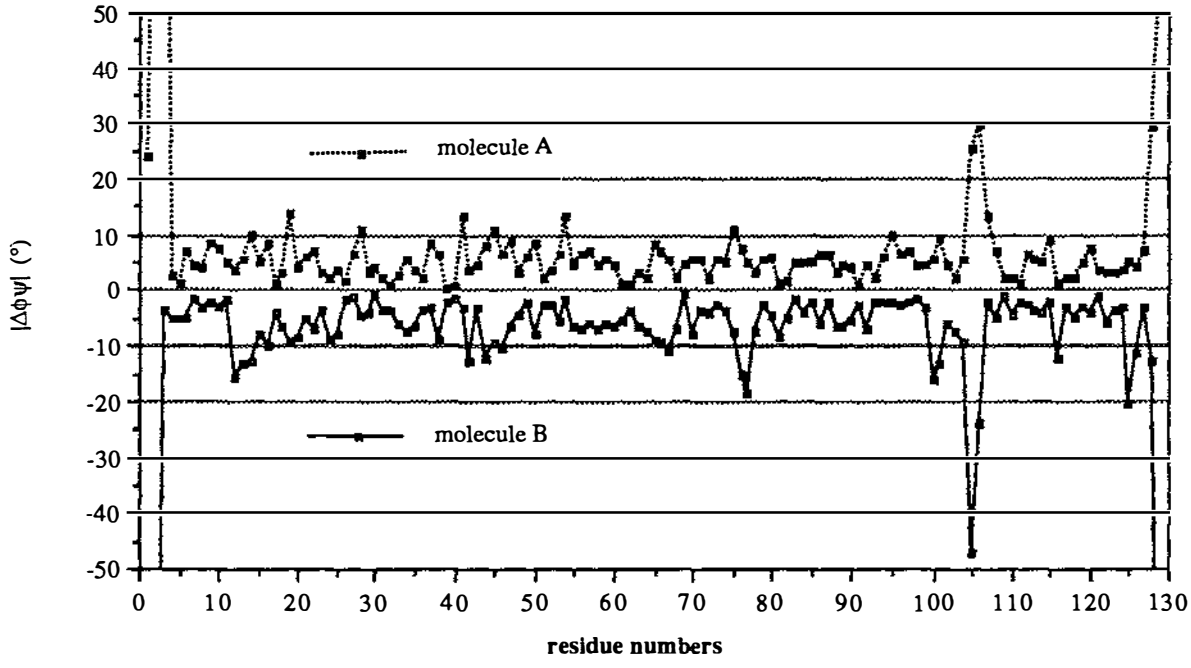

Figure 3.2.2.2. Change in the main-chain torsion angles, $|\Delta\phi\psi|$, between reduced and oxidised azurins, where $|\Delta\phi\psi|=\sqrt{((\Delta\phi^2+\Delta\psi^2)/2)}$. Values off the scale are at residues 1B (148°), 2A (122°), 2B (122°), 3A (151°), 129A (66°) and 129B (172°).

The changes are evident in both molecules of the asymmetric unit, and are above the error in ϕ, ψ for this stretch in the oxidised and reduced structures (r.m.s. $\Delta\phi\psi$ are 6.9° and 6.1° for oxidised and reduced azurins, respectively). Results from the consistent shift analysis (see below) also suggest changes in the main-chain atom positions for Gly-45 and His-46, and consequently these changes in the main-chain torsion angles may be real. The changes in the region Met-44 to Asn-47 are discussed further in Section 3.2.6, dealing with the copper site.

Table 3.2.2.1. The largest differences in the backbone conformational angles, except for those at the N and C-termini, between oxidised and reduced azurin. The differences are given in terms of r.m.s. deviations in $\Delta\phi\psi$ for each segment along with the average B-value of the main-chain atoms for each section.

residue segment	r.m.s. $\Delta\phi\psi$ (°)	<B> mainchain atom (Å^2)
53-54	10.7	39
74-78	11.7	40
105-106	25.1	56

Table 3.2.2.2. Shifts in the ϕ and ψ angles in the stretch of residues from Met-44 to Asn-47 between oxidised and reduced azurin (Oxidised - reduced).

	Molecule A		Molecule B		Average change	
	$\Delta\phi$	$\Delta\psi$	$\Delta\phi$	$\Delta\psi$	$\langle\Delta\phi\rangle$	$\langle\Delta\psi\rangle$
Met-44	0	-11	+7	-16	+4	-14
Gly-45	+6	-14	+11	-8	+9	-12
His-46	+3	-9	+5	-14	+4	-12
Asn-47	+9	-9	+6	-7	+8	-8

Side-chain torsion angles (χ_1-χ_5)

As was found for the main-chain torsion angles (ϕ,ψ), the torsion angles for the side-chain groups in azurin are also essentially unchanged after reduction to the Cu(I) form. As a general rule, the side-chain conformational torsion angles vary more than the main-chain torsion angles, and and the variation tends to increase for those torsion angles which are further away from the backbone of the polypeptide chain. This is presumably because there are fewer constraining forces acting on the side-chain atoms than the main-chain atoms, and any constraints on the side-chain atoms generally diminish further out from the backbone of the protein chain.

The r.m.s. deviations in the side-chain torsion angles between the oxidised and reduced forms of azurin are 16.1° for 92% of χ_1 angles, 22.7° for 89% of χ_2 angles, 46.6° for 78% of χ_3 angles and 48.6° for 79% of χ_4 angles. (Large differences were omitted from the calculation of the r.m.s. $\Delta\chi$, if $\Delta\chi_1 \geq 60°$, $\Delta\chi_2 \geq 60°$, $\Delta\chi_3 \geq 90°$ and $\Delta\chi_4 \geq 120°$.) For buried side-chains, defined as those residues which have a solvent accessibility less than 5Å^2 per atom[235], the conformational torsion angles are less variable, with r.m.s.

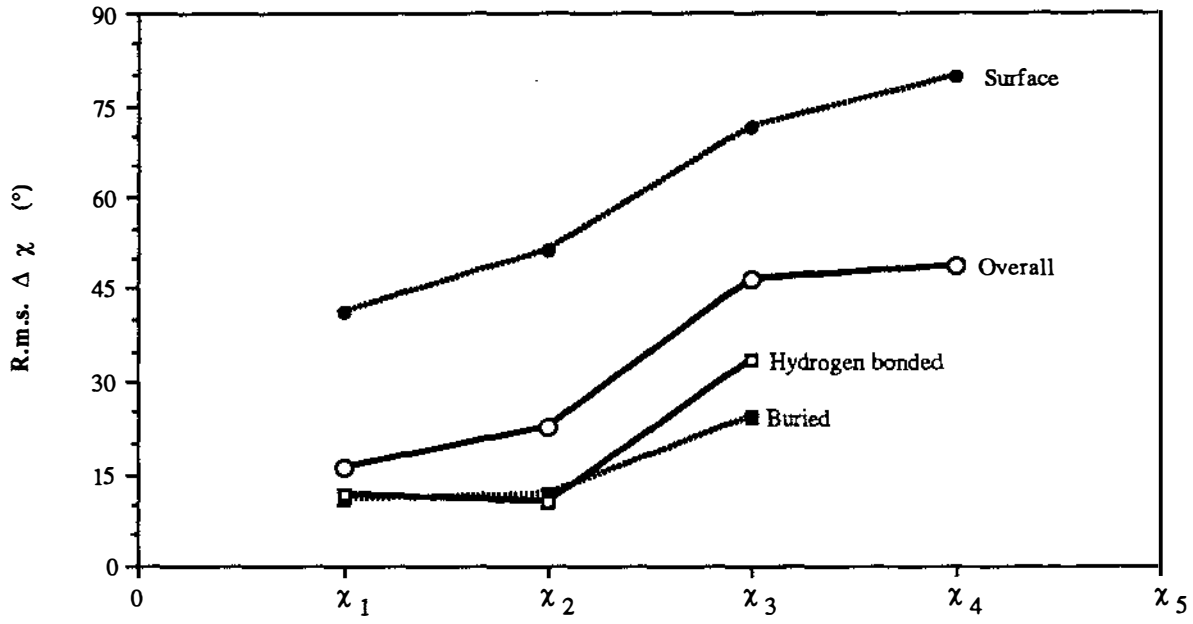

Figure 3.2.2.3. Plot of the r.m.s. deviations in χ angles between oxidised and reduced azurins.

deviations in $\Delta\chi_1$-$\Delta\chi_3$ of 10.9°, 22.6° and 24.4°, respectively. Similarly, those side-chains which make strong hydrogen bonds also have more rigid side-chain torsion angles. For χ_1-χ_3 of these side-chains, the r.m.s. deviation is 11.8°,10.5° and 33.6°, respectively. These side-chains are restricted by packing interactions and hydrogen bonds, and consequently their conformational angles show less difference between the two redox forms. At the other end of the spectrum, the largest changes in the side-chain conformational angles occur in the those located on the surface of the protein. These are almost certainly not associated with reduction. The r.m.s. deviations between the oxidised and reduced azurin structures, for angles of surface side-chains, are 41.4°, 51.5°, 71.1° and 79.4° for χ_1-χ_4 angles, respectively.

Changes which may be due to reduction are seen only in some of the side-chains near the copper site. These are at His-46 ($<\Delta\chi_1> = +9°$), Ser-113 ($<\Delta\chi_1> = +13°$), Phe-114 ($<\Delta\chi_1> = -10°$) and His-117 ($<\Delta\chi_2> = -6°$), see Table 3.2.2.1. The majority of these changes are lower than the r.m.s. deviation in torsion angles for buried side-chains, but what distinguishes them from those which occur in the more mobile parts of the structure is that these changes are located in the most well ordered part of the protein, and appear in both molecules of the asymmetric unit. More importantly though, many of the above changes in the side-chain torsion angles are associated with other changes observed in the

Table 3.2.2.1. Changes in side-chain torsion angles (oxidised-reduced) between oxidised and reduced azurin.

	Molecule A		Molecule B		Average $\Delta\chi$	
	$\Delta\chi_1$	$\Delta\chi_2$	$\Delta\chi_1$	$\Delta\chi_2$	$<\Delta\chi_1>$	$<\Delta\chi_2>$
His-46	**+8**	-3	**+9**	-9	**+9**	-6
Ser-113	**+15**	-	**+11**	-	**+13**	-
Phe-114	+2	**-10**	0	**-10**	+1	**-10**
His-117	+4	**-7**	+5	**-5**	+5	**-6**

structure, such as the hydrogen bond geometry. The effect of these changes with respect to the reduction of the copper atom will be discussed in Section 3.2.6.

3.2.3 Hydrogen bonds

Virtually all of the potential hydrogen bond donors and acceptors of reduced azurin form hydrogen bonds either with other parts of the protein or with the solvent. Only 12.5% of potential donors and acceptors are not involved in explicit hydrogen bonds. Most of these are polar groups on the surface of the molecule, and are in contact with the bulk solvent. All internal polar atoms are involved in hydrogen bonds except for three; the carbonyl oxygen of Gly-45, which is directed towards the copper atom, the side-chain imide group of Trp-48, which is surrounded by hydrophobic groups, and the carbonyl oxygen of Pro-115 which is effectively buried by crystal packing in the interface between the hydrophobic patches of the two protein molecules.

To analyze the hydrogen bonds, hydrogen atom positions were calculated and input into the coordinate set for all non-amino nitrogens using the programs DISTANG[236] and ORDER[237] (amino hydrogens are excluded because of the free rotation about the N-C bond). The criteria for the hydrogen bond geometry were taken from the review of Baker and Hubbard[238]. An acceptor-donor pair is considered a hydrogen bond if; 1) O...N, O...O and N...N distances, without a calculated hydrogen atom, are less than 3.5Å, or O...H and N...H distances, with a calculated hydrogen atom, are less than 2.5Å, and 2) if the hydrogen bond angle at both donor and acceptor atoms is greater than 90° (i.e. O(N)...H-N angle > 90° or O(N)...O(N)-C angle > 90°).

Main-chain...main-chain hydrogen bonds

β-sheets

Most of the hydrogen bonds found in azurin are main-chain...main-chain interactions.

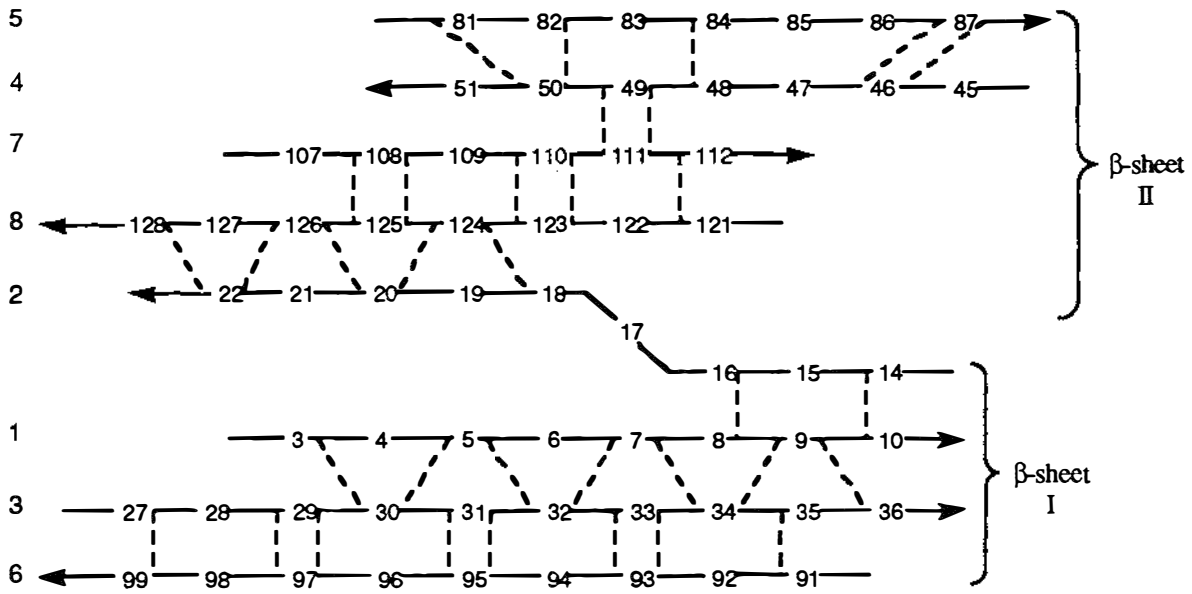

Figure 3.2.3.1. Schematic diagram of the main-chain...main-chain hydrogen bonds in the β-sheets of reduced azurin. β-strand numbers are given on the left, and β-sheet numbers are given on the right.

The hydrogen bonds are made between the β-strands, linking these strands together to form two β-sheets. The β-sandwich is then created by bringing together the hydrophobic faces of the two β-sheets. Sheet I comprises four strands, 1, 3, 6, and the first half of strand 2, while Sheet II is made up of five strands 4, 5, 7, 8, and the second half of strand 2. Both β-sheets contain parallel and anti-parallel β-strands. Connections between the sheets, apart from the hydrophobic interactions in the interior of the protein, are limited to a "kink" in strand 2 (residues 16-18) which joins the two halves of that strand, and two main-chain...side-chain hydrogen bonds between strands 5 and 6 (N 85...$O_{\delta 2}$ 93 and N 88...$O_{\varepsilon 1}$ 91). Figure 3.2.3.1 portrays the main-chain...main-chain hydrogen bonding structure in the β-sandwich.

Helices

The structure of azurin contains only one significant length of helix and a few loops which can be classed as single helical turns. The principal helix is found in the "flap" region and has three turns between residues 55-67. The hydrogen bonds made within the α-helix are classical 1-5 hydrogen bonds between the main-chain atoms, which then tighten at the final turn into a 3_{10}-helix. Figure 3.2.3.2 shows the hydrogen bonds of this helix schematically. Two loops, residues 40-44 and 117-121, contain a single 1-5 hydrogen bond, and can be regarded as single α-helical turns (α-turns). A double turn, which contains two consecutive 1-4 hydrogen bonds, is found at residues 98-102, and can also be classed as a single turn of a 3_{10}-helix[239].

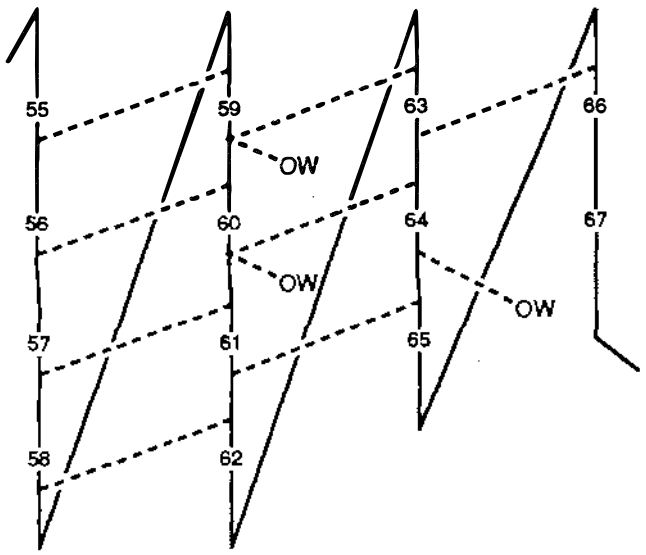

Figure 3.2.3.2. Schematic diagram of the main-chain...main-chain hydrogen bonds in the α-helix of the "flap" region of reduced azurin.

Loops and turns

The remaining structure of reduced azurin consists of loops and turns which are found between the individual β-strands and in the non-helical sections of the flap region. The majority of the loops are 3_{10}-bends (β-turns), which contain a single 1-4 main-chain...main-chain hydrogen bond. This is by far the most common type of turn in globular proteins[238]. Only two loops (40-44 and 117-121) have 1-5 main-chain...main-chain hydrogen bonds, and as was mentioned above can be considered as single turns of α-helix. In fact, the main-chain...main-chain hydrogen bonds of these loops are bifurcated and show both 1-4 and 1-5 type interactions, which are somewhat more frequent in loops than a single 1-5 type hydrogen bond[238]. There is only one example of a π-turn in azurin, a 1-6 type hydrogen bond followed by a 2-5 hydrogen bond, which occurs after the α-helix of the "flap" region. Consecutive turns appear in two parts of the protein structure; in the "flap" region where a type II (residues 74-77) and then a type III (residues 77-80) turn follow the π-turn (residues 67-72), and near the copper site (residues 114-121) where a type-II turn (residues 114-117) is followed by an α-turn (residues 117-121). The only part of the structure which can not be classified as either turn, helix or β-structure is the short segment of residues 37-39. Here, the only main-chain...main-chain hydrogen bond formed is between the carbonyl oxygen of Met-39 and the amide group of Gly-89. Presumably, these interactions in the loops of the polypeptide chain help to stabilise the conformation of the backbone, allowing it to fold back upon itself. Table 3.2.3.1 lists types of secondary structural elements along with their corresponding residues.

Table 3.2.3.1. The secondary structure elements of reduced azurin.

β-strands	Strand no.	Helices	type	Turns	type
3-10	1	55-67	α	10-13	type-I
14-22	2	98-102	3_{10}	23-26	type-I
27-36	3			40-44	α-turn
45-51	4			52-55	type-III
81-87	5			67-72	π-turn
91-99	6			68-71	type-I
107-112	7			70-73	type-III'
121-128	8			74-77	type-II
				77-80	type-III
				88-91	type-II
				103-106	type-II
				114-117	type-II
				117-121	α-turn

Main-chain...side-chain hydrogen bonds

Thirty-one main-chain...side-chain hydrogen bonds exist in the structure of reduced azurin.These interactions may be divided into two groups; "local" hydrogen bonds between groups within four residues of each other, and long range or "crosslinking" hydrogen bonds between residues that are sequentially far apart. Table 3.2.3.2 gives the main-chain...side-chain hydrogen bonds of reduced azurin.

Nearly half (14) of the main-chain...side-chain hydrogen bonds are local; most of these (10) occur in reverse turns of the structure, and probably help to direct and stabilise the conformation of the main-chain. Six main-chain...side-chain hydrogen bonds (Asn-10, Asp-23, His-35, Asp-77, Asp-98 and Cys-112) may be classified as Asx turns, where the side-chain of residue *n* makes a hydrogen bond with the main-chain NH of residue *n*+2 [238,240,241]. Four of these Asx turns are associated with β-turns (Asn-10, Asp-23, Asp-77 and Asp-98), and similar turns involving cysteines have been noted previously in the iron-sulphur proteins[242,243].

The next most common feature are four *n*...O*n+1* interactions, which appear at Thr-51, His-83, Thr-84 and Ser-128. His-83 and Thr-84 are located in the middle β-strand, and their interactions may help to orient the side-chain. In particular, the hydrogen bond for His-83 is probably important for forming part of the sulphate binding site. There is only one main-chain...side-chain hydrogen bond in the α-helix of azurin ($O_{\gamma 1}$ 61...O 57), and it is typical of a *n...(n-4)* hydrogen bond to the main-chain carbonyl.

Crosslinking hydrogen bonds, formed between residues that are sequentially distant, play an important role in drawing together different parts of the structure and stabilising the

Table 3.2.3.2. Main-chain...side-chain hydrogen bonds in reduced azurin, divided into "local" and "crosslinking" interactions. Side-chains invariant in other azurins are double underlined, while those replaced by similar hydrogen bonding groups are singly underlined. The terminology for the location of crosslinking interactions is "North", referring to the copper site end of the protein molecule, and "South" referring to the opposite end.

Local	Type	Cross-linking	Location
Asn-10 $O_{\delta1}$...HN 12	n...HN(n+2)	Ser-9 O_{γ}...O 34	North
Asn-10 $O_{\delta1}$...HN 14	n...HN(n+4)	Asp-11 $O_{\delta1}$...HN 39	North
Asp-16 $O_{\delta2}$...HN 16	n...HN(n)	Asp-11 $O_{\delta2}$...HN 38	North
Asp-23 $O_{\delta1}$...HN 25	n...HN(n+2)	Tyr-15 O_{η}...O 47	North
His-35 $N_{\delta1}$...HN 37	n...HN(n+2)	Asn-16 $O_{\delta1}$...HN 8	Middle
Thr-51 $O_{\gamma1}$...HN 52	n...O(n+1)	His-35 $N_{\varepsilon2}$...O 44	North
Thr-61 $O_{\gamma1}$...HN 57	n...O(n-4)	His-46 $N_{\varepsilon2}$...O 10	North
Asp-77 $O_{\delta1}$...HN 79	n...HN(n+2)	Asn-47 $O_{\delta1}$...HN 113	North
His-83 $N_{\delta1}$...O 84	n...O(n+1)	Asn-47 $N_{\delta2}$...O 71	North
Thr-84 $O_{\gamma1}$...O 85	n...O(n+1)	Asp-71 $O_{\delta1}$...HN 86	North
Glu-91 $O_{\varepsilon1}$...HN 88	n...HN(n-3)	Thr-84 $O_{\gamma1}$...N 48	Middle
Asp-98 $O_{\delta2}$...HN 100	n...HN(n+2)	Asp-93 $O_{\delta2}$...HN 85	Middle
Cys-112 S_{γ}...HN 114	n...HN(n+2)	Tyr-108 O_{η}...NH 103	South
Ser-128 O_{γ}...O 129	n...O(n+1)	Tyr-110 O_{η}...O 17	Middle
		Cys-112 S_{γ}...HN 47	North
		Ser-113 O_{γ}...O 72	North

final folding pattern of the protein[244]. Sixteen crosslinking hydrogen bonds appear in the structure of azurin. The hydrogen bonds made to the side-chain of Asn-47 are good examples of this, joining together the two loops containing the copper ligands and the "flap" region to the bulk of the β-sandwich. Many of the side-chains involved in crosslinking hydrogen bonds are internal, with the exception of the Asp side-chains, which are on the surface of the molecule, presumably because of their negative charge. Asp and Tyr are the most common side-chains in crosslinking interactions in azurin.The Tyr OH binds to carbonyl oxygens and the Asp carboxylate oxygens bind to the peptide NH groups of the main-chain.

Four crosslinking hydrogen bonds join adjacent β-strands. The hydrogen bond O_{γ} 9...O 34 bridges strands 1 and 3, and $O_{\gamma1}$ 84...N 48 links strands 4 and 5. There is also a link from the end of the strand 7 to strand 4 (S_{γ} 112...N 47) and another just prior to the "kink" in strand 2 to strand 1 (N 8...$O_{\delta1}$ 16). No crosslinking hydrogen bonds are made to the α-helix in the "flap" region.

The majority (11) of the crosslinking hydrogen bonds are found in the "northern" end of the molecule in the vicinity of the copper site, providing for the extra stability and rigidity of this region of the structure[31]. At the "southern" end of the molecule, only one cross-

linking hydrogen bond (Tyr-108 O_{η}...HN 103) is found, linking residues that belong to the same extended loop. Consequently, the "southern" region of the molecule exhibits higher mobility and poorer agreement between the two independent molecules.

Conservation of the main-chain...side-chain hydrogen bonds in azurins

The importance of main-chain...side-chain hydrogen bonds is apparent when the sequences of different azurins are compared. Of the 31 hydrogen bonds, 17 involve side-chains which are invariant in all azurin sequences. A further eight side-chains are conservatively changed with the residues replaced by similarly hydrogen bonding groups. The conservation also extends to other blue copper proteins. For instance the neighbouring residues of Cys-112, Asn-47 and Ser(Thr)-113, are conserved in all azurins, and their corresponding residues in plastocyanin, Asn-38 and Ser-85, are also invariant[10]. The cross-linking hydrogen bond of Tyr-15, which is near the copper ligand, Met-121, does not appear in most azurins, however, as this residue is usually Phe[31].

Side-chain...side-chain hydrogen bonds

A total of eleven side-chain...side-chain hydrogen bonds appear in the structure of azurin. These are listed in Table 3.2.3.3. This number is very low considering the number of polar residues in the sequence. Some of the side-chains involved in such hydrogen bonds have high thermal parameters (e.g. Glu-4, Asp-98 and Glu-106), and their interactions may not be important, but a few interactions, for instance $N_{\delta 2}$ 47...O_{γ} 113, probably do help to stabilise the surrounding structure. Three side-chain...side-chain hydrogen bonds appear in the β-structure. These are concentrated in one region of β-sheet I; one interaction joins strands 1 and 3 ($O_{\varepsilon 1}$ 4...$N_{\varepsilon 2}$ 32), while the other two join strands 3 and 6 ($O_{\gamma 1}$ 30...$O_{\gamma 1}$ 96 and $N_{\delta 1}$ 32...$O_{\gamma 1}$ 94). These hydrogen bonds may help stabilise the β-structure, since Thr-30, Ser-94 and Thr-96 are invariant in other azurins. The remaining interactions of this type are associated with the loops and turns of the polypeptide chain. One salt bridge is found, a set of three hydrogen bonds from Asp-62 and Asp-77 to Arg-79. These three residues, Asp-62, Asp-77 and Arg-79, are invariant in azurins, and may help to stabilise this part of the flap region.

Hydrogen bonds involving sulphur

The structure of azurin contains two hydrogen bonds which involve a sulphur atom as an acceptor. Both of these hydrogen bonds are made to the thiolate sulphur of Cys-112, which is strongly bound to the copper, and their implications will be discussed in section

3.2.7. Here, a description of the general nature of sulphur hydrogen bonds will be given, since these hydrogen bonds are affected by the reduction of azurin.

Table 3.2.3.3. Side-chain...side-chain hydrogen bonds in reduced azurin. Invariant side-chains are double underlined, while those replaced by similar hydrogen bonding groups in other azurins are singly underlined.

Side-chain...side-chain hydrogen bonds	
$O_{\varepsilon 1}$ 4...$N_{\varepsilon 2}$ 32	$O_{\delta 1}$ 62...$N_{\eta 2}$ 79
$N_{\delta 2}$ 10...$O_{\varepsilon 2}$ 14	$O_{\delta 1}$ 77...N_{ε} 79
$O_{\delta 1}$ 23...O_{γ} 25	$O_{\delta 2}$ 77...$N_{\eta 2}$ 79
$O_{\gamma 1}$ 30...$O_{\gamma 1}$ 96	$O_{\delta 2}$ 98...O_{γ} 100
$N_{\delta 1}$ 32...O_{γ} 94	$O_{\varepsilon 1}$ 106...O_{η} 108
$N_{\delta 2}$ 47...O_{γ} 113	

Hydrogen bonds involving sulphur atoms are longer than those involving nitrogen or oxygen, because of the greater radius of the sulphur atom (van der Waals radius of 1.80Å compared to 1.55Å and 1.50Å, respectively[256]). They are also weaker because of the lower electronegativity of sulphur[245-250]. In proteins, sulphur containing side-chains are not usually hydrogen bonded, except for some cysteines. The average cysteine sulphur hydrogen bond length is 3.5(±0.1)Å for 54 possible interactions found in the Protein Data Bank by Ippolito *et al.*[245] (S...D or S...A, where A=acceptor and D=donor). The average C-S...D/A angle is 104±27°, and the C-C-S...D/A torsion angle shows a slight preference for donors/acceptors in the gauche orientation. The average hydrogen bond length is long when compared to S...HN interactions in crystal structures of sulphur-containing organic compounds examined by Donohue[247] where the S...HN hydrogen bonds have S...N distances in the range 3.25-3.55Å.

Several S...HN hydrogen bonds have been found in the metal sites of the FeS proteins ferredoxin[242,243,251], rubredoxin[252] and high potential iron protein (HiPIP)[243]. Adman *et al.* calculate an average distance of 3.6Å for these interactions, which range from 3.1Å to 4.0Å. These include some long interactions where the amide hydrogen points directly at the sulphur and are considered "incipient" hydrogen bonds[242]. Five types of S...HN hydrogen bonds have been identified. In two types, the cysteinyl sulphur atom binds to the amide hydrogen two residues along the sequence, i.e. *n...n+2*. These two types are geometrically similar to NH...O hydrogen bonds in type I and type II (3_{10}) turns[253]. The third type of hydrogen bond involves sequentially distant parts of the protein, as in crosslinking hydrogen bonds, and this often completes a nearly tetrahedral arrangement about the cysteinyl sulphur. In the fourth type of S...HN hydrogen bond, the amide hydrogen is directed towards an inorganic sulphur atom (S^{2-}), while the fifth type is a *n...n+3* interaction, which is found in the copper site of pseudoazurin[34].

In azurin, the two S...HN hydrogen bonds belong to the type I, $n...n+2$, category (S_γ 112...HN 114), and the crosslinking category (S_γ 112...HN 47). The amide hydrogens are directed towards the sulphur atom in such a way as to complete a tetrahedral arrangement about the sulphur with the copper and C_β atoms (see Figure 3.2.3.3). No hydrogen bonds involving methionine sulphur as a hydrogen bond acceptor are found in the strucure of azurin. Methionine as a hydrophobic residue, however, has been found to prefer dipole-quadrupole interactions with aromatic side-chains[254]. This type of interaction occurs between Met-121 and Tyr-15 in azurin.

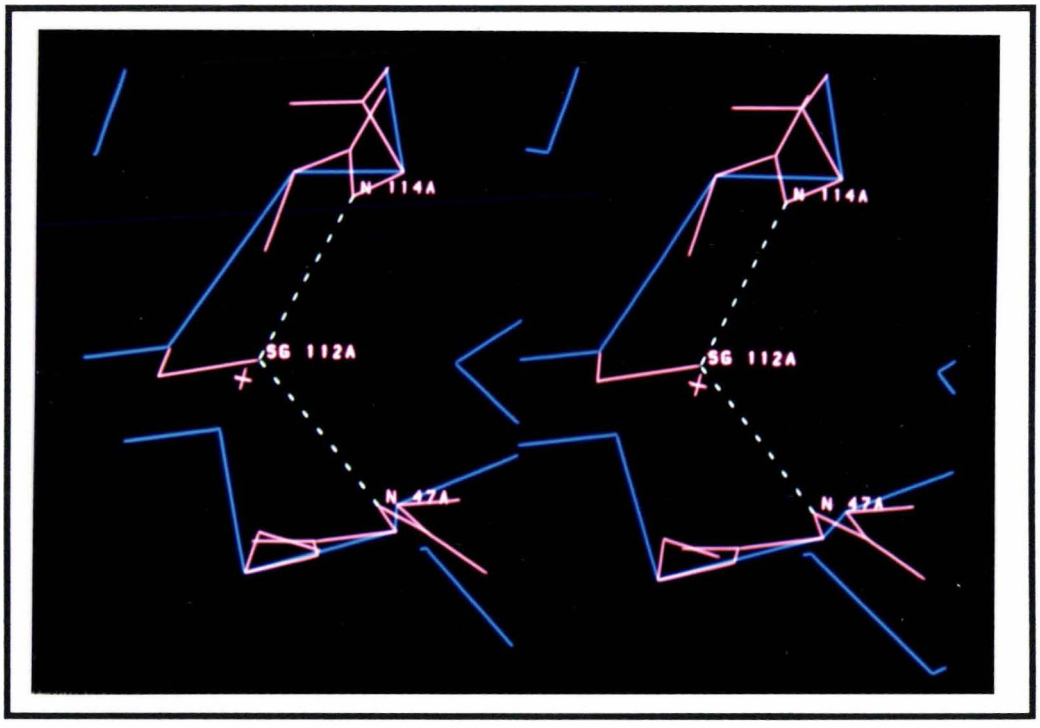

Figure 3.2.3.3. S...HN hydrogen bonds of the copper site viewed down the Cu-S(Cys) bond. C_α trace in blue, and selected atoms in pink (copper as a pink cross).

Changes in the hydrogen bonds upon reduction

The only hydrogen bonds which undergo reduction dependent changes are the two S...HN interactions between the side-chain of Cys-112 and two peptide NH groups. Since Cys-112 is part of the copper site, these changes will be discussed in section 3.2.7. Changes in the rest of the hydrogen bonds of azurin upon reduction are small, and probably not significant.

There are only a few hydrogen bonds which do not appear in both redox forms of azurin, and these are restricted to regions of the molecule which have higher flexibility (as judged

Table 3.2.3.4. Differences in hydrogen bonding between oxidised and reduced forms of azurin. A "✓" indicates the presence of a hydrogen bond. Those in parentheses are "marginal" hydrogen bonds.

Hydrogen bond	Oxidised azurin		Reduced azurin	
	A	B	A	B
main-chain...main-chain				
O 10...N 13		✓	(✓)	
O 41...N 45			(✓)	
O 53...N 56		(✓)		(✓)
O 61...N 65	(✓)	(✓)		
O 64...N 67	(✓)			
O 67...N 70	(✓)		(✓)	(✓)
O 70...N 73		(✓)	(✓)	(✓)
O 74...N 77	✓		✓	
O 77...N 80		✓		(✓)
O 128...N 24			✓	
main-chain...side-chain				
2 $O_{\varepsilon 1}$...3 N		✓		
10 $O_{\delta 1}$...10 N	(✓)			
23 $O_{\delta 1}$...25 N	✓		✓	✓
47 $O_{\delta 1}$...47 N				(✓)
86 O...41 N_{ζ}			✓	
93 $O_{\delta 1}$...94 N		(✓)		(✓)
98 $O_{\delta 2}$...100 N	✓		✓	
123 O...122 N_{ζ}	✓	(✓)		
128 O...24 N_{ζ}				(✓)
128 O_{γ}...129 N			(✓)	
129 O_{ε}...24 N_{ζ}		✓		
side-chain...side-chain				
$O_{\varepsilon 1}$ 4...$N_{\varepsilon 2}$ 32	✓		✓	✓
$O_{\varepsilon 1}$ 8...N_{ζ} 34	✓			
$O_{\delta 1}$ 23...O_{γ} 25	✓	(✓)	✓	
$O_{\delta 2}$ 23...O_{γ} 128		(✓)		(✓)
$O_{\varepsilon 1}$ 53...N_{ζ} 56				(✓)
$O_{\varepsilon 1}$ 53...N_{ζ} 122	✓	(✓)		
$O_{\delta 1}$ 62...N_{ζ} 74	✓		✓	
$O_{\delta 1}$ 77...N_{ε} 79	✓	✓		✓
$O_{\varepsilon 1}$ 91...N_{ζ} 41	✓			
$O_{\delta 1}$ 93...N_{ζ} 85		(✓)		✓
$O_{\delta 2}$ 98...N_{ζ} 27			✓	
$O_{\delta 1}$ 98...O_{γ} 100		✓		✓
$O_{\gamma 1}$ 124...N_{ζ} 122		(✓)		

by B-values) than the rest of the structure. Hydrogen bonds which do not appear in both molecules of the oxidised and reduced structures are listed in Table 3.2.3.4. Ten of these are main-chain...main-chain interactions, 13 are main-chain...side-chain interactions and 14 are side-chain...side-chain interactions. Many of these show poor agreement between the two reduced azurin molecules, and have "marginal" geometry; where either 1) O...N

or O...H distances are greater than 3.3Å or 2.3Å, respectively, or 2) an angle is less than 100°. In contrast, those hydrogen bonds which are common to both redox states exhibit only minor differences in hydrogen bond geometry.

Most of the non-conserved main-chain...main-chain hydrogen bonds appear in the more poorly defined, flexible parts of the polypeptide chain. One is at the C-terminus, where there is a conformational variation from crystal packing effects, while another two are located at the "southern" end of the molecule, where B-values are high. Most (14 out of 19) are interactions which have "marginal" hydrogen bond geometry.

Non-conserved hydrogen bonds involving side-chain atoms are all on the surface of the molecule; many (19) involve side-chains of residues in loops and a few (5) are associated with the termini of the polypeptide chain. In particular, 22 out of 24 of these interactions involve the side-chains of lysines, glutamic acids and aspartic acids. These charged groups are exposed to the solvent, and generally have high thermal parameters ($<B>\approx 50Å^2$). Surprisingly, many of these hydrogen bonds (11) involve sequentially distant regions of the protein; three are main-chain...side-chain interactions (all involving lysine side-chains), and nine are side-chain...side-chain interactions (six of which involve lysine side-chains). All but two of the 11 crosslinking variety are between loops that are spatially adjacent in the structure. As for the main-chain...main-chain hydrogen bonding, many of the differences in the side-chain hydrogen bonding are hydrogen bonds with "marginal" geometry.

For the main-chain...main-chain interactions common to all molecules of both redox forms, the hydrogen bond distances (O...H) and angles (O...H-N) have r.m.s. deviations of 0.13Å and 6.4°, respectively, for 110 pairs. Those main-chain...main-chain hydrogen bonds that make up the β-sheets and α-helix show comparable differences (r.m.s. deviations for distances and angles are 0.12Å and 6.1° for β-sheets, and 0.14Å and 6.3° for the α-helix, respectively), whereas those hydrogen bonds involved in loops and turns show larger differences; r.m.s. deviations of 0.19Å and 8.7° for distances and angles, respectively.

Overall, main-chain...side-chain hydrogen bonds have r.m.s deviations of 0.18Å for distances and 6.1° for angles. When these are separated into local (within four residues) and crosslinking interactions, the local interactions are more varied with r.m.s. deviations of 0.21Å and 6.5° for distance and angles, respectively; while those for crosslinking are much less varied, r.m.s. deviations is 0.14Å for distances and 5.8° for angles. The reason for crosslinking hydrogen bonds being less varied between the redox forms of

azurin is that most of these interactions are buried in the protein interior, whereas virtually all local hydrogen bonds are found on the surface of the protein in loops and turns.

Side-chain...side-chain hydrogen bond geometry shows the least agreement between the oxidised and reduced forms. The r.m.s. deviation in distances is 0.22Å, while for angles the r.m.s. deviation is 9.6°. Since side-chain atoms are usually less constrained than main-chain atoms, the poorer agreement seen for side-chain...side-chain interactions than for main-chain...side-chain or main-chain...main-chain interactions is expected.

3.2.4 Superposition of the reduced and oxidised azurin structures

To give an indication of the size of the overall changes in the structure of azurin after reduction, the two molecules of oxidised azurin were superimposed onto the corresponding molecules of reduced azurin. The method of superposition used here is that of Kabsch[255], which minimises the square of the deviation in atom positions. Superposition of the oxidised molecules on to the corresponding reduced molecules (i.e. oxidised A on to reduced A and oxidised B on to reduced B) using all of the atoms in the protein gives an r.m.s. deviation in atom positions of 0.81Å and 0.88Å for molecules A and B, respectively. For main-chain atoms (residues 3-127, omitting the N- and C-termini) the corresponding figures are 0.17Å and 0.18Å. Table 3.2.4.1 gives the r.m.s. deviations of atom positions for different sets of atoms.

Table 3.2.4.1. Rms values from superimposing oxidised and reduced azurins. Superposition of the β-strands uses the main-chain atoms of residues 3-10,14-16,18-22,27-36,45-51,81-87,91-99,108-112,121-127. The "Copper environment" atom set consists of the main-chain atoms of residues 9-15,35-37,41-48,85-88,111-122 and the sidechain atoms of 9,11,15,35,37,45-48,86-88,111-117,121 (i.e. internal side-chains). The "Copper site" set includes Gly-45,His-46,Cys-112,His-117 and Met-121.

Atom Set	R.m.s. Δx molecule A	R.m.s. Δx molecule B
All protein atoms (977 atoms refined)	0.811Å	0.880Å
Main-chain atoms of residues 3 - 127 (500 atoms refined)	0.174Å	0.182Å
β-strand main-chain atoms (244 atoms refined)	0.154Å	0.134Å
Copper enviroment (215 atoms refined).	0.160Å	0.171Å
Copper site (38 atoms refined)	0.153Å	0.162Å

It should be noted that the agreement between molecule A of the oxidised structure and molecule A of the reduced structure (and similarly for molecule B) is significantly better than the agreement between molecules A and B of either the oxidised or reduced forms (r.m.s. deviations of 0.30Å and 0.28Å for reduced and oxidised, respectively, see Section 3.3). This implies that the changes to the structure upon reduction are actually smaller than those differences which are due to crystal packing effects, microheterogeneity or to error in the structure.

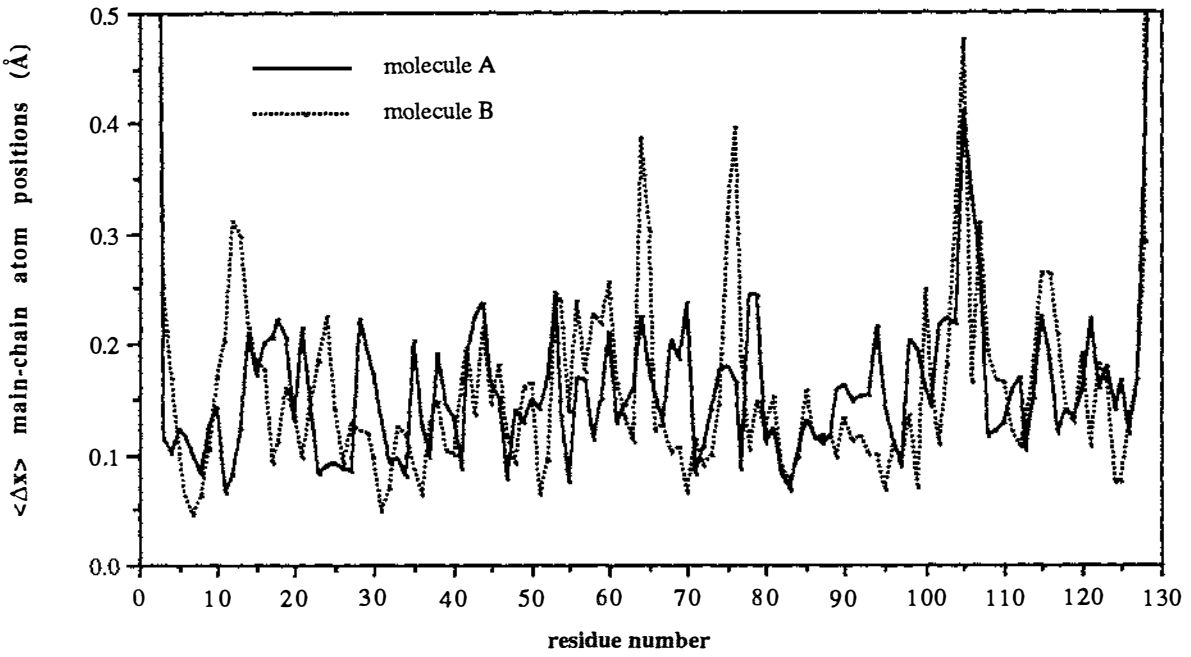

Figure 3.2.4.1. Average main-chain atom displacement between oxidised and reduced azurin.

Main-chain atom positions

The average deviations in main-chain atom positions for each residue are plotted in Figure 3.2.4.1, and show that very few differences exist between the polypeptide chains of reduced and oxidised azurin. The largest displacements appear at the N- and C-termini, which are poorly defined in the electron density maps, and are involved in lattice contacts causing variations in the main-chain conformation. Otherwise there are no major differences in the polypeptide folding between the oxidised and reduced structures. Displacements greater than 0.25Å in average main-chain atom position occur in the some of the loops that interconnect the β-strands and α-helix. These regions are residues 11-13, 53-55, 64, 75-76 and 103-107, and are located on the surface of the molecule where the thermal parameters are high (average B=41Å^2). Residues 103-107 show particularly poor agreement between the oxidised and reduced forms, perhaps because there are very few constraints from packing effects or hydrogen bonding to other parts of the protein. Consequently this region is less well ordered than other parts of the structure, resulting in poor definition of the electron density. Regions of the main-chain which have the lowest average deviation in atom positions are the β-strands, the α-helix and the copper site. The r.m.s. deviation for such areas is 0.14Å, 0.18Å and 0.16Å for the β-strands, the α-helix and the copper site, respectively.

Comparison of the β-structure in reduced and oxidised azurin

The copper atom in azurin lies between the loops at one end of the β-sandwich. This raises the question of whether there is any expansion or contraction of the distance between the two β-sheets when the protein is reduced. Visual inspection on an interactive graphics system shows no obvious change, but to be sure, distances were measured between opposing C_α atoms from each β-sheet†, and were then compared between the oxidised and reduced forms. Differences in 52 pairs of C_α-C_α distances on average increase by 0.014Å and decrease by 0.004Å in molecules A and B, respectively. Such differences are effectively nil when compared to the r.m.s. deviations of the C_α-C_α distances between molecules A and B of the reduced protein (r.m.s. = 0.11Å), and suggest no expansion in the distance between the β-sheets. As a further test, the differences in C_α-C_α distances were divided into three regions, those at the "north" end of the β-sandwich near the copper site, those in the middle and those at the "south" end of the β-sandwich. This should indicate whether reduction has caused the relative distance between the β-sheets to increase locally near the copper site, but not elsewhere. C_α-C_α distances between the β-sheets on average change upon reduction in the "north" by +0.03Å (21 distances), in the middle by 0.00Å (16 distances) and in the "south" by -0.02Å (15 distances). These results imply that there is no significant change in the separation distance between the β-sheets after reduction.

Side-chain atom positions

Changes in the side-chain atom positions were determined by first superimposing the main-chain atoms (residues 3-127) of the oxidised and reduced structures and then calculating the average deviation in side-chain atom positions. Figure 3.2.4.2 illustrates the average shift in side-chain atom position for each residue. The largest changes in position, those greater than 1.0Å, occur at Ala-1, Gln-2, Lys-18, Lys-27, Gln-28, Lys-34, Lys-41, Lys-52, Gln-57, Met-64 and Asn-129 for molecule A, and Ala-1, Gln-2, Glu-4, Met-13, Lys-18, Glu-19, Lys-27, Lys-41, Glu-53, Gln-57, Lys-122 and Asn-129 for molecule B. Average shifts in side-chain atom positions of 0.5-1.0Å are seen at Glu-19, Val-21, Lys-24, Lys-38, Met-39, Met-44, Lys-52, Lys-85, Lys-101, Met-120, Lys-122 and Lys-126 for molecule A, and Glu-14, Val-21, Lys-24, Met-44,

† C_α-C_α distances used were; 1) 14-121, 14-112, 14-46, 15-122, 15-111, 15-47, 10-45, 10-46, 9-112, 9-46, 33-48, 33-112, 33-84, 34-47, 34-86, 35-46, 35-87, 36-45, 91-87, 92-87 and 92-47 for "top" region; 2) 8-47, 8-111, 7-48, 7-110, 7-123, 6-110, 6-123, 32-48, 32-84, 93-85, 93-47, 94-84, 94-48, 95-83 and 95-49 for "middle" region; 3) 5-19, 5-20, 5-125, 4-22, 4-21, 3-22, 3-23, 29-126, 29-22, 30-21, 30-21, 30-125, 31-110, 31-49, 96-82, 96-50 and 97-81 for "bottom" region.

Lys-52, Lys-56, Met-64, Glu-70, Lys-74 and Lys-85 for molecule B. Approximately half of these residues are lysines (21 out of 45), and another 11 are either glutamic acids or glutamines. All of these side-chains, which have an average displacement in their atom positions above 0.5Å, are located on the surface of the protein molecule, are in contact with the solvent (except for Met-13) , and are usually associated with high B-values. This includes the seven methionines, except for Met-13B for which changes are due to a crystal lattice contact with the opposing protein molecule. Changes elsewhere in azurin upon reduction are smaller (<0.5Å), and occur in side-chains which are buried or well defined in the structure. In particular, the shifts in side-chain atom positions which make up the copper site are among the smallest in the protein (see Figure 3.2.4.2).

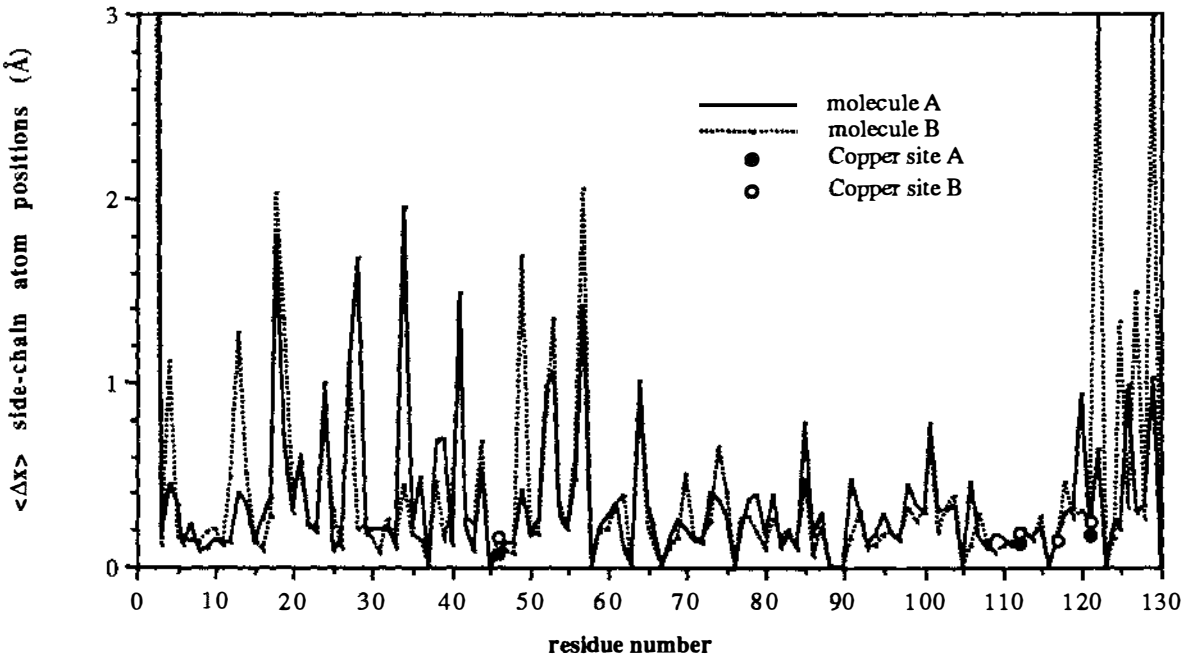

Figure 3.2.4.2. Average side-chain atom displacement between oxidised and reduced azurin. The four main copper ligands (His-46, Cys-112, His-117 and Met-121) are indicated as either hollow (molecule A) or filled (molecule B) dots. The filled dot for His-117B is not evident because it is covered by the hollow dot of His-117A.

The superposition studies clearly indicate that the largest shifts in atom positions occur in those parts of the structure which are at the surface of the molecule. These changes, however, are probably not significant and are not a result of reduction. Instead, these changes presumably reflect either the poor definition or flexibility of these regions. Changes in the other parts of the structure are much smaller, and those which may be due to reduction can not be clearly identified by this method. Consequently, other methods are required to determine the structural changes (if any) which occur upon reduction.

3.2.5 Consistent Shift Vector Analysis

Since the changes upon reduction of azurin were shown to be small, compared to the error in the structure and the differences due to crystal packing effects, a method is required for identifying those areas where reduction does cause small but consistent changes. The two independent molecules of the asymmetric unit can be utilised for this purpose. A shift vector can be calculated for each atom of the protein molecule, describing the movement of the atom upon reduction, and then these vectors of molecule B can be superimposed on to those of molecule A to compare the shifts in the atom positions between the two molecules. This was done using the two molecules of reduced and oxidised azurin to search for the regions in the structure where the shift upon reduction is consistent.

A function was developed to highlight the atoms and residues which undergo consistent shifts in both molecules when azurin is reduced. This function uses the lengths of the shift vectors for both molecules, and the angle between them (see Figure 3.2.5.1). Weights are also set in order emphasize those regions of the structure which are well defined (low B-values) and down-weight those which are poorly defined (high B-values). Additional weights were also used to down-weight shift vectors which are very different in length between the two molecules, and those atoms that might be well defined in one molecule but not in the other (i.e. if ΔB is large between the two molecules, then the atom position is well defined in one molecule but not the other, and similarly for the shift vector). The empirical function below was used to express the consistency in shift vectors of an atom when the protein is reduced.

$$\Xi = \frac{10000\ \Delta x_A \Delta x_B\ (\mathrm{Cos}\ \theta + 1)^4}{(\Delta x_{max}/\Delta x_{min})(B_{max\text{-}ox}/B_{min\text{-}ox})(B_{max\text{-}red}/B_{min\text{-}red})\langle B_A\rangle\langle B_B\rangle}$$

where

Δx_A, Δx_B	= length of the shift vector for an atom in molecule A or B (Å).
θ	= angle between the shift vector pairs (°).
$\langle B_A\rangle$, $\langle B_B\rangle$	= mean B-value of an atom between the oxidised and reduced forms for molecule A or B.
$B_{max\text{-}ox}/B_{min\text{-}ox}$	= ratio of the B-value for an atom between molecules A and B of oxidised azurin.
$B_{max\text{-}red}/B_{min\text{-}red}$	= ratio of the B-value for an atom between molecules A and B of reduced azurin.
$\Delta x_{max}/\Delta x_{min}$	= ratio of the shift vector lengths.

The $(Cos\theta + 1)^4$ term acts as a weight to give those vector pairs that are virtually parallel ($\theta \approx 0°$) a high value, those pairs that are orthogonal ($\theta \approx 90°$) a value close to unity, and those that point in opposite directions ($\theta \approx 180°$) a value close to zero. Down-weighting vector pairs which have a large difference in length is handled by the $\Delta_{max}/\Delta_{min}$ term. The weight for regions in the structure which are very clear in one molecule (low B-value), but not clear in the other molecule (high B-value), is expressed by the $B_{max\text{-}ox}/B_{min\text{-}ox}$ and $B_{max\text{-}red}/B_{min\text{-}red}$ term.

To determine the shift vector in the transition from oxidised to reduced azurin, the superposition of the protein molecules was done in two steps. First, molecule B of reduced azurin was superimposed on to molecule A of the same form (using the main-chain atoms of residues 3-127). Then oxidised molecule A was superimposed on to reduced molecule A, and oxidised molecule B was superimposed on to the new coordinates of reduced molecule B. This eliminates any effects due to the differences in unit cell dimensions of oxidised and reduced azurin crystals.

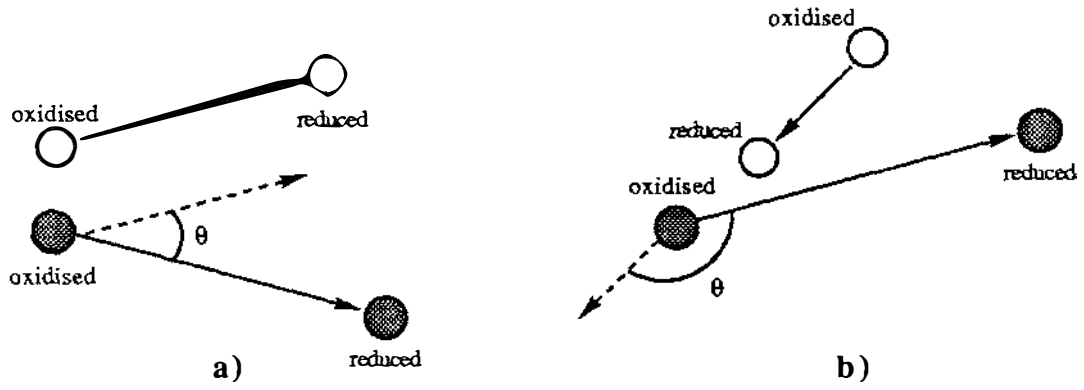

Figure 3.2.5.1. Schematic diagram describing the 2-dimensional case of an atom shifting position in molecule A (hollow circles) and in molecule B (filled circles). In **a)**, the shift vectors in molecules A and B are very similar in size and direction (i.e. high consistency), whereas in **b)**, the shift vectors are very different (i.e. low consistency).

Shift vectors were then calculated for both molecules, A and B, for the transition from oxidised to reduced structures. Theoretically, in the regions where the structure is dependent on the redox state, the shift vectors of molecule A should be roughly parallel to those of molecule B. The values of Ξ and the angle between the shift vectors (θ) were inspected to identify regions with consistantly high Ξ values and low θ values. Regions where only a single atom scored high in Ξ, while the surrounding structure has low scores, were usually ignored.

Upon reduction of azurin, areas of high Ξ scores ($\Xi > 50$) and parallel vectors are listed

Table 4.2.5.1. Results from the consistent shift analysis between reduced and oxidised azurin structures.

Residue		Ξ	Average angle between shift vectors (°)	Average distance shifted (Å)
Ξ > 100				
Gln-2	(s.c.)	1647.07	69.96	5.509
Val-21	(s.c.)	208.34	20.85	0.575
Met-44	(m.c.)	114.06	42.41	0.226
Met-44	(s.c.)	100.81	40.66	0.611
Glu-53	(s.c.)	192.89	102.32	1.200
Gln-57	(s.c.)	583.19	70.07	1.753
Met-64	(s.c.)	213.62	58.49	0.976
Ser-92	(s.c.)	112.82	39.18	0.294
Pro-115	(m.c.)	186.16	23.24	0.244
Pro-115	(s.c.)	212.45	20.94	0.249
Gly-116	(m.c.)	119.92	41.87	0.244
Trp-118	(s.c.)	122.05	22.86	0.383
100 > Ξ > 50				
Tyr-15	(m.c.)	63.58	24.73	0.177
Tyr-15	(s.c.)	50.15	47.52	0.145
His-32	(s.c.)	62.28	31.14	0.230
His-35	(s.c.)	58.81	44.25	0.197
Gly-45	(m.c.)	80.62	40.52	0.153
His-46	(m.c.)	62.82	69.91	0.166
Val-49	(s.c.)	56.63	41.89	0.143
Thr-51	(s.c.)	80.50	35.87	0.221
Lys-56	(s.c.)	91.96	79.77	0.552
His-83	(s.c.)	72.47	54.15	0.191
Val-99	(s.c.)	98.34	46.82	0.290
Lys-101	(s.c.)	74.29	59.38	0.740
Leu-102	(s.c.)	73.93	63.39	0.246
Phe-114	(m.c.)	52.13	45.72	0.162
His-117	(m.c.)	75.72	29.90	0.164
His-117	(s.c.)	62.50	33.12	0.150
Trp-118	(m.c.)	65.34	17.28	0.141

in Table 3.2.5.1. These regions were then checked visually to see if the shifts did appear to be significant. In general, the results show that consistent changes during reduction are small, and comparable to the differences between the two molecules of the asymmetric unit.

The residues with the highest scores in Ξ (Ξ > 100 for either the main-chain atoms or side-chain atoms) are Gln-2, Val-21, Lys-38, Met-44, Glu-53, Gln-57, Met-64, Ser-92, Pro-115, Gly-116 and Trp-118. Some of these shifts can be eliminated, because the large value of Ξ is caused by a flexible side-chain of one redox form having a different conformation which, however, still occupies the same general space. For instance, the side-chain of Lys-38 has a high Ξ score because in the reduced form the conformation is different at C_ε-N_ζ with respect to the oxidised form (see Figure 3.2.5.2). Presumably this is the result of flexibility. Furthermore, for many of these groups the average

deviation in atom positions between the two reduced azurin molecules is considerably greater than their average consistent shift, and the significance of their shifts is doubtful. All of the shifts with Ξ scores above 100 can all be eliminated for these reasons, except possibly for those at Pro-115, Gly-116 and Trp-118.

The residues Pro-115, Gly-116 and Trp-118, show definite shifts of 0.2-0.4Å that appear to be dependent on the redox state of the protein. The most obvious of these is the shift in the indole ring of Trp-118 shown in Figure 3.2.5.3, where the side-chain group moves in the plane of the ring. At Pro-115, the pyrrolidene ring appears to move away from the copper centre upon reduction (see Figure 3.2.5.4), and this movement seems to be coupled to the shifts in Gly-116. The changes in Pro-115 and Gly-116 are more difficult to describe than those at Trp-118, but seem to be consistent and part of a movement of the loop as a whole. Interestingly, all three residues are part of the loop between Cys-112 and Met-121, and are also part of the hydrophobic patch surrounding His-117. These shifts will be further discussed in Section 3.2.7.

Other regions which have high Ξ scores ($100 > \Xi > 50$) are at Tyr-15, Lys-24, His-32, His-35, Gly-45, His-46, Val-49, Thr-51, Lys-56, His-83, Lys-101, Leu-102, Phe-114, and His-117. Many of these residues are buried (Tyr-15, His-35, Gly-45, His-46, Val-49, Thr-51, Leu-102, Phe-114 and His-117), and all of them, except for Leu-102, are at or near the copper site. These shifts (0.1-0.2Å) will be treated in the section describing the environment surrounding the copper site

The remaining residues with Ξ scores in the range 50-100 are located on the surface of the protein (Lys-24, His-32, Lys-56, His-83, and Lys-101), and their shifts may not be significant. The shifts in His-32 and His-83 are in the plane of the imidazole ring, and are illustrated in Figures 3.2.5.5 and 3.2.5.6. The significance of these shifts is doubtful because they are smaller than the average deviation in atom positions between the two reduced azurin molecules (average deviations of 0.57Å and 0.24Å compared to average shifts of 0.23Å and 0.19Å, respectively). The shifts in the atoms of the side-chain of Lys-56 are surprisingly consistent since lysine side-chains are generally flexible. However, it is interesting to note that the shift in the side-chain of Trp-118, a neighbour 3-4Å away, is in the same direction as that of Lys-56 (see Figure 3.2.5.7). At Lys-24 and Lys-101 the shifts are a result of the side-chains being built differently in electron density ("out-of-phase") between the oxidised and reduced structures, but still occupy the same general region of space (Figure 3.2.5.8).

Since most of the consistent shifts are small, and are of the order of the deviation in atom

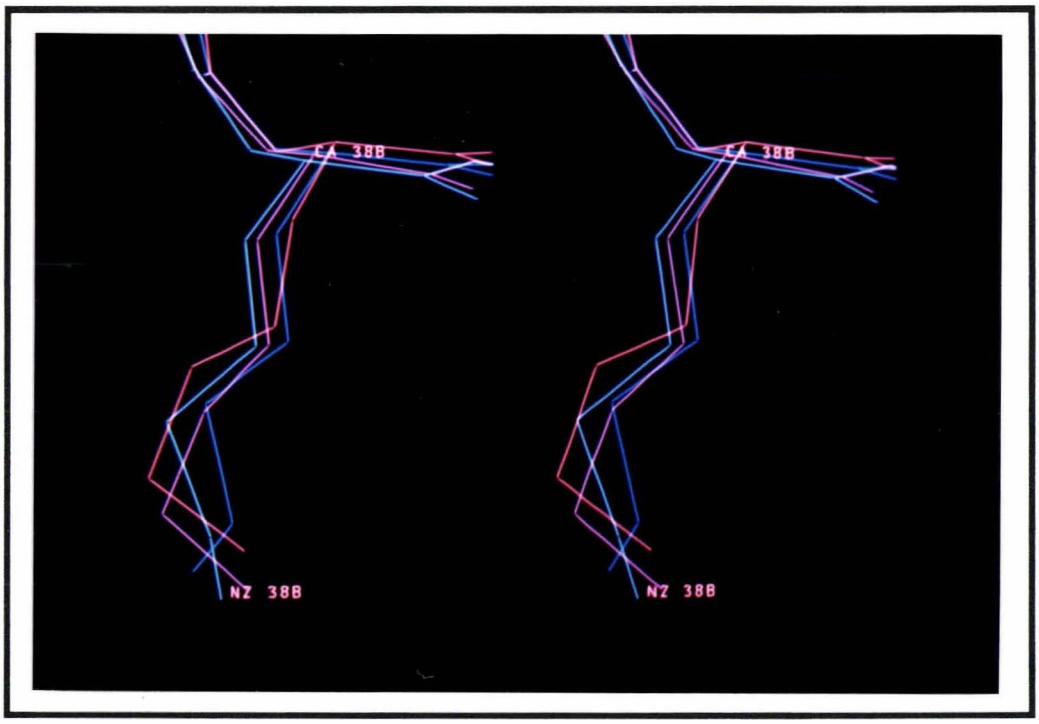

Figure 3.2.5.2. Side-chain conformation of Lys-38 in the four molecules of reduced (A/B=red/pink) and oxidised (A/B=blue/light blue) azurins, notice the differences in the C_{ε}-N_{ζ} region which has caused a high score in Ξ.

Figure 3.2.5.3. Shift in the side-chain of Trp-118. Oxidised azurin molecules in blue (A) and light blue (B), and reduced azurin molecules in red (A) and pink (B).

Figure 3.2.5.4. Shift in the residues Pro-115 and Gly-116. Oxidised azurin molecules in blue (A) and light blue (B), and reduced azurin molecules in red (A) and pink (B).

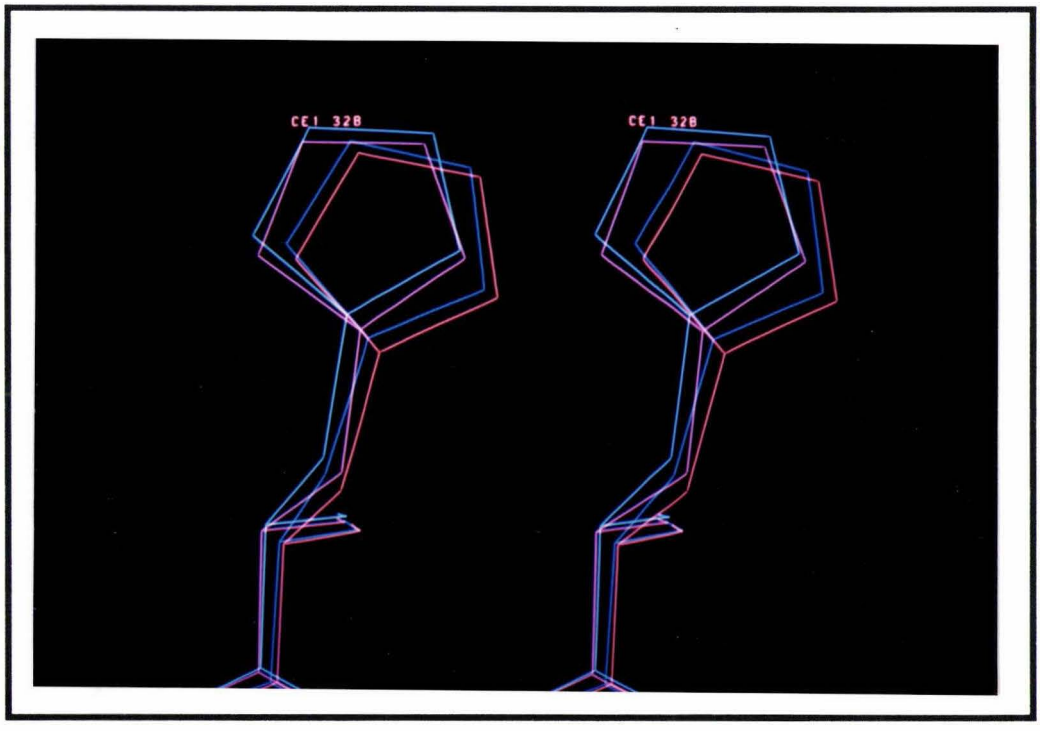

Figure 3.2.5.5. Shift in the side-chain of His-32. Oxidised azurin molecules in blue (A) and light blue (B), and reduced azurin molecules in red (A) and pink (B).

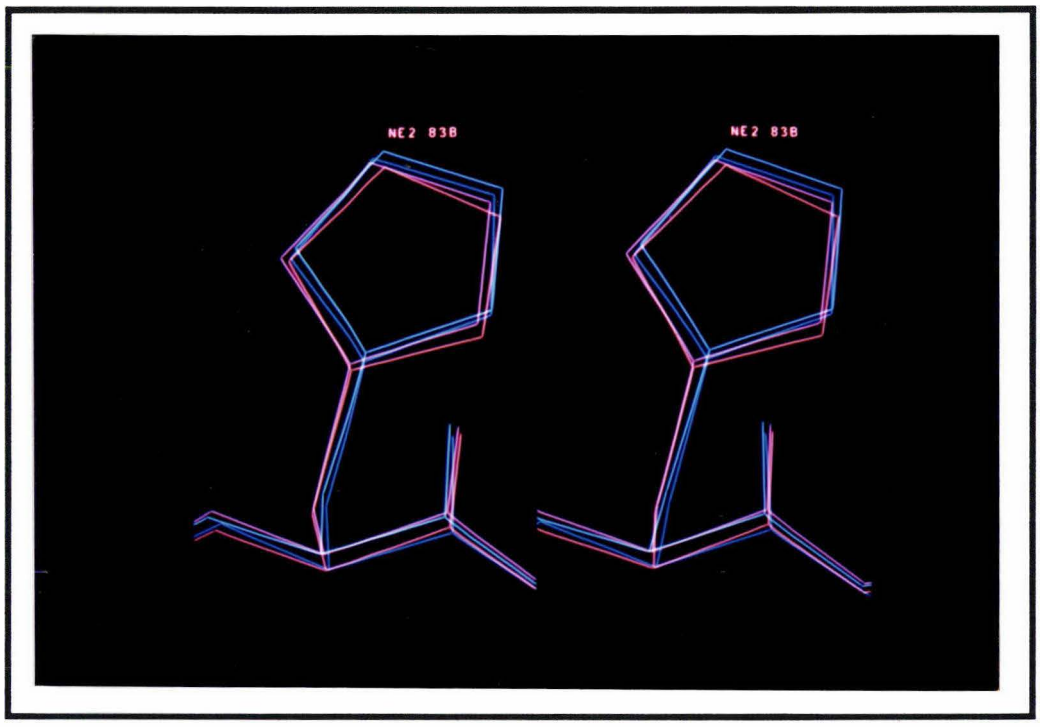

Figure 3.2.5.6. Shift in the side-chain of His-83. Oxidised azurin molecules in blue (A) and light blue (B), and reduced azurin molecules in red (A) and pink (B).

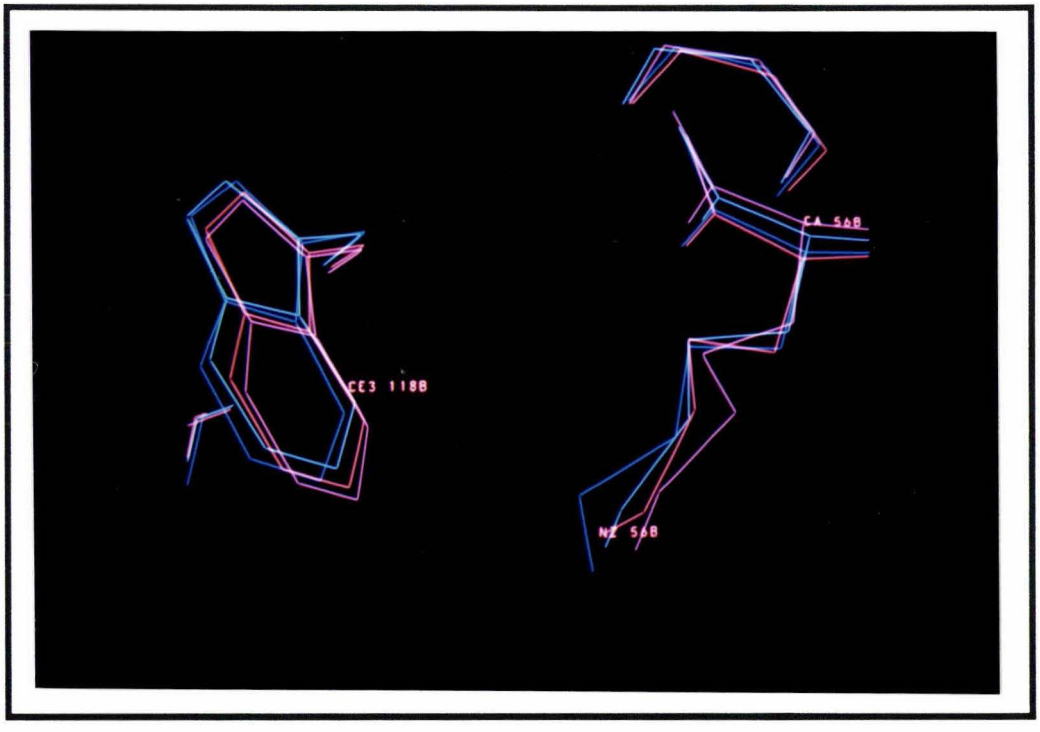

Figure 3.2.5.7. Shift in the side-chain of Lys-56, note the similar shift and proximity of the side-chain of Trp-118. Oxidised azurin molecules in blue (A) and light blue (B), and reduced azurin molecules in red (A) and pink (B).

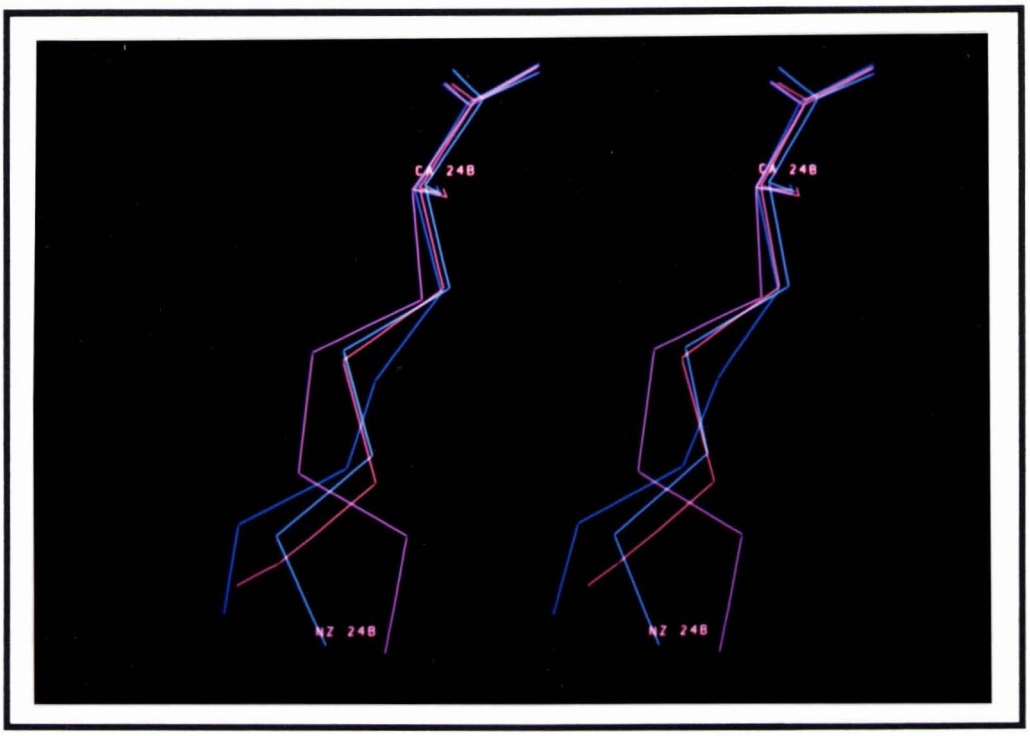

Figure 3.2.5.8. Shift in the side-chain of Lys-24, note how the side-chain atoms of the reduced structure are "out-of-phase" with the oxidised structure. A similar situation appears with the side-chain of Lys-101. Oxidised azurin molecules in blue (A) and light blue (B), and reduced azurin molecules in red (A) and pink (B).

positions between the two molecules, this type of analysis of the shift of atom positions can not stand on its own as conclusive evidence for structural changes upon reduction. However, in the other sections describing the reduced structure, the shifts noted by this analysis will be used as support in clarifying the changes in the structure upon reduction.

3.2.6 The Copper Site

The copper site of reduced azurin is very similar to that of the oxidised form. However, small, but important, differences are apparent. The overall copper geometry can be described as either distorted trigonal or trigonal bipyramidal. Three ligands bind the copper strongly in a distorted trigonal plane about the copper; two of these are imidazole nitrogens ($N_{\delta 1}$) from the sidechains of His-46 and His-117, and the other is the thiolate sulphur (S_{γ}) from Cys-112. Approaches are made by the carbonyl oxygen of Gly-45 and the sulphur of Met-121 to the axial positions of the copper on either side of this equatorial plane. Both axial groups (Gly-45 and Met-121) make angles which deviate away from the normal of the equatorial plane of the copper site. Whether the copper geometry is considered trigonal or trigonal bipyramidal depends on to what extent the axial groups are considered to interact with the copper atom. Figure 3.2.6.1 illustrates the overall changes to the copper site.

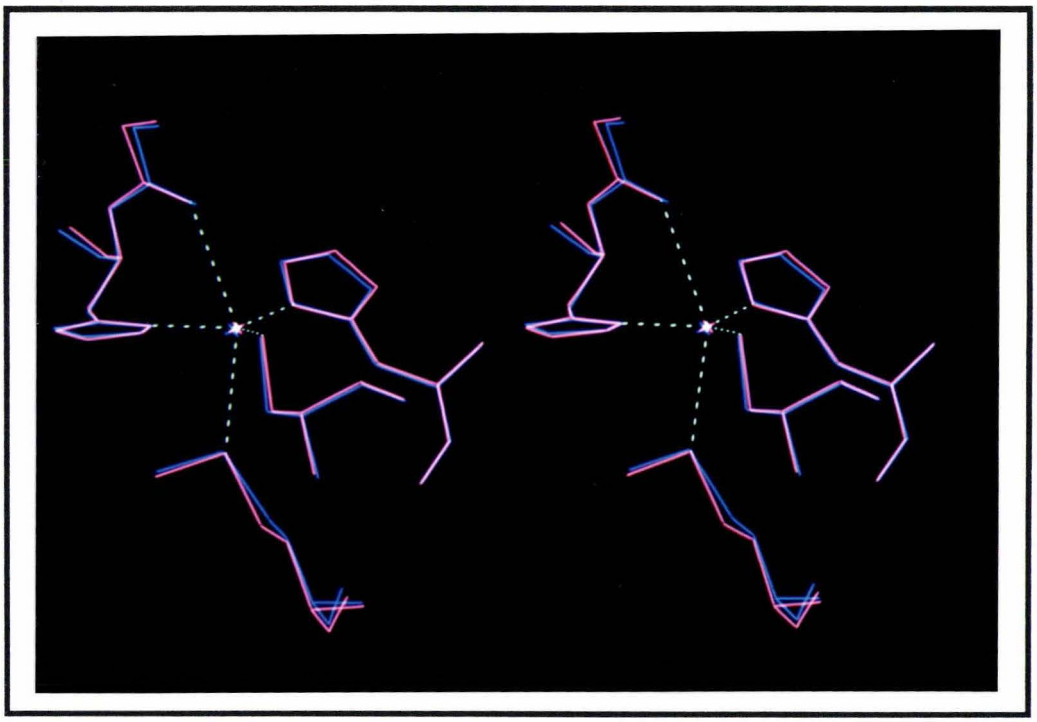

Figure 3.2.6.1. The superimposed oxidised (blue) and reduced (red) copper sites of azurin (molecule A).

In both molecules the copper site undergoes a general expansion, with distances to the copper increasing on average by 0.05-0.12Å. Table 3.2.6.1 lists the distances to the copper atom in both oxidised and reduced azurins. The average increase in the Cu-N(imidazole) bonds of His-46 and His-117 is 0.05Å, which gives mean bond lengths of 2.18Å and 2.05Å, respectively. The average Cu-S(thiolate) bond distance lengthens by 0.12Å to an average value of 2.27Å. Both of the axial groups shift roughly 0.10Å further away from the copper atom to give mean copper distances of 3.22 and 3.23Å, for Gly-45 and Met-121, respectively.

Table 3.2.6.1. Copper distances (Å) of oxidised and reduced forms of azurin.

Ligand	Oxidised		Reduced		Average
	molecule A	molecule B	molecule A	molecule B	change
O 45	3.16	3.09	3.25	3.19	**+0.10**
$N_{\delta 1}$ 46	2.08	2.09	2.17	2.09	**+0.05**
S_{γ} 112	2.12	2.17	2.22	2.31	**+0.12**
$N_{\delta 1}$ 117	2.01	1.99	2.05	2.05	**+0.05**
S_{δ} 121	3.12	3.10	3.21	3.25	**+0.12**

Angles about the copper atom in reduced azurin are very similar to those in the oxidised structure. These are listed in Table 3.2.6.2, and a comparison shows that most changes between the redox forms are below 5°. The copper atom rests on average 0.14Å below

Table 3.2.6.2. Angles at the copper atom in oxidised and reduced azurins reduction.

Angle (°)	Oxidised		Reduced		Average change
	molecule A	molecule B	molecule A	molecule B	
O 45-Cu-Nδ1 46	72	76	69	68	-6
O 45-Cu-Sγ 112	103	104	105	103	+1
O 45-Cu-Nδ1 117	78	81	82	85	+4
O 45-Cu-Sδ 121	146	148	142	144	-4
Nδ1 46-Cu-Sγ 112	135	135	132	131	-4
Nδ1 46-Cu-Nδ1 117	101	108	100	108	-1
Nδ1 46-Cu-Sδ 121	79	75	77	79	-1
Sγ 112-Cu-Nδ1 117	122	116	126	119	+4
Sγ 112-Cu-Sδ 121	109	105	109	109	+2
Nδ1 117-Cu-Sδ 121	94	98	90	94	-4

the plane defined by the three atoms Nδ1 46, Sγ 112 and Nδ1 117 towards Met-121 in reduced azurin, essentially the same as the mean displacement in the oxidised structure (0.13Å).

In comparing the two molecules of the asymmetric unit, the r.m.s. differences in the copper distances and angles are 0.063Å and 3.7° for the reduced structure, and 0.041Å and 3.9° for the oxidised structure, respectively (see Section 3.3.6). The changes in copper distances upon reduction are either slightly larger than or equal to the r.m.s. deviation of the copper distances, and it could be argued that because the changes upon reduction are of similar magnitude, these changes are not signifcant. It is important to note, however, that the differences in the copper site are seen in both molecules of the asymmetric unit, which were refined independently. This suggests that the changes are a real effect of the change in oxidation state.

The overall changes at the copper centre upon reduction from Cu(II) to Cu(I) make physical and chemical sense. Reduction introduces an electron to the copper site, which causes an expansion in the copper radius by 0.05Å[256,172], and the changes in the copper equatorial bond lengths reflect this trend. With respect to the axial groups, the increase in the copper distances is greater, suggesting that the closer approaches made in oxidised azurin reflect the ability of Cu(II) to make long axial interactions, so that the Cu...O and Cu...S(Met) distances actually decrease when azurin is oxidised to the Cu(II) form. In this respect, the copper site can be considered to change upon reduction from a more trigonal bipyramidal geometry, characteristic of Cu(II), to a more trigonal geometry, preferred by Cu(I).

The basic configuration of the copper ligands is also maintained during reduction. Apart

from the increase in the distances to the copper atom, other small changes occur in the side-chain and main-chain atoms. As the distance between the carbonyl oxygen of Gly-45 and the copper atom increases during reduction, the segment of atoms from C_α 45 to N 47, rotates in a fashion such that the carbonyl group of Gly-45 swings away from the copper atom, with N 46 as the axis of rotation. Figure 3.2.6.2 illustrates the change in conformation of this segment of the main-chain. This may explain changes found in the main-chain torsion angles and in the consistent shift analysis, where the ϕ and ψ angles of Gly 45 change on average by +9° and -12°, respectively, and the length of the mean shift vector of Gly-45 is 0.15Å, (θ=41°, Ξ=81). The shift in O 45 away from the copper atom combined with the other changes suggests that an interaction does exist between O 45 and Cu(II) in oxidised azurin.

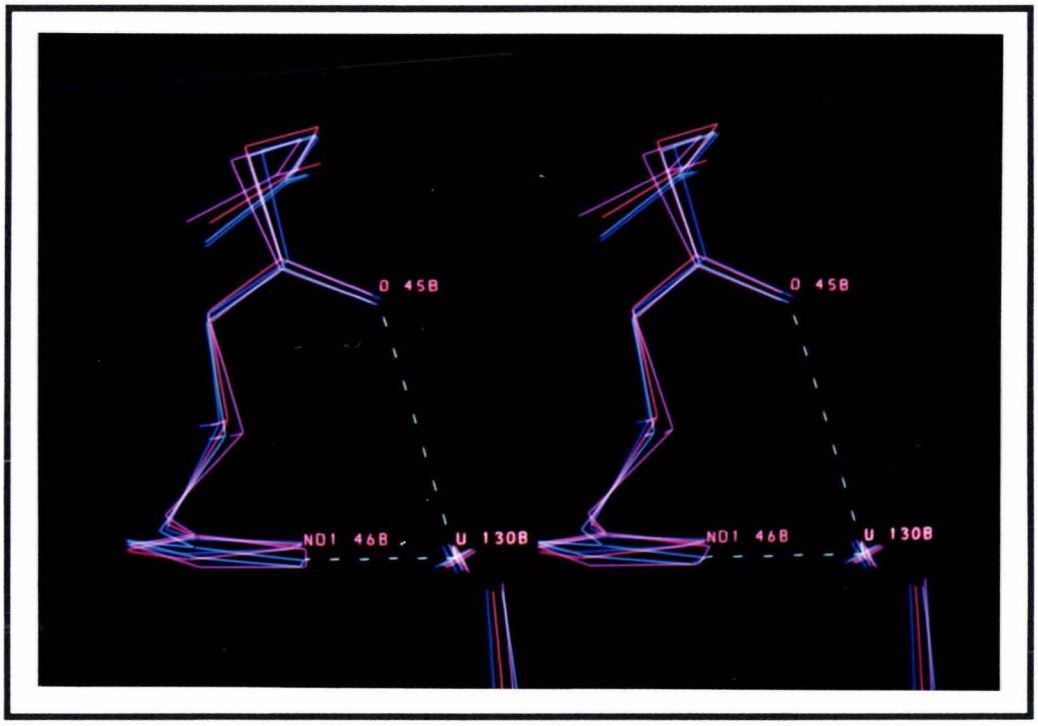

Figure 3.2.6.2. Shift in the carbonyl oxygen of Gly-45 upon reduction of azurin. Oxidised azurin molecules in blue (A) and light blue (B), and reduced azurin molecules in red (A) and pink (B).

The configuration of the His-46 side-chain does not change during reduction; the lone pair of electrons of $N_{\delta 1}$ remains directed at the copper atom to within 4° of the ideal (where the ideal is 0°, such that the angles C_γ-$N_{\delta 1}$-Cu and $C_{\varepsilon 1}$-$N_{\delta 1}$-Cu are equal). The copper atom is displaced on average 0.27Å out of the plane of the imidazole ring of His-46, compared to 0.24Å in oxidised azurin, and the imidazole ring is roughly coplanar with the N_2S plane (average 23°, virtually identical to the oxidised value of 25°). The side-chain atoms of His-46 do not move during reduction. Lengthening of the Cu-$N_{\delta 1}$ distance is achieved by a small shift of the copper atom.

The lone pair of electrons at $N_{\delta 1}$ 117 are also directed at the copper to within 4°. In contrast to His-46, however, the imidazole ring of His-117 makes an angle of 41° to the N_2S plane of the copper site, while the copper atom lies on average 0.35Å further out of the plane of the imidazole ring in reduced azurin (mean 0.42Å) than in oxidised azurin (mean 0.07Å). This difference is seen in both molecules and is possibly a consequence of a 6° rotation in χ_2 (see Figure 3.2.6.3). The net result is that the torsion angle, which is virtually eclipsed in oxidised azurin ($<\chi_2>$ = -169°), becomes less so in the reduced form ($<\chi_2>$ = -163°). Two possible effects could explain this change. One is that an electronic interaction such as π-bonding between the Cu(II) and imidazole ligand has been altered by reduction, but a more likely explanation is that steric effects from the side-chains of Phe-114 and Met-13, which tightly sandwich the imidazole ring, force this 6° change as the Cu-$N_{\delta 1}$ distance increases, pushing the imidazole ring away from the copper.

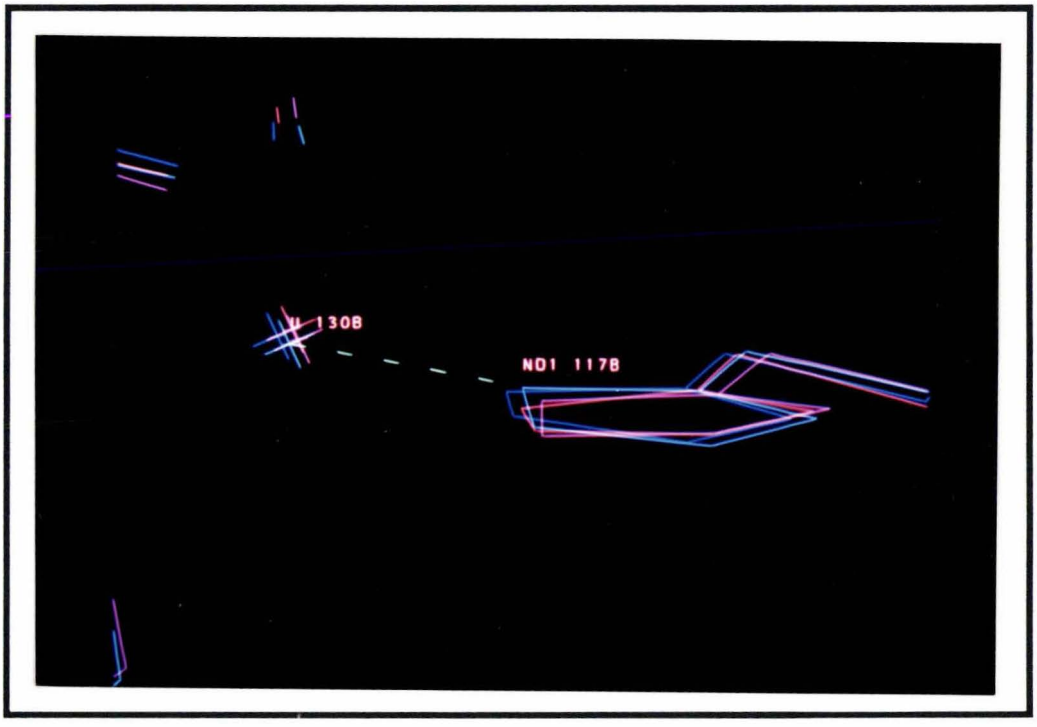

Figure 3.2.6.3. Structural changes at His-117 upon reduction of azurin. Oxidised azurin molecules in blue (A) and light blue (B), and reduced azurin molecules in red (A) and pink (B).

Although the configuration of the thiolate side-chain of Cys-112 is very similar between the oxidised and reduced forms, several small changes are noticeable. In both redox states, the average Cu-S_γ-C_β angle is very close to tetrahedral, so that a lone pair of electrons of the sulphur is directed towards the copper atom. The angle is more acute in reduced azurin (average of 102° compared to 107°), however, becoming distorted from the ideal value of 109.5° because the C_β and main-chain atoms do not move on reduction, while S_γ does. At the same time the average C_α-C_β-S_γ angle becomes more acute on reduction, from 105.5° to the low value of 102.4°, and S_γ 112 moves towards the amide

nitrogens of residues 47 and 114. This produces a shortening of the two S...HN hydrogen bonds (see Section 3.2.7). The average χ_1 torsion angle also changes slightly (+5°) on reduction, from 173° in the oxidised to 178° in the reduced structure. However, the average torsion angle Cu...S_γ-C_β-C_α does not alter (190° reduced and 191° oxidised). This metal side-chain conformation is common in other proteins containing metal-thiolate bonding, and is preferred because the fully extended conformation places the copper atom the furthest from the main-chain atoms[257].

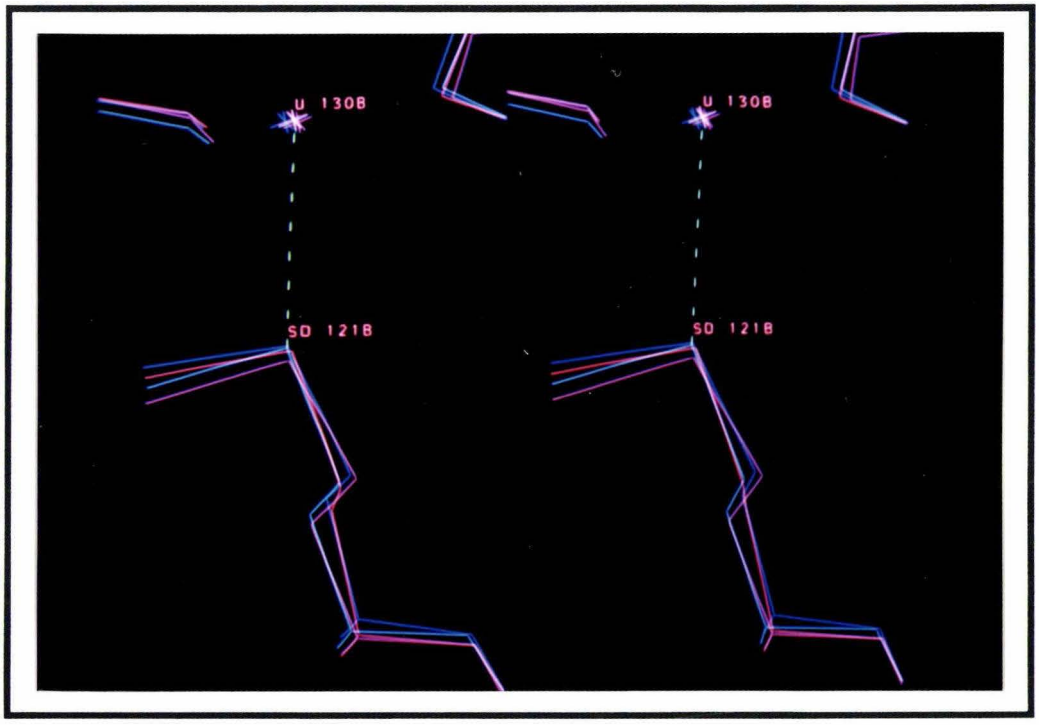

Figure 3.2.6.4. Shifts in the side-chain of Met-121 and the copper upon reduction in azurin. Oxidised azurin molecules in blue (A) and light blue (B), and reduced azurin molecules in red (A) and pink (B).

The configuration of the Met-121 side-chain is little affected by the reduction of the copper. The orientation of the sulphur of Met-121 is such that neither lone pair of electrons points directly at the copper (assuming tetrahedral sulphur). In the reduced structure, the mean C_γ-S_δ...Cu and C_ε-S_δ...Cu angles are 103° and 138°, respectively, no different from the average values of 102° and 142°, respectively, in the oxidised structure. The conformational angles of the side-chain of Met-121 in the reduced state are also similar to those of the oxidised structure, but the variation between the two molecules of the asymmetric unit of both redox forms obscures any changes which may have occurred. The increase in the Cu...S(Met) distance, however, is a result of a small shift in the position of S_δ 121, combined with the shift in the copper atom away from S_δ 121 (see Figure 3.2.6.4). This shift is also seen in the separation between O 45 and S_δ 121, which increases on average by 0.13Å from 5.99Å in the oxidised form to 6.12Å in the reduced form, further confirming that the axial groups move away from the copper on

reduction.

Comparison with EXAFS results

As noted in Section 3.1, distances to the copper agree with those from EXAFS experiments[161] except for the value of the Cu...S(Met) distance for which the EXAFS distance is probably incorrect. Prior to the determination of the crystal structure of reduced azurin, the results from the EXAFS experiments implied that the Cu...S(Met) distance shortens considerably on reduction, changing from 3.1Å (the crystallographic oxidised distance[31]) to 2.7Å (the reduced EXAFS distance[161]). Such a change could occur if the copper atom moved towards the methionine sulphur, to change the copper geometry from distorted trigonal bipyramidal to distorted tetrahedral, which is favoured by Cu(I) (see Figure 3.2.6.5). However, the crystallographic results here clearly show that such a change upon reduction does not occur in azurin. Rather, the Cu...S(Met) distance increases from 3.11Å to 3.23Å, and the copper geometry changes from more trigonal bipyramidal-like to more trigonal-like.

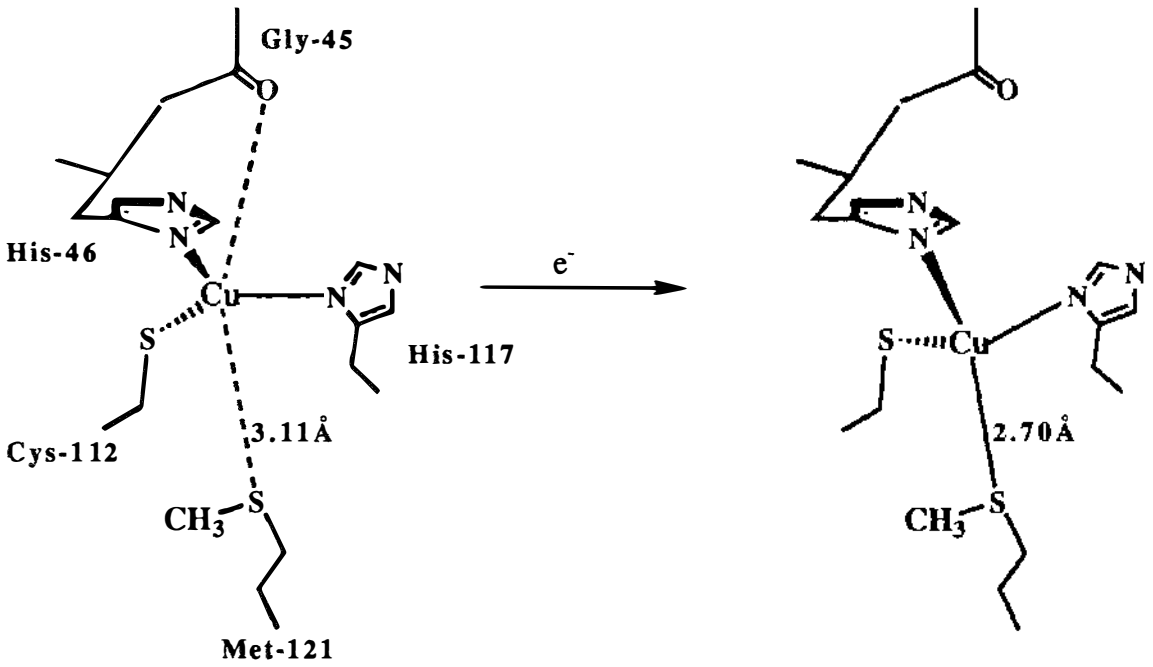

Figure 3.2.6.5. Schematic diagram of the change in the copper geometry upon reduction as implied by the EXAFS results.

Comparison of Copper(I) distances with model compounds

There are very few examples of model compounds which contain the particular coordination characteristics of the copper site of azurin. Mononuclear model complexes which contain the N_2S configuration usually have Cu-N(imidazole) and Cu-S(thioether)

coordination, but few with thiolate coordination have yet been synthesised. This is in part because Cu(I) thiolate systems have a strong tendency to form CuS clusters instead of mononuclear complexes, making their synthesis difficult. In the following section, the copper distances in reduced azurin will be compared with those determined from small molecule Cu(I) complexes. For an extensive review of copper chemistry see Hathaway[258], and for blue copper site model complexes see Bouwman *et al.*[94].

Cu(I)...O distances

Only a small number of crystal structures have been determined on Cu(I) complexes which contain Cu(I)-O coordination. This is not surprising since the hard Lewis base characteristics of oxygen ligands are not compatible with the soft Lewis acid character of Cu(I), which prefers ligands containing sulphur, phosphorous or aromatic nitrogen atoms. Cu(I)-O bond lengths range from 1.828Å to 2.43Å[259-276]. Bond lengths below 2.0Å are uncommon, and are usually found in Cu(I) centers which are either two-coordinate (linear) or three-coordinate (trigonal)[259,269,271]. The majority of Cu(I)-O distances fall in the 2.0-2.3Å range, many involving oxygen atom(s) from either oxyanions or carboxylate groups[260-266]. Virtually all of these copper centres have tetrahedral or C_2 geometry. Oxygen ligands also bridge Cu(I) centres in multi-nuclear complexes[267-276], and here the Cu-O distances vary between 1.828Å[271] and 2.31Å[272]. The longest Cu(I)-O distance reported is 2.43Å in a carbon monoxide complex involving a coordinated perchlorate group[275]. Longer Cu(I)...O distances, as are found in Cu(II) complexes, are presumably not formed because of the difference in the electronic configuration (d^{10} for Cu(I) and d^9 for Cu(II))[258]. However, two long Cu(I)...N distances of 2.77Å and 2.92Å, and one long Cu(I)...O distance of 3.56Å have been reported[277,278]. The 2.77Å distance is found in a binuclear Cu(I) complex, where the coppers have near linear geometry, and the Cu(I)...N(amino) distance is an approach caused by steric effects of the configuration of the ligand[277]. The other distance (2.92Å) is found in a mixed valence Cu(I)Cu(II) cluster where one Cu(I) centre, which has two imidazole nitrogen donors coordinated in a linear fashion, is approached by a methylcyanide solvent molecule to complete a "T-shaped" geometry[277]. The Cu(I)...O distance of 3.56Å is much too long to be considered an interaction, but it is an extreme case of a counter ion (a perchlorate) being forced to approach the copper centre by crystal packing forces. In this case the perchlorate anion occupies the vacant axial site of the trigonal pyramidal Cu(I) centre[278].

The Cu(I)...O 45 distance in reduced azurin (average 3.23Å) is much longer than any known bonding Cu(I)...O distance. When compared to the sum of the van der Waals

radii of Cu(0) and oxygen (2.90Å)[256], the Cu(I)...O 45 distance is too long to be considered a bond. This suggests that the Cu(I)...O 45 distance is the result of a steric effect, as is seen above in the long Cu(I)...O and Cu(I)...N distances. Furthermore, the charge on the Cu(I) ion is neutralised by the thiolate anion of Cys-112, effectively removing any possibility of an electrostatic attraction between the Cu(I) ion and the carbonyl oxygen. In the oxidised form, the charge on the Cu(II) ion is not neutralised, so that this charge combined with the partial negative charge on the carbonyl oxygen can form a weak electrostatic interaction. Also, because the Cu(II) ion has a d^9 electronic configuration its shape is considered to be ellipsiodal rather than spherical, favouring the weak bonding of axial groups and leading to the term "semi-coordinated" [279,280]. Consequently there is a difference of 0.6Å in the covalent radii of the major and minor axes of Cu(II), putting the in-plane colvalent radius at 1.30Å and the out-of-plane radius at 1.90Å[281].

Cu(I)-N(imidazole) bond lengths

Cu(I)-N(imidazole) and Cu(I)-N(benzimidazole) bond lengths range from 1.867 to 2.064Å [95,277,282-288]. The Cu-N bond length is dependent on the coordination number of the copper, with values of 1.867-1.92Å for linear 2-coordinate[95,277,283], 1.910-1.92Å for trigonal planar or "T-shaped" 3-coordinate[283], and 1.977-2.100Å for tetrahedral 4-coordinate complexes[95,282,286-288]. This trend of increase in the Cu(I)-N(imidazole) bond length with increasing coordination number is found for other nitrogen ligands, where the average Cu(I)-N distances are 1.88Å, 1.97Å and 2.04Å for 2, 3 and 4-coordinate complexes, respectively[258]. In reduced azurin, the average Cu-N(imidazole) bond lengths are 2.13Å and 2.05Å for His-46 and His-117, respectively, and although the Cu-$N_{\delta 1}$ 46 bond length is a bit long, the Cu-$N_{\delta 1}$ 117 bond length is typical when compared to model complexes. The extra length in the Cu-$N_{\delta 1}$ 46 distance is attributed to a steric repulsion from the hydrogen atom of C_α 46, pointing directly at the copper making an average H...Cu contact of ≈2.6Å.

Cu(I)-S(thiolate) bond lengths

The Cu(I)-S(thiolate) bond distance in reduced azurin (average 2.27Å) is similar to those found in many small molecule Cu(I) complexes (2.134-2.474Å)[288-307]. Unfortunately, however, there are very few examples of Cu(I)-S(thiolate) complexes which contain one copper coordinated to a single thiolate sulphur[288]. This is understandable since Cu(I)-S(thiolate) systems strongly prefer to form clusters rather than single mononuclear complexes, and the thiolate sulphurs aid the cluster formation by acting as bridging

ligands between copper centers. The copper geometry in Cu(I)-S(thiolate) clusters is usually trigonal[289-299,301-303], but some clusters do contain tetrahedral[288,302,304,305] and/or linear[290,300,306,307] Cu(I) centers. Only a few mononuclear Cu(I)-S(thiolate) complexes exist, for which the copper geometry is either linear[300], trigonal[301] or tetrahedral[288,304]. The bridging ability of thiolate sulphur seems to have little effect on the Cu(I)-S(thiolate) bond length, but the coordination number of the copper center does. Trigonal Cu(I) centers have Cu(I)-S bond lengths ranging from 2.186-2.368Å[289,303], whereas linear Cu(I) centers have shorter bonds between 2.134-2.175Å[306,307], and tetrahedral Cu(I) centres have longer bonds between 2.308-2.358Å[304] (except for one tetrahedral complex with a Cu-S(thiolate) distance of 2.19Å[288]). The Cu(I)-S(Cys) bond lengths of the two molecules of reduced azurin (2.22-2.31Å) lie in the range found for trigonal Cu(I)-S(thiolate) clusters and mononuclear complexes (2.19-2.37Å). In all of the Cu(I)-S(thiolate) clusters, the sulphurs bind and bridge to the copper centres in a pyramidal (sp^3) disposition, which points the sulphur lone pairs of electrons at the metal centers[289-297,302-307]. This geometry is also found for the thiolate sulphur of Cys-112 in reduced azurin, where one lone pair of electrons of the sulphur is directed at the copper, while the other two lone pairs form hydrogen bonds with the backbone amide nitrogens of residues 47 and 114 (see scection 3.2.7 below). Overall, the stereochemistry of the Cu(I)-S(thiolate) interaction in reduced azurin is very similar to that found in small molecule thiolate complexes.

Cu..S(thioether) distances

Many crystal structures have been completed on Cu(I) complexes containing coordinated thioether sulphur. The most common copper geometry for these complexes is tetrahedral, although some have trigonal pyramidal geometry[308-311], while very few have trigonal geometry[283]. Cu(I)-S(thioether) bond lengths vary from 2.221Å to 2.469Å[258,287,308,309,312-321]. The Cu...S(Met) distance in reduced azurin of 3.23Å (average) is much longer than the typical Cu(I)-S(thioether) bond length found in small molecule Cu(I) complexes. The longest reported Cu(I)-S(thioether) distance, which can only be considered a weak bond, is 2.66Å (average) and is found in a tetranuclear cluster where the thioether sulphur bridges two Cu(I) centres (see Figure 3.2.6.5a)[322]. However, a few Cu(I) complexes do have Cu(I)...S(thioether) distances longer than 2.66Å, the result of "steric approaches" where the sulphur atom is forced to be near the copper centre by the configuration of the ligand. In a bent CuN_2 chromophore (N-Cu-N=168°), a Cu(I)...S(thioether) distance of 2.867Å has been described as "at best weakly interacting" (see Figure 3.2.6.5b)[94,284]. A long Cu(I)...S(thioether) distance of 3.039Å is seen in the dimer of $[Cu(2,2'\text{-bithiazolidinyl})]_2(ClO_4)_2$, which involves a

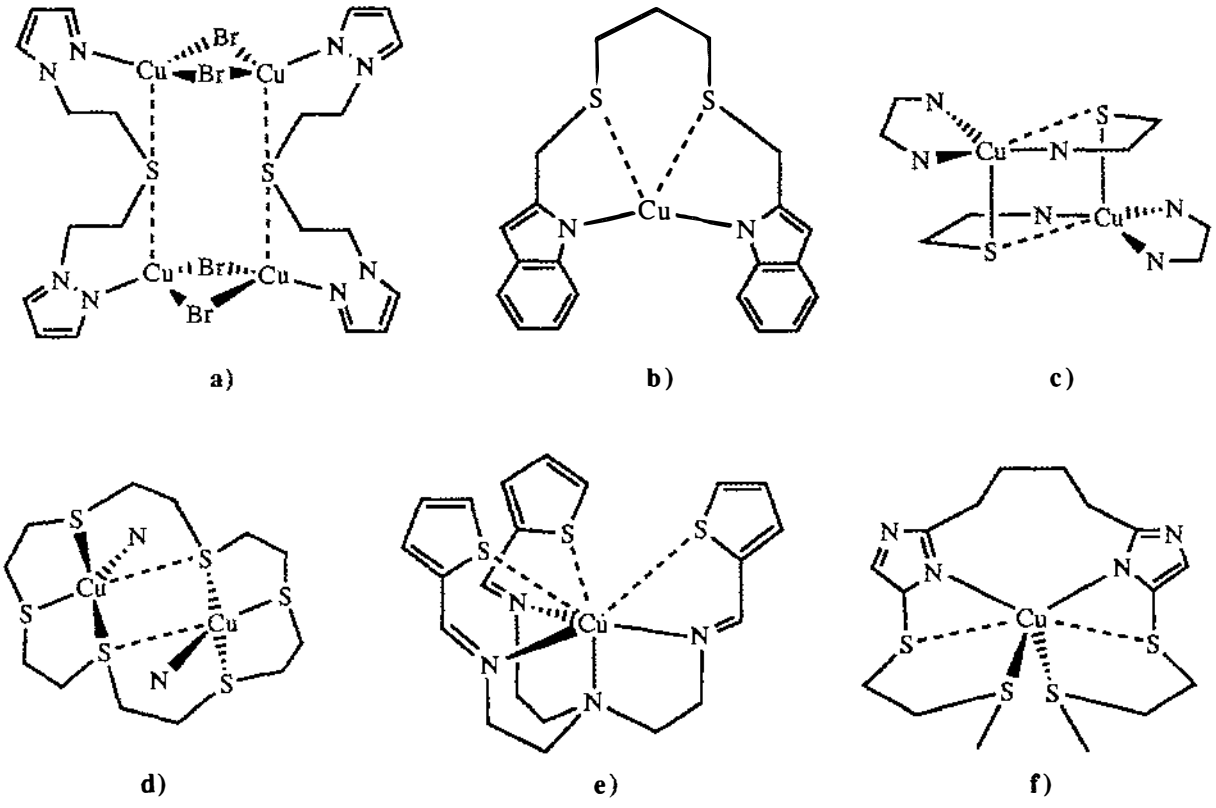

Figure 3.2.6.5. Schematic diagrams illustrating some of the long Cu(I)...S(thioether) distances found in small molecule complexes. a) Cu(I)...S=2.64-2.68Å[322] b) Cu(I)...S=2.867Å[284] c) Cu(I)...S=3.039Å[323] d) Cu(I)...S=3.318Å[311] e) Cu(I)...S=3.276-3.396Å[324] f) Cu(I)...S=3.660-3.614Å[287]

tetrahedral CuN_3S centre with an approach by a sulphur atom bound to the other copper centre (see Figure 3.2.6.5c)[323]. In another binuclear Cu(I) complex, $[Cu_2([18]aneS_6)(NCMe)_2]^{2+}$, the coppers are coordinated to three thioether donors and one methylcyanide nitrogen in a tetrahedral fashion, but there is a Cu(I)...S approach of 3.318Å, which is described as a "long range interaction", distorting the copper geometry towards trigonal bipyramidal (see Figure 3.2.6.5d)[311]. Distances of 3.276-3.396Å are made to a mononuclear Cu(I) centre by three separate thienyl sulphur atoms, and are described as "too great for any bonding interaction" (see Figure 3.2.6.5e)[324]. However, this copper centre is coordinated in a trigonal pyramidal geometry to four nitrogens, and the copper centre rests 0.275Å above the equatorial plane, away from the apical nitrogen and towards these sulphurs. The longest reported Cu(I)...S(thioether) distance (3.614-3.660Å) appears in a distorted tetrahedral CuN_2S_2 chromophore, where the Cu...S approach is very clearly the result of the ligand configuration forcing the sulphur atom close to the copper atom (see Figure 3.2.6.5e)[287].

Whether these long Cu(I)...S(thioether) distances represent actual interactions is unclear for some of the complexes. In the examples **a** and **b** (see Figure 3.2.6.5), the possibility

of an interaction between the copper and sulphur is relatively certain, because the Cu...S distance (2.6-2.9Å) is significantly shorter than the sum of the van der Waals radii of Cu(0) and sulphur (3.20Å), which can be used as an upper limit[256] and a definite distortion exists in the copper geometry. For the longer Cu...S distances in the complexes **c** to **e** (3.0-3.4Å), it is doubtful whether these are real interactions, but two points are noteworthy; 1) the ligands of these complexes are neutral, and 2) the copper atoms are displaced in a direction towards the sulphur atom. Consequently, the possibility that these distances are weak electrostatic interactions can not be totally dismissed. In the last case, the Cu...S distance (3.6Å) is much longer than the sum of the van der Waals radii, and the copper geometry is not distorted towards the sulphur, and thus no interaction exists between the copper and the sulphur. The situation for reduced azurin falls into the marginal category, since the Cu...S(Met) distance (average 3.23Å) is equal to the sum of the van der Waals radii. But, unlike the ligands discussed above, there can be no electrostatic interaction, because the charge on the copper is neutralised by the charge on the thiolate sulphur. Hence the possibility of any interaction between the copper and methionine sulphur is rather doubtful.

3.2.7 Constraints on the copper site

In the region surrounding the copper ligands there are several hydrogen bonds and steric packing constraints which appear to impose the observed ligand configuration and copper geometry on to the copper site. Upon reduction, only minimal changes are observed in these contacts (the r.m.s. deviation in atom positions is 0.17Å). Nevertheless, there are some important small changes which appear to be due to reduction.

S_γ..HN Hydrogen bonds at Cys-112

The most significant change in the protein structure around the copper site occurs in the two hydrogen bonds from the peptide nitrogens N 47 and N 114 to the thiolate sulphur of Cys-112. These hydrogen bonds restrain the position of the sulphur atom. In the oxidised form, they are nearly linear (average S...HN angles of 168° and 158°, respectively) and have mean S...N distances of 3.49Å and 3.58Å, respectively. Upon reduction of the copper site, both of these S...HN hydrogen bonds shorten by approximately 0.2Å,the largest consistent structural change to occur near the copper site. Table 3.2.7.1 lists the S...HN hydrogen bond geometry, and Figure 3.2.7.1 illustrates this change.

S...H-N hydrogen bonds have also been found in other blue copper proteins. In the structure of oxidised pseudoazurin, which has been refined to very high resolution

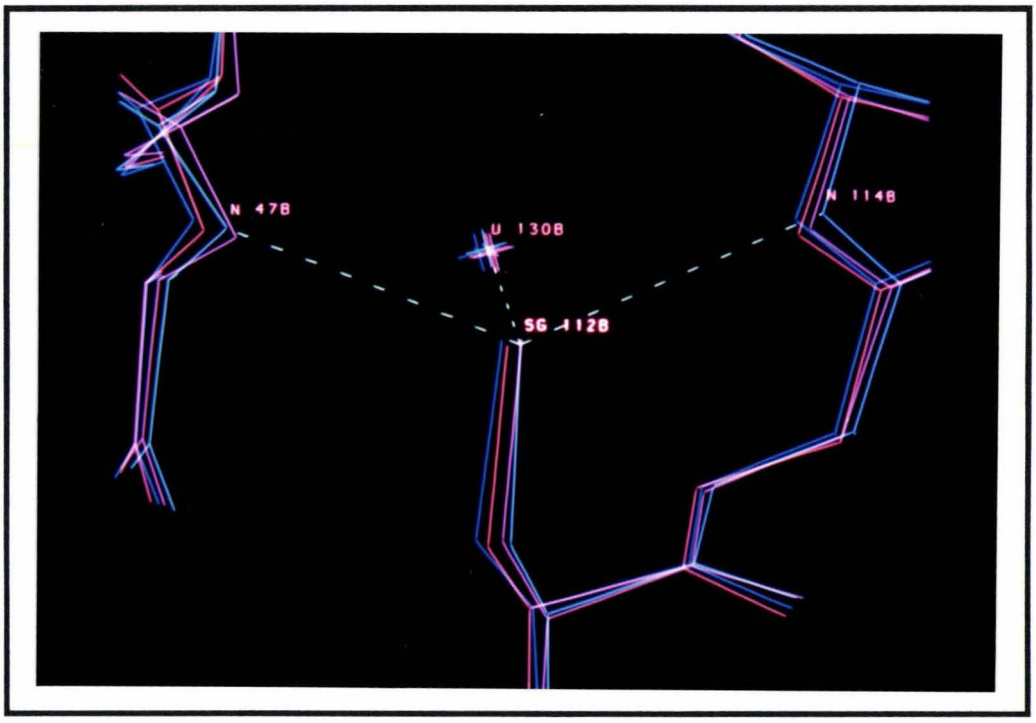

Figure 3.2.7.1. Changes in the S...HN hydrogen bonds at Cys-112. Superposition was done using the all of the main-chain atoms of residues 3-127. Oxidised azurin molecules in blue (A) and light blue (B), and reduced azurin molecules in red (A) and pink (B).

Table 3.2.7.1. Cys-112 S...HN hydrogen bond geometries of reduced and oxidised azurin. Differences in distances and angles are as reduced-oxidised.

	Cβ-Sγ...H angle (°)		Sγ...H distance (Å)		Sγ...N distance (Å)		Sγ...H-N angle (°)	
	A	B	A	B	A	B	A	B
Sγ...HN 47								
oxidised	104	110	2.53	2.48	3.52	3.45	170	167
reduced	104	105	2.41	2.34	3.37	3.29	160	159
change	**0**	**-5**	**-0.12**	**-0.14**	**-0.15**	**-0.16**	**-10**	**-8**
Sγ...HN 114								
oxidised	117	116	2.54	2.72	3.50	3.66	161	155
reduced	115	116	2.40	2.43	3.36	3.37	163	158
change	**-2**	**0**	**-0.14**	**-0.29**	**-0.14**	**-0.29**	**+2**	**+3**

(1.55Å)[34], the copper ligand sulphur of Cys-78 makes two S...H-N hydrogen bonds; one to N-H 41 and another to N-H 81. The S...HN hydrogen bond geometry of oxidised pseudoazurin is given in Table 3.2.7.2, and these bonds are longer by 0.1-0.2Å than those in oxidised azurin. In the blue copper protein plastocyanin, for which crystal structures have been determined in both the reduced and oxidised states[32,122], the corresponding thiolate sulphur makes only one hydrogen bond (S_γ 84...H-N 38) to a peptide nitrogen instead of two. The geometries of these interactions in plastocyanin and pseudoazurin have been calculated from coordinates deposited with the Brookhaven Protein Data Bank[210], and are given in Table 3.2.7.2.

Table 3.2.7.2. S...H-N hydrogen bond geometries of plastocyanin and pseudoazurin. Hydrogen atom positions at ≈1.0Å from the nitrogens were determined manually by using an interactive graphics system.

Plastocyanin					Pseudoazurin	
angle / distance	oxidised	reduced pH 3.8	reduced pH 7.0	apo	angle / distance	oxidised
S_γ 84...N 38	3.41Å	3.59Å	3.46Å	3.55Å	S_γ 78...N 41	3.61Å
S_γ 84...N 87	4.19Å	3.83Å	3.94Å	4.21Å	S_γ 78...N 81	3.76Å
Cu...S_γ 84...N 38	110°	97°	104°	-	Cu...S_γ 78...N 41	105°
Cu...S_γ 84...N 87	86°	108°	93°	-	Cu...S_γ 78...N 81	89°
S_γ 84...H-N 38	165°	170°	167°	167°	S_γ 78...H-N 41	161°
S_γ 84...H-N 87	126°	141°	146°	131°	S_γ 78...H-N 81	151°
S_γ 84...H 38	2.44Å	2.59Å	2.49Å	2.60Å	S_γ 78...H 41	2.65Å
S_γ 84...H 87	3.51Å	2.99Å	3.08Å	3.50Å	S_γ 78...H 81	2.86Å
Cu...S_γ 84...H 38	114°	99°	105°	-	Cu...S_γ 78...H 41	108°
Cu...S_γ 84...H 87	97°	117°	101°	-	Cu...S_γ 78...H 81	96°

In the structure of plastocyanin, there is no hydrogen bond directly analogous to the S...HN 114 hydrogen bond in azurin, because the residue equivalent to Phe-114 is a proline. However, the peptide nitrogen of residue 87, adjacent to Pro-86, is nearby and is directed at the sulphur of Cys-84 (S_γ 84...N 87 = 4.19Å). During the reduction of the copper site of plastocyanin, the S...H-N 38 hydrogen bond does not shorten, but appears to lengthen slightly by 0.18Å in the low pH form and by 0.05Å in the high pH form. In contrast, the distance between N 87 and S_γ 84 shortens considerably by 0.36Å in the low pH form and by 0.25Å in the high pH form. Although the S_γ 84...N 87 distances are long in the reduced plastocyanin (3.83-3.94Å), they are just outside the upper limit of a S...HN hydrogen bond (3.75Å)[242].

Shortening of S...HN hydrogen bonds on reduction has been previously reported in the $Fe_4S_4S(Cys)_4$ clusters of high potential iron protein (HiPIP)[242,243,325]. In HiPIP, the S...N hydrogen bond distances decrease by 0.07-0.19Å and the S...N-C angles change by as much as 10° when the metal cluster is reduced[325]. The overall change in the S...HN hydrogen bond geometry upon reduction is a shortening of the S...N distance to a similar extent to that seen in azurin. Although the S...HN angles do change slightly on reduction, they do not necessarily become more linear, another sign of increased hydrogen bond strength.

The shortening of the S...HN hydrogen bonds made to cysteine sulphurs in HiPIP has been explained as a response to the increase in negative charge at the redox site[325,326]. By increasing the electron density on the sulphur through the reduction of the metal site, the electrostatic interaction with the H-N group[326,327] is strengthened. *Ab initio* calculations conducted on S...HN hydrogen bond systems (where the sulphur is bound to an arbitrary atom in place of a metal), show that the increase in electronic charge at the

metal centre is transmitted on to the sulphur atom. This in turn, polarises the hydrogen bond further, thereby increasing the electrostatic interaction between donor and acceptor, and strengthening the hydrogen bond[327]. Strengthening of an S...H-N hydrogen bond also arises if the S...H-N angle becomes more linear[325], but there is no obvious change in the S...H-N angles in azurin. Figure 3.2.7.2 is a diagrammatic representation of the change in hydrogen bond stereochemistry at the thiolate sulphur in the copper site of azurin; note also that the sulphur atom appears to lift above the equatorial plane of the oxidised structure.

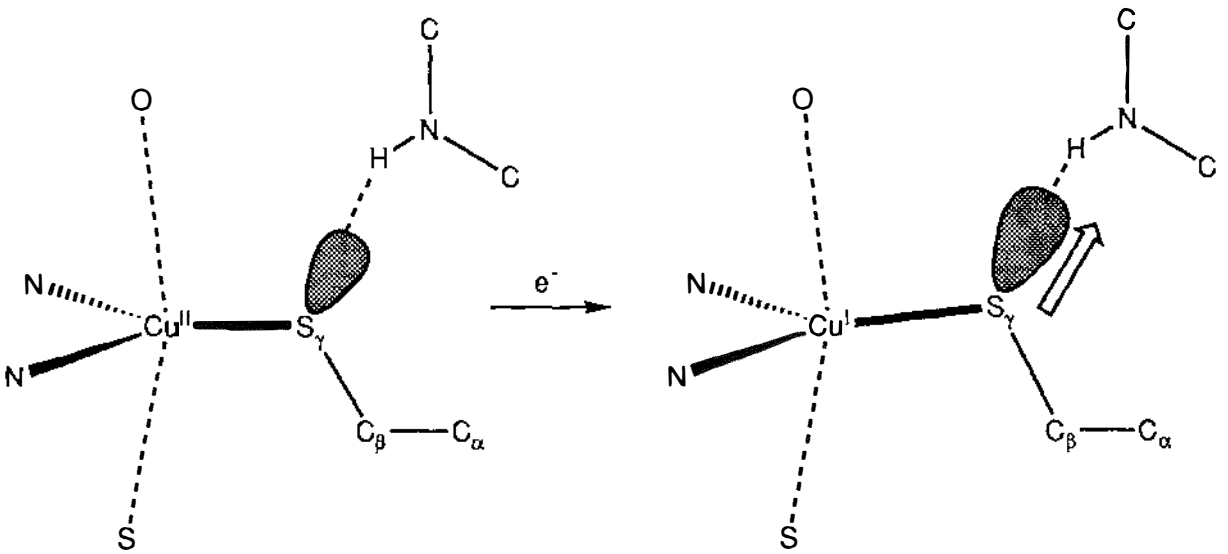

oxidised copper site **reduced copper site**

Figure 3.2.7.2. S...HN shift in azurin upon reduction. The shaded area represents a lone pair of electrons and shows an increase in the electron density on the sulphur atom.

One interesting point to note is that the decrease in S...N distances is roughly the same between HiPIP and azurin, but in HiPIP there is one electron distributed over four iron centres, while in azurin the electron is distributed over only a single copper centre. The shortening of the S...N distances would be expected to be smaller in HiPIP because the net increase in electronic charge is 1/4 electron, yet the change is comparable to that found in azurin. A possible explanation for this is that the Fe(III) centres are more electrostactic in nature than the Cu(II) centres which are more covalent, and thus the increase in charge is more influential. Also, the covalency of the Cu-S(Cys) bond is promoted by an extra S...HN hydrogen bond at the sulphur which draws away electronic charge from the lone pair of electrons that interact with the copper.

Carter *et al.* have proposed that the S...HN hydrogen bonds might stabilise the reduced state of FeS proteins by raising the redox potential[243]. The number of S...HN hydrogen bonds is considered to be one factor which could increase the redox potential of the Fe_4S_4

cluster by stabilising the extra negative charge on the redox site[326,328,329]. The effect is presumably partly responsible for the difference in redox potentials† of 400mV in ferredoxin (16 hydrogen bonds[242]) and -350mV in HiPIP (5 hydrogen bonds[242])[325,328]. For the blue copper proteins, the situation is reversed. Where azurin contains two S...HN hydrogen bonds and a reduction potential of 276mV[82], plastocyanin has only one S...HN hydrogen bond and a reduction potential of 370mV[122]. This difference is explainable since the $Fe_4S_4(Cys)_4$ clusters in ferredoxin and HiPIP are negatively charged sites, while the copper sites of azurin and plastocyanin are positively charged sites, and both redox sites reside in the hydrophobic interior of the protein. Consequently, the S...HN hydrogen bonds can only exert a stabilising effect when an extra negative charge is added to a negatively charged redox site[325]. The effect of S...HN interactions at a positively charged redox site, such as azurin, is the reverse, i.e. the extra S...HN hydrogen bonds destabilise the reduced state, because these hydrogen bonds withdraw electronic charge from the metal, creating a higher positive charge for the whole redox centre. However, the relative number of S...HN hydrogen bonds is not the only factor determining the redox potential, and work by Krishnamoorthi and Markley on different HiPIPs shows that the redox potentials are influenced by a combination of factors of which the number of S...HN hydrogen bonds is only one[328].

$N_{\varepsilon 2}$-H(His)...O Hydrogen bonds at His-46 and His-117

A similar effect between the oxidation state and hydrogen bond strength has also been proposed for those hydrogen bonds made to imidazole rings which are bound to a metal[330]. In the systems examined, the imidazole ring is bound to a haem iron through $N_{\varepsilon 2}$, while $N_{\delta 1}$ makes a hydrogen bond with a peptide carbonyl oxygen. The *ab initio* calculations done on this system indicated that the strength of the hydrogen bond is sensitive to the charge on the imidazole ring and therefore also the oxidation state of the metal. It was predicted that a more favourable hydrogen bond geometry would result in a greater stabilisation of the oxidised form. However, out of three haem proteins for which X-ray structural data is available in both oxidation states, only one protein (tuna cytochrome c) shows a significant difference in the $N_{\delta 1}$...O distance (≈1.0Å) between the oxidised and reduced forms. In the other cases, the differences in hydrogen bond geometry are comparable to or smaller than the level of error in the protein coordinates

† Note that the redox potentials of ferredoxin (Fd) and HiPIP are usually given as -400mV and +350mV, respectively, for oxidation:

$$Fd(Fe_4S_4Cys_4^{3-}) \rightarrow Fd(Fe_4S_4Cys_4^{2-}) + e^- \qquad E°=-400mV$$
$$HiPIP(Fe_4S_4Cys_4^{2-}) \rightarrow HiPIP(Fe_4S_4Cys_4^{1-}) + e^- \qquad E°=+350mV$$

However, the redox potentials given in the text are for reduction.

(≈0.1Å).

In azurin any changes in hydrogen bonds to the imidazole ligands are barely detectable considering the magnitude of the error in atom positions. For His-46, the $N_{\varepsilon 1}...O$ distance increases by 0.17Å in one protein molecule, but decreases by 0.05Å in the other, while the $N_{\varepsilon 1}$-H...O angle becomes more linear in both molecules. (Note that the imidazole ring binds through $N_{\delta 1}$ to the metal in the blue copper proteins, not $N_{\varepsilon 2}$ as for the haem proteins.) No indication of a change is apparent for the hydrogen bond between the His-117 and OW 162. This is not surprising since the error in position of a water molecule at this resolution is probably more than 0.2Å. Tables 3.2.7.3 & 3.2.7.4 list the hydrogen bond geometries for the side-chains of His-46 and His-117 of azurin. Overall there are no changes seen in the hydrogen bonds of the side-chains of His-46 and His-117 during reduction, except for possibly the $N_{\varepsilon 1}$ 46-H...O 10 angle.

Table 3.2.7.3. Changes in the hydrogen bond geometry of His-46 $N_{\varepsilon 2}$-O 10.

	C-$N_{\varepsilon 2}$...O angle (°)		$N_{\varepsilon 2}$...O distance (Å)		H...O distance (Å)		$N_{\varepsilon 2}$-H...O angle (°)	
	A	B	A	B	A	B	A	B
oxidised	119	121	2.81	2.60	1.85	1.67	161	154
reduced	121	125	2.76	2.77	1.77	1.80	169	165
Δ	+2	+4	-0.05	+0.17	-0.08	+0.13	+8	+9

Table 3.2.7.4. Changes in the hydrogen bond geometry of His-117 $N_{\varepsilon 2}$-OW 162.

	C-$N_{\varepsilon 2}$...OW angle (°)		$N_{\varepsilon 2}$...OW distance (Å)		H...OW distance (Å)		$N_{\varepsilon 2}$-H...OW angle (°)	
	A	B	A	B	A	B	A	B
oxidised	126	119	2.65	2.78	1.65	1.79	177	170
reduced	120	123	2.72	2.72	1.75	1.74	161	166
Δ	-6	+3	+0.07	-0.06	+0.10	-0.05	-16	-4

Changes at His-35 and Met-44

Much interest has focussed on His-35 in azurin because it has been suggested to be involved in electron transfer and to play a role in the pH dependence of the electron transfer rate with cytochrome c_{551} [153]. Although site directed mutagenesis studies have now shown that His-35 is not involved in electron transfer with cytochrome c_{551} [156], and crystallographic studies have identified the pH dependent structural change as being due to a peptide flip[41] (see Chapter 1), this residue is structurally important since it provides a packing constraint for the copper ligand of His-46. Results from the consistent shift analysis show a net average shift of 0.20Å (θ=44°) in the side-chain of His-35. Changes in this region show that the side-chain of His-35 forms a more linear hydrogen bond with the carbonyl oxygen of Met-44 (see Table 3.2.7.5). The change in the geometry appears

as shifts in the $N_{\varepsilon 2}$-H...O and H...O-C angles of +18° and +9°, respectively. The O-C... $N_{\varepsilon 2}$ angle also changes on average by 9° (14° and 5° in oxidised and reduced azurin, respectively). At the same time the mean planes of the Met-44-Gly-45 peptide and the imidazole ring of His-35 become more coplanar upon reduction (the angle between them decreasing from 11° to 5°). Inspection of this region by superimposing all of the molecules of oxidised and reduced forms illustrates that the changes are actually due to the shifts in the main-chain of Met-44 (mean shift of 0.23Å, θ=41°) rather than the shifts in His-35 (see Figures 3.2.7.3 and 3.2.7.4). Although the changes in orientation seem consistent, the H...O hydrogen bond length change, however, is far from consistent (Table 3.2.7.5), suggesting some error in this region.

Table 3.2.7.5. Changes in the hydrogen bond geometry of His-35 $N_{\varepsilon 2}$-O 44. Differences in distances and angles are given as reduced-oxidised.

	$N_{\varepsilon 2}$-H...O angle (°)		$N_{\varepsilon 2}$...O distance (Å)		H...O distance (Å)		H...O-C angle (°)	
	A	B	A	B	A	B	A	B
oxidised	154	155	2.91	2.91	2.02	1.99	148	151
reduced	168	176	3.00	2.62	2.07	1.65	155	162
Δ	+14	+21	+0.09	-0.29	+0.05	-0.34	+7	+11

The net shift in the carbonyl group of Met-44 is also apparent in the main-chain torsion angle ψ. Upon reduction, the ψ angle for Met-44 decreases on average by 14° (11° and 16° for molecules A and B, respectively). This change in the ψ angle of Met-44 is also accompanied by other nearby changes in the main-chain torsion angles from Met-44 to Asn-47. Table 3.2.7.6 lists these changes between the the oxidised and the reduced forms of azurin, which presumably result from changes in the O 45 interaction to copper, and the S...HN hydrogen bond between Cys-112 and Asn-47. Although the changes are small (the r.m.s. deviation in main-chain torsion angles is 6° and 7° for the reduced and oxidised structures, respectively), they are the same in both molecules of the asymmetric unit. Figure 3.2.7.5 illustrates these changes in the segment of residues from Met-44 to Asn-47.

Table 3.2.7.6. Main-chain torsion angle changes in the stretch of residues from Met-44 to Asn-47. Changes above 10° in magnitude are given in bold. Differences are oxidised-reduced values.

	Molecule A		Molecule B		Average Δ	
	Δφ	Δψ	Δφ	Δψ	<Δφ>	<Δψ>
Met-44	0	**+11**	-7	**+16**	-4	**+14**
Gly-45	-6	**+14**	**-11**	+8	-9	**+12**
His-46	-3	**+9**	-5	**+14**	-4	**+12**
Asn-47	-9	+9	-6	+7	-8	+8

Figure 3.2.7.3. View of the side-chain of His-35, normal to the imidazole ring, showing the shift in the imidaziole ring away from the copper site. Oxidised azurin molecules in blue (A) and light blue (B), and reduced azurin molecules in red (A) and pink (B).

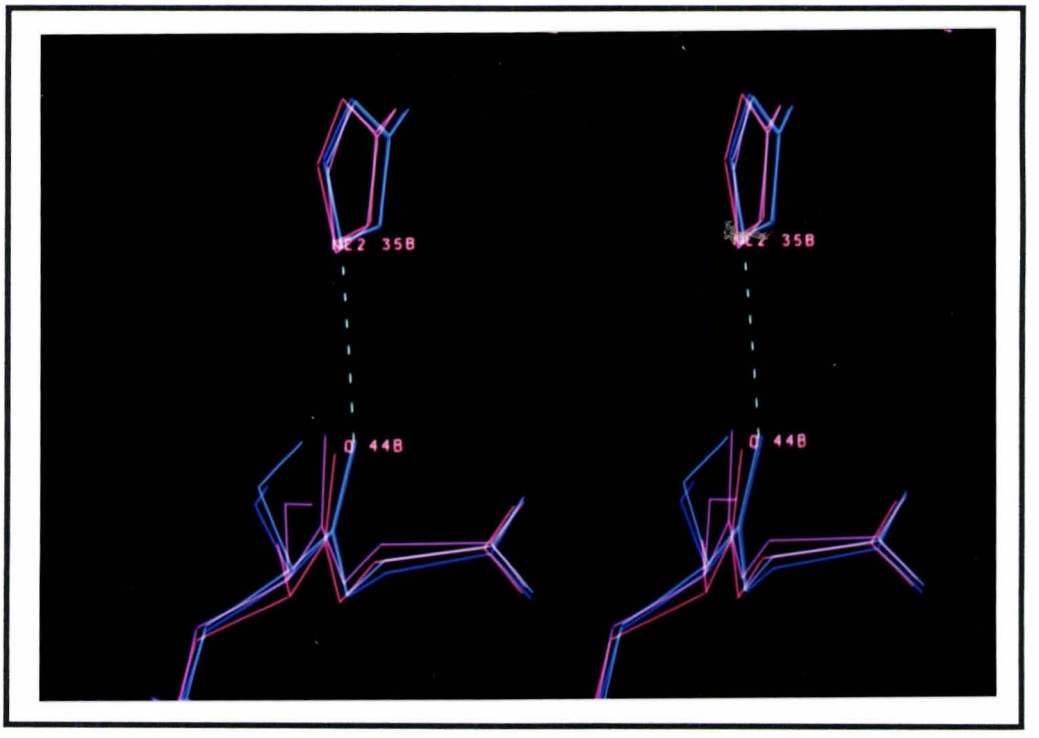

Figure 3.2.7.4. View of the $N_{\varepsilon 2}$ 35...O 44 hydrogen bond showing the twist in the Met-44 main-chain. Oxidised azurin molecules in blue (A) and light blue (B), and reduced azurin molecules in red (A) and pink (B).

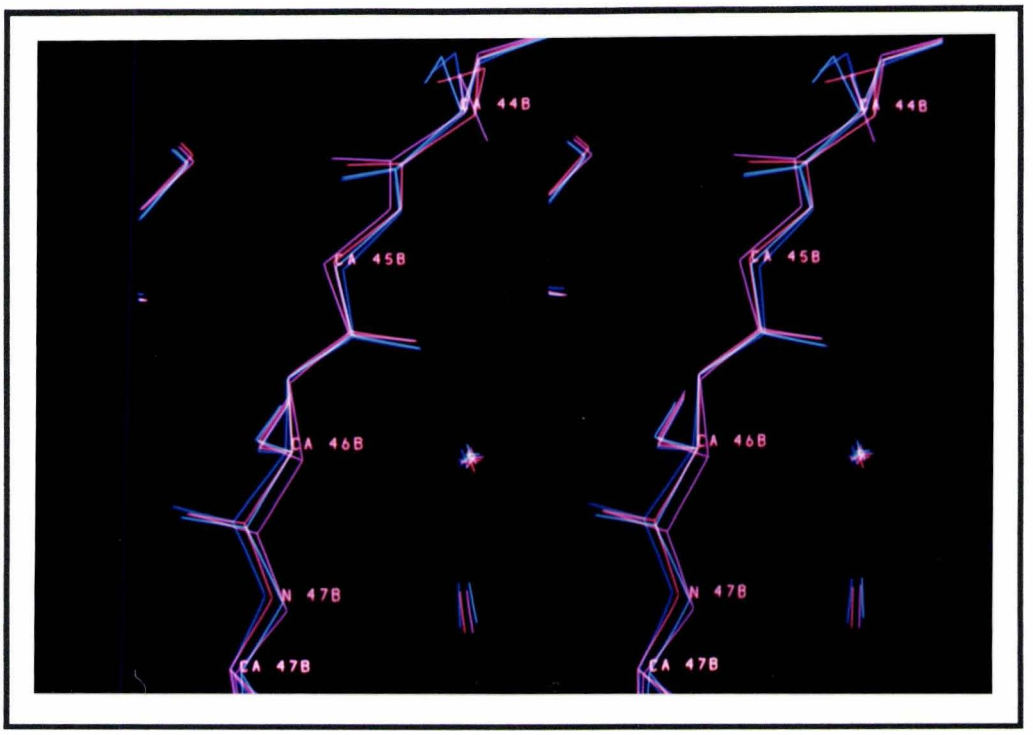

Figure 3.2.7.5. Stereo view of the changes in the stretch of residues from Met-44 and Asn-47. Oxidised azurin molecules in blue (A) and light blue (B), and reduced azurin molecules in red (A) and pink (B).

Figure 3.2.7.6. Change in the Pro-115-Gly-116 section of the polypeptide chain upon reduction of the copper site of azurin. Oxidised azurin molecules in blue (A) and light blue (B), and reduced azurin molecules in red (A) and pink (B).

Changes in residues 115-116

Another change in the copper environment occurs in the loop between Phe-114 and His-117, which forms part of the hydrophobic patch. For Pro-115 and Gly-116, the atoms move on average 0.24Å in the direction away from the copper site (θ=29°). The change is illustrated in Figure 3.2.7.6. A plausible explanation for this change is that the shift is a consequence of the increase in the Cu-$N_{\delta 1}$ 117 bond length on reduction. On the opposite side of the imidazole ring of His-117 from the copper atom, a contact is made between $C_{\delta 2}$ 117 and O 115 (average distance 3.22Å and 3.14Å in oxidised and reduced azurins, respectively). Upon reduction, as the Cu-$N_{\delta 1}$ 117 bond length increases, and the imidazole ring shifts away from the from the copper atom, it is possible that the $C_{\delta 2}$ atom of His-117 pushes against the carbonyl oxygen of Pro-115, and hence the 115-116 peptide, causing the change seen in Figure 3.2.7.6.

Other changes

The remaining residues which can be considered to constrain the configuration of the copper site, do not show any significant changes upon reduction. The side-chain of His-117 is sandwiched between the side-chains of Phe-114 and Met-13. Despite the shift in the imidazole ring of His-117 caused by the increase in the bond to the copper, neither of the side-chains of Phe-114 or Met-13 moves significantly in any way. This supports the view that the His-117 ligand to the copper is constrained by these contacts. Similarly, the surrounding environment of Met-121 also shows little change on reduction. The only change, as suggested by the consistent shift analysis, is at Tyr-15, where the average shift is 0.15Å (θ=25°) and 0.18Å (θ=48°), for the main-chain and side-chain atoms, respectively. However, the shift appears to have little or no effect on the other parts of the protein (see Figure 3.2.7.7).

Overall, some changes are observed in the protein environment surrounding copper site when the protein is reduced. These changes, however, are small, but can be detected by comparing the changes in the two independent molecules of the asymmetric unit. The largest change is in the hydrogen bonding of the thiolate sulphur of Cys-112, where the N...S(thiolate) distances shorten on average by 0.2Å upon the reduction of the copper site. Elsewhere, smaller changes are observed. A consistent shift is seen in the region of Pro-115 to Gly-116, which may be a result of the increase in the Cu-$N_{\delta 1}$ 117 bond. Other changes appear in the section of chain around Gly-45.

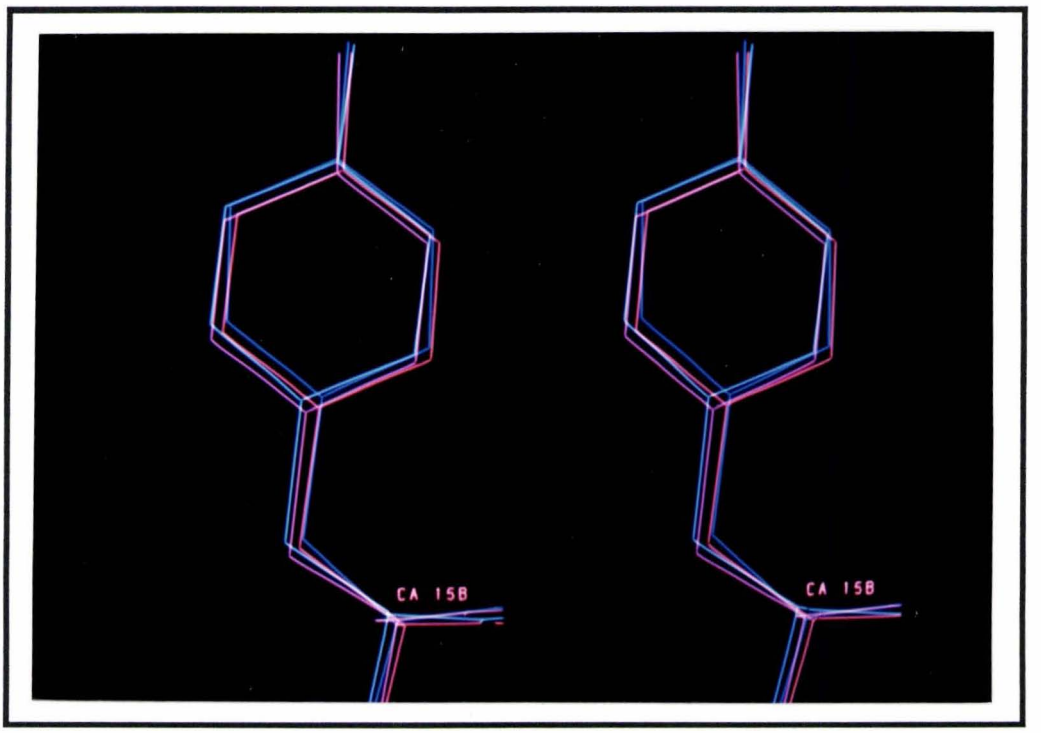

Figure 3.2.7.7. Stereoview of the small shift in Tyr-15, which packs against the copper ligand Met-121, upon reduction. Oxidised azurin molecules in blue (A) and light blue (B), and reduced azurin molecules in red (A) and pink (B).

3.2.8 Surface features of reduced azurin

All of the surface features of reduced azurin are essentially the same as in the oxidised structure. A few minor changes which may be due to the oxidation state change appear in the hydrophobic patch. The distance between the opposing side-chains of His-117 of the two molecules in the asymmetric unit has shrunk by 0.12Å to a value of 6.50Å. This is expected since the increase in Cu-$N_{\delta 1}$ 117 bond length pushes the imidazole rings of the opposing molecules towards each other (see Figure 3.2.8.1). Also, the angle between the mean planes defined by the imidazole rings of His-117 increases from 25.8° to 35.9°. Other changes in the hydrophobic patch are at Pro-115, Gly-116 and Trp-118, previously described.

At the sulphate site of reduced azurin, the anion is bound by the same two hydrogen bonds as in the oxidised structure, from the $N_{\varepsilon 2}$ atom of His-83 and the peptide NH of Gly-76. As the thermal parameters suggest, the sulphate anion is probably only partially occupied or disordered in the site (average B=91$Å^2$). Figure 3.2.8.2 shows the orientation of the sulphate in the binding site of azurin for four separate protein molecules, two from reduced azurin and two from oxidised azurin. Much variation exists in the position and orientation of the anion, but most of the water structure which surrounds the sulphate anion is maintained upon reduction. Twenty-eight water molecules

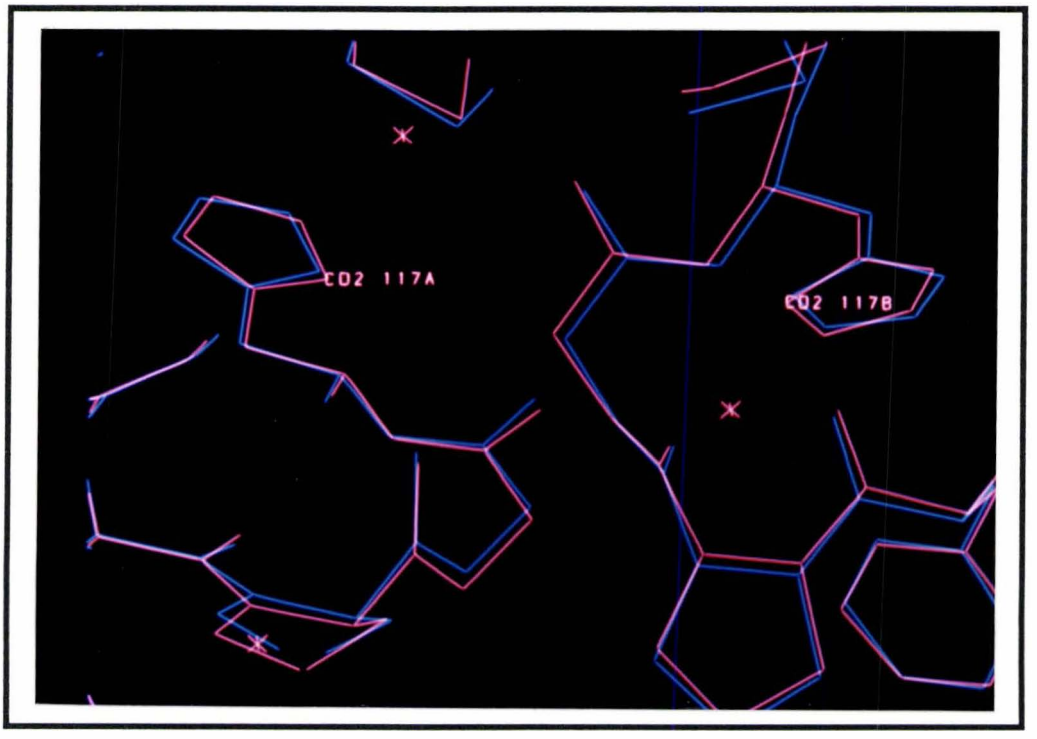

Figure 3.2.8.1. Changes in the orientation of the two opposing His-117 side-chains which are at the centre of the hydrophobic patches. Oxidised azurin molecules in blue and reduced azurin molecules in red.

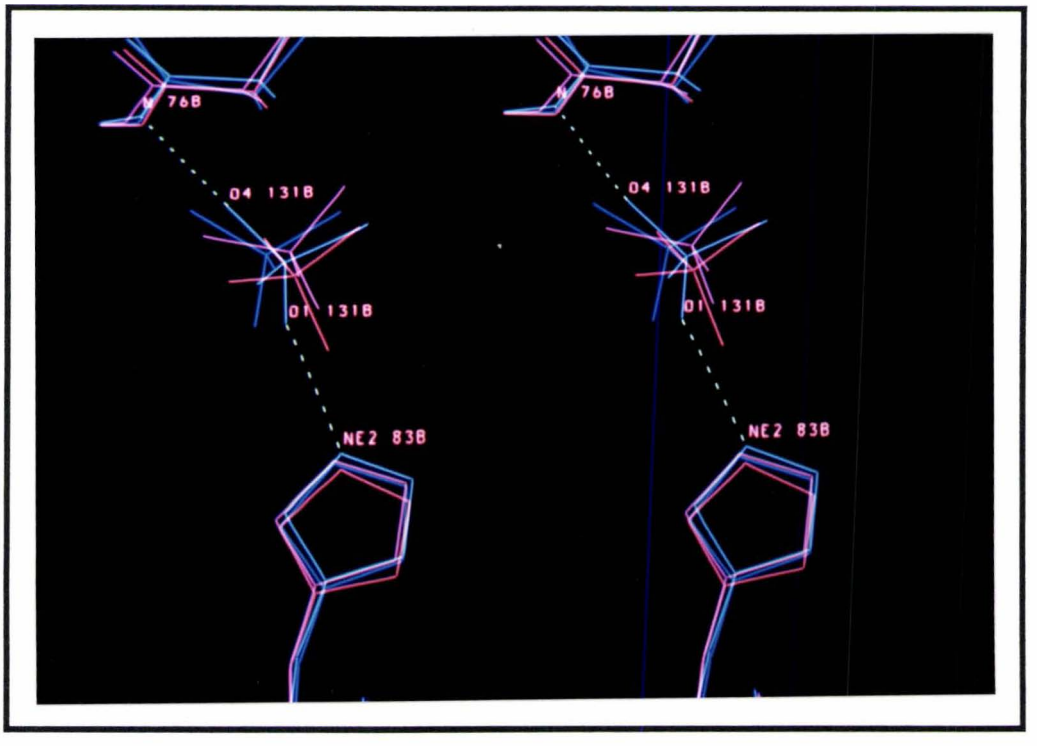

Figure 3.2.8.2. The sulphate site of oxidised and reduced azurin. Oxidised azurin molecules in blue (A) and light blue (B), and reduced azurin molecules in red (A) and pink (B).

associated with the sulphate sites are found in both redox forms of azurin (15 in molecule A and 13 in molecule B). These waters are in the crevice formed between the "flap" and the β-sandwich, and are hydrogen bonded to the protein and/or to the sulphate anion. The few water molecules which are not found in both forms of azurin are located further away from the protein in the solvent medium (see section 3.2.10 for the analysis of the solvent structure).

Table 3.2.8.1. Salt bridge geometries in oxidised and reduced azurin. Distances (Å) are H...O, and angles (°) are N-H...O and H...O-C; or if no hydrogen atom position could be calculated N...O, C-N...O and N...O-C. Values in bold belong to salt bridges which are common between all molecules of oxidised and reduced azurin.

Salt bridge	Oxidised azurin						Reduced azurin					
	molecule A			molecule B			molecule A			molecule B		
	angle	dist	angle	angle	dist	angle	angle	dist	angle	angle	dist	angle
Nζ 34...Oε1 8	155	3.08	116	-	-	-	-	-	-	-	-	-
Nζ 126...Oε1 19	-	-	-	87	2.64	117	-	-	-	-	-	-
Nζ 24...129 Oε	-	-	-	117	2.90	161	-	-	-	-	-	-
Nζ 27...98 Oδ1	-	-	-	-	-	-	160	2.70	104	-	-	-
Nζ 41...91 Oε1	120	3.24	126	-	-	-	-	-	-	-	-	-
Nζ 56...Oε1 53	-	-	-	-	-	-	-	-	-	97	3.47	138
Nζ 122...Oε1 53	129	2.61	128	112	3.40	134	-	-	-	-	-	-
Nζ 74...Oδ1 62	166	2.79	125	-	-	-	177	2.64	124	-	-	-
Nη2 79...Oδ1 62	**106**	**1.74**	**132**	**138**	**2.13**	**112**	**113**	**2.03**	**101**	**139**	**2.30**	**95**
Nε 79...Oδ1 77	**151**	**2.02**	**104**	**168**	**1.64**	**131**	**107**	**2.92**	**121**	**163**	**2.03**	**108**
Nη2 79...Oδ1 77	**136**	**1.71**	**116**	**155**	**1.82**	**102**	**124**	**2.18**	**108**	**151**	**1.52**	**114**
Nζ 85...93 Oδ1	-	-	-	128	3.38	113	-	-	-	134	3.03	107

In the structure of oxidised azurin, charged side-chains are evenly distributed over the surface of the protein, yet only one salt bridge is common to the two independent protein molecules[31]. This involves three residues; Asp-62, Asp-77 and Arg-79. A similar situation exists in reduced azurin. The same salt bridge appears in both reduced azurin molecules, although the precise nature of the interaction appears to vary. The difference, however, is probably a result of poor definition in this region. The other salt bridges in azurin are distributed over the rest of the structure (see Table 3.2.8.1), but all involve poorly defined side-chains.

3.2.9 Thermal parameters

In general, the thermal parameters of reduced azurin are very similar to those of the oxidised structure. Figure 3.2.9.1 illustrates the extent of the similarities in the average main-chain B-values for each residue between the oxidised and reduced structures. The thermal parameters of reduced azurin are on average higher by 2.83Å^2, which is a reflection of the overall B-value of the reduced crystal structure with respect to the

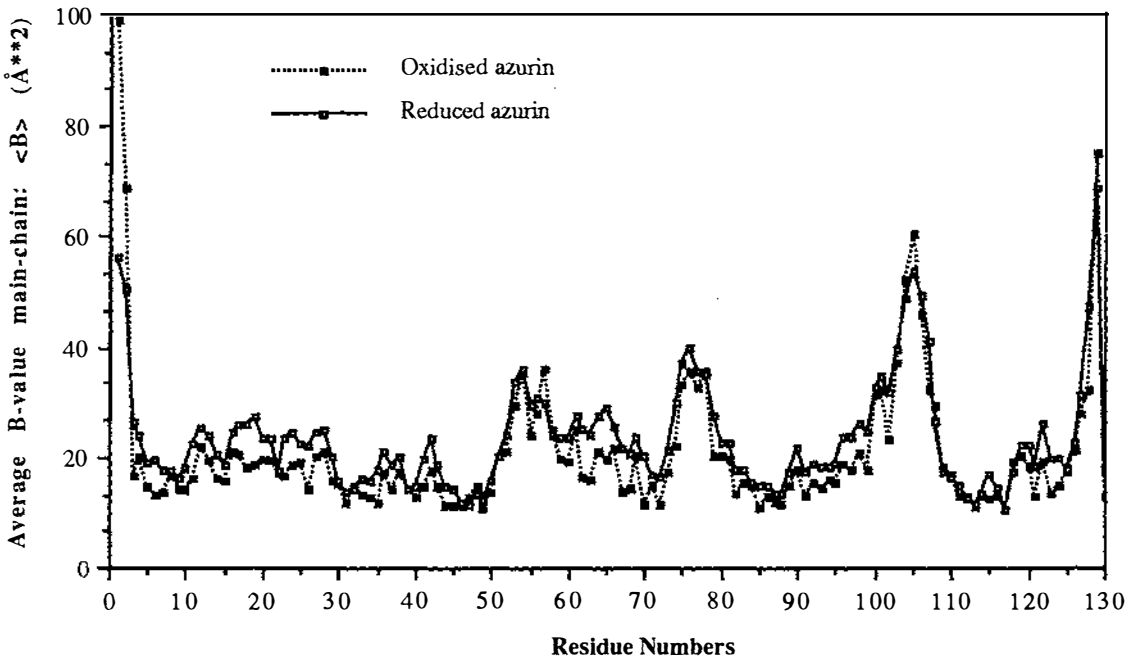

Figure 3.2.9.1. Plot of the average main-chain B-value against residue number for oxidised and reduced azurins.

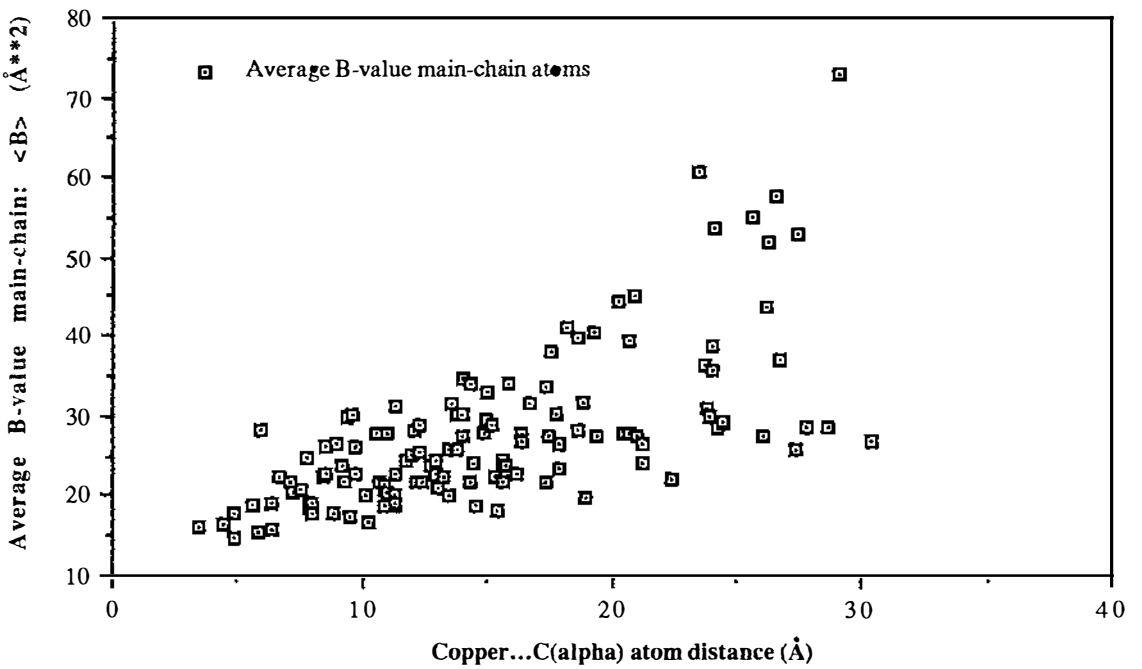

Figure 3.2.9.2. Plot of average main-chain B-value against the distance to the copper atom for reduced azurin.

oxidised structure.

The thermal parameters of both redox forms make structural sense. The lowest B-values occur for internal atoms, which are constrained by the steric packing forces of surrounding atoms. Thermal parameters are also low for main-chain atoms of the β-strands and the loops surrounding the copper site (averages of 24Å^2 and 22Å^2, respectively). When the average main-chain B-value is plotted against the distance from the copper atom to the C_α atom of each residue, it is apparent that the protein becomes more constrained closer to the copper site.

The largest differences in the thermal parameters of reduced azurin compared with oxidised azurin are at the N-terminus of the polypeptide chain. Here the B-values are lower in the reduced structure than in the oxidised structure; 56Å^2 compared to 99Å^2. The reason for this is unclear, but it suggests that the conformation in oxidised azurin could be in error.

3.2.10 Solvent structure

The solvent molecules in the crystal structure of reduced azurin have been modelled as water molecules except for three sulphate anions, one in the sulphate site of each protein molecule (see section 3.2.8), and one which is tentatively assigned as a sulphate ion on a 2-fold crystallographic axis. No water molecules are located in the protein interior, but two are buried in pockets created by the packing of the hydrophobic patches of the two independent azurin molecules. These two water molecules are related by the 2-fold non-crystallographic axis, and each makes three hydrogen bonds bridging the two protein molecules; two interactions to one protein molecule ($N_{\varepsilon 2}$ 117 and O 43) and another to the opposing protein molecule (O 116) (see Figure 3.2.10.1). Similarly, many of the other water molecules (140 of 258 in total) are also related by the same 2-fold non-crystallographic axis (these are discussed further in section 3.3.10).

The differences in solvent structure between oxidised and reduced azurin are few and small, not surprisingly since the two crystal forms are isomorphous. As compared to oxidised azurin[31], slightly fewer solvent molecules have been located in the crystal structure of reduced azurin (258 verses 281 molecules). Of these, 195 (94 in molecule A and 101 in molecule B) are within 2.0Å of a solvent molecule position in the oxidised structure. These "common" solvent molecules are labelled with the corresponding solvent number in oxidised azurin. Figure 3.2.10.2 illustrates the even distribution of the solvent

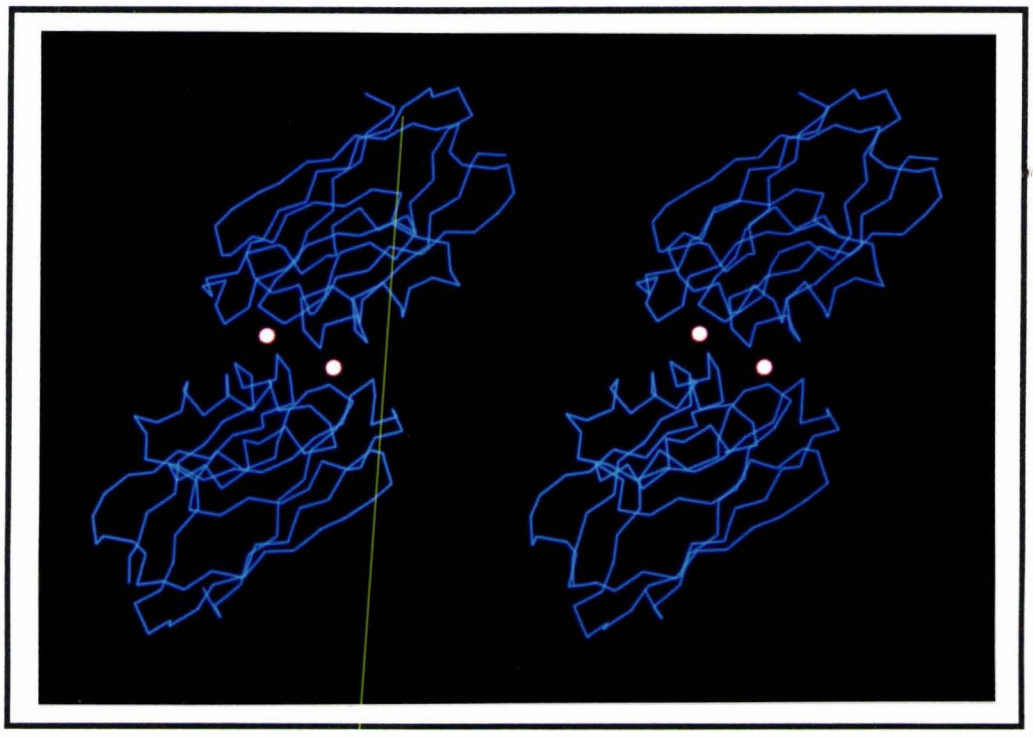

Figure 3.2.10.1. The two solvent molecules in reduced azurin buried in the pockets between the hydrophobic patches of the two independent azurin molecules. C_α trace in blue, and solvent molecules in white.

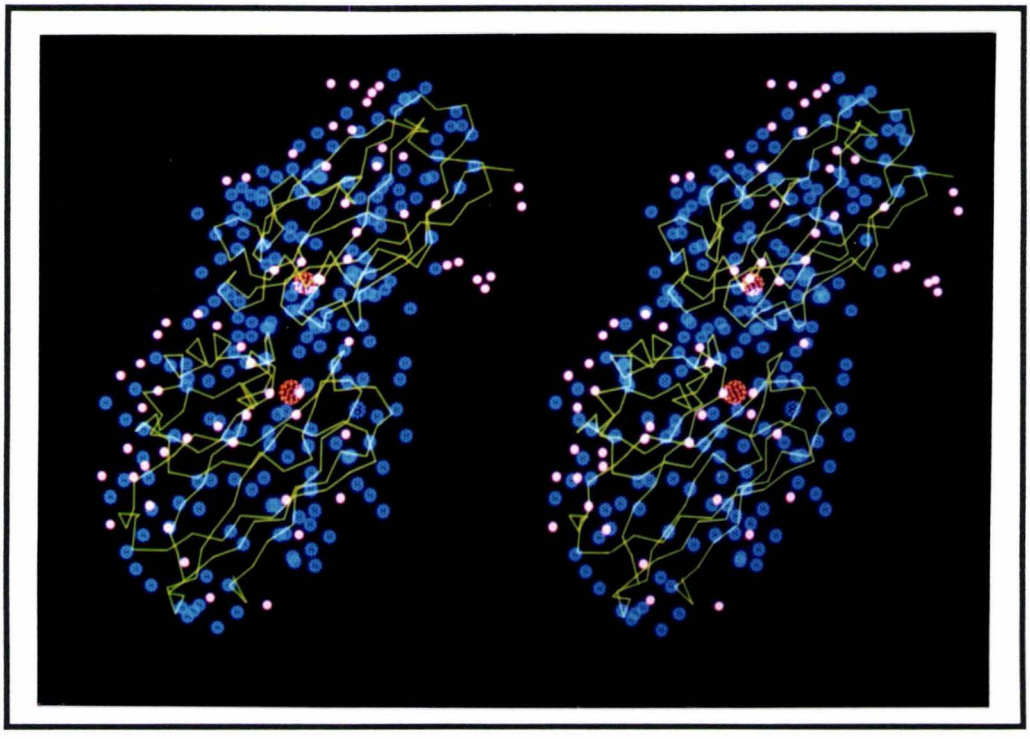

Figure 3.2.10.2. Solvent structure of reduced azurin. Large blue spheres are solvent molecules which are "common" to oxidised azurin, and small pink spheres are those which are "unique" to reduced azurin. The copper atoms are shown in orange, and the C_α trace in green..

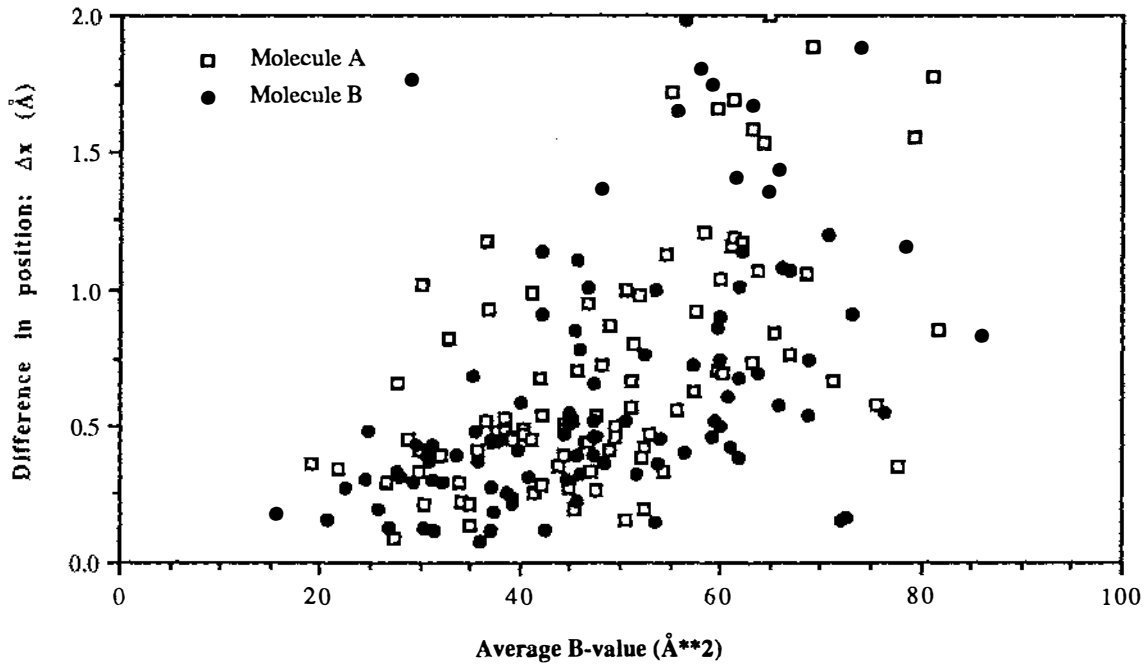

Figure 3.2.10.3. Plot of the differences in position of the solvent molecules between oxidised and reduced azurin.

around the two reduced azurin molecules. Those solvent molecules which are not close to a corresponding solvent molecule position in oxidised azurin, i.e. are "unique" to reduced azurin, are relatively few (total 63) and are more poorly defined than the other solvent molecules. The average B-value of these "unique" solvent molecules is higher (74Å^2) than those that are "common" (52Å^2). Of these, 28 are associated with molecule A and 35 with molecule B (see Figure 3.2.10.2). They are also distributed evenly over the surface of the protein. Possible reasons for these "unique" solvent molecules not being found in oxidised azurin are 1) their electron density is too close to the noise level to be detected, 2) they were missed in the oxidised structure or 3) they are errors in the reduced structure. (In the coordinate file, these solvent molecules are numbered above 300.)

The differences in the positions of the solvent molecules which are "common" between reduced and oxidised azurin are correlated with the average B-value of the solvent molecule (see Figure 3.2.10.3). Solvent molecules with a low average B-value typically show smaller differences in position betwen the two redox forms than those with a high average B-value. This suggests that the differences in the solvent structure between the two redox forms are smallest for those solvent molecules which are well ordered in both structures.

3.3 Comparison of the two independent molecules

As for oxidised azurin, the crystal structure of reduced azurin contains two independent molecules in the asymmetric unit[31]. These two molecules are related by a 2-fold non-crystallographic axis and are essentially identical in structure. Although this effectively doubles the size of the crystallographic problem, a comparison between the two independent molecules can give an indication of the accuracy of the structure and the reliability of different regions. The usual method for determining the overall accuracy of the model is from an analysis of the agreement between the observed and calculated structure factors (i.e. a Luzzati plot[232], see section 3.1), but this method assumes that all errors in the structure are randomly distributed through out the structure[232]. However, more detailed information on the accuracy of the structure is available from the comparison of the two reduced azurin molecules since they were treated independently during refinement. Differences between the two independent molecules may indicate errors, regions of flexible structure, or regions affected by crystal packing forces. The analyses presented below show, as expected, that flexibility in the protein structure occurs at the surface and in the loops between secondary structural elements, while the structure around the copper site appears to be better defined than the rest of the protein.

3.3.1 Intermolecular Contacts

Since the two molecules of reduced azurin are found in a pseudo-tetragonal cell (see section 3.2.1), many of the lattice contacts to adjoining molecules are similar between the two independent molecules. Fourteen intermolecular hydrogen bonds are made between molecule A and other protein molecules of the crystal lattice, while 15 intermolecular hydrogen bonds are found for molecule B. Differences between the two molecules occur only at residues 2,4,24,36,57,61,65,92 and 129. For many of the differences in the lattice contacts between the two molecules, either one or both of the groups involved are associated with regions of the protein structure which have high thermal parameters and poorly defined electron density (e.g. the N- and C-termini). None of the lattice contacts are salt bridges. Table 3.3.1.1 lists the intermolecular hydrogen bonds of reduced azurin and the symmetry operations required to generate the neighboring molecules.

There are other intermolecular contacts less than 3.5Å, which are not hydrogen bonds. Four of these occur across the interface between the hydrophobic patches of the molecules A and B. A further two intermolecular contacts are more isolated; between the side-chains of residues Ser-94A and His-32B, and between the main-chain of residue

Table 3.3.1.1. Intermolecular hydrogen bonds in reduced azurin

Hydrogen bond	Distance (Å)	Symmetry operation	Hydrogen bond	Distance (Å)	Symmetry operation
			$N_{\varepsilon 2}$ 2B-O 57B	3.25	1-x,-1/2+y,1/2-z
			$N_{\varepsilon 2}$ 2B-OG1 61B	2.85	1-x,-1/2+y,1/2-z
			$O_{\varepsilon 2}$ 4B-O_{γ} 92A	3.17	-1/2+x,1/2+y,z
$O_{\delta 2}$ 23A-$N_{\delta 2}$ 65A	2.73	-1/2+x, 1/2-y,-z	$O_{\delta 2}$ 23B-$N_{\delta 2}$ 65B	2.79	1-x,-1/2+y,1/2-z
O 24A-N 68B	2.89	-1/2+x, 1/2-y,-z	O 24B-N 68A	2.88	-x,1/2+y,1/2-z
N_{ζ} 24A-$O_{\delta 1}$ 129B	3.12	1/2-x,-y,-1/2+z	N_{ζ} 24B-$O_{\delta 1}$ 129A	2.80	1/2-x,-y,-1/2+z
O 38A-N 40A	2.77	1/2-x,y,1/2-z	O 38B-N 40B	2.76	x,-y,-z
N 40A-O 38A	2.77	1/2-x,y,1/2-z	N 40B-O 38B	2.76	x,-y,-z
			O 57B-$N_{\varepsilon 2}$ 2B	3.25	1-x,-1/2+y,1/2-z
			$O_{\gamma 1}$ 61B-$N_{\varepsilon 2}$ 2B	2.85	1-x,-1/2+y,1/2-z
$N_{\delta 2}$ 65A-$O_{\delta 2}$ 23A	2.73	-1/2+x, 1/2-y,-z	$N_{\delta 2}$ 65B-$O_{\delta 2}$ 23B	2.79	1-x,-1/2+y,1/2-z
$N_{\delta 2}$ 65A-O 129A	3.20	1/2+x,1/2-y,-z			
N 68A-O 24B	2.88	-x,1/2+y,1/2-z	N 68B-O 24A	2.89	-1/2+x, 1/2-y,-z
O_{γ} 92A-$O_{\varepsilon 2}$ 4B	3.17	-1/2+x,1/2+y,z			
O 129A-$N_{\delta 2}$ 65A	3.20	1/2+x,1/2-y,-z			
$O_{\delta 1}$ 129A-N_{ζ} 24B	2.80	1/2-x,-y,-1/2+z	$O_{\delta 1}$ 129B-N_{ζ} 24A	3.12	1/2-x,-y,-1/2+z

Table 3.3.1.2. Non-hydrogen bonding lattice contacts of reduced azurin. [a] Disordered side-chain of Gln-57.

Lattice Contact	Distance (Å)	Symmetry operation	Lattice Contact	Distance (Å)	Symmetry operation
			C_{β} 1B-N_{ζ} 34A	3.29	-1/2+x,1/2+y,z
			S_{δ} 13B-C_{ε} 120A	3.14	x,y,z
C_{ε} 13A-C_{ε} 13B	3.06	x,y,z	C_{ε} 13B-C_{ε} 13A	3.06	x,y,z
			$C_{\varepsilon 1}$ 32B-O_{γ} 94A	3.24	-1/2+x,1/2+y,z
N_{ζ} 34A-C_{β} 1B	3.29	-1/2+x,1/2+y,z			
			O 43B-C_{β} 119A	3.43	x,y,z
			[a]$N_{\varepsilon 1}$ 57B-C_{α} 90A	3.42	-x,y,1/2-z
C_{α} 90A-$N_{\varepsilon 1}$ 57B[a]	3.42	-x,y,1/2-z			
O_{γ} 94A-$C_{\varepsilon 1}$ 32B	3.24	-1/2+x,1/2+y,z			
O 115A-C_{α} 116B	3.39	x,y,z	O 115B-C_{α} 116A	3.30	x,y,z
C_{α} 116A-O 115B	3.30	x,y,z	C_{α} 116B-O 115A	3.39	x,y,z
C_{β} 119A-O 43B	3.43	x,y,z			
C_{ε} 120A-S_{δ} 13B	3.14	x,y,z			

90A and the disordered side-chain of Gln-57B. Table 3.3.1.2 lists those lattice contacts which are not hydrogen bonds.

Many intermolecular contacts are made via bridging water molecules. Twenty-six solvent molecules link together crystallographically different protein molecules in the crystal structure. Of these 26, only three are found for both of the molecules of the asymmetric unit, OW 137, OW 139 and OW 162.

3.3.2 Conformational angles

Main-chain torsion angles (ϕ,ψ)

The main-chain conformational angles for the two molecules of reduced azurin are represented as Ramachandran plots in Figures A.1 and A.2 of Appendix A. The ϕ and ψ angles of the two molecules agree well for the bulk of the structure. The r.m.s. deviation for 95% of the main-chain structure is 8.5° for ϕ angles, and 7.7° for ψ angles. The largest differences in the main-chain torsion angles, where $\Delta\phi$ or $\Delta\psi > 30°$, appear at residues 2-3, 74-75, 105-106 and 127-128. The differences at residues 2-3 and 127-128 are associated with the polypeptide chain termini, which have high thermal parameters and appear to have different conformations. The other regions are associated with loops of the structure. Residues 105-106 and 74-75 are parts of long unrestrained loops on the surface of the protein, and are poorly resolved in electron density maps. Figure 3.3.2.1 plots the differences in ϕ, ψ angles between the two molecules of reduced azurin.

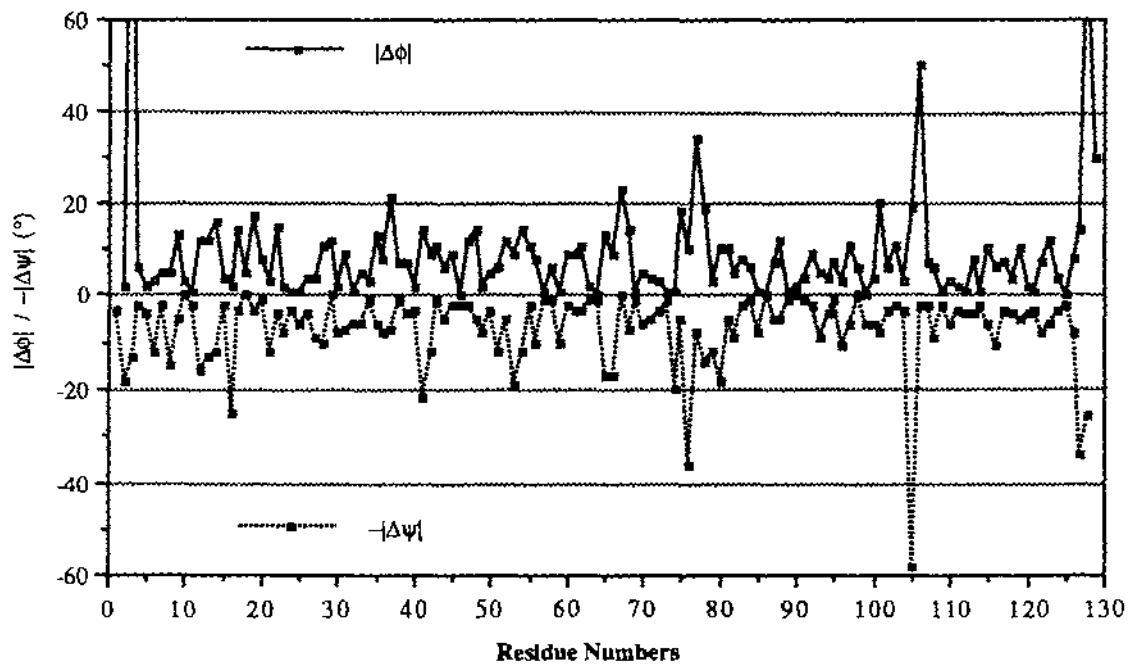

Figure 3.3.2.1. Absolute differences in the main-chain torsion angles between the two molecules of reduced azurin. Differences in (ϕ,ψ) for those residues off the scale are at residues 3 ($|\Delta\phi|$=165°) and 128 ($|\Delta\phi|$=86°).

Side-chain torsion angles

Differences also occur in the conformational angles of the side-chains (χ_{1-5}). A plot of the average difference in side-chain torsion angles (see Figure 3.3.2.2) shows that the largest differences appear in those side-chains which are located on the surface of the protein and are not involved in hydrogen bonds. The r.m.s. deviation in side-chain conformational angles is 13.2° for internal side-chains, 15.7° for hydrogen bonded side-chains and 63.2° for external side-chains. Overall, the r.m.s. deviation is 26.4°.

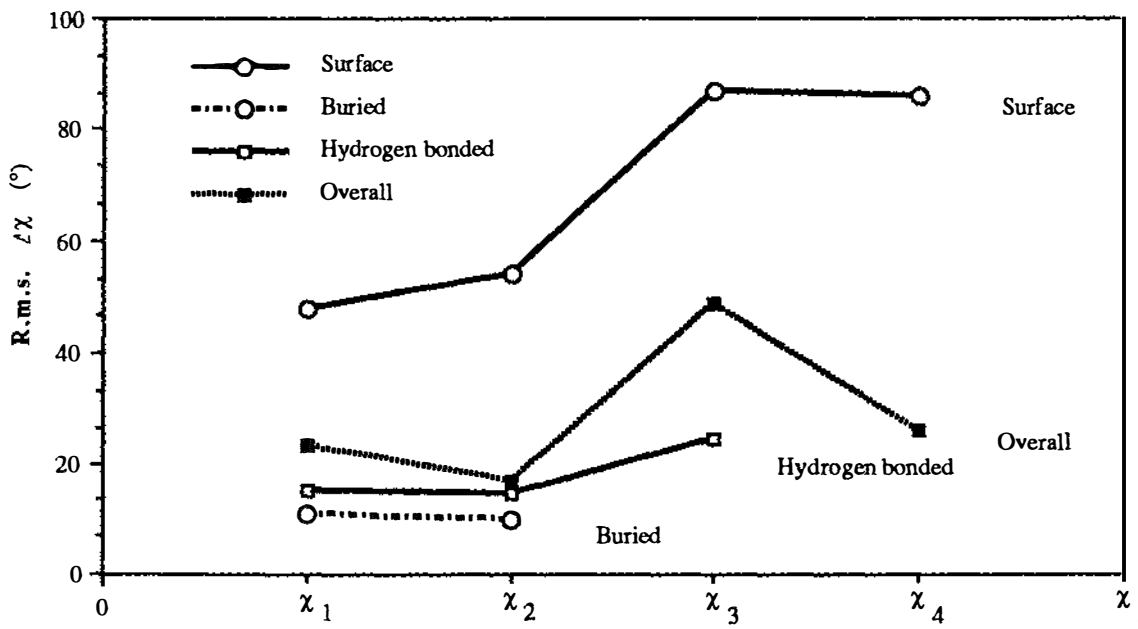

Figure 3.3.2.2. Plot of r.m.s. deviation in side-chain torsion angles (χ_{1-4}) between the two reduced azurin molecules.

Variations in side-chain torsion angles increase further away from the backbone of the protein molecule for flexible fuctional groups such as lysines and glutamic acids. The r.m.s. deviations for the individual torsion angles χ_1-χ_4 are 48.1°, 53.7°, 91.1° and 86.0°, respectively, for all lysines, asparagines, glutamines, methionines, aspartic acids and glutamic acids. There are notable exceptions to this trend in the case of side-chains which are internal or form strong hydrogen bonds. For example, Asn-47 is an internal side-chain and its functional group makes three hydrogen bonds. Other exceptions in reduced azurin are Asp-11, Asp-55, Arg-79 and Asp-93 which also make important contacts linking different parts of the structure.

3.3.3 Comparison of the Hydrogen bonds

Similar hydrogen bonding occurs in the two reduced azurin molecules in the asymmetric unit. A few hydrogen bonds are found in only one or the other molecule; these are listed in Table 3.3.3.1. These hydrogen bonds are found in the loops and at the C-terminus of the polypeptide chain. All are on the surface of the protein, and many belong to the most flexible regions, with high B-values. Most hydrogen bonds of this group are far from the copper site, only two being near the copper site, i.e. O 10...N 13 and O 41...N 45, both in molecule A.

Table 3.3.3.1 Hydrogen bonds found only in one or other molecule. O...H distances are in ångstroms (Å), and C-O...H and O...H-N angles are in degrees (°). Where no hydrogen atom position was calculated, distances and angles are either O...N, C-O...N and O...N-C, or O...O, C-O...O and O...O-C. Values in italics are considered marginal hydrogen bonds.

	molecule A			molecule B		
	C-O...H	O...H	O...H-N	C-O...H	O...H	O...H-N
main-chain...main-chain						
O 10...N 13	*108*	*2.36*	*163*			
O 41...N 45	*128*	*2.42*	*113*			
O 53...N 56				*107*	*2.50*	*164*
O 74...N 77	153	2.03	128			
O 77...N 80				*96*	*2.40*	*156*
O 128...N 24	162	2.18	123			
main-chain...side-chain						
$O_{\delta 1}$ 10...N 14	*157*	*2.48*	*153*			
$O_{\delta 1}$ 47...N 47				*104*	*2.34*	*100*
O 86...N_{ζ} 41	147	2.98	102			
$O_{\delta 1}$ 93...N 94				*101*	*2.32*	*126*
O 127...N_{ζ} 24	*97*	*3.00*	*144*			
O 128...N_{ζ} 24				*112*	*3.23*	*91*
$O_{\gamma 1}$ 128...N 129	*98*	*1.73*	*135*			
side-chain...side-chain						
$O_{\delta 1}$ 77...N_{ε} 79				108	2.03	163
$O_{\delta 1}$ 23...O_{γ} 25	150	2.54	106			
$O_{\delta 2}$ 23...O_{γ} 128				*105*	*3.37*	*110*
$O_{\varepsilon 1}$ 53...N_{ζ} 56				*138*	*3.47*	*97*
$O_{\delta 1}$ 62...N_{ζ} 74	124	2.64	177			
$O_{\delta 1}$ 93...N_{ζ} 85				107	3.03	134
$O_{\delta 1}$ 98...O_{γ} 100				132	2.78	136
$O_{\delta 1}$ 98...N_{ζ} 27	104	2.70	160			

Some of these differences can be attributed to perturbations in the structure due to crystal packing effects. Six of these hydrogen bonds are close to (within one residue) or are involved in intermolecular contacts; O 41A...N 45A, O 53B...N 56B, O 128A...N 24A, $O_{\gamma 1}$ 128A...N 129A, $O_{\delta 2}$ 23B...O_{γ} 128B and $O_{\delta 1}$ 23A...O_{γ} 25A. The difference at $O_{\delta 2}$ 23, is a good example of a hydrogen bond affected by crystal packing. In both molecules $O_{\delta 2}$ 23 forms a hydrogen bond with $N_{\delta 2}$ 65 of an adjacent

Table 3.3.3.2. Lattice contacts near the hydrogen bonds which differ between the two molecules.

Hydrogen bonds	Nearby lattice contacts	Hydrogen bonds	Nearby lattice contacts
$O_{\delta 1}$ 23A...O_{γ} 25A	$O_{\delta 2}$ 23A...$N_{\delta 2}$ 65A	O 127A...N_{ζ} 24A	$O_{\delta 2}$ 23A...$N_{\delta 2}$ 65A
$O_{\delta 2}$ 23B...O_{γ} 128B	$O_{\delta 2}$ 23B...$N_{\delta 2}$ 65B	O 128A...N 24A	$O_{\delta 2}$ 23B...$N_{\delta 2}$ 65B
	O 24A...N 68B	O 128B...N_{ζ} 24B	O 24A...N 68B
	O 24B...N 68A		O 24B...N 68A
	N_{ζ} 24A...$O_{\delta 1}$ 129B		N_{ζ} 24A...$O_{\delta 1}$ 129B
	N_{ζ} 24B...$O_{\delta 1}$ 129A		N_{ζ} 24B...$O_{\delta 1}$ 129A
	O 129A...$N_{\delta 2}$ 65A		O 129A...$N_{\delta 2}$ 65A
	$O_{\delta 1}$ 129A...N_{ζ} 24B		$O_{\delta 1}$ 129A...N_{ζ} 24B
	$O_{\delta 1}$ 129B...N_{ζ} 24A		$O_{\delta 1}$ 129B...N_{ζ} 24A
O 41A...N 45A	N 40A...O 38A	$O_{\gamma 1}$ 128A...N 129A	O 129A...$N_{\delta 2}$ 65A
	N 40B...O 38B		$O_{\delta 1}$ 129A...N_{ζ} 24B
O 53B...N 56B	O 57B...$N_{\varepsilon 2}$ 2B		$O_{\delta 1}$ 129B...N_{ζ} 24A

molecule, but in molecule B, $O_{\delta 2}$ 23 also forms a hydrogen bond with O_{γ} 128. The hydrogen bonds which are affected by lattice contacts are listed in Table 3.3.3.2.

About half (12 out of 21) of these differences in the hydrogen bonding structure are due to interactions which are "marginal", i.e. O...H distances greater than 2.3Å, or an angle less than 100°. For instance, the O 41...N 45 hydrogen bond is marginal with an O...H distance of 2.42Å, close to the defined maximum of 2.50Å. Other apparent differences arise because the geometry in one molecule falls just short of the defined criteria for a hydrogen bond[238], and hence there is actually little difference. For example, O 10...H-N 14 has a distance of 2.36Å in molecule A, but is 2.53Å in molecule B, just beyond the defined criteria.

Agreement of hydrogen bond geometry

The majority of hydrogen bonds in reduced azurin, though, are found in both molecules of the asymmetric unit. A comparison of these hydrogen bond pairs demonstrates the agreement of hydrogen bond geometry. The hydrogen bond geometry was unconstrained during refinement, and variation in it gives an indication of accuracy of the structure. The r.m.s. deviation of all the hydrogen bonds lengths in the reduced structure (excluding those made to water molecules) is 0.20Å for 94 pairs. A breakdown of these results into main-chain...main-chain, main-chain...side-chain, and side-chain...side-chain bonds (Table 3.3.3.3) shows that interactions with the side-chain atoms are associated with larger differences. This is because side-chains are typically more flexible than main-chain groups, as judged by their higher thermal parameters. Conversely, better agreement is

Table 3.3.3.3. Hydrogen bond geometry r.m.s. deviations for reduced azurin

	R.m.s. Δ values	
	distance (Å)	angle (°)
main chain-main chain atoms (60 pairs)	0.17	9.2
main chain-side chain atoms (25 pairs)	0.23	7.6
side chain-side chain atoms (9 pairs)	0.33	19.5
copper environment (23 pairs)	0.15	8.2
overall (94 pairs)	0.20	10.3

seen in hydrogen bonds with main-chain atoms, presumably because these atoms are more tightly constrained.

Around the copper site, the r.m.s. deviation in hydrogen bond lengths is 0.15Å, less than the r.m.s. deviations for other regions, showing that the copper site enviroment is better defined and more rigid than the rest the protein structure. The largest differences in hydrogen bond geometry at the copper site are seen at $N_{\varepsilon 2}$ 35...O 44, N 44...O 40 and $N_{\delta 1}$ 35...N 37. An examination of the thermal parameters of these residues shows that the residues 35-40 have consistently higher B-values in molecule A (average B = 26Å^2) than in molecule B (21Å^2). This may indicate that this section of the structure has not refined completely. Table 3.3.3.4 lists the geometry of hydrogen bonds made to copper ligands.

Table 3.3.3.4. Hydrogen bond distances and angles made to copper ligands of reduced azurin

Hydrogen bond distances (Å)	N-H...O angle (°)			N-H...O distance (Å)		
	A	B	Δ	A	B	Δ
O 10-$N_{\varepsilon 2}$ 46	169	165	4	1.77	1.80	0.03
S_γ 112-N 47	160	159	1	3.37	3.29	0.08
S_γ 112-N 114	163	158	5	3.36	3.37	0.01

3.3.4 Comparison of the main-chain atom positions

Superposition of the polypeptide backbone of the two independent molecules using the same transformation as in section 3.3.1 (i.e. the main-chain atoms of residues 3-127) shows that the two molecules are essentially identical, and gives an r.m.s. deviation in main-chain atom positions of 0.30Å. A stereoview of the C_α plot of the two superposed molecules of reduced azurin is shown in Figure 3.3.4.1, and the average deviation in main-chain atom positions (<Δx>) is plotted against residue number in Figure 3.3.4.2. The positions where there are differences in the backbone atoms above the r.m.s.

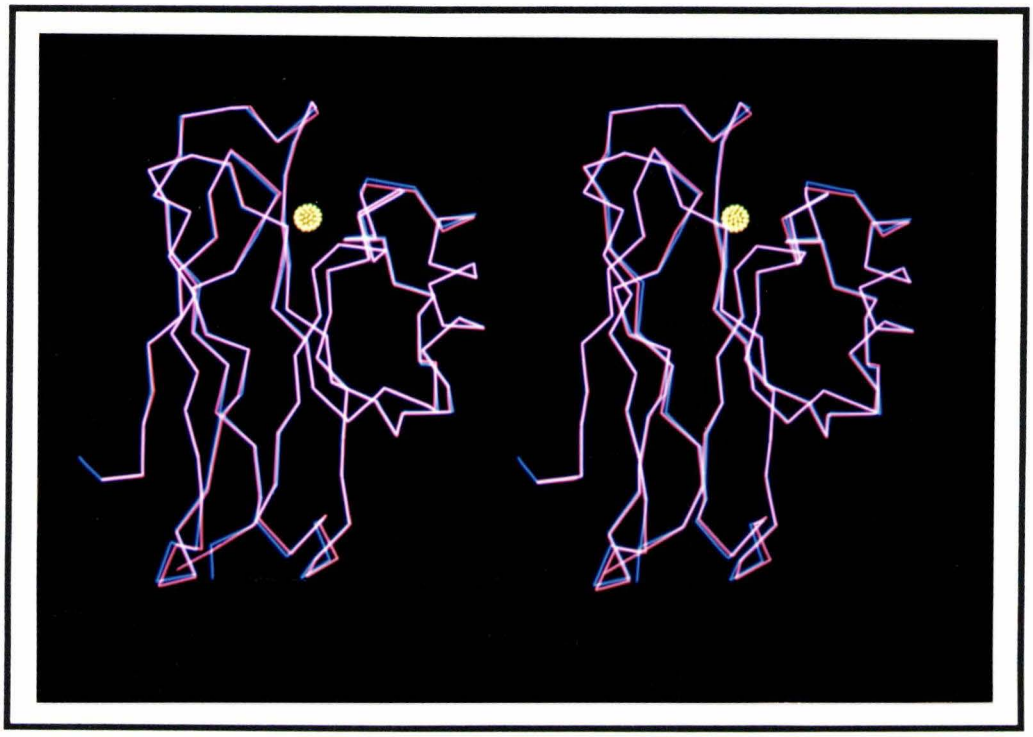

Figure 3.3.4.1. A stereo view of the C_α plot of the two superimposed molecules of reduced azurin. Copper atom in yellow, molecule A in red and molecule B in blue. Sections which are white are overlapping regions between the two molecules.

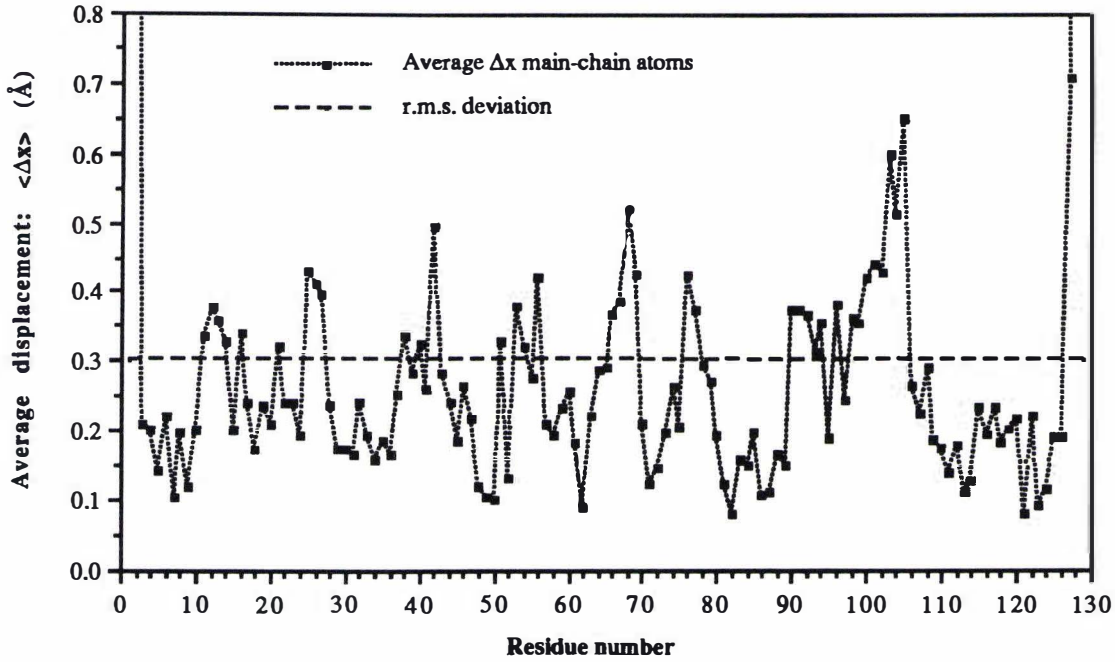

Figure 3.3.4.2. Average difference in the main-chain atom positions after superposition plotted against residue number.

deviation, are similar to those found in structure of oxidised azurin[31], namely at the chain termini and in certain connecting loops between secondary structure elements.

More specifically, these differences in the reduced structure occur at residues 1 to 2, 11 to 14, 25 to 27, 38 to 42, 51 to 56, 66 to 69, 76 to 77, 90 to 94, 96 to 105 and 127 to 129, and their average deviations for the main-chain atoms are listed in Table 3.3.4.1. All of these residues are located on the surface of the protein, and most are found at the southern end of the molecule. The largest differences, those greater than 1.0Å, are located at the termini of the polypeptide chain. Deviations in the N-terminus of the polypeptide chain, residues 1 to 2, are probably the result of disorder or high flexibility in this region which is characterised by weak electron density. At the C-terminus, residues 127 to 129, crystal intermolecular contacts have forced two distinctly different conformations between the two molecules. Other differences can also be ascribed to crystal intermolecular contacts. These occur at residues 25 to 27, 38 to 42, and 66 to 69, where intermolecular contacts presumably cause small fluctuations in the structure. The remaining regions of the main-chain structure which show variations above 0.3Å (residues 11 to 14, 51 to 56, 76 to 77 and 90 to 105), however, are not involved in intermolecular contacts, and their differences probably are the result of the flexibility of these regions, error or conformational microheterogeneity.

Table 3.3.4.1. Residues whose average main-chain atom deviations are above the r.m.s. value for reduced azurin, along with the differnces in main-chain torsion angles and the average B-value.

Residue	Δx (Å)	Δφ (°)	Δψ (°)	<B> (Å^2)	Residue	Δx (Å)	Δφ (°)	Δψ (°)	<B> (Å^2)
1	6.418	-	-	61	76	0.425	36	10	44
2	2.142	2	18	55	77	0.374	8	34	40
11	0.337	2	1	27	90	0.375	1	2	26
12	0.380	16	12	30	91	0.376	1	4	21
13	0.359	13	12	28	92	0.366	2	9	23
14	0.327	12	16	25	93	0.314	9	5	23
16	0.340	25	2	29	94	0.354	4	4	22
21	0.320	12	3	28	96	0.383	11	3	28
25	0.432	6	1	27	98	0.363	0	6	30
26	0.413	4	4	26	99	0.355	6	0	29
27	0.399	9	4	29	100	0.422	6	4	37
38	0.336	1	7	24	101	0.440	8	20	39
40	0.323	3	2	19	102	0.430	3	6	36
42	0.496	12	9	28	103	0.598	2	11	44
51	0.330	12	6	24	104	0.515	3	3	53
53	0.377	19	9	38	105	0.650	58	19	58
54	0.322	12	14	40	127	0.706	34	14	36
56	0.421	10	8	35	128	1.556	170	26	52
66	0.368	17	9	29	129	2.893	-	-	73
67	0.386	0	23	26					
68	0.523	7	14	25					
69	0.427	1	1	28					

The thermal parameters for many of the main-chain atoms whose positions deviate more than 0.3Å, are above the average B-value for all main-chain atoms (B=27.5Å^2). This correlation is consistent, since B-values physically represent the thermal motion of an atom, or any positional disorder. Similarly, these sections of the polypeptide chain, also correspond to the large differences in main-chain torsion angles (ϕ and ψ). Differences in ϕ or ψ angles between the two molecules have an r.m.s. deviation of 30° for these residues, which is well above the r.m.s. value for the overall protein (r.m.s.=8°).

The sections of the main-chain structure which superpose best occur in the β-sheets and α-helix, and around the environment of the copper. Most of the average deviations for residues in the β-sheets and α-helices are less than 0.3Å. The exception to this is the β-strand 91-98 which forms an edge of a β-sheet. This strand is less constrained than the other edge strands, because it makes fewer contacts to other parts of the protein or to adjoining protein molecules of the crystal lattice.

For main-chain atoms of the β-sheet (residues 3-10, 14-16, 18-22, 27-36, 45-51, 81-87, 91-99, 108-112 and 121-127) the r.m.s. deviation is 0.25Å, while the r.m.s. deviation for the main-chain atoms of the α-helix is 0.21Å. Similarly, the main-chain torsion angles of residues in the β-sheets and α-helix agree very well between the two molecules of reduced azurin. The r.m.s. deviation of ψ,ϕ are lower than the overall molecule (r.m.s. $\Delta\psi$=6.5°, r.m.s. $\Delta\phi$=7.3°). The better agreement in secondary structural elements is understandable since β-strands and α-helices form the structural framework of the protein and are often tightly constrained by packing effects and hydrogen bonding.

3.3.5 Comparison of the side-chain atom positions

In general, much larger deviations are found in the side-chain atom positions than in the main-chain atom positions. This is expected, because side-chains have more conformational flexibility than the main-chain. The side-chains can be separated into three groups; those side-chains with an average deviation in atomic positions above 1Å, those between 0.6Å and 1Å, and those below 0.6Å. The side-chains of the two molecules were superposed using the same transformation as for the main-chain (i.e. superimposed using the main-chain atoms of residues 3-127). The average deviation in side-chain atom positions is plotted against residue number in Figure 3.3.5.1.

Twenty-one residues have side-chains for which the average deviation in atomic positions is greater 1.0Å (see Table 3.3.5.1). All of these are located on the surface of the azurin molecule, and are associated with high thermal parameters (average B=48Å^2). Nine of

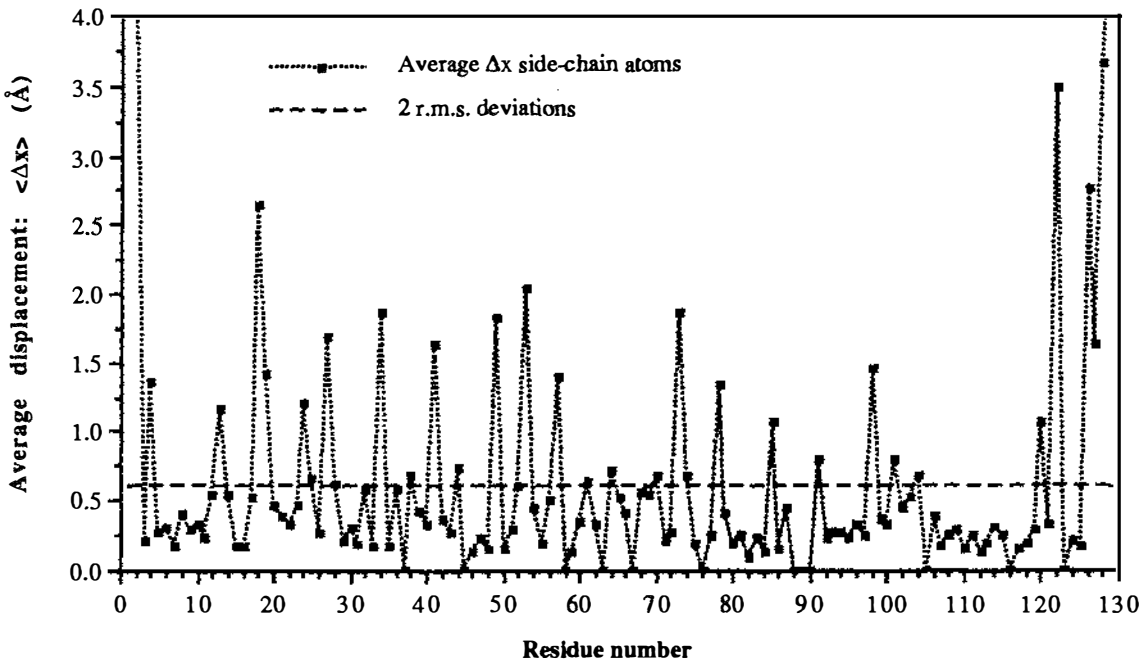

Figure 3.3.5.1. Plot of the average deviation in side-chain atom position against residue number. Values off the scale are residues 1 (9.692Å), 2 (4.612Å) and 129 (5.520Å).

these side-chains are involved in lattice contacts (residues 1, 2, 4, 13, 24, 34, 57, 120 and 129), most of them lysines, glutamines, or other residues which have long side-chains that are flexible and can occupy different conformations (3 Gln, 2 Lys, 2 Met, 1 Asn and 1 Ala). The difference in Ala-1 is an anomaly, since it is due to differences in the conformation of the main-chain. Large differences are apparent in these side-chain torsion angles. The overall rms $\Delta\chi$ of these torsion angles is 91°, while separate values of rms $\Delta\chi_1$-$\Delta\chi_4$ are 69°,80°,118° and 98° respectively; this illustrates the way that the torsion angles of these sidechains become more variable further out from the backbone of the molecule.

A further 12 residues have average deviations in side-chain atom positions of 0.6Å to 1.0Å. These side-chains are also located on the surface of the protein molecule, and have a relatively high average B-value (39 $Å^2$). Only the side-chains of residues 38 and 61 are invloved in lattice contacts. Four side-chains are involved in hydrogen bonds (Ser-25, Thr-61, Lys-74 and Glu-91), most of which are local interactions, and a further four make contacts to water molecules (Gln-28, Lys-38, Gln-70 and Lys-101). The variation in torsion angle is less than the previous group, as expected since there are more constraining interactions. The overall rms $\Delta\chi$ is 47°, and the separate r.m.s. $\Delta\chi_1$-$\Delta\chi_4$ values are 32°, 28°, 70° and 52°, respectively.

Table 3.3.5.1. Average difference in side-chain atom positions greater than 1Å (residues labelled with a "*" are involved in intermolecular contacts in one or both molecules).

Residue	<Δx> (Å)	<B> ($Å^2$)	$\Delta\chi_1$ (°)	$\Delta\chi_2$ (°)	$\Delta\chi_3$ (°)	$\Delta\chi_4$ (°)
Ala-1 *	9.69	58	-	-	-	-
Gln-2 *	4.61	72	32	62	4	-
Glu-4 *	1.36	42	92	40	163	-
Met-13 *	1.17	38	34	6	174	-
Lys-18	2.63	52	8	20	55	64
Glu-19	1.42	56	88	60	41	-
Lys-24 *	1.21	42	10	26	179	103
Lys-27	1.70	47	57	128	56	40
Lys-34 *	1.87	31	17	158	175	155
Lys-41	1.62	35	160	10	148	147
Glu-53	2.03	53	21	111	79	-
Gln-57 *	1.39	43	28	34	13	-
Thr-78	1.35	43	40	-	-	-
Lys-85	1.07	40	15	1	67	137
Asp-98	1.45	49	62	60	-	-
Met-120 *	1.06	41	1	46	175	-
Lys-122	3.47	46	179	166	9	6
Lys-126	2.76	45	9	74	138	81
Leu 127	1.64	36	58	111	-	-
Ser-128	3.64	53	13	-	-	-
Asn-129 *	5.52	77	69	21	-	-

Table 3.3.5.2. Average side-chain differences between 0.6Å and 1Å for reduced azurin. (Residues labelled with a "*" are involved in lattice contacts in either or both molecules).

Residue	<Δx> (Å)	<B> ($Å^2$)	$\Delta\chi_1$ (°)	$\Delta\chi_2$ (°)	$\Delta\chi_3$ (°)	$\Delta\chi_4$ (°)
Ser-25	0.658	31	30	-	-	-
Gln-28	0.629	46	16	19	21	-
Lys-38*	0.681	30	15	24	17	5
Met-44	0.742	30	69	61	139	-
Lys-52	0.607	46	2	33	99	28
Thr-61*	0.638	31	13	-	-	-
Met-64	0.715	35	3	1	62	-
Gln-70	0.689	33	2	0	27	-
Lys-74	0.682	40	22	31	6	100
Glu-91	0.791	33	49	9	99	-
Lys-101	0.794	55	44	22	19	4
Pro-104	0.689	52	(4)	-	-	-

By comparison, side-chains which are buried or are make strong hydrogen bonds are more constrained. Completely or partially buried sidechains have a average difference in atom positions of 0.29Å, while those side-chains which make strong hydrogen bonds have a average difference of 0.48Å. Differences in torsion angles for both of these groups are small (r.m.s. $\Delta\chi_1$-$\Delta\chi_3$ = 10.8°, 9.7° for buried side-chains and 15.2°, 14.7°, 24.7° for those involved in hydrogen bonds, respectively, see above). The difference in atom postions is comparable to the difference found in main-chain atoms.

3.3.6 Comparison of the Copper site and its surrounds

Superposition of the copper site and its surrounding enviroment show that this is the most well ordered part of the reduced azurin molecule. The r.m.s. deviation of the atom positions after superposing the copper site atoms and residues 10-12, 15, 35, 44-47, 112-117 and 121 is 0.21Å, while for the copper site (residues 45, 46, 112, 117, 121 and copper atom) it is even less at 0.16Å. Both of these values are significantly lower than for the main-chain atoms (residues 3-127, r.m.s.=0.30Å). Figure 3.3.6.1 is a stereoview of the copper site of reduced azurin after superposing the two molecules and shows how well the two independent molecules agree.

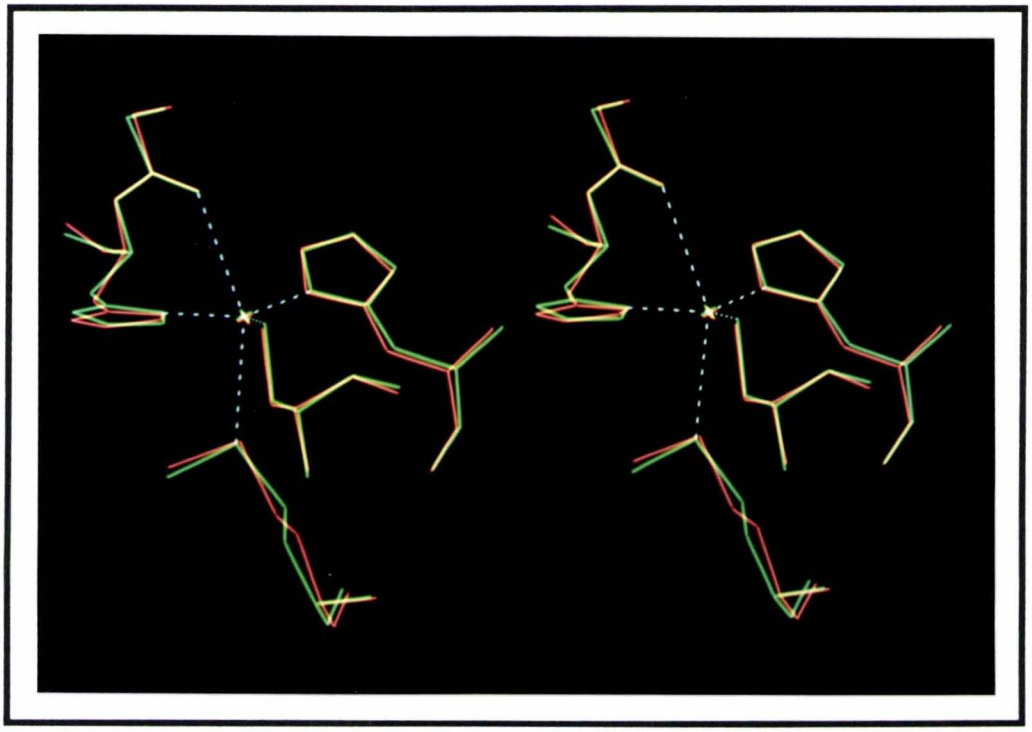

Figure 3.3.6.1. Stereo view of the copper site of reduced azurin after superposition. Molecule A in red and molecule B in green.

The individual copper distances and angles to the ligands are listed in Tables 3.3.6.1 and 3.3.6.2. The differences in the copper geometry between the two molecules are small, with r.m.s. deviation of 0.06Å for distances and 3.7° for angles. This level of agreement suggests that the changes seen in the copper distances upon reduction (0.05-0.12Å) are not large enough to be considered statistically significant, because the changes are only 1-2 times the level of the r.m.s. deviation in copper distances. However, it is important to note that the changes observed are consistent in both protein molecules, implying that these changes are in fact real. The only structural change upon reduction which is truly significant is the shortening of the two S...HN hydrogen bonds by 0.2Å (r.m.s. deviation in S...N distances of 0.06Å, see Table 3.3.6.3).

Table 3.3.6.1. Copper to ligand distances (Å) for reduced (Cu(I)) azurin.

	Molecule A	Molecule B	Average	Difference
Cu...O 45	3.25	3.19	3.22	0.06
Cu...$N_{\delta 1}$ 46	2.17	2.09	2.13	0.08
Cu...S_{γ} 112	2.22	2.31	2.27	0.09
Cu...$N_{\delta 1}$ 117	2.05	2.05	2.05	0.00
Cu...S_{δ} 121	3.21	3.25	3.23	0.04

Table 3.3.6.1. Angles at the copper atom (°) for reduced (Cu(I)) azurin.

	Molecule A	Molecule B	Average	Difference
O 45-Cu-$N_{\delta 1}$ 46	68.5	68.0	68.3	0.5
O 45-Cu--S_{γ} 112	105.2	102.9	104.1	2.3
O 45-Cu--$N_{\delta 1}$ 117	82.0	84.7	83.4	2.7
O 45-Cu--S_{δ} 121	142.5	144.4	143.4	1.9
$N_{\delta 1}$ 46-Cu-S_{γ} 112	132.3	131.3	131.8	1.0
$N_{\delta 1}$ 46-Cu--$N_{\delta 1}$ 117	100.2	108.1	104.2	7.9
$N_{\delta 1}$ 46-Cu--S_{δ} 121	77.3	78.9	78.1	1.6
S_{γ} 112-Cu-$N_{\delta 1}$ 117	126.4	118.	122.7	7.5
S_{γ} 112-Cu--S_{δ} 121	109.1	108.7	108.9	0.4
$N_{\delta 1}$ 117-Cu-S_{δ} 121	89.5	93.8	91.7	4.3

Table 3.3.6.3. Cys-112 S...HN hydrogen bond geometries of reduced and oxidised azurin.

	S_{γ} 112...N 47 distance (Å)		S_{γ} 112...H-N 47 angle (°)		S_{γ} 112...N 114 distance (Å)		S_{γ} 112...H-N 114 angle (°)	
	A	B	A	B	A	B	A	B
oxidised	3.52	3.45	170	167	3.50	3.66	161	155
reduced	3.37	3.29	160	159	3.36	3.37	163	158

The agreement of the copper geometry in the two reduced azurin molecules is similar to that of the two copper sites of oxidised azurin[31], where the r.m.s. deviations for copper bond distances and angles are 0.04Å and 3.9°, respectively, and the r.m.s. deviation in the atom positions of the oxidised copper site and its surrounds is 0.17Å.

3.3.7 Comparison of B-values

Thermal parameters for the reduced azurin structure were refined individually for each atom and independently for each of the two protein molecules. Figure 3.3.7.1 is a plot of the average B-value for the main-chain atoms and Figure 3.3.7.2 is a plot of the average B-value for the side-chain atoms of both molecules. As can be seen, there is a good correlation of the B-values of the two molecules. The r.m.s. deviation in average B-value is 3.94$Å^2$ for all residue pairs.

The agreement between the thermal parameters of both molecules is best where the protein structure is clearly defined. At the copper site, the r.m.s. deviation in B-value is 2.16Å^2. Main-chain atoms associated with the β-strands also show good agreement (rms ΔB=3.23Å^2). Many of the thermal parameters in the loops between the β-strands and in the "flap" region are more varied. This is reasonable, since these loops are at the surface of the molecule, and are apt to show more flexibility due to a lack of constraining forces.

Differences in thermal parameters of side-chains are closely tied to the differences found in the main-chain. Virtually all side-chains have the same sign and similar magnitude of ΔB as their corresponding main-chain atoms. The largest differences in the thermal parameters of side-chains occur at residues which are on the surface of the protein molecule and extend out into the solvent. Typical examples are Glu-4, Lys-24, Lys-38, residues 75-80, Val-99 and residues 126-128. These are also areas of the protein which are better resolved in electron density maps of one molecule than of the other.

Valuable information on the structural model is also held in the differences of the thermal parameters between the two molecules. Consistently large differences in B-values may indicate that a section in one molecule is misplaced. An example of this for reduced azurin is at residues 55 to 72, where the B-values are consistently lower in molecule A than in molecule B, suggesting that this region of structure in molecule B may be misplaced. This type of error may not be detected when inspecting electron density maps. Such subtle errors could be caused by the region refining to a local minimum near to the correct structure. A possible means of rectifing the situation would be to superpose the better of the two molecules onto this region, and use the better molecule as a guide in rebuilding the poorer molecule. However, this technique was attempted during the refinement of apo-azurin with limited success (see Section 4.1).

Comparison of thermal parameters and deviations of the main-chain atom positions of reduced azurin shows that the smallest deviations in atom positions occur where the thermal parameters are lowest. Figure 3.3.7.4 shows this trend in the main-chain and side-chain atoms for each residue. The larger average deviations in side-chain positions compared to main-chain positions is due to the higher conformational flexibility of side-chains (see Section 3.3.5).

3.3.8 Solvent structure

Since the crystal structure of azurin contains two independent molecules in the asymmetric unit, related by a non-crystallographic two-fold axis, much of the solvent

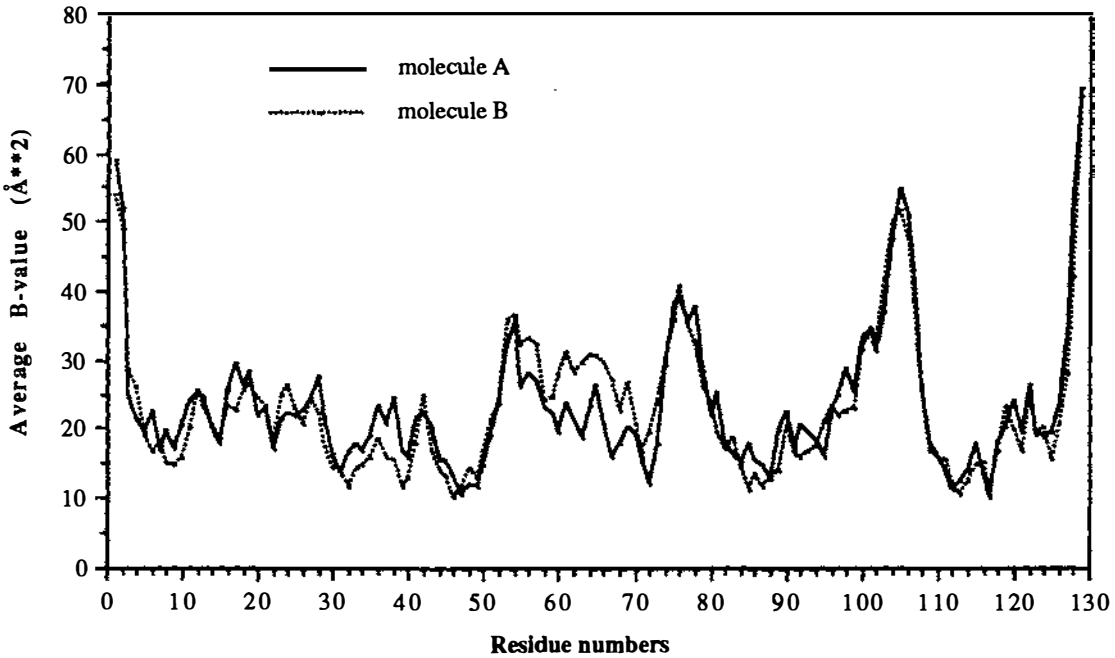

Figure 3.3.7.1. Comparison of the average main-chain B-values against residue number.

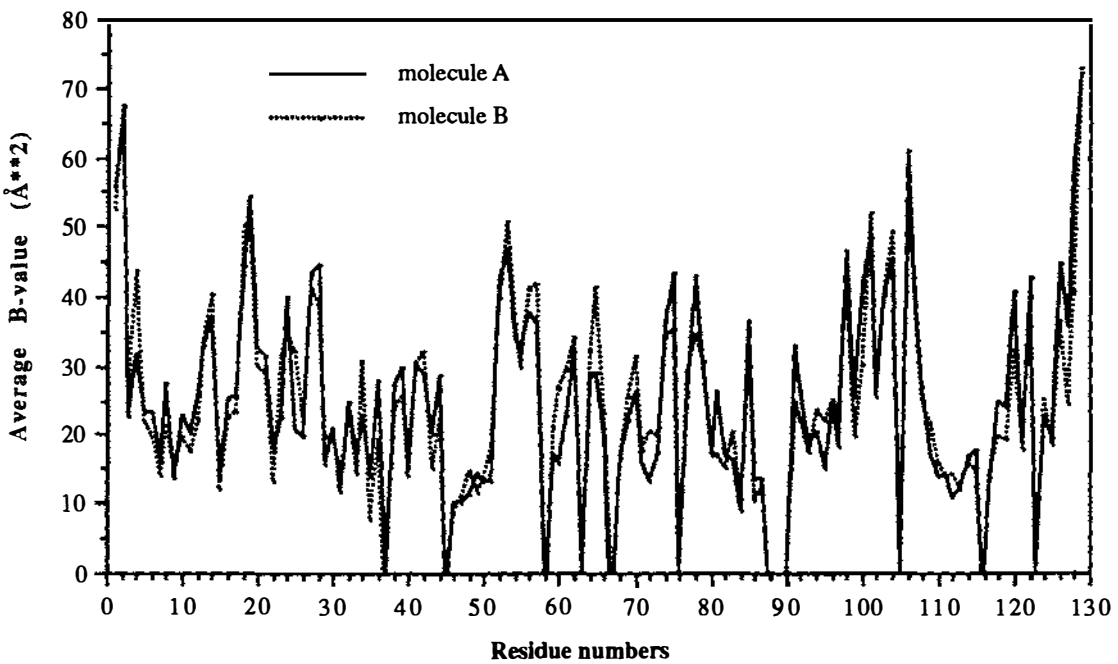

Figure 3.3.7.2. Comparison of the average side-chain B-values against residue number.

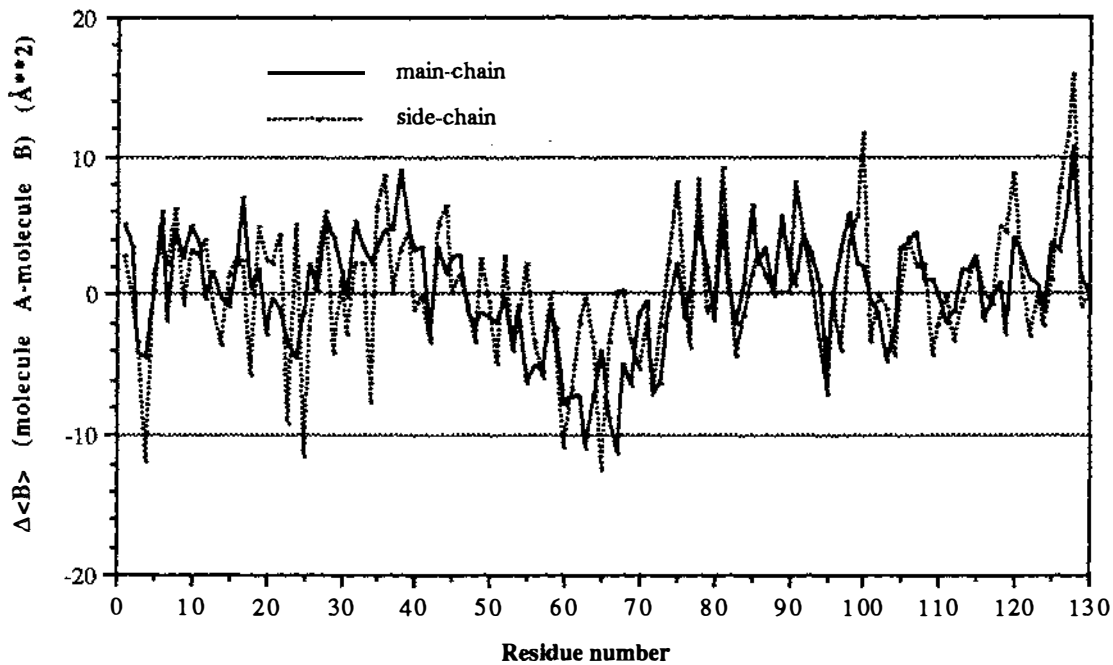

Figure 3.3.7.3. Difference in average B-value between the two molecules in the asymmetric unit of reduced azurin.

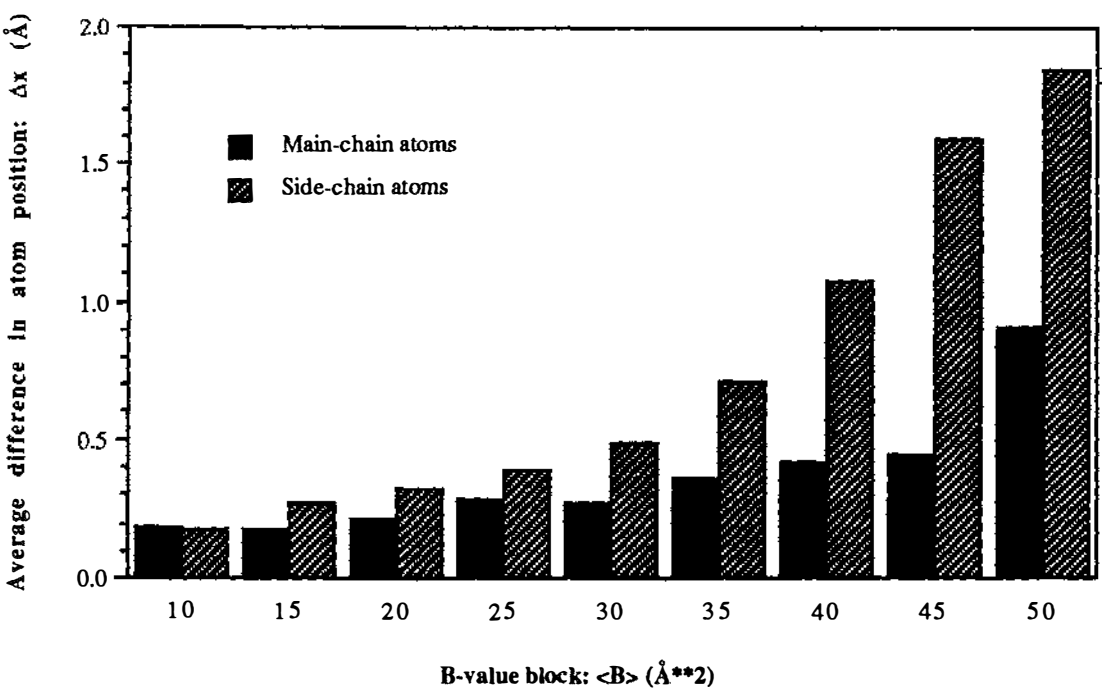

Figure 3.3.7.4. Plot of the average deviation in atom position against the B-value separated into blocks of 5Å^2. Main-chain and side-chain atoms have been separated to show the difference in these two groups of atoms.

structure is also related by the same two-fold axis. To determine which solvent molecules have equivalent partners, solvent molecules of protein molecule B were superimposed on those of protein molecule A using a transformation calculated from the main-chain atoms of residues 3-127. Where a superimposed solvent molecule of protein molecule B had a position within 1.5Å of a solvent molecule associated with protein molecule A, the pair of solvent molecules were considered related to each other by the two-fold non-crystallographic axis. Solvent molecules were also considered related if they made hydrogen bonds to the same parts of the protein and are within 3.0Å of each other after superposition. Using these criteria, 70 solvent molecule pairs have been identified as related by the two-fold non-crystallographic axis. Figure 3.3.10.1 shows the regions which contain solvent molecules that are related by the non-crystallographic two-fold axis, and those which are not.

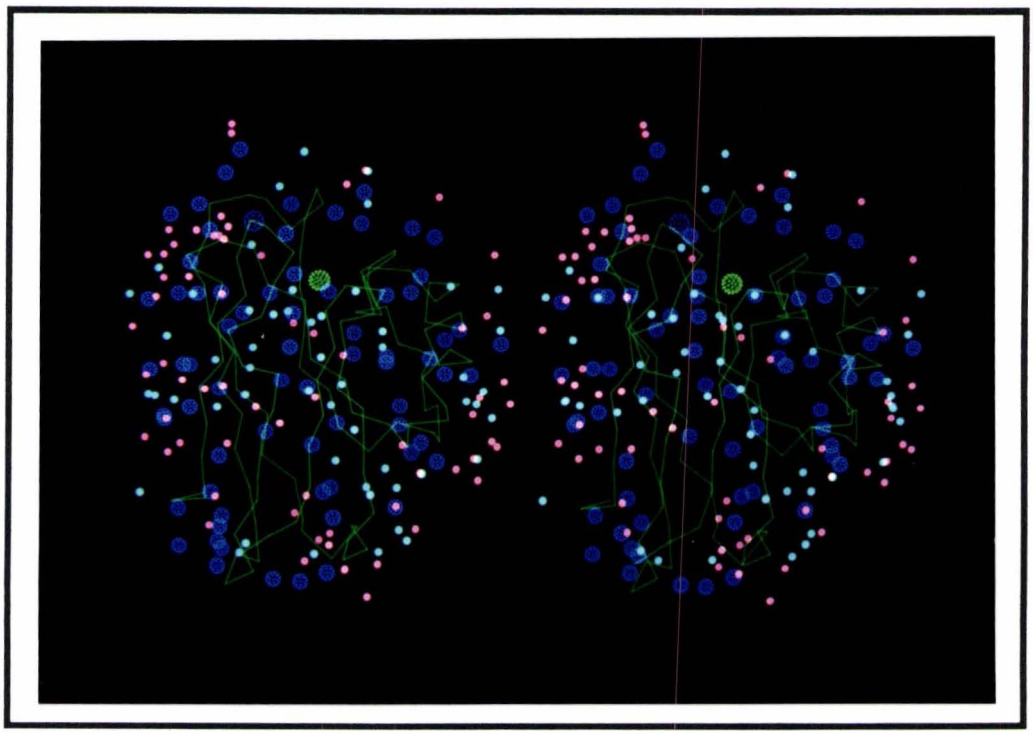

Figure 3.3.10.1. Solvent molecules in reduced azurin which are related by the two-fold non-crystallographic axis are shown in blue, while those that are "unique" are shown in smaller spheres, light blue for molecule A and pink for molecule B.

Differences in the relative positions of the 2-fold related solvent molecules, after superposition, show a correlation with the number of hydrogen bonds made by the solvent molecule to the protein. Solvent molecule pairs which make three or more hydrogen bonds to the protein show the best agreement in their relative positions, whereas those that make only one or no hydrogen bonds to the protein have the largest differences (see Figure 3.3.10.2). This correlation reflects the better agreement seen in 2-fold related solvent molecules which make more contacts to protein and are

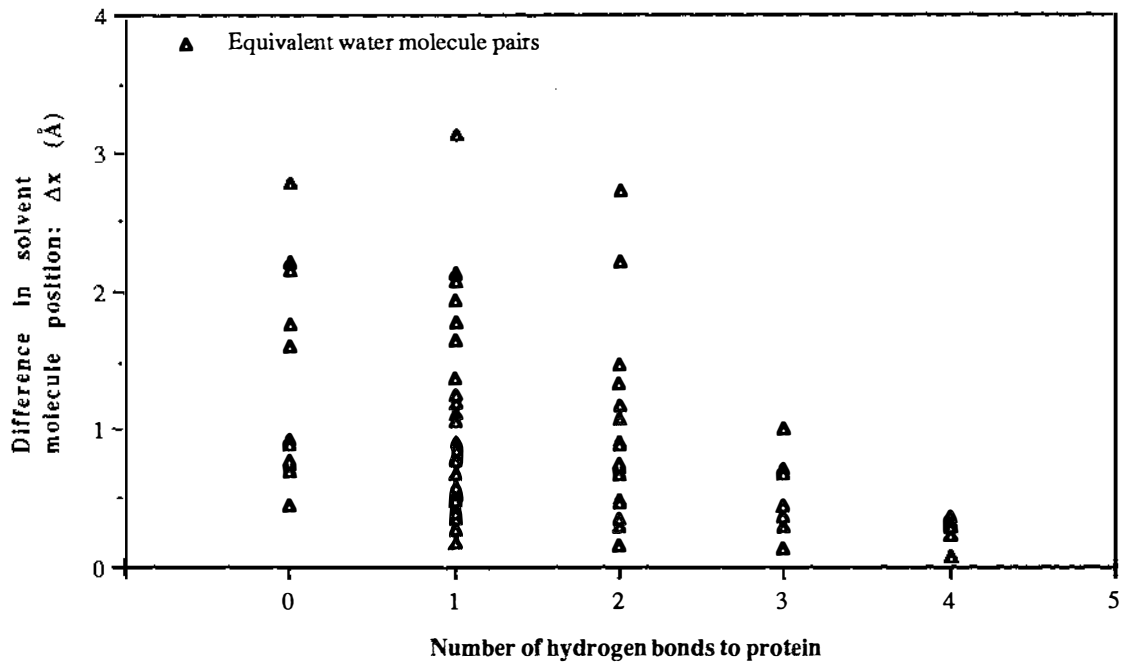

Figure 3.3.10.2. Plot of the correlation between the number of contacts made to the protein by the solvent molecule and the agreement in position after superposition.

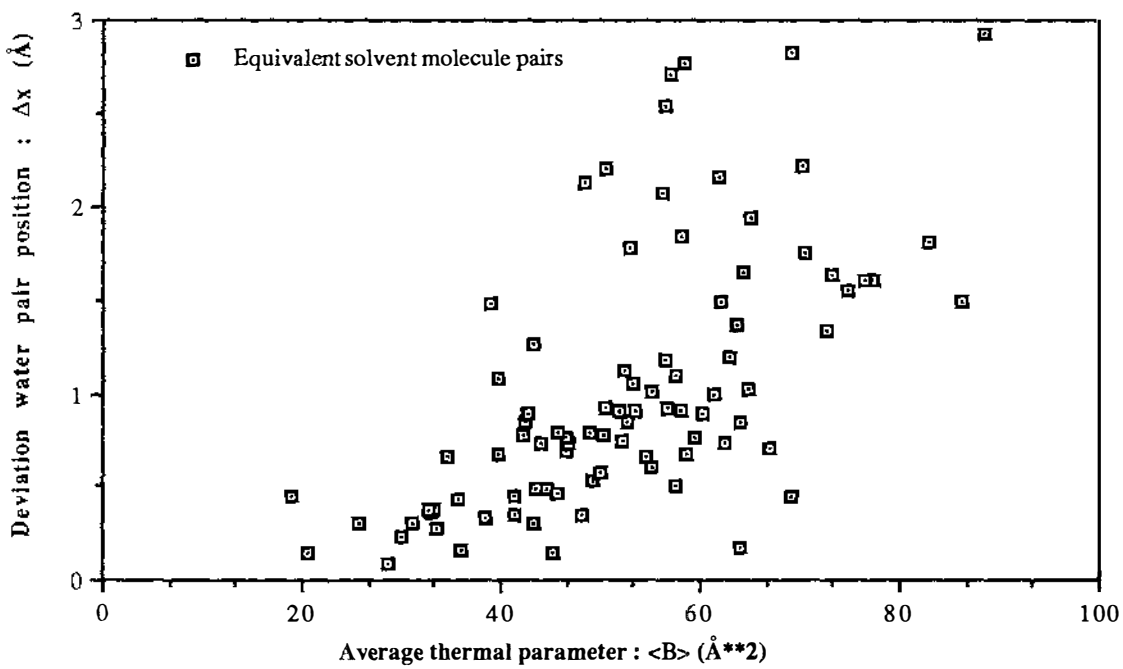

Figure 3.3.10.3. Deviation in position between non-crystallographic two-fold equivalent solvent molecules of reduced azurin.

consequently more tightly constrained.

A similar correlation is seen in the average B-value of the solvent molecule pair. Where the B-value is low the difference between the positions is small, while for higher average B-values the deviation is larger (see Figure 3.3.10.2). This correlation is understandable, since those solvent molecules with lower B-values are more clearly defined in the structure (i.e. higher occupancy, less disorder and less thermal motion) due to greater number of interactions with the protein.

Chapter 4 : Apo-azurin

4.1 Refinement of apo-azurin

Since the crystals of apo-azurin are isomorphous with those of oxidised azurin, the coordinates of the latter structure could be used as a starting model. The program HKPROLSQ was used throughout the refinement, except when the residual copper occupancies were refined with the program TNT[230]. The geometrical constraints used were similar to those used for the reduced azurin refinement, and are listed in Table 4.1.1 along with the r.m.s. deviations from ideal geometry of the final structure. Torsion angles and the hydrogen bond distances were left unrestrained except where the hydrogen bond distance was short (i.e. N...O less than 2.6Å). The course of the refinement is summarised in Table 4.1.2.

Table 4.1.1. Values of geometrical constraints and the r.m.s. deviations in the final model of apo-azurin. [a]An upper limit for shifts in the atom coordinates and thermal parameters was set to prevent any excessive shifts in the model. The values under "R.m.s. deviations" here represent the r.m.s. shift in the positions and B-values in the last cycle of refinement.

Geometry	Restraint	R.m.s. deviation
Distances		
1-2 bonded distances	0.020Å	0.013Å
1-3 angle distances	0.040Å	0.047Å
1-4 intraplanar distances	0.050Å	0.049Å
Planar groups		
deviation from plane	0.020Å	0.012Å
Chiral centers		
chiral volume	0.15Å^3	0.154Å^3
Non-bonded contacts		
single torsion	0.50Å	0.210Å
multiple torsion	0.50Å	0.267Å
Thermal factors		
main-chain bond	2.50Å^2	2.707Å^2
main-chain angle	3.50Å^2	4.370Å^2
side-chain bond	3.00Å^2	3.957Å^2
side-chain angle	3.50Å^2	6.143Å^2
Excessive shifts[a]		
positional parameters	0.30Å	0.005Å
thermal parameters	3.00Å^2	0.07Å^2

The initial R-factor for the starting model (oxidised protein atoms minus the copper, its ligands and the solvent molecules) was 0.302, which dropped to 0.257 (r.m.s. $\Delta_{distance}$=0.015Å) after 13 cycles against data to 2.2Å resolution (13233 observations I>0 between 5Å and 2.2Å resolution). To encourage further refinement, the geometrical restraints were relaxed for six cycles (r.m.s. $\Delta_{distance}$=0.078Å), and then gradually retightened over 16 cycles to R=0.240 (r.m.s. $\Delta_{distance}$=0.014Å, cycle 35). The copper ligands were then built in from F_o-F_c maps using the interactive graphics system[231,331].

The configurations of the copper ligands were clear and found to be similar to those in the oxidised structure. The R-factor dropped from 0.225 to 0.204 after nine cycles (r.m.s. $\Delta_{distance}$=0.014Å, cycle 51). Geometrical restraints were relaxed again for five cycles (r.m.s. $\Delta_{distance}$=0.046Å), and retightened over 18 cycles bringing the R-factor to 0.191 (r.m.s. $\Delta_{distance}$=0.016Å, cycle 69).

At this stage of refinement, solvent molecules were identified from F_o-F_c maps, and were included as water molecules in the model if the peak height was greater than 2σ. 191 solvent molecules (189 waters and the sulphur atoms of two sulphate anions) were clearly identified, and the R-factor dropped to 0.164 after 10 cycles (cycle 79). Another 39 water molecules were found, while 9 were removed. The geometrical restraints were then relaxed over 12 cycles (cycle 92, R=0.151, rms $\Delta_{distances}$=0.063Å), and gradually retightened over 35 cycles (cycle 127, R=0.165, rms $\Delta_{distance}$=0.014Å). Several parts of the protein were then rebuilt (regions with high B-values and short van der Waals contacts), more solvent molecules found (58 waters), and the structure further refined to R=0.163 (cycle 139). Solvent molecules were checked against F_o-F_c maps after omitting those with B>60Å^2 and were removed if the F_o-F_c peak did not reappear. A total of 13 water molecules were removed using this method, while a sulphate anion on a 2-fold axis was added as a sulphur atom (see below). Distance restraints were imposed on some poor hydrogen bonding contacts involving protein atoms, and the structure refined for eight cycles (R=0.161). Residual copper was then accounted for (see below) by introduction of copper atoms with occupancies visually estimated from F_o-F_c maps (5% and 10% for molecules A and B, respectively). With the residual copper atoms included, the R-factor dropped, over six cycles, to 0.160. Six cycles of TNT refinement were conducted to refine the residual copper occupancies, which converged quickly, to 18% and 22% for molecules A and B, respectively (cycle 160, R=0.159). Refinement was terminated after 12 cycles with a final R-factor of 0.158 (cycle 172, rms $\Delta_{distances}$=0.013Å). The final model contained 1954 protein atoms, two copper atoms, two sulphate anions as SO_4^{2-}, one sulphate as S and 264 water molecules.

The apo protein structure was rebuilt at three stages during refinement (at cycles 80, 128 and 148), and the experience gained in rebuilding the reduced structure was used to avoid pitfalls. While rebuilding, particular attention was given to the torsion angles (χ_1-χ_5), especially when rebuilding poorly defined side-chains for which the omit density could be satisfied by more than one conformation, or which did not provide a clear configuration. In these cases, energetically unfavorable configurations (e.g. χ_1=0°) were avoided, so that a structurally realistic model could be built. Although non-crystallographic symmetry restraints were never imposed on the two protein molecules during refinement, at cycle

128 advantage was taken of this symmetry to help rebuild two sections of the main-chain in molecule A (residues 51-58 and 104-107) by comparing the sections in molecule B which had consistently lower B-values. Towards the end of the refinement (cycles 140 and 167), a few hydrogen bond lengths remained below 2.5Å, despite continued attempts at rebuilding. As a final solution, these distances were rebuilt and tightly restrained to realistic values. These hydrogen bonds were $O_{\delta 1}$ 23...O_{γ} 25, $O_{\gamma 1}$ 30...$O_{\gamma 1}$ 96, $N_{\delta 1}$ 32...O_{γ} 94, $O_{\delta 1}$ 62...$N_{\eta 2}$ 79, O 72...O_{γ} 113, and $O_{\delta 2}$ 11...N 38.

Virtually all of the solvent molecules in the structure were included as water molecules. Water molecules were input to the model at cycles 71, 80 and 128, while some were removed at cycles 80 and 140. Near the end of refinement (cycle 148), a difference Fourier map was checked against the solvent structure of oxidised azurin[31], and no assignable peaks were found close to positions of oxidised azurin water molecules. Two sulphate anions found in sites corresponding to the sulphate binding sites of oxidised and reduced azurin, and were included into the structure at cycle 71, as sulphur atoms, while another one, lying on a two-fold axis, was included as a sulphur atom at cycle 140. Later, oxygen atoms were added to the former two sulphate anions, after their positions were found from difference Fourier maps (cycle 148 for molecule A and cycle 154 for molecule B).

Residual Copper in the binding site

Early in the refinement, it became apparent from difference Fourier maps that not all of the copper was removed from the protein, since a small peak of positive density existed at the original copper position after the ligands were built in. Initially, it was thought that this peak may be a result of bias towards the starting model, but continued refinement did not see the peak disappear, suggesting that it was real. The possibility that the peak could be a water molecule was dismissed, since the cavity size is too small (average radius of 1.21Å).

Attempts to account for the peak by including a hydrogen atom on the cysteine ligand, or rebuilding the copper ligands into the residual density as a disordered site, failed to satisfactorily remove it from the difference map. The best model for this peak was as a metal ion in the active site, possibly copper, although substitution of another metal can not be ruled out. The initial visual estimation of the copper occupancies was made by comparing this residual density with that of a nearby water molecule (OW 162) which is well ordered and bound to the ligand His-117, after first omitting this water molecule from the model. By this method, the residual peak appeared to be half the height of the

peak of the water molecule, suggesting an occupancy of 3-4 electrons or a copper occupancy of ≈10%. The two partial copper atoms were given B-values which were averages of the B-values from $N_{\delta 1}$ 46, S_{γ} 112 and $N_{\delta 1}$ 117. Including these residual copper atoms, with occupancies 5% and 10% for molecules A and B, respectively, reduced the R-factor from 0.163 to 0.160. Difference Fourier maps from this model revealed that most of the residual peak was removed. The copper occupancies and positions were then refined (B-values fixed) using the program TNT[230], while the rest of the structure was frozen (positions and B-values). After six cycles of TNT, the occupancies converged quickly from 5 and 10% to 18% and 22% for molecules A and B, respectively, with negligible shifts in position. It is interesting to note that an average copper occupancy of ≈20% (≈6 electrons) does not agree with the visual estimation of half a water molecule. Difference Fourier maps suggest that the residual peak shape is elliptical, which may indicate that the density would be more appropriately modelled with anisotropic B-values. This has not been attempted.

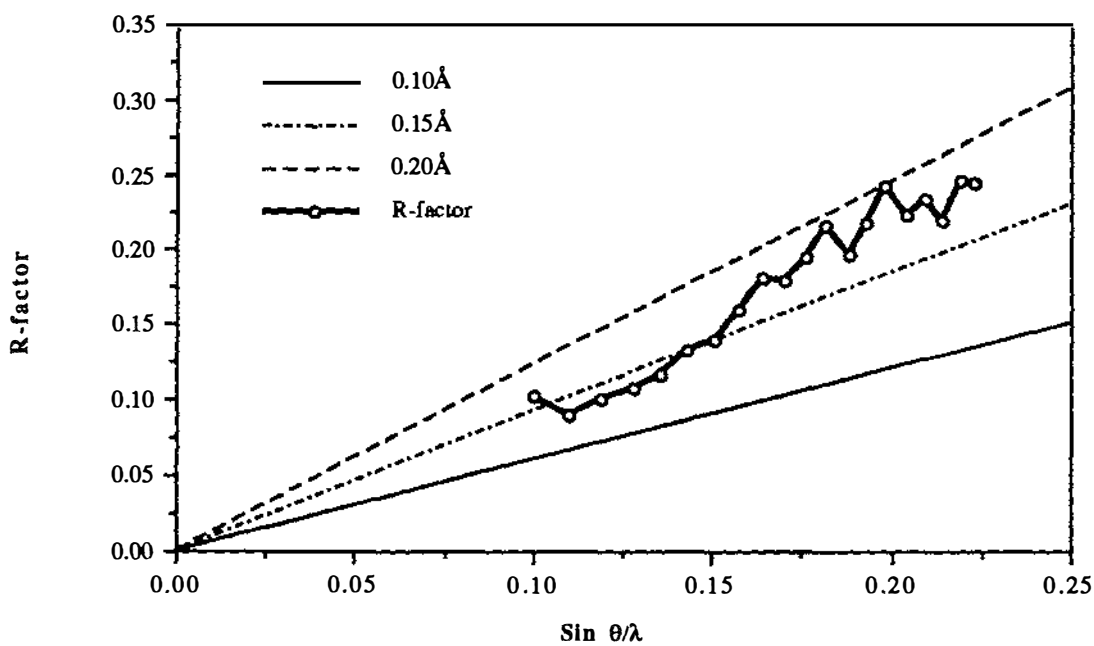

Figure 4.1.1. Luzzati plot for the refined structure of apo-azurin to 2.2Å resolution. Error lines of 0.10Å, 0.15Å and 0.20Å are for acentric data.

Accuracy of the model

A Luzzati plot for the refined structure of apo-azurin is shown in Figure 4.1.1[232]. The plot of the R-factor against resolution indicates that the maximum average error in the atomic coordinates is between 0.15Å and 0.20Å. However, as was seen in structural

Table 4.1.2. Summary of the refinement of apo-azurin.

Cycle	R-factor	Rms Δ_{dist}	Comments
0	0.302	0.015	Starting coordinates taken from the refined model of oxidised azurin, minus the solvent molecules, copper atoms and ligands (main-chain of Gly-45, and side-chains of His-46, Cys-112, His-117 and Met-121).
13	0.257	0.015	13 cycles
20	0.225	0.078	Geometric restraints loosened over 7 cycles.
35	0.240	0.014	Geometry gradually retightened, over 15 cycles.
36	0.223	0.015	Copper ligands built in (main-chain of Gly-45, and side-chains of His-46, Cys-112, His-117 and Met-121).
46	0.204	0.014	10 cycles
54	0.182	0.044	Geometry loosened over 8 cycles.
63	0.188	0.016	Geometry retightened over 9 cycles.
69	0.191	0.016	Geometry involving planar groups tightened (rms Δ_{planes} from 0.016Å to 0.011Å).
71	0.175	0.016	1954 protein atoms, 189 H_2O, 2 sulphates as sulphur atoms.
79	0.164	0.013	8 cycles
80	0.185	0.013	All solvent molecules checked with omit maps, 9 removed and 39 added; poor van der Waals contacts rebuilt, side-chains rebuilt and copper ligands checked and rebuilt
83	0.178	0.013	3 cycles
92	0.151	0.063	9 cycles with relaxed geometric restraints
127	0.165	0.014	35 cycles, geometry gradually retightened. Lowest R-factor in past cycles, R=0.1484 with rms Δ_{dist}=0.053Å.
128	0.175	0.020	Short van der Waals contacts and some protein rebuilt. Copper binding site checked. 58 waters input. Superposition of the two protein molecule main-chain atoms (residues 3-127) gives an r.m.s. deviation in atom positions of 0.296Å.
139	0.163	0.013	11 cycles
140	0.166	0.015	Checked water molecules with B-values above 60Å^2, removed 13 and added 1 sulphate as a sulphur atom. Restraints imposed on a few very short hydrogen bonding contacts.
148	0.161	0.014	8 cycles
	0.163	0.017	Rebuilt C-termini and sulphate(A) input as SO_4^{2-} (B=80Å^2). Checked solvent structure against oxidised azurin solvent structure.
149	0.162	0.017	Input copper atoms at 5% and 10% occupancies for molecules A & B, respectively. Occupancies estimated from omit maps of a nearby water molecule. At this point, attempted to the model residual density with a disordered Cys-112 side-chain, and a thiol hydrogen atom.
154	0.160	0.013	6 cycles
160	0.159	0.013	Refined copper occupancy values and position over 6 cycles of TNT refinement, all other atoms frozen.
166	0.158	0.013	6 cycles. Copper occupancies at 18% and 22%.
167	0.160	0.017	Short van der Waals contacts rebuilt, and sulphate(B) input as SO_4^{2-} (B=80Å^2).
172	0.158	0.013	5 cycles Final model 1954 protein atoms 2 copper atoms 2 sulphates as SO_4^{2-}. 1 sulphate as a sulphur atom 264 water molecules

analysis of reduced azurin, the actual error in the apo-azurin structure may be lower than this, because all of the weak X-ray data were included in the refinement, and this breaks down the assumption of the Luzzati analysis that the discrepancies between the observed and calculated structure factors are solely due to errors in the model[233,234]. In section 4.3, the two independent apo-azurin molecules are compared to give an indication of the level of error in the structure.

4.2 The Structure of Apo-azurin

The general organisation of the apo-azurin molecule is essentially the same as for the oxidised and reduced forms of azurin[31]. The bulk of the polypeptide chain folds into an eight-stranded β-sandwich. The β-strands run the length of the molecule, with the hydrophobic residues occupying the space between the two β-sheets, and the charged residues on the surface. A cavity is formed at the "top" of the molecule between the two β-sheets, where the copper atom resides in the oxidised and reduced forms of azurin. The 30 residue segment, referred to as the "flap" region, packs against the side of the β-sandwich, and contains the only piece of α-helix in the structure. A hydrophobic patch on the surface of the molecule surrounds the copper ligand, the side-chain of His-117. In the following sections, the structure of apo-azurin at 2.2Å resolution will be discussed with respect to the oxidised, Cu(II), and reduced, Cu(I), forms. Many of the structural differences simply reflect flexibility or poor definition of certain parts of the structure, but there are some consistent changes which appear to be real effects caused by the the removal of the copper.

4.2.1 Crystal packing

The crystal packing arrangement of the apo-azurin molecules in the crystal lattice is essentially identical to that of the crystal structures of oxidised and reduced azurin. This is expected, since the apo form of the protein was prepared in the crystalline state from oxidised azurin crystals and was found to be isomorphous with the other forms of azurin. To verify that the crystalline state does not restrain the apo structure from its preferred conformation, crystals were also prepared from solutions of the apo-protein. Precession photographs show that the crystals from apo-protein solutions are also isomorphous to those produced by soaking in cyanide solutions (see Table 4.2.1.1). Consequently, it is presumed that the crystal packing arrangement has no major effect on the protein folding.

Table 4.2.1.1 Unit cell parameters of apo-azurin crystals produced by two methods, one from crystals soaked in cyanide solutions and another from crystals grown from the apo-protein solution.

	a (Å)	b (Å)	c (Å)
Cyanide soaked crystals	75.13	74.33	99.05
Solution grown crystals	75.05	74.10	99.50

The asymmetric unit of the crystal structure of apo-azurin contains two independent protein molecules related by a local two-fold axis passing through the interface between the hydrophobic patches of the two molecules, as in the oxidised and reduced forms. Using the method of Kabsch[255], the transformation for superimposing molecule B on to

molecule A with the best fit from 97% of the main-chain atoms (excluding the N- and C-termini) is ;

$$\begin{bmatrix} -0.11692 & 0.99285 & 0.02389 \\ 0.99249 & 0.11593 & 0.03908 \\ 0.03603 & 0.02828 & -0.99895 \end{bmatrix} \times \begin{bmatrix} x_B \\ y_B \\ z_B \end{bmatrix} + \begin{bmatrix} 20.08621 \\ -16.96780 \\ -12.74946 \end{bmatrix} = \begin{bmatrix} x_A \\ y_A \\ z_A \end{bmatrix}$$

where the transformation is expressed as a rotation matrix ($\underline{R}$) and translation vector ($\underline{T}$), such that $\underline{R}.\underline{x}_B + \underline{T} = \underline{x}_A$, with $\underline{x}_A$ and $\underline{x}_B$ as the orthogonal coordinates of the protein molecules A and B, respectively. This transformation equates to a rotation of 179.5° between the two protein molecules, which is similar to the values found for oxidised and reduced azurins (179.7° and 179.8°, respectively).

4.2.2 Conformational angles

The main-chain torsion angles (ϕ,ψ) for the two molecules of apo-azurin are essentially the same as those in the oxidised and reduced structures of azurin,with two highly populated regions representing the β-strands (-120°, 135°) and the interconnecting loops and helices (-60°, -30°) of the molecule. The only residues which lie outside the allowable regions are glycines, and the same three residues which occupy the left handed α region in the oxidised and reduced structures also appear in the apo structure (Met-13, Asp-71 and Tyr-72). Ramachandran plots of (ϕ,ψ) for the two apo-azurin molecules are given in Appendix A, Figures A.3 and A.4.

The combined r.m.s. deviation in the (ϕ,ψ) angles is 6.4° between the apo and oxidised forms, and 7.6° between the apo and reduced forms. The largest differences in (ϕ,ψ) are found in the residues which make up the more flexible loops of the structure. Figures 4.2.2.1 and 4.2.2.2 show the changes in the main-chain torsion angles between the apo and oxidised and between the apo and reduced structures, respectively, for each residue as $|\Delta\phi\psi|$ (where $|\Delta\phi\psi| = \sqrt{((\Delta\phi^2+\Delta\psi^2)/2)}$).

The largest differences in the apo structure with respect to either redox form are at the termini of the polypeptide chain, while other smaller differences are located in residues at the more flexible loops of the structure (e.g. residues 53-56 and 103-106). Differences at these loops are similar to those found in the comparison between the oxidised and reduced structures (see Section 3.2.2). The plots of $|\Delta\phi\psi|$ also illustrate that the main-chain torsion angles of apo-azurin are more similar to the oxidised form than the reduced form. This may just reflect the fact that the oxidised structure was used as a starting model in the refinement of apo-azurin. However, using the reduced structure as a starting

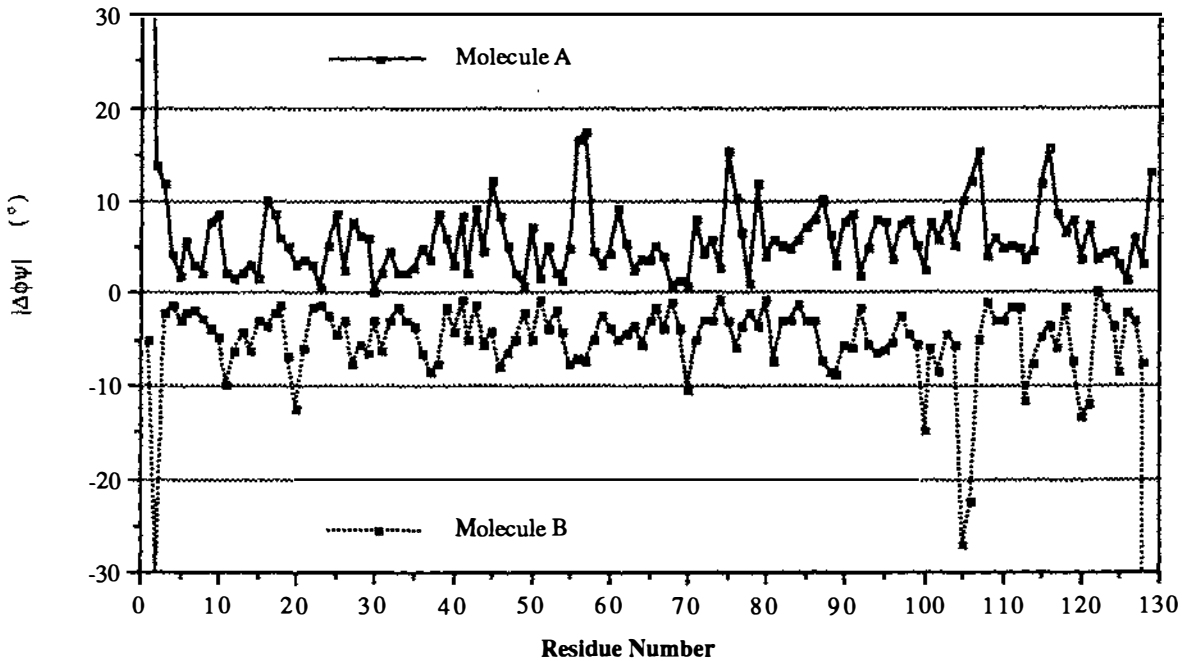

Figure 4.2.2.1. Change in the main-chain torsion angles |Δφψ| between apo and oxidised azurins.

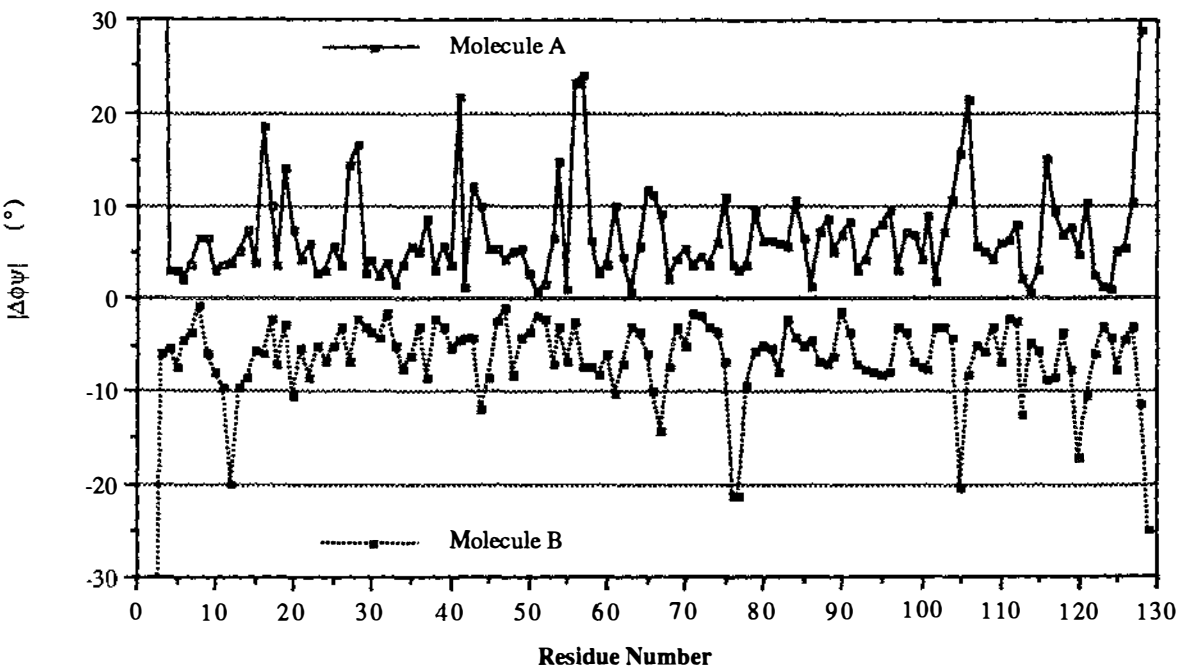

Figure 4.2.2.2. Change in main-chain torsion angles |Δφψ| between apo and reduced azurins.

model gives a higher initial R-factor (see Section 4.2.4). Of particular interest is that there appear to be some small changes in (ϕ,ψ) in the sections of the polypeptide chain containing the copper ligands (Met-44 to Asn-47 and Cys-112 to Met-121).

Comparison of apo and oxidised azurins

Consistent changes in the main-chain torsion angles upon removal of the copper from the oxidised protein are isolated to a few residues. In the entire structure, changes greater than 9° (1.5 r.m.s.) which occur in both protein molecules are restricted to the residues Lys-27, Gln-57, Glu-106, Ala-119 and Met-121 (see Table 4.2.2.1). Three of these residues (Lys-27, Gln-57 and Glu-106) are found in flexible or poorly defined parts of the polypeptide chain, and their differences are probably not due to the removal of the copper. The changes in Ala-119 and Met-121 may be the result of copper removal, because they belong to a loop of the copper binding site. However, there are other large changes in this loop (residues 113-121) which are <u>not</u> consistent (r.m.s. deviation in (ϕ,ψ) of 8.6°, see Table 4.2.2.2). In fact, a number of non-consistent changes occur in the residues 45-46 and 112-121, which supply the copper ligands, suggesting that these sections of the polypeptide chain may have become more flexible upon the removal of the metal (see Section 4.2.8 on thermal parameters).

Table 4.2.2.1. Consistent changes in the main-chain torsion angles between apo and oxidised azurins. Differences are as apo - oxidised, and those greater than 9° are highlighted in bold.

	Molecule A		Molecule B		Average change	
	$\Delta\phi$	$\Delta\psi$	$\Delta\phi$	$\Delta\psi$	$<\Delta\phi>$	$<\Delta\psi>$
Lys-27	-1	**-11**	+4	**-10**	+2	**-11**
Gly-57	-19	**+15**	-3	**+10**	-11	**+13**
Glu-106	+11	**+13**	-30	**+11**	-10	**+12**
Ala-119	**-9**	+7	**-10**	+3	**-10**	+5
Met-121	**+10**	-3	**+17**	-2	**+14**	-3

Table 4.2.2.2. Changes in the main-chain torsion angles of apo and oxidised azurins, including non-consistent changes, for residues near the copper binding site. Differences are apo - oxidised, and those greater than 9° are highlighted in bold.

	Molecule A		Molecule B	
	$\Delta\phi$	$\Delta\psi$	$\Delta\phi$	$\Delta\psi$
Gly-45	+1	**+17**	+1	+6
His-46	**-10**	+6	-3	**+11**
Ser-113	-1	+5	-5	**+16**
Phe-114	-4	-5	**-11**	0
Pro-115	**+16**	-5	+6	-3
Gly-116	**-11**	**+19**	+3	-4
His-117	**-11**	-5	-7	+5
Trp-118	+2	**+9**	-1	+2
Ala-119	**-9**	+7	**-10**	+3
Met-120	-5	+1	**+9**	**-17**
Met-121	**+10**	-3	**+17**	-2

Table 4.2.2.3. Consistent changes in the main-chain torsion angles of apo and reduced azurins. Values in bold are changes above 10° (apo - reduced).

	Molecule A		Molecule B		Average change	
	Δφ	Δψ	Δφ	Δψ	<Δφ>	<Δψ>
Met-44	-6	**-13**	-1	**-17**	-4	**-15**
Thr-61	0	**-14**	-4	**-14**	-2	**-14**
Ser-94	**-10**	+1	**-10**	+5	**-10**	+3
Val-95	-2	**+11**	-6	**+10**	-4	**+11**
Thr-96	**-13**	+3	**-10**	-5	**-12**	-1
Gly-116	-9	**+19**	-4	**+12**	-7	**+16**
Ala-119	**-11**	0	**-11**	+1	**-11**	+1
Met-121	**+12**	-8	**+15**	-2	**+14**	-6

Table 4.2.2.4. Changes in the main-chain torsion angles of apo and reduced azurins, including non-consistent changes, for residues near the copper binding site. Differences are apo - reduced, and those greater than 10° are highlighted in bold.

	Molecule A		Molecule B	
	Δφ	Δψ	Δφ	Δψ
Ala-43	-8	**+15**	0	+6
Met-44	-6	**-13**	-1	**-17**
Gly-45	+1	**+17**	+1	+6
Cys-112	**-11**	-2	+2	+3
Ser-113	0	-3	**-10**	**+15**
Phe-114	0	+1	-6	+3
Pro-115	+4	-2	+5	-6
Gly-116	-9	**+19**	-4	**+12**
His-117	**-13**	-3	-8	+9
Trp-118	+5	+8	0	-5
Ala-119	**-11**	0	**-11**	+1
Met-120	+3	-6	**+14**	**-20**
Met-121	**+12**	-8	**+15**	-2

Comparison of apo and reduced azurins

More consistent changes in the main-chain torsion angles occur between apo and reduced azurins than between apo and oxidised azurins. Changes above 10° (1.5 r.m.s.) in both independent molecules are in residues Met-44, Thr-61, Ser-94, Val-95, Thr-96, Gly-116, Ala-119 and Met-121 (see Table 4.2.2.3). Some of these residues are not near the copper binding site; Thr-61 is in the α-helix of the "flap" region, while residues 94-96 are in a β-strand. The changes in these sections are not understood; however all of these residues are on the surface of the protein, and Ser-94 is near an intermolecular contact in molecule A. The changes in Met-44, Gly-116, Ala-119 and Met-121 are near the copper binding site, and thus may be related to the removal of the copper. However, as was seen in the comparison of apo and oxidised azurins, there are other large (>10°) non-consistent changes in the two copper binding loops of azurin (see Table 4.2.2.4). The r.m.s. deviations in (φ,ψ) for residues 43-45 and 112-121 are 9.3° and 8.5°, respectively, and the changes in these loops may be a sign of increased flexibility, as was suggested earlier.

4.2.3 Hydrogen Bonding

The hydrogen bonding of apo-azurin is very similar to that of the reduced and oxidised forms. Figures 3.2.3.1 and 3.2.3.2, which are schematic diagrams illustrating the hydrogen bonding of the β-sheets and α-helix of reduced azurin, apply equally well to the structure of apo-azurin. A complete list of the hydrogen bonds in apo-azurin, as well as their geometries, is given in Appendix B. The r.m.s. differences in the hydrogen bond geometry between the apo-azurin and the other two forms are given in Table 4.2.3.1, and show that the changes are small for most of the structure. The differences are similar to those found between reduced and oxidised forms in Section 3.2.3. The larger differences in the side-chain...side-chain geometries was also seen in the comparison of the reduced and oxidised forms; these differences result from the less well defined positions of the side-chain atoms.

Table 4.2.3.1. R.m.s. differences in hydrogen bond geometry between apo and oxidised azurins and apo and reduced azurins. The number of hydrogen bond pairs for each category is in brackets. For hydrogen bonds which do not have a calculated hydrogen atom position, the distances are X...Y, and the angles are X...Y-C.

	Apo & Oxidised		Apo & Reduced	
	O...H-N (°)	O...H (Å)	O...H-N (°)	O...H (Å)
Main-chain...main-chain	6.1 (114)	0.12 (106)	6.3 (109)	0.12 (107)
Main-chain...side-chain	6.5 (54)	0.13 (49)	6.5 (51)	0.13 (44)
Side-chain...side-chain	11.6 (20)	0.21 (19)	9.4 (17)	0.21 (17)

Main-chain...main-chain hydrogen bonds

Only a few minor changes occur in the hydrogen bonding of azurin upon removal of the copper. The differences in main-chain...main-chain hydrogen bonding are listed in Table 4.2.3.2, where a tick (✓) represents the presence of a "non-marginal" hydrogen bond (i.e. where O...H is less than 2.3Å and all angles are greater than 100°). Two thirds (4 out of 6) of the differences in the main-chain...main-chain hydrogen bond between the three forms of azurin occur in the "flap" region. Of these differences, only one appears in the α-helix (O 61...N 65), while the rest appear in the set of loops between residues 67-81. Other differences are in the loops inter-connecting the β-strands, and only one involves a main-chain...main-chain hydrogen bond in the "northern" part of the molecule (O 10...N 13). Overall, the changes in hydrogen bonding between the apo, oxidised and reduced forms are located on the surface of the protein in the loops of the polypeptide chain, and may represent structural microheterogeneity.

Table 4.2.3.2. Differences in the hydrogen bonding structure of apo, oxidised and reduced azurins. A tick "✓" signifies the presence of a "non-marginal" hydrogen bond, and one in parentheses signifies a "marginal" hydrogen bond.

	oxidised		apo		reduced	
	A	B	A	B	A	B
main-chain...main-chain						
O 10...N 13		✓			(✓)	
O 61...N 65	(✓)	(✓)	✓	(✓)		
O 67...N 70	(✓)		✓	(✓)	(✓)	(✓)
O 74...N 77	✓		✓		✓	
O 77...N 80		✓		(✓)		(✓)
O 128...N 24			(✓)		✓	
main-chain...side-chain						
$O_{\varepsilon 1}$ 2...N 3		✓		✓		
$O_{\delta 1}$ 11...N 39	(✓)	✓		(✓)	✓	(✓)
O 16...N_{ζ} 18	✓					
O 57...$O_{\gamma 1}$ 61	(✓)	✓			✓	✓
O 81...N_{ζ} 101		✓		✓		
O 86...N_{ζ} 41		✓		✓	✓	
$O_{\delta 2}$ 98...N 100	✓		✓		✓	
O_{ε} 129...N_{ζ} 24		✓				
side-chain...side-chain						
$O_{\varepsilon 1}$ 4...$N_{\varepsilon 2}$ 32	✓				✓	✓
$O_{\varepsilon 1}$ 14...$N_{\delta 2}$ 10	✓	✓		✓	✓	✓
$N_{\delta 1}$ 46...112 Sγ			✓	✓		
$O_{\varepsilon 1}$ 53...N_{ζ} 122	✓	(✓)		(✓)		
$O_{\delta 1}$ 62...N_{ζ} 74	✓		✓		✓	
$O_{\delta 1}$ 77...N_{ε} 79	✓	✓	✓	✓		✓
$O_{\varepsilon 1}$ 91...N_{ζ} 41	✓		(✓)			
$O_{\delta 1}$ 93...N_{ζ} 85		(✓)		✓		✓
$O_{\delta 1}$ 98...N_{ζ} 27					✓	
$O_{\delta 1}$ 98...Oγ 100		✓		✓		✓
$N_{\delta 1}$ 117...Sγ 112			✓	✓		
O_{ε} 129...Oγ 128			✓			

Main-chain...side-chain hydrogen bonds

Eight differences in the main-chain...side-chain hydrogen bonding are observed between apo, oxidised and reduced forms of azurin. Two of these differences are due to "non-marginal" hydrogen bonds which occur in only one out of the six molecules (from the three forms of azurin). The majority (7) of these differences are in or near loops (5), or involve the termini (2) of the polypeptide chain. One difference appears in the "kink" of β-strand 2 (O 16...N_{ζ} 18). Four differences are crosslinking hydrogen bonds, of which two are located at the "northern" part of the molecule ($O_{\delta 1}$ 11...N 39 and O 86...N_{ζ} 41). The reasons for the differences in the main-chain...side-chain hydrogen bonding are the not same as those found for the main-chain...main-chain hydrogen bonding, instead the

differences are mostly the result of poor definition for these parts of the structure, since five out of eight interactions involve lysine side-chains or the termini of the polypeptide chain.

Side-chain...side-chain hydrogen bonds

A similar situation occurs with the side-chain...side-chain hydrogen bonds as with the main-chain...side-chain hydrogen bonds, where most of the differences in the hydrogen bonding are at the surface of the molecule in poorly defined regions. Many of the these hydrogen bonds involve lysine side-chains which are poorly defined in the structure (5 out of 12), a trend also seen in the differences between the reduced and oxidised structures. At the copper binding site, however, two new hydrogen bonds are formed, linking at the sulphur of Cys-112, presumed to be a thiol, to the imidazole nitrogens of His-46 and His-117. These are discussed in detail in Section 4.2.6.

Although there are many differences (12) in side-chain...side-chain hydrogen bonding, there are six hydrogen bonds which are common to all of the molecules in the three forms of azurin. Two are located in the flap region ($O_{\delta 1}$ 62...$N_{\eta 2}$ 79 and $O_{\delta 2}$ 77...$N_{\eta 2}$ 79), and two are found on β-sheet 1 ($O_{\gamma 1}$ 30...$O_{\gamma 1}$ 96 and $N_{\delta 1}$ 32...O_{γ} 94). Of the remaining two, one is in the loop that links β-strands 1 and 2 ($O_{\delta 1}$ 23...O_{γ} 25), and the other is an internal hydrogen bond near the metal binding site ($N_{\delta 2}$ 47...O_{γ} 113). Other common side-chain...side-chain hydrogen bonds, appearing in five of the six protein molecules, are $N_{\delta 2}$ 10...$O_{\varepsilon 1}$ 14, $O_{\delta 1}$ 77...N_{ε} 79 and $O_{\varepsilon 1}$ 106...●$_{\eta}$ 108. The only salt bridge which is common to all of the molecules in the three forms, is that formed between the side-chains of Asp-62, Asp-77 and Arg-79. Other salt bridge interactions which exist in at least half of the six molecules are between $O_{\varepsilon 1}$ 53...N_{ζ} 122, $O_{\delta 1}$ 62...N_{ζ} 74 and N_{ζ} 85...$O_{\delta 1}$ 93. Interestingly, of the side-chain...side-chain hydrogen bonds, those that are found in most of the molecules of the three forms usually involve at least one hydrogen bonding partner which is invariant in all azurins, and may indicate that the these hydrogen bonds are important for stabilising local configurations in the structure[31].

4.2.4 Superposition

When the apo protein is superimposed on the oxidised and reduced structures using all the protein atoms (method of Kabsch[255]), the r.m.s. deviation in the atom positions is 0.57Å between the apo and the oxidised structures and 0.85Å between the apo and the reduced structures. For the main-chain atoms, excluding the polypeptide chain termini, the r.m.s. deviation in atom positions is less at 0.16Å between the apo and oxidised

structures and 0.21Å between the apo and reduced structures. The differences between apo-azurin and the other two forms of azurin are less than those between the two apo-azurin molecules of the asymmetric unit, a result also found in the structural analysis of reduced azurin.

Although all three forms are very similar to each other, the r.m.s. deviation in atom positions suggests that the apo structure is more like the oxidised than the reduced structure. To test that this is not an artefact of starting the refinement with the oxidised azurin coordinate set, two R-factors were calculated against the X-ray data of apo-azurin; one with the oxidised azurin coordinates and the other with the reduced azurin coordinates[†] . The R-factor from the oxidised set (R = 0.276) was much lower than the reduced set (R = 0.322), supporting the suggestion that the apo-azurin structure is more like oxidised azurin. Ideally, parallel refinements starting from both oxidised and reduced coordinates could have been done to determine if the convergence is towards the same structure. Other aspects of this structural analysis also show that the apo form is more like the oxidised structure of azurin.

Comparison with the oxidised structure

To compare the apo with the oxidised structure, the same method of superposition was used as in the analysis of the reduced structure (i.e. the best fit was obtained using all of the main-chain atoms, except for the N- and C-termini)[255]. Figure 4.2.4.1 illustrates the average differences in main-chain atom position between the apo and oxidised structures. The largest differences clearly occur at the termini of the polypeptide chain, while other large deviations (>0.3Å or 2 r.m.s.) appear at residues which belong to loops of the structure.

Among side-chains, the largest differences between the apo and oxidised structures occur for those groups which are on the surface of the protein molecule. Twenty-seven side-chains between the two structures have an average difference in atom positions above 0.5Å; these include 9 Lys, 5 Glu, 3 Met, 3 Thr, 2 Gln, 1 Ala and 4 at the N and C-termini. Those where differences are seen for both molecules, apart from the N- and C-termini, are Lys-52, Glu-53, Thr-61, Met-64, Glu-106 and Lys-122. These differences are due to poor definition in the structure for these regions, a result of the flexibilty of these side-chains (e.g. Glu-53, Glu-106 and Lys-122).

[†] Note that the fractional coordinates were used to account for the differences in the unit cell dimensions between apo, oxidised and reduced azurins.

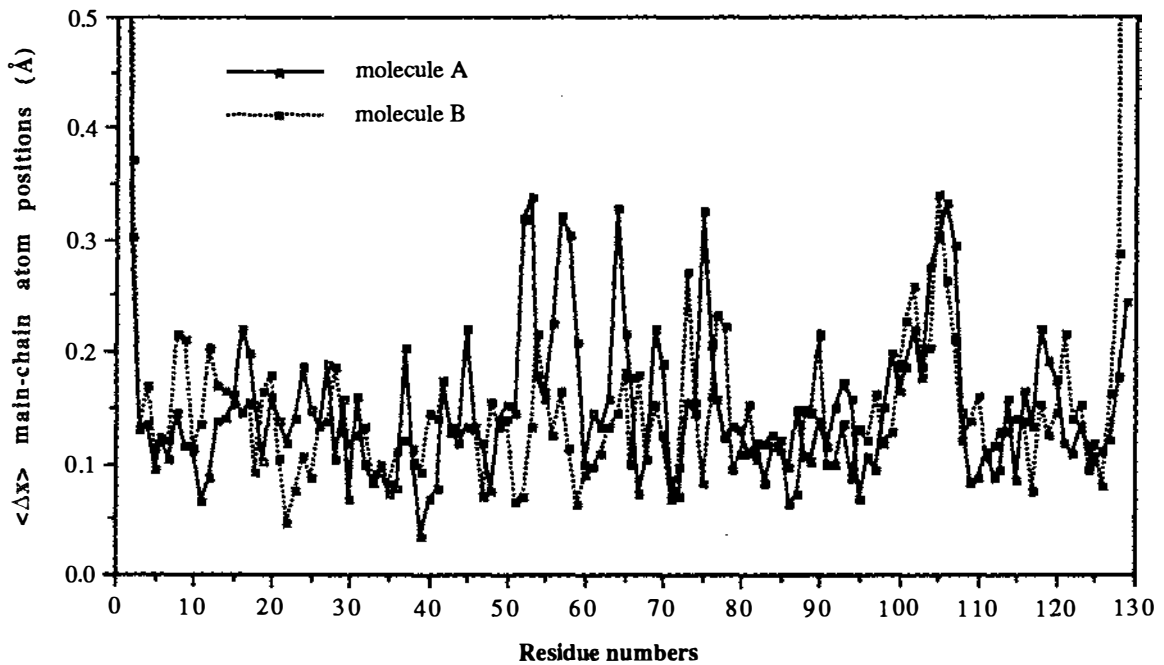

Figure 4.2.4.1. Average difference in main-chain atom positions for each residue between apo and oxidised azurins. Off scale values are at residues 1A (1.071Å), 1B (1.833Å) and 129B (1.859Å).

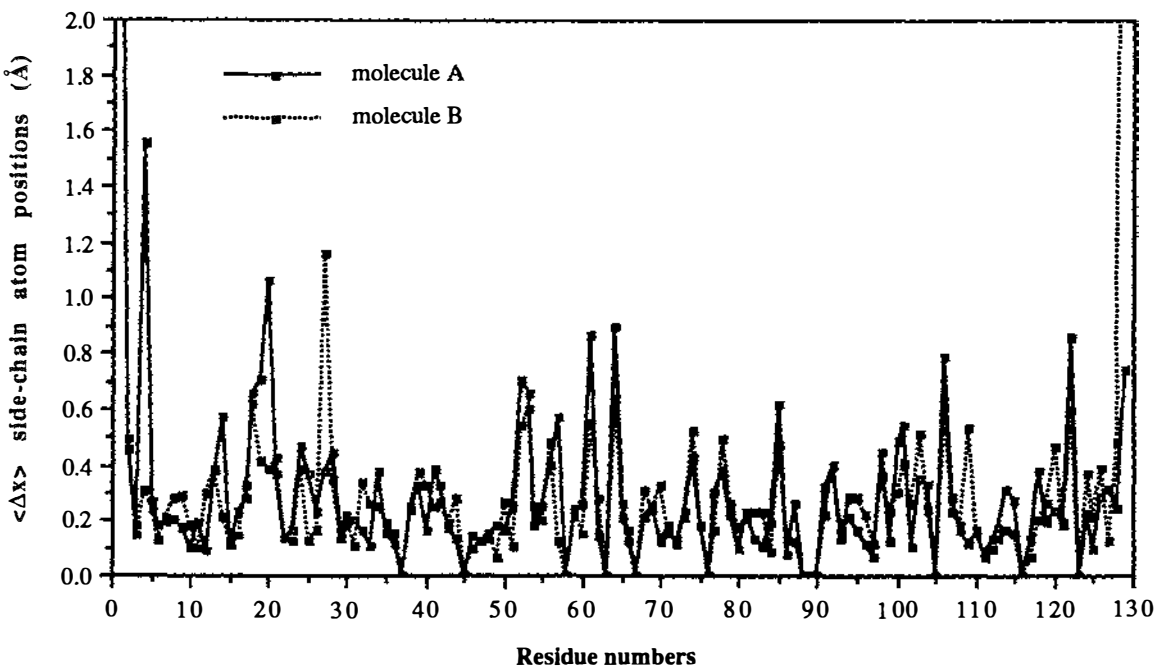

Figure 4.2.4.2. Average difference in side-chain atom positions for each residue between apo and oxidised azurins. Off scale values are at residues 1A (2.490Å), 1B (3.266Å) and 129B (4.096).

Comparison with reduced azurin

There are larger differences between the apo and reduced structures than between the apo and oxidised structures (see Figure 4.2.4.3). This is apparent in the greater number of residues which have an average devation in main-chain atom positions above 0.3Å. All of these residues are at the surface of the protein, and most are located in the loops of the polypeptide chain. An unexpected difference in the main-chain structure is in the loop of residues 112-121 which supplies three of the copper ligands, where several of the residues have an average difference in main-chain atom positions between 0.25-0.35Å. Differences in this region between the apo and oxidised structures are less.

A comparison of the side-chains of apo and reduced azurins also shows that the largest differences appear on the surface of the protein. There are approximately twice as many side-chains whose average difference in position is greater than 0.5Å as there are between the apo and oxidised structures. These consist of 21 Lys, 9 Glu, 8 Gln, 7 Met and 10 Val/Thr, including both molecules of the asymmetric unit.

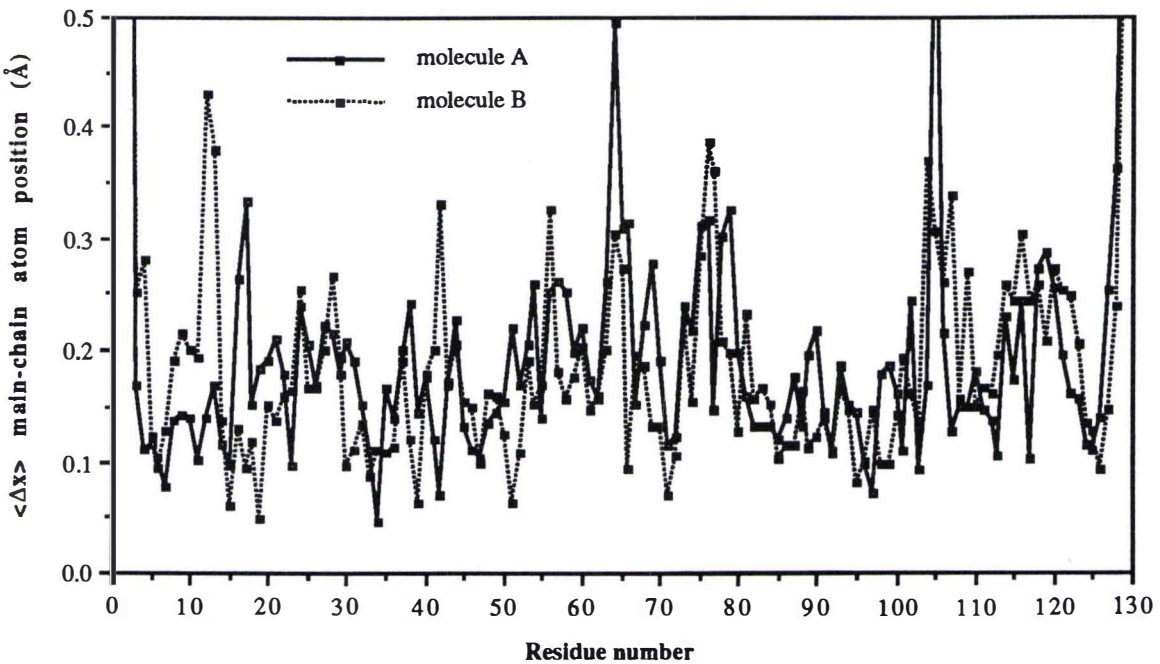

Figure 4.2.4.3. Average difference in main-chain atom positions for each residue between apo and reduced azurins. Off scale residues are at 1A (5.085Å), 1B (5.674Å), 2A (1.924Å), 2B (1.073Å), 105A (0.628), 129A (0.761Å) and 129B (0.756Å).

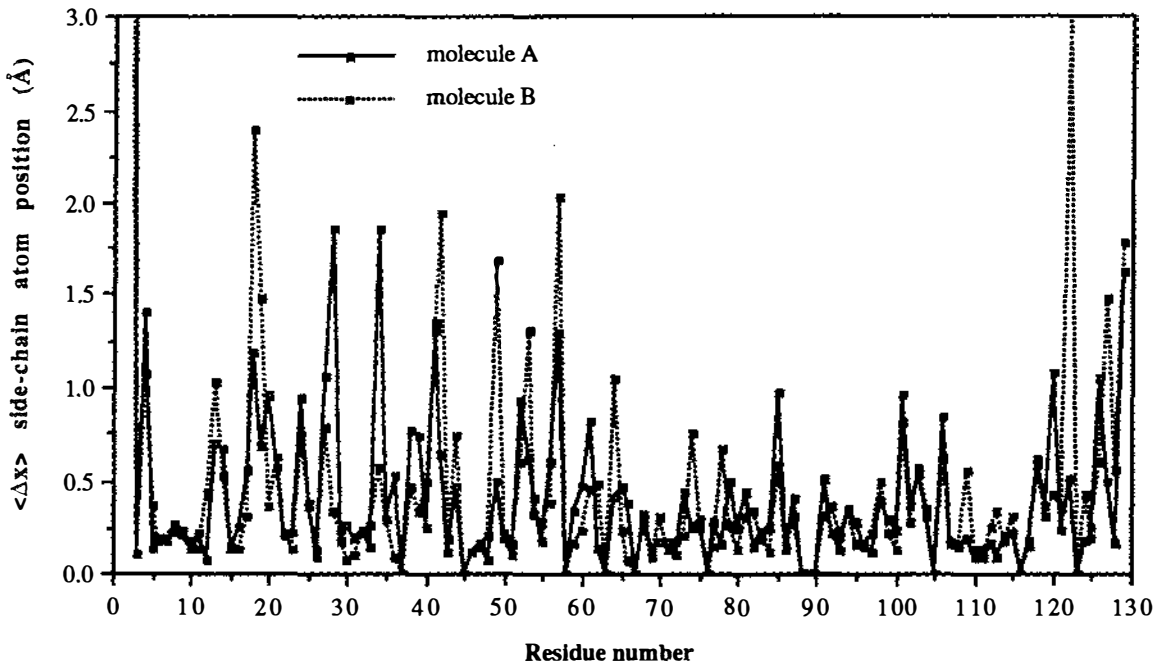

Figure 4.2.4.4. Average difference in side-chain atom positions for each residue between apo and reduced azurins. Off scale values are at residues 1A (8.170Å), 1B (6.882Å), 2A (5.915Å), 2B (5.023Å) and 122A (3.234Å)

4.2.5 Consistent Shift Analysis

In the previous section, the largest differences between the structures of apo-azurin and the two redox forms of azurin were attributed to the flexible nature and poor definition of those residues which were located on the surface of the protein. However, to identify the more subtle changes in the structure which result from removal of the copper, the consistency of shifts in the atom positions must be examined. The method used is described in the consistent shift analysis section for reduced azurin (Section 3.2.5). Here, two sets of consistent shift vectors are calculated, one between the apo and oxidised structures and the other between the apo and reduced structures.

Consistent shifts between apo and oxidised azurins

When the apo protein molecules are analysed for consistent shifts between the apo and oxidised forms, eight side-chains give Ξ scores above 100. Most of these shifts are small (<0.5Å), and appear unrelated to the removal of the copper from the protein. These small changes are normally the result of small changes in the torsion angles. One shift, however, may be related to the removal of the copper, since it is a translation in the

phenyl ring of Phe-114, which forms part of the surrounding environment of the copper site (see Figure 4.2.5.1).

A further sixteen consistent shifts in the oxidised to apo transition have Ξ scores between 50 and 100. Most of these shifts also appear unrelated to the removal of the copper, except possibly the changes in the main-chain atoms of Ala-43, Met-44 and Gly-45. Here the average shifts are small (0.12-0.18Å), but as Figure 4.2.5.2 illustrates, these shifts may be caused by the carbonyl oxygen of Gly-45 moving away from the space vacated by the copper.

Table 4.2.5.1. Results from the consistent shift analysis between apo and oxidised azurin structures.

Residue		Ξ	Average angle between shift vectors (°)	Average distance shifted (Å)
Ξ > 100				
Ala-1	(s.c.)	474.06	48.27	2.878
Val-21	(s.c.)	160.43	20.30	0.395
Val-31	(s.c.)	114.79	38.89	0.152
Thr-61	(s.c.)	191.67	67.68	0.708
Leu-68	(s.c.)	241.94	15.28	0.259
Ser-92	(s.c.)	208.72	38.66	0.398
Val-95	(s.c.)	101.58	34.34	0.223
Phe-114	(s.c.)	174.67	12.95	0.235

Table 4.2.5.2. Results from the consistent shift analysis between apo and oxidised azurin structures.

Residue		Ξ	Average angle between shift vectors (°)	Average distance shifted (Å)
100 > Ξ > 50				
Leu-17	(s.c.)	73.36	34.44	0.306
Met-20	(s.c.)	53.38	41.36	0.725
Cys-26	(s.c.)	62.60	37.03	0.197
Lys-27	(s.c.)	54.93	86.89	0.770
Val-31	(m.c.)	56.48	44.27	0.143
Ala-43	(m.c.)	52.05	33.16	0.132
Met-44	(m.c.)	84.74	25.58	0.122
Gly-45	(m.c.)	56.32	49.46	0.176
Trp-48	(s.c.)	59.06	41.69	0.144
Val-73	(m.c.)	69.71	80.99	0.212
Val-73	(s.c.)	96.03	25.16	0.222
Ala-82	(s.c.)	68.09	31.53	0.184
Ile-87	(s.c.)	52.81	64.05	0.197
Ser-94	(s.c.)	95.49	27.69	0.245
Lys-122	(s.c.)	67.17	76.06	0.726

Figure 4.2.5.1. The small shift in the phenyl ring of Phe-114, which is part of the surrounding structure of the copper binding site. Oxidised azurin is in two shades of blue; dark blue (molecule A) and light blue (molecule B), while apo-azurin is in yellow (molecule A) and light yellow (molecule B).

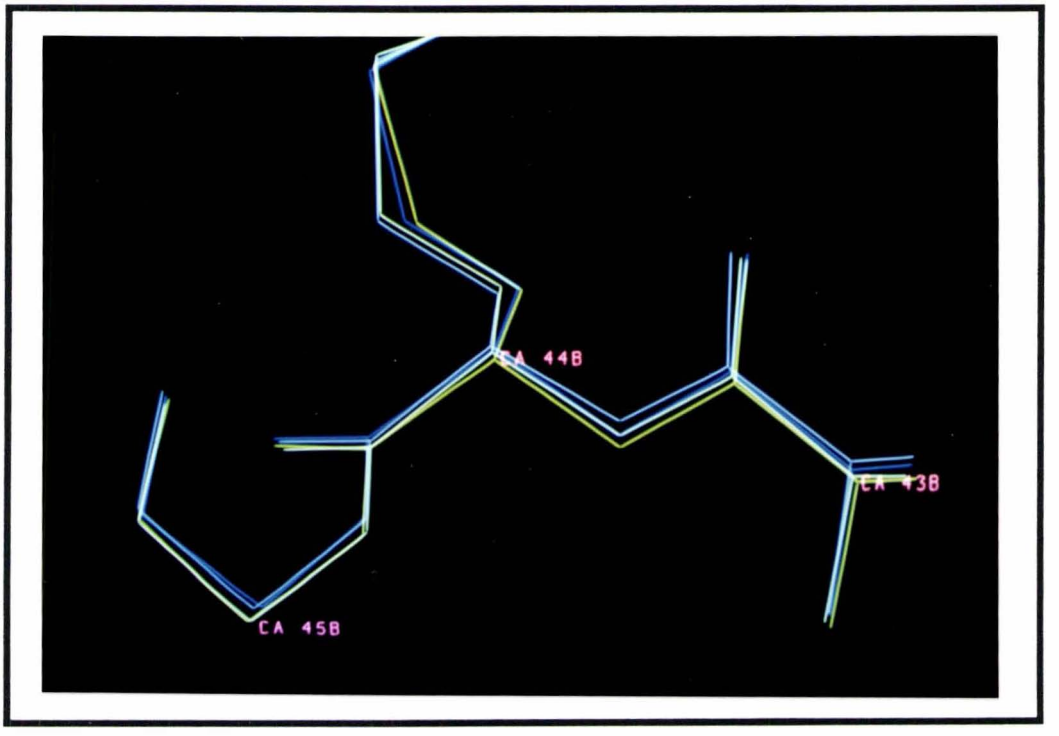

Figure 4.2.5.2. The shift in the main-chain atoms of Ala-43, Met-44 and Gly-45, possibly a result of the movement in the carbonyl oxygen of Gly-45. Oxidised azurin is in two shades of blue; dark blue (molecule A) and light blue (molecule B), while apo-azurin is in yellow (molecule A) and light yellow (molecule B).

Consistent shifts between reduced and apo-azurin

The analysis of the consistent shifts between the apo and reduced forms of azurin shows more changes in the structure than between the apo and the oxidised forms. As was shown before for the oxidised to apo transition, the majority of the consistent shifts are changes unrelated to the removal of the copper and are the result of small movements of flexible groups. However, three noteworthy shifts, with Ξ scores above 100, are seen at Cys-112, Pro-115 and Gly-116. The change in Cys-112 is very clear as the S_γ 112 atom moves towards the position vacated by the copper atom (see Figure 4.2.5.3), while the shifts at Pro-115 and Gly-116 seem to be in the direction away from the copper binding site (see Figure 4.2.5.4).

Table 4.2.5.3. Results from the consistent shift analysis between apo and reduced azurin structures.

Residue		Ξ	Average angle between shift vectors (°)	Average distance shifted (Å)
Ξ > 100				
Ala-1	(s.c.)	108.03	112.58	7.526
Gln-2	(s.c.)	1609.00	76.32	5.469
Ile-7	(s.c.)	101.82	63.66	0.174
Val-21	(s.c.)	321.10	46.89	0.589
Lys-38	(s.c.)	146.94	68.39	0.609
Met-44	(s.c.)	149.35	27.28	0.597
Val-49	(s.c.)	169.40	103.54	1.088
Lys-52	(s.c.)	127.42	47.99	0.759
Gln-57	(s.c.)	343.65	69.41	1.654
Leu-68	(s.c.)	154.96	36.68	0.291
Ile-87	(s.c.)	307.69	40.97	0.356
Ser-94	(s.c.)	180.78	30.44	0.342
Lys-101	(s.c.)	153.43	43.76	0.889
Leu-102	(s.c.)	168.21	65.74	0.315
Thr-103	(s.c.)	204.49	25.16	0.548
Cys-112	(s.c.)	129.49	56.92	0.207
Pro-115	(s.c.)	119.67	40.27	0.267
Gly-116	(m.c.)	184.73	19.82	0.274
Trp-118	(s.c.)	135.58	58.22	0.597

Other smaller indications of consistent shifts (Ξ = 50-100) are also seen near the copper binding site. These are at Ala-40, Met-44, Phe-114, Pro-115, Trp-118, Ala-119 and Met-121. The changes at Ala-40 and Met-44 result in a subtle change in the bifurcated hydrogen bond made from O 40 to N 44 and N 43. Figure 4.2.5.5 shows the carbonyl oxygen of O 44 changing orientation to point more toward N 44 than N 43 in the apo structure. The changes in Phe-114 are a small translation in the phenyl ring, and a movement in the peptide nitrogen which makes a hydrogen bond to S_γ 112 (see Figure 4.2.5.6). The shifts in Trp-118 (main-chain) and Ala-119 are less clear, but may be due to the changes in the loop structure that forms part of the copper binding site. Finally, the shift in Met-121 is actually the result of the C_ε 121 atom shifting on average by 0.3Å

Table 4.2.5.4. Results from the consistent shift analysis between apo and reduced azurin structures.

Residue		Ξ	Average angle between shift vectors (°)	Average distance shifted (Å)
100 > Ξ > 50				
Met-13	(s.c.)	74.91	71.82	0.863
Lys-24	(s.c.)	58.67	99.61	0.838
Ala-40	(m.c.)	53.30	91.47	0.177
Met-44	(m.c.)	83.49	47.97	0.216
Glu-53	(s.c.)	76.64	100.71	0.966
Thr-61	(s.c.)	62.04	82.48	0.627
Met-64	(s.c.)	86.71	53.65	0.727
Val-73	(m.c.)	77.24	24.69	0.233
Ala-82	(s.c.)	83.55	14.27	0.238
Lys-85	(s.c.)	50.25	72.17	0.776
Ala-109	(s.c.)	69.70	15.81	0.363
Phe-114	(m.c.)	70.89	57.08	0.244
Phe-114	(s.c.)	70.61	37.97	0.189
Pro-115	(m.c.)	96.89	24.29	0.209
Trp-118	(m.c.)	63.82	50.47	0.265
Ala-119	(s.c.)	64.54	46.73	0.335
Met-121	(s.c.)	50.45	62.14	0.290

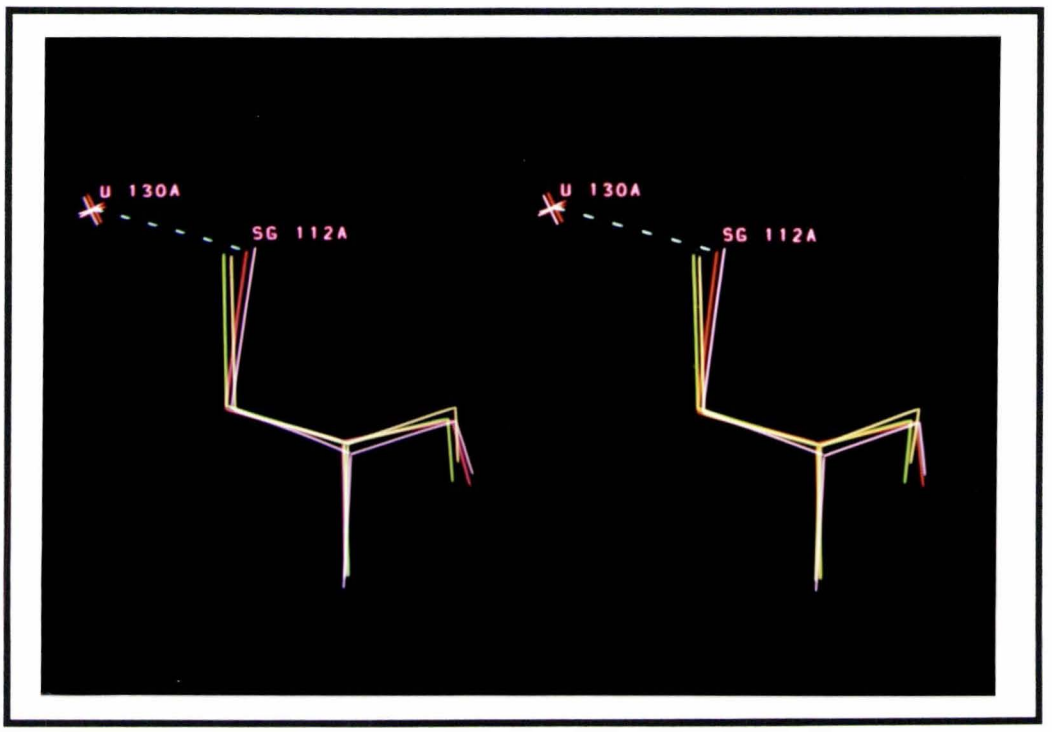

Figure 4.2.5.3. The shift of S_γ 112 into the space vacated by the copper. Reduced azurin is in red (molecule A) and pink (molecule B), while apo-azurin is in yellow-green (molecule A) and yellow (molecule B).

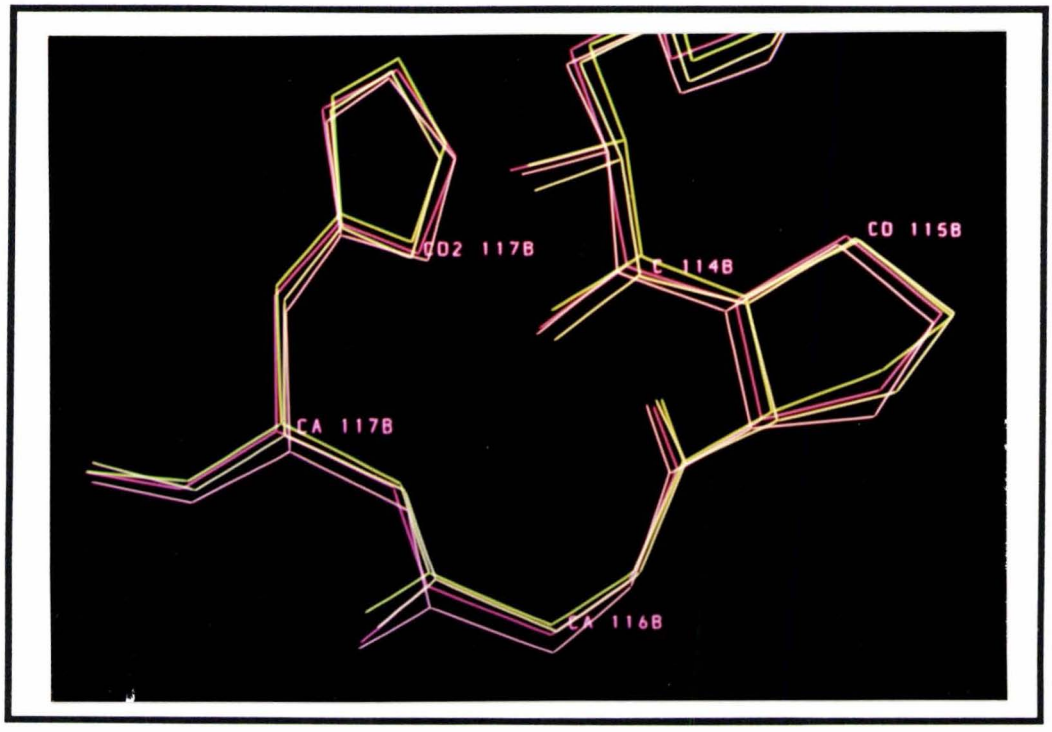

Figure 4.2.5.4. The shifts in Pro-115 to Gly-116 away from the copper binding site. Reduced azurin is in red (molecule A) and pink (molecule B), while apo-azurin is in yellow-green (molecule A) and yellow (molecule B).

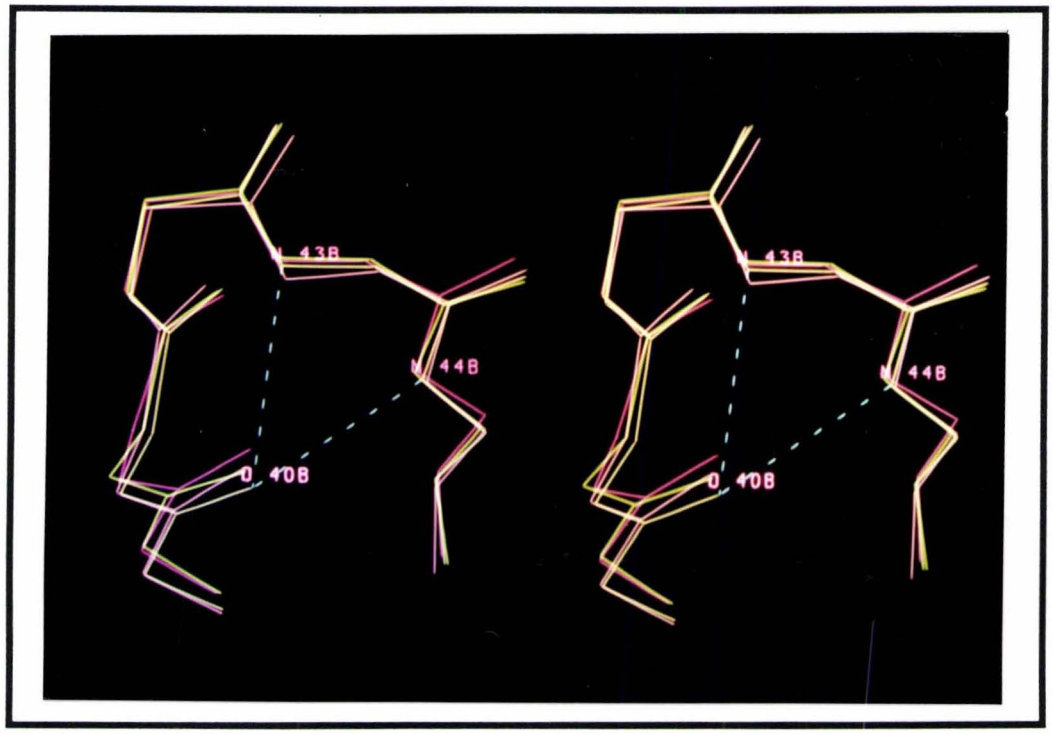

Figure 4.2.5.5. The shifts in the O 40...N 44 and O 40...N 43 hydrogen bonds. Reduced azurin is in red (molecule A) and pink (molecule B), while apo-azurin is in yellow-green (molecule A) and yellow (molecule B).

between the reduced and apo forms.

4.2.6 The Copper binding site

The copper binding site of apo-azurin is structurally very similar to the oxidised and reduced sites, except for the absence of the copper ion. The site is well buried in the protein interior, and contains a cavity which could accomodate an ellipsiod of dimensions 1.2Å × 1.2Å × 3.0Å. The same residues which are the copper ligands in the oxidised and reduced azurins, also form the border of the cavity (Gly-45, His-46, Cys-112, His-117 and Met-121). As with the oxidised and reduced forms of azurin, the side-chains of His-46, Cys-112 and His-117, are arranged in a trigonal fashion around the cavity, while the carbonyl oxygen of Gly-45 and the side-chain of Met-121 cap off either the end of the cavity. Figures 4.2.6.1 and 4.2.6.2 are two views rotated 90° degrees with respect to each other, and show the van der Waals surfaces of the copper binding site. Figure 4.2.6.1 looks down the long axis normal to the N_2S plane of His-46, Cys-112 and His-117, while Figure 4.2.6.2 looks along this plane.

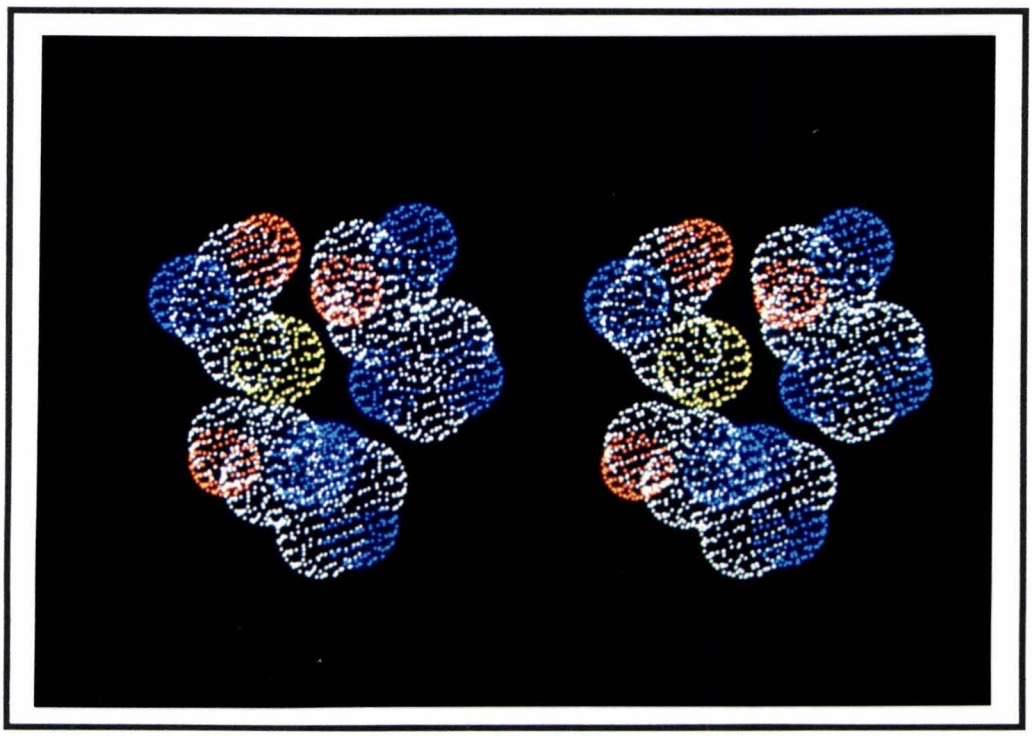

Figure 4.2.6.1. Van der Waals surface (75%) of the copper binding site of apo-azurin, looking down the O 45...Sδ 121 axis normal to the N_2S plane of His-46, Cys-112 and His-117. (Sulphur atoms in yellow, nitrogen atoms in blue, oxygen atoms in red and carbon atoms in white.)

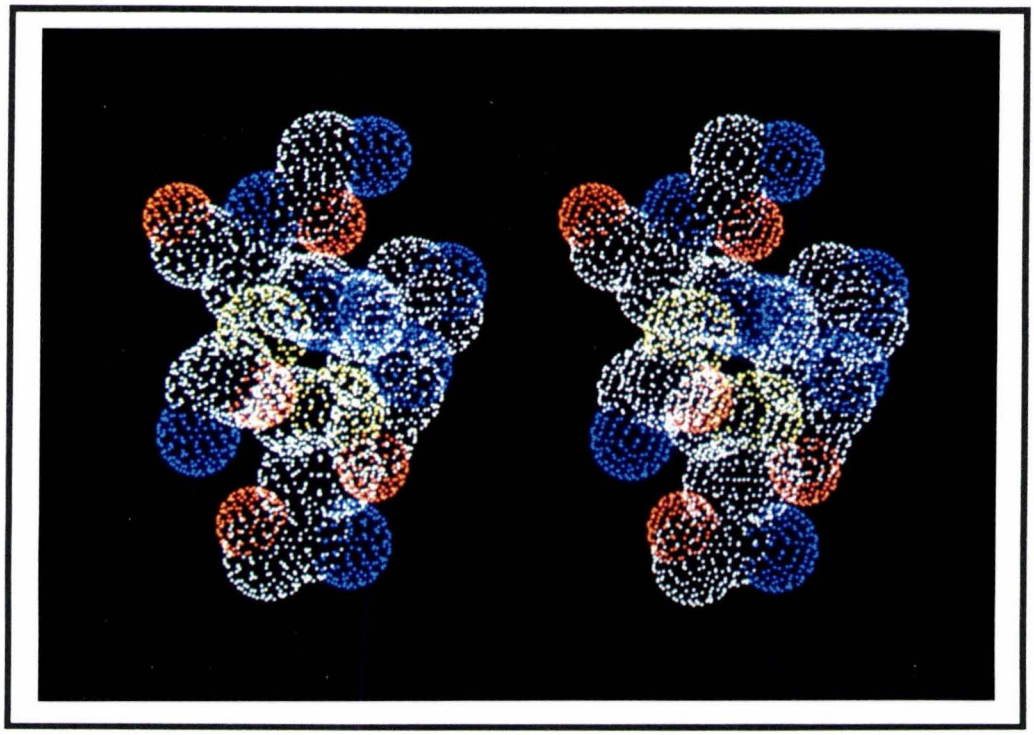

Figure 4.2.6.2. Van der Waals surface (75%) of the copper binding site of apo-azurin, along the N_2S plane of His-46, Cys-112 and His-117, and 90° to Figure 4.2.6.1. (Sulphur atoms in yellow, nitrogen atoms in blue, oxygen atoms in red and carbon atoms in white.)

With the removal of the copper atom from the active site, there are several reasons to believe that the sulphur of Cys-112 is protonated. First, thiol groups have a $pK_a \approx 8.2$, and under the pH conditions at which the crystals were soaked (≈pH 6.0), the cysteine sulphur should be protonated. Second, Cys-112 is buried in the interior of the protein, and if the thiolate was left unprotonated, this would leave a negative charge in the hydrophobic core of the protein, and would effectively destabilise the protein configuration. Unfortunately, the resolution of the X-ray data from the apo-azurin crystals (2.2Å) is too low to observe any hydrogens in electron density maps, but the configuration of the surrounding structure near the side-chain of Cys-112 suggests that a thiol hydrogen in a staggered conformation is feasible, since no unfavorable contacts to the surrounding structure would be made.

With the side-chain of Cys-112 protonated as a thiol, this group is found to be positioned such that it can act as a hydrogen bond donor to two other residues. Three distinct possibilities arise for thiol hydrogen bonding by Cys-112; 1) a hydrogen bond to $N_{\delta 1}$ of His-46, 2) a hydrogen bond to $N_{\delta 1}$ of His-117, or 3) bifurcated forming hydrogen bonds to His-46 and His-117. Figure 4.2.6.3 shows schematically the different possibilities for the formation of a thiol hydrogen bond between Cys-112, His-46 and His-117. Note that for both imidazoles the $N_{\varepsilon 2}$ atom is assumed to be protonated, because both of these atoms bind to hydrogen bond acceptors; for His-46, $N_{\varepsilon 2}$ binds to the carbonyl oxygen of

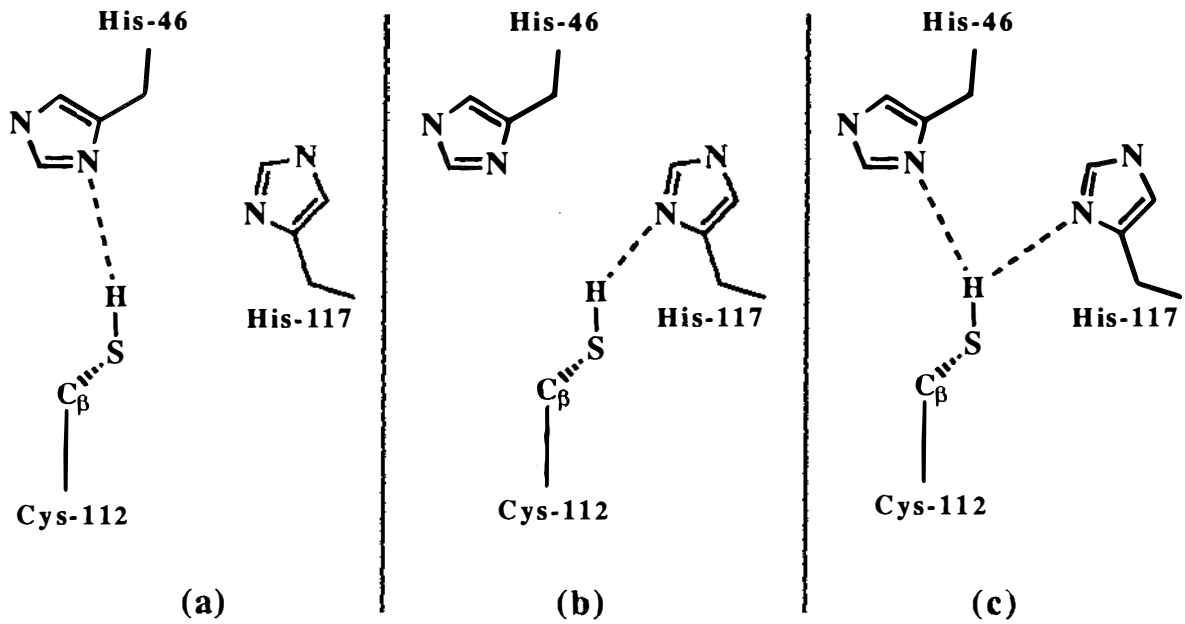

Figure 4.2.6.3. Schematic representations of possible thiol-type hydrogen bonds at the copper binding site of apo-azurin. The SH group interacts with a) His-46 only, b) His-117 only or c) both as a bifurcated interaction.

Table 4.2.6.1. Distances (Å) between the atoms of the copper binding site.

	Molecule A	Molecule B	Average
O 45...$N_{\delta 1}$ 46	3.16	3.25	3.21
O 45...S_{γ} 112	4.29	4.24	4.27
O 45...$N_{\delta 1}$ 117	3.42	3.57	3.50
O 45...S_{δ} 121	6.01	6.08	6.05
$N_{\delta 1}$ 46...S_{γ} 112	3.67	3.87	3.77
$N_{\delta 1}$ 46...$N_{\delta 1}$ 117	3.19	3.36	3.28
$N_{\delta 1}$ 46...S_{δ} 121	3.31	3.38	3.35
S_{γ} 112...$N_{\delta 1}$ 117	3.59	3.49	3.54
S_{γ} 112...S_{δ} 121	4.12	4.17	4.15
$N_{\delta 1}$ 117...S_{δ} 121	3.89	3.92	3.91

residue 10, while for His-117, $N_{\varepsilon 2}$ makes a hydrogen bond to a solvent molecule which is also hydrogen bonded to two carbonyl oxygens (O 43 and O 116), one of which is in the other protein molecule (O 116).

Table 4.2.6.1 gives the "inter-ligand" distances of the copper binding site, and shows that the average distances between the cysteine sulphur and the two $N_{\delta 1}$ atoms of His-46 and His-117 are 3.77Å and 3.54Å, respectively. Both of these distances are within the theoretical limits for a sulphur to nitrogen hydrogen bond; thus the thiol group appears to form a bifurcated hydriogen bond. Since $N_{\delta 1}$ of His-117 is on average ≈0.2Å closer to the cysteine sulphur than $N_{\delta 1}$ of His-46, this suggests that a slightly stronger interaction

is made to His-117 than to His-46. The possibilities of the thiol forming a hydrogen bond to either the carbonyl oxygen of Gly-45 or the thioether sulphur of Met-121 are remote since these atoms are too far from the thiol sulphur and make unfavorable orientations for a hydrogen bond (average distances of O 45...S_γ 112 = 4.27Å and S_δ 121...S_γ 112 = 4.15Å).

The orientation of the side-chains of His-46, Cys-112 and His-117 also supports the possibility of a bifurcated thiol hydrogen bond. All of the C-N...S and N...S-C angles are sufficiently close to 120° or 109°, respectively, to consider the interactions as hydrogen bonds (see Table 4.2.6.2). This geometry is comparable to those of thiol hydrogen bonds found in two surveys on hydrogen bonds involving sulphur in high resolution protein structures[245,246]. These surveys report that S-H groups can be involved in hydrogen bonds, but that this is not a frequent occurrence since free S-H groups usually form disulphide bridges. For those S-H groups found, however, the surveys revealed similar results, i.e. that the average S_γ...X (X = O or N) distance is 3.5±0.1Å[245], and can be as large as 3.7Å[246].

Table 4.2.6.2. SH...N thiol hydrogen bond geometries of the two molecules of apo-azurin. S...N-C angles defined by C_γ atom.

	Molecule A			Molecule B		
SH...N	C-S...N (°)	S...N (Å)	S...N-C (°)	C-S...N (°)	S...N (Å)	S...N-C (°)
S_γ 112...$N_{\delta1}$ 46	113	3.67	142	112	3.87	138
S_γ 112...$N_{\delta1}$ 117	119	3.59	144	112	3.49	144

Table 4.2.6.3. SH...N thiol hydrogen bond geometries of apo-azurin with calculated thiol hydrogen atom positions. H...N-C angles defined by C_γ atom.

	Molecule A			Molecule B		
SH...N	S-H...N (°)	H...N Å	H...N-C (°)	S-H...N (°)	H...N Å	H...N-C (°)
S-H 112...$N_{\delta1}$ 46	156	2.42	116	144	2.71	121
S-H 112...$N_{\delta1}$ 117	121	2.72	114	132	2.45	115

Since the S_γ-C_β bond is free to rotate, there is no restraint on the position of the thiol hydrogen atom. Potential energy calculations could determine a theoretical hydrogen atom position which would place it in the best position for a hydrogen bond, but this was not done. Instead, as an approximation, a hydrogen atom position was determined from the coordinates of S_γ 112, C_β 112 and C_α 112, assuming the torsion angle of C_α-C_β-S-H is 180° (S-H bondlength of 1.34Å and C_β-S-H angle of 100° [332], see Table 4.2.6.3) The possibility of thiol hydrogen bonding at the copper binding site was not discussed in the structure of apo-plastocyanin[191], although the geometry can easily be calculated from the Protein Data Bank coordinates (see Table 4.2.6.4 and refer below).

Table 4.2.6.4. SH...N thiol hydrogen bond geometries of apo-plastocyanin with calculated thiol hydrogen atom positions. H...N-C angles defined by C_γ atom.

	Molecule B		
SH...N	S-H...N (°)	H...N Å	H...N-C (°)
S-H 84...$N_{\delta 1}$ 37	141	2.34	116
S-H 84...$N_{\delta 1}$ 87	111	3.11	111

Table 4.2.6.5. Distances and angles at the residual copper atom in apo-azurin.

	Molecule A	Molecule B	Average
Copper distances (Å)			
O 45...Cu	2.96	3.11	3.04
$N_{\delta 1}$ 46...Cu	1.94	2.13	2.04
S_γ 112...Cu	2.10	2.18	2.14
$N_{\delta 1}$ 117...Cu	2.02	1.88	1.95
S_δ 121...Cu	3.33	3.21	3.27
Copper angles (°)			
O 45-Cu-$N_{\delta 1}$ 46	77	74	76
O 45-Cu-S_γ 112	115	105	110
O 45-Cu-$N_{\delta 1}$ 117	85	88	87
O 45-Cu-S_δ 121	146	148	147
$N_{\delta 1}$ 46-Cu-S_γ 112	130	128	129
$N_{\delta 1}$ 46-Cu-$N_{\delta 1}$ 117	107	114	111
$N_{\delta 1}$ 46-Cu-S_δ 121	73	75	72
S_γ 112-Cu-$N_{\delta 1}$ 117	121	118	120
S_γ 112-Cu-S_δ 121	96	99	98
$N_{\delta 1}$ 117-Cu-S_δ 121	90	98	94

Residual metal in the copper binding site

The peak of residual electron density found at the position previously occupied by the copper in the oxidised and reduced structures implies either that the removal of the copper was not complete, or that another metal(s) has gained access to the copper binding site. The crystals are colourless, suggesting that if copper is present, either its occupancy is extremely low, or it is present as Cu(I). With the latter possibility in mind, an apo-azurin crystal was treated with potassium ferricyanide, to re-oxidise any remaining copper in the protein. Despite treatment for six months, no blue colouration developed. Thus the possibility of a partially substituted metal(s) other than copper must be considered, although every effort was made to remove all metal ions from the soaking solutions. Metals which have a high affinity for thiol groups (e.g. Hg), would be possible candidates for a substituted metal in the metal binding site.

For the purposes of refinement, the peak of residual electron density was treated as a

partial copper atom. The relative occupancy of the residual copper is also an unresolved question. Of the two methods used, one gives an occupancy of ≈20% (TNT refinement), while the other gives a value closer to ≈10% (as estimated from a comparison of the electron density of a nearby solvent molecule). Whether the occupancy is closer to 10% or 20% does not change the fact that the at least 80% of the protein molecules in the crystal lattice are metal free, which is sufficient to consider the structure as that of the apo protein. Table 4.2.6.5 lists the distances between the residual metal and the copper ligands. Note that the agreement of these distances and angles is rather poor between the two independent molecules (r.m.s. deviations are 0.14Å and 5.1°, respectively), which is not surprising since the metal atom has a low occupancy, and has not been well refined.

Comparison with the copper sites of oxidised and reduced azurins

As noted earlier, the configuration of the copper ligands in apo-azurin is essentially unchanged from the oxidised and reduced forms of azurin. The r.m.s. deviations in the atom positions of the five residues at the copper site are 0.14Å between the apo and oxidised structures, and 0.17Å between the apo and the reduced structures. This reinforces the earlier observation that the apo structure is more like the oxidised form than the reduced form. In the next two sections it will be shown that small movements do occur upon removal of the copper atom, and that these are different between the oxidised and reduced structures of azurin.

Comparison with the oxidised copper site

Upon removal of the copper atom from the oxidised protein, all of the metal ligands shift 0.1-0.2Å from their oxidised positions. The mean differences in main-chain and side-chain atom positions are shown in Table 4.2.6.6. Figure 4.2.6.4 is a stereo view of the apo-azurin site superimposed on to the oxidised copper site.

Table 4.2.6.6. Average differences in position of the metal ligands between apo and oxidised forms of azurin. The superposition was done using all atoms of residues Gly-45, His-46, Cys-112, His-117 and Met-121.

	Molecule A		Molecule B	
	main-chain atoms	side-chain atoms	main-chain atoms	side-chain atoms
Gly-45	0.19	-	0.09	-
His-46	0.13	0.16	0.10	0.07
Cys-112	0.11	0.13	0.09	0.11
His-117	0.12	0.10	0.08	0.11
Met-121	0.10	0.20	0.16	0.11

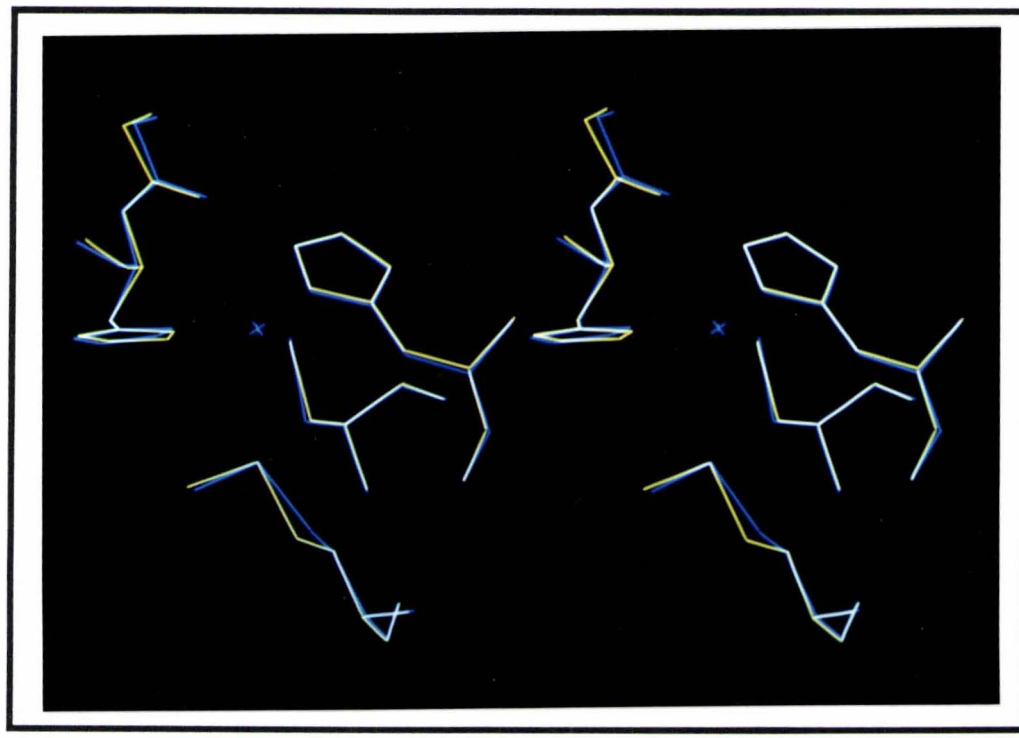

Figure 4.2.6.4. Stereo view of the superposition of the apo (yellow) and oxidised (blue) copper sites of azurin (molecule A).

Table 4.2.6.7. Distances (Å) between the atoms of the copper binding site.

	Apo-azurin			Oxidised azurin			Change
	A	B	Average	A	B	Average	(apo-ox)
O 45...$N_{\delta 1}$ 46	3.16	3.25	**3.21**	3.18	3.27	**3.23**	**-0.02**
O 45...S_{γ} 112	4.29	4.24	**4.27**	4.17	4.19	**4.18**	**+0.09**
O 45...$N_{\delta 1}$ 117	3.42	3.57	**3.50**	3.36	3.39	**3.38**	**+0.12**
O 45...S_{δ} 121	6.01	6.08	**6.05**	6.01	5.96	**5.99**	**+0.06**
$N_{\delta 1}$ 46...S_{γ} 112	3.67	3.87	**3.77**	3.88	3.94	**3.91**	**-0.14**
$N_{\delta 1}$ 46...$N_{\delta 1}$ 117	3.19	3.36	**3.28**	3.15	3.30	**3.23**	**+0.05**
$N_{\delta 1}$ 46...S_{δ} 121	3.31	3.38	**3.35**	3.39	3.26	**3.33**	**+0.02**
S_{γ} 112...$N_{\delta 1}$ 117	3.59	3.49	**3.54**	3.60	3.53	**3.57**	**-0.03**
S_{γ} 112...S_{δ} 121	4.12	4.17	**4.15**	4.31	4.21	**4.26**	**-0.11**
$N_{\delta 1}$ 117...S_{δ} 121	3.89	3.92	**3.91**	3.81	3.90	**3.86**	**+0.05**

Several small changes are noticeable between the apo and oxidised sites, and these changes can be expressed by comparing the average inter-ligand distances between the two structures (see Table 4.2.6.7). All of the changes in the inter-ligand distances are less than 0.15Å, with shifts of 0.1Å or greater occurring in the distances of O 45...S_{γ} 112, O 45...$N_{\delta 1}$ 117, $N_{\delta 1}$ 46...S_{γ} 112 and S_{γ} 112...S_{δ} 121. Although most of these shifts are consistent between the two protein molecules, they are not truly significant, because they are comparable to the r.m.s. differences in inter-ligand distances between the two apo-azurin molecules (0.11Å, see Section 4.3.5). Small changes in the side-chain torsion angles of the residues at the copper binding site are also seen upon the removal of the

Table 4.2.6.8. Changes in the side-chain torsion angles (°) between apo and oxidised azurins of the residues at the apo site (apo - oxidised)

	$\Delta\chi_1$ (°)		$\Delta\chi_2$ (°)		$\Delta\chi_3$ (°)	
Molecule	A	B	A	B	A	B
His-46	-10	-5	+2	+2		
Cys-112	+4	+4				
His-117	-5	-2	-4	+4		
Met-121	-15	-5	-12	-1	+25	+3

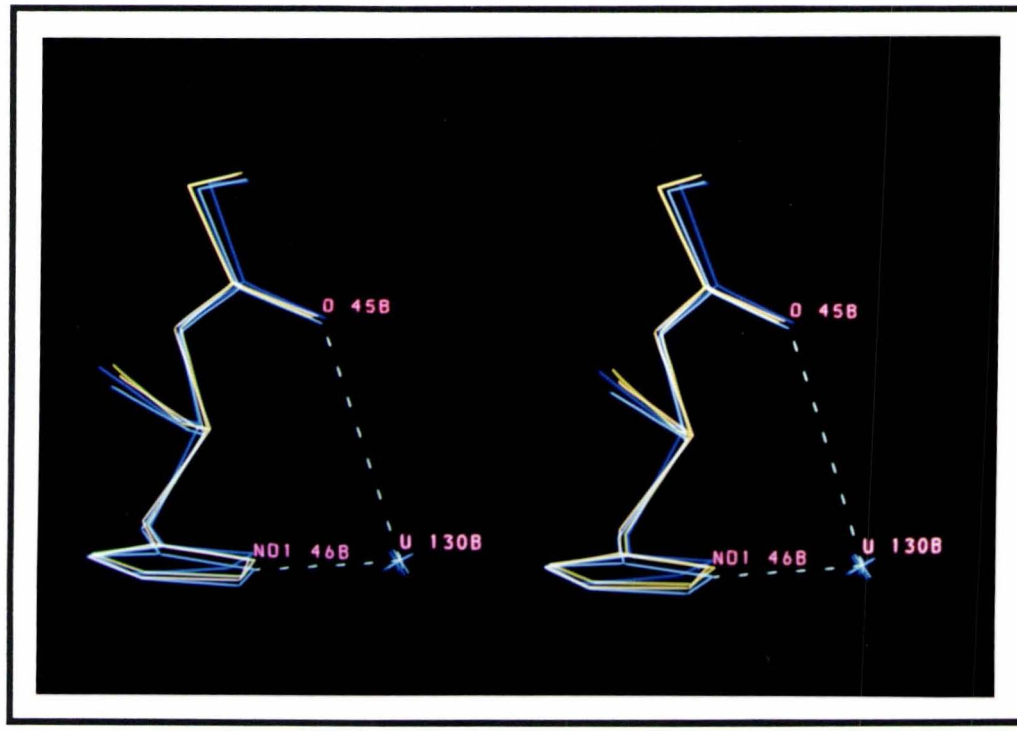

Figure 4.2.6.5. Stereo view of the structural change at Gly-45 between apo and oxidised azurins. The two independent molecules of the asymmetric unit from both apo and oxidised azurins are superimposed on each other. Oxidised azurin molecules in blue (A) and light blue (B), and apo-azurin molecules in yellow-green (A) and yellow (B).

metal (see Table 4.2.6.8); while the directions of some of these changes are consistent, the magnitudes are not.

The changes in the inter-ligand distances can be accounted for by two structural movements. One is a movement of the carbonyl oxygen of Gly-45 away from the centre of the copper binding site (see Figure 4.2.6.5). This increases the distances to the other ligands, except for His-46. However, it should be noted that the O 45...Sδ 121 distance increases (oxidised $\rightarrow$ apo) in only one protein molecule of the asymmetric unit (no change in molecule A and an increase of 0.12Å in molecule B). A movement of O 45 would be significant because in the crystallographic analysis of oxidised azurin the extent to which the carbonyl oxygen of Gly-45 interacted with the copper centre was

questioned[31,155]. It was suggested that a Cu...O distance of 3.1Å was probably at the limit of any interaction, although it was also pointed out that the carbonyl oxygen was 1) buried in a hydrophobic environment, 2) not close to any potential hydrogen bonding partners and 3) oriented in such a way that a lone pair of electrons from the oxygen was directed towards the copper. If the carbonyl oxygen of Gly-45 does move away upon the removal of the copper, this is then suggestive of a weak interaction between O 45 and Cu in oxidised azurin.

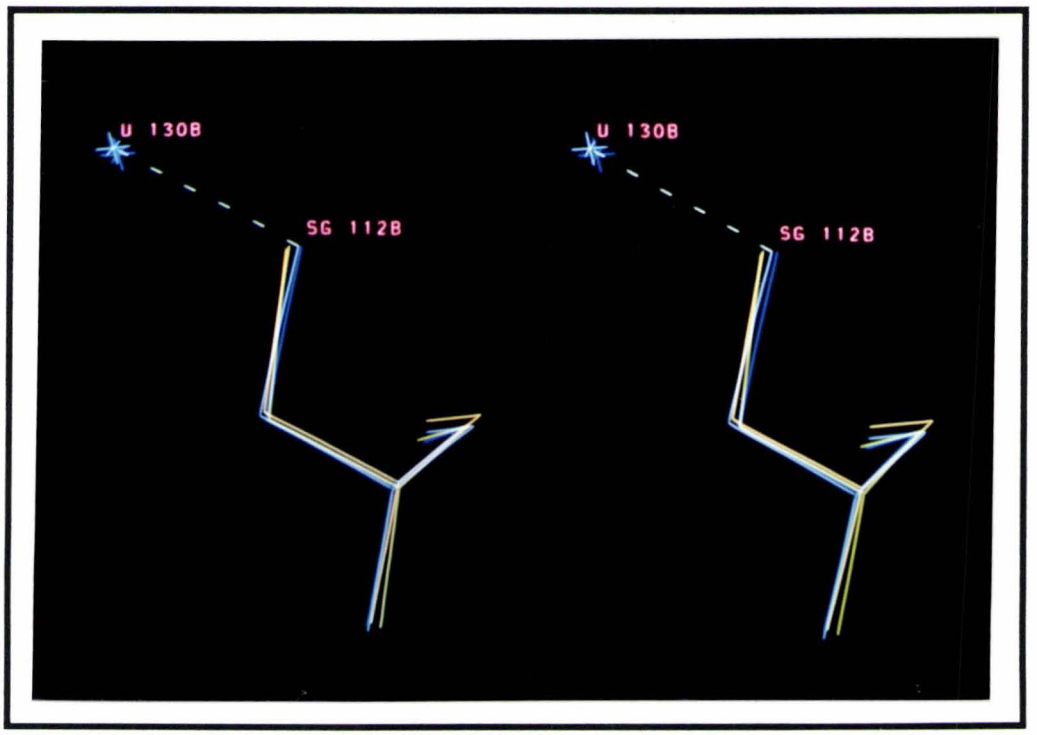

Figure 4.2.6.6. Superposition of the active sites of apo and oxidised azurins, illustrating the small shift in S_γ 112 upon removal of the copper. Oxidised azurin molecules in blue (A) and light blue (B), and apo-azurin molecules in yellow-green (A) and yellow (B).

The second shift in the active site occurs in the side-chain of Cys-112. This movement is a shift of the Sγ atom into the space left by the copper atom, and shortens the $N_{\delta 1}$ 46...S_γ 112 distance by 0.14Å (average). Again, this movement is consistent, but the magnitude is below the level of significance. Interestingly, the histidine ligands do not shift into space left by the copper atom, since the $N_{\delta 1}$ 117...S_γ 112 distance does not shorten significantly (average of 0.03Å) and the $N_{\delta 1}$ 46...$N_{\delta 1}$ 117 distance actually increases on average by 0.05Å. The changes at Cys-112 are shown in Figure 4.2.6.6. From the analysis of consistent shifts between the apo and oxidised forms (Section 4.2.5), the Ξ score of the Cys-112 side-chain is low (Ξ = 44) compared to the other changes described, but the small angle between the shift vectors (θ = 28°) is a strong suggestion that this change occurs in both of the independent molecules, although the shift is small (average of 0.13Å for S_γ 112). The shift in Cys-112 was not discussed in section 4.2.5, because

the Ξ score was just below the threshold of 50 points. Note that no other consistent shifts are observed in the ligands His-46, His-117 or Met-121 (see Table 4.2.6.9). The movement of S_γ 112 is presumably to fill the void left by the removal of the copper. This movement may also be affected by the formation of thiol to nitrogen hydrogen bonds, since the lone pair of electrons of both $N_{\delta 1}$ 46 and $N_{\delta 1}$ 117 point directly towards the position of a thiol hydrogen atom.

Table 4.2.6.9. Consistent shifts in the residues of the copper binding site of azurin between apo and oxidised forms.

	Ξ		Theta (°)		Mean shift (Å)	
	main-chain	side-chain	main-chain	side-chain	main-chain	side-chain
Gly-45	56.32	-	49.46	-	0.176	-
His-46	34.78	1.84	59.44	93.83	0.132	0.120
Cys-112	10.81	44.21	54.84	28.38	0.102	0.118
His-117	2.88	5.35	106.82	79.54	0.104	0.098
Met-121	7.06	10.83	79.90	88.95	0.167	0.188

The largest changes which occur in the side-chain torsion angles of the residues of the copper binding site are in Met-121. These changes, however, are not consistent in magnitude, (see Figure 4.2.6.7).

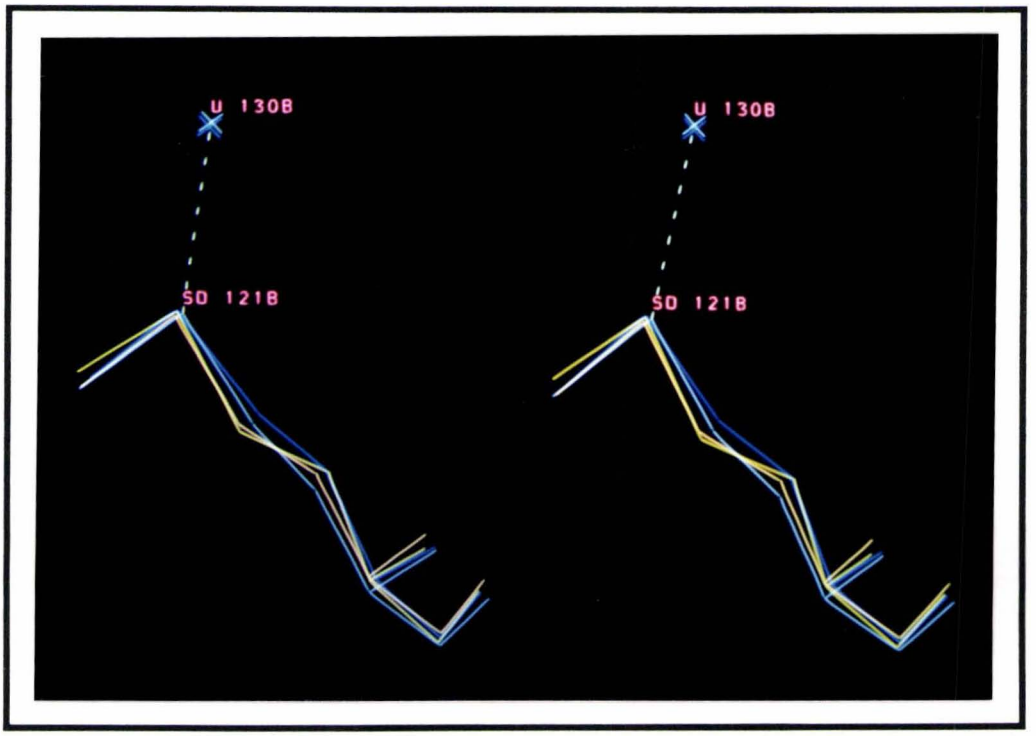

Figure 4.2.6.7. Stereo view of the changes at Met-121 between apo and oxidised azurins. Oxidised azurin molecules in blue (A) and light blue (B), and apo-azurin molecules in yellow-green (A) and yellow (B).

Comparison with the reduced copper site

The overall differences between the apo and reduced sites are larger than betweeen the apo and oxidised sites. These differences are shown in Figure 4.2.6.8, as a stereo diagram with the copper binding sites of the apo and reduced forms superimposed. The mean deviations for the main-chain and side-chain of each residue are listed in Table 4.2.6.10. Table 4.2.6.11 shows that most of the changes in the side-chain torsion angles, which are similar to those seen between the apo and oxidised structures, do not appear to be significant.

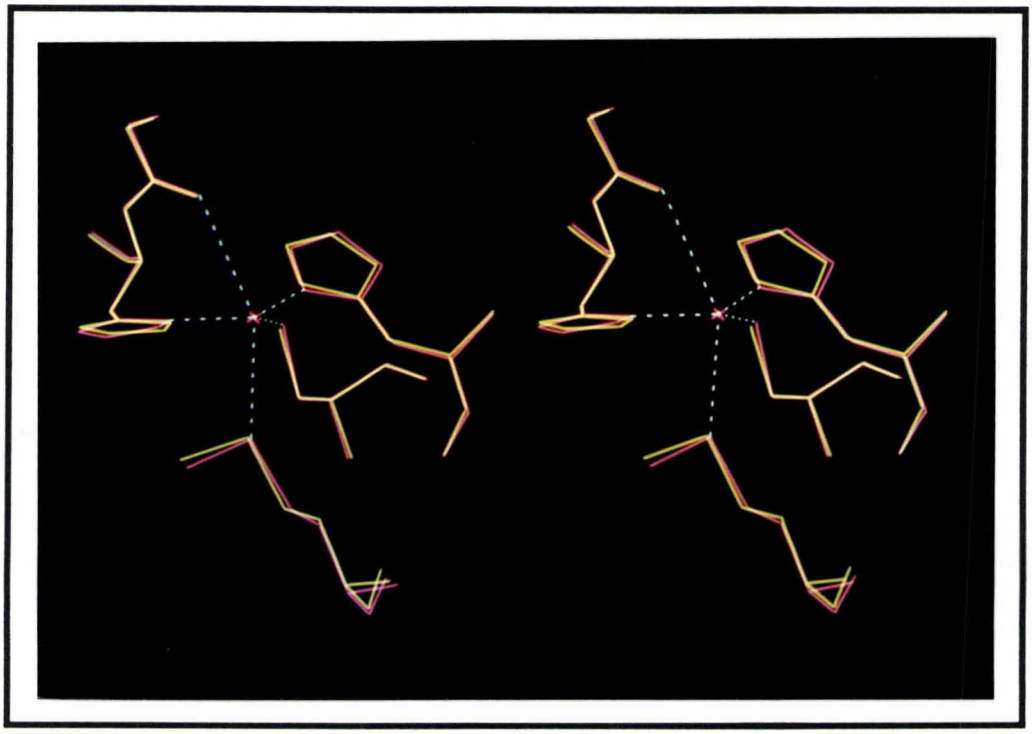

Figure 4.2.6.8. Stereo view of the superposition of the copper binding sites of apo and reduced azurins (molecule A). Reduced azurin in red and apo-azurin in yellow.

Table 4.2.6.10. Average deviations (Å) in position of the metal ligands between apo and reduced forms of azurin. Superposition done using the atoms of residues Gly-45, His-46, Cys-112, His-117 and Met-121.

	Molecule A		Molecule B	
	main-chain atoms	side-chain atoms	main-chain atoms	side-chain atoms
Gly-45	0.10	-	0.14	-
His-46	0.11	0.16	0.11	0.10
Cys-112	0.14	0.16	0.12	0.29
His-117	0.10	0.11	0.21	0.14
Met-121	0.16	0.20	0.19	0.25

Table 4.2.6.11. Changes in the side-chain torsion angles (°) of the copper ligands between apo and reduced azurins.

Molecule	$\Delta\chi_1$ (°)		$\Delta\chi_2$ (°)		$\Delta\chi_3$ (°)	
	A	B	A	B	A	B
His-46	-2	+4	-1	-7		
Cys-112	-3	+2				
His-117	-1	+3	-11	-1		
Met-121	-1	-19	**-7**	**-13**	**+10**	**+32**

Table 4.2.6.12. Distances in ångstroms (Å) between the atoms of the copper binding site.

	Apo-azurin			Reduced azurin			change
	A	B	Average	A	B	Average	(apo-red)
O 45...$N_{\delta 1}$ 46	3.16	3.25	**3.21**	3.18	3.09	**3.14**	**+0.07**
O 45...S_{γ} 112	4.29	4.24	**4.27**	4.39	4.34	**4.37**	**-0.10**
O 45...$N_{\delta 1}$ 117	3.42	3.57	**3.50**	3.59	3.63	**3.61**	**-0.11**
O 45...S_{δ} 121	6.01	6.08	**6.05**	6.11	6.13	**6.12**	**-0.07**
$N_{\delta 1}$ 46...S_{γ} 112	3.67	3.87	**3.77**	4.02	4.01	**4.02**	**-0.25**
$N_{\delta 1}$ 46...$N_{\delta 1}$ 117	3.19	3.36	**3.28**	3.24	3.35	**3.30**	**-0.02**
$N_{\delta 1}$ 46...S_{δ} 121	3.31	3.38	**3.35**	3.46	3.51	**3.49**	**-0.14**
S_{γ} 112...$N_{\delta 1}$ 117	3.59	3.49	**3.54**	3.81	3.75	**3.78**	**-0.24**
S_{γ} 112...S_{δ} 121	4.12	4.17	**4.15**	4.46	4.55	**4.51**	**-0.36**
$N_{\delta 1}$ 117...S_{δ} 121	3.89	3.92	**3.91**	3.79	3.96	**3.88**	**+0.03**

A comparison of the inter-ligand distances shows that the copper binding site is contracted relative to the reduced site, since virtually all of the distances decrease upon removal of the metal. The average changes (apo → reduced) in the inter-ligand distances range from +0.07Å to -0.36Å between the apo and reduced forms. The largest of these all involve the side-chain of Cys-112, and are S_{γ} 112...S_{δ} 121 (-0.36Å), $N_{\delta 1}$ 46...S_{γ} 112 (-0.25Å) and S_{γ} 112...$N_{\delta 1}$ 117 (-0.24Å).

Inspection of the two superimposed structures shows that the largest atom shift in the active site is seen at the side-chain of Cys-112, where the S_{γ} atom moves on average 0.31Å into the space vacated by the copper atom. This shift accounts for most of the decrease in the inter-ligand distances, and is also accompanied by a change in the average S_{γ}-C_{β}-C_{α} angle from 102°, which is rather acute, in the reduced form, to 109°, which is virtually a tetrahedral angle, in the apo form. The movement of S_{γ} 112 between the apo and reduced forms is similar to the movement seen between the apo and oxidised forms except that it is larger (0.31Å versus 0.13Å, respectively). The shifts in Cys-112 imply that the distance from S_{γ} 112 to the center of the active site gradually increases from apo to oxidised to reduced forms of azurin. This is understandable as a steric effect, since the the larger Cu(I) ion will cause S_{γ} to move away (apo → reduced), and the S_{γ}-C_{β}-C_{α} angle to become more acute. Figure 4.2.6.9 shows the changes in the side-chain of Cys-112.

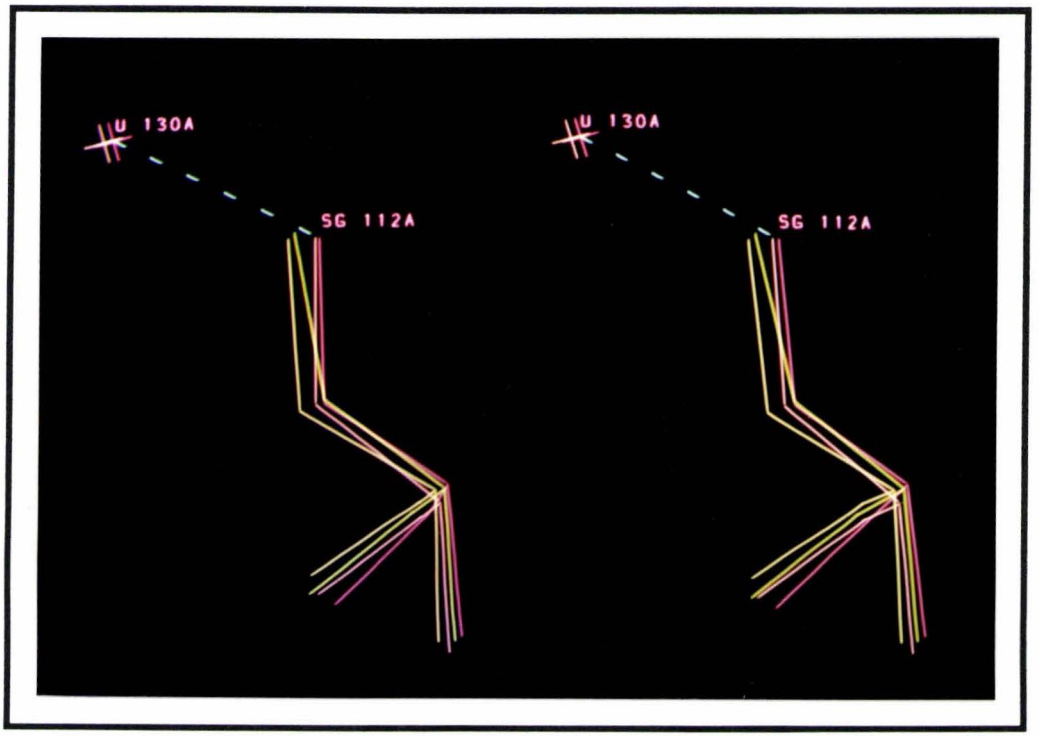

Figure 4.2.6.9. Stereo view of the movement of Cys-112 between apo and reduced azurin. Reduced azurin molecules in red (A) and pink (B), and apo-azurin molecules in yellow-green (A) and yellow (B).

Movements of the other copper ligands are much smaller than that of Cys-112 (see Table 4.2.6.13). No consistent shifts are evident at Gly-45, which was shown to shift when the apo form was compared to the oxidised form. At His-46 and His-117, the shifts in the atom positions suggest that these ligands are essentially static, which seems to be confirmed by the small changes in the inter-ligand distances. Some consistent changes seem to occur in the side-chain torsion angles of Met-121 (see Table 4.2.6.11); these would be considered significant except that the average difference in $\chi_{1\text{-}3}$ for Met-121 between the two reduced azurin molecules is 22°. Despite this, these changes may be related to a small shift in $S\delta$ 121 which moves towards the space vacated by the copper, and causes an average decrease in the O 45...$S\delta$ 121 distance of 0.07Å (see Figure 4.2.6.10).

Table 4.2.6.13. Consistent changes in the residues of the active site of azurin between apo and reduced azurin.

	Ξ		Theta (°)		Mean shift (Å)	
	main-chain	side-chain	main-chain	side-chain	main-chain	side-chain
Gly-45	1.15	-	112.22	-	0.145	-
His-46	4.52	11.84	103.42	80.14	0.131	0.119
Cys-112	32.11	129.49	67.93	56.92	0.150	0.207
His-117	12.60	28.06	61.84	48.03	0.174	0.158
Met-121	48.70	50.45	46.72	62.14	0.225	0.290

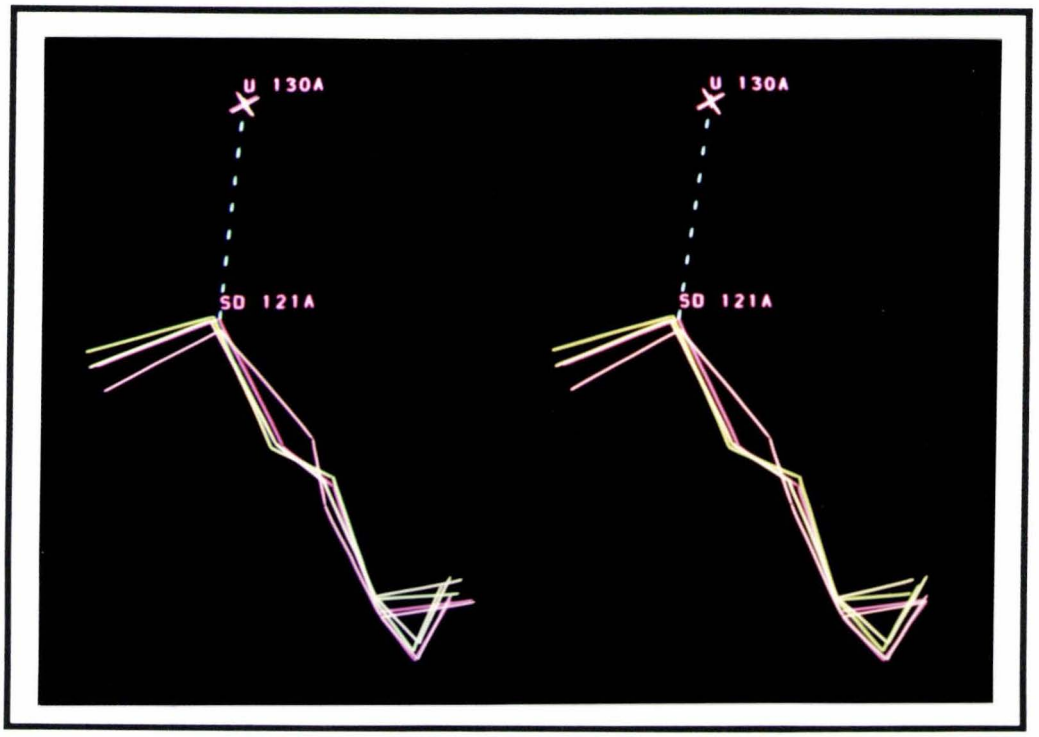

Figure 4.2.6.10. Changes in the side-chain torsion angles between apo and reduced azurin at Met-121. Reduced azurin molecules in red (A) and pink (B), and apo-azurin molecules in yellow-green (A) and yellow (B).

Overall the copper binding site of apo-azurin is remarkably similar to the copper sites of the two redox forms of azurin. Atom positions agree to within 0.2Å between these structures, which implies that the copper binding site of azurin is maintained in a configuration dictated by the protein. The only effects that the copper atom has on the protein configuration are very small, the most significant being a movement of the side-chain of Cys-112.

Comparison with apo-plastocyanin

One striking difference between the structures of apo-azurin and apo-plastocyanin is the conformation of the histidine ligand at the surface of the protein. In plastocyanin, the side-chain of His-87 undergoes a 180° rotation so that $N\delta 1$ is exposed to the solvent medium. In azurin, this corresponding sidechain (His-117) does not rotate, but stays in the same conformation as found in the oxidised and reduced forms.

There are two possible reasons for this difference in behaviour between azurin and plastocyanin. The first is that the histidine side-chain in azurin is more tightly constrained (sandwiched between the side-chains of Phe-114 and Met-13) than the corresponding residue in plastocyanin. The shortest contacts to Phe-114 and Met-13 from His-117, in azurin, are ≈3.3Å and ≈3.6Å, respectively; whereas the distances to the two residues

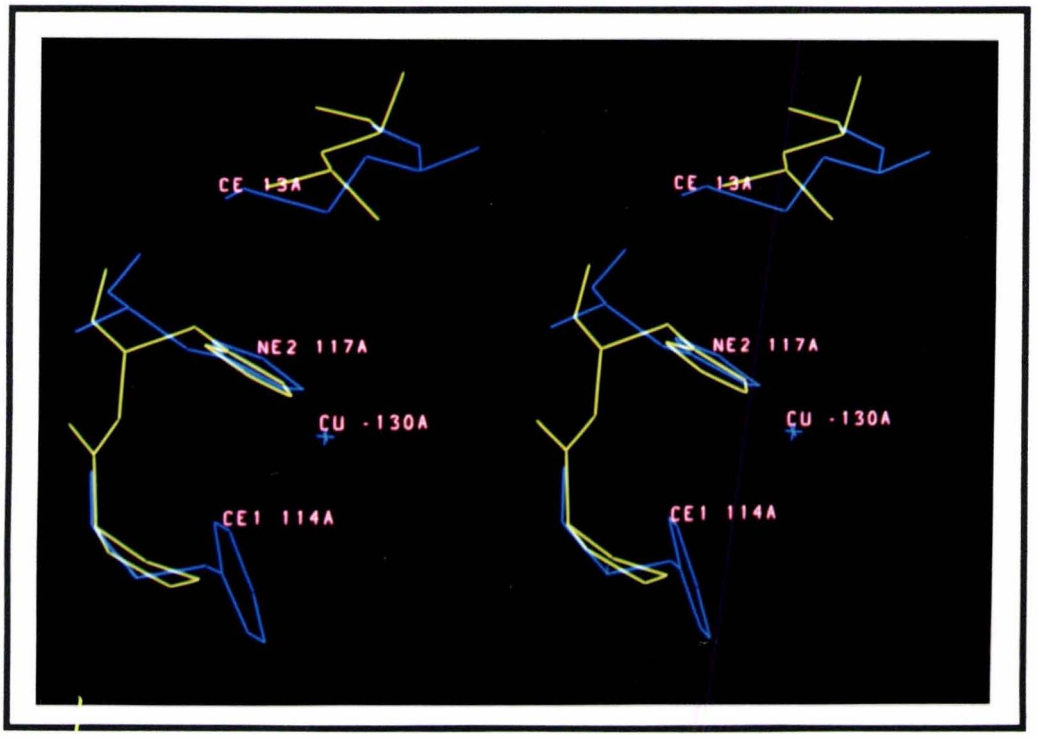

Figure 4.2.6.11. Superposition of apo-azurin (blue) and apo-plastocyanin (yellow) showing the differences in packing of the copper ligands His-87 (plastocyanin) and His-117 (azurin).

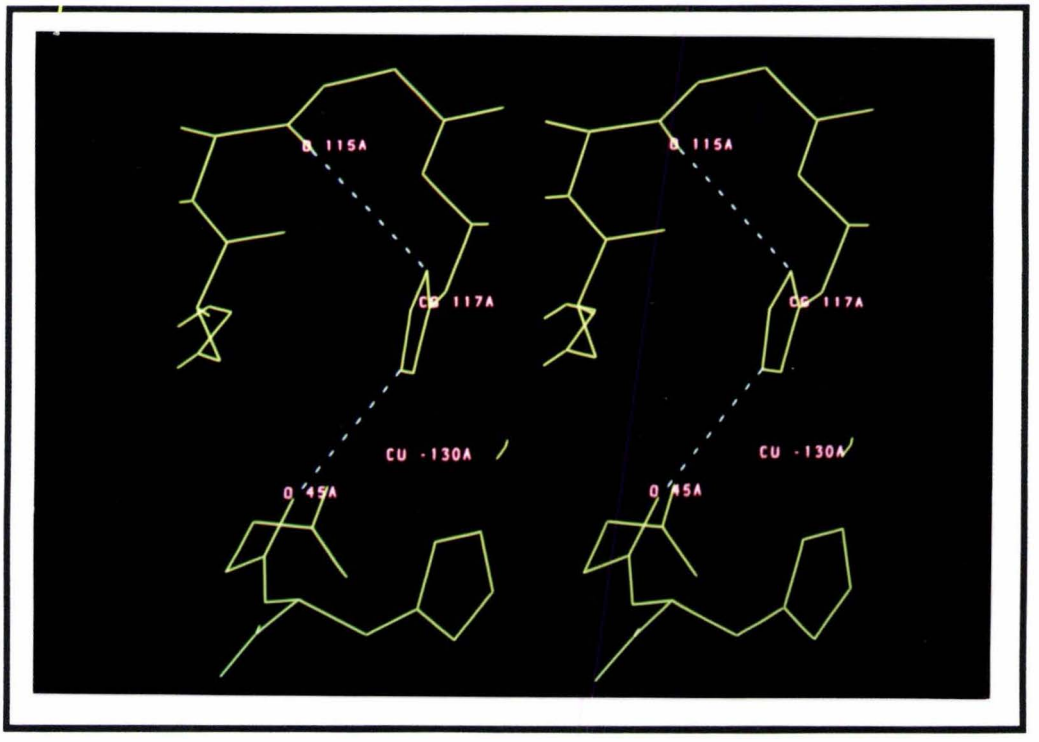

Figure 4.2.6.12. Two possible hydrogen bonds at His-117, if its side-chain rotated 180°.

which sandwich the side-chain of His-87 of plastocyanin, Leu-12 and Pro-86, are longer at ≈3.9Å and ≈4.5Å, respectively. Figure 4.2.6.11 illustrates the differences between the ligands.

The second reason involves the different crystal packing arrangements between azurin and plastocyanin. In plastocyanin, His-87 is exposed to a solvent channel of the crystal lattice, while the side-chain of His-117 in azurin is linked to another protein molecule through a solvent molecule which is buried in the interface between the two azurin molecules (see Section 3.2.9). A rotation of the His-117 side-chain, as in apo-plastocyanin, could make two possible hydrogen bonds to other parts of the protein (O 45 and O 115), but these interactions may be too long (O...H>2.5Å), and this rotation would destroy the favourable hydrogen bond geometry of the buried solvent molecule and would also direct a C-H group towards it. The possible hydrogen bonds of a rotated His-117 side-chain are shown in Figure 4.2.6.12, along with the buried solvent molecule.

A further difference betweeen apo-azurin and apo-plastocyanin is the presence of a peak of residual electron density at the centre of the copper binding site of apo-azurin. In apo-plastocyanin, no residual electron density was found in the binding site, and a "revolving door" mechanism, which facilitated the entry and exit of the copper to and from the binding site, was proposed for plastocyanin[191]. The incomplete removal of the copper from azurin is presumably due to the tighter packing of the His-117 side-chain in azurin and the crystal lattice contacts made in this area, which effectively exclude all but two solvent molecules. The combined effect is to make the removal of the copper in azurin more difficult than in plastocyanin. In solution, however, removal of the copper from azurin is complete within 8-12 hours (see Section 2.2), suggesting that the crystal packing is the main factor which hinders the removal of the copper. However, the tight packing around the side-chain of His-117 also suggests that the mode of copper removal may not be a facile "revolving door" mechanism.

The overall changes in the protein structure when the copper is removed from either azurin or plastocyanin show several similarities. Table 4.2.6.14 gives the inter-ligand distances of the three forms of plastocyanin (apo, oxidised and reduced (pH 7.0)) to compare changes with those of azurin.

In particular, the movement of the cysteine sulphur atom of plastocyanin is almost identical to the ≈0.3Å shift of S_γ 112 in azurin. From superposition of the three forms of plastocyanin, the S_γ atom shifts ≈0.2Å between apo and oxidised structures and ≈0.4Å

Table 4.2.6.14. Inter-ligand distances of apo, oxidised and reduced (pH 7.0) plastocyanins. Distances to the carbonyl oxygen of Pro-36 are given to compare with the corresponding distances of Gly-45 in azurin. All distances were obtained from Protein Data Bank coordinates.

Distance (Å)	apo plastocyanin	oxidised plastocyanin	reduced plastocyanin
O 36...$N_{\delta 1}$ 37	3.47	3.44	3.51
O 36...S_{γ} 84	4.83	4.68	4.81
O 36...$N_{\delta 1}$ 87 ($C_{\delta 2}$ 87)	4.02	3.81	3.91
O 36...S_{δ} 92	6.81	6.46	6.60
$N_{\delta 1}$ 37...S_{γ} 84	3.48	3.81	3.98
$N_{\delta 1}$ 37...$N_{\delta 1}$ 87 ($C_{\delta 2}$ 87)	3.35	3.09	3.44
$N_{\delta 1}$ 37...S_{δ} 92	3.65	3.41	3.51
S_{γ} 84...$N_{\delta 1}$ 87 ($C_{\delta 2}$ 87)	3.79	3.72	3.73
S_{γ} 84...S_{δ} 92	4.01	4.10	4.23
$N_{\delta 1}$ 87 ($C_{\delta 2}$ 87)...S_{δ} 92	4.33	3.94	4.22

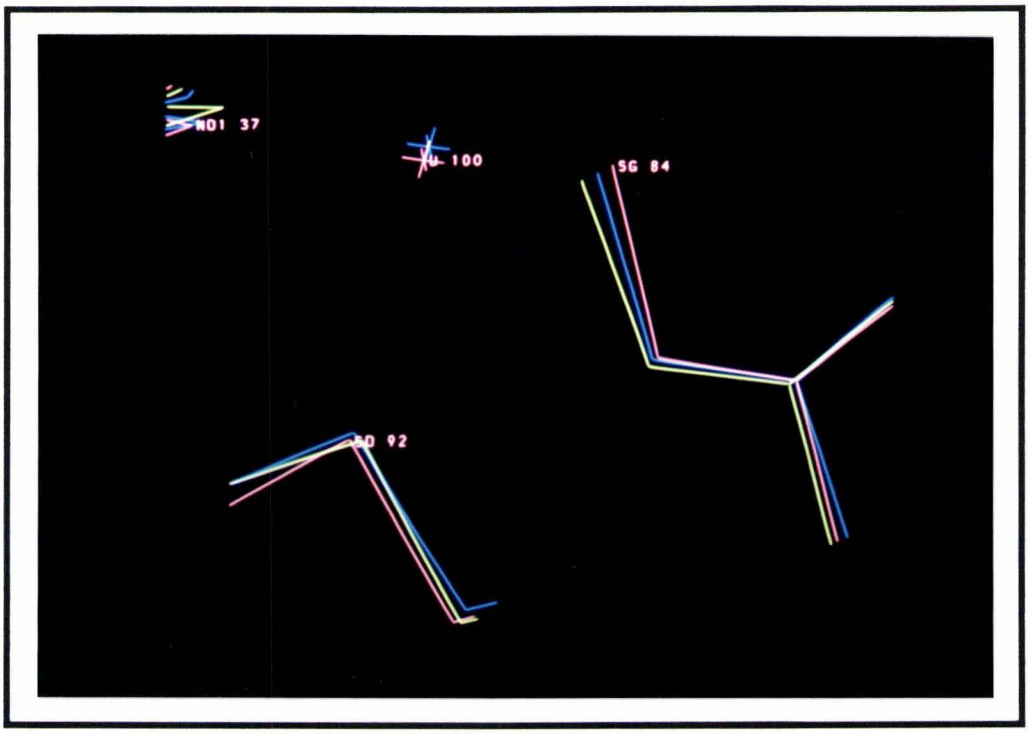

Figure 4.2.6.13. Superposition of the apo (yellow), oxidised (blue) and reduced, pH 7.0 (red), sites of plastocyanin showing the shift of the S_{γ} atom between each form.

between apo and reduced structures. Figure 4.2.6.13 illustrates these movements. It is also interesting to note that the S_{γ} 84... $N_{\delta 1}$ 37 distance in apo-plastocyanin (3.48Å) is short enough to imply a single, strong thiol (SH...N) hydrogen bond, whereas in azurin two weaker thiol hydrogen bonds are possible. The copper ligands in apo-plastocyanin differ in position by 0.1-0.3Å from the oxidised Cu(II) plastocyanin structure[191]. The size of the shifts is similar in apo-azurin and shows that in both proteins the polypeptide chain enforces this configuration of copper ligands. The copper ligands in apo-azurin

shift by 0.1-0.3Å compared to the reduced azurin structure, and 0.1-0.2Å compared to the oxidised structure.

The binding site of azurin is changed less than that of plastocyanin when the copper is removed. The r.m.s. deviation of the copper ligands of apo-azurin is 0.135Å between the apo and oxidised forms, and 0.168Å between the apo and reduced forms; while for plastocyanin the corresponding values are 0.183Å and 0.183Å, respectively. The smaller changes may be the result of a more deeply buried copper site in azurin than in plastocyanin.

4.2.7 The surrounding environment of the binding site of apo-azurin

In the previous section , it was shown that the copper ligands made only small shifts upon removal of the copper. In the crystallographic analyses of several blue copper proteins it has been proposed that the distorted geometry of the copper centre is imposed by the protein through hydrogen bonds and steric packing effects from the surrounding structure[31-34,39,40,155]. This surrounding environment is very similar between the three forms of azurin. The r.m.s. deviation in atom positions (main-chain and side-chain) for the structure around the binding site is 0.150Å between the apo and oxidised forms, and is 0.196Å between the apo and reduced forms[†]. The greater likeness of the apo form to the oxidised form as opposed to the reduced form, noted previously, also applies to this region.

Changes in the S...HN hydrogen bonds

Despite the similarities in the protein environment of the active site in the three forms of azurin, subtle changes are apparent upon removal of the copper. The most significant of these changes occur in the S...HN hydrogen bonds involving the S_γ atom of Cys-112. These hydrogen bonds are weaker in the structure of apo-azurin, compared to oxidised and reduced azurins. Table 4.2.7.1 lists the geometries of the two S...HN hydrogen bonds for all three forms of azurin along with the net change between them.

When the S...HN hydrogen bond geometries of apo-azurin are compared to those of the oxidised form, in going from oxidised to apo, a small decrease in the strength of both interactions is observed. The S...N distance of the S_γ 112...N 114 hydrogen bond increases on average by 0.17Å, while the S_γ 112...N 47 hydrogen bond only increases

[†] Residues used for the superposition are 9, 10*, 11, 12*-14*, 15, 35, 36*, 37, 41*-44*, 45-48, 85*, 86, 88*, 111-117, 118*-120*, 121, and 122*; where * indicates main-chain atoms only.

Table 4.2.7.1. S_γ 112...HN 47 and S_γ 112...HN 114 hydrogen bond geometries at Cys-112 for apo, oxidised and reduced azurins.

	molecule A				molecule B			
	C-S...H (°)	S...H (Å)	S...N (Å)	S...H-N (°)	C-S...H (°)	S...H (Å)	S...N (Å)	S...H-N (°)
S_γ 112...HN 47								
apo	101	2.62	3.57	160	109	2.54	3.51	163
oxidised	104	2.53	3.52	170	110	2.48	3.46	167
apo-oxidised	-3	+0.09	+0.05	-10	-1	+0.06	+0.06	-4
reduced	104	2.41	3.37	160	105	2.34	3.29	159
apo-reduced	-3	+0.21	+0.20	0	+4	+0.20	+0.22	+4
S_γ 112...HN 114								
apo	111	2.76	3.72	160	106	2.80	3.77	163
oxidised	117	2.54	3.50	161	116	2.72	3.65	155
apo-oxidised	-6	+0.22	+0.22	-1	-10	+0.08	+0.12	+8
reduced	115	2.40	3.36	163	116	2.43	3.37	158
apo-reduced	-4	+0.36	+0.36	-3	-10	+0.37	+0.40	+5

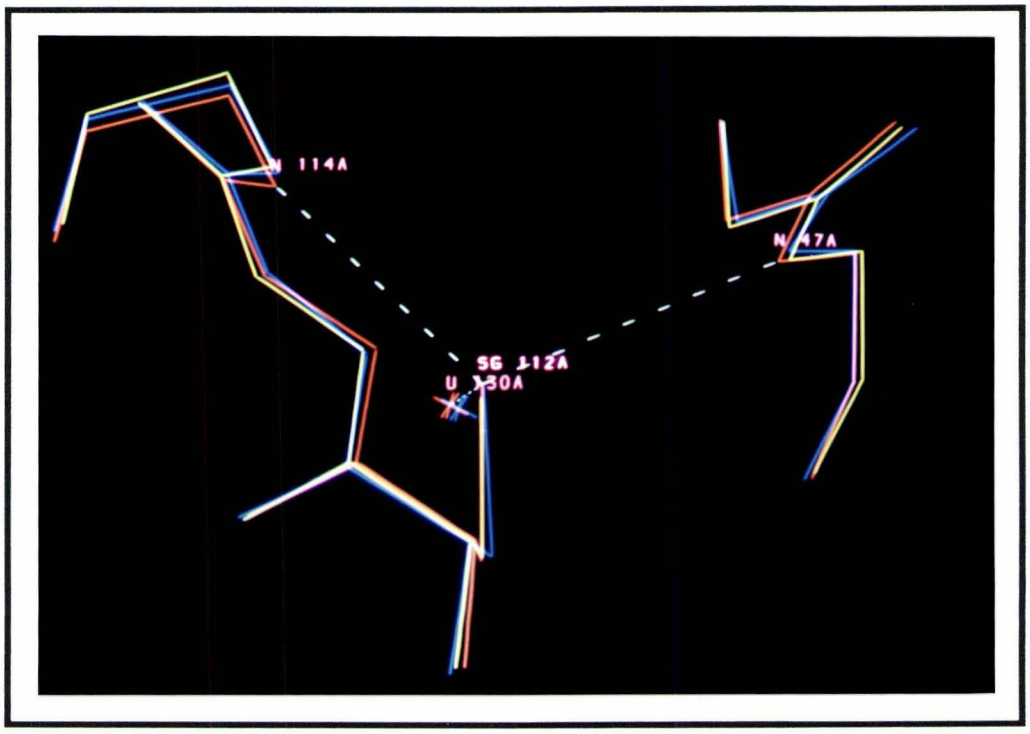

Figure 4.2.7.1. Stereo view of the changes in the S...HN hydrogen bonds at Cys-112 upon removal of the copper from azurin. Oxidised in blue, reduced in red and apo-azurin in yellow.

by 0.06Å on average. The changes in these interactions between the apo and the reduced forms (reduced → apo) are even more pronounced, with the S...N distance increasing by 0.21Å for S_γ 112...N 47, and even further by 0.38Å for S_γ 112...N 114. These changes in the S...HN hydrogen bonds are seen in both molecules of apo-azurin, and are very consistent in magnitude

In plastocyanin, for which crystal structures are available for apo, oxidised and reduced

forms[32,122,191], the single S...HN hydrogen bond shows changes between the apo and oxidised structures similar to those in azurin (see Table 4.2.7.2). The increase (oxidised → apo) in the S...N distance of 0.14Å in plastocyanin is comparable to the average increase of 0.17Å in azurin. Changes in the S...N distances between the apo and reduced structures of plastocyanin are different from those in azurin, because the reduced site of plastocyanin exists in two different pH-dependent conformations. At low pH (3.8), the S...N distance actually decreases (reduced → apo) by 0.04Å upon removal of the copper, and this change is probably affected by the change in the configuration of the copper site at low pH. The change in the S...N distance from the high pH (7.0) reduced to the apo form of plastocyanin is similar to that seen in azurin, except that the increase (reduced → apo) in the S...N distance is significantly less (0.09Å in plastocyanin compared to the average of 0.30Å in azurin).

The changes observed in the S...HN hydrogen bond lengths upon removal of the copper from azurin are caused by the shift of the S_γ 112 atom into the space vacated by the copper. As the S_γ 112 atom moves into this void, it shifts away from the hydrogen bond donors, N 47 and N 114. In addition, any interaction between the thiol hydrogen of Cys-112 and the side-chains of His-46 and His-117 would encourage the shift of S_γ 112 and the lengthening of the S...HN hydrogen bonds. The protonation of S_γ on the removal of the copper atom would also deplete some of the electronic charge on S_γ, thereby diminishing its electrostactic interaction with the amide nitrogens and increasing the S...N distances. It is interesting to note that the electronic effect is the reverse of that seen upon the reduction of Cu(II) azurin, where an increase in the electronic charge on S_γ following reduction causes a decrease in the S...N distances. These changes in S...N distances (oxidised → apo and oxidised → reduced) are consistent with the change in the electronic charge on S_γ. The changes in the S...HN hydrogen bonds are shown in Figure 4.2.7.1.

Changes in the polypeptide loop preceding Gly-45

Any changes to the protein structure near Gly-45 are of special interest because these changes may indicate whether O 45 interacts with the copper. When the apo and oxidised structures are compared, small consistent changes are observed in the α-turn preceding Gly-45 (residues 40-45). These were noted in earlier sections, in the analyses of the consistent atom shifts, the hydrogen bonds and the main-chain torsion angles. All of the changes are small (shifts of 0.12-0.18Å in main-chain atom positions and 7-12° in (ϕ,ψ)), and are of the order of the average difference in main-chain atom positions between the two apo-azurin molecules (0.1-0.2Å). In addition, changes in the hydrogen bonds of this region (see Table 4.2.7.2) are below 0.20Å and 10°, and do not

Table 4.2.7.2. Changes in the hydrogen bonds O 41...N 45 and O 40...N 43 between apo and oxidised azurins.

	molecule A			molecule B		
	C-O...H (°)	O...H (Å)	O...H-N (°)	C-O...H (°)	O...H (Å)	O...H-N (°)
O 41...HN 45						
apo	118	2.44	124	119	2.45	122
oxidised	126	2.60	110	123	2.57	117
apo-oxidised	**-8**	**-0.16**	**+14**	**-4**	**-0.12**	**+5**
O 40...HN 43						
apo	105	2.32	140	109	2.37	147
oxidised	107	2.26	134	117	2.26	148
apo-oxidised	**-3**	**+0.06**	**+6**	**-8**	**+0.11**	**-1**

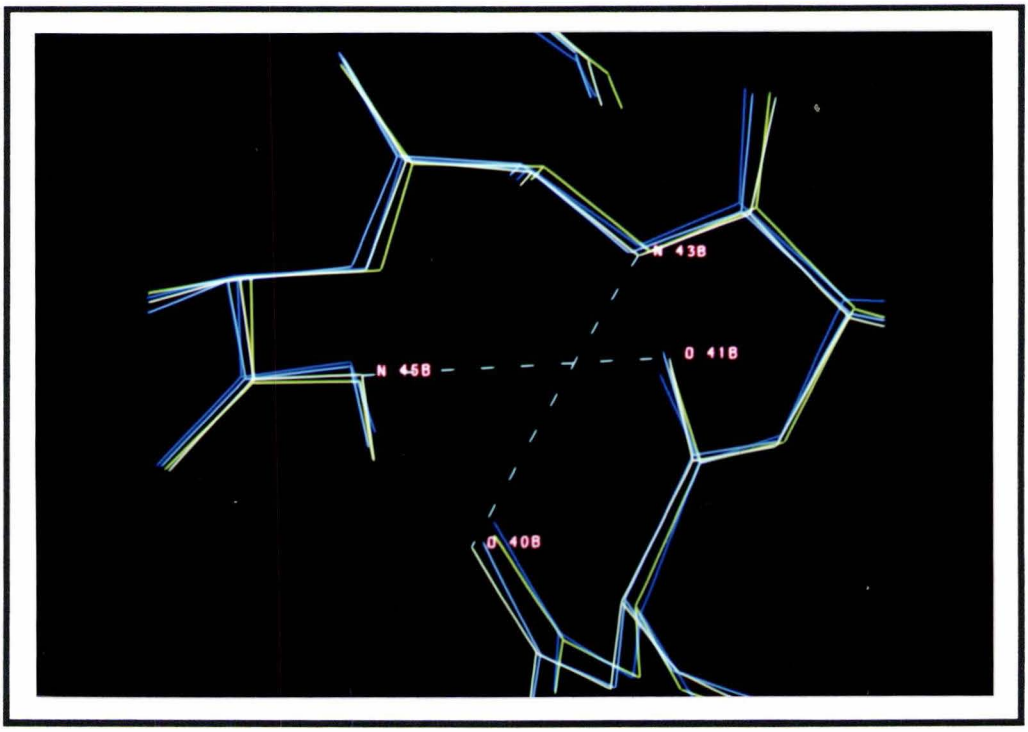

Figure 4.2.7.2. Changes in the hydrogen bonds O 41...N 45 and O 40...N 43 between apo and oxidised azurins. Oxidised azurin molecules in blue (A) and light blue (B), and apo-azurin molecules in yellow-green (A) and yellow (B).

significantly alter the strengths of these interactions.

Most of the changes in this region between the apo and the reduced structures are of the same order of magnitude as those between the apo and oxidised forms. Consistent shifts of 0.18-0.22Å are seen for Ala-40 and Met-44, while changes in angles as large as 10-15° are apparent for Met-44 and Gly-45. A larger change, however, is seen in the hydrogen bond O 40...HN 43, where the O...H distance increases by ≈0.4Å on removal of copper, and is accompanied by consistent changes in the angles of another hydrogen bond (O 40...HN 44) of 10-18° (see Table 4.2.7.3). The significance of these changes

Table 4.2.7.3. Changes in the hydrogen bonds O 40...N 43 and O 40...N 44 between apo and reduced azurins.

	molecule A			molecule B		
	C-O...H (°)	O...H (Å)	O...H-N (°)	C-O...H (°)	O...H (Å)	O...H-N (°)
O 40...HN 43						
apo	105	2.32	140	109	2.37	147
reduced	114	1.97	137	125	1.90	152
apo-reduced	**-9**	**+0.35**	**+3**	**-16**	**+0.47**	**-5**
O 40...HN 44						
apo	151	2.00	149	150	2.01	160
reduced	159	1.72	173	161	2.00	172
apo-reduced	**-8**	**+0.28**	**-24**	**-11**	**+0.01**	**-12**

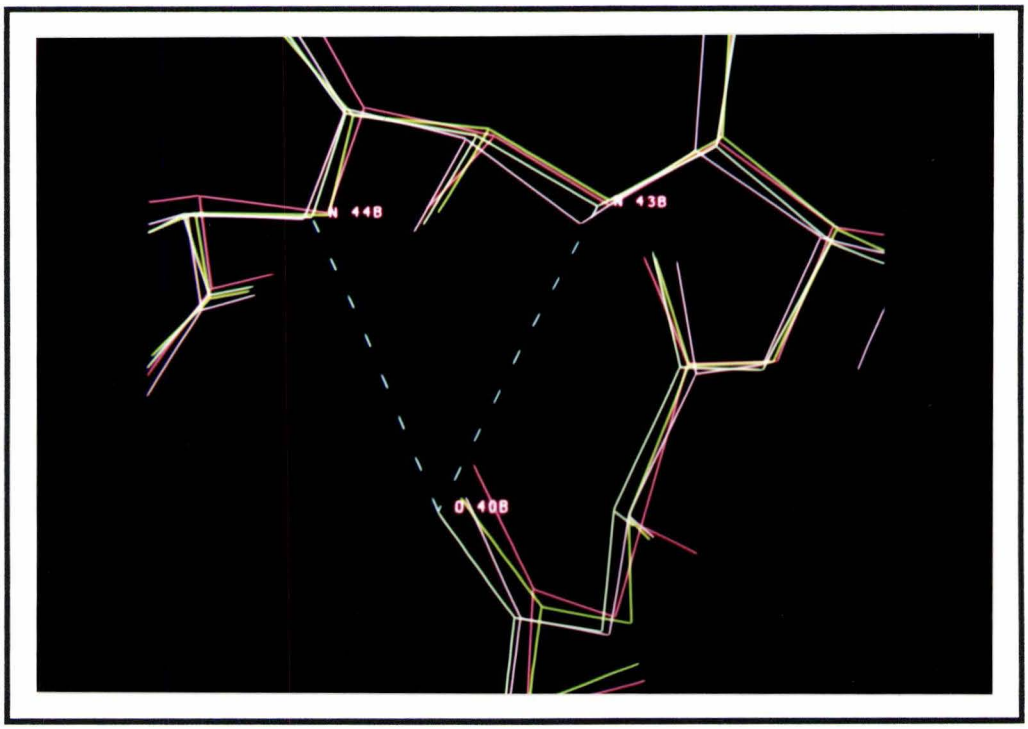

Figure 4.2.7.3. Stereo view showing the changes in the hydrogen bonds O 40...N 43 and O 40...N 44 between apo and reduced azurins. Reduced azurin molecules in red (A) and pink (B), and apo-azurin molecules in yellow-green (A) and yellow (B).

is not clear. They could be related to the movement of Gly-45, but they could also simply identify this as a region in which small adjustments in the copper site can be taken up.

Increased flexibility of the 112-121 loop

In the discussion of the thermal parameters of apo-azurin (section 4.2.8), the relative B-values of residues 117-121 are shown to be significantly higher in the apo structure than in the oxidised and reduced structures. This is graphically shown as a plot of the average main-chain B-value against the residue number (see Figures 4.2.8.3-4), and

suggests that the 117-121 loop is somewhat more flexible in the absence of the copper.

Other indications of the increased flexibility of this loop upon the removal of the copper are given by the average deviation in the atom positions of residues 112-121, and in the weakening of the $N_{\delta 2}$ 47...O_{γ} 113 hydrogen bond. The average difference in main-chain atom positions of residues 112-121 between the two protein molecules of the asymmetric unit for apo-azurin is 0.22Å compared to 0.17Å and 0.18Å for oxidised and reduced azurins, respectively. Although the agreement in this region is only slightly less in apo-azurin, it may perhaps indicate that this region is less well defined in the absence of the copper ion. Another possible indication that the 112-121 loop has become more flexible is the small change of the hydrogen bond $N_{\delta 2}$ 47...O_{γ} 113 which links the two loops providing the ligands of the copper site. Although the changes are small, they are consistent between both independent protein molecules (see Table 4.2.7.3), and more importantly occur for a hydrogen bond between two buried residues. The H...O distance increases on average by 0.18Å from the oxidised to the apo form, and by 0.23Å from the reduced to apo form.

Table 4.2.7.4. $N_{\delta 2}$ 47...O_{γ} 113 hydrogen bond geometries for apo, oxidised and reduced azurins.

	Molecule A			Molecule B		
	N-H...O	H...O	H...O-C	N-H...O	H...O	H...O-C
apo	150	2.12	166	141	2.07	174
oxidised	148	1.89	169	143	1.94	175
apo-oxidised	**+2**	**+0.23**	**-3**	**-2**	**+0.13**	**-1**
reduced	148	2.00	172	146	1.74	177
apo-reduced	**+2**	**+0.12**	**-6**	**-5**	**+0.33**	**-3**

If the loop of residues 112-121 is really more flexible in the apo structure, then this may be related to certain observations made on azurin in ^1H NMR experiments[126], Fourier-transform infrared spectra[205] and differential scanning calorimetry[204]. In ^1H NMR experiments, a small number of NH protons observed to be inert to $^1H \rightarrow ^2H$ exchange in Cu(I) azurin, were found to be more labile upon the removal of the copper. Studies of the infrared spectra of azurin also found that $^1H \rightarrow ^2H$ exchange could be thermally induced in apo-azurin at 55°C, and that the thermal stability of the apo form is significantly reduced from the native form[205]. Furthermore, calorimetric experiments show that apo-azurin melts with an additional transition prior to the single main transition (assigned to the unfolding of the main secondary structural element, the β-sheets) seen in oxidised azurin and all other metal-substituted derivatives of azurin[204]. Although the additional melting transition in apo-azurin could not be specifically assigned to any structural element, the authors did suggest that this transition may involve the "flap" region of the protein molecule, since it is near the copper binding site. The "flap" region, however, is not

directly linked to the copper binding site of azurin, but rather makes only a small contribution to its surrounding environment. Instead, this extra melting transition is more likely to involve the unfolding of some or all of the loops surrounding copper binding site because they supply the metal ligands. Since the loop 117-121 has increased B-values in the apo form, it may be involved in the additional melting transition seen in the calorimetric scans, and could also be responsible for the lower thermal stability of apo-azurin.

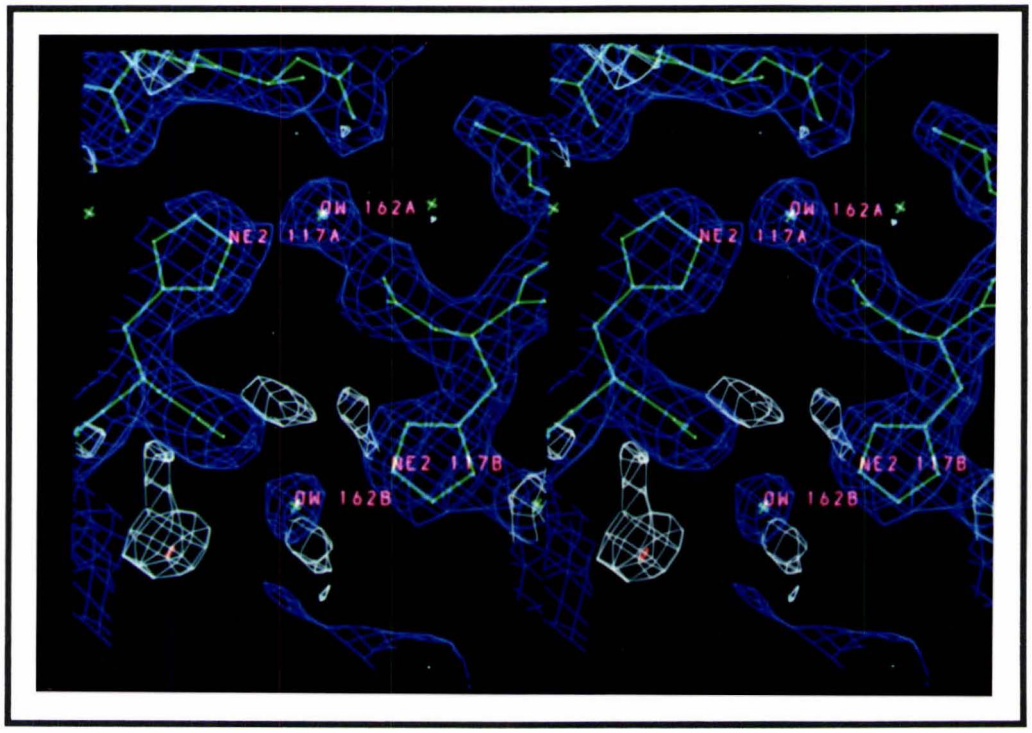

Figure 4.2.7.4. Stereo view of the interface between the hydrophobic patches of the two protein molecules of the asymmetric unit. Note the relative absence of any residual electron density peaks (white and red) between the two protein molecules.

Conservation of the solvent structure near the side-chain of His-117

In plastocyanin, changes in the conformation of the copper ligand His-87, which is at the surface of the molecule, were discovered because of a change in the solvent structure associated with this copper ligand. No change in the solvent structure, however, is apparent near the corresponding side-chain, His-117, in azurin (see Figure 4.2.7.4). The single solvent molecule, OW 162, which is bound to the side-chain of His-117 is well ordered in the structure (<B> = 23Å^2), and makes three strong hydrogen bonds arranged in a trigonal geometry (average OW...O or N ≈ 2.7Å to hydrogen bonding partners). In fact, the hydrogen bonding environment of this solvent molecule is virtually identical between apo, oxidised and reduced azurins (see Figure 4.2.7.5). This solvent molecule is also present in the crystal structures of wild type and mutant azurins from *Ps. aeruginosa*

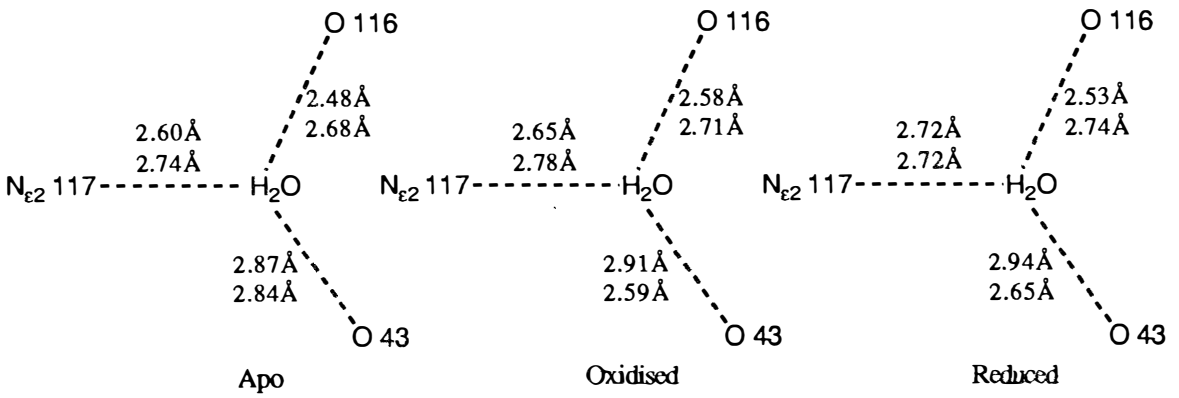

Figure 4.2.7.5. Hydrogen bond distances of the water molecule OW 162. Note top distances are for molecule A, bottom distances are for molecule B. The water molecule bridges to the carbonyl oxygen of residue 116 of a neighbouring protein molecule.

[41,155], and has been identified in solution by NMR studies[333], suggesting that this solvent molecule is a conserved feature in the structure of azurins.

4.2.8 Thermal parameters

The patterns and trends in the B-values for apo-azurin are very similar to those for the oxidised and reduced structures. The average difference in the main-chain B-values is 3.4Å^2 between the apo and oxidised forms and 0.6Å^2 between the apo and reduced forms. The average B-value for each residue is shown in Figure 4.2.8.1, along with the corresponding B-values of the oxidised and reduced structures. The close similarity between the apo and reduced structures is especially interesting since different algorithms were used in the refinement of the two structures (HKPROLSQ and PROLSQ).

B-values are generally low for residues which make up the β-strands (average main-chain B = 19.8Å^2), whereas the loops of the polypeptide chain on the surface of the protein have higher B-values (average main-chain B = 24.6Å^2). An exception to this, however, are the loops which suround the copper-binding site. These loops have low B-values (average main-chain B = 19.5Å^2), compared to the loops furthest from the copper binding site (average main-chain B = 31.5Å^2). This feature is also seen in the oxidised and reduced forms of azurin, where the structure is more restrained closer to the copper binding site. Figure 4.2.8.2 shows that the average B-value increases as a function of the distance of each residue (C_α position) from the centre of the copper binding site.

Another feature of the thermal parameters of the apo structure is that the B-values of the 117-121 loop (an α-turn), which supplies two of the ligands to the copper binding site, increase upon the removal of the copper. When the B-values of this section are compared

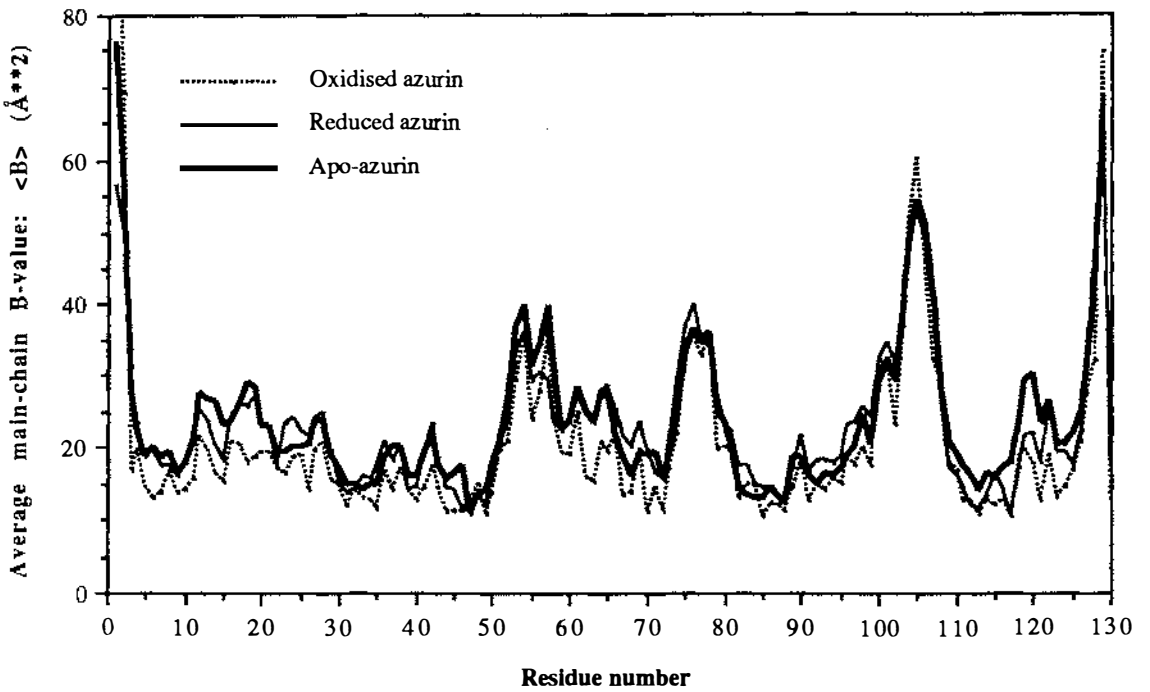

Figure 4.2.8.1. Average B-value as a function of residue number for apo, oxidised and reduced azurins. B-values are an average of the two independent molecules of the asymmetric unit.

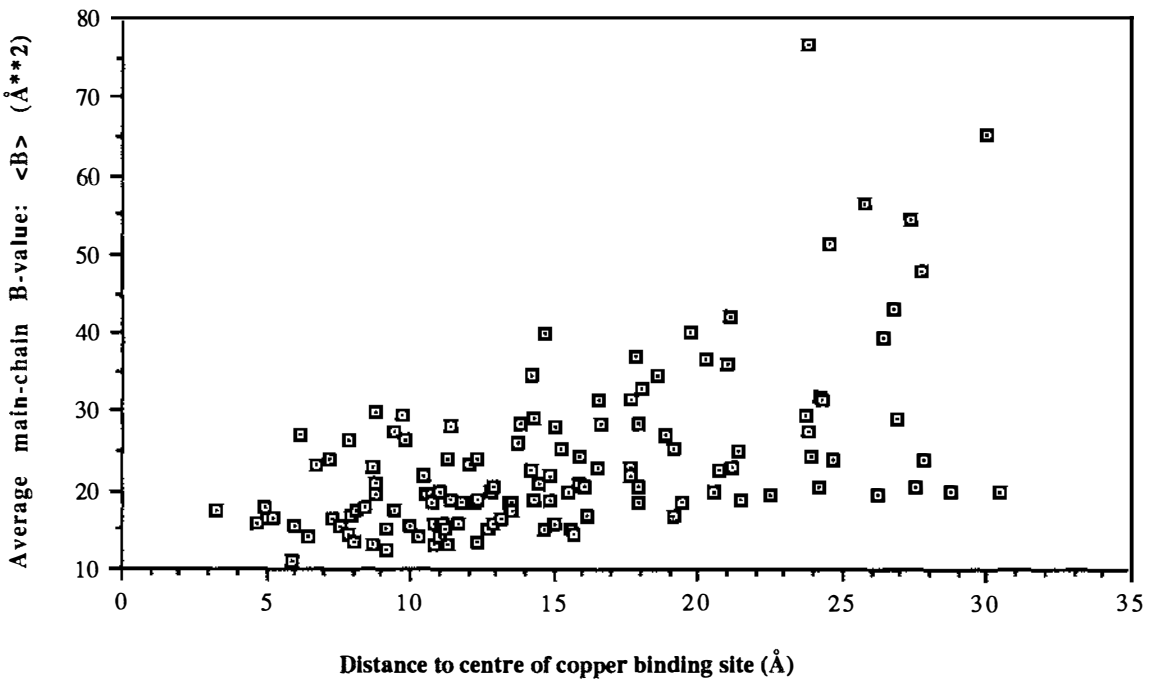

Figure 4.2.8.2. Average B-factors of main-chain atoms for both molecules of apo-azurin plotted against the distance between the center of the copper binding site and the position of C_α.

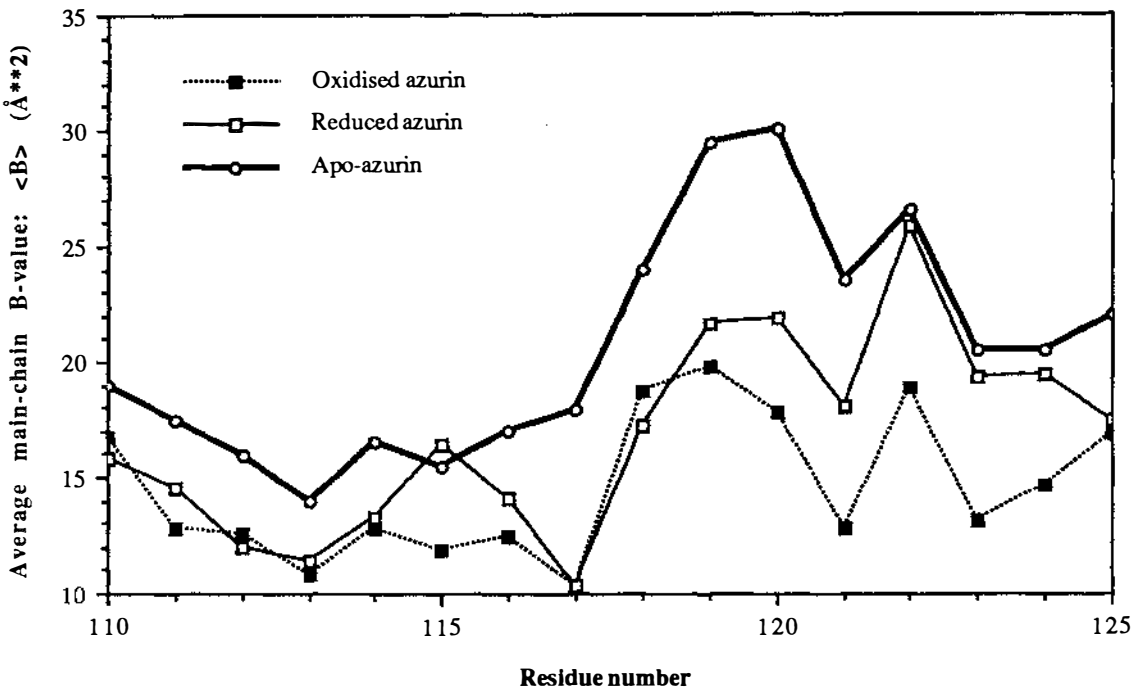

Figure 4.2.8.3. Plot of the average main-chain B-value for the section of residues between 110 and 125.

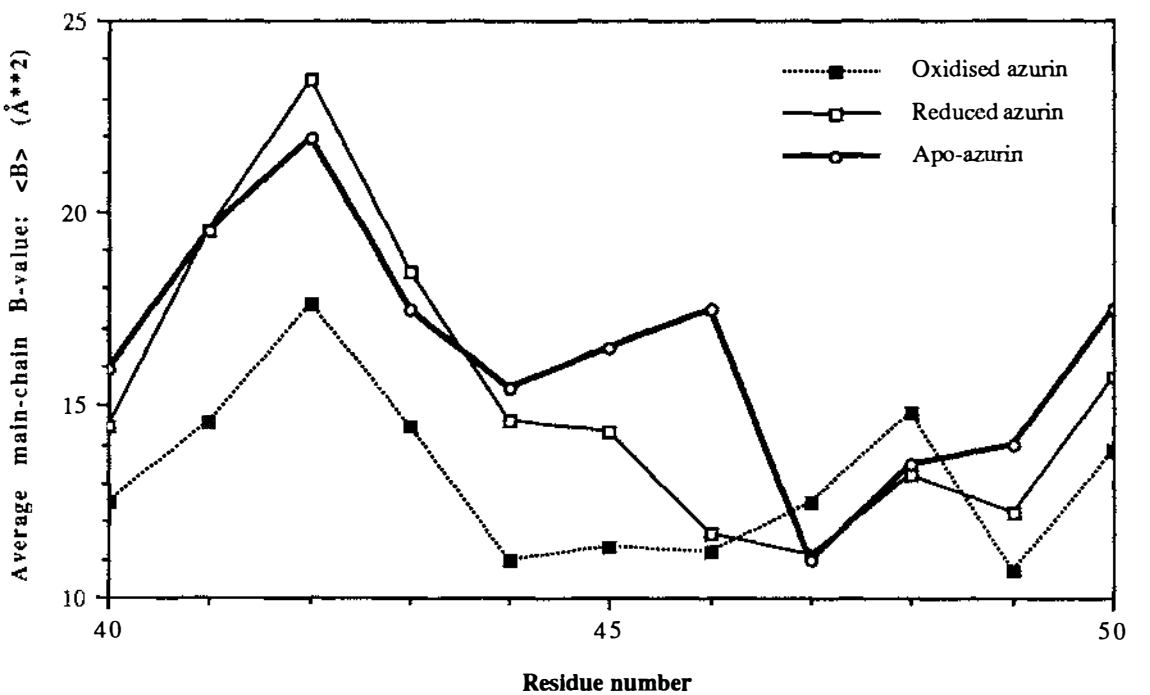

Figure 4.2.8.4. Plot of the average B-value for the section of residues between 40 and 50.

to the oxidised and reduced structures, they are found to be higher in the apo form by 9.1Å^2 (apo-oxidised) and 7.1Å^2 (apo-reduced) (see Figure 4.2.8.3). A similar effect is seen for the other copper ligand, His-46, where the main-chain B-values increase by 6.3Å^2 (apo-oxidised) and 5.8Å^2 (apo-reduced) on copper removal (see Figure 4.2.8.4). However, the average B-values in residues 112-117, the type II turn which procedes loop 117-121, are only slightly higher, by ≈3Å^2, than those of oxidised and reduced azurins (see Figure 4.2.8.3). These increases in B-values may be related to the removal of the copper since they supply the copper ligands. Also, the 117-121 loop is on the surface of the protein and does not make any hydrogen bonds to sequentially distant parts of the protein, which might restrain the thermal motion of this loop. Furthermore, the side-chain of His-117 is the only copper ligand which is not hydrogen bonded to another part of the protein, and it is thus possible that it could become more free upon removal of the copper, as judged by the increase in the B-values. Other indications that the 117-121 turn has become more flexible are also seen in the agreement between the two apo-azurin molecules of the asymmetric unit; especially in the main-chain torsion angles and in the deviation of atom positions after superposition (see Section 4.3.2).

4.2.9 Solvent structure

As in oxidised and reduced azurins, most of the solvent structure of apo-azurin has been modelled as water molecules. The exceptions are the sulphate anions in the sulphate binding sites of the two protein molecules, and one possible disordered sulphate anion on a 2-fold crystallographic axis. Most of the solvent molecules in the apo form are located within 2Å of a position which corresponds to a solvent molecule in the oxidised form (201 out of 269). In the atom coordinates, these are given the same labels as their counterparts in oxidised azurin (132 to 283). When compared to the solvent structure of reduced azurin, there are fewer solvent molecules (167) in the apo form that are within 2Å of a corresponding position in reduced azurin. Of these solvent molecules which are common to the reduced form, only 13 are not found in the solvent structure of oxidised azurin (these are 193B, 199B, 217A, 240B and those with labels above 300). In fact, only 51 solvent molecules have positions which are "unique" to the solvent structure of apo-azurin (labelled as 401 to 451). The average B-value for these "unique" solvent molecules (<B> = 70Å^2) is higher than those which are at positions corresponding to solvent molecules in oxidised and reduced azurins (<B> = 56Å^2). Figure 4.2.9.1 shows the differences in the positions of solvent molecules between the apo, oxidised and reduced azurins as a function of the average B-value.

The resemblance of the solvent structure between the three forms of azurin is expected

since the crystal forms are isomorphous with each other. The few differences which do occur could be the result of small changes in the unit cell parameters between oxidised, reduced and apo azurins. It is possible, however, that the differences could simply reflect the fact that these are mostly the more poorly defined water molecules whose density is close to the noise level in electron density maps; their appearence would therefore be very sensitive to small errors in the data, or the model, and differences in refinement, etc. It is interesting to note that the greater similarity between the protein structures of apo and oxidised azurins when compared to those of apo and reduced azurins, as shown in earlier sections, also extends to the solvent structure.

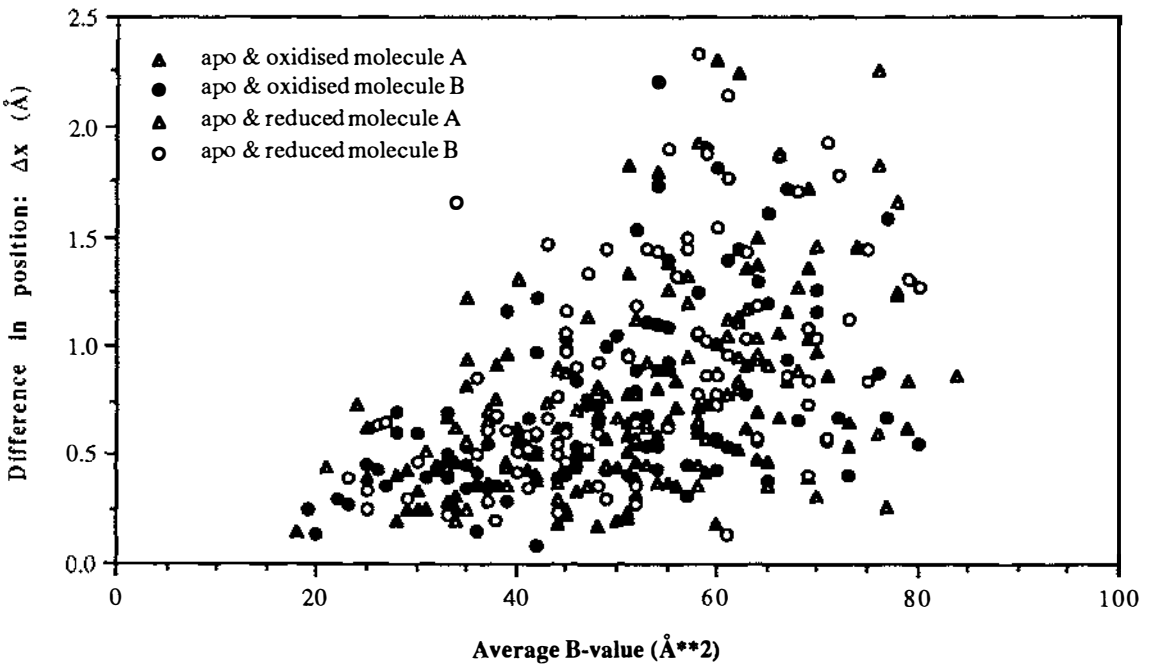

Figure 4.2.9.1. Plot of the differences in position of the solvent molecules between apo, oxidised and reduced azurins.

4.3 Comparison of the two apo-azurin molecules

As for reduced azurin, the two independent protein molecules in the asymmetric unit of apo-azurin crystals can be compared to estimate the reliability of the structure, because no non-crystallographic symmetry restraints were imposed on them during refinement. Since the structure of apo-azurin has been refined at a lower resolution than reduced azurin, the agreement between the two independent molecules of apo-azurin is expected to be poorer than that found for reduced azurin.

4.3.1 Lattice contacts

Since the crystal packing arrangement in apo-azurin is similar to the oxidised and reduced forms of azurin, with the pseudo-tetragonal symmetry of the crystals maintained, the two independent molecules of apo-azurin have similar lattice contacts. These contacts are listed in Tables 4.3.1.1 and 4.3.1.2. The criteria used to define a lattice contact are the same as for the reduced structure (i.e. any non-hydrogen atom distance below 3.5Å). Of a total of 46 intermolecular hydrogen bonds in the crystal structure, 10 pairs are found in corresponding regions of the two protein molecules. These contacts which are common to both molecules involve residues 23-24, 38, 40, 65, 68 and 129. Differences between the two molecules occur at residues 2A, 4B, 24A, 28A, 34B, 92A, 92B, 128A, 129A and 129B; these differences involve the side-chains of Glu, Gln and Lys residues, and the chain termini, for which the structure is poorly defined.

Eighteen of the 46 lattice contacts in the structure of apo-azurin correspond to contacts found in the structure of reduced azurin, and 25 correspond to contacts in the oxidised structure. Hydrogen bonds which are underlined in Table 4.3.1.1 indicate that a similar contact is made in reduced azurin, while those in bold are found in the oxidised structure. The differences in the lattice contacts between the apo- and two other redox forms involve flexible or poorly defined parts of the structure (e.g. 9 of these hydrogen bond contacts involve the C-termini of the polypeptide chains).

The crystal structure of apo-azurin contains twenty-two non-hydrogen bonding lattice contacts (<3.5Å) of which only three are common to both protein molecules. Many of the these lattice contacts are associated with intermolecular hydrogen bonds but five contacts are made between atoms in the hydrophobic patches of the two molecules. Of special interest is the absence of contacts between the main-chain atoms of residues 115 and 116, which are present in the oxidised and reduced forms of azurin. In apo-azurin these contacts are >3.5Å, but are 3.18-3.38Å and 3.30-3.39Å in the oxidised and reduced

structures, respectively. This suggests there could be a slight repacking of the molecules, accompanying the small change in the unit cell dimensions. Table 4.3.1.2 lists the non-hydrogen bonding contacts of apo-azurin, and includes some additional contacts with distances beyond 3.5Å (in italics) for comparison with the oxidised and reduced forms. In addition to the lattice contacts made between protein molecules, 29 lattice contacts are made through bridging water molecules. Of these water molecules, only three pairs of solvent molecules (OW 137, OW 139 and OW 162) make hydrogen bonds to equivalent regions of the two protein molecules.

Table 4.3.1.1. Intermolecular hydrogen bonds in the crystal structure of apo-azurin.

Hydrogen bond	Distance (Å)	Symmetry operation	Hydrogen bond	Distance (Å)	Symmetry operation
$O_{\varepsilon 1}$ 2A-N_{ζ} 34B	3.01	-1/2+x,1/2+y,z			
			$O_{\varepsilon 1}$ 4B-O_{γ} 92A	3.04	-1/2+x,1/2+y,z
			$O_{\varepsilon 2}$ 4B-O_{γ} 92A	3.26	-1/2+x,1/2+y,z
			$O_{\varepsilon 2}$ 4B-O_{γ} 94A	3.10	-1/2+x,1/2+y,z
$O_{\delta 2}$ 23A-$N_{\delta 2}$ 65A	2.80	-1/2+x, 1/2-y,-z	**$O_{\delta 2}$ 23B-$N_{\delta 2}$ 65B**	2.95	1-x,-1/2+y,1/2-z
O 24A-N 68B	3.00	-1/2+x, 1/2-y,-z	**O 24B-N 68A**	2.84	-x,1/2+y,1/2-z
N_{ζ} 24A-O 65B	2.66	-1/2+x, 1/2-y,-z	**N_{ζ} 24B-O 65A**	3.08	-x,1/2+y,1/2-z
N_{ζ} 24A-O 129B	3.21	1/2-x,-y,-1/2+z			
			N_{ζ} 24B-$O_{\delta 1}$ 129A	2.90	1/2-x,-y,-1/2+z
N_{ζ} 24A-O_{ε} 129B	2.77	1/2-x,-y,-1/2+z			
$O_{\varepsilon 1}$ 28A-N 92B	3.05	-1/2+x,1/2+y,z			
$N_{\varepsilon 2}$ 28A-O 92B	3.12	-1/2+x,1/2+y,z			
			N_{ζ} 34B-$O_{\varepsilon 1}$ 2A	3.01	-1/2+x,1/2+y,z
O 38A-N 40A	2.92	1/2-x,y,1/2-z	**O 38B-N 40B**	2.80	x,-y,-z
N 40A-O 38A	2.92	1/2-x,y,1/2-z	**N 40B-O 38B**	2.80	x,-y,-z
O 65A-N_{ζ} 24B	3.08	-x,1/2+y,1/2-z	**O 65B-N_{ζ} 24A**	2.66	-1/2+x, 1/2-y,-z
$N_{\delta 2}$ 65A-$O_{\delta 2}$ 23A	2.80	-1/2+x, 1/2-y,-z	**$N_{\delta 2}$ 65B-$O_{\delta 2}$ 23B**	2.95	1-x,-1/2+y,1/2-z
N 68A-O 24B	2.84	-x,1/2+y,1/2-z	**N 68B-O 24A**	2.80	-1/2+x, 1/2-y,-z
			N 92B-$O_{\varepsilon 1}$ 28A	3.05	-1/2+x,1/2+y,z
			O 92B-$N_{\varepsilon 2}$ 28A	3.12	-1/2+x,1/2+y,z
O_{γ} 92A-$O_{\varepsilon 1}$ 4B	3.04	-1/2+x,1/2+y,z			
O_{γ} 92A-$O_{\varepsilon 2}$ 4B	3.26	-1/2+x,1/2+y,z			
O_{γ} 94A-$O_{\varepsilon 2}$ 4B	3.10	-1/2+x,1/2+y,z			
O_{γ} 128A-$N_{\delta 2}$ 129B	3.11	1/2-x,-y,-1/2+z			
O 129A-N_{ζ} 24B	2.75	1/2-x,-y,-1/2+z	O 129B-N_{ζ} 24A	3.21	1/2-x,-y,-1/2+z
			O 129B-$N_{\delta 2}$ 129A	2.71	1/2-x,-y,-1/2+z
$O_{\delta 1}$ 129A-N_{ζ} 24B	2.90	1/2-x,-y,-1/2+z	**$O_{\delta 1}$ 129B-N_{ζ} 24A**	3.12	1/2-x,-y,-1/2+z
			$N_{\delta 2}$ 129B-O_{γ} 128A	3.11	1/2-x,-y,-1/2+z
$N_{\delta 2}$ 129A-O 129B	2.71	1/2-x,-y,-1/2+z			
			O_{ε} 129B-N_{ζ} 24A	2.77	1/2-x,-y,-1/2+z

Table 4.3.1.2. Non-hydrogen bonding lattice contacts in the crystal structure of apo-azurin.

Lattice Contact	Distance (Å)	Symmetry operation	Lattice Contact	Distance (Å)	Symmetry operation
			N 1B-$C_{\gamma 2}$ 61B	2.89	1-x,-1/2+y,1/2-z
			C_β 1B-C_α 58B	3.16	1-x,-1/2+y,1/2-z
C_ε 13A-C_ε 13B	2.67	x,y,z	C_ε 13B-C_ε 13A	2.67	x,y,z
O 25A-CD2 68B	3.36	-1/2+x, 1/2-y,-z	O 25B-$C_{\delta 2}$ 68A	3.24	-x,1/2+y,1/2-z
			$C_{\varepsilon 1}$ 32B-OG 94A	3.39	-1/2+x,1/2+y,z
C_ε 38A-O 119B	*3.53*	1/2-x,y,1/2-z	C_ε 38B-O 119A	3.37	x,-y,-z
			C_β 40B-O 89B	3.29	x,-y,-z
O 43A-C_β 119B	*3.61*	x,y,z	O 43B-C_β 119A	3.45	x,y,z
			$N_{\varepsilon 1}$ 57B-C_α 90A	3.14	-x,y,1/2-z
			C_α 58B-C_β 1B	3.16	1-x,-1/2+y,1/2-z
			$C_{\gamma 2}$ 61B-N 1B	2.89	1-x,-1/2+y,1/2-z
			C_ε 64B-C_γ 115A	3.20	x,y,z
$C_{\delta 2}$ 68A-O 25B	3.24	-x,1/2+y,1/2-z	$C_{\delta 2}$ 68B-O 25A	3.36	-1/2+x, 1/2-y,-z
			O 89B-C_β 40B	3.29	x,-y,-z
C_α 90A-$N_{\varepsilon 1}$ 57B	3.14	-x,y,1/2-z			
O_γ 94A-$C_{\varepsilon 1}$ 32B	3.39	-1/2+x,1/2+y,z			
C_γ 115A-C_ε 64B	3.20	x,y,z			
O 115A-C_α 116B	*3.65*	x,y,z	O 115B-C_α 116A	*3.55*	x,y,z
C_α 116A-O 115B	*3.55*	x,y,z	C_α 116B-O 115A	*3.65*	x,y,z
O 119A-C_ε 38B	3.37	x,-y,-z	O 119B-C_ε 38A	*3.53*	1/2-x,y,1/2-z
C_β 119A-O 43B	3.45	x,y,z	C_β 119B-O 43A	*3.61*	x,y,z

4.3.2 Comparison of the main-chain structure

Overall, the differences in the main-chain between the two apo-azurin molecules follow the same pattern as for the two molecules of reduced azurin. To avoid repetition, these will not be dicussed in detail.

Superposition of the main-chain

Superposition of the two molecules of apo-azurin was done as for reduced azurin (section 3.3)[255]. All main-chain atoms were used except for the N- and C-termini (residues 1-2 and 128-129), since these regions have large differences in their main-chain conformations between the two molecules. The transformation for superimposing molecule B on to molecule A with the best fit is given below, such that $\underline{R}.\underline{x}_B + \underline{T} = \underline{x}_A$, where $\underline{R}$ is the rotation matrix, $\underline{T}$ the translation vector, and $\underline{x}_A$, $\underline{x}_B$ the orthogonal coordinates of molecule A and B, respectively. i.e.

$$\begin{bmatrix} -0.11692 & 0.99285 & 0.02389 \\ 0.99249 & 0.11593 & 0.03908 \\ 0.03603 & 0.02828 & -0.99895 \end{bmatrix} \times \begin{bmatrix} x_B \\ y_B \\ z_B \end{bmatrix} + \begin{bmatrix} 20.08621 \\ -16.96780 \\ -12.74946 \end{bmatrix} = \begin{bmatrix} x_A \\ y_A \\ z_A \end{bmatrix}$$

Alternatively, the transformation can be expressed as a rotation of 179.5° about the local 2-fold axis. Figure 4.3.2.1 plots the average deviation in main-chain atom position as a function of residue number. The r.m.s. deviation for main-chain atom positions between residues 3 and 127 is 0.288Å. The regions with the least agreement between the two apo-azurin molecules ($\Delta x > 0.5$Å) are at residues 1-2, 25, 69, 103-104 and 127-129, which belong to the termini and certain loops on the surface of the protein. The best agreement between the main-chain atoms appears in the residues which correspond to the β-strands and the single α-helix of the structure, where average deviations in main-chain atom positions range from 0.05Å to 0.25Å. When separated into secondary structural elements, the r.m.s. deviation in main-chain atom positions is 0.22Å for residues of the β-strands, and 0.21Å for residues of the α-helix.

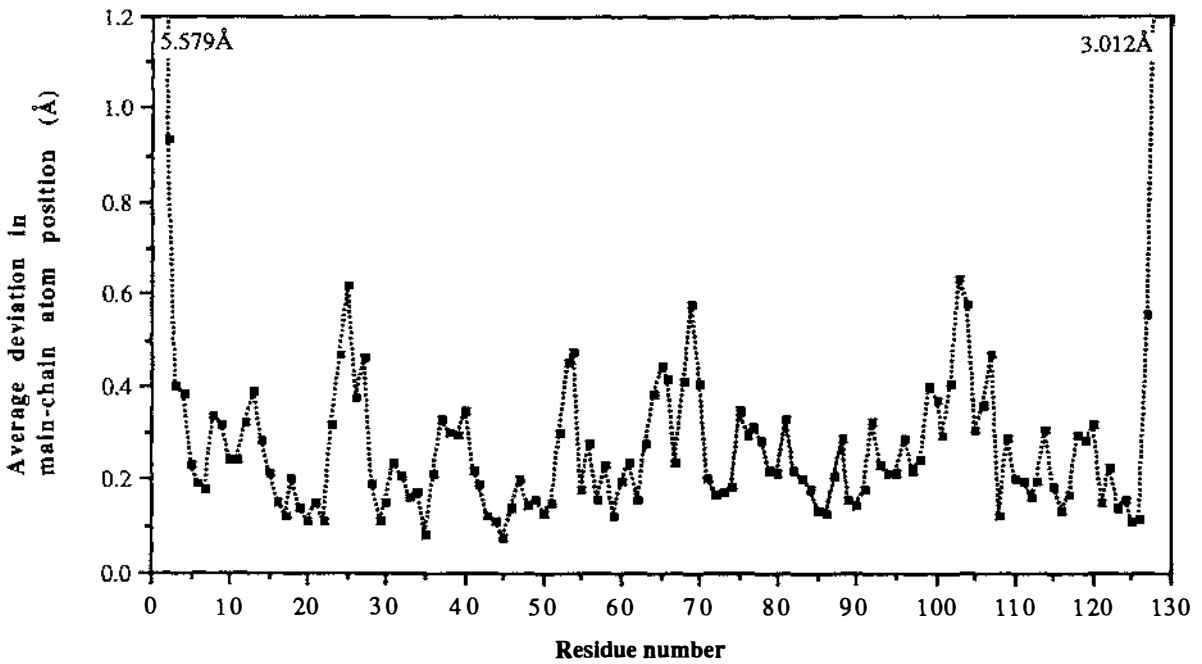

Figure 4.3.2.1. Average deviation in main-chain atom positions between the two superimposed molecules of apo-azurin.

Comparison of the main-chain torsion angles

The main-chain torsion angles (ϕ,ψ) agree well between the two apo-azurin molecules. The r.m.s. deviation in torsion angles calculated from all residues is 19.3°, but this value drops to 7.0° when residues 1-2 and 128-129 are excluded. Figure 4.3.2.2 shows the differences in ϕ and ψ between the two molecules of apo-azurin. While for the majority of

the residues torsion angles agree within 10°, a few isolated values disagree by as much as 20°. These poorly agreeing sections include residues 56-57 and 105-106, which are loops on the surface of the protein and are remote from the copper binding site. The sections of the main-chain with the best agreement in ϕ and ψ are in the β-strands with an r.m.s. deviation in (ϕ,ψ) of 6.0°, and the α-helix, for which the agreement is slightly less (r.m.s. $\Delta\phi\psi$ = 8.0°).

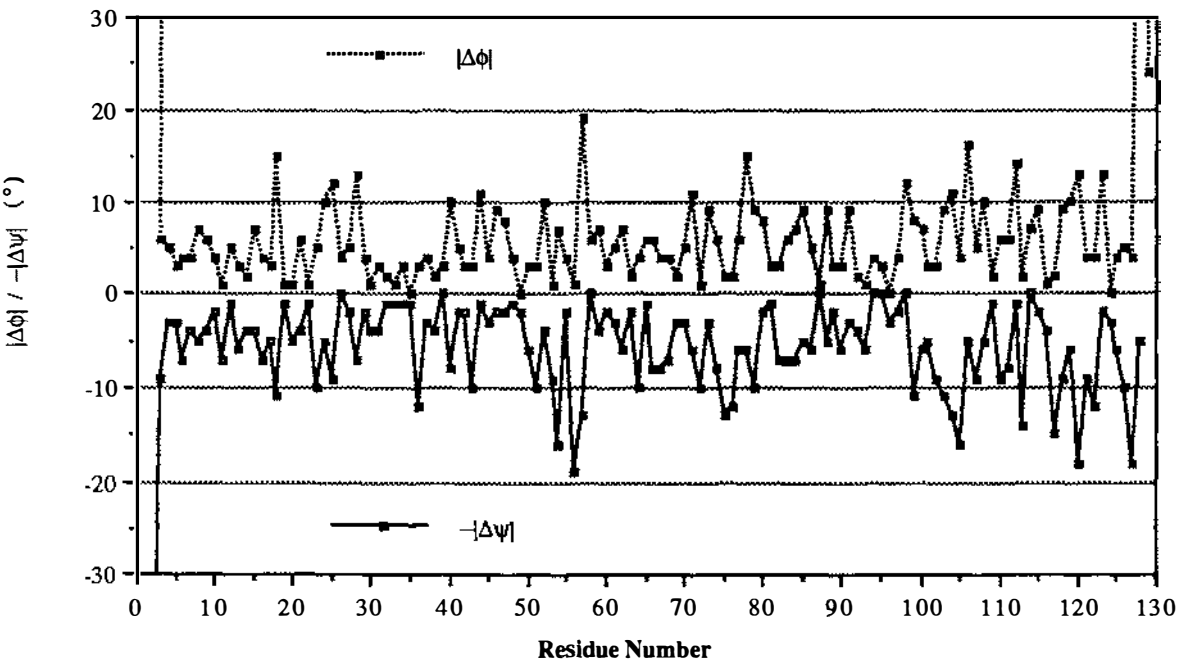

Figure 4.3.2.2. Deviation in the main-chain torsion angles (ϕ,ψ). Values for ($|\Delta\phi|$,$|\Delta\psi|$) for the N- and C- termini are Ala-1 = (-, 173), Gln-2 = (164, 110), Ser-128 = (102, 5), Asn-129 = (24, -).

Thermal parameters

Figure 4.3.2.3 shows the level of agreement in the average main-chain atom B-values between the two apo-azurin molecules. These give an r.m.s. deviation of only 4.2Å^2. Since the B-values were refined independently for each protein molecule, the agreement testifies to the validity of these parameters as a representation of the thermal motion and disorder of the structure. As in the reduced structure, the highest B-values correspond to those sections of the main-chain which have the largest deviation in atom position. Similarly, the lowest B-values in the main-chain correspond to those residues with the smallest deviations in atom position.

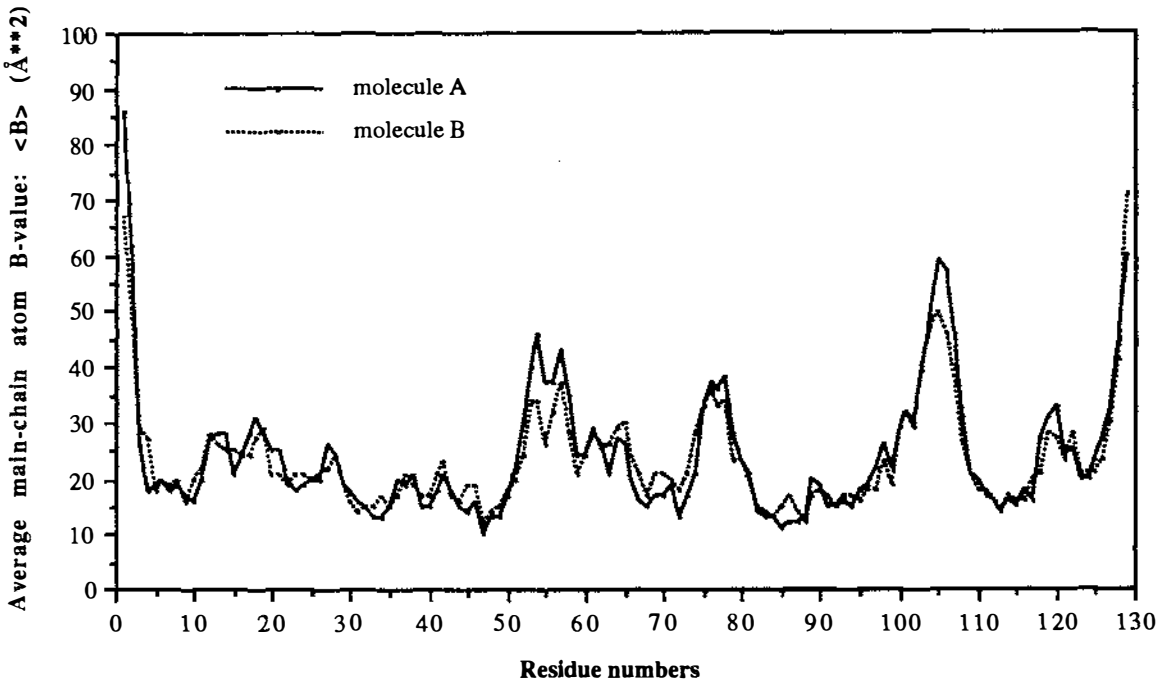

Figure 4.3.2.3. Average B-values for main-chain atoms of apo-azurin.

4.3.3 Comparison of the side-chain structure

Superposition of the side-chains

The same transformation matrix used to superimpose the main-chain structure was used to compare the side-chains between the two apo-azurin molecules. Figure 4.3.3.1 shows the average deviation in side-chain atom positions for each residue, and as in the reduced structure, the agreement between the two molecules can be divided into three general categories, i.e. with the average deviation 1) <0.6Å (1 r.m.s.), 2) 0.6-1.2Å (2 r.m.s.) and 3) >1.2Å.

The first category (<0.6Å) contains most of the sidechains which are buried in the interior of the molecule, and in particular, includes the side-chains of the binding site. The next category (0.6-1.2Å) comprises many side-chains which reside on the surface of the protein molecule, and are in contact with the solvent. Of charged residues in this group, there are 8 Lys, 4 Glu and 1 Asp. The last division (>1.2Å) contains the N- and C-termini, 3 Lys, 3 Glu, 2 Met and 1 Asp. Virtually all of these side-chains are poorly defined in electron density maps of either one or both protein molecules, with the exception of Met-13 and Met-64 for which the differences are caused by intermolecular contacts (see section 4.3.1).

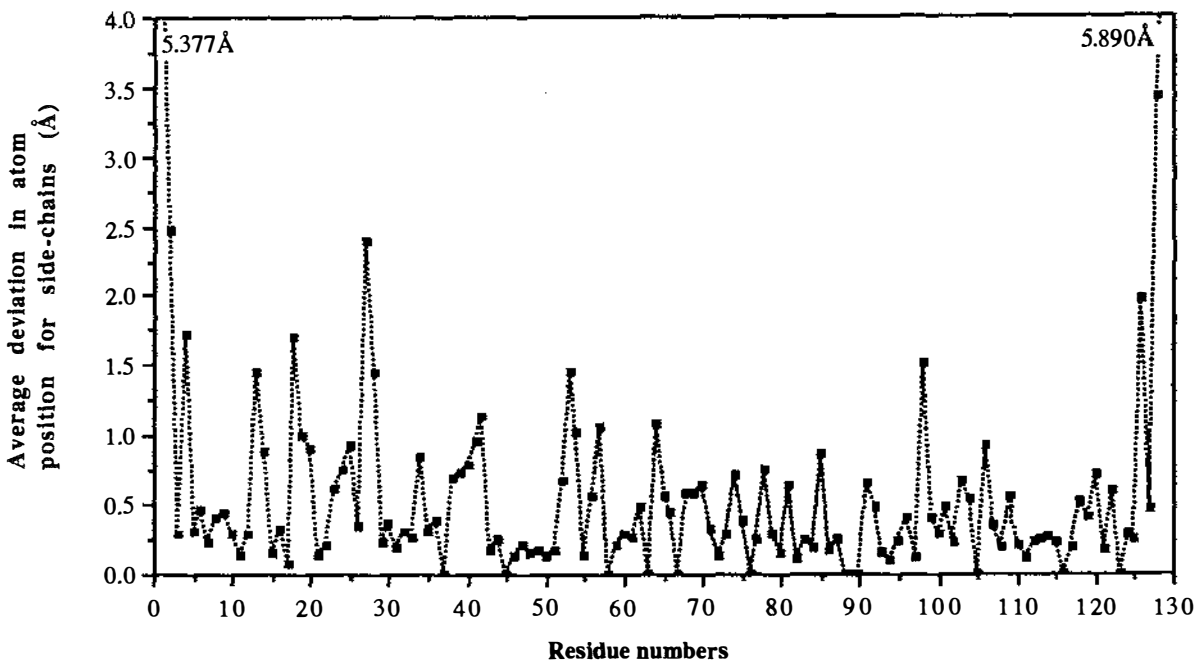

Figure 4.3.3.1. Average deviation in side-chain atom positions between the two molecules of apo-azurin.

Overall the differences in the positions of the side-chains of apo-azurin are similar to those found in reduced azurin, i.e. the largest deviations in position occurring in side-chains on the surface of the protein, and the smallest in the most well defined or buried side-chains. However, some exceptions are apparent, since a few side-chains on the surface of the protein show good agreement between both molecules, despite being poorly defined in the electron density maps. For several of these, however, the side-chains were rebuilt during refinement according to the conformation observed for whichever molecule had clearer electron density (e.g. Glu-53, Glu-55, Thr-61 and Lys-101).

Comparison of side-chain torsion angles

As expected, the side-chain torsion angles, which were left unrestrained during refinement, are very similar between the two protein molecules. The r.m.s. deviations in χ_1-χ_4 are 12.8° (95 pairs), 19.1° (62 pairs), 40.7° (24 pairs) and 42.1° (13 pairs), respectively. This shows the same trend as was observed in the reduced azurin structure, where the agreement is best for χ_1 and gradually deteriorates until χ_4. The relationship between buried side-chains (defined as those residues with a solvent accessibility less

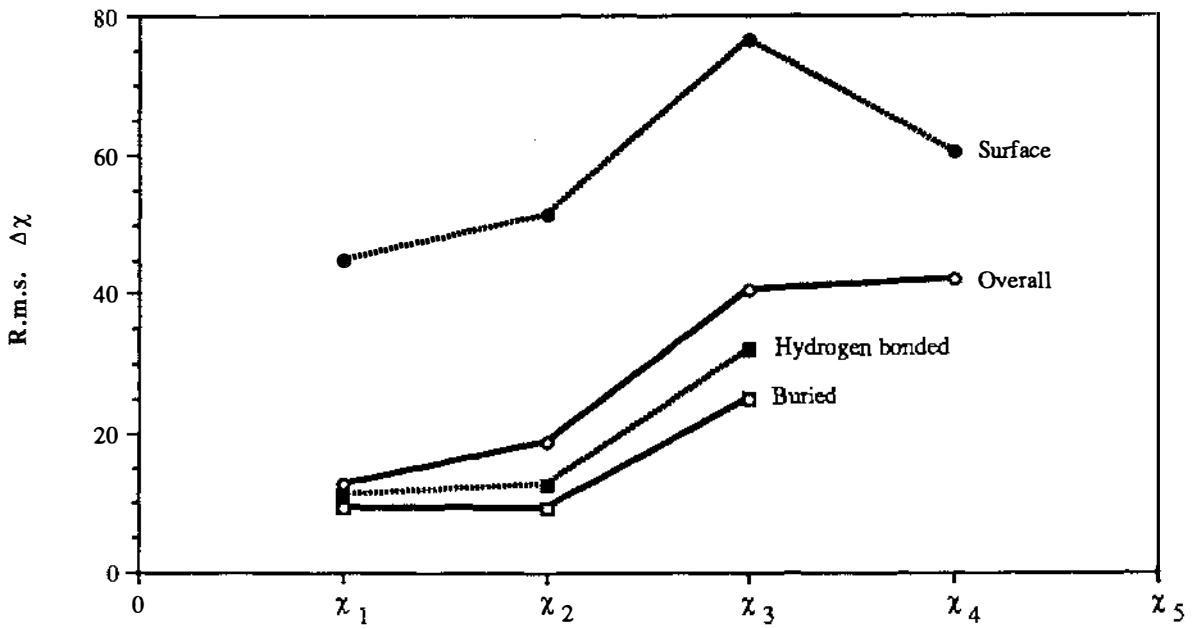

Figure 4.3.3.2. R.m.s. deviations in side-chain torsion angles (χ_{1-4}) of apo-azurin for buried, hydrogen bonded, surface and overall side-chains.

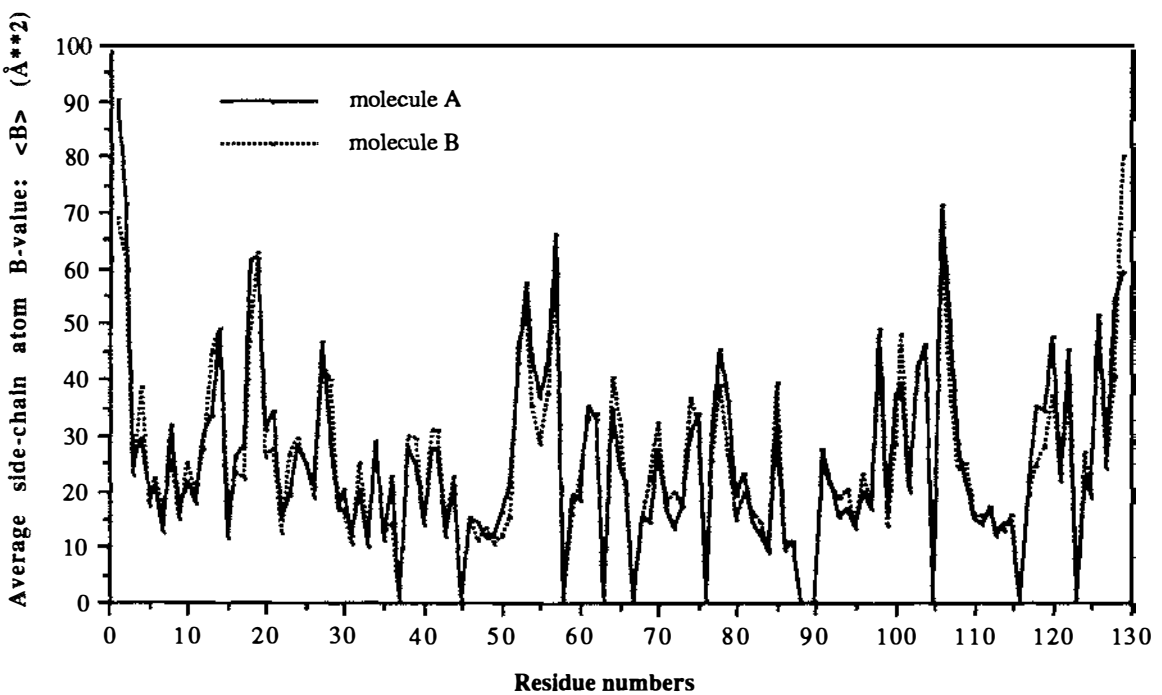

Figure 4.3.3.3. Average B-values for the side-chain atoms of the two apo-azurin molecules.

than 5Å^2 per atom[235]), hydrogen bonded side-chains and surface side-chains in apo-azurin is identical to that found in reduced azurin (see Figure 4.3.3.2). R.m.s. deviations in χ_1-χ_3 for buried residues are 9.2°,9.4° and 25.2°, respectively; for hydrogen bonded side-chains are 11.4°,12.7° and 31.9°, respectively; and for surface side-chains are 44.9°, 51.5°, 76.4° and 60.3°, respectively.

Thermal parameters

Analysis of the side-chain B-values of apo-azurin gives a similar conclusion to that found for the main-chain B-values. The B-values between the two protein molecules agree well (r.m.s deviation for the average B-value of side-chains is 6.11Å^2), and also confirms their validity as physical parameters (see Figure 4.3.3.3). As was noted before, the largest differences in the B-values occur in those parts of the protein which are more clearly defined in one molecule than the other (e.g. residues 53-56).

4.3.4 Comparison of the hydrogen bonds

Since most of hydrogen bonds were not geometrically restrained during refinement, a comparison of the hydrogen bonds between the two independent molecules will give another indication of the accuracy of the structure. The hydrogen bonds were calculated and analysed in the same manner as for reduced azurin. The same criteria for defining a hydrogen bond were also used, (i.e. distances less than 3.5Å without a hydrogen atom or 2.5Å with hydrogen atom, and hydrogen bond angles greater than 90°).

Hydrogen bonding structure

There are very few differences in the hydrogen bonding structure between the two apo-azurin molecules. These differences are listed in Table 4.3.4.1, and those hydrogen bonds which have "marginal" geometry (i.e. O...H>2.3Å or O...N>3.3Å for distances, or any angle less than 100°) are in italics. All of the residues involved in these hydrogen bonds reside on the surface of the protein molecule, and are either in regions where the electron density is poorly defined or belong to flexible parts of the molecule. About half (10 of 22) of the hydrogen bonds are "marginal". Some of the differences may be the result of differences between the crystal lattice contacts of the two molecules, especially at Gln-2, Met-39, Ser-128 and Asn-129.

Table 4.2.3.1. Differences in the hydrogen bonding between the two apo-azurin molecules. Where there are O...H-O interactions the geometry is listed as C-O...O, O...O and O...O-C.

	molecule A			molecule B		
	N-H...O (°)	H...O (Å)	H...O-C (°)	N-H...O (°)	H...O (Å)	H...O-C (°)
main-chain...main-chain						
N 24...O 128	*132*	*2.32*	*134*			
N 56...O 53				*160*	*2.39*	*103*
N 73...O 70				*160*	*2.45*	*120*
N 77...O 74	134	2.10	148			
N 80...O 77				*162*	*2.40*	*109*
main-chain...side-chain						
N 3...$O_{\varepsilon 1}$ 2				151	1.84	129
N 10...$O_{\delta 1}$ 10	*102*	*2.45*	*98*			
N 14...$O_{\delta 1}$ 10	*146*	*2.37*	*157*			
N 39...$O_{\delta 1}$ 11				*141*	*2.34*	*114*
N_{ζ} 41...O 86				125	3.08	146
N 47...$O_{\delta 1}$ 47				*109*	*2.39*	*101*
N 94...$O_{\delta 1}$ 93				*133*	*2.33*	*90*
N 100...$O_{\delta 2}$ 98	158	1.48	146			
N_{ζ} 101...O 81				135	2.96	143
side-chain...side-chain						
$N_{\delta 2}$ 10...$O_{\varepsilon 1}$ 14				161	2.22	146
N_{ζ} 41...$O_{\varepsilon 1}$ 91	*173*	*3.30*	*117*			
N_{ζ} 74...$O_{\delta 1}$ 62	167	2.65	126			
N_{ζ} 85...$O_{\delta 1}$ 93				116	3.23	114
O_{γ} 100...$O_{\delta 1}$ 98				126	2.83	131
O_{η} 108...$O_{\varepsilon 1}$ 106	100	3.28	103			
N_{ζ} 122...$O_{\varepsilon 1}$ 53				93	2.66	125
O_{γ} 128...O_{ε} 129	128	3.15	125			

Variation in the hydrogen bond geometry

The variation in the hydrogen bond geometry between the two apo-azurin molecules is similar to that found in the reduced structure. The r.m.s. deviation between 60 pairs of main-chain...main-chain hydrogen bond distances and angles, is 0.16Å (58 pairs) and 7.1° (57 pairs), respectively. Main-chain...side-chain interactions, both local and crosslinking (total 25 pairs) show less agreement, with r.m.s. deviations of 0.22Å for distances (22 pairs) and 7.3° for angles (23 pairs). In contrast, side-chain...side-chain hydrogen bonds, including salt bridges (total 9 pairs), show rather good agreement, r.m.s. deviations of 0.12Å for distances and 8.6° for angles. However these latter are few in number, and several had to be restrained during refinement as they were otherwise too short. Thus their level of agreement is probably artificially low (see Section 4.1).

When the hydrogen bonds are analyzed with respect to their secondary structure assignment, the r.m.s. deviation of hydrogen bond distances and angles in the β-sheets is

0.17Å and 5.9°, respectively. The values are similar for the hydrogen bonds in the α-helix, 0.14Å for distances and 10.4° for angles. In contrast, hydrogen bonds associated with the loops of the structure agree somewhat less well between the two molecules; r.m.s. deviations in distances and angles of 0.19Å and 10.9°, respectively.Generally, the agreement in the hydrogen bond geometries between the two molecules of apo-azurin is similar to that found in the structure of reduced azurin.

4.3.5 Comparison of the binding sites and their surrounds

Like the copper sites of the other forms of azurin, the binding site of apo-azurin shows less variation in structure between the two protein molecules than the rest of the protein. Superposition of the residues which make up the binding site (Gly-45, His-46, Cys-112, His-117 and Met-121) gives an r.m.s. deviation in atom positions of 0.15Å. Figure 4.3.5.1 is a superposition of the two binding sites, illustrating the good level of agreement. This level of agreement is comparable to that found for the copper sites of the other two forms of azurin (0.14Å oxidised and 0.16Å reduced azurin). The r.m.s. deviation in the atom positions for the protein structure surrounding the binding site is 0.20Å, a value comparable to the agreement in the reduced form of azurin (r.m.s. = 0.21Å). Of the hydrogen bonds which surround the binding site (22 pairs), the r.m.s. deviation in their geometries is 0.19Å and 7.9° for hydrogen bond lengths and angles, respectively. Omitting three "outliers" reduces these r.m.s. deviations down to 0.13Å and 6.0°, respectively.

The agreement in the torsion angles between the two binding sites is also comparable to the agreement found in the copper site of the reduced structure. The r.m.s. deviation for main-chain torsion angles (ϕ,ψ) and side-chain torsion angles (χ) of the binding site (Gly-45, His-46, Cys-112, His-117 and Met-121) is 8.0° and 6.6°, respectively. Note, however, that the r.m.s. $\Delta\phi\psi$ drops to 5.1° if the two largest values are omitted (Cys-112 $\Delta\phi$ = 14° and His-117 $\Delta\psi$ = 15°).

In the structural analyses of oxidised and reduced azurins, the copper distances were compared between the two molecules of the asymmetric unit to give an indication of the accuracy at the active site. Although copper distances can not be given for the binding site of apo-azurin, distances can be measured between the copper binding atoms, i.e. O 45, $N_{\delta 1}$ 46, S_{γ} 112, $N_{\delta 1}$ 117 and S_{δ} 121. Table 4.3.5.1 lists these distances for both molecules. The r.m.s. deviation for all of these distances is 0.11Å, which drops to 0.08Å if the two largest differences are omitted. In comparison, the r.m.s. deviation in copper distance is 0.06Å for the reduced azurin and 0.04Å for the oxidised azurin. Similarly, an

Figure 4.3.5.1. Stereo view of the copper binding sites from the two apo-azurin molecules superimposed on each other using the atoms of Gly-45, His-46, Cys-112, His-117 and Met-121. Molecule A in yellow and molecule B in blue.

Table 4.3.5.1. Distances in ångstroms (Å) between the atoms of the apo-azurin binding site.

	Molecule A	Molecule B	Average
O 45...$N_{\delta 1}$ 46	3.16	3.25	3.21
O 45...S_{γ} 112	4.29	4.24	4.27
O 45...$N_{\delta 1}$ 117	3.42	3.57	3.50
O 45...S_{δ} 121	6.01	6.08	6.05
$N_{\delta 1}$ 46...S_{γ} 112	3.67	3.87	3.77
$N_{\delta 1}$ 46...$N_{\delta 1}$ 117	3.19	3.36	3.28
$N_{\delta 1}$ 46...S_{δ} 121	3.31	3.38	3.35
S_{γ} 112...$N_{\delta 1}$ 117	3.59	3.49	3.54
S_{γ} 112...S_{δ} 121	4.12	4.17	4.15
$N_{\delta 1}$ 117...S_{δ} 121	3.89	3.92	3.91

indication of the agreement in the angles of the binding site can be obtained by comparing the angles between the various ligands (e.g. O 45...S_{γ} 112...S_{δ} 121). This gives an r.m.s. deviation in angles of 3.0°, compared to 3.9° and 3.7° for the copper angles of oxidised and reduced azurins, respectively.

Hydrogen bonds involving the sulphur of Cys-112

With the absence of a copper atom in the active site, the sulphur at Cys-112 is assumed to

be protonated at pH 6.0, resulting in two extra possible hydrogen bonds. The occurrence of these thiol (SH...N) hydrogen bonds was discussed in section 4.2.7. Here, a comparison between the two protein molecules is presented. Table 4.3.5.2 lists the hydrogen bond geometries for the S...HN and SH...N interactions. The geometry of the S...HN interactions agrees well, with differences of 0.04-0.08Å for S...H distances and 3-8° for S...H-N angles. Including a thiol hydrogen atom in a staggered conformation (torsion angle of C_α-C_β-S_γ-H = 180°), the variation in SH...N geometry is greater than that for the S...HN hydrogen bonds with differences of 0.29Å for H...N distances, and 5-12° for S-H...N angles. Note that with a calculated thiol hydrogen atom, the H...N hydrogen bond distances suggest that the thiol hydrogen binds more strongly to His-46 in molecule A, but more strongly to His-117 in molecule B, whereas the S...N distances suggest that the thiol binds more strongly to His-117 in both molecules. This is presumably due to slight variations in the orientation of the C_α and C_β atoms of Cys-112, and the consequent difficulty in defining the hydrogen position.

Table 4.3.5.2. S...HN and SH...N hydrogen bond geometries of the two apo-azurin molecules.

	Molecule A			Molecule B		
S...HN	C-S...H	S...H	S...H-N	C-S...H	S...H	S...H-N
S_γ 112...H-$N_{\delta1}$ 47	101°	2.62Å	160°	109°	2.54Å	163°
S_γ 112...H-$N_{\delta1}$ 114	111°	2.76Å	160°	106°	2.80Å	163°
SH...N	C-N...H	N...H	N...H-S	C-N...H	N...H	N...H-S
$N_{\delta1}$ 46...H-S_γ 112	116°	2.46Å	149°	121°	2.75Å	140°
$N_{\delta1}$ 117...H-S_γ 112	117°	2.78Å	117°	112°	2.49Å	129°

4.3.6 Comparison of the solvent structure

Of the 265 solvent molecules in the asymmetric unit of apo-azurin, there are 78 pairs in which the two molecules are related to each other, within 2Å, by the 2-fold non-crystallographic axis. Only three of these pairs are "unique" to the crystal structure of apo-azurin (labelled 401-403), while the remaining pairs are located in positions which correspond to solvent molecules in either oxidised or reduced azurin. Those solvent molecules which do not have a 2-fold equivalent (109) generally have large B-values (>60Å^2).

Three sulphate anions are present in the asymmetric unit. Two of these are equivalent, located in the sulphate binding site of each molecule, and show the same level of variation in position (average difference in atom positions is 0.65Å) as was seen in reduced azurin (see Figure 4.3.6.1). The other anion lies on a 2-fold crystallographic axis.

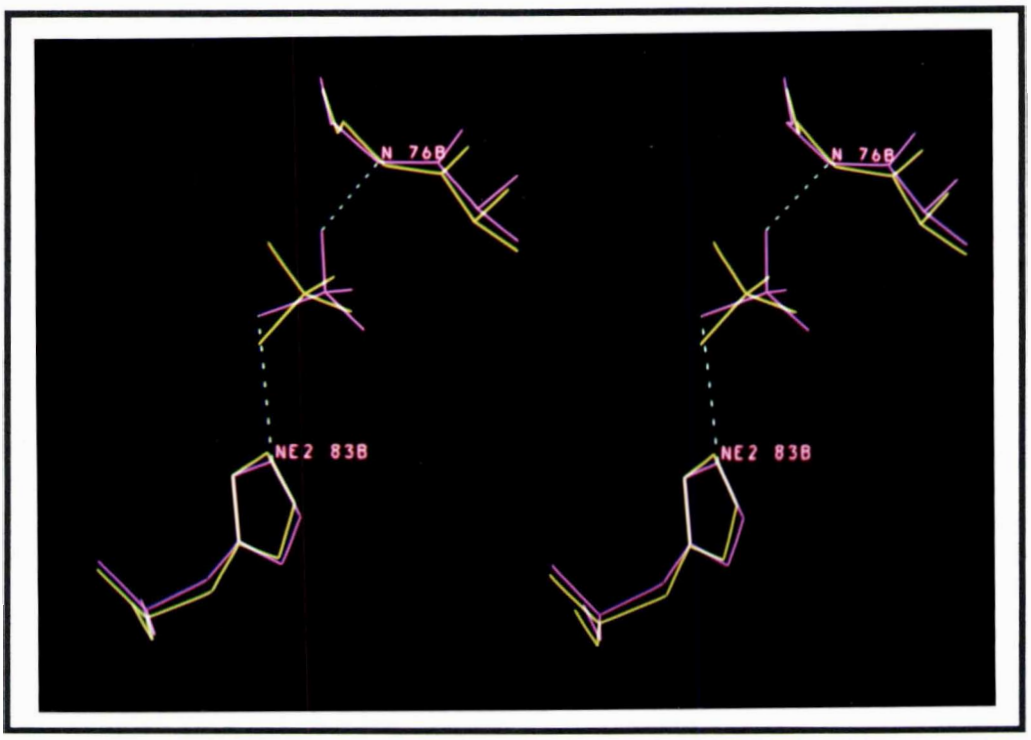

Figure 4.3.6.1. Variation in the positions of the sulphate anions in the sulphate binding site of the two molecules of apo-azurin. Molecule A in yellow and molecule B in purple.

Chapter 5 : Conclusions and Discussion

The crystal structures of apo and reduced azurins have been determined by X-ray diffraction methods, and refined to high resolution (2.2Å and 1.9Å, respectively). Analysis and comparison of these structures show that they are virtually identical with the structure of oxidised azurin[31]. Of the differences which are apparent in structure between the three forms, most are small with the largest appearing in the more flexible and poorly defined regions of the protein. Such differences can not be considered *real* changes caused by the reduction of the protein or the removal of the copper. Instead, they reflect the low accuracy of the structure for these regions. There are, however, some small changes near the copper binding site, a well ordered part of the protein, which may be dependent on the redox state or presence of the copper. These changes are just above the level of accuracy, and because of the limited resolution of these structures, most of them can not be considered truly significant. However, these changes are *consistent* between the two independent molecules of the asymmetric unit, and are discussed and summarized in the sections below.

The structural differences between apo, oxidised and reduced azurins also have implications for protein function. The comparison of the three structures has presented an opportunity to relate the changes made upon reduction or copper removal to the ability of azurin to provide fast, efficient, electron transfer. In Section 5.3, this is discussed in terms of how the protein utilises the copper at the active site to achieve its functional role. Finally, some suggestions are made in Section 5.4 for future research into the structure and properties of azurin.

5.1 Conclusions from the structure of reduced azurin

5.1.1 Structural changes upon reduction

The structure of reduced azurin and its comparison with the oxidised form, show that upon reduction the protein undergoes minimal change either at the copper site or elsewhere. The majority of the changes in the structure are located on the surface of the protein either in loops of the polypeptide chain or in side-chains which extend out into the solvent. Since these regions are associated with high B-values or are unclear in electron density maps, their differences are probably not significant and can not be regarded as real changes related to the process of reduction.

Although the majority of the differences in the protein structure between the oxidised and

reduced forms can not in all probability be attributed to the process of reduction, there are a few small changes which can, especially since these changes are consistent between the two independent molecules of the asymmetric unit. All of the reduction dependent changes are at or near the copper site, and include 1) an increase in all of the copper-ligand distances by 0.05-0.10Å, 2) a decrease in the S...N distances by ≈0.2Å for the two S...HN hydrogen bonds involving Cys-112, 3) small changes in the main-chain torsion angles for the α-turn which precedes Gly-45, and 4) small shifts in the main-chain atom positions of the 112-117 loop. The overall copper geometry and the general arrangement of the copper ligands, however, remains essentially unaltered upon reduction.

All of the structural changes which occur at the copper site upon reduction can be explained in terms of the chemical coordination preferences of the two oxidation states, Cu(I) and Cu(II). The copper geometry alters slightly from trigonal bipyramidal in the Cu(II) state towards a more trigonal geometry in the Cu(I) state. The increases in the Cu-N(His) and Cu-S(Cys) distances are typical of the differences in the metal-ligand bond lengths between Cu(II) and Cu(I) complexes[47,172,258]. This expansion can also be seen as a steric effect in response to the increase in the metal radius by 0.05Å[256], where the physically larger Cu(I) ion effectively pushes these ligands further out from the center of the active site. The increases in the copper distances to the carbonyl oxygen of Gly-45 and the thioether sulphur of Met-121 also reflect the change in the preferences of the metal oxidation state. The ability of Cu(II) centres to form long metal-ligand bonds is well known, a result of the Jahn-Teller effect on its d^9 electronic configuration. Cu(I) centres on the other hand, do not have this tendency to form long metal-ligand interactions because their electronic configuration is d^{10}. Furthermore, the loss of a positive charge at the copper would cause a reduction in any electrostatic interaction between the metal and these groups.

Other changes near the copper site, however, were less expected than those above. The most prominent change is the shortening of the S...HN hydrogen bonds made to Cys-112. This change can not be a steric effect, because the increase in the Cu-S(Cys) bond length (≈0.1Å) is less than the distance shortened in these hydrogen bonds (≈0.2Å), and the direction of the Cu-S(Cys) bond is nearly perpendicular to the direction of the S...HN hydrogen bonds. Instead, this change is explicable on electrostatic grounds. As the copper site is reduced, the electron density on the S_γ 112 increases due to the extra electron which is delocalised between the sulphur and copper. This in turn strengthens the electrostatic interaction between the sulphur and amide hydrogens. Such shifts in S...HN hydrogen bonds have been previously noted in high potential iron protein, where the

$Fe_4S_4Cys_4$ cluster expands by 0.16Å upon reduction, and the S...HN hydrogen bond lengths shorten by 0.1-0.2Å[243,325]. The magnitude of the S...HN shift might be expected to be greater in azurin because the additional electron is confined to one metal centre rather than being distributed over four metal centres as in HiPIP. That it is not could be due to chemical or structural differences between the two redox centres, although it should also be remembered that the changes concerned are small.

Another unexpected structural change upon reduction occurs in the polypeptide loop preceding Gly-45. Here, some of the main-chain torsion angles (ϕ,ψ) were shown to alter by up to 15° (the r.m.s. deviation for the whole molecule is 8°). Presumably, these changes are related to the increase of ≈0.1Å in the Cu...O 45 distance. If so, then these changes could be viewed as a re-adjustment of the protein structure after being released from a weak interaction between O 45 and the Cu(II) centre. The shifts in the main-chain torsion angles are very small, and consequently, the magnitude of the interaction between O 45 and Cu(II) can probably not be considered a covalent bond, however weak. Rather the Cu(II)...O 45 interaction is more likely to be electrostatic, since in the oxidised form the +2 charge on the copper is only countered by the -1 charge of the thiolate sulphur of Cys-112. Upon reduction, the charge is effectively neutralised by the reducing electron, and most of the electrostatic interaction between the copper and O 45 is lost.

Finally, small shifts are also observed in the two residues Pro-115 and Gly-116, which form part of the loop between the copper ligands Cys-112 and His-117, and reside on the surface of the protein. The shift is small (≈0.2Å), and like the changes in the loop preceding Gly-45, they are probably a re-adjustment of the protein structure due to the changes at the copper site. In particular, the movements may be related to the increase in the Cu-$N_{\delta 1}$ 117 bond length, because the carbonyl oxygen of Pro-115 makes a van der Waals contact of ≈3Å with the imidazole ring of His-117.

Comparison with plastocyanin

When comparing the structural changes in azurin upon reduction with those in plastocyanin, it should be noted that the structures of reduced plastocyanin are complicated by the presence of two pH-dependent forms of the copper site; one redox "inactive" and the other redox "active". At intermediate pH values, the copper site of plastocyanin is a weighted average of the two pH forms. Consequently, to determine the actual Cu(I) geometry of the redox "active" form, since the crystals could not withstand basic pH conditions, the copper distances were extrapolated from those obtained at intermediate pH values. In the reduced structure of azurin, however, the copper site is not

complicated by the presence of a redox "inactive" form, and hence the "active" Cu(I) geometry can be determined directly.

Some of the changes in the copper geometry of plastocyanin, as determined by extrapolation, are comparable to those found in azurin. Both Cu-N(His) bonds in plastocyanin lengthen by ≈0.05-0.10Å upon reduction, similar to the increases in the corresponding ligands in azurin (≈0.05Å). The copper-sulphur distances on the other hand do not change significantly in plastocyanin, in definite contrast to the ≈0.10Å increase in Cu-S(Cys) and Cu-S(Met) in azurin. Although no comment was made by Guss *et al.*[122], there are also changes to the S...HN hydrogen bond (S_γ 84...N 38) upon reduction. At both pH extremes the S...N distance increases rather than decreases as in azurin. At pH 3.8, the lengthening of the S...HN hydrogen bond (≈0.18Å) can be attributed to the shift in the S_γ 84 atom as the copper site changes from the "active" to the "inactive" form, while the increase in the S...N distance in the pH 7.0 form is smaller at 0.05Å. Although, the S_γ 84...HN 38 hydrogen bond appears to increase upon reduction, an "incipient" S...HN interaction between residues 84 and 87 does decrease in distance upon reduction by ≈0.2-0.4Å in both "active" and "inactive" forms.

5.1.2 The Cu...S_δ 121 distance and EXAFS

One important finding from the crystal structure of reduced azurin is the relationship (or lack of it) between the copper distances determined crystallographically and those from EXAFS experiments. Copper distances determined from EXAFS experiments have identified a possible Cu-S(Met) distance of 2.7Å for reduced azurin[161]. The results from the crystallographic refinement, however, disagree with this distance, and instead, put the Cu-S(Met) distance at ≈3.2Å. Two different attempts at refining the Cu-S(Met) distance to the EXAFS value of ≈2.7Å, saw the distance return to the original value of ≈3.2Å, despite tightly restraining it in both cases. Note that for plastocyanin and oxidised azurin, EXAFS experiments could not determine any value for the Cu-S(Met) distances [160,162,163]. Consequently, in light of the difficulties in determining this distance and the crystallographic evidence, the Cu-S(Met) distance of ≈2.7Å from the EXAFS experiments is incorrect. (It must be noted, however, that the authors only *tentatively* assigned this distance at ≈2.7Å[161].)

Certain conclusions can be drawn from the EXAFS experiments on reduced azurin and the other blue copper proteins. Copper distances to the three strongest binding ligands, the two imidazole nitrogens and the thiolate sulphur, are probably close to the true copper distances as there is good agreement between crystallography and EXAFS. Beyond this

though, especially where weak bonds to the copper are concerned, EXAFS techniques have failed to resolve the correct distance between the copper and ligand. Reasons for this may be 1) the inability of atoms involved in such weak bonds to backscatter sufficiently to be detected, or 2) interference by the atoms of other ligands, especially when these atoms are at a distance from the metal centre similar to that of the weakly bonded ligand. This means that EXAFS experiments can probably provide reasonable metal-ligand distances for the primary coordination sphere, where the ligands are bound tightly to the metal, but for weaker bonds or interactions, the method fails to give reliable results.

EXAFS techniques, however, show promise of being able to detect pH-dependent changes in the copper sites of blue copper proteins. This has already been shown for amicyanin[165] and umecyanin[164] for which crystal structures are not yet available. The copper site of amicyanin appears to undergo a pH-dependent change similar to that seen in plastocyanin, where the Cu(I) geometry changes to NS_2 coordination at low pH, whereas the copper coordination of umecyanin was shown to independent of pH, as for azurin[161].

5.1.3 pH-independent redox activity

As noted previously, one of the most significant differences between azurin and plastocyanin is that the redox activity of plastocyanin is pH-dependent, switching off at low pH, whereas the redox activity for azurin is pH-independent. This raises the question of what structural elements of these proteins lead to the pH-dependence or independence in the redox activity. Although it is not possible give a definitive answer to this yet, some of the differences between the blue copper proteins may help in the understanding this "switching off" behaviour, and eventually lead to designing experiments which could provide an answer.

Of the blue copper sites which to date have been structurally determined at high resolution (plastocyanin, azurin and pseudoazurin), all show the same basic ligand arrangement. Superimposing the main-chain and side-chain atoms of the four residues which make up the copper site (i.e. those corresponding to His-46, Cys-112, His-117 and Met-121 in azurin) gives r.m.s. deviations in the atom positions of 0.44Å between azurin and plastocyanin, 0.49Å between azurin and pseudoazurin and 0.21Å between plastocyanin and pseudoazurin (see Figures 5.1.3.1 - 5.1.3.3). The agreement between these three different copper sites reveals that there are only small differences in the arrangement of the copper ligands, and that the sites are so similar that the copper geometry is probably

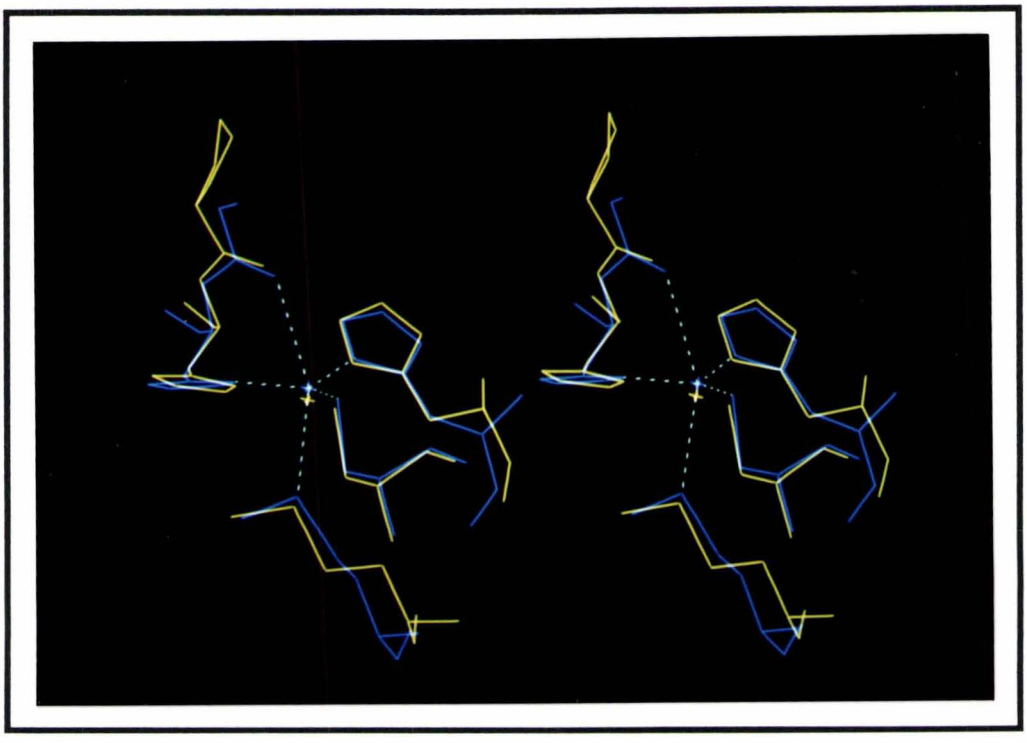

Figure 5.1.3.1. Superposition of the copper sites from azurin (blue) and plastocyanin (yellow).

Figure 5.1.3.2. Superposition of the copper sites from azurin (blue) and pseudoazurin (orange).

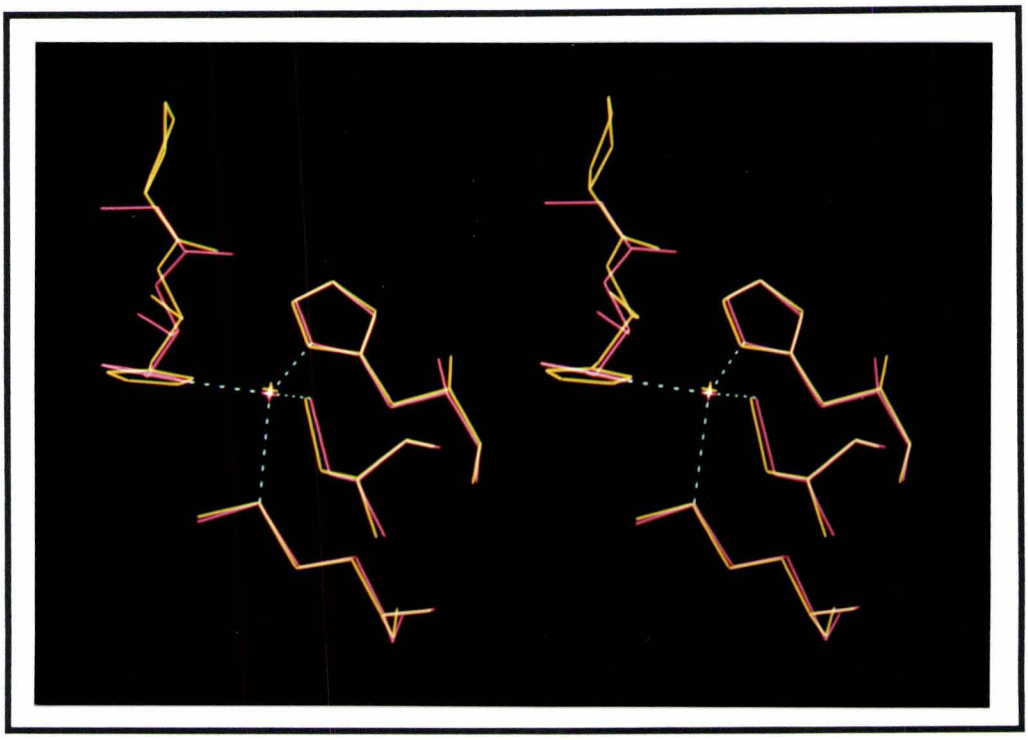

Figure 5.1.3.3. Superposition of the copper sites from pseudoazurin (red) and plastocyanin (yellow).

not responsible for the pH-dependent/independent redox activity. Thus if the redox activity with respect to pH is not determined by the copper geometry the next option is to consider the protein structure surrounding the copper site.

In plastocyanin, the pH-dependence of the redox activity is associated with the protonation and rotation of the copper ligand His-87 (equivalent to His-117 in azurin). Thus the most obvious candidates which may affect the pH-dependence of the redox activity are the residues which flank either side of the imidazole ring of His-87(117) on the surface of the protein. In plastocyanin, these groups are Leu-12 and Pro-86, and pack around the copper ligand rather loosely (contacts of 3.9-4.1Å and 4.5-4.9Å, respectively). The corresponding residues in azurin, Met-13 and Phe-114, make much shorter contacts of ≈3.6Å and ≈3.3Å, respectively, and this results in a tighter constraint on His-117, which may not allow rotation and protonation of the ring. These differences between azurin and plastocyanin, may explain the pH-dependence of the redox activity in plastocyanin and the lack of such an effect in azurin.

An observation which bears on this question is that in site directed mutagenesis experiments on azurin, the Phe-114→Ala mutant does not show significant pH-dependent redox activity between pH 6.0 and pH 7.0[188]. Removing the phenyl ring which packs against His-117 would be expected to loosen the constraint on this copper ligand if the structure is maintained. However, this mutant was noted to have perturbed

optical and EPR spectra, and to be considerably slower in picking up Cu(II) than the wild type[334], suggesting there has been some rearrangement of the structure.

The only other blue copper protein with confirmed pH-dependent redox activity is amicyanin[165,335-337]. Unfortunately the 3-dimensional structure of amicyanin has not been determined yet, but a comparison of the amino acid sequences shows that the loop between the cysteine and the second histidine is almost identical to those in plastocyanin and pseudoazurin (see Table 5.1.3.1). Furthermore, the following loop is also small, suggesting that these two tight loops in amicyanin may leave the histidine less constrained.

Table 5.1.3.1. Sequence alignments of the main binding loops in plastocyanin, azurin, pseudoazurin and amicyanin.

plastocyanin[10]	84					87							92
poplar	**C**	A	-	P	-	**H**	-	Q	G	A	G		**M**
azurin[10]	112					117							121
Alc. denitrificans	**C**	S	F	P	G	**H**	-	W	-	A	M		**M**
pseudoazurin[37]	78					81							86
Alc. faecalis S-6	**C**	T	-	P	-	**H**	-	Y	A	M	G		**M**
amicyanin[165,337]	93					96							99
Thiobacillus versutus	**C**	T	-	P	-	**H**	P	F	-	-	-		**M**

Consideration of the above loop sequences, together with the 3-dimensional structures of azurin[31], plastocyanin[32] and pseudoazurin[34], further suggests that plastocyanin, pseudoazurin and amicyanin form part of a larger family which is distinct from the azurins. The presence of a proline at the *"n+2"* position following the cysteine prevents the formation of a hydrogen bond directly analogous to the S_γ 112...HN 114 interaction in azurin. However, in both plastocyanin and pseudoazurin there is a weaker interaction involving the *"n+3"* amide (S_γ 84...HN 87=3.83Å in plastocyanin and S_γ 78...HN 81 =3.76Å in pseudoazurin). Similarly, pseudoazurin[34] shows the same rather loose packing around the imidazole ring of His-81 (closest contacts; Met-16 3.8-4.0Å and Pro-80 4.1-4.3Å) as is seen in plastocyanin.

Given these structural relationships it seems likely that amicyanin will show the same looser packing around His-96 as is shown by plastocyanin and pseudoazurin, and that this contributes to the pH-dependence of its redox activity. Further it seems likely that pseudoazurin will show the same pH-dependence, becoming redox inactive at low pH. The answers to these speculations, however, must await careful measurements of the effect of pH on the redox activity of pseudoazurin.

It is also worth noting that the relative strengths of the S...HN hydrogen bonds at the

copper site probably do *not* play a role in the pH-dependence of its redox activity. Although the thiolate sulphur position may be more constrained in azurin as compared to plastocyanin (two strong interactions versus one strong interaction) and thereby preventing the formation of the redox "inactive" form, the shift in the position of S_γ between the redox "active and "inactive" forms of plastocyanin is less than 0.1Å[122]; a movement too small to be prevented by an extra S...HN interaction.

5.2 Conclusions from the structure of apo-azurin

5.2.1 Structural changes upon copper removal

The basic configuration of the copper ligands is maintained after the removal of the copper atom. Although the copper binding site is very similar to the oxidised and reduced sites of azurin, there are small changes which are consistent between the two independent molecules of the asymmetric unit. The largest structural change occurs at the side-chain of Cys-112, where the S_γ 112 atom moves towards the space vacated by the copper atom. This shift results in a lengthening and presumed weakening of the S...HN hydrogen bonds made to the polypeptide chain. Also associated with the shift in S_γ 112 is the formation of two weak bifurcated SH...N hydrogen bonds between the SH group of Cys-112 and the $N_{\delta 1}$ atoms of His-46 and His-117. The contraction of the distances between the copper ligands, His-46, Cys-112 and His-117, is primarily due to the shifts in side-chain atoms of Cys-112.

Other changes at the copper binding site are smaller, and were identified by searching for the consistent shifts between the two independent molecules of the asymmetric unit. The carbonyl oxygen of Gly-45 moves away from the space vacated by the copper atom, with a resulting small increase in the O 45...S_δ 121 distance. Also observed are subtle changes in the main-chain structure of the α-turn preceding Gly-45, which cause slight changes in the geometries of the hydrogen bonds made at O 40. A possible implication of the small increase in the O 45...S_δ 121 distance and the changes at the α-turn are that the carbonyl oxygen of Gly-45 does interact, albeit weakly, with the Cu(II) centre in oxidised azurin. Since shifts similar to this occur upon reduction of oxidised azurin, it seems likely that some form of a weak electrostatic interaction between the Cu(II) centre and O 45 exists. Furthermore, in apo-azurin the orientation of Gly-45 is more like that of reduced azurin than oxidised azurin. This is the only part of the apo-azurin structure which is more like the reduced form than the oxidised form and fits with the suggestion of a weak electrostatic interaction between Cu(II) and O 45. Removal of the Cu(II) ion would remove a net +1 charge from the active site, just as occurs in the reduction of azurin. Figure 5.2.1.1 illustrates the differences at Gly-45 between apo, oxidised and reduced azurins.

The overall structure of apo-azurin shows greater similarity to the oxidised structure than to the reduced structure. This is also the case for the copper binding site, as is most clearly shown in the conformation of the side-chain of Cys-112 and in the S...HN hydrogen bond distances. In fact, a trend is apparent in the geometry of the side-chain of

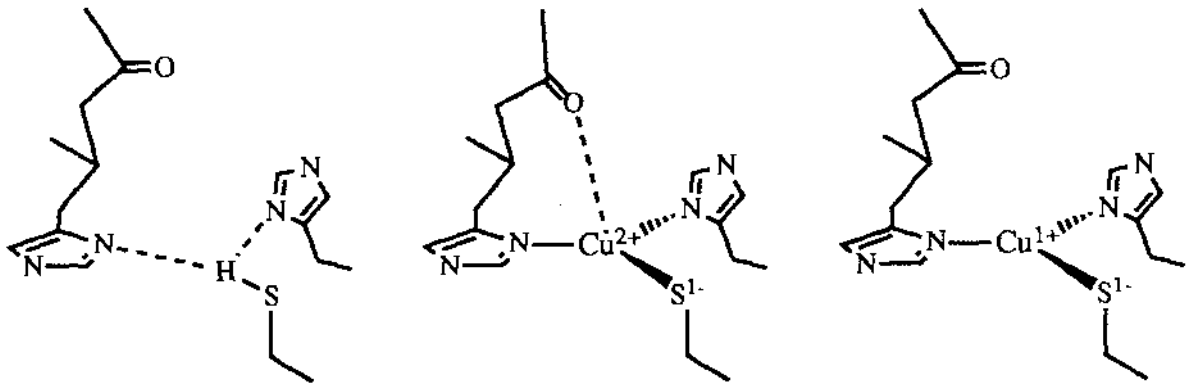

Figure 5.2.1.1. Schematic diagram illustrating the changes in Gly-45 with respect to the protein form. Met-121 has been omitted for clarity.

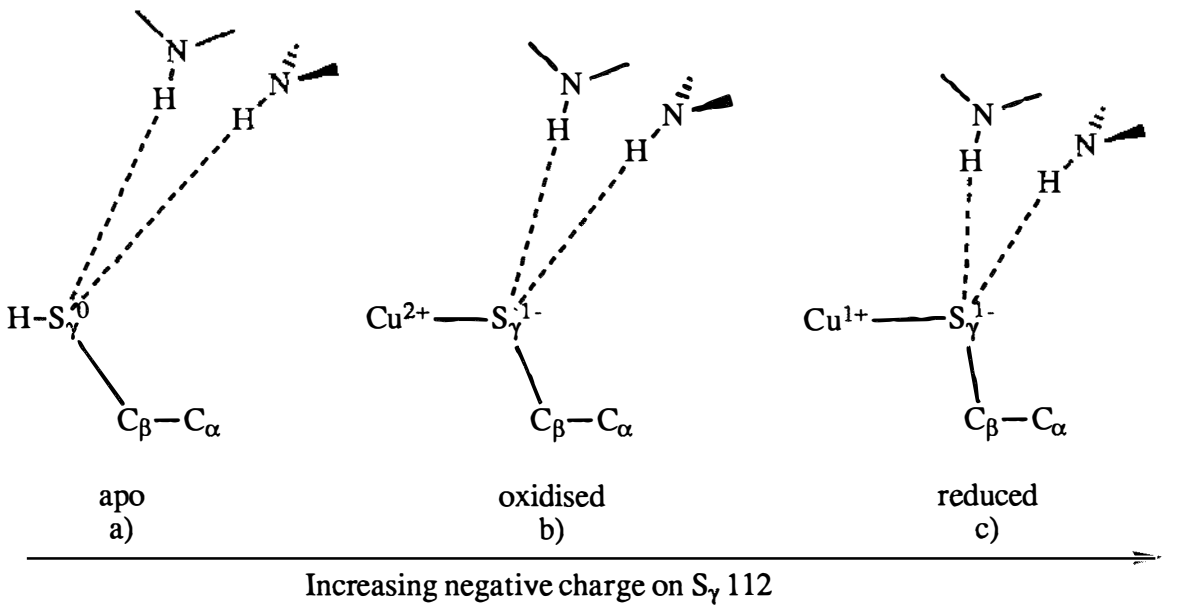

Figure 5.2.1.2. Schematic diagram illustrating the trend of increasing electronic charge on the S_γ 112 atom between the apo, oxidised and reduced forms of azurin.

Cys-112, relating the hydrogen bond lengths and the position of the sulphur atom to the charge density on S_γ 112. In the apo form there is no charge on S_γ 112 because the side-chain is protonated (see Figure 5.2.1.2a), and this results in only a weak interaction with the amide nitrogens of residues 47 and 114. With the incorporation of the copper, S_γ 112 becomes deprotonated, giving it a formal charge of -1. This negative charge, however, is reduced by the formal +2 charge on the Cu(II) ion, but still results in stronger hydrogen bonding interactions between the S_γ 112 atom and the amide nitrogens

(see Figure 5.2.1.2b). In the reduced state, the formal charge of -1 on S_γ 112 is less reduced than in oxidised azurin, because of the lower formal charge on the Cu(I) ion, and the S...HN hydrogen bonding interactions are further strengthened (see Figure 5.2.1.2c).

Finally, an increase in the thermal parameters of the polypeptide loop between residues 117 and 121 upon the removal of the copper atom suggests that this loop, which is on the surface of the protein, becomes more flexible. This indicates that although the copper atom does not influence the configuration of the protein structure, it does tighten this part of the structure. The flexibility of the 117-121 loop may account for the decrease in the thermal stability of apo-azurin compared to most other metallated forms of the protein. The first of two melting transitions in the differential calorimetric scans of apo-azurin was tentatively assigned by Engeseth and McMillin[204] to an unfolding of the "flap" region in azurin. However, this transition may be better assigned to the 117-121 loop, since it is actually bound to the copper atom, whereas the "flap" region is not.

5.2.2 Rate of copper removal

Despite the rigorous conditions required to remove the copper ion from crystals of oxidised azurin (several months in cyanide solutions), only a slow rate of copper loss is observed. The reasons for this are obvious when the crystal packing for azurin is considered. With the two molecules packing via their hydrophobic patches, virtually all of the solvent is excluded from the most direct route to the copper atom, i.e. through the side-chain of His-117 (see Figure 5.2.3.1). This contrasts with plastocyanin where the corresponding region in the crystal structure[191] is exposed to a solvent channel, and would be directly accessible by chelating agents. This probably explains 1) why the copper atom in plastocyanin can be completely removed from crystals within a matter of hours[191], and 2) the difficulty experienced in completely removing copper from azurin, indicated by the presence of residual electron density at the center of the copper binding site (as much as 20% copper). In solution, however, there may be little difference in the rate of copper removal, as the copper is removed from azurin solutions within 12 hours.

5.2.3 Mechanism for copper incorporation

Copper binding to apo-plastocyanin has been proposed to occur via a "revolving door" mechanism. This suggests that the copper enters the active site in a two step mechanism, where it first binds to the imidazole ring of His-87, on the surface of the protein, and then the ring and its bound copper rotate to allow the copper to bind to the other ligands. Two step mechanisms consisting of a fast complexation step and a slow rearrangement have

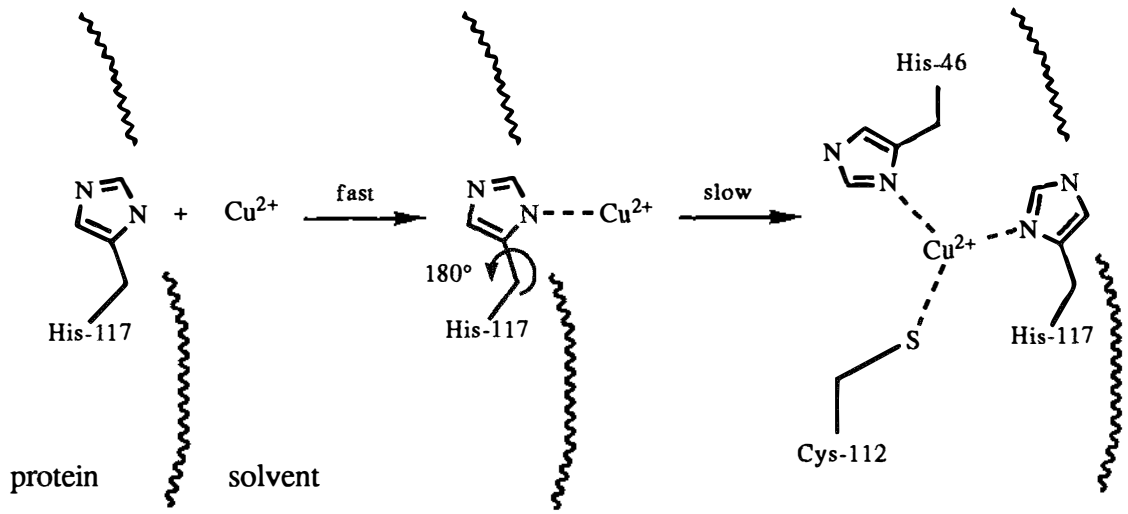

Figure 5.2.3.1. Schematic diagram of the proposed "revolving door" mechanism of apo-plastocyanin for incorporation of the copper into the active site as applied to azurin.

been observed in kinetics studies of azurin[201] and stellacyanin[338], and it is possible that the same mechanism applies to these proteins also. However, an interesting aspect of the "revolving door" mechanism is that the side-chain of His-117 in azurin is more tightly sandwiched than the side-chain of His-87 in plastocyanin. It then follows from this mechanism, that the second slow rearrangement step should be slower in azurin than in plastocyanin, and this should be reflected in the kinetics of copper uptake. Unfortunately, there have been no reports in the literature on the kinetics of the uptake of copper by plastocyanin to compare with those on azurin[201,202] to verify this mechanism.

5.3 Implications for Biological Function

The structures of apo and reduced azurins have several implications for its biological function and for the function of proteins generally. In particular, the structures provide evidence for the theoretical concept of the entatic state, by which a protein is designed to optimise its activity. The concept of the entatic state is introduced below, and the implications of this concept are discussed in relation to the structure and function of azurin.

The Entatic State

In 1968 Vallee and Williams introduced the concept of the *entatic state* to explain aspects of the catalytic behaviour of certain enzymes[208]. In essence, the concept considers that the reactivity of the enzyme is the result of the active parts of the protein containing "atypical" chemical or structural character as compared to simple small molecules or catalytically "inert" regions of the protein. These "atypical" regions are described as structural and/or electronic abnormalities which are intimately associated with the catalytic activity of the enzyme, making it a better catalyst.

In enzyme catalysis, the enhancement of the reaction rate is attributed to stabilisation of the transition state, which reduces the activation energy, and thereby makes it easier for the transition state to be reached by the reactants (see Figure 5.3.1)[339]. The idea of transition state stabilisation asserts that the catalytic action arises from the enzyme binding the transition state of the substrate more strongly than its ground state (see Kraut[339] for a recent discussion of this and references therein). This is the fundemental concept behind rack-type mechanisms whereby the enzyme forces the substrate into a conformation resembling the transition state. A good example of this is lysozyme, where the saccharide is forced into the "half chair" conformation as opposed to the ground state "chair" conformation[340].

The idea of the entatic state, however, differs from this by going a step futher. It is proposed that a region of a protein is "energised" or "activated" relative to the ground state of a catalyst or simple molecule, so that the reaction starts at a *ground* state which is *closer* to the transition state, thus reducing the activation energy even further in a manner somewhat different from simple stabilisation of the transition state (see Figure 5.3.2)[341-343].

Since the entatic region is an "activated" part of the protein, it is thus a property of the

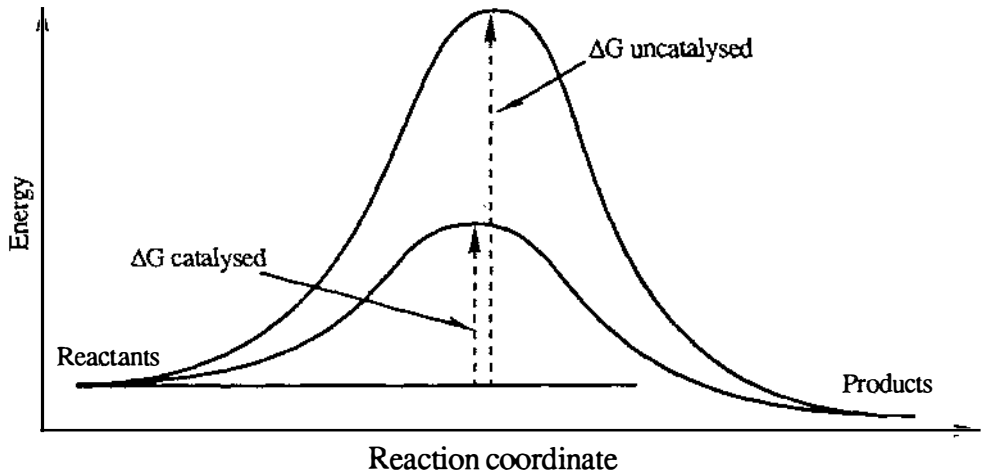

Figure 5.3.1. The potential energy diagram for a "normal" reaction, and the lowering of its transition state energy in an catalysed reaction.

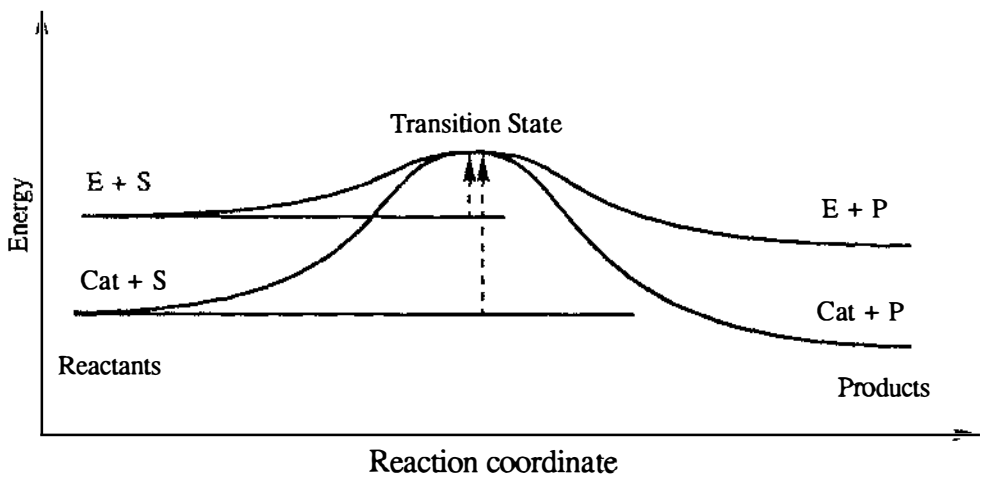

Figure 5.3.2. Potential energy diagram showing how the entatic region of a protein is "activated" or "energised" relative to a catalyst, leading to a lower activation energy. E=entatic protein or enzyme, Cat=catalyst, S=substrate and P=products.

protein, and should be present in the absence of any substrate. Therefore, if a substrate molecule enters the entatic region, it comes under attack by "activated" groups resulting in a small activation energy. Note, however, that the entatic state is not the only source of catalytic activity, although it may provide an important component to catalysis. Furthermore, the concept of an entatic state does not give any information about the role the substrate plays in complexing to the enzyme or lowering the activation energy.

As such, Vallee and Williams defined the entatic state as a site which is "poised for catalytic action in the absence of a substrate"[208]. This is not to be confused with the rack-type mechanisms, where the protein molecule applies a strain on to the substrate as a means of catalyzing the reaction[341]. The question remains, however, as to how enzymes generate such "activated" or "poised" regions? The "activation" of the entatic region of the

protein is attributed to the protein as a whole, such that in order to minimise the free energy of the whole protein (in its most stable conformation) some regions adopt unusual conditions relative to simple molecules. For example, this may occur in the creation of a hydrophobic pocket in the protein, which is a high energy region for the solvent (presumably water). In other words, the free energy of the protein molecule as a whole is at a minimum, but some parts of the protein fold into conformations which are "activated" or less favourable to achieve this minimum free energy[208,341-343]. A yet fuller definition of the entatic state given by Vallee and Williams[208] is:

"...a state of entasis: the existence in the enzyme of an area with energy closer to that of a unimolecular transition state than to that of a conventional, stable molecule, thereby constituting an energetically poised domain.""

The difference between such an enzyme and simple molecules which act as models, is that these conventional molecules do not have the geometry of the transition state of the chemical reaction. Instead, they are relaxed into conventional stable geometries and electronic configurations. Such differences might also reflect the different constraints on the active centre, such that in the enzyme this may occur as a specific type of tertiary structure. For example, the constraints of the protein may provide an unusual disposition of metal ligands, thereby forcing an irregular geometry on to a metal centre. Thus the metal and its ligands (the protein) generate the entatic state jointly. Note that the term "rack-induced bonding" [129,207] applies equally as well to this type of situation.

In electron transfer, the exchange of an electron between two redox sites results in a subsequent change in the electronic charge on both centres. This would be expected to cause a re-arrangement of the bond lengths and and angles of both redox centres so that the geometry of the system conforms to the new oxidation state. Thus an entatic region which is well suited for electron transfer should then be a redox centre in which the bond lengths and angles provide a ground state which is a compromise between the two oxidation state preferences, and is thus closer to the transition state[341].

For a metal centre such as iron, in the low spin state, this only involves forming a metal site which has Fe-ligand bond lengths between those typically found for Fe(II) and Fe(III) complexes, since the preferred geometry of both oxidation states is the same (octahedral). Consequently, the activation energy can be lowered by developing a ground state iron complex which has Fe-ligand bond lengths between the values for the Fe(II) and Fe(III).

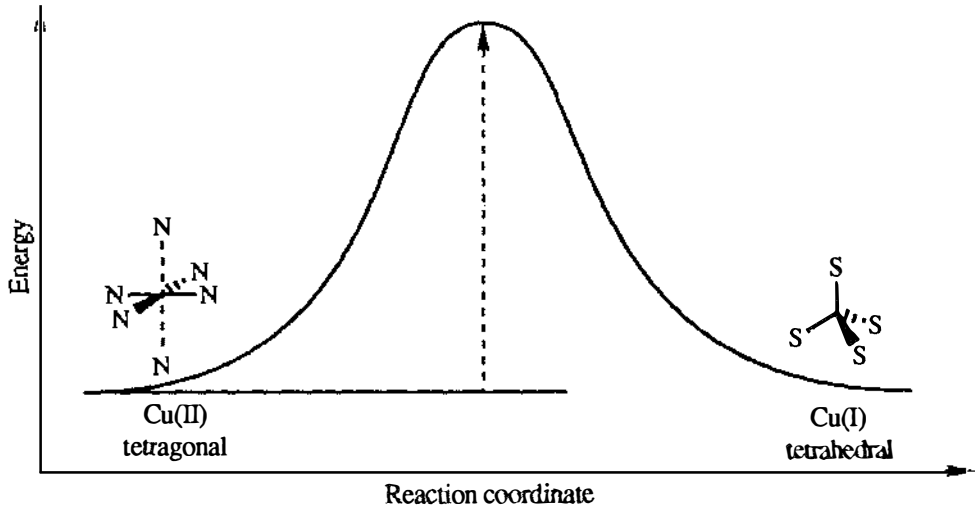

Figure 5.3.3. Potential energy diagram for the oxidation-reduction process of a copper system which heeds the coordination preferences between Cu(I) and Cu(II) centres.

For a system which uses copper as its redox centre, such as azurin, the differences in the coordination preferences between Cu(I) and Cu(II) are much greater than those for Fe(II) and Fe(III). Where Cu(I) centres prefer tetrahedral geometry (4-coordinate) with "soft" Lewis base donors (e.g. sulphur ligands), Cu(II) centres prefer tetragonal geometry (6-coordinate) with "moderate" Lewis base donors (e.g. nitrogen ligands). This large difference in oxidation state preferences would be expected to create a particularly large activation energy barrier for electron transfer (see Figure 5.3.3) because in order to satisfy the preferences of both oxidation states, the system must 1) alter the coordination number by two (either bond formation or bond cleavage), 2) change the ligand type, and 3) drastically alter the metal geometry. The final result is a system, if it conforms to these preferences, which can only transfer electrons slowly.

In the redox system of azurin, however, the copper site only undergoes *minimal* changes ($\leq$0.2Å) in its structure. This was clearly shown in the comparison of the structures of oxidised and reduced azurins (Section 3.2). Such minimal changes upon reduction are consistent with the fast elctron transfer ability of azurin, and imply that the active site of azurin is specifically designed for this function.

An inspection of the active site of azurin shows that the copper site is in a state of entasis. The copper site can be viewed as a compromise of Cu(I) and Cu(II) oxidation state preferences in the following ways: 1) The coordination number of the copper centre is between 3 and 5, depending on the extent to which the apical groups are considered to interact or coordinate with the metal. 2) A mixture of aromatic nitrogen and sulphur ligands provides a combination of soft and moderate Lewis base donors. 3) A

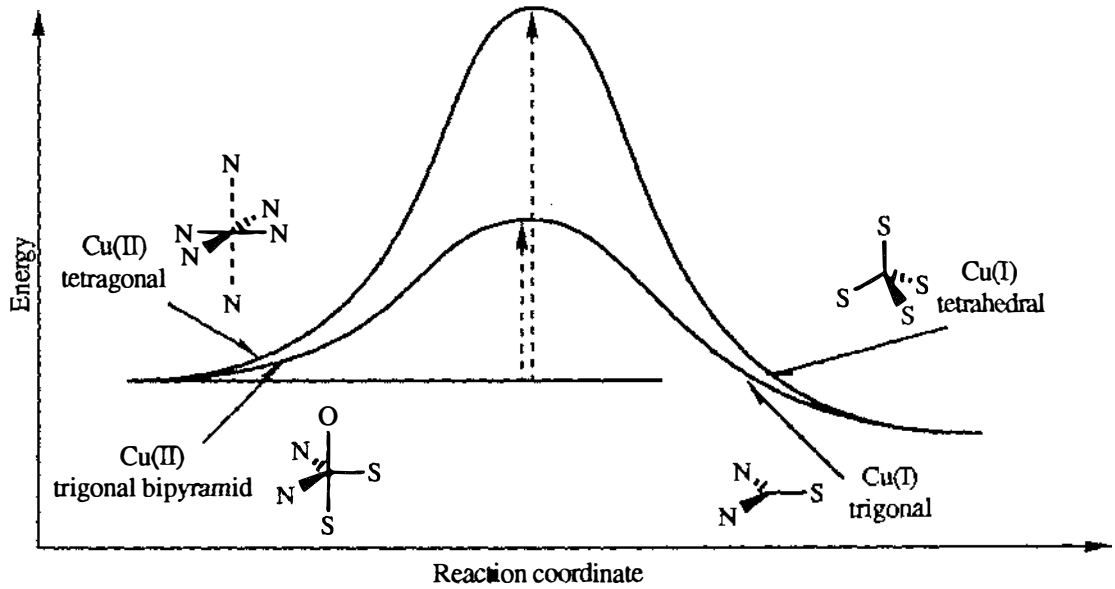

Figure 5.3.4. Potential energy diagram showing the reduction in the activation energy when changing the redox system from tetragonal-tetrahedral to trigonal bipyramid-trigonal with mixed sulphur and nitrogen ligands.

compromise in the copper geometry is apparent, not between tetragonal and tetrahedral, but between the less frequently observed geometries of trigonal bipyramid (Cu(II)) and trigonal (Cu(I)). Thus a copper redox centre which contains a mixture of nitrogen and sulphur ligands, and forms into a trigonal bipyramidal geometry for Cu(II) and trigonal geometry for Cu(I), effectively lowers the energy level of the transition state as compared to the tetragonal-tetrahedral system. With these two geometries in use, the only barrier to electron transfer is the cleavage (or formation) of two copper-ligand bonds, since the bond angles and ligand types remain the same. In other words, such a system is a better catalyst for the process of electron transfer than the tetragonal-tetrahedral copper system (see Figure 5.3.4).

However, the copper distances to the apical groups in azurin are not those of strong bonds. Instead these groups interact with the copper at a much weaker level, where the Cu...S(Met) and the Cu...O(Gly) distances may be considered a weak bond and a weak electrostatic attraction, respectively, at best. Thus the copper site of azurin employs a copper geometry which is basically trigonal with weak to marginal apical interactions, and can be viewed as an "activated" or "energised" state of a trigonal bipyramidal (or trigonal) geometry, as is postulated for the entatic state. Thus by utilising these characteristics of copper coordination chemistry, the active site of azurin reduces the activation energy by *raising* the *ground* state of the redox centre (see Figure 5.3.5). In other words, the copper site of azurin is very close to the transition state between the trigonal bipyramid of Cu(II) and the trigonal of Cu(I). It is effectively in a state of entasis, reducing the activation

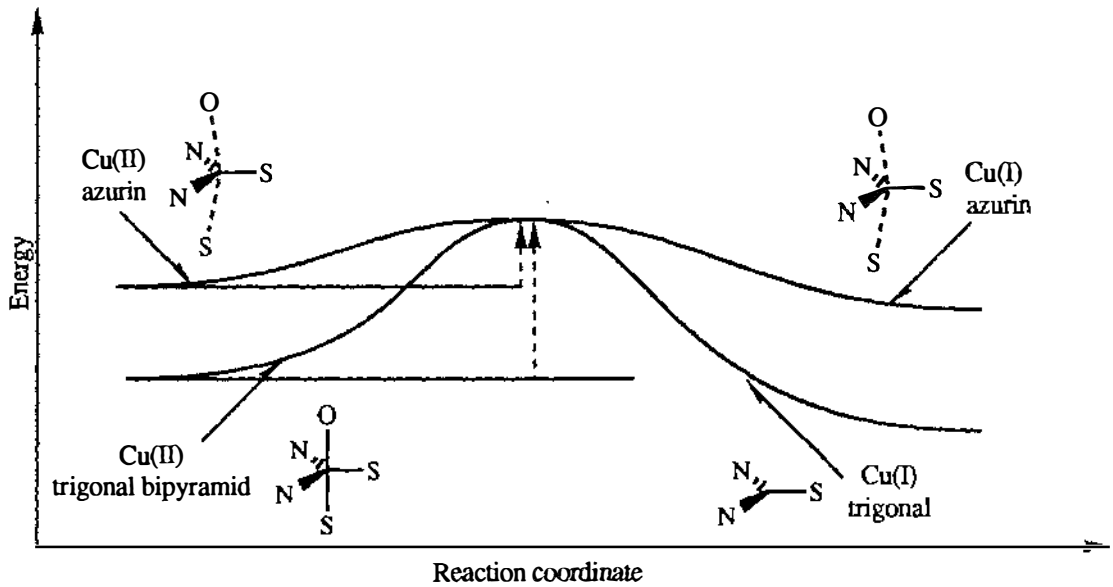

Figure 5.3.5. Potential energy diagram of the reaction coordinates of the electron transfer process of the trigonal bipyramidal-trigonal redox system and that of azurin which is "activated" towards the transition state.

energy for electron transfer and giving a functional advantage to the protein.

The structure of apo-azurin shows that the configuration of the copper ligands is essentially identical to that of the oxidised and reduced forms of the protein. This implies that the protein conformation determines the geometry of the copper site of azurin, forcing the copper to accept a ground state geometry which is like the transition state for the electron transfer reaction. Thus, the active site is a consequence of "rack-induced bonding" [129,207], where the distorted geometry of the copper is the result of a "rack" mechanism (note that the copper atom is not the substrate, rather the substrate is the electron). The protein does this through a network of hydrogen bonds and packing effects which orient the copper ligands into position. The only effect on the protein which is induced by the binding of the copper is a tightening of the polypeptide loop from His-117 to Met-121, containing two of the copper ligands.

Finally, the structure of apo-azurin shows that the overall folding of the polypeptide chain is a stable configuration. This is in accord with the concept that the protein molecule as a whole is at minimum free energy. It should be noted that no part of apo-azurin contains strained geometry, but that the entatic region of the protein is generated by the metal and the protein jointly.

Tuning of the redox potential

The blue copper proteins as a family show a diverse range of redox potentials, from +184mV through to +680mV. Even among the different strains of the same protein, the redox potential can vary; for example, for azurins E° ranges from 230mV to 308mV[82]. As the protein imposes a distorted geometry on to the copper centre, it also tunes the redox potential of the active site to the required value for electron transfer with its physiological redox partner.

The redox potential is determined by three factors. The first two are associated with the copper site; 1) the copper geometry and 2) the nature of the copper ligands. These two factors probably explain the consistently higher E° values in plastocyanins (340-370mV[10]) as compared to the azurins (230-308mV[82]), since the copper geometry in plastocyanin is more tetrahedral, a geometry preferred by Cu(I). The approach of the carbonyl oxygen to the copper centre in azurin would also lower the E° relative to plastocyanin.

Since the structure of the copper site of *Ps. aeruginosa* azurin[41] is virtually identical to that of *Alc. denitrificans* azurin[31], the variation in the redox potential must also be controlled by other factors beyond the copper site. Electrostatic contributions from the surrounding environment contribute to the value of E°, and site directed mutagenesis studies show that single amino acid changes can alter the E° by as much as 70mV[98,155,156,188,189]. The exent of the effect is dependent on the distance between the residue and the copper centre, so that a charged residue far from the active site will have only a small contribution to E°, while a residue closer will have a larger contribution. It should also be noted that the copper binding site of apo-azurin is structurally more similar to the copper site of oxidised azurin than reduced azurin. This suggests that the high E° value, relative to the copper-aquo complex, is not a result of a structural preference for Cu(I) over Cu(II) by the protein.

Models for the association complex of the electron self-exchange reaction

The crystal packing arrangement of azurin provides a model for the association complex of two azurin molecules during the electron self-exchange reaction. The two independent molecules of the asymmetric unit are arranged in the unit cell with their hydrophobic patches facing each other, and the copper atoms making a closest approach to each other of ≈14Å. As has been confirmed by site directed mutagenesis studies, this hydrophobic patch is the main candidate for the site of electron transfer in the electron self-exchange

reaction[189]. Using the hydrophobic patch as the site of electron transfer has other advantages as well as the bringing of the copper sites as close together as possible, since it provides a secure intermolecular environment free from charged residues which might perturb the medium through which the electron must travel or prevent the formation of the association complex.

At the centre of each hydrophobic patch in azurin is the side-chain of the copper ligand His-117. In the crystal packing arrangement, the side-chains of the His-117 residues of the two molecules oppose each other, separated by a gap of ≈6.5Å. This gap could accommodate a water molecule except that there are no potential hydrogen bonding partners directed towards it (see Figure 5.3.6). The distance between the side-chains of the two histidines is suitable for a "through-space" electron transfer mechanism[344-346] according to Marcus theory[347]. This explains the fast electron transfer rate observed, and also accounts for the discrepancy between the electron transfer rate and the large separation distance of the two copper atoms. Thus it appears that the protein extends the electron transfer molecular orbital on the copper atom through the conjugated imidazole ring, so extending the reach of the redox site by 3-4Å. Furthermore, the orientation of the two imidazole rings is approximately coplanar (an angle of 26-36° between the mean planes of the imidazole rings), which is favourable for optimising the overlap between the molecular orbitals of the two groups.

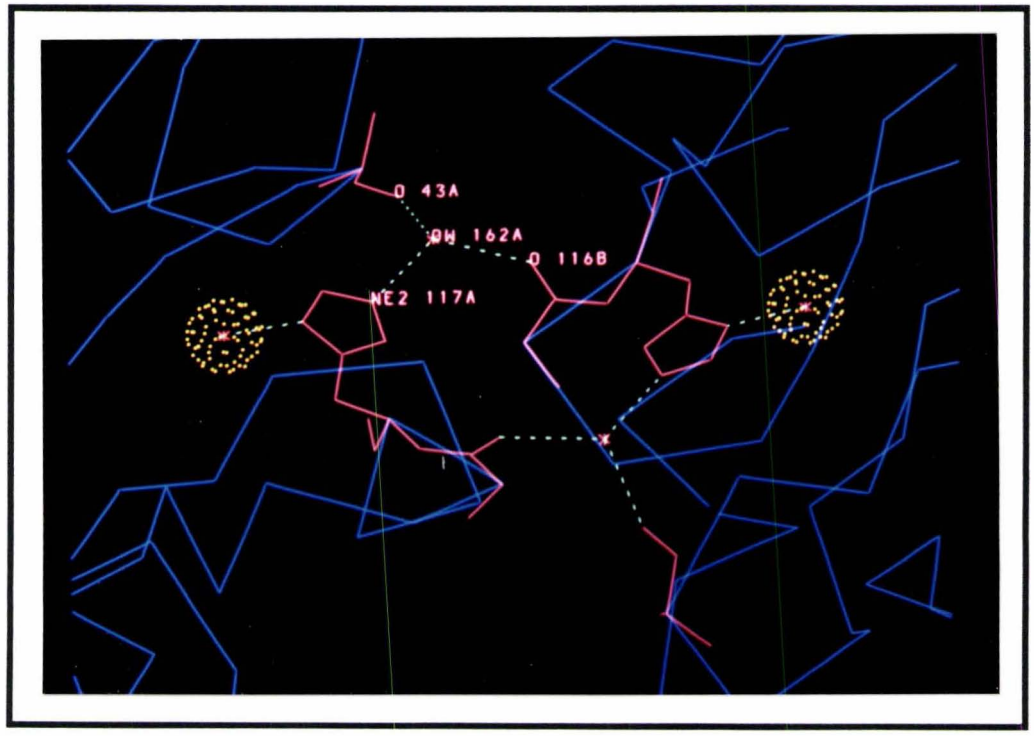

Figure 5.3.6. View of the gap between the two opposing His-117 imidazole rings at the interface between the two hydrophobic patches. Copper atoms in yellow, C_α trace in blue and selected atoms in pink.

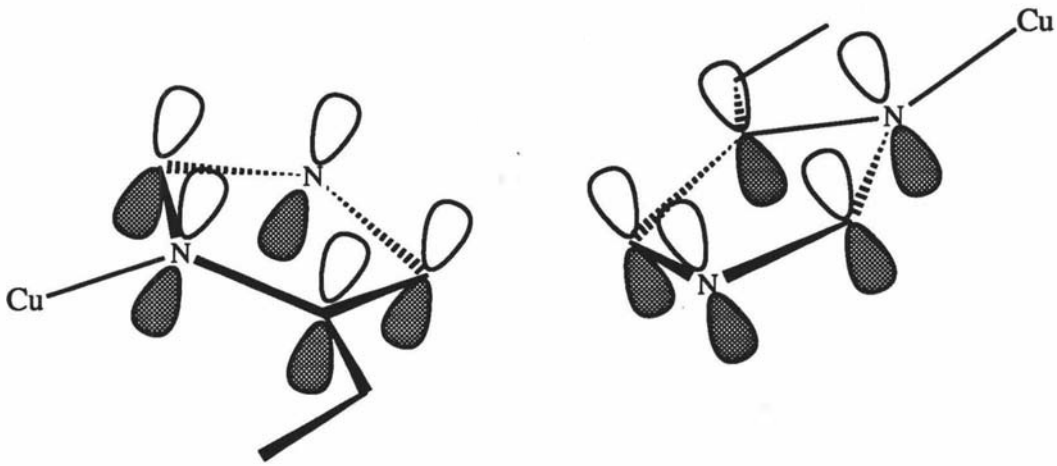

Figure 5.3.7. Orientation of the atomic orbitals of the His-117 side-chain in *Alc. denitrificans* azurin, where the π molecular orbitals are nearly coplanar to provide "maximum" overlap for electron transfer.

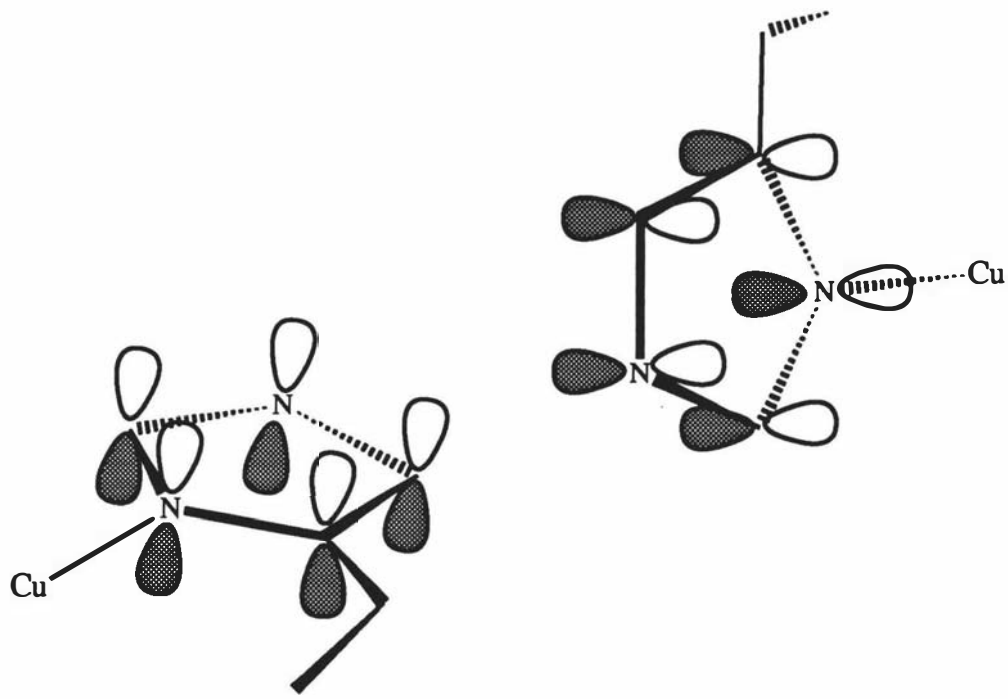

Figure 5.3.8. Orientation of the atomic orbitals of His-117 in *Ps. aeruginosa* azurin, where the π molecular orbitals are set perpendicular to one another, thus minimising the overlap for electron transfer.

A similar model for the association complex between two azurin molecules has been proposed from the crystal structure of azurin from *Ps. aeruginosa*[155]. Although the crystal packing arrangement of *Ps. aeruginosa* azurin is not quite the same as that in *Alc. denitrificans* azurin crystals, in both cases there are intermolecular contacts between two protein molecules at their hydrophobic patches. The distance of 6.6Å between the imidazole rings of the two His-117 residues for *Ps. aeruginosa* azurin still agrees with

the theoretical distance from Marcus theory[347]. However, the molecules are differently oriented, so that the two imidazole rings of His-117 in *Ps. aeruginosa* crystals are almost perpendicular to each other (the dihedral angle being 80-85°), very different from the near coplanar arrangement seen in *Alc. denitrificans* azurin (see Figures 5.3.7 and 5.3.8). Presumably, this difference between the two packing arrangements is a result of the differences in the crystal packing between these two proteins (in turn caused by differences in structure and sequence), and simply reflects the rather non-specific nature of the interactions between the hydrophobic surfaces.

The near perpendicular orientation of the imidazole rings in *Ps. aeruginosa* azurin is not conducive for a "through-space" electron transfer mechanism, because this orientation minimises the orbital overlap between these groups, hindering electron transfer (see Figure 5.3.8). Instead, the orbitals in the *Alc. denitrificans* model are better orientated to provide the overlap necessary for electron transfer (see Figure 5.3.7). The gap or cavity between the two *Ps. aeruginosa* azurin molecules, however, is filled by two solvent molecules, presumably water. Two such solvent molecules are also found buried between the hydrophobic patches, bound to His-117, in *Alc. denitrificans* azurin, but here the solvent molecules do not lie in the direct path between the two imidazole rings. These two solvent molecules in *Ps. aeruginosa* azurin bridge the gap between the imidazole rings through a set of three hydrogen bonds ($N_{\varepsilon 2}$ 117...OW...OW...$N_{\varepsilon 2}$ 117, see Figure 5.3.9)[155]. This means that although the *Ps. aeruginosa* model is not suitable for a through-space electron transfer mechanism, it is conducive for a "through-bond" electron transfer mechanism[155,348,349].

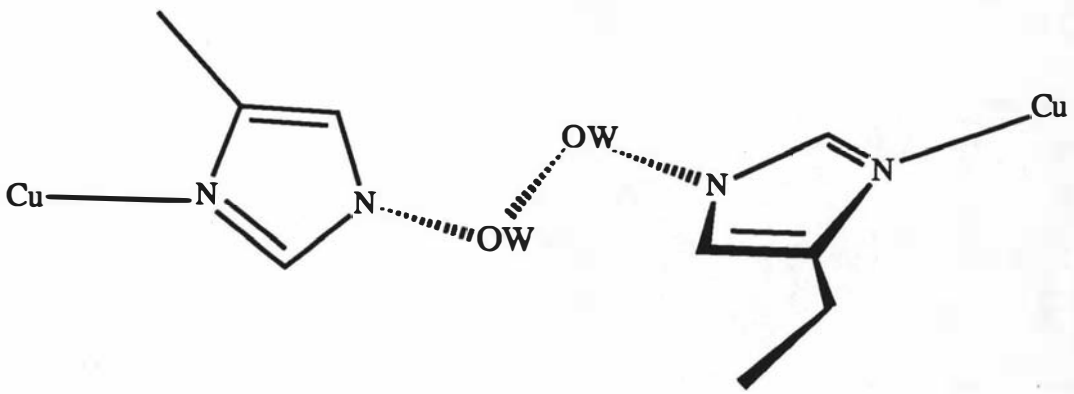

Figure 5.3.9. Orientation of the two solvent molecules bound to the side-chains of His-117 in *Ps. aeruginosa* azurin, allowing electron transfer to proceed via a "through-bond" mechanism..

Although the "through-bond" mechanism for electron transfer normally applies to covalent bonds, the mechanism still applies to hydrogen bonds. This is because electron transfer through a hydrogen bond is similar to electron transfer through two OH covalent bonds where one bond is slightly longer than the other[344]. Compared to a "through-

space" mechanism, a "through-bond" mechanism is considered to be more efficient for electron transfer, but the zig-zag nature of the pathway in the "through-bond" mechanism creates a longer distance between azurin molecules than in the "through-space" mechanism. Consequently, the rates of electron transfer are expected to be roughly equal between the two models.

With two models for the ESE association complex equally valid, it is apparent that instead of only one structural model for the ESE reaction, there are many, where the two azurin molecules are shifted and rotated with respect to each other. In particular, the through hydrogen bond mechanism, overcomes the problem of a poor orientation between the imidazole rings, and suggests that either "through-space" or "through-bond" mechanisms can be employed to transfer the electron, depending on the orientation of the two protein and two solvent molecules. Finally, it is also interesting to note that NMR studies have shown that this particular solvent molecule can be detected in the spectra, indicating that it is a conserved feature in solution[333].

5.4 Future directions for research on azurin

With the cloning of the gene for *Alc. denitrificans* azurin there is now an opportunity to further investigate the relationships between structure and function through site directed mutagenesis[179]. Mutants of azurin can be made and characterised, with the intention of determining their crystal structures to investigate their properties compared to the native molecule. Other directions for future research should also include X-ray crystal structure analyses of metal substituted azurins, as well as analyses of minor variations of the apo, oxidised and reduced forms of azurin.

5.4.1 Suggestions for site directed mutants

Site directed mutagenesis studies have already been initiated for *Ps. aeruginosa* azurin (see Section 1.2.8). Several of the mutants from these studies have contributed answers to some long-standing questions. Mutations such as Met-121→Leu[98], have shown that the second sulphur is not essential for the spectral properties characteristic of the blue copper proteins, while mutating Met-44→Lys[189] has given direct evidence for the hydrophobic patch as the site of electron transfer in the electron self-exchange reaction.

Creating a pH-dependent copper site of azurin

Many other possibilities exist for site directed mutagenesis experiments, which may provide more information on the origin of the structural basis of the properties of azurin and other blue copper proteins. One aspect worth probing is to attempt to create mutants which will change the copper site of azurin from pH-independent to pH-dependent, and thus determine which parts of the protein are responsible for this difference in azurin and plastocyanin. The first suggestion is to mutate the two side-chain residues (Met-13 and Phe-114) which tightly sandwich the copper ligand His-117, to smaller side-chain groups such as alanine. This will test whether the restraints on this ligand prevent the imidazole ring from undergoing the rotation seen in inactive plastocyanin. The Phe-114→Ala mutation has already been made[188], and preliminary results show a pH-independent redox activity between pH 6-7, but this pH range is probably to narrow to be conclusive, and further investigations are needed to establish the effects of this mutation. A Met-13→Ala mutation would test the constraint on His-117 as above. Since the residue is also semi-conserved as Leu in plastocyanin, and Met in pseudoazurin, however, removing this bulky side-chain would probe the overall role this residue plays in orienting His-117. The double mutant Met-13→Ala, Phe-114→Ala, could also be made. Crystal structures of these mutants would be required, however, to determine the extent to which

the restraints on the His-117 side-chain are loosened.

Another possible strategy for creating a pH-dependent azurin mutant would be to replace either or both of the two loops which provide the copper ligands in azurin, with those in plastocyanin and amicyanin. Since these are the only two blue copper proteins known to "switch off" their redox activity at low pH, this would determine if either of these loops are responsible for this type of redox behavior. This mutation would also shorten the loops, and make the copper more accessible to the solvent.

Redox potential and spectra studies

The determinants of the spectroscopic properties and redox potential of azurin could be investigated by mutating various residues so as to alter the geometry of the copper site. The most obvious of these is to mutate Met-121 into other side-chains to alter the ligand type bound to the metal. In particular, altering Met-121→Gln would place an oxygen in range of the copper. Such a stereochemistry could mimic the copper site in stellacyanin, which has no methionine in its sequence, and the lowest redox potential of the blue copper proteins, and is thought to have an oxygen as a fourth ligand to the copper. Although cassette mutagenesis of Met-121 has been done for *Ps. aeruginosa* azurin[185], it should be remembered that according to ^{113}Cd NMR studies the cadmium site of stellacyanin is slightly more like *Alc. denitrificans* azurin than *Ps. aeruginosa* azurin[143].

The effect of the carbonyl oxygen of Gly-45 on the copper of azurin is unknown. Insertion or deletion of residues in the loop preceding Gly-45 (residues 39-44) may alter the distance to the copper centre. Of special interest would be to insert residues in the α-turn preceding Gly-45 in an effort to move the carbonyl oxygen closer to the copper, and observe the changes in the redox potential and spectra. These experiments may indicate how the Gly-45 oxygen contributes to the properties of azurin.

Other site directed mutagenesis studies could include altering one of the copper ligands to a second cysteine sulphur. This would be of interest because recent EXAFS studies have suggested that the copper denoted Cu_A in the membrane bound protein cytochrome c oxidase[2] and some of the copper atoms in nitrous oxide reductase[350], which has a high redox potential of ≈+700mV, have two thiolate sulphurs[351]. Again careful design is necessary, because the proximity of two cysteine side-chains may cause the formation of an unwanted disulphide bridge.

Finally, replacing the thiolate sulphur of Cys-112 with a selenium atom may highlight

some important chemistry between sulphur and selenium. Also this may point out differences in the metal binding of the active site.

Other targets for site directed mutagenesis

Another suggestion is to create an azurin mutant which has only one S...HN hydrogen bond as in plastocyanin, by making the changes Asn-47→Pro and/or Phe-114→Pro. Of these two, changing Phe-114 may be a simpler option, because the Asn-47 side-chain makes several hydrogen bonds to different parts of the protein. However, both mutants and even a double mutant which blocks off both S...HN hydrogen bonds, should be made to test the proposal that these hydrogen bonds can effect E°. It would be interesting to see if a copper site could be created which has no S...HN hydrogen bonds, or if the structure would rearrange itself to make a S...HN hydrogen bond to a different residue.

Site directed mutagenesis experiments should also be carried out on those residues which are conserved in the blue copper proteins. For example, all of the structures determined to date contain an aryl residue which caps the methionine copper ligand (Tyr-15 in azurin). Changes in this residue would test the extent to which it constrains the copper site and in particular the Cu...S(Met) distance. Suggested mutants to try are Tyr-15→Ala, removing the phenol ring with a small group, or Tyr-15→Trp, replacing the side-chain with a larger group. Other possible experiments should include changing Asn-47 and Ser-113 to non-polar side-chain groups. These two residues, through their side-chains, make hydrogen bonds which link together the two loops containing the copper ligands, and removing the hydrogen bonds here would determine their role in maintaining the configuration of the copper site.

5.4.2 Metal substitution of azurin

Cd(II) azurin

Future experiments on azurin could include crystallographic analyses on other metal substituted forms of the protein. In particular, the three dimensional structure of Cd(II) substituted azurin would be of interest since ^{113}Cd NMR experiments on azurin and stellacyanin show single resonances at nearly identical chemical shifts[143]. Hence, if Cd(II) binds in the active site, a crystallographic analysis of Cd(II) azurin would give some insight into the structure of the blue copper site of stellacyanin which lacks methionine in its amino acid sequence[102]. The fourth ligand of the copper site in stellacyanin has been suggested as either an oxygen from a glutamine[102], and/or a

sulphur from a disulphide bridge[170,174-178]. Work on this is currently underway in our laboratory, and results are awaited with interest.

Hg(II) azurin

Apart from the high binding ability of Hg(II) to apo-azurin, calorimetric scans of the Hg(II) substituted protein as a function of the metal ion/protein ratio show that a species appears at about the 1:2 (metal:protein) molar ratio point prior to the formation of the stoichiometric 1:1 metal substituted protein[204]. An analogous set of scans for Cu(II) azurin also reveals the possibility of intermediate forms at substoichiometric levels of Cu(II)[204]. The shorter retention time of the 1:2 Hg(II) azurin on a Sephadex G-75 column as compared to Cu(II), 1:1 Hg(II) and apo-azurins, which all have the same retention time, suggests that the intermediate species has a higher molecular weight, consistent with the formation of a dimer bridged by a single Hg(II) ion. A structure analysis of this Hg(II) substituted dimer would be of interest because it may provide an insight into the intermediates formed during the incorporation of the metal into the active site. The crystal packing arrangement in azurin crystals suggests that possible binding sites for this Hg(II) dimer may be in the cavities formed between the two hydrophobic patches of two protein molecules. In particular, a possible candidate is the cavity occupied by the solvent water molecule which makes hydrogen bonds to $N_{\varepsilon 2}$ 117, O 43 and O 116' in a near perfect trigonal arrangement. Preparation of this Hg(II) dimer could be attempted by co-crystallizing the apo protein with a half molar equivalent of Hg(II).

5.4.3 Further structural studies on azurin

Reduced azurin

Although the results from the crystallographic analysis of reduced azurin suggest that the copper site does not undergo a pH-dependent conformational change which switches off the redox activity, X-ray crystallographic analysis should also be carried out on this form at high and low pH conditions (≈pH 8 and ≈pH 4). These analyses will determine if the protein structure shows any pH-dependent conformers at the copper site. The low pH study should be below pH 4.5, because NMR experiments[27,28,123,128] suggest that His-35 is protonated below this, rather than at the usual pK_a of imidazole groups. This would also determine whether the pH-dependent change in oxidised *Ps. aeruginosa* azurin, a peptide flip, occurs in *Alc. denitrificans* azurin[41].

Apo-azurin

In the analysis of the structure of apo-azurin described here, the copper was removed from oxidised azurin in the crystalline state. Crystal packing forces, however, may then prevent the protein from relaxing into its preferred conformation. Consequently, it was decided that crystallographic analysis should be carried out on crystals grown from apo-azurin solutions. As mentioned earlier (Section 2.1.3), such crystals have been grown and were found to be isomorphous with the cyanide soaked crystals. The crystallographic analysis of the solution grown apo-azurin crystals is currently underway in our laboratory.

Oxidised azurin

Finally, at high pH (10.5-11.4) small changes the electronic and EPR spectra are observed which suggest that the blue copper site is modified slightly without losing the essential components for a blue copper site[82]. Such small changes in the electronic and EPR spectra have been noticed for other blue copper proteins[86,87,89,90]. The spectral changes are reversible, and identification of the associated structural changes would give a clearer indication of the parts of the protein which influence the characteristic spectra of the blue copper proteins. Many protein crystals, however, can not withstand such high pH values. If oxidised azurin crystals are robust enough to withstand these alkaline conditions (they have withstood several months of soaking in cyanide solutions up to pH 8.5), an analysis of an oxidised azurin crystal structure at high pH could be seriously considered.

Appendix A.1. Ramachandran plot of main-chain torsion angles (ϕ,ψ) for reduced azurin molecule A. Glycine residues indicated as squares.

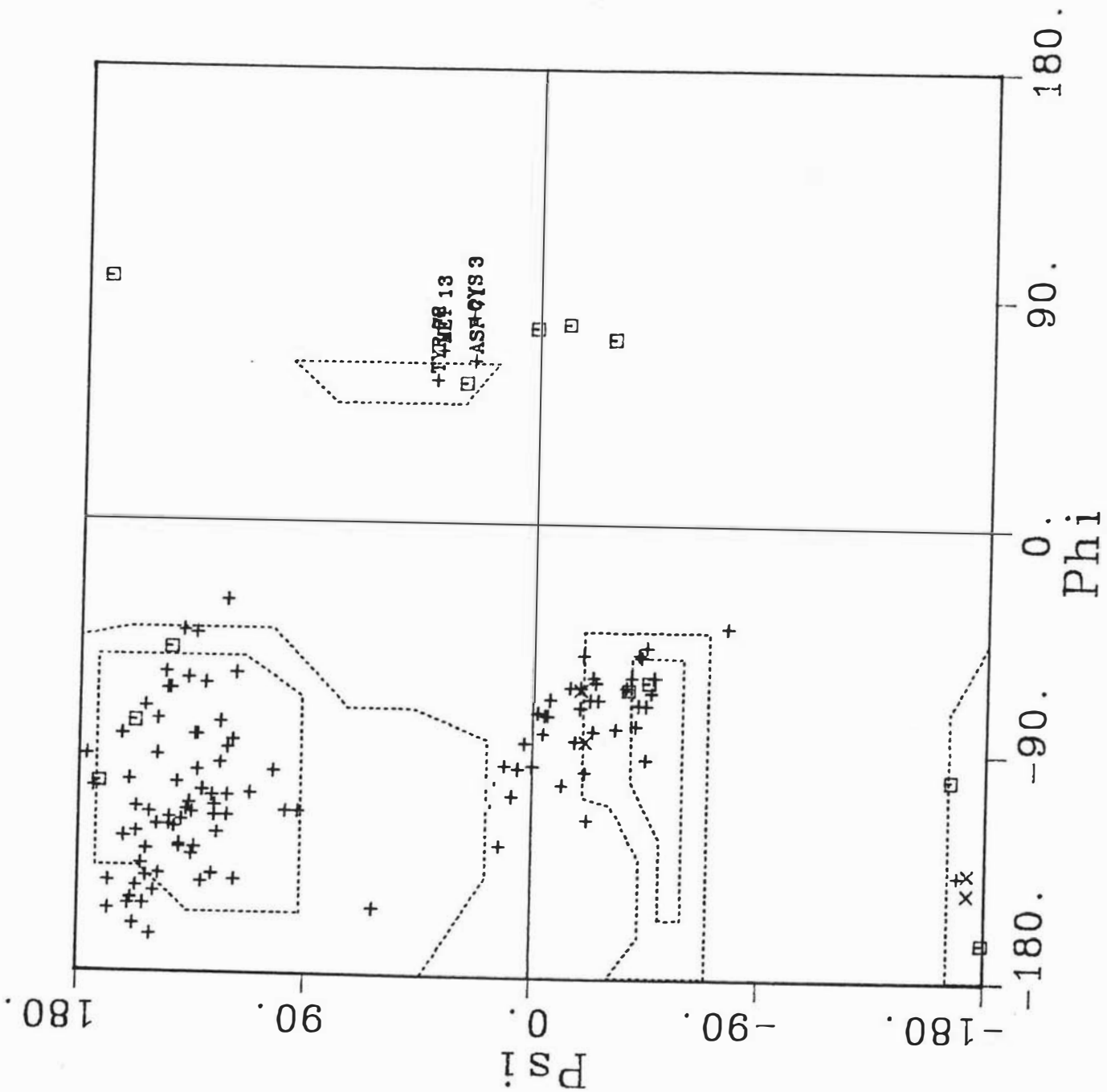

Appendix A.2. Ramachandran plot of main-chain torsion angles (ϕ,ψ) for reduced azurin molecule B. Glycine residues indicated as squares.

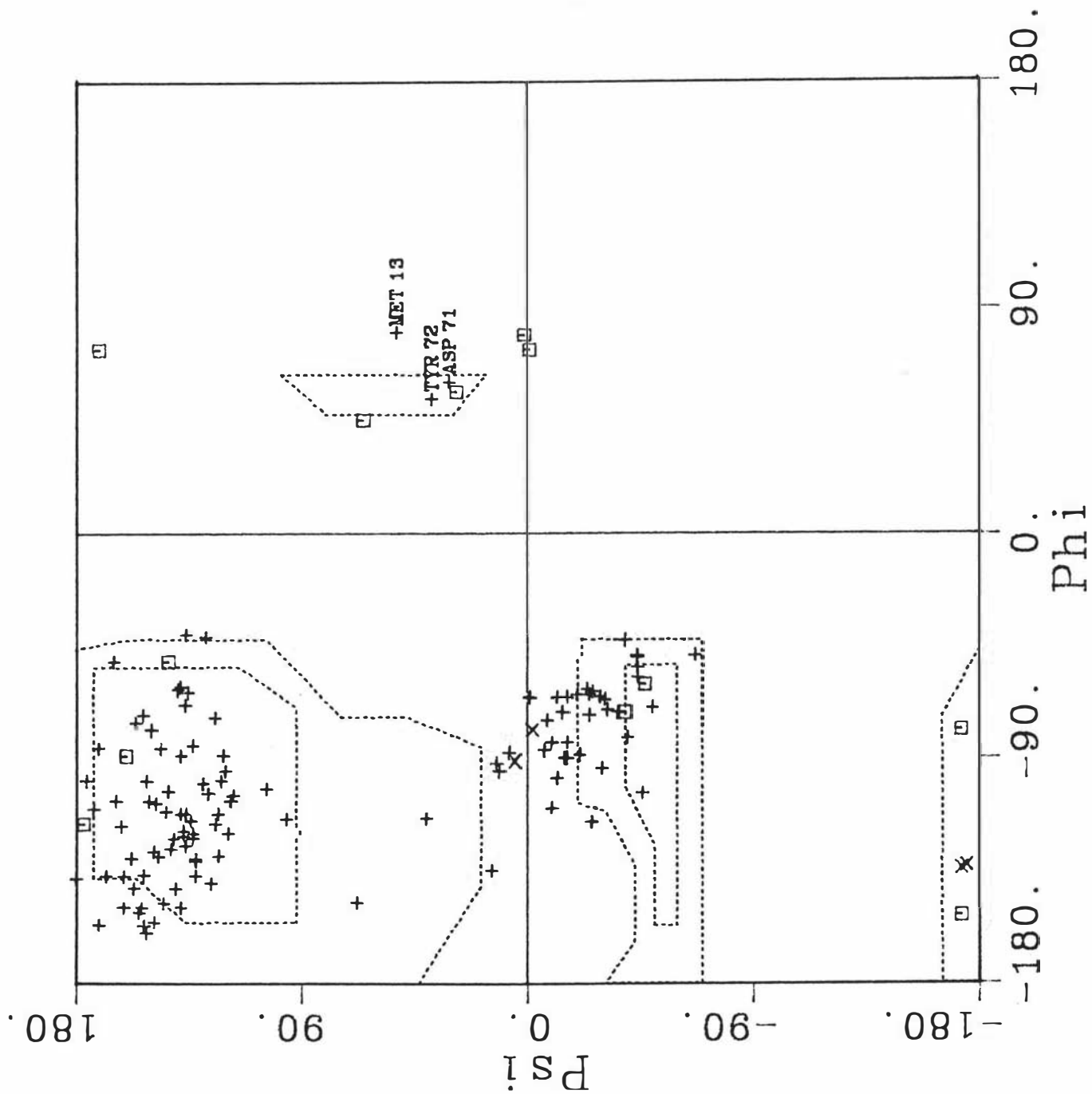

Appendix A.3. Ramachandran plot of main-chain torsion angles (ϕ,ψ) for apo-azurin molecule A. Glycine residues indicated as squares.

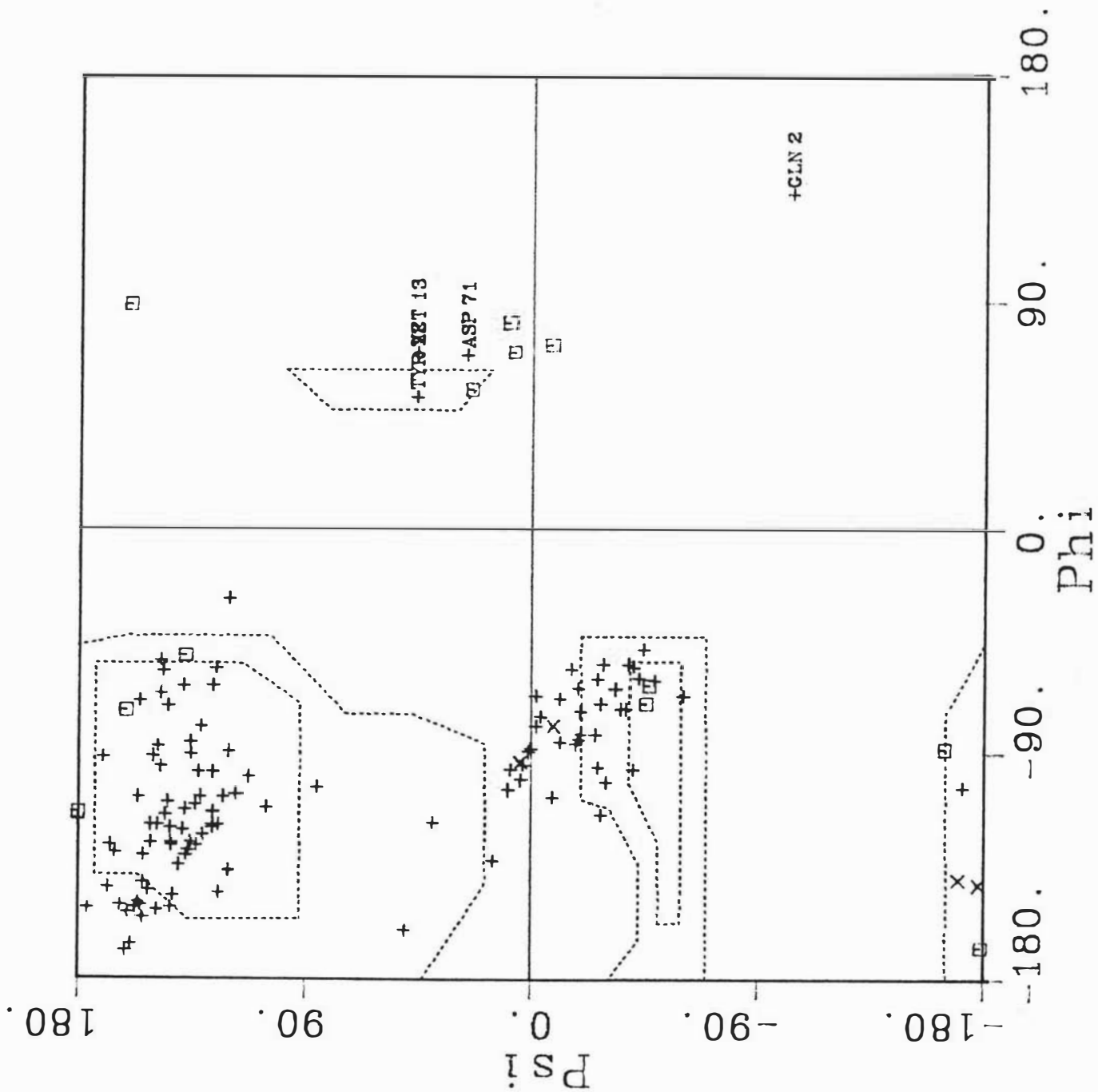

Appendix A.4. Ramachandran plot of main-chain torsion angles (ϕ,ψ) for apo-azurin molecule B. Glycine residues indicated as squares.

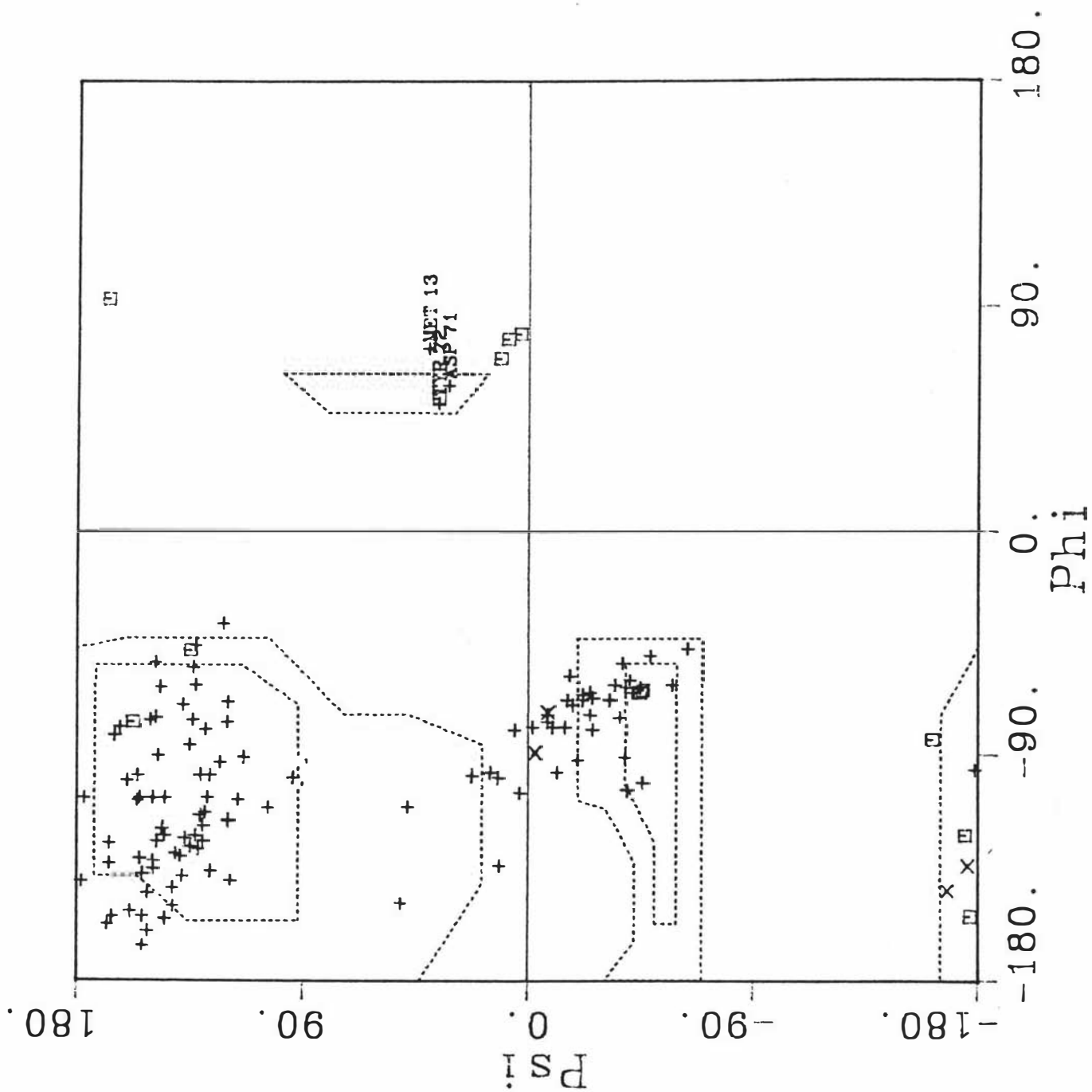

Appendix B.1. Main-chain...main-chain hydrogen bonds of azurin. The geometry is given in the order C-O...H angle, O...H distance and O...H-N angle.

	Oxidised A			Oxidised B			Apo A			Apo B			Reduced A			Reduced B		
	(°)	Å	(°)	(°)	Å	(°)	(°)	Å	(°)	(°)	Å	(°)	(°)	Å	(°)	(°)	Å	(°)
3 O-30 N	137	2.06	155	138	2.04	161	142	2.03	156	127	2.18	151	139	2.09	158	134	2.04	160
5 O-32 N	159	1.85	169	164	1.90	177	146	1.81	162	154	1.85	167	161	1.79	168	153	1.99	167
7 O-34 N	168	2.06	158	155	2.03	160	154	2.01	156	154	2.26	162	158	2.06	163	156	2.09	167
8 O-16 N	147	2.27	129	145	2.09	137	145	2.23	131	150	1.89	131	146	2.07	126	141	2.08	134
9 O-36 N	168	1.83	152	108	2.46	160	168	1.89	162	166	2.05	167	169	2.17	159	173	2.02	153
10 O-13 N				178	1.98	162							108	2.36	163			
14 O-10 N	147	2.36	144	151	2.39	135							151	2.45	136	156	2.44	142
18 O-124 N	144	1.90	156	138	1.90	151	136	1.84	158	142	1.88	157	151	1.70	162	139	1.85	150
20 O-126 N	151	2.16	155	156	2.15	157	152	2.15	157	150	2.39	154	153	1.99	152	160	2.33	154
22 O-128 N	151	1.98	165	171	1.88	140	164	1.90	165	166	1.84	137	142	1.96	153	171	1.81	132
23 O-26 N	123	1.99	156	127	1.86	161	116	2.30	152	119	1.91	153	120	2.06	157	120	2.02	156
27 O-99 N	134	2.12	165	131	2.03	166	139	1.83	151	137	2.14	162	127	1.88	162	135	1.87	160
29 O-97 N	155	1.66	154	161	2.02	164	162	1.83	157	171	1.95	158	151	1.82	151	157	1.92	157
30 O-5 N	157	2.18	151	161	1.96	145	158	2.13	149	156	2.23	137	164	2.13	153	151	2.15	141
31 O-95 N	149	1.92	157	144	1.98	150	150	2.07	153	150	1.98	149	146	2.09	147	143	2.03	152
32 O-7 N	158	1.88	170	161	1.95	164	160	1.87	165	150	1.91	157	155	1.75	163	164	1.87	165
33 O-93 N	147	1.91	161	150	2.09	162	149	1.96	154	152	1.98	154	148	1.87	150	154	1.99	154
34 O-9 N	154	1.90	155	159	2.05	148	156	1.91	150	155	2.16	150	163	1.85	164	153	2.14	147
35 O-90 N	138	2.18	136	139	2.02	149	133	2.08	139	136	2.21	136	132	1.86	132	140	2.12	139
39 O-89 N	163	1.94	152	157	1.76	151	167	1.79	155	163	1.82	149	170	1.92	161	167	1.67	155
40 O-43 N	107	2.26	134	117	2.26	148	105	2.32	140	109	2.37	147	114	1.97	137	125	1.90	152
40 O-44 N	163	1.89	159	163	2.07	171	151	2.00	149	150	2.01	160	159	1.72	173	161	2.00	172
41 O-45 N							118	2.44	124	119	2.45	122	128	2.42	113			
46 O-87 N				143	1.97	171	152	1.89	159	150	1.90	162	145	1.84	153	144	2.05	166
48 O-84 N	150	1.77	170	155	2.06	157	150	2.17	146	156	2.11	154	150	2.08	158	159	2.10	158
49 O-111 N	151	2.13	153	140	1.94	147	144	2.03	149	139	2.19	151	159	1.84	157	156	2.05	158
50 O-81 N	144	1.97	147	154	1.86	148	154	1.80	145	160	1.71	148	152	2.10	147	147	1.80	156
51 O-109 N	162	1.88	150	145	2.12	149	164	1.85	159	146	2.15	146	168	1.71	161	148	2.00	146
52 O-55 N	158	1.90	155	111	2.03	140	114	2.35	128	108	2.26	127	112	2.04	130	123	1.92	146
53 O-56 N	114	1.90	130	109	2.41	167				103	2.39	160				107	2.50	164
55 O-59 N	161	2.00	162	146	2.25	153	174	2.09	171	159	2.11	162	167	2.07	157	155	1.99	153

Appendix B.1. (continued). Main-chain...main-chain hydrogen bonds of azurin. The geometry is given in the order C-O...H angle, O...H distance and O...H-N angle.

	Oxidised A			Oxidised B			Apo A			Apo B			Reduced A			Reduced B		
	(°)	Å	(°)	(°)	Å	(°)	(°)	Å	(°)	(°)	Å	(°)	(°)	Å	(°)	(°)	Å	(°)
56 O-60 N	143	2.14	143	149	2.02	151	124	2.42	142	145	2.20	151	160	2.24	164	159	2.01	151
57 O-61 N	139	1.98	147	147	2.10	158	128	2.22	141	140	2.12	156	141	2.15	155	142	2.16	160
58 O-62 N	141	2.03	167	140	2.06	160	143	2.11	163	149	2.03	169	135	2.26	164	129	2.24	147
59 O-63 N	131	1.98	142	135	1.95	138	139	1.73	146	131	1.93	139	140	1.84	147	129	2.03	140
60 O-64 N	146	2.07	167	139	1.99	157	130	2.00	156	141	1.98	153	151	1.98	163	150	2.06	166
61 O-65 N	139	2.49	148	139	2.36	148	144	2.21	143	149	2.43	154						
63 O-66 N	106	1.89	145	112	1.80	150	110	1.98	147	112	1.88	155	112	1.81	155	111	1.66	154
64 O-67 N	110	2.49	148															
67 O-70 N	109	2.39	149				104	2.20	146	102	2.30	138	101	2.44	141	118	2.40	137
67 O-72 N	149	2.12	150	150	2.05	154	148	2.13	149	149	2.03	157	145	2.20	148	141	2.27	156
68 O-71 N	108	2.05	151	107	2.03	152	107	1.86	162	106	2.08	148	106	1.77	152	118	2.02	150
70 O-73 N				111	2.47	149				120	2.45	160	115	2.42	153	115	2.47	152
74 O-77 N	146	2.22	124				148	2.10	134				153	2.03	128			
77 O-80 N				104	2.27	153				109	2.40	162				96	2.40	156
82 O-50 N	173	2.02	161	176	2.16	155	174	1.92	165	173	1.91	157	171	1.93	158	168	1.90	161
87 O-46 N	149	2.07	165	151	2.05	162	150	2.17	154	153	1.93	156	158	1.99	161	151	2.11	154
88 O-91N	131	2.33	147	143	2.38	141	150	2.27	141	151	2.03	148	135	2.41	140	145	2.18	148
91 O-35 N	169	1.84	164	160	2.02	173	172	1.93	165	159	2.09	172	163	2.01	169	161	2.00	172
93 O-33 N	169	1.75	151	176	1.86	160	156	1.82	151	160	1.91	148	169	1.93	153	168	1.86	164
95 O-31 N	163	1.77	156	162	1.97	172	173	1.72	161	173	1.83	164	162	1.61	159	165	1.93	170
97 O-29 N	156	1.71	164	147	1.96	147	158	1.95	160	157	2.14	158	155	1.84	164	143	1.89	147
98 O-101 N	113	2.33	147	109	2.34	155	119	2.10	154	113	2.12	155	117	2.21	161	118	2.19	142
99 O-102 N	109	2.13	142	115	1.89	149	125	1.98	164	107	2.18	152	113	2.05	155	115	1.95	150
103 O-106 N	138	2.32	147	129	2.24	154	129	2.27	151	159	2.06	150	129	2.01	140	155	2.22	135
108 O-125 N	133	1.77	161	133	1.87	166	141	1.86	163	143	1.82	162	134	1.92	161	136	1.94	167
109 O-51 N	164	1.95	173	170	2.21	172	168	2.00	174	169	2.26	174	171	1.90	174	165	2.01	167
110 O-123 N	158	1.86	146	151	1.91	149	164	2.07	134	160	1.69	150	149	2.10	140	153	1.86	151
111 O-49 N	143	2.10	141	151	2.11	144	152	1.85	144	143	2.07	141	151	1.89	142	142	2.03	132
114 O-117 N	144	2.10	166	153	1.86	157	155	2.08	148	161	1.84	154	152	1.98	164	151	1.96	148
117 O-120 N	118	2.33	151	108	2.45	146	129	2.12	162	107	2.47	142	116	2.10	154	122	2.32	158
117 O-121 N	154	2.09	146	155	2.09	151	161	2.08	157	167	1.99	166	146	2.14	142	153	2.16	151

Appendix B.1. (continued). Main-chain...main-chain hydrogen bonds of azurin. The geometry is given in the order C-O...H angle, O...H distance and O...H-N angle.

	Oxidised A			Oxidised B			Apo A			Apo B			Reduced A			Reduced B		
	(°)	Å	(°)	(°)	Å	(°)	(°)	Å	(°)	(°)	Å	(°)	(°)	Å	(°)	(°)	Å	(°)
121 O-112 N	152	2.07	146	147	2.16	152	158	2.29	147	152	2.16	155	146	2.46	157	149	2.23	158
123 O-110 N	143	1.99	168	135	2.08	163	139	2.22	162	132	1.97	161	139	1.92	170	137	2.26	172
124 O-20 N	152	1.81	156	160	1.92	156	153	1.87	156	149	2.02	153	145	1.92	155	154	1.89	161
125 O-108 N	153	1.96	144	158	1.93	167	159	2.16	153	162	1.76	171	152	2.12	154	159	1.85	160
126 O-22 N	150	1.78	167	146	1.98	168	149	1.82	169	151	1.92	170	162	2.18	123	148	2.16	172
128 O-24 N							133	2.32	132				162	2.18	123			

Appendix B.2. Main-chain...side-chain hydrogen bonds of azurin. The geometry is given in the order C-O...H angle, O...H distance and O...H-N angle; or C-A...D angle, A...D distance and A...D-C angle for those without a calculated hydrogen atom (where, A=acceptor and D=donor).

	Oxidised A			Oxidised B			Apo A			Apo B			Reduced A			Reduced B		
	(°)	Å	(°)	(°)	Å	(°)	(°)	Å	(°)	(°)	Å	(°)	(°)	Å	(°)	(°)	Å	(°)
2 $O_{\varepsilon 1}$-3 N				106	2.07	165				129	1.84	151						
10 O-46 $N_{\varepsilon 2}$	139	1.85	161	138	1.67	154	146	1.92	157	148	1.64	152	137	1.77	169	143	1.80	165
10 $O_{\delta 1}$-10 N	95	2.39	107				98	2.45	102									
10 $O_{\delta 1}$-12 N	100	2.17	142	113	2.07	145	101	2.14	145	113	2.07	150	103	2.16	143	109	2.10	146
10 $O_{\delta 1}$-14 N	159	2.48	140	144	2.46	151	157	2.37	146				157	2.48	153			
11 $O_{\delta 1}$-39 N	106	2.32	157	116	2.29	144				114	2.34	141	114	2.28	154	111	2.35	142
11 $O_{\delta 2}$-38 N	109	1.75	176	113	1.86	174	110	1.90	168	107	1.98	169	109	1.66	176	105	1.80	164
16 $O_{\delta 1}$-8 N	128	1.93	167	119	1.80	178	114	2.06	173	118	1.59	169	120	1.83	174	118	1.71	174
16 $O_{\delta 1}$-16 N	104	2.27	116	103	2.44	110	108	1.95	111	101	2.19	115	108	2.10	113	102	2.15	113
16 O-18 N_{ζ}	131	3.04	100															
17 O-110 O_{η}	106	2.68	134	104	2.63	124	98	2.62	125	112	2.64	130	109	2.48	131	110	2.54	134
23 $O_{\delta 1}$-25 N	126	2.02	162				116	2.08	159	114	2.19	156	120	2.09	157	112	2.50	150
34 O-9 O_{γ}	124	2.89	117	119	3.25	120	126	2.76	127	121	3.29	117	123	3.02	112	126	3.05	129
35 $N_{\delta 1}$-37 N	109	2.20	151	115	2.24	145	108	2.33	150	114	1.89	147	117	2.10	149	121	2.38	143
44 O-35 $N_{\varepsilon 2}$	154	2.02	148	155	1.99	151	159	1.82	156	159	2.17	140	168	2.07	155	176	1.65	162
47 O-15 O_{η}	138	2.59	127	150	2.59	137	142	2.63	124	140	2.71	131	140	2.64	128	146	2.79	127
47 $O_{\delta 1}$-47 N										109	2.39	101				104	2.34	100
47 $O_{\delta 1}$-113 N	133	1.93	165	119	2.02	153	130	2.01	155	112	2.04	144	130	1.96	164	112	2.04	150
52 O-51 $O_{\gamma 1}$	120	2.94	95	125	2.81	108	129	2.85	100	126	2.86	108	124	2.90	97	121	3.07	109
57 O-61 $O_{\gamma 1}$	152	2.94	95	148	2.66	116							160	3.08	105	152	2.62	105
71 O-47 $N_{\delta 2}$	154	2.20	123	150	2.32	128	149	2.17	119	155	2.39	125	153	2.14	130	158	2.20	134
71 $O_{\delta 1}$-86 N	114	1.91	168	105	1.89	173	122	1.84	164	98	2.11	172	123	1.80	168	109	1.96	173
72 O-113 O_{γ}	132	2.64	111	134	2.50	113	136	2.57	111	131	2.54	116	132	2.72	109	129	2.62	103
77 $O_{\delta 1}$-79 N	161	1.89	150	129	2.17	156	137	2.29	167	139	1.95	163	156	1.82	149	160	2.03	146

Appendix B.2.(continued). Main-chain...side-chain hydrogen bonds of azurin. The geometry is given in the order C-O...H angle, O...H distance and O...H-N angle; or C-A...D angle, A...D distance and A...D-C angle for those without a calculated hydrogen atom (where, A=acceptor and D=donor).

	Oxidised A			Oxidised B			Apo A			Apo B			Reduced A			Reduced B		
	(°)	Å	(°)	(°)	Å	(°)	(°)	Å	(°)	(°)	Å	(°)	(°)	Å	(°)	(°)	Å	(°)
81 O-101 $N\zeta$				134	2.72	148				143	2.96	135						
84 O-83 $N\delta1$	137	1.82	154	130	1.77	163	137	1.66	161	138	1.73	147	134	1.64	153	134	1.82	152
84 $O\gamma1$-85 O	114	2.88	133	107	2.87	127	109	2.91	130	107	2.92	128	113	2.88	131	111	2.93	127
84 $O\gamma1$-48 N	131	2.44	135	136	2.20	136	133	2.37	135	137	2.40	132	129	2.46	126	134	2.21	141
86 O-41 $N\zeta$				136	2.77	141				146	3.08	125	147	2.98	102			
91 $O\varepsilon1$-88 N	101	1.87	144	112	1.80	176	92	2.23	143	121	1.64	167	100	2.39	149	98	2.03	162
93 $O\delta1$-94 N				93	2.50	128				90	2.33	133				101	2.32	126
93 $O\delta2$-85 N	129	2.00	165	132	1.88	166	135	1.84	159	145	1.90	177	131	2.10	168	133	1.98	169
98 $O\delta2$-100 N	128	2.04	168				146	1.48	158				109	1.78	174			
108 $O\eta$-103 N	121	2.17	158	113	2.29	141	126	1.79	163	117	2.31	136	126	1.90	160	118	2.23	142
112 $S\gamma$-47 N	104	2.53	170	110	2.48	167	101	2.62	160	106	2.80	163	104	2.41	160	105	2.34	159
112 $S\gamma$-114 N	117	2.54	161	116	2.72	155	111	2.76	161	109	2.54	163	115	2.40	163	116	2.43	158
123 O-122 $N\zeta$				99	3.12	95												
127 O-24 $N\zeta$													97	3.00	144			
128 O-24 $N\zeta$																112	3.23	91
128 $O\gamma$-129 N													98	1.73	135			
129 $O\varepsilon$-24 $N\zeta$				161	2.90	117												

Appendix B.3. Side-chain...side-chain hydrogen bonds of azurin. The geometry is given in the order C-O...H angle, O...H distance and O...H-N angle; or C-A...D angle, A...D distance and A...D-C angle for those without a calculated hydrogen atom (where, A=acceptor and D=donor).

	Oxidised A			Oxidised B			Apo A			Apo B			Reduced A			Reduced B		
	(°)	Å	(°)	(°)	Å	(°)	(°)	Å	(°)	(°)	Å	(°)	(°)	Å	(°)	(°)	Å	(°)
4 $O_{\varepsilon 1}$-32 $N_{\varepsilon 2}$	101	2.09	166										110	1.83	169	102	1.73	151
14 $O_{\varepsilon 1}$-10 $N_{\delta 2}$	123	2.21	168	144	1.97	173				146	2.22	161	138	2.16	159	152	2.11	162
23 $O_{\delta 1}$-25 O_{γ}	146	2.57	103	141	2.67	99	149	2.64	101	141	2.62	104	150	2.54	106			
23 $O_{\delta 2}$-128 O_{γ}				118	3.42	99										105	3.37	110
30 $O_{\gamma 1}$-96 $O_{\gamma 1}$	125	2.54	119	119	2.39	116	114	2.79	117	120	2.75	110	126	2.53	115	116	2.49	122
53 $O_{\varepsilon 1}$-56 N_{ζ}																138	3.47	97
53 $O_{\varepsilon 1}$-122 N_{ζ}	128	2.61	129	134	3.40	112				125	2.66	93						
62 $O_{\delta 1}$-74 N_{ζ}	125	2.79	166				126	2.65	167				124	2.64	177			
62 $O_{\delta 1}$-79 $N_{\eta 2}$	106	1.74	132	112	2.13	138	101	1.82	132	120	1.67	150	101	2.03	113	95	2.30	139
77 $O_{\delta 1}$-79 N_{ε}	104	2.02	151	131	1.64	168	109	1.71	166	115	1.66	167				108	2.03	163
77 $O_{\delta 2}$-79 $N_{\eta 2}$	116	1.71	136	102	1.82	155	111	1.80	140	107	1.64	151	108	2.18	124	114	1.52	151
91 $O_{\varepsilon 1}$-41 N_{ζ}	126	3.24	120				117	3.30	173									
93 $O_{\delta 1}$-85 N_{ζ}				128	3.38	113				116	3.23	114				134	3.03	107
94 O_{γ}-32 $N_{\delta 1}$	145	2.08	129	118	1.38	169	134	1.89	151	125	1.76	153	156	1.98	136	117	1.60	152
98 $O_{\delta 1}$-27 N_{ζ}													104	2.70	160			
98 $O_{\delta 1}$-100 O_{γ}				139	2.49	145				131	2.83	126				132	2.78	136
106 $O_{\varepsilon 1}$-108 O_{η}	134	3.22	93	118	3.16	95	103	3.28	100				137	3.08	93	110	3.27	99
113 O_{γ}-47 $N_{\delta 2}$	148	1.89	169	143	1.94	175	150	2.12	166	141	2.07	174	148	2.00	172	146	1.74	177
112 S_{γ}-46 $N_{\delta 1}$							113	3.67	142	112	3.87	138						
112 S_{γ}-117 $N_{\delta 1}$							119	3.59	144	112	3.49	144						
124 $O_{\gamma 1}$-122 N_{ζ}				132	3.45	149												
129 O_{ε}-128 O_{γ}							125	3.15	128									

Appendix C.1. Unit cell details for the various forms of azurin.

Crystal system[c] **:** Orthorhombic

Cell dimensions :

	a (Å)	b (Å)	c (Å)	α (°)	β (°)	γ (°)
Oxidised azurin (Cu(II))	75.0	74.2	99.6	90	90	90
Reduced azurin (Cu(I))	75.1	73.8	100.1	90	90	90
Copper-removed azurin[a] (Cyanide soaked crystals)	75.1	74.3	99.1	90	90	90
Apo-azurin[b] (Solution grown crystals)	75.1	74.1	99.5	90	90	90

Space group[c] **:** $C222_1$

Molecules per unit cell[c] **:** 16

V_M[c,d] **:** 2.39 $Å^3$/dalton

Solvent content[c,d] **:** 48.5%

---

[a] See p42.

[b] See p44.

[c] All forms.

[d] Matthews, B.W. (1968) *J. Mol. Biol.*, **33**, 491-497.

Appendix C.2.1. A C_α plot of azurin showing the location of specific residues.

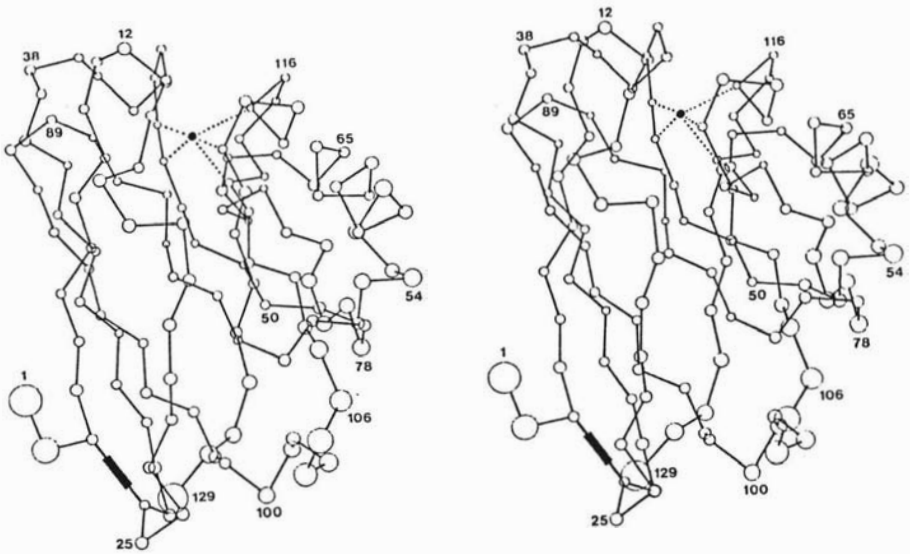

Appendix C.2.2. The amino acid sequence of *Alcaligenes denitrificans* azurin. Amino acid residues are given as one letter codes†.

Residue number	1	.	.	.	5	.	.	.	.	10	Residue number
0	A	Q	C	E	A	T	I	E	S	N	10
10	D	A	M	Q	Y	N	L	K	E	M	20
20	V	V	D	K	S	C	K	Q	F	T	30
30	V	H	L	K	H	V	G	K	M	A	40
40	K	V	A	M	G	H	N	W	V	L	50
50	T	K	E	A	D	K	Q	G	V	A	60
60	T	D	G	M	N	A	G	L	A	Q	70
70	D	Y	V	K	A	G	D	T	R	V	80
80	I	A	H	T	K	V	I	G	G	G	90
90	E	S	D	S	V	T	F	D	V	S	100
100	K	L	T	P	G	E	A	Y	A	Y	110
110	F	C	S	F	P	G	H	W	A	M	120
120	M	K	G	T	L	K	L	S	N		130

† IUPAC-IUB Commission on Biochemical Nomenclature (1968) *J. Biol. Chem.*, **243**, 3557-3559.

Bibliography

1 Ettinger, M.J. (1984) in *Copper Proteins and Copper Enzymes* (Lontie, R., ed.) vol. 3, pp. 175-229, CRC Press, Boca Raton, Florida.

2 Adman, E.T. (1990) *Advances in Protein Chemistry*, in press.

3 Lontie, R., ed. (1984) in *Copper Proteins and Copper Enzymes,* vol. 1-3, CRC Press, Boca Raton, Florida.

4 Cass, A.E.G., and Hill, H.A.O. (1980) *Biological roles of copper (Ciba Foundation Symposium)* **79**, 71-91.

5 Fee, J.A. (1975) *Structure and Bonding* **23**, 1-60, and refences therein.

6 Malkin, R. and Malmström, B.G. (1970) *Adv. Enzymol.* **33**, 177-244.

7 Lappin, A.G. (1981) in *Metal ions in Biological Systems* (Sigel, H., ed.), vol. 13, pp. 15-71, Dekker, New York.

8 Farver, O. and Pecht, I. (1984) in *Copper Proteins and Copper Enzymes* (Lontie, R., ed.), vol. 1, pp. 183-214, CRC Press, Boca Raton, Florida.

9 Ryden, L. (1984) in *Copper Proteins and Copper Enzymes* (Lontie, R., ed.), vol. 1, pp. 157-182, CRC Press, Boca Raton, Florida.

10 Adman, E.T. (1985) in *Topics in Molecular Biology, Metalloproteins* (Harrison, P., ed.) vol. 1, pp. 1-42, VCH, Weinheim, New York.

11 Ryden, L.(1984) in *Copper Proteins and Copper Enzymes* (Lontie, R., ed.), vol. 3, 37-100, CRC Press, Boca Raton, Florida.

12 Deinum, J., Reinhammar, B., and Marchesini, A. (1974) *F.E.B.S. Lett.* **42**, 241-245.

13 Marchesini, A., and Kroneck, P.M.H. (1979) *Eur. J. Biochem.* **101**, 65-76.

14 Messerschmidt, A., Rossi, A., Ladenstein, R., Huber, R., Bolognesi, M., Guiseppina, G., Marchesini, Petruzzelli, R. and Finazzi-Agro (1989) *J. Mol. Biol.* **206**, 513-529.

15 Ambler, R.P., and Tobari, J. (1985) *Biochem. J.* **232**, 451-457.

16 Tobari, J. (1984) in *Microbial Growth on C_1 Compounds. Proceedings of the 4th International Symposium* (Crawford, R.L., and Hanson, R.S., eds.), pp. 106-112, American Society for Microbiology, Washington.

17 Van Houwelingen, T., Canters, G.W., Stobbelaar, G., Duine, J.A., Frank, J., and Tsugita, A. (1985) *Eur. J. Biochem.* **153**, 75-80.

18 Husain, M., and Davidson, V.L. (1986) *Biochemistry* **25**, 2431-2436.

19 Lawton, S.A., and Anthony, C. (1985) *Biochem. J.* **228**, 719-726.

20 Gray, K.A., Davidson, V.L., and Knaff, D.B. (1988) *J. Biol. Chem.* **263**, 13987-13990.

21 Katoh, S., and Takamiya, A. (1961) *Nature* **189**, 665

22 Kakutani, T., Watanabe, H., Arima, K., and Beppu, T. (1981) *J. Biochem.* **89**, 463-472.

23 Sivestrini, M.C., Brunori, M., Tegoni, M., Gervais, M., Labeyrie, F. (1986) *Eur. J. Biochem.* **161**, 465-472.

24 Antonini, E., Finazzi-Agro, A., Avigliano, L., Guerrieri, P., Rotilio, G., and Mondovi, B. (1970) *J. Biol. Chem.* **245**, 4847-4856.

25 Augustin, M.A., Chapman, S.K., Davies, D.M., Watson, A.D., and Sykes, A.G. (1984) *J. Inorg. Biochem.* **20**, 281-289.

26 Mondovi, B., and Avigliano, L. (1984) in *Copper Proteins and Copper Enzymes* (Lontie, R., ed.), vol 3, pp. 101-118, CRC Press, Boca Raton, Florida.

27 Groeneveld, C.M., and Canters, G.W. (1985) *Eur. J. Biochem.* **153**, 559-564.

28 Groeneveld, C.M., and Canters, G.W. (1988) *J. Biol. Chem.* **263**, 167-173.

29 Norris, G.E., Anderson, B.F., and Baker, E.N. (1983) *J. Mol. Biol.* **165**, 501-521.

30 Norris, G.E., Anderson, B.F., and Baker, E.N. (1986) *J. Am. Chem. Soc.* **108**, 2784-2785.

31 Baker, E.N. (1988) *J. Mol. Biol.* **203**, 1071-1095.

32 Guss, J.M., and Freeman, H.C. (1983) *J. Mol. Biol.* **169**, 521-563.

33 Collyer, C.A., Guss, J.M., Sugmura, Y., Yoshizaki, F., and Freeman, H.C. (1990) *J. Mol. Biol.* **211**, 617-632.

34 Petratos, K., Dauter, Z., and Wilson, K.S. (1988) *Acta Cryst.* **B44**, 628-636.

35 Korzun, Z.R. (1987) *J. Mol. Biol.* **196**, 413-419.

36 Adman, E.T., Stenkamp, R.E., Sieker, L.C., and Jensen, L.H. (1978) *J. Mol. Biol.* **123**, 35-47.

37 Petratos, K., Banner, D.W., Beppu, T., Wilson, K.S., and Tsernoglou, D. (1987) *F.E.B.S. Lett.* **218**, 209-214.

38 Colman, P.M., Freeman, H.C., Guss, J.M., Murata, M., Norris, V.A., Ramshaw, J.A.M., and Venkatappa, M.P. (1978) *Nature* **272**, 319-324.

39 Adman, E.T., Turley, S., Bramson, R., Petratos, K., Banner, D., Tsernoglou, D., Beppu, T., and Watanbe, H. (1989) *J. Biol. Chem.* **264**, 87-99.

40 Guss, J.M., Merritt, E.A., Phizackerley, R.P., Hedman, B., Murata, M., Hodgson, K.O., and Freeman, H.C. (1988) *Science* **241**, 806-811.

41 Nar, H., Messerschmidt, A., Huber, R., van de Kamp, M., and Canters, G.W. (1991) *J. Mol. Biol.* **221**, in press.

42 Lontie, R., ed. (1984) in *Copper Proteins and Copper Enzymes* vol. 2-3, CRC Press, Boca Raton, Florida.

43 Knowles, P.F., and Yadav, K.D.S. (1984) in *Copper Proteins and Copper Enzymes* (Lontie, R., ed.) vol. 2, 103-130, CRC Press, Boca Raton, Florida.

44 Kosman, D.J. (1984) in *Copper Proteins and Copper Enzymes* (Lontie, R., ed.) vol. 2, 1-26, CRC Press, Boca Raton, Florida.

45 Reinhammer, B. (1984) in *Copper Proteins and Copper Enzymes* (Lontie, R., ed.) vol. 3, 1-36, CRC Press, Boca Raton, Florida.

46 Fielden, E.M., and Rotilio, G. (1984) in *Copper Proteins and Copper Enzymes* (Lontie, R. ed.) vol. 2, 27-62, CRC Press, Boca Raton, Florida.

47 Hathaway, B.J., and Billing, D.E. (1970) *Coord. Chem. Rev.* **5**, 143-207.

48 Boas, J.F. (1984) in *Copper Proteins and Copper Enzymes* (Lontie, R. ed.) vol. 1, 5-62, CRC Press, Boca Raton, Florida.

49 Halliwell, B. (1984) in *Copper Proteins and Copper Enzymes* (Lontie, R. ed.) vol. 2, 63-102, CRC Press, Boca Raton, Florida.

50 Tainer, J.A., Getzoff, E.D., Beem, K.M., Richardson, J.S., and Richardson, D.C. (1982) *J.Mol.Biol.* **160**, 181-217.

51 Ito, N., Phillips, S.E.V., Stevens, C., Ogel, Z.B., McPherson, M.J., Keen, J.N., Yadav, K.D.S., and Knowles, P.F. (1991) *Nature* **350**, 87-90.

52 Preaux, G., and Gielens, C.(1984) in *Copper Proteins and Copper Enzymes* (Lontie, R., ed.), vol 2, pp. 159-206, CRC Press, Boca Raton, Florida.

53 Robb, D.A. (1984) in *Copper Proteins and Copper Enzymes* (Lontie, R., ed.) vol. 2, pp. 207-240, CRC Press, Boca Raton, Florida.

54 Lerch, K., and Germann, U.A. (1988) in *Oxidases and Related Redox Systems* (King, T.E., Manson, H.S., and Morrison, M., eds.), pp. 331-348, Alan R. Liss, New York.

55 Solomon, E.I., Cole, J.L., and Baldwin, M.J. (1990) *Pure Appl. Chem.* **62**, 1063-1066.

56 Volbeda, A., and Hol, W.G.J. (1989) *J. Mol. Biol.* **209**, 249-279.

57 Eickman, N.C., Himmelwright, R.S., and Solomon, E.I. (1979) *Proc. Natl. Acad. Sci. U.S.A.* **76**, 2094.

58 Solomon, E.I., Penfield, K.W., and Wilcox, D.E. (1983) *Structure and Bonding* **53**, 1-57.

59 Volbeda, A., and Hol, W.G.J. (1989) *J. Mol. Biol.* **206**, 531-546.

60 Loehr, J.S., Freedman, T.B., and Loehr, T.M. (1974) *Biochem. Biophys. Res. Commun.* **56**, 510.

61 Thamann,T.J., Loehr, J.S., and Loehr, T.M. (1977) *J. Am. Chem. Soc.* **99**, 4187.

62 Klotz, I.M., Duff, L.L., Kurtz, D.M., Jr., and Shriver, D.F. (1981) in *Invertebrate Oxygen-Binding Proteins: Structure, Active site and Function,*

(Lamy, J., and Lamy, J.,eds.), p. 469, Marcel Dekker, New York.

63 Calabrese, L., Carbonaro, M., and Musci, G. (1989) *J. Biol. Chem.* **264**, 6183-6187.

64 Weser, U., and Hartmann, H.-J. (1984) in *Copper Proteins and Copper Enzymes* (Lontie, R., ed.) vol. 3, pp. 151-174, CRC Press, Boca Raton, Florida.

65 Buse, G. (1984) in *Copper Proteins and Copper Enzymes* (Lontie, R., ed.) vol. 3, pp. 119-150, CRC Press, Boca Raton, Florida.

66 Capaldi, R.A. (1990) *Ann. Rev. Biochem.* **59**,569-596.

67 Riester, J., Zumft, W.G., and Kroneck, P.M.H. (1989) *Eur. J. Biochem.* **178**, 751-762.

68 Jin, H., Thomann, H., Coyle, C.L., and Zumft, W.G. (1989) *J. Am. Chem. Soc.* **111**, 4262-4269.

69 Lontie, R., ed. (1984) in *Copper Proteins and Copper Enzymes,* vol. 1, 1-4, CRC Press, Boca Raton, Florida.

70 Nersissian, A.M.,.Melkonyan, V.Z., and Nalbandyan, R.M. (1991) *Biochim. Biophys. Acta* **1076**, 337-342.

71 Bordas, J., Koch, M.H.J., Hartmann, H.-J., and Weser, U. (1982) *F.E.B.S. Lett.* **140**, 19.

72 Aasa, R., Albracht, S.J.P., Falk, K.-E., Lanne, B., and Vänngård, T. (1976) *Biochim. Biophys. Acta* **422**, 260-272.

73 Stevens, T.H., Martin, C.T., Wang, H., Brudvig, G.W., Scholes, C.P., and Chan, S.I. (1982) *J. Biol. Chem.* **257**, 12106-12113.

74 Froncisz, W., Scholes, C.P., Hyde, J.S., Wei, Y.-H., King, T.E., Shaw, R.W., and Beinert, H. (1979) *J. Biol. Chem.* **254**, 7482-7484.

75 Li, P.M., Gelles, J., Chan, S.I., Sullivan, R.J., and Scott, R.A. (1987) *Biochemistry* . **26**, 2091-2095.

76 Martin, C.T., Scholes, C.P., and Chan, S.I. (1988) *J. Biol. Chem.* **263**, 8420-8429.

77 Palmer, G., Babcock, G.T., and Vickery, L.E. (1976) *Proc. Natl. Acad. Sci. U.S.A.* **73**, 2206.

78 Blumberg, W.E., and Peisach, J.(1979) in *Cytochrome Oxidase* (King, T.E., Orii, Y., Cance, B., and Okunuki, K., eds.), p. 153 Elsevier/North Holland Biomedical Press, Amsterdam.

79 Reed, C.A., and Landrum, J.T. (1979) *F.E.B.S. Lett.* **106**, 265.

80 Brudvig, G.W., Stevens, T.H., and Chan, S.I. (1980) *Biochemistry* . **19**, 5275.

81 Solomon, E.I., Hare, J.W., Dooley, D.M., Dawson, J.H., Stevens, P.J., and

Gray, H.B., (1980) *J. Am. Chem. Soc.* **102**, 168-178.

82 Ainscough, E.W., Bingham, A.G., Brodie, A.M., Ellis, W.R., Gray, H.B., Loehr, T.M., Plowman, J.E., Norris, G.E., and Baker, E.N. (1987)*Biochemistry* **26**, 71-82.

83 Penfield, K.W., Gay, R.R., Himmelwright, R.S., Eickman, N.C., Norris, V.A., Freeman, H.C., and Solomon, E.I. (1981) *J. Am. Chem. Soc.* **103**, 4382-4388.

84 Gray, H.B., and Solomon, E.I., (1981) in *Copper Proteins* (Spiro, T., ed.), p. 1, John Wiley, New York.

85 Lever, A.B.P. (1984) in *Inorganic Electronic Spectroscopy*, pp. 203-208, Elsevier, New York.

86 Peisach, J., Levine, W.G., and Blumberg, W.E. (1967) *J. Biol. Chem.* **242**, 2847-2858.

87 Malmström, B.G., Reinhammar, B., and Vänngård, T. (1970) *Biochim. Biophys. Acta* **205**, 48-57.

88 Sakurai, T., Suzuki, S., and Chikira, M. (1990) *J. Biochem.* **107**, 37-42.

89 Marchesini, A., Minelli, M., Merkle, H., and Kroneck, P.M.H. (1979) *Eur. J. Biochem.* **101**, 77-84.

90 Stigbrand, T., and Sjoholm, I. (1972) *Biochim. Biophys. Acta* **263**, 244-257.

91 Ainscough, E. W., Bingham, A.G., Brodie, A.M., Husbands, J.M., and Plowman, J.E. (1981) *J. Chem. Soc., Dalton Trans.*, 1701-1707.

92 Penfield, K.W., Gewirth, A.A., and Solomon, E.I. (1985) *J. Am. Chem. Soc.* **107**, 4519-4529.

93 Groeneveld, C.M., Aasa, R., Reinhammar, B., and Canters, G.W. (1987) *J. Inorg. Biochem.* **31**, 143-154.

94 Bouwman, E., Driessen, W.L., and Reedjik, J. (1990) *Coord. Chem. Rev.* **104**, 143-172.

95 Agnus, Y., Louis, R., and Weiss, R. (1980) *J. Chem. Soc., Chem. Comm.*, 867-869.

96 Brader, M.L., and Dunn, M.F. (1990)*J. Am. Chem. Soc.* **112**, 4585-4587.

97 den Blaauwen, T., van de Kamp, M., and Canters, G.W. (1991) *J. Am. Chem. Soc.* **113**, 5050-5052.

98 Karlsson, B.G., Aasa, R., Malmström, B.G., and Lundberg, L.G. (1989) *F.E.B.S. Lett.* **253**, 99-102.

99 Cox, J.C., Aasa, R., and Malmström, B.G. (1978) *F.E.B.S. Lett.* **93**, 157.

100 Katoh, S., Shiratori, I., and Takamiya, S. (1962) *J. Biochem. (Tokyo)* **51**, 32-40.

101 Stigbrand, T., Malmström, B.G., and Vänngård, T. (1971) *F.E.B.S. Lett.* **12**,

260.

102 Murata, M., Begg, G.S., Lambruo, F., Leslie, B., Simpson, R.J., Freeman, H.C., and Morgan, F.J. (1982) *Proc. Natl. Acad. Sci. U.S.A.* **79**, 6434-6437.

103 Takabe, T., Niwa, S., and Ishikawa, H. (1980) *J. Biochem.* **87**, 1335-1339.

104 Malmström, B.G., Reinhammar, B., and Vänngård, T. (1968) *Biochim. Biophys. Acta* **156**, 67-76.

105 Sakurai, T., Okamoto, H., Kawahara, K., and Nakahara, A. (1982) *F.E.B.S. Lett.* **147**, 220-224.

106 Sarkissian, L., and Nalbandyan, R.M. (1983) *Biosci. Rep.* **3**, 915-20.

107 Ingledew, W.J., and Cobley, J.C. (1980) *Biochim. Biophys. Acta*, **590**, 141-158.

109 Taniguchi, V.T., Sailasuta-Scott, N., Anson, F.C., and Gray, H.B. (1980) *Pure Appl. Chem.* **52**, 2275-2281.

110 Rosen, P., Segal, M., and Pecht, I. (1981) *Eur. J. Biochem.* **120**, 339-344.

111 Stigbrand, T. (1972) *F.E.B.S. Lett.* **23**, 41-43.

112 Addison, A.W. (1983) in *Copper Coordination Chemistry: Biochemical and Inorganic Perspectives* (Karlin, K.D., Zubieta, J., eds.), pp. 109-128, Adenine Press, New York.

113 Augustin, M.A., Yandell, J.K., Addison, A.W., and Karlin, K.D. (1981) *Inorg. Chim. Acta* **55**, L35-L37.

114 Addison, A.W. (1989) *Inorg. Chim. Acta* **162**, 217-220.

115 Pavlishchuk, V.V., Yatsimirskii, K.B., Strizhak, P.E., and Lubuda, J. (1989) *Inorg. Chim. Acta* **164**, 65-68.

116 Yokoi, H., and Addison, A.W. (1977) *Inorg. Chem.* **16**, 1341-1349.

117 Atkinson, N., Blake, A.J., Drew, M.G.B., Forsyth, G., Lavery, A.J., Reid, G., and Schroder, M. (1989) *J. Chem. Soc., Chem. Comm.*, 984-986.

118 Frank, P., Licht, A., Tullius, T.D., Hodgson, K.O., and Pecht, I. (1985) *J. Biol. Chem.* **260,** 5518-5525.

119 Sakurai, T., Ikeda, O., and Suzuki, S. (1990) *Inorg.Chem.* **29**, 4715-4718.

120 Petigrew, G.W., Leitch, F.A., and Moore, G.R. (1983) *Biochim. Biophys. Acta* **725**, 409-416.

121 Ellis, W.R., and Corin, A.F. (1981) unpublished work.

122 Guss, J.M., Harrowell, P.R., Murata, M., Norris, V.A., and Freeman, H.C. (1986) *J. Mol. Biol.* **192**, 361-387.

123 Adman, E.T., Canters, G.W., Hill, H.A.O., and Kitchen, N.A. (1982) *F.E.B.S. Lett.* **143**, 287-292.

124 Ugurbil, K., and Bersohn, R. (1977) *Biochemistry* **16**, 3016-3023.

125 Ugurbil, K., Norton, R.S., Allerhand, A., and Bersohn, R. (1977) *Biochemistry* **16**, 886-894.

126 Hill, H.A.O., and Smith, B.E. (1979) *J. Inorg. Biochem.* **11**, 79-93.

127 Farver, O., and Pecht, I. (1981) *Isr. J. Chem.* **21**, 13-17.

128 Groeneveld, C.M., Ouwerling, M.C., Erkelens C., and Canters, G.W., (1988) *J. Mol. Biol.* **200**, 189-199.

129 Blair, D.F., Campbell, G.W., Schoonover, J.R., Chan, S.I., Gray, H.B., Malmström, B.G., Pecht, I., Swanson, B.I., Woodruff, W.H., Cho, W.K., English, A.M., Fry, H.A., Lum, V., and Norton, K.A. (1985) *J. Am. Chem. Soc.* **107**, 5755-5766.

130 Dooley, D.M., Moog, R.S., Liu, M.-Y., Payne, W.J., and LeGall, J. (1988) *J. Biol. Chem.* **263**, 14625-14628.

131 Agnew, S.F., Schoonover, J.R., Swanson, B.I., and Woodruff, W.H. (1985) *J. Am. Chem. Soc.* **107**, 6716-6718.

132 Woodruff, W.H., and Norton, K.A. (1983) *J. Am. Chem. Soc.* **105**, 657-658.

133 Belhadj, M., Jean, J.M., Friesner, R.A., Schoonover, J., and Woodruff, W.H. (1990) *J. Phys. Chem.* **94**, 2160-2166.

134 Thamann, T.J., Frank, P., Willis, L.J., and Loehr, T.M. (1982) *Proc. Natl. Acad. Sci. U.S.A.* **79**, 6396-6400.

135 Urushiyama, A., and Tobari, J. (1990) *Bull. Chem. Soc. Jpn.* **63**, 1563-1571.

136 Miskowski, V., Tang, S.-P.W., Spiro, T.G., Shapiro, E., and Moss, T.H. (1975) *Biochemistry* **14**, 1244-1250.

137 Nestor, L., Larrabee, J.A., Woolery, G., Reinhammer, B., and Spiro, T.G. (1984) *Biochemistry* **23**, 1084-1093

138 Thompson, T.J., Marks, T.B., and Ibers, J.A. (1977) *Proc. Natl. Acad. Sci. U.S.A.* **74**, 3114-3118.

139 Ferris, N.S., Woodruff, W.H., Rorabacher, D.B., Jones, T.E., and Ochrmowycz, L.A. (1978) *J. Am. Chem. Soc.* **100**, 5939-5942.

140 Siiman, O., Young, N.M., and Carey, P.R. (1976) *J. Am. Chem. Soc.* **98**, 244-247.

141 Dahlin, S., Reinhammar, B., and Ångstrom, J. (1989) *Biochemistry* **28**, 7224-7233.

142 Bagby, S., Driscoll, P.C., Goodall, K.G., Redfield, C., and Hill, H.A.O. (1990) *Eur. J. Biochem.* **188**, 413-420.

143 Engeseth, H.R., McMillin, D.R., and Otvos, J.D. (1984) *J. Biol. Chem.* **259**, 4822-4826.

144 Babayan, M.A., Nersissian, A.M., and Nalbandyan, R.M. (1988) *F.E.B.S.*

Lett. **238**, 167-170.

145 Driscoll, P.C., Hill, H.A.O., and Redfield, C. (1987) *Eur. J. Biochem.* **170**, 279-292.

146 King, G.C., and Wright, P.E. (1986) *Biochemistry* **25**, 2364-2374.

147 Hill, H.A.O., Smith, B.E., Storm, C.B., and Ambler, R.P. (1976) *Biochem. Biophys. Res. Commun.* **70**, 783-790.

148 Hill, H.A.O., Leer, J.C., Smith, B.E., Storm, C.B., and Ambler, R.P. (1976) *Biochem. Biophys. Res. Commun.* **70**, 331-338.

149 Moore, J.M., Case, D.A., Chazin, W.J., Gippert, G.P., Havel, T.F., Powls, R., and Wright, P.E. (1988) *Science* **240**, 314-317.

150 Moore, J.M., Chazin, W.J., Powls, R., and Wright, P.E. (1988) *Biochemistry* **27**, 7806-7816.

151 Moore, J.M., Lepre, C.A., Gippert, G.P., Chazin, W.J., Case, D.A., and Wright, P.E. (1991) *J. Mol. Biol.* **221**, 533-555.

152 Mulkley, J.L., Ulrich, E.L., Bergh, J.P., and Kroymann, D.W. (1975) *Biochemistry* **14**, 4428-4433.

153 Silvestrini, M.C., Brunori, M., Wison, M.T., and Darley-Usmar, V.M. (1981) *J.Inorg.Biochem.* **14**, 327-338

154 Mitra, S., and Bersohn, R. (1982) *Proc. Natl. Acad. Sci. U.S.A.* **79**, 6807-6811.

155 Nar, H., Messerschmidt, A., Huber, R., van de Kamp, M., and Canters, G.W. (1991) *J. Mol. Biol.* **218**, 427-447.

156 van de Kamp, M., Silvestrini, M.C., Brunori, M., Van Beeumen, J., Hali, F.C., and Canters, G.W. (1990) *Eur. J. Biochem.* **194**, 109-118.

157 Armstrong, F.A., Driscoll, P.C., Hill, H.A.O., and Redfield, C. (1987) *Biochem Soc. Trans.* **15**, 767.

158 Ackerman, J.J.H., Orr, T.V., Bartuska, V.J., and Maciel, G.E. (1979) *J. Am. Chem. Soc.* **101**, 341-347.

159 Mennitt, P.G., Shatlock, M.P., Bartuska, V.J., and Maciel, G.E. (1981) *J. Phys. Chem.* **85**, 2087-2091.

160 Tullius, T.D., Frank, P., and Hodgson, K.O. (1978) *Proc. Natl. Acad. Sci. U.S.A.* **75**, 4069-4073.

161 Groeneveld, C.M., Feiters, M.C., Hasnain, S.S., van Rijn, J., Reedijk, J., and Canters, G.W. (1986) *Biochim. Biophys. Acta* **873**, 214-227.

162 Penner-Hahn, J.E., Murata, M., Hodgson, K.O., and Freeman, H.C. (1989) *Inorg. Chem.* **28**, 1826-1832.

163 Scott, R.A., Hahn, J.E., Doniach, S., Freeman, H.C., and Hodgson, K.O. (1982) *J. Am. Chem. Soc.* **104**, 5364-5369.

164 Chapman, S.K., Orme-Johnson, W.H., McGinnis, J., Sinclair-Day, J.D., Sykes, A.G., Ohlsson, P.-I., and Paul, K.-G. (1986) *J. Chem. Soc., Dalton Trans.*, 2063-2068.

165 Lommen, A., Pandya, K.I., Koningsberger, D.C., and Canters, G.W. (1991) *Biochim. Biophys. Acta* **1076**, 439-447.

166 Feiters, M.C., Dahlin, S., and Reinhammar, B. (1988) *Biochim. Biophys. Acta* **955**, 250-260.

167 Peisach, J., Powers, L., Blumberg, W.E., and Chance, B. (1982) *Biophys. J.* **38**, 277-285.

168 Holt, S.D., Piggott, B., Ingledew, W.J., Feiters, M.C., and Diakun, G.P. (1990) *F.E.B.S. Lett.* **269**, 117-121.

169 Co, M.S., and Hodgson, K.O. (1984) in *Copper Proteins and Copper Enzymes* (Lontie, R., ed.), vol. 1, pp. 93-113, CRC Press, Boca Raton, Florida.

170 Wherland, S., Farver, O., and Pecht, I. (1988) *J. Mol. Biol.* **204**, 407-415.

171 Ryden, L., and Lungren, J. (1976) *Nature* **261**, 344-346.

172 Clegg, W., Acott, S.R., and Garner, C.D. (1984) *J. Chem. Soc., Dalton Trans.* 2581-2583

173 Angus, Y., Louis, R., and Weiss, R. (1980) *J. Chem. Soc., Chem. Comm.*, 867-869.

174 Ferris, N.S., Woodruff, W.H., Rorabacher, D.B., Jones, T.E., and Ochrymowycz, L.A. (1978) *J. Am. Chem. Soc.* **100**, 5939-5942.

175 Tennent, D.L., and McMillin, D.R. (1979) *Science* **101**, 2307.

176 McMillin, D.R., and Morris, M.C. (1981) *Proc. Natl. Acad. Sci. U.S.A.* **78**, 6567.

177 Farver, O., Licht, A., and Pecht, I. (1987) *Biochemistry* **26**, 7317.

178 Farver, O., and Pecht, I. (1988) in *Oxidases and related Redox Systems* (King, T.E., Mason, H.S., and Morrison, M., eds.), pp. 270-283, Liss, New York.

179 Hoitink, C.W.G., Woudt, L.P., Turenhout, J.C.M., van de Kamp, M., and Canters, G.W. (1990) *Gene* **90**, 15-20.

180 Arvidsson, R.H.A., Nordling, M., and Lundberg, L.G. (1989) *Eur. J. Biochem.* **179**, 195-200.

181 Canters, G.W. (1987) *F.E.B.S. Lett.* **212**, 168-172.

182 Yamamoto, K., Uozumi, T., and Beppu, T. (1987) *J. Bacteriol.* **169**, 5648-5652.

183 van de Kamp, M., Hali, F.C., Rosato, N., Finazzi-Agro, A., and Canters, G.W. (1990) *Biochim. Biophys. Acta* **1019**, 283-292.

184 Henry, Y., and Bessieres, P. (1984) *Biochimie* **66**, 259-289.

185 Karlsson, B.G., Nordling, M., Pascher, T., Tsai, L.-C., Sjolin, L., and Lundberg, L.G. (1991) *Protein Eng.* **4**, 343-349.

186 Farver, O., Blatt, Y., and Pecht, I (1982) *Biochemistry* , **21**, 3556-3561.

187 Horio, T. (1958) *J. Biochem. (Tokyo)* **45**, 195.

188 Pascher, T., Bergström, J., Malmström, B.G., Vänngård, T., and Lundberg, L.G. (1989) *F.E.B.S. Lett.* **258**, 266-268.

189 van de Kamp, M., Floris, R., Hali, F.C., and Canters, G.W. (1990) *J. Am. Chem. Soc.* **112**, 907-908.

190 Nar, H., Messerschmidt, A., Huber, R., van de Kamp, M., and Canters, G.W. (1991) unpublished material.

191 Garrett, T.P.J., Clingeleffer, D.J., Guss, J.M., Rogers, S.J., and Freeman, H.C. (1984) *J. Biol. Chem.* **259**, 2822-2825.

192 Ryden, L. (1984) in *Copper Proteins and Copper Enzymes* (Lontie, R., ed.) vol. 1, pp. 157-182, CRC Press, Boca Raton, Florida.

193 Boulter, D., Haslett, B.G., Peacock, D., Ramshaw, J.A.M., and Scawen, M.D. (1977) *Plant Biochemistry II, International Rev. Biochem.*, **13**, 1.

194 Sykes, A.G. (1985) *Chem. Soc. Rev.* **14**, 283-315.

195 Wynn, R.M., and Malkin, R. (1988) *Biochemistry* **27**, 5863-5869.

196 Chothia, C., and Lesk, A.M. (1982) *J.Mol.Biol.* **160**, 309-323.

197 Yamanaka, T., Ota, A., and Okunuki, K. (1961) *Biochim. Biophys. Acta* **53**, 294-308.

198 Rosenberg, R.C., Wherland, S., Holwerda, R.A., and Gray, H.B. (1976) *J. Am. Chem. Soc.* **98**, 6364.

199 Lappin, A.G., Segal, M.G., Weatherburn, D.C., Henderson, R.A., and Sykes, A.G., (1979) *J. Am. Chem. Soc.***101**, 2302-2306.

200 Wherland, S., Holwerda, R.A., Rosenberg, R.C., and Gray, H.B. (1975) *J. Am. Chem. Soc.* **97**, 5260.

201 Marks, R.H.L., and Miller, R.D. (1979) *Arch. Biochem. Biophys.* **195**, 103-111.

202 Blaszak, J.A., McMillin, D.R., Thornton, A.T., and Tennent, D.L. (1983) *J. Biol. Chem.* **258**, 9886-9892.

203 Markley, J.L., Ulrich, E.L., Berg, J.P., and Krogman, D.W. (1975) *Biochemistry* **14**, 4428-4433.

204 Engeseth, H.R., and McMillin, D.R. (1986) *Biochemistry* **25**, 2448-2455.

205 Surewicz, W.K., Szabo, A.G., and Mantsch, H.H. (1987) *Eur. J. Biochem.* **167**, 519-523.

206 Ambler, R.P., and Brown, L.H. (1967) *Biochem. J.* **104**, 784.

207 Gray, H.B., and Malmström, B.G. (1983) *Comments Inorg. Chem.* **2**, 203-

209.

208 Vallee, B.L., and Williams, R.J.P. (1968) *Proc. Natl. Acad. Sci. U.S.A.* **59**, 498-505.

209 Norris, G.E. (1982) Ph.D. Thesis, Massey University, Palmerston North, New Zealand.

210 Bernstein, F.C., Koetzle, T.F., Williams, G.J.B., Meyer, E.F., Brice, M.D., Rodgers, J.R., Kennard, O., Shimanouchi, T., and Tasumi, M. (1977) *J. Mol. Biol.* **112**, 535-542.

211 Yamanaka, T., Kijimoto, S., and Okunuki, K. (1963) *J. Biochem. (Tokyo)* **53**, 256-259.

212 Birknes, B. (1983) *J. Appl. Crystallogr.* **16**, 11-13.

213 Diamond, R. (1969) *Acta Cryst.* **A25**, 43-55.

214 Hanson, J.C., Watenpaugh, K.D., Sieker, L., and Jensen, L.H. (1979) *Acta Cryst.* **A35**, 616-621.

215 North, A.C.T., Phillips, D.C., and Mathews, F.S. (1968) *Acta Cryst.* **A24**, 351-359.

216 Programs PREPRO, FITC3 and REDUCER obtained from Washington University, St. Louis.

217 Baker, E.N., and Dodson, E.J. (1980) *Acta Cryst.* **A36**, 559-572.

218 Ford, G.C. (1974) *J. Appl. Cryst.* **7**, 555-564.

219 Rae, A.D. (1965) *Acta Cryst* **19**, 683.

220 Konnert, J.H. (1976) *Acta Cryst.* , **A32**, 614-617.

221 Hendrickson, W.A., and Konnert, J.H. (1980) in *Biomolecular Structure, Function, Conformation and Evolution* (Srinivasan, R., ed.), vol. 1, pp. 43-57, Pergamon, Oxford.

222 Hendrickson, W.A., and Konnert, J.H. (1980) in *Computing in Crystallography*, (Diamond, R., Ramaseshan, S., and Venkatesan, K., eds.), pp. 13.01-13.23, Indian Institute of Science, Bangalor.

223 Konnert, J.H., and Hendrickson, W.A. (1980) *Acta Cryst.* , **A36**, 344-350.

224 Hendrickson, W.A., and Konnert, J.H. (1980) *Biophys. J.* , **32**, 645-47.

225 Cooley, J.W., and Tukey, J.W. (1965) *Math. Comput.* **19**, 297-301.

226 Agarwal, R.C. (1978) *Acta Cryst.* **A34**, 791-809.

227 Rollett, J.S. (1982) in *Computational Crystallography* (Sayre, D., ed.), pp. 338-353, Clarendon Press, Oxford.

228 Rollett, J.S. (1984) in *Methods and Applications in Crystallographic Computing* (Hall, S.R., and Ashida, T., eds.), pp. 161-173, Clarendon Press, Oxford.

229 Isaacs, N. (1984) in *Methods and Applications in Crystallographic Computing*

(Hall, S.R., and Ashida, T., eds.), pp. 193-205, Clarendon Press, Oxford.

230 Ten Eyck, L.F. (1973) *Acta Cryst.* **A29**, 183-191.

231 Jones, T.A. (1978) *J. Appl. Cryst.* **11**, 268-272.

232 Luzzati, P.V. (1952) *Acta Cryst.* **5**, 802-810.

233 Derewenda, Z.S., Brzozowski, A.M., Stepein, A. and Grabowski, M.J. (1982) *Acta Cryst.* **A38**, 432-438.

234 Fermi, G. (1975) *J. Mol. Biol.* **97**, 237-256.

235 Kabsch, W., and Sander, C. (1983) *Biopolymers* **22**, 2577-2637.

236 Program DISTANG from Dodson, E. (1985) Daresbury Laboratory.

237 Program ORDER selects and reformats the hydrogen atom positions output from DISTANG.

238 Baker, E.N., and Hubbard, R.E. (1984) *Prog. Biophys. Molec. Biol.* **44**, 97-179.

239 Isogai, Y., Nemethy, G., Rackovsky, S., Leach, S.J., and Scheraga, H.A. (1980) *Biopolymers* **19**, 1183-1210.

240 Richardson, J.S. (1981) *Advan. Protein Chem.* **34**, 167-339.

241 Rees, D.C., Lewis, M., and Lipscomb, W.N. (1983) *J. Mol. Biol.* **168**, 367-387.

242 Adman, E.T., Watenpaugh, K.D., and Jensen, L.H. (1975) *Proc. Natl. Acad. Sci. U.S.A.* **72**, 4854-4858.

243 Carter, C.W., Jr., Kraut, J., Freer, S.T., and Alden, R.A. (1974).*J. Biol. Chem.* **249**, 6339-6346.

244 Alber, T., Dao-pin, S., Wilson, K., Wozniak, J.A., Cook, S.P., and Matthews, B.W. (1987) *Nature (London)* **330**, 41-46.

245 Ippolito, J.A., Alexander, R.S., and Christianson, D.W. (1990) *J. Mol. Biol.* **215**, 457-471.

246 Gregoret, L.M., Rader, S.D., Fletterick, R.J., and Cohen, F.E. (1991) *PROTEINS: Structure, Function and Genetics* **9**, 99-107.

247 Donohue, J. (1969) *J. Mol. Biol.* **45**, 231-235.

248 Walters, M.A., Dewan, J.C., Min, C., and Pinto, S. (1991) *Inorg. Chem.* **30**, 2656-2662.

249 Hamilton, W.C., Ibers, J.A. (1968) in *Hydrogen bonding in Solids*, Chapter 5, Benjamin, New York.

250 Chung, W.P., Dewan, J.C., and Walters, M.A. (1991) *J. Am. Chem. Soc.* **113**, 525-530.

251 Kissinger, C.R., Sieker, L.C., Adman, E.T., and Jensen, L.H. (1991) *J. Mol. Biol.* **219**, 693-715.

252 Watenpaugh, K.D., Sieker, L.C., Herriott, J.R., and Jensen, L.H. (1973)

Acta Cryst. **B29**, 943-956.

253 Venkatachalam, C.M. (1968) *Biopolymers* **6**, 1425-1436.

254 Reid, K.S.C., Lindley, P.F., and Thornton, J.M. (1985) *F.E.B.S. Lett.* **190**, 209-213.

255 Kabsch, W. (1976) *Acta Cryst.* **A32**, 922-923.

256 Bondi, A. (1964) *J. Phys. Chem.* **68**, 441.

257 Chakrabarti, P. (1989) *Biochemistry* **28**, 6081-6085.

258 Hathaway, B.J. (1989) *Comprehensive Coordination Chemistry* **5**, 533-774.

259 Coucouvanis, D., Swenson, D., Baenziger, N.C., Pedelty, R., Caffery, M.L., and Kanodia, S. (1989) *Inorg. Chem.* **28**, 2829-2836.

260 Olmstead, M.M., Musker, W.K., and Kessler, R.M.(1982). *Transition Met. Chem.* **7**, 140.

261 Musker, W.K., Olmstead, M.M., Kessler, R.M., Murphey, M.B., Neagly, C.H., Roush, P.B., Hill, N.L., Wolford, T.L., Hope, H., Delker, G., Swanson, K., and Gorewit, B.V. (1980). *J. Am. Chem. Soc.* **102**, 1225.

262 Cariati, F., Naldini, L., Panzanelli, A., Demartin, F., and Manassero, M. (1983) *Inorg. Chim. Acta* **69**, 117.

263 Messmer, G.G., and Palenik, G.J. (1969) *Inorg. Chem.* **8**, 2750.

264 Drew, M.G.B., Othman, A.H.B., Edwards, D.A., and Richards, R. (1975) *Acta Cryst.* **B31**, 2695.

265 Bartlett, M.W.(1970) Ph.D. Thesis, University of Waterloo.

266 Restivo, R.J., Costin, A., Ferguson, G., and Carty, A.J. (1975) *Can. J. Chem.* **53**, 1949.

267 Pasquali, M., Fiaschi, P., Floriani, C., and Gaetani-Manfredotti, A. (1983) *J. Chem. Soc., Chem. Comm.*, 197.

268 Gagne, R.R., Kreh, R.P., and Dodge, J.A. (1979) *J. Am. Chem. Soc.* **101**, 6917.

269 Rauchfuss, T.B., Wilson, S.R., and Wrobleski, D.L. (1981) *J. Am. Chem. Soc.* **103**, 6769.

270 Ho, D.M., and Bau, R. (1983) *Inorg. Chem.* **22**, 4079.

271 Rodesiler, P.F., and Amma, E.L. (1974) *J. Chem. Soc., Chem. Comm.*, 599.

272 Mounts, R.D., Ogura, T.,and Fernando, Q. (1974) *Inorg. Chem.* **13**, 802.

273 Geerts, R.L., Huffman, J.C., Folting, K., Lemmen, T.H., and Caulton, K.G. (1983) *J. Am. Chem. Soc.* **105**, 3503.

274 Pasquali, M., Fiaschi, P., Floriani, C., and Zanazzi, P.F. (1983) *J. Chem. Soc., Chem. Comm.* 613.

275 Thompson, J.S., and Whitney, J.F. (1984) *Inorg. Chem.* **23**, 2813.

276 Doyle, G., Erikson, K.A., and van Engen, D. (1983) *Inorg. Chem.* **22**, 2892.

277 Hendriks, H.M.J., Birker, P.J.M.W.L., Van Rijn, J., Verschoor, G.C., and Reedijk, J. (1982). *J. Am. Chem. Soc.* **104**, 3607.

278 Oshio, H. (1990) *J. Chem. Soc., Dalton Trans.*, 2985-2989.

279 Brown, D.S., Lee, J.D., Melson, B.G.A., Hathaway, B.J., Procter, I.M., and Tomlinson, A.A.G. (1967) *Chem. Commun.* 369.

280 Procter, I.M., Hathaway, B.J., and Nicholls, P. (1968) *J. Chem. Soc. (A)*, 1678.

281 Tomlinson, A.A.G., Hathaway, B.J., Billing, D.E., and Nicholls, P. (1969) *J. Chem. Soc.(A)*, 65.

282 Clegg, W., Acott, S.R., and Garner, C.D. (1984) *Acta Cryst.* **C40**, 768.

283 Dagdigan, J.V., McKee, V., and Reed, C.A. (1982) *Inorg. Chem.* **21**, 1332.

284 Schilstra, M.J., Birker, P.J.M.W.L., Verschoor, G.C., and Reedjik, J. (1982) *Inorg. Chem.* **21**, 2637.

285 Nishida, Y., Takahashi, K., Kuramoto, H., and Kida, S. (1981) *Inorg. Chim. Acta* . **51**, L103.

286 Jeannin, S., Jeannin, Y., and Lavigne, G. (1979) *Inorg. Chem.* **18**, 3528.

287 Knapp, S., Keeman, T.P., Liu, J., Potenza, J.A., and Schugar, H.J. (1990) *Inorg. Chem.* **29**, 2189-91.

288 Thompson, J.S., Marks, T.J., and Ibers, J.A. (1979) *J. Am. Chem. Soc.* **101**, 4180-4192.

289 Knotter, D.M., van Koten, G., van Maanen, H.L., Grove, D.M., and Spek, A.L. (1989) *Angew. Chem. Int. Ed. Engl.* **28**, 341-342.

290 Dance, I.G., Fitzpatrick, L.J., Craig, D.C., and Scudder, M.L. (1989) *Inorg. Chem.* **28**, 1853-1861.

291 Chadha, R., Kumar, R., and Tuck, D.G. (1986) *J. Chem. Soc., Chem. Comm.*, 188-189.

292 Bharadwaj, P.K., John, E., Xie, C.-L., Zhang, D., Hendrickson, D.N., Potenza, J.A., and Schugar, H.J. (1986) *Inorg.Chem.* **25**, 4541-4546.

293 Khan, M.A., Kumar, R., and Tuck, D.G. (1988) *Polyhedron* **7**, 49-55.

294 Birker, P.J.M.W.L., and Freeman, H.C. (1977) *J. Am. Chem. Soc.* **99**, 6890.

295 Schugar, H.J., Ou, C.-C., Thich, J.A., Potenza, J.A., Felthouse, T.R., Haddad, M.S., Hendrickson, D.N., Furey, W., Jr., and Lalancette, R.A. (1980) *Inorg. Chem.* **19**, 543-552.

296 Coucouvanis, D., Murphy, C.N., and Kanodia, S.K. (1980) *Inorg. Chem.* **19**, 2993-2998.

297 Dance, I.G., Bowmaker, G.A., Clark, G.R., and Seadon, J.K. (1983) *Polyhedron* **2**, 1031-1043.

298 Nicholson, J.R., Abrahams, I.L., Clegg, W., and Garner, C.D. (1985) *Inorg. Chem.* **24**, 1092-1096.

299 Dance, I.G. (1986) *Polyhedron* **5**, 1037-1104.

300 Koch, S.A., Fikar, R., Millar, M., O'Sullivan, T. (1984) *Inorg. Chem.* **23**, 121-122.

301 Garner, C.D., Nicholson, J.R., and Clegg, W. (1984) *Inorg. Chem.* **23**, 2148-2150.

302 Annan, T.A., Kumar, R., and Tuck, D.G. (1990) *Inorg. Chem.* **29**, 2475-2479.

303 Matsubayashi, G., and Yokozawa, A. (1991) *J. Chem. Soc., Chem. Comm.*, 68-69.

304 Ball, J.M., Boorman, P.M., Fait, J.F., and Ziegler, T. (1989) *J. Chem. Soc., Chem. Comm.* 1989, 722-723.

305 Karagiannidis, P., Hadjikakou, S.K., Aslanidis, P., and Hountas, A. (1990) *Inorg. Chim. Acta* **178**, 27-34.

306 Block, E., Kang, H., Ofori-Okai, G., and Zubieta, J. (1990) *Inorg. Chim. Acta* **167**, 147-148.

307 Becker, B., Wojnowski, W., Peters, K., Peters, E.-M., and von Schnering, H.G. (1990) *Polyhedron* **9**, 1659-1666.

308 Karlin, K.D., Dahlstrom, P.L., Stanford, M.L., and Zubieta, J. (1979) *J. Chem. Soc., Chem. Comm.*, 465-467.

309 Karlin, K.D., Dahlstrom, P.L., Hyde, J.R., and Zubieta, J. (1980) *J. Chem. Soc., Chem. Comm.*, 906-908.

310 Birker, P.J.M.W.L., and Reedjik, J. (1983) in *Copper Coordination Chemistry: Biochemical and Inorganic Perspectives* (Karlin, K.D., Zubieta, J., eds.), pp. 409-424, Adenine Press, New York.

311 Blake, A.J., Gould, R.O., Holder, A.J., Lavery, A.J., and Schröder, M. (1990) *Polyhedron* **9**, 2919-2924.

312 Brubaker, G.R., Brown, J.N., Yoo, M.K., Kinsey, R.A., Kutchan, T.M., and Mottel, E.A. (1979) *Inorg. Chem.* **18**, 299-302.

313 Clarkson, J.A., Yagbasan, R., Blower, P.J., and Cooper, S.R. (1989) *J. Chem. Soc., Chem. Comm.*, 1244-1245.

314 Balakrisnan, K.P., Riesen, A., Zuberbühler, A.D., and Kaden, T.A. (1990) *Acta Cryst.* **C46**, 1236-1238.

315 Adman, E.T., and Jensen, L.H. (1981) *Isr. J. Chem.* **21**, 8.

316 Addison, A.W., and Sinn, E. (1983) *Inorg. Chem.* **22**, 1225.

317 Anderson, O.P., Perkins, C.M., and Brito, K.K. (1983) *Inorg. Chem.* **22**, 1267.

318 Toftlund, H., Becher, J., Oleson, P.H., and Pedersen, J.Z. (1985) *Isr. J. Chem.* **25**, 56.

319 Blake, A.J., Taylor, A., and Schröder, M. (1990) *Polyhedron* **9**, 2911-2918.

320 Baker, E.N., and Norris, G.E. (1977) *J. Chem. Soc., Dalton Trans.*, 877-882.

321 de Groot, B., Giesbrecht, G.R., Loeb, S.J., and Shimizu, G.K.H. (1991) *Inorg. Chem.* **30**, 177-182.

322 Stoffels, A.L.E., Haanstra, W.G., Driessen, W.L., and Reedjik, J. (1990) *Angew. Chem. Int. Ed. Engl.* **29**, 1419-1420.

323 Raper, E.S. (1985) *Coord. Chem. Rev.* **11**, 115.

324 Alyea, E.C., Ferguson, G., Jennings, M., Li, B., Xu, Z., You, X., Liu, S. (1990) *Polyhedron* **9**, 2463-2467.

325 Sheridan, R.P., Allen, L.C., and Carter, C.W., Jr. (1981) *J. Biol. Chem.* **256**, 5052-5057.

326 Sheridan, R.P., Knight, E.T., and Allen, L.C. (1984) *Biopolymers* **23**, 195-200.

327 Sheridan, R.P., and Allen, L.C. (1980) *Chem. Phys. Lett.* **69**, 600-604.

328 Krishnamoorthi, R., and Markley, J.L. (1986) *Biochemistry* **25**, 60-67.

329 Carter, C.W., Jr. (1977) *J. Biol. Chem.* **252**, 7802-7811.

330 Valentine, J.S., Sheridan, R.P., Allen, L.C., and Kahn, P.C. (1979). *Proc. Natl. Acad. Sci. U.S.A.* **76**, 1009-1013.

331 Evans & Sutherland PS-330 interactive graphics system.

332 *Handbook of Chemistry and Physics*, 63rd edition (1982-1983), p. F-184, CRC Press.

333 Canters, G.W. (1991) personal communication. (OW162 in NMR studies.)

334 Karlsson, B.G., Pascher, T., Nordling, M., Arvidsson, R.H.G., and Lundberg, L.G. (1989) *F.E.B.S. Lett.* **246**, 211-217.

335 Lommen, A., Canters, G.W., and van Beeuman, J. (1988) *Eur. J. Biochem.* **176**, 213-223.

336 Lommen, A., and Canters, G.W.(1990) *J. Biol. Chem.* **265**, 2768-2774.

337 Canters, G.W., Lommen, A., van de Kamp, M., and Hoitink, C.W.G. (1989) in *Symposium on Biochemical approaches to the study of Copper Proteins*, pp. 1-10, Camerino, 10-11 July 1989.

338 Morpugo, L., Rotilio, G., Finazzi-Agro, A., and Mondovi, B. (1974) *Arch. Biochem. Biophys.* **161**, 291-296.

339 Kraut, J. (1988) *Science* **242**, 533-540.

340 Blake, C.C.F., Johnson, L.N., Mair, G.A., North, A.C.T., Phillips, D.C., Sharma, V.R. (1967) *Proc. Royal Soc.* **B167**, 378.

341 Williams, R.J.P. (1971) *Inorg. Chim. Acta Rev.* **5**, 137-155.

342 Williams, R.J.P. (1971) *Cold Spring Harbour Symposia on Quantitative Biology* **36**, 53-62.

343 Williams, R.J.P. (1985) *J. Mol. Catal.* **30**, 1-26.

344 Onuchic, J.N., and Beratan, D.N. (1990) *J. Chem. Phys.* **92**, 722-733.

345 Beratan, D.N., Onuchic, J.N., and Hopfield, J.J. (1987) *J. Chem. Phys.* **86**, 4488.

346 Beratan, D.N., Onuchic, J.N., and Hopfield, J.J. (1985) *J. Chem. Phys.* **83**, 5325.

347 Marcus, R.A. (1964) *Ann. Rev. Phys. Chem.* **15**, 155.

348 Beratan, D.N., and Hopfield, J.J. (1984) *J. Am. Chem. Soc.* **106**, 1584-1594.

349 Ohta, K., Closs, G.L., Morokuma, K., and Green, N.J. (1986) *J. Am. Chem. Soc.* **108**, 1319-1320.

350 SooHoo, C.K., Hollocher, T.C., Kolodziej, A.F., Orme-Johnson, W.H., and Bunker, G. (1991) *J. Biol. Chem.* **266**, 2210-2218.

351 Li, P.M., Malmström, B.G., and Chan, S.I. (1989) *F.E.B.S. Lett.* **248**, 210-211.